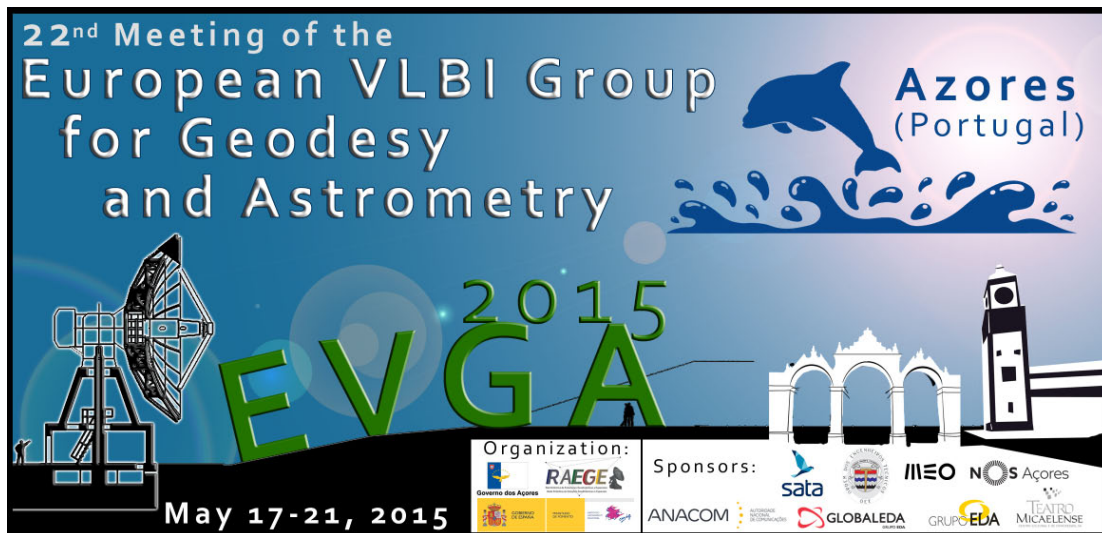


Proceedings of the 22nd European VLBI
Group for Geodesy and Astrometry
Working Meeting
18-21 May 2015
Ponta Delgada, Azores

edited by R. Haas and F. Colomer



ISBN: 978-989-20-6191-7

**Proceedings of the 22nd European VLBI Group for Geodesy and Astrometry
Working Meeting**

edited by
Rüdiger Haas and Francisco Colomer

The authors are responsible for the content of their papers.
The use of the contents has to follow the laws of copyright and ownership.

ISBN 978-989-20-6191-7

Preface

The 22nd Working Meeting of the European VLBI Group for Geodesy and Astrometry was a very special meeting. Besides the perfect organisation by the local hosts, the very nice venue in the Teatro Micaelense at Ponta Delgada, and a very intense and interesting scientific program, it was to my knowledge the first EVGA working meeting ever that included the inauguration of new radio telescopes (!). The EVGA participants witnessed both the inauguration of the new VGOS radio telescope at Zelenchukskaya (Caucasus, Russia) and the new VGOS radio telescope at Santa Maria (Azores, Portugal).

The 13.2 m VGOS-telescope at Zelenchuskaya was inaugurated on 19 May by a short speech of Prof. Alexander Ipatov given via internet and the immediately following first VLBI observations with the new telescope and partner telescopes in Yebes, Wettzell and Badary, see Fig. 1 left. The observed data were correlated at the correlators in Bonn and St. Petersburg and fringes could be reported already a short time after during the ongoing EVGA meeting. This was a very impressive demonstration of the new telescope and its receiving equipment, and I want to congratulate everyone involved in the project and this impressive inauguration!

The 13.2 m VGOS-telescope at Santa Maria was inaugurated on 20 May when all EVGA participants flew early in the morning from São Miguel to Santa Maria. After a nice breakfast the actual ceremony took place at the RAEGE station with speeches given by Mr. Vasco Alves Cordeiro, the President of the Azores, and Mr. Amador Elena Córdoba the General Director of the Instituto Geográfico Nacional (IGN) of Spain. The new telescope and the complete RAEGE site could be visited and inspected by all EVGA participants. After a nice lunch and an island tour on Santa Maria during the afternoon, the conference participants took the plane back to São Miguel.



Figure 1: Left: Picture of the telescopes active in VLBI observations during the inauguration of the Zelechukskaya radio telescope. Right: Inauguration of the Santa Maria radio telescope.

The inaugurations of two new radio telescopes following the VLBI2010 design is a very strong indication that the VLBI Global Observing System (VGOS) era now really has started. Several VGOS telescopes are coming online now. It is in particular very good to see that the European VLBI community is very active in the VGOS development. Several further European VGOS telescopes are planned and/or under construction and we hopefully see further inaugurations in the near future.

The large number of participants at the EVGA 2015 working meeting, see Fig. 2, and the high quality and interesting oral and poster presentations are another indication that European VLBI community is on a good track. The proceedings are available electronically at http://evga2015.raege.net/EVGA2015_proceedings.pdf. I think and hope we can count on a strong contribution of the EVGA to VGOS!

November 2015

Rüdiger Haas (EVGA chair)



Figure 2: Picture of the EVGA 2015 participants in front of the conference venue, the Teatro Micaelense in Ponta Delgada.

Message by the Regional Government

On behalf of the Regional Government of the Azores, I would like to convey to all of those who participated in the 22nd European Very Long Baseline Interferometry (VLBI) Group for Geodesy and Astrometry Meeting our sincere appreciation. We strongly believe the Azores are an excellent location, in the middle of the Atlantic Ocean, to host international scientific events, such as this meeting, held in São Miguel last May.

While making the most of our geostrategic position, the Government of the Azores has implemented an investment policy in technological infrastructures, including stations for space and earth observation, climatology and detection of nuclear tests and we encourage our research centres to actively engage with international networks. Space technologies and methodologies are critical in terms of knowledge and competitiveness of industry, and its applications are crucial in areas such as transports (positioning systems and fleet management), defense, and even health (image technology used by satellites is now used in hospitals to detect diseases).

For the Azores it is essential to be included in the routes of spatial development and to ensure a role in the space technologies development, thus the public support to this end. The Azores are the Portuguese region with more investment in this field, through the installation of important infrastructures, which are expected to be catalysts for scientific and technological development, and to provide a sound basis for competitiveness and economic growth in our region. The transatlantic vocation of the Azores and its geographical location is an attraction factor to the implementation of projects in the space policy domain.

Boosting synergies with several stakeholders – such as companies, universities, scientific associations and public authorities – will, so we trust, lead to the creation of a new economic cluster on space technologies. Projects on the spatial domain represent opportunities for technological and scientific development while contributing to the creation of skilled jobs in our Region on areas such as high-tech engineering systems. It is easy to understand, given the nature of the Azores Region, the importance of satellite imagery for the monitoring of ocean and coastal areas, for volcanic and seismological monitoring, for climatology and the study the atmosphere, and also for habitat mapping. Against this background the projects that EVGA's participants presented and shared are fundamental for the answers we need to the emerging challenges of space technologies, worldwide, and in the Azores as well.

Thank you!

November 2015

Fausto Abreu

Regional Secretary of the Sea, Science and Technology of the Regional Government of Azores

EVGA 2015 organising committees

Scientific Organising Committee (SOC)

- Sabine Bachmann, Bundesamt für Kartographie und Geodäsie, Germany
- Alessandra Bertarini, Universität Bonn, Germany
- Géraldine Bourda, Université Bordeaux 1, France
- Johannes Böhm, Technische Universität Wien, Austria
- Francisco Colomer, Instituto Geográfico Nacional, Spain
- Rüdiger Haas (Chair), Chalmers Tekniska Högskola, Sweden

Local Organising Committee (LOC)

- Luis Ramalhais Santos (Chair)
- Sara de Viveiros Pavão
- Francisco Luis Wallenstein Faria e Maia de Macedo
- Maria Luciana Lisboa Ananias
- Hélder Filipe Martins de Medeiros
- Mónica Paulo de La Cerda
- Francisco Colomer
- Susana García Espada
- Rubén Bolaño González
- José Antonio López Fernández

Acknowledgements

We thank all participants of the EVGA 2015 for sharing their findings with the meeting audience during interesting oral and poster presentations. We thank the scientific organising committee for putting together a very interesting meeting program. The program and the list of participants are provided in Appendix-A. And we are of course grateful to all authors for preparing their proceedings contributions.

We thank the local organising committee for an excellent organisation of this EVGA meeting! Everything worked perfectly and we are convinced that all participants enjoyed their stay in Ponta Delgada.

The support by the local sponsors Autoridade Nacional de Comunicações, SATA, GlobalEDA, MEO, NOS Açores, GrupoEDA, Teatro Micaelense, and Ordem dos Engenheiros Técnicos is gratefully acknowledged. More details on the sponsors are provided in Appendix-B.

Rüdiger Haas and Francisco Colomer
Editors
November 2015

This page is intentionally left blank.

Contents

Technology

VGOS Operational Readiness	1	A. Neidhardt, J. Lovell, K. Kirschbauer, M. Schönberger, E. Himwich, J. McCallum, Ch. Plötz, J. Quick
B. Petrachenko		
Broadband VLBI at 6 GHz to 14 GHz frequency range between Kashima 34 m and Ishioka 13 m	6	Current Operations of the Bonn Correlator and Preparations for VGOS 35
K. Takefuji, T. Kondo, H. Hideki, M. Sekido		W. Alef, T. Schüler, A. Müskens, A. Nothnagel, A. Bertarini, H. Rottmann, L. La Porta, S. Bernhart, G. Bruni
Technological Developments for VGOS from IGN Yebes Observatory	11	IAA VGOS GPU-based Software Correlator: current status and broadband processing 40
J. A. López-Fernández, F. Tercero-Martínez, J. A. López-Pérez, J. M. Serna-Puente, P. de Vicente, J. D. Gallego, L. R. Santos		V. Ken, I. Surkis, Y. Kurdubova, A. Melnikov, N. Mishina, V. Mishin, V. Shantyr
Results from the TWIN Commissioning Phase	15	Wideband Cryogenic Feed Receivers for VLBI 43
T. Schüler, G. Kronschnabl, A. Neidhardt, C. Plötz, A. Bertarini, L. La Porta, S. Bernhart, A. Müskens, S. Halsig, A. Nothnagel		R. Rayet, S. Rawson, T. Bonhoure, M. Sevrin, A. Martellosio, M. Pasian
The Yebes RAEGE telescope control, commissioning tests and first results	20	Ultra Wide-Band HTS filter for new geodetic VLBI front-ends 48
P. de Vicente, R. Bolaño, L. Barbas, A. Moreno, A. Díaz, S. García-Espada		A. Caddemi, E. Cardillo, G. Tuccari
Development of Multipurpose Digital Backend for "Quasar" network radio telescopes	25	The German Antarctic Receiving Station O'Higgins - upgrades of the VLBI-capabilities for future challenges 52
E. Nosov		Ch. Plötz, A. Neidhardt, T. Klügel, R. Wojdziak, J. Serna-Puente, B. Vaquero-Jiménez, T. Schüler, VLBI Team Wettzell, DFD Team DLR
Results from a test realization of a system monitoring for seamless auxiliary data	30	Status of the Spanish-Portuguese RAEGE project 55
		J. Gómez-González, L. Santos, J. A. López- Fernández, F. Colomer

Observations

The southern hemisphere AUSTRAL program: A pathway to VGOS	59	GLONASS-VLBI: Onsala-Wettzell test observations	107
J. Lovell, J. McCallum, L. Plank, E. Rastorgueva-Foi, S. Shabala, D. Mayer, J. Böhm, O. Titov, J. Quick, S. Weston, S. Gulyaev, T. Natusch, C. Reynolds, H. Bignall, J. Sun, A. Neidhardt		R. Haas, T. Hobiger, A. Hellerschmied, A. Neidhardt, J. Kodet	
GSI's regional stations and AOV activities	64	Hb-Ho: Observations with the sibling telescope in Hobart	112
R. Kawabata, T. Wakasugi		L. Plank, J. Lovell, J. McCallum, J. Böhm, D. Mayer	
First Geodetic Result of Ishioka VGOS Station	67	The Asia-Oceania VLBI Group for Geodesy and Astrometry	117
Y. Fukuzaki, K. Wada, R. Kawabata, M. Ishimoto, T. Wakasugi		J. Lovell, R. Kawabata, S. Kurihara, F. Shu, J. Cho	
On the Role of Tianma Radio Telescope for Improving Celestial Reference Frames	71	Twin Telescopes at Onsala and Wettzell and their contribution to the VGOS System	120
F. Shu, J. Wang, W. Jiang, G. Wang, Z. Shen		C. Schönberger, P. Gnielsen, J. Böhm, R. Haas	
Russian Radio Interferometer of New Generation	75	Contributions of Onsala Space Observatory to GGOS	125
A. Ipatov, D. Ivanov, G. Ilin, V. Olifirov, V. Mardyshkin, I. Surkis, L. Fedotov, I. Gayazov, V. Stempkovsky, Y. Bondarenko		R. Haas, G. Elgered, T. Hobiger, H.- G. Scherneck, J. Johansson	
Status report on the GGAO-Westford VGOS systems	80	Local Tie Works in Yebes Observatory	130
A. E. Niell		B. Córdoba, J. López-Ramasco, S. García-Espada	
Contributions of HartRAO to Space Geodesy, Astrometry and related disciplines	85	Coordinate-Based Bundle Adjustment – Advanced Network Adjustment Model for Polar Measurement Systems	135
L. Combrinck, R. Botha, P. Mey, A. de Witt, J. Quick		M. Lösler, C. Eschelbach, R. Haas	
Geodetic Italian VLBI: first tests	90	Determining HartRAO antenna parameters with VieVS	140
M. Stagni, M. Negusini		M. Nickola, A. de Witt, H. Krásná, W. L. Combrinck, J. Böhm	
A Vision for VGOS Observations and Analysis in 2020	93	Continuous VLBI Scheduling: The CONT14 Example	145
H. Hase, D. Behrend, A. Nothnagel, H. Schuh		D. Behrend	
Practical Uses of VGOSDB Format	97	Implementation of the vgosDb format	150
J. Gipson		S. Bolotin, K. Baver, J. Gipson, D. Gordon, D. MacMillan	
Scheduling of VLBI observations to satellites with the Vienna VLBI Software (VieVS)	102	Observing GNSS L-band Signals: Ionospheric Corrections by co-located GNSS Measurements	153
A. Hellerschmied, J. Böhm, R. Haas, J. Kodet, A. Neidhardt, L. Plank		B. Männel, M. Rothacher	

Analysis

VLBI-like GNSS delays in the analysis of CONT11	158	Comparison of VLBI nutation time series	205
Y. Kwak, J. Böhm, T. Hobiger, L. Plank		C. Gattano, S. Lambert, C. Bizouard	
Influence of the horizontal resolution of numerical weather models on ray-traced delays for VLBI analysis	162	Estimating a Celestial Reference Frame in the Presence of Source Structure	210
A. Hofmeister, D. Landskron, J. Böhm		L. Plank, S. Shabala, J. McCallum, H. Krásná, E. Rastorgueva-Foi, J. Lovell, B. Petrachenko	
Augmenting the stochastic model in VLBI data analysis by correlations from atmospheric turbulence models	167	Imaging the IYA09 VLBI Super-session	215
S. Halsig, T. Artz, A. Iddink, A. Nothnagel		A. Collioud, P. Charlot	
Short-term station coordinate variations from Kalman filtering VLBI data	172	Aligning VLBI and Gaia Extragalactic Celestial Reference Frames	220
B. Soja, M. Karbon, T. Nilsson, K. Balidakis, S. Glaser, R. Heinkelmann, H. Schuh		G. Bourda, P. Charlot, A. Collioud	
Antenna axis offsets estimated in VLBI data analysis	177	Estimating the velocity of the barycenter of the solar system from VLBI observations	224
T. Nilsson, M. Karbon, J. A. Mora-Diaz, V. Raposo-Pulido, B. Soja, R. Heinkelmann, H. Schuh		M. H. Xu, J. Anderson, R. Heinkelmann, H. Schuh, G. L. Wang	
Numerical Issues of VLBI Data Analysis	181	The CVN Geodetic Observation and its Result	228
T. Artz, S. Halsig, A. Iddink, A. Nothnagel		G. Wang, M. Xu, Z. Zhang, S. Xu, L. Li, F. Shu	
Sophistication in UT1-Intensive Scheduling by Using Impact Factors - First Results of Field Tests	185	Minimization of the UT1 Formal Error Through a Minimization Algorithm	230
A. Nothnagel, J. Leek, M. Beier, T. Artz, D. Ullrich		J. Gipson, K. Bayer	
The CONT Campaigns as a Precursor to VGOS Observing	189	Automated analysis of Kokee–Wetzell intensive sessions	235
D. MacMillan		N. Kareinen, T. Hobiger, R. Haas	
Investigation of Earth Orientation Parameters for VLBA Calibrator Survey sessions	193	Comparison of tropospheric delays from GPS and Kalman filtered VLBI data	240
D. Mayer, J. Böhm, H. Krásná		B. Soja, T. Nilsson, M. Karbon, C. Lu, X. Li, K. Balidakis, J. Anderson, S. Glaser, L. Liu, J. Mora-Diaz, M. Xu, R. Heinkelmann, H. Schuh	
Revisiting the VLBA Calibrator Surveys, VCS-II	198	Combining VLBI and GPS for inter-continental frequency transfer	245
D. Gordon		T. Hobiger, C. Rieck, R. Haas, Y. Koyama	
Assessment of CRF Solutions from Session-wise Normal Equation Systems	201	Baseline dependent weights in VieVS	249
A. Iddink, T. Artz, S. Halsig, A. Nothnagel		M. Uunila, H. Krásná, J. Gipson	
		Combination of common parameters for co-located VLBI antennas	252
		T. Nilsson, R. Heinkelmann, S. Glaser, B. Soja, M. Karbon, H. Schuh	
		VLBI Analysis at BKG	256
		V. Thorandt, G. Engelhardt, D. Ullrich	

Combination products and the IVS contribution to ITRF2014	259
L. Messerschmitt, S. Bachmann, D. Thaller	
Analysis of GPS, VLBI and DORIS input time series for ITRF2014	263
V. Tornatore, E. Tanır Kayıkçı, M. Roggero	
VLBI Phase-referencing Experiments for Deep Space Probes	268
W. Zheng, F. Tong, J. Zhang, F. Shu, L. Liu	
A Celestial Reference Frame at 22 GHz (K-band)	272
A. de Witt, A. Bertarini, C. S. Jacobs, J. Quick, S. Horiuchi, J. E. J. Lovell, J. M. McCallum, T. Jung, G. Bourda, P. Charlot	
Observing Gaia transfer sources in R&D and RDV sessions	277
K. Le Bail, D. Gordon, J. M. Gipson, D. S. MacMillan	

VGOS Operational Readiness

B. Petrachenko

Abstract The state of VGOS operational readiness will be discussed from the point of view of the IVS Technology Development Coordinator

Keywords VGOS operations broadband

1 Introduction

In 2003 the International VLBI Service for Geodesy and Astrometry (IVS) began investigating options for a next generation VLBI system. By 2005 the organization had made a commitment to a bold new vision for the future that promised nearly an order of magnitude improvement in geodetic/astrometric precision, continuous observing, and the production of initial results within 24 hours of taking data (Niell et al., 2005). [The new system was initially referred to as the VLBI2010 System but has since been renamed the VLBI Global Observing System (VGOS).]

Over the next years, the VLBI2010 Committee (V2C) developed the requirements for the next generation system (Petrachenko et al., 2009). The specifications set by the committee were to a large degree based on the conclusions of Monte Carlo simulations that showed that the most effective strategy for improving performance was to increase the observation rate per site to about one observation every 30 s. This required the construction of fast slewing antennas and the use of a completely new broadband observing mode that involved four 1 GHz bands

optimally placed in the frequency range 2–14 GHz. The VGOS requirements were further elaborated at the IVS VLBI2010 Workshop on Technical Specifications (2012).

In the meantime a significant number of fast slewing antennas have been funded with several already constructed or under construction. Simultaneously broadband signal chains have been developed and tested. More recently, the IVS generated an observing plan (Petrachenko et al., 2014) to guide the ramp up of VGOS observations. The plan begins with a series of three test campaigns in 2015 and a pilot project in 2016; it ends with full global 24/7 operations in 2020.

2 Current Status

The VGOS Observing Plan indicates that (at the time that this paper was being written) two test campaigns should already have been completed. However execution of the test campaigns requires the pre-existence of efficient end-to-end operational processes and the existence of a small VGOS network, both of which were not available at the time the test campaigns were scheduled to begin. To remedy this situation, intensive work is underway to get VGOS operational processes and a larger number of broadband signal chains into a workable state. It is now estimated that the first steps of the VGOS Observing Plan will be delayed by about a year to the start of 2016; however this delay is not expected to have a significant impact on the target date for the start of full VGOS operations.

Bill Petrachenko
Natural Resources Canada, 588 Booth St., Ottawa, ON, K1A 0Y7

2.1 Operational Process Development

Beginning in late 2014, short bi-weekly sessions on the the Westford/GGAO baseline have been used as a test bed for VGOS operational process development. At the start, the tests were 1 hour in duration but the length has recently been increased to 6 hours.

The efficiency of the test sessions continues to improve due to progress in a number of areas:

1. The VEX2 definition is now complete. This update to the original VEX language was needed to describe new hardware functionality associated with the VGOS broadband observing mode. It is a prerequisite to the efficient automation of VGOS processes.
2. Automatic control of VGOS station equipment is progressing well with all major broadband hardware subsystems now under the control of the Field System.
3. Significant progress has been made in the automation of software processes such as Sked, Drudge, Correlation, Fringing and Analysis but significantly more work needs to be done in this area.
4. A complete parallel set of operational files equivalent to those related to the SX master schedules has been set up for VGOS. It is referred to as the VGOS “Parallel Universe”. This approach has the benefit of giving the VGOS sessions the same top level look and feel as legacy SX sessions.

2.2 Broadband Signal Chains

The establishment of VGOS broadband signal chains is lagging behind antenna construction with only GGAO and Westford up and running in broadband mode. A number of other stations are however working to establish broadband signal chains so that seven stations expect to be operational by mid-2016, those stations being GGAO, Hobart, Kokee, Noto, Westford, Wettzell, and Yebes.

3 VGOS Technical Challenges

3.1 Compliance

The VGOS technical specifications were laid out in detail at the IVS VLBI2010 Workshop on Technical Specifications (2012). However, some systems and stations are not fully compliant with the recommendations, e.g.:

1. The VGOS input frequency range is 2.3–14 GHz. However, most stations have problems with the 2.3–3 GHz range due to RFI. In some cases RFI in that range is strong enough to risk saturating the front end and hence completely incapacitating the system. In those cases receivers will have little choice but to use a low frequency cut-off of 3 GHz. Furthermore, even in cases where saturation is not a concern, it will be difficult to find useable spectral regions below 3 GHz. As a result it is recommended that the 2.3–3 GHz range not be used for sessions that include VGOS stations only. However, for stations where S-band saturation is not an issue, inclusion of the 2.3–3 GHz range will have the benefit of allowing “mixed mode” observing with SX or S/X/Ka band stations.
2. VGOS specifies the use of four 1 GHz bands that can each be placed anywhere in the input frequency range. Currently some stations (e.g. those using RDBEs) can only achieve a maximum bandwidth of 512 MHz. However, in the case of the RDBE, a firm plan is in place to design and build, during the next 18 months, a next generation RDBE, the R2DBE, which will have a maximum input bandwidth of at least 1024 MHz.
3. By convention, VGOS systems typically divide each band into 32 MHz channels. Some systems however use a single monolithic band covering the full 1024 MHz bandwidth. Compatibility modes are available in the correlator so that both data types can be processed together but those modes are awkward to use and may lead to data transmission inefficiency if the whole band is not used. In at least one case plans are in place to build a new version of the monolithic bandwidth system that *can* produce 32 MHz channels.
4. VGOS specifies an instantaneous data acquisition rate of 16 Gbps. Currently the GGAO/Westford bi-weekly tests use a Mk6 system acquiring data at 8

Gbps. This could easily be increased to 16 Gbps if two record modules were installed in the Mk6 but this would have the unwanted side effect, in some situations, of increasing the number of modules that need to be shipped per session. However if care is taken during scheduling to ensure that the Mk6 internal RAM buffer does not overflow, then data can be acquired at 16 Gbps into RAM while the antenna is on source and recorded more slowly onto a *single* module while the antenna slews.

5. To achieve its intended accuracy, VGOS requires the use of phase, cable, *and* amplitude calibration. All of the VGOS calibration systems are being upgraded to achieve better precision and stability.

3.2 Continuity of Broadband with Legacy Network

In order to ensure continuity of SX and VGOS results it is necessary that the two networks be accurately tied together. The most obvious way to do this is to have the VGOS antennas observe along with the SX network in “mixed mode”. But for VGOS antennas that cannot observe below 3 GHz it will not be possible to co-observe at S-band so the direct tie cannot be made. For those antennas three options are available for tying into the SX network.

1. In some cases an S/X/Ka-band feed will also be available at an antenna. In those cases, the S/X/Ka-band feed can be swapped in periodically to co-observe with the legacy SX network.
2. If the VGOS antenna is co-located with a legacy SX antenna then a short baseline tie can be established using X-band only since the ionosphere delay will be nearly the same for both antennas, making an S-band tie unnecessary.
3. If all else fails, indirect ties can be established by observing with VGOS broadband antennas that have already been tied to the legacy SX network.

3.3 Compatibility of Band Structures

Although broadband is the agreed upon observing mode for VGOS, a number of antennas have chosen to use S/X/Ka as their standard. Unfortunately the

two modes do not work well together. For example if observations are taken in the spectral overlap regions of broadband and S/X/Ka-band then what remains is in effect an expanded SX mode, which does not take advantage of the unique benefits of either the broadband or S/X/Ka approaches. What is clear is that the best results will be produced when all VGOS antennas observe in a single unified network with all sites using the same band structure. In this regard, broadband remains the standard agreed upon mode for VGOS, although periodic mixed mode observing is encouraged to tie the broadband and S/X/Ka-band stations together.

3.4 Interoperability of Systems

Many different versions of subsystems exist. For example the RDBE and DBBC are well known examples of systems that were both designed to meet the VGOS digital back end (DBE) recommendation. However, even if systems are designed to meet the same specification, it is still possible that they may not work well together due to, for example:

1. incompatibility of local oscillator (LO) parameters,
2. misunderstood sideband, format, or bit encoding definitions,
3. unaccounted system delays.

Such problems may be due to either a poorly written or incomplete spec or to an error in the design. The best way to reveal these incompatibilities is to operate the systems together and then study the correlated output. This has been the purpose of the zero baseline tests supported by the IVS. Fortunately, most incompatibility issues can be corrected easily, often through an upgrade to field programmable gate array (FPGA) bit code. Alternatively, once the interoperability issue has been identified, it can often be corrected in the correlator. However this increases the complexity of correlator setup and leads to a proliferation of correlator “mixed mode” features. If possible interoperability issues should be resolved in the subsystem where they occur.

3.5 Network Connections

An important VGOS requirement is to provide initial results within 24 hours of taking data, which requires at least some electronic transmission of data to the correlator. Furthermore, a number of SX stations have come to use eTransfer for the majority of their data transmission needs and now view module shipment as an operational inconvenience.

At earlier times, the major impediment to electronic transmission of VLBI data was the so called last mile problem, in which fiber still needed to be installed between a nearby fiber trunk line and the radio telescope. In the majority of cases this problem has been solved. For VGOS, the problem is now predominantly an issue of capacity.

Full 24/7 operation of a VGOS station requires a sustained data transmission rate of about 5 Gbps (Petrachenko et al., 2014). Most stations have fiber connections capable of between 1 and 10 Gbps so it is conceivable that by 2020, when full VGOS operations are scheduled to begin, the majority of stations will be able to handle the VGOS data transmission requirement.

However, since data from all stations needs to be concentrated at the correlator, its data transmission requirement is considerably higher. For example to handle a 20 station network, a correlator will require a fiber connection capable of roughly 100 Gbps. Currently no IVS correlator has a plan in place to upgrade its network capacity to 100 Gbps. However network costs continue to drop so it is anticipated that the VGOS network requirement will eventually be affordable at correlators. However it is difficult to predict exactly when this will happen.

In the meantime it is recommended that all stations maintain at least a *capability* to handle removable media so that modules can be shipped if necessary. It needs to be kept in mind that even if a station will have no problem eTransferring all of its data, correlators may not be able to receive it (especially if the majority of stations prefer to use eTransfer). As a result, it is expected that module shipment will continue to play a significant role at least into the foreseeable future. Fortunately, data record equipment is not particularly expensive.

3.6 Correlation

Significant progress has been made towards satisfying VGOS correlator requirements:

1. It is now possible to correlate and fringe both polarizations and all VGOS bands simultaneously to give a single value for ionosphere and group delay for each observation (which is a major departure from the processes required to correlate and fringe legacy SX data).
2. A number of IVS correlators have recently been (or will soon be) upgraded. After the upgrades, enough computer cores will be available to satisfy correlator computational requirements for the next few years as VGOS operations ramp up; however they will not be adequate to handle full 24/7 VGOS operations.

At the same time, challenges remain:

1. Significant hand work is required to set up correlator jobs (although the completion of the VEX2 definition makes it possible to at least start the work required to automate this process).
2. The process of getting data off of modules (or the internet) and into a place where they can actually be correlated is currently a correlator bottleneck. Considerable work has been done to improve this situation but more is required.
3. Network bandwidth into correlators is significantly below what is required if all stations eTransfer data to the correlator during full VGOS operations (see previous section).
4. VGOS correlator processes need to be exported to other correlators so that experience can be gained at those correlators with broadband processing.
5. By the time full 24/7 VGOS operations begin, more correlator cores will be required.

3.7 Monitor/Control Interface

Automation and remote control are priorities for VGOS. Many station parameters need to be acquired to support analysis or to evaluate the health of a station and the success of an observations, e.g. weather parameters, calibrations, voltages, motor currents, temperatures, to name a few.

To be fully useful the data should be:

1. logged 24 hours a day and 7 days per week (24/7).
2. easily available via Internet.
3. conveniently distilled into succinct status reports and alarms.
4. meaningfully displayed at the control centre.

Significant work has been done on this by Alexander Neidhardt and Chris Beaudoin and a few solutions are being considered. A coherent (standardized) plan needs to be put in place so that all stations can be conveniently monitored from *any* control centre.

K. D. Baver, D. Behrend and K. L. Armstrong (eds.), *IVS 2013 Annual Report*, NASA/TP-2014-217522, 70–79.
 Petrachenko B, Bertarini A, Alef W, Behrend D, Cappallo R, Hase H, Ma C, Niell A, Nothnagel A, Zhang X (2015) VGOS Data Transmission and Correlation Plan, November, 2014. In: K. D. Baver, D. Behrend K. L. Armstrong (eds.), *IVS 2014 Annual Report*, NASA/TP-2015-217532, 11–19.

4 Summary and Conclusions

1. Daily VGOS observations will likely be delayed by about 1 year relative to the VGOS Observing Plan.
2. Some challenges lie ahead but none appear to be insurmountable.
3. All the right steps are being taken to achieve daily VGOS operations as soon as possible, e.g.
 - a. Efficient operational processes are being put in place.
 - b. VGOS signal chains are being established at a number of sites.
4. Within about a year it is anticipated that the first global scale VGOS observations will be carried out.

References

- Niell A, Whitney A, Petrachenko B, Schlüter W, Vandenberg N, Hase H, Koyama Y, Ma C, Schuh H, Tuccari G (2006) VLBI2010: Current and Future Requirements for Geodetic VLBI Systems. In: D. Behrend and K. Baver (eds.), *IVS 2005 Annual Report*, NASA/TP-2006-214136, 13–40.
- Petrachenko B, Niell A, Behrend D, Corey B, Böhm J, Charlot P, Collioud A, Gipson J, Haas R, Hobiger T, Koyama Y, MacMillan D, Malkin Z, Nilsson T, Pany A, Tuccari G, Whitney A, Wresnik J (2009) Design Aspects of the VLBI2010 System: Progress Report of the IVS VLBI2010 Committee. NASA/TM-2009-214180, pp. 58.
- IVS VLBI2010 Workshop on Technical Specifications (TecSpec)*, Bad Kötzing/Wetzell (Germany), March 1-2, 2012. www.fs.wetzell.de/veranstaltungen/vlbi/tecspec2012.
- Petrachenko B, Behrend D, Hase H, Ma C, Niell A, Nothnagel A, Zhang X (2014) Proposal for VGOS Observing Plan. In:

Broadband VLBI at 6 GHz to 14 GHz frequency range between Kashima 34 m and Ishioka 13 m

K. Takefuji, T. Kondo, H. Hideki, M. Sekido

Abstract First results from the Japanese broad band VLBI between Kashima 34 m and Ishioka 13 m are shown. We have been developing a broad-band system for the Kashima 34 m antenna. Broadband feed for 6.5 GHz to 15 GHz and broadband receivers were installed to 34 meter and high-speed direct samplers K6/OCTAD-G was also installed to the observation room since 2014. From the session a coherent phase connection over six frequencies were performed. Then quite fine delay resolution function were obtained. An error of delay resolution function by the super bandwidth synthesis is estimated 0.1 ps. Thus, we report more details e.g. the delay variation behavior from the broadband VLBI.

Keywords Broad-band, Super bandwidth synthesis

1 Introduction

To establish next generation geodetic VLBI, called VGOS (VLBI Global Observing System) which is based on the so-called broadband delay which uses four 1 GHz bandwidth in the range from 2.5 GHz to 14 GHz, we have been developing a broad-band system for the Kashima 34 m radio telescope which is the third largest radio telescope with Cassegrain optics in Japan. There are several antennas which meet the requirement VGOS specification, e.g. Westford and GGAO in United States, Yebes, Santa Maria in Spain and Portugal, Ishioka in Japan, Wettzell in

Kazuhiro Takefuji, Tetsuro Kondo, Hideki Hideki and Mamoru Sekido
893-1 Hirai, Kashima, Ibaraki, Japan

Germany, Badary and Zelenchukskaya in Russia. However, currently existing VGOS antennas have installed (or will install) Eleven feeds or QRFH feeds to realize receiving the 2 GHz to 14 GHz frequency range. Since these feeds have wide opening angles, the sub-reflector of the antenna needs to be close to the feed. Thus, ring focus optics are required to gain a high efficiency. Therefore, it is very challenging to develop a feed which has sharp beam width and broad band sensitivity for Cassegrain optics. We started to develop the feed since 2011, and a prototype feed (IGUANA-H) was installed at the Kashima 34 m telescope. To demonstrate broad-band VLBI, feasible VLBI sessions with Kashima 34 m and the new VGOS-type Ishioka 13 m were carried out from end of 2014 to January 2015.

2 Development broadband system for Kashima 34 meter

Currently we have installed two type of broadband feeds (IGUANA-H and NINJA). Figure 1 shows the two type of feeds. The smaller feed shown in the left of the picture is the IGUANA-H covering 6.5 GHz to 15 GHz frequency range, and the bigger feed in the right of the picture is the NINJA feed covering 3.2 GHz to 14.4 GHz frequency range. Since December 2013 the IGUANA-H feed has already been installed and evaluated by VLBI. The second brand new NINJA feed was recently deployed in July 2015. The lowest frequency of VGOS the specification is 2.5 GHz, but the NINJA feed has a cut-off frequency at 3.2 GHz to prevent highly strong RFI. Since strong RFI from stations for mobile telephony is emitted around 2 GHz,

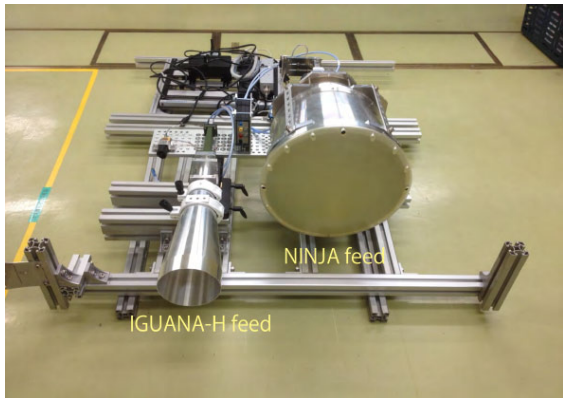


Fig. 1 The Iguana-H feed (left) and the NINJA feed (right) mounted to the trolley bed.

the broad-band LNA will be easily saturated by receiving such strong signals. Our broad-band system has an ambient temperature receiver system with a system temperature below 200 K until 14 GHz. The efficiency of the IGUANA-H feed is over 40 % in the frequency range of 6 GHz to 13 GHz. Above 13 GHz the efficiency is reduced and has 30 % at 15 GHz (see Fig. 2). The signal after the LNA is transferred over optical fiber, then the high-speed direct sampler called K6/GALAS converts the analog stream to digital signals with a digital baseband conversion (Takefuji, 2013). There has also conventional analog down-converters, these analog signals are sampled ADS3000+ (see Fig. 4).

3 Broad band VLBI between Kashima 34 meter and Ishioka 13 meter

Full VGOS radio telescope is built by The Geospatial Information Authority of Japan in Ishioka, Ibaraki, Japan, about 50 km north-west of Kashima. Broad-band VLBI sessions with the Kashima 34 m (IGUANA-H feed) and the new VGOS-type Ishioka 13 m (Eleven feed) were carried out on January and July 2015. We carried out intensive sessions for 6 to 14 GHz (6-bands, 2048 Msps, 1 bit) during four hours. The backend was made up two parts. One was the direct sampling system K6/GALAS covering 6 GHz, 7 GHz, 8 GHz and 9 GHz. The another was the analog frequency converter for 10 GHz and 13 GHz. Two bands were sampled with the ADS3000+ after analog

down-conversion. Both systems were set up for both antennas. We carried out intensive sessions for 6 to 14 GHz (6-bands, 2048 Msps, 1 bit). Unfortunately there was no internet connection. Then, the recorded data were transferred from Ishioka to Kashima by car. Fringes from all six frequency bands could be immediately detected after transferred by software correlator GICO3 (Kimura, 2007).

4 Super bandwidth synthesis from Kashima-Ishioka session

A coherent phase connection with six frequencies bands were performed. The bandwidth synthesis will be processed following the procedures,

1. Choose single scan as a template: At first we chose a single scan which has high SNR as a template. The template scan does not change whole observations. The apriori information (e.g. station position, clock delay and rate) of each frequency bands were necessary to uniform in correlation.
2. Inter-band delay correction: Among the frequency bands, a few nano second delay differences were unavoidably included through the analog systems. The differences will be normalized by using the 1st band (or any frequency bands)
3. Intra-band delay correction: Since a phase curvature on 1 GHz bandwidth is usually waved, the curvature is fitted to use as template.
4. Ionospheric delay correction: After inter and intra delay correction, the ionospheric delay still included. The whole bandwidth will be re-analyzed to measure ionospheric delay $\propto 1/f^2$.

A delay resolution function of the super bandwidth synthesis after previous procedures is shown in Fig. 5. This is the first achievement in the world and its theoretical delay precision reaches 2.7×10^{-14} s after 60 s integration. Figure 6 shows the delay observable of 1 s integration every over 700 seconds. The different colors of the plot (red, green, and blue) indicate delay data bandwidth of 1 GHz, 2 GHz and 4 GHz of #1 to #4 band respectively. This figure indicates the scattering become smaller as increasing the bandwidth with keeping systematic behavior unchanged. The root-mean-square (RMS) of delay observable at 1 s integration are calculated to be 3.08 ps, 2.01 ps and 0.96 ps in 1 GHz,

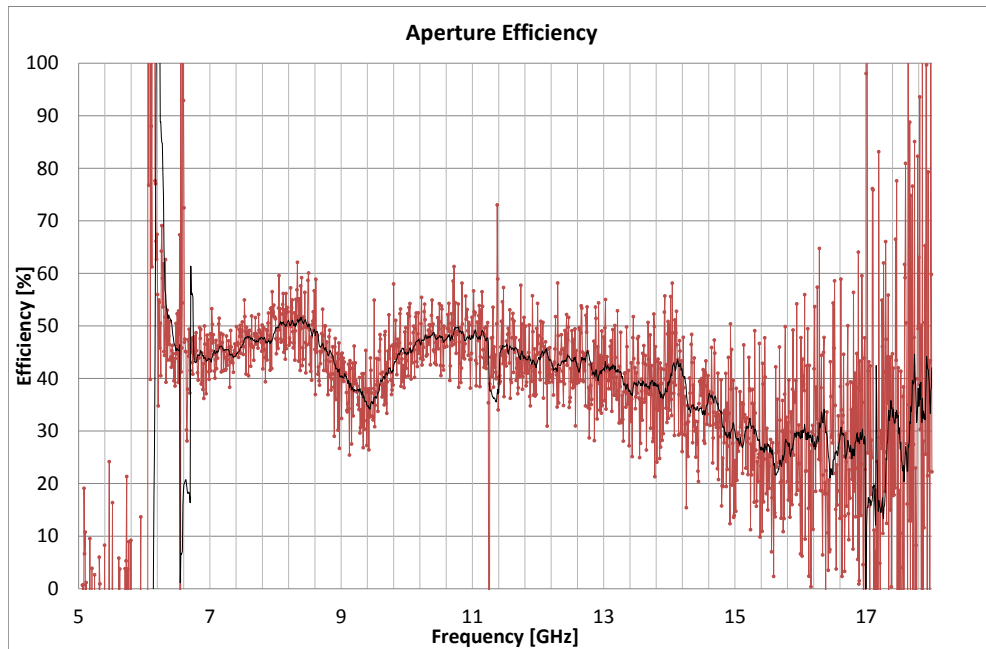


Fig. 2 Aperture efficiency of Kashima 34 m telescope deployed with IGUANA-H feed.



Fig. 3 The K6/Galas sampler, a direct sampling (16 GHz speed) system including DBBC signal processing.



Fig. 4 The K5/ADS3000+ sampler. The maximum sampling speed is 4 GHz, having DBBC signal processing for conventional geodetic VLBI

2 GHz and 4 GHz bandwidth, respectively. It shows that the delay precision improved as the bandwidth becomes wider. However, Fig. 7 depicts a power spectrum of Fig. 6. The plot bends around 20 s, which indicates that the while noise component continues only for

20 s. When we observe longer than 20 s, flicker noise will be dominating. Thus, the delay fluctuation might be limited mainly caused by atmospheric delay in this case.

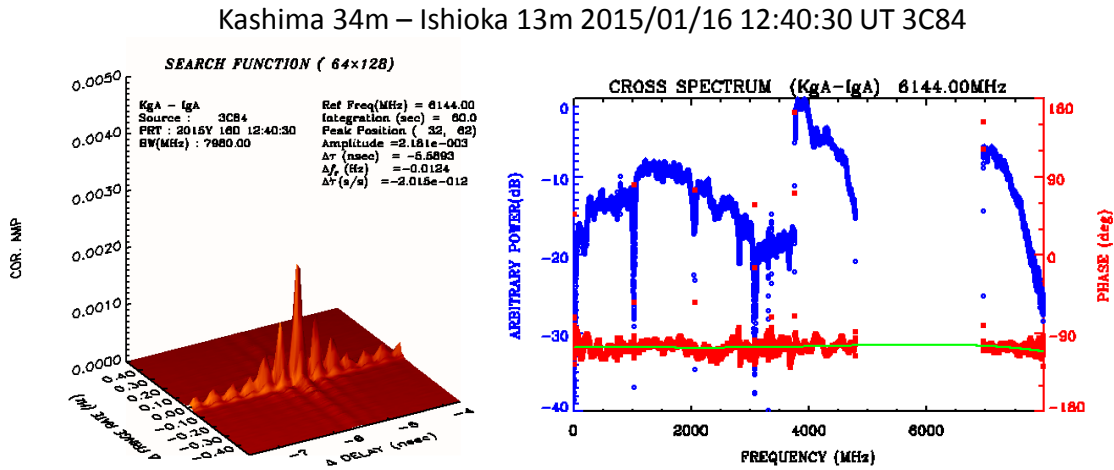


Fig. 5 Super bandwidth synthesis over 8 GHz bandwidth between Kashima 34 m and Ishioka 13 m.

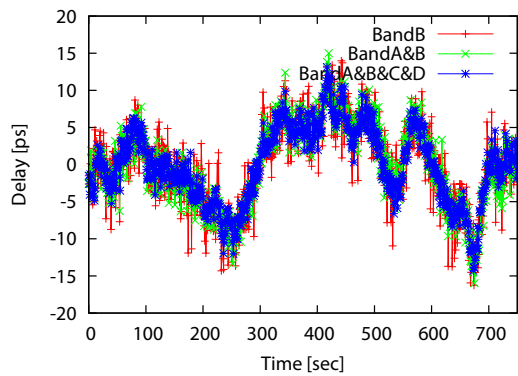


Fig. 6 Delay comparison with 1 GHz, 2 GHz, 4 GHz bandwidth in a 700 s scan.

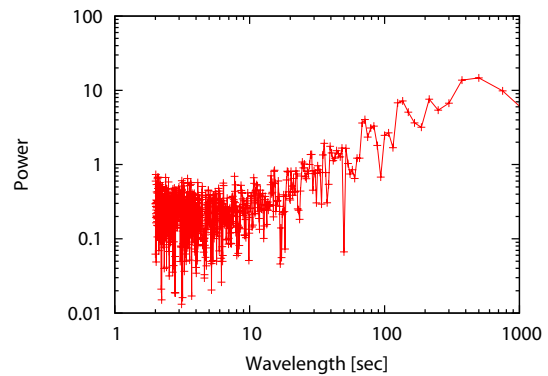


Fig. 7 A power spectrum of the delays presented in Fig.6.

5 Conclusions

We developed broad-band and sharp width feeds (IGUANA-H and NINJA). We carried out broad-band

VLBI experiments covering the 6 GHz to 14 GHz frequency range between Kashima 34 m and Ishioka 13 m. The six frequency bands over 8 GHz were synthesized with correcting for inter and intra delays.

The delay precision improves as a bandwidth becomes wider, however improvement will be limited because of atmospheric delays. The limitation in this case was about 20 s.

Acknowledgements

We thanks to GSI staff, especially Mr. Fukuzaki for supporting antenna control and monitoring experiments. The development of Gala-V is supported by a jointed development of National Astronomical Observatory Japan (NAOJ). It is entitled “Development of ultra broadband system for Kashima 34 meter antenna”.

References

- Kimura M (2007) Development of the software correlator for the VERA system II. *IVS NICT-TDC News 2007 No. 28*, 22–25. Web document http://www2.nict.go.jp/aeri/sts/stmg/ivstdc/news_28/pdf/\tdcnews_28.pdf.
- Takefuji K, Ujihara H (2013) Technology Development Center at NICT. In: K. D. Baver, D. Behrend, K. L. Armstrong (eds.), *IVS 2012 Annual Report*, NASA/TP-2013-217511, 342–345.

Technological Developments for VGOS from IGN Yebes Observatory

J. A. López–Fernández, F. Tercero–Martínez, J. A. López–Pérez, J. M. Serna–Puentes, P. de Vicente, J. D. Gallego, L. R. Santos

Abstract Several technological development activities at Yebes Observatory have been focused on different topics related to VGOS. Our low noise amplifiers can cover the S and X geodetic bands but also the 2–14 GHz band new ones (that yield average 7.5 K noise temperatures) for the broad band delay experiments. Our Tri-band receiver (S, X and Ka bands) is now installed at Yebes and Ishioka 13.2 radiotelescopes. We are also working in our first broad band receiver which will cover the mentioned 2–14 GHz band with a conical log-spiral feed, DYQSA.

Keywords VGOS, DYQSA, ALMA, LNA, MMIC

1 LNA Development

During 2014, several Yebes developed low noise amplifiers at S, X and Ka bands were developed and integrated into the tri-band receivers built for Yebes, Santa Mara and Ishioka 13.2 m VGOS radiotelescopes. The S-band LNA construction has been transferred to the industry. X-band is based on our ALMA IF LNAs 4-12 GHz design. Ka-band amplifiers are the fruit of a long-term successful collaboration with the Fraunhofer IAF and the University of Cantabria, they include mGaAs

José Antonio López–Fernández, Félix Tercero–Martínez, José Antonio López–Pérez, José Manuel Serna–Puentes, Pablo de Vicente, Juan Daniel Gallego

Yebes Observatory, IGN, Cerro de la Palera s/n, E-19141 Yebes, Spain

Luis R. Santos

DROPC/SRTT, Rua Conselheiro Dr. Luis Bettencourt 16, 9500-058 Ponta Delgada, Azores, Portugal

MMICs with good cryogenic performance. A remarkable new development in Ka-band was made together with the ETH Zurich in the framework of an ESA contract. The amplifier is a compact hybrid design with interchangeable I/O outputs 2.9 mm coaxial or WR-28 waveguide. The LNA shows noise temperatures of 10 K averaged in the 25.5–35.5 GHz band, extremely high gain, and very low power dissipation.

We are working towards an ultra-wideband amplifier covering the 2–14 GHz band, following two approaches: an MMIC-based version and a hybrid amplifier. The first hybrid units produced were tested with different transistors in the first stage, see Fig. 1. The best results, obtained with NGST transistors, yield average noise temperatures of 7.5 K.

2 Triband (S/X/Ka) receiver

A cryogenically cooled tri-band receiver has been successfully designed and developed. Currently three of these receivers have been built: two of them for the RAEGE radio telescopes in Yebes and Santa Mara, and one for the GSIs Ishioka station. This receiver allows simultaneous dual circular polarization observations at S, X and Ka bands. The Tri-band feed is actually made of three feeds in a coaxial arrangement. The S and X band feeds are fed by four symmetric ports at 90 degrees apart. The Ka-band feed output is a circular waveguide that interfaces to a septum polarizer coupler developed in house. The cryostat is built over a two-stage Sumitomo closed cycle refrigerator inside a cylindrical dewar made of steel with suitable multi-layer insulation. The LNAs and 90 hybrid circuits are in-house designs performed at Yebes Labs. The aver-

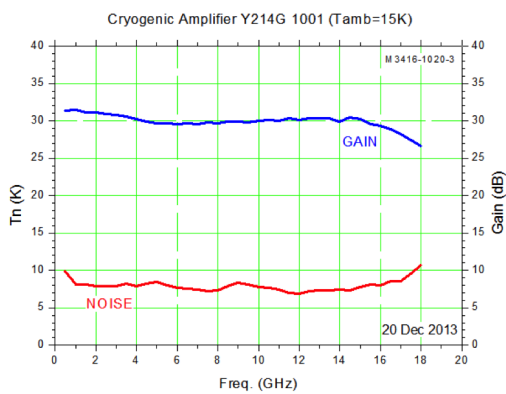
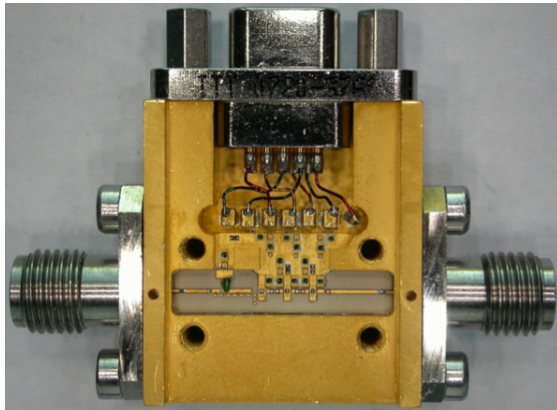


Fig. 1 Picture of the 2–14 GHz LNA (top) and results from noise and gain measurement (bottom).

aged receiver noise temperatures are below 25 Kelvin. The receiver, see Fig. 2, is fully integrated in a frame box positioner that facilitates the installation at the radio telescope feed cone.



Fig. 2 Tri-band receiver. Detail of the interior.

3 Broadband Feed

The geometry of the broadband feed is based on a conical log-spiral antenna. This is the origin of the name of the solution we have selected, devoted to the work on this kind of antennas developed by Prof. Dyson in the 50s. The explanation of the radiation mechanism is totally explained by Dyson (1965). The proposed feed uses four antennas as shown in Fig. 3. Two antennas are devoted to one polarization and the other two antennas are devoted to the opposite one. The angle between the axis of the cones and the z-axis is 16° . The radiation pattern of the antenna was analyzed using CST Microwave Studio and HFSS Ansoft softwares, obtaining from both softwares the same results (see Fig. 4).

A pretty high symmetry in the radiation patterns at all frequencies is obtained with a maximum CP-XP level in broadside > 15 dB with a gain of 10 dB. Efficiencies, estimated following Kildal (1985) are presented in Fig. 5 and the phase center in Fig. 6.

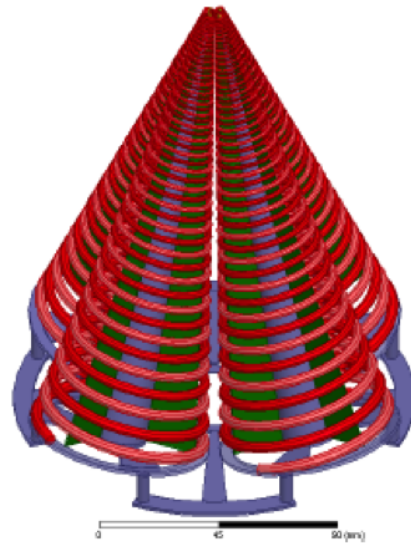


Fig. 3 Configuration of the proposed broadband feed.

For the DYQSA feed it is possible to radiate the calibration signal directly into the feed or to couple it into the signal chain after the LNA. However, due to the combining network and multiple LNAs needed for the DYQSA Feed, it is not practical when using this feed to inject calibration signals between the feed and LNA. Due to the differential port configuration of the

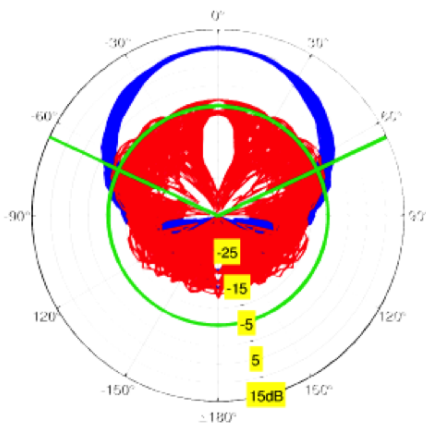


Fig. 4 Radiation patterns of the complete feed system from 2 GHz up to 14 GHz (step of 2 GHz) at the planes ϕ with steps of 15° from $\phi = 0^\circ$ up to $\phi = 180^\circ$. Blue line is copolar polarization and red line is cross-polar polarization. Circular polarization is assumed. Green lines remark the subtended angle from the focus of the subreflector.

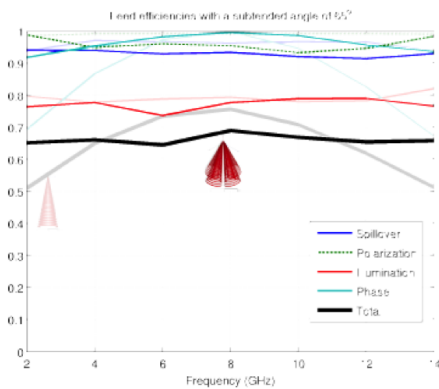


Fig. 5 Efficiencies of the proposed broadband feed.

DYQSA Feed, each polarization output requires a network to combine the output from four antenna ports. To avoid noise degradation from the combining network, LNAs are required directly on each antenna port for a total of 4 LNAs per polarization or 8 LNAs per DYQSA feed. Furthermore, since mismatches in the LNAs degrade feed performance, it is necessary that the LNAs be matched within specified limits.

The solution has been manufactured in Titanium following a 3D printing growing technique and then the antenna was silvered, see Fig. 7. It has been measured in the anechoic chamber of Centro Astronómico de Yebes. Also, the first cooling test are being carried

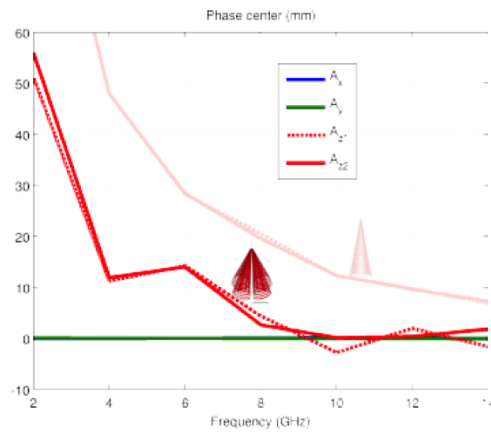


Fig. 6 Estimated phase center of of the proposed broadband feed.

out with good results. In Fig. 8, finally, the radiation patterns for one circular polarization are plotted from 2 up to 14 GHz, showing and excellent stability on their characteristics.

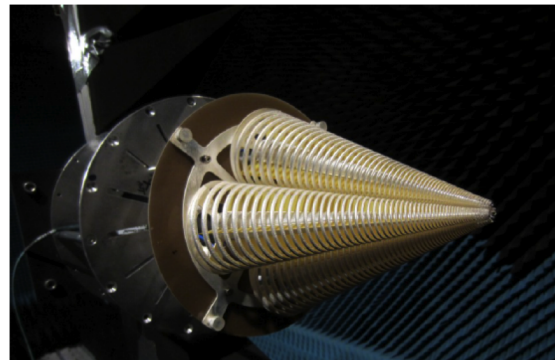


Fig. 7 Manufactured and measured DYQSA feed and first tests.

4 Control software developments

We also undertook several software developments related to the radio telescope control. The connection between the Field System and the control system developed at Yebes is done via UDP sockets. Information from the weather station and the gps-maser comparison uses the same protocol. The Field System also transfers

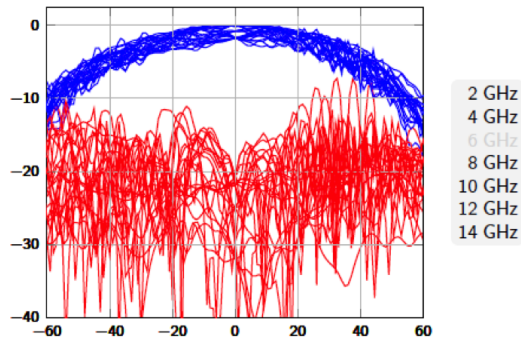


Fig. 8 DYQSA Measured radiation patterns from 2 up to 14 GHz for circular polarization. Copolar and cross-polar components are plotted Left, $\phi = 0^\circ$, right, $\phi = 45^\circ$.

commands for the receivers: local oscillator frequency, attenuation and noise diode switching on/off.

A DBBC2 equipped with 4 IFs/ADB2s/CORE2s was connected to a Mark5B+ recorder and we performed a 24 hour VLBI observation (R1656) with the 40-m telescope in parallel with the VLBA5 system. Fringes were found and hence, both the 13-m DBBC2 and the Mark5B+, were validated. OnOff sessions controlled by the Field System were also conducted to determine the SEFD of the telescope at S and X bands and to fine tune the calibration from the noise diodes. These tests were also important to debug the control software and the communication between the Field System and the local control system.

Finally, in November 2014, selected scans from an IVS session (R4663) were observed in parallel with the VLBA5 system connected to the 40-m telescope and the DBBC2 connected to the 13-m antenna. Fringes were found at X band. The lack of fringes at S band was due to a problem with the signal from the IF. Our near term goal is to have the 13-m be scheduled in 2015 as tag along in some IVS sessions the 40-m antenna takes part. This will allow to test thoroughly the whole receiving chain, detect problems and correct them. It will also determine the position of the 13-m antenna and prepare the telescope for standard IVS observations.

5 Other activities

During 2014, several activities have been carried out for the upgrade of cryogenic receivers belonging to BKG (Germany). One of the S/X Wettzell dewars was upgraded by fixing some bugs (vacuum leaks, multi-layer insulation,...) that deteriorate the cryogenic performance. The OHiggins station in Antartida was also fully upgraded by installing new LNAs and a custom waveguide coupler designed and built in our labs. Several receiver modules like the down converter, noise calibration and LOs have been also upgraded. The functionalities of the receiver (setting and monitor output power level, LOs lock status, noise cal, phase cal and LNAs bias) can be controlled via Ethernet, using a remote control system developed in our labs.

Acknowledgements

The development related have been supported by project FIS2012-38160 financed by the Spanish Ministry of Economy and Competitiveness (MINECO).

References

- Dyson J D (1965) The characteristics and design of the conical log-spiral antenna. *IEEE Trans Antennas Propag*, 13(4), 488–499, doi: 10.1109/TAP.1965.1138471.
- Kildal P S (1985) Factorization of the feed efficiency of paraboloids and Cassegrain antennas. *IEEE Trans Antennas Propag*, 33(8), 903–908, doi: 10.1109/TAP.1985.1143689

Results from the TWIN Commissioning Phase

T. Schüler, G. Kronschnabl, A. Neidhardt, C. Plötz, A. Bertarini, L. La Porta, S. Bernhart, A. Müskens, S. Halsig, A. Nothnagel

Abstract The TWIN radio telescope pair at the Geodetic Observatory Wettzell features two identical antenna constructions reserved for geodetic VLBI within the International VLBI Service for Geodesy and Astrometry with slightly different receiving systems. The first telescope, TTW1, owns a tri-band feed horn for S-, X- and Ka-band with dual-polarization capabilities and a broad X-band window from 6.8 to 9.8 GHz. This system entered its commissioning phase in 2014. Results obtained with the final tri-band receiver configuration are being presented here. The positioning performance evaluated over the 123 m baseline between TTW1 and the existing 20 m RTW telescope is rather satisfactory in X-band. Nevertheless, some initial problems with the backend hardware had to be resolved as soon as the final tri-band down-converter was introduced into the measurement chain. In the end, the 3D position deviations are at the level of a few millimeters compared to the local tie vector from terrestrial surveying. Unfortunately, S-band group delays suffer from increased radio frequency interference. This possibly requires additional measures to be taken. However, the negative impact of RFI tends to get neutralized over long distances. Indeed, long baseline vector processing results indicate a high level of agreement as well.

Torben Schüler, Gerhard Kronschnabl, Christian Plötz
Geodetic Observatory Wettzell, Federal Agency for Cartography and Geodesy (BKG), Sackenrieder Str. 25, D-93444 Bad Kötzing, Germany
Alexander Neidhardt
Geodetic Observatory Wettzell, Technische Universität München, Sackenrieder Str. 25, D-93444 Bad Kötzing, Germany
Alessandra Bertarini, Laura La Porta, Simone Bernhart, Arno Müskens, Sebastian Halsig, Axel Nothnagel
Rheinische Friedrich-Wilhelms Universität Bonn, IGG, Nußallee 17, D-53115 Bonn, Germany

Keywords TWIN, TTW1 Wettzell, VGOS, Short Baseline Group Delay Analysis

1 Introduction

The TWIN radio telescope pair at the Geodetic Observatory Wettzell was officially inaugurated in May 2013. The interior of the telescopes currently differs in terms of the receiving system. TWIN Telescope Wettzell 1 (TTW1) was finalized between June 2013 and May 2014 and entered its commissioning phase in June 2014. The two antennas were designed to match the VGOS requirements (Niell et al. 2006) and are identical, except for the receiving systems: TTW1 is equipped with a triple band feed horn featuring S-, X- and Ka-band frequency ranges in dual circular polarization mode. The X-band receiving capabilities of TTW1 are broad ranging from approximately 6.8 up to 9.8 GHz.

The initial performance evaluation is carried out at the local level for the short baseline between the existing 20 m RTW and the new 13.2 m TTW1, see Fig. 1. Due to the limitations of RTW, the usable frequencies and subsequent correlation and data analysis is fixed to traditional S- and X-band frequencies in single-polarization mode. Nevertheless, an initial performance evaluation is possible.

This paper features the latest results from the commissioning phase obtained with the final receiving system. For an exhaustive discussion of initial results obtained predominantly with a legacy dual-band legacy down-converter, please refer to Schüler et al. (2015).

The local baseline between RTW and TTW1 can be determined with an accuracy of a few millimeters (3D



Fig. 1 Image of the 13.2 m TTW1 (left), the first of the two TWIN telescopes at Wetzell, and the 20 m RTW. The baseline between the two reference points has a length of 123 m.

distance) in most cases using X-band data. S-band results are about 10 times less precise. Its frequency window is smaller compared to X-band due to the technical limitations of the RTW. This naturally leads to a decreased precision of the group delay, but does only partially explain the precision decrease actually observed. Radio frequency interference (RFI) is obviously playing an important role as far as the poor results obtained at local level are concerned. Long baseline processing is apparently less influenced by RFI-problems as summarized in this paper.

2 Tri-Band Feed System

The currently implemented feed system for TTW1 is a tri-band feed (López-Pérez et al., 2012; Tercero et al., 2012). It consists of an interleaved coaxial waveguide system that enables a moderate bandwidth at the following frequency bands:

1. S-band: 2.0 to 2.8 GHz
2. X-band: 6.8 to 9.8 GHz
3. Ka-band: 27 to 34 GHz

We decompose the radio signal into a right (RHCP) and left hand circular polarized (LHCP) fraction. The signals received in the S- and X-band waveguide sections are extracted by radially mounted turnstile junctions and then combined to right and left hand circular polarized signals via a 90° hybrid. For the Ka-band section, a circular waveguide tube acts as a feed horn in the center of the tri-band feed. The Ka-band signal

is directly divided into RHCP and LHCP waves by a septum polarizer.

3 Down-Converter

The down-converter developed for the tri-band TTW1 receiving system has the same design as the one foreseen for the 2-14 GHz broadband feed in TTW2. As a matter of fact, the VGOS requirements defined for VLBI receiving systems (Niell et al., 2006) are very demanding. A continuous 12 GHz broad frequency spectrum is to be covered, and within this frequency range, an arbitrary selection of multiple bands with a bandwidth of 1 GHz shall be selectable. Additionally, both microwave polarizations (LHCP and RHCP) must be available.

These requirements lead to a substantially more complex hardware for the new broadband receiver compared to that of the existing 20 m RTW. In essence, it is necessary to use an up-down-converter for X-band and a down-down-converter for the Ka-band to transfer all bands into the requested IF-bands. The key point is to achieve an effective and selectable down conversion of the microwave signals to different Nyquist zones (0-512, 512-1024, 1024-1536, 1536-2046 MHz).



Fig. 2 Picture of the complete down-converter for the tri-band receiving system of TTW1.

A quadruple phase stable synthesizer is used as variable first local oscillator (LO) for the up-conversion. It is directly locked to a 1 00 MHz frequency reference derived from a hydrogen maser. Moreover, a receiver with an excellent spurious and

cross-talk rejection (better than 60 dB) is needed. For further details including block diagrams of the down-converter and the intermediate-frequency (IF) converter as well as the backend, please refer to Schüler et al. (2015). See Fig. 2 for an image of the down-converter.

4 Experiments

The initial results from 26 experiments carried out between June 2014 and March 2015 are presented in Schüler et al. (2015). In this contribution, we set the focus on the results obtained from experiments starting by the end of February 2015 using the final tri-band down-converter, whereas most of the initial results are based on the legacy S-/X-band down-converter, but using the same feed horn.

All experiments dealt with in this paper are so-called Intensives (Nothnagel and Schnell, 2008). TTW1 measured the associated radio sources synchronously with RTW, so it is a matter of convenience to use the group delay observations for a first performance assessment. The sessions last one hour and target at the determination of $\Delta UT1 = UT1 - UTC$. Although this type of experiment is certainly not optimized for baseline vector determination, it is still possible to estimate the vector components between TTW1 and RTW and to quality-check the group delay observations.

The backend setup is standard for Intensive experiments. The digital backend in use is a DBBC-2 (Tucari et al., 2010). Results obtained with an ADS3000+ (Takefuji et al., 2010) can be found in Schüler et al. (2015) where the reader can also find more details on the actual backend configuration, and results for three experiments covering a period of 24 hours.

5 VLBI Correlation

All experiments during the TTW1 commissioning phase were correlated at the Bonn Correlator operated by the Max-Planck-Institute for Radio Astronomy (MPIfR) together with the University Bonn (IGG) and in partnership with the Federal Agency for Cartography and Geodesy (BKG).

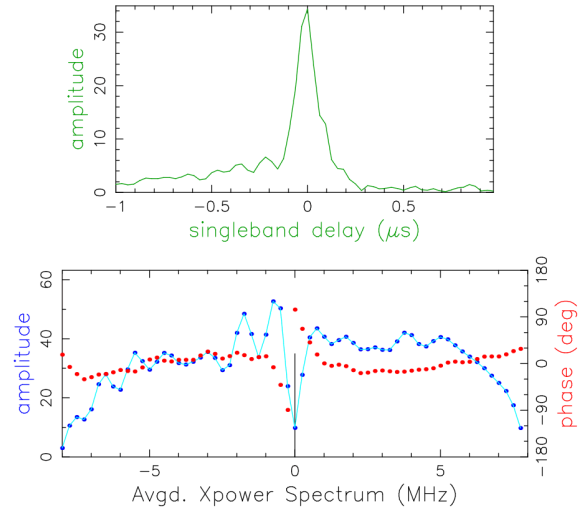


Fig. 3 Correlator output for the baseline Tsukuba/TTW1 at 8.4 GHz. Upper part: single band delay (SBD); bottom part: Fourier transform of the SBD, i.e., averaged power spectrum. The red line corresponds to the phase and the blue line to the amplitude of the fringe visibilities.

An example for an X-band correlation result is presented in Fig. 3 for the baseline between TTW1 and Tsukuba. The upper part shows the single band delay (SBD) in μs (cross-correlator coefficient amplitude). The averaged power spectrum is plotted below. This is the Fourier transform of the SBD into the frequency domain. The peak of the SBD is well defined and centered at zero as expected after the correlation and the residual delay correction. Moreover, to have good fringes we should see the phase (red line) well aligned, as actually visible in the plot. The signal-to-noise ratio (SNR) obtained from this scan was 101.

We then calculated the theoretical SNR for the source observed within the scan considered (example: radio source ICRF J175132.8+093900, flux density at X-band is about 3 Jy). Given the effective sampled bandwidth of 64 MHz (8 BBC channels each 8 MHz wide) and the integration time of 15 s, the *a priori* SNR is about 100, indicating that the TTW1 performed well.

Correlation analysis for the band at 2.3 GHz (S-band) indicates contamination by radio frequency interference (RFI), typically caused by telecommunication satellites. Such contamination is present on almost all the baselines. On the long baselines, the correlator fringe rotator wraps the RFI phases many times within

one integration period (one second). In most cases, this reduces the amplitudes of the RFI close to zero. Consequently, long baselines between TTW1 and (in this case) Tsukuba, are well-usable for further geodetic analysis as also proven for long baseline vector component estimation by Schüler et al. (2015). In contrast, on the short 123 m baseline between TTW1 and RTW, the correlator fringe rotator does not wind up the phases of the RFI, hence the RFI is not attenuated and corrupts the data.

Fig. 4 shows the S-band part of the RFI spectrum common to the TTW1 and RTW as obtained using the astronomical image processing system AIPS¹. Some lines are thin in frequency and are present for the whole experiment (possibly signals broadcast from telecommunication satellites). Some others appear only for a certain period of time (possibly nearby interference).

6 Local Baseline Results

The short baseline analysis results for the vector between TTW1 and RTW are presented in Tab. 1. The percentage of the accepted scans (i.e., group delay observations) is given in column 3, $\Sigma(0)$ is the standard deviation of unit weight à posteriori and à priori (in brackets). The *3D Difference* is the difference between the estimated baseline vector length and the distance obtained from precision terrestrial surveying (123.3070 m). The number in brackets is the empirically determined standard deviation from the vector adjustment procedure.

The agreement between the surveyed local tie and the VLBI analysis result was usually at the level of a few millimeters as long as the S-/X-legacy down-converter was in use (Schüler et al., 2015). In contrast, we can identify relatively large deviations of 2–6 cm with the new tri-band down-converter. The analysis of the Intensive conducted on 30 March 2015 also suffers from a very small number of delay observations initially available for the adjustment procedure.

This indicates problems with the receiving system: The installation of the new tri-band down-converter introduced two main changes of the S-/X-band IF sig-

¹ National Radio Astronomy Observatory. Astronomical Image Processing System (Homepage). Available online: <http://www.aips.nrao.edu/index.shtml> (accessed on 15 March 2015).

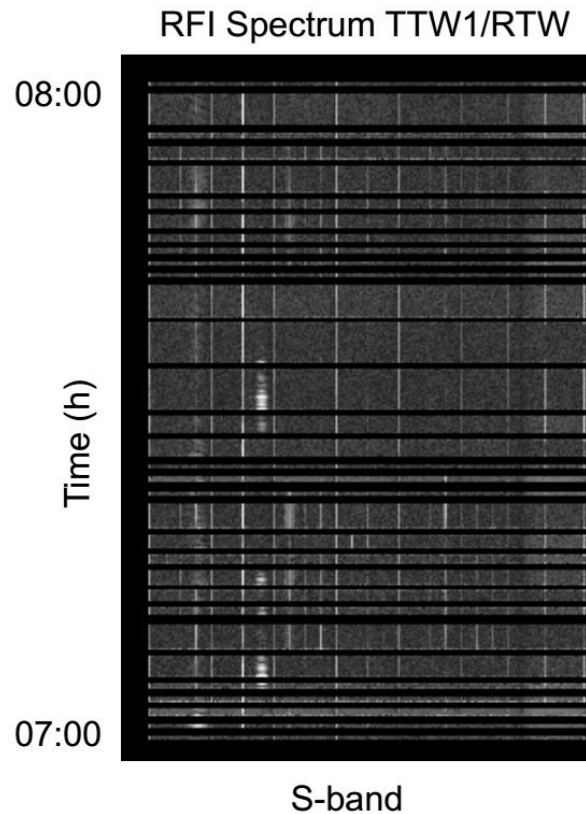


Fig. 4 RFI spectrum common to TTW1 and RTW (ordinate: time in hours; abscissa: frequency).

nals compared to the setup used for the previous VLBI measurements. The initial output power levels of the new tri-band down-converter are lower than the ones of the S-/X-legacy down-converter. This caused lower input power levels for signal processing of the DBBC-2, which resulted in an insufficient overall signal-to-noise ratio (SNR). Moreover, the frequency band of the IF X-band output (up-down-converter for X-Band) is shifted by 500 MHz to higher frequencies. This implies that another Nyquist filter (1024–1536 MHz) within the DBBC-2 is used with slightly more attenuation. Hence, optimizing the IF input power levels for the DBBC-2 re-established a well-adjusted backend system including the new tri-band down-converter.

Consequently, the results for the Intensives starting on 20 April 2015 until 4 May 2015 illustrate a very satisfactory level of agreement in the range of 1.6–3.6 mm. Moreover, the number of accepted scans was 100 %, i.e., no observations were identified as outliers. Such outliers are present in other experiments and can

Table 1 Short baseline results obtained from X-band group delays using the DBBC backend. Numbers in parenthesis: À priori standard deviation of unit weight $\Sigma(0)$ and empirical standard deviation of the 3D difference.

Date	Scans	Accepted	$\Sigma(0)$	3D Difference
2015-02-23	29	97%	6.7 (2.5) mm	8.8 (6.4) mm
2015-03-02	17	94%	7.4 (6.0) mm	20.8 (12.9) mm
2015-03-09	29	100%	10.8 (4.3) mm	19.9 (10.3) mm
2015-03-30	11	73%	3.1 (2.8) mm	57.9 (51.2) mm
2015-04-13	25	100%	2.4 (1.8) mm	8.1 (5.7) mm
2015-04-20	32	100%	3.4 (2.0) mm	2.6 (4.2) mm
2015-04-27	31	100%	5.8 (3.0) mm	1.6 (8.0) mm
2015-05-04	32	100%	4.1 (2.6) mm	3.6 (5.1) mm
2015-05-11	19	89%	3.7 (3.0) mm	13.7 (7.4) mm
2015-05-18	30	73%	6.1 (3.8) mm	0.6 (6.1) mm

have a magnitude of several centimeters up to decimeters. In the latter case, we assume that the correlation process effectively failed. The experiment on 11 May features a somewhat larger deviation, but this seems to be partially related to a poorer geometrical constellation of the radio sources available for baseline analysis, because the standard deviation of the length is already at a level of 7.4 mm, whereas the standard deviation of unit weight (a measure for the precision of a single group delay) is at a relatively low level of 3.7 mm.

All à priori standard deviations are slightly smaller than the à posterioris, though at an acceptable level in our opinion, since the à prioris do not cover the complete error budget. Note that the phase calibration unit of TTW1 had to be disabled throughout all these local experiments. Otherwise, the VLBI correlation process would have been impacted in a negative way.

7 Conclusions

TTW1, the first of the two TWIN telescopes at the Geodetic Observatory Wettzell, is currently in its commissioning phase. Initial results using both a legacy S-/X-band as well as tri-band down-converter manufactured at the Observatory show promising results after some initial problems could be successfully resolved. Furthermore, and not yet mentioned in this contribution, first positive Ka-band correlation results were obtained with the large astronomical telescope at Effelsberg (27 March 2015, fringe quality 5, bad weather conditions) as well as at Yebes (29 April 2015, fringe quality 7).

Some work still has to be performed in order to fully qualify the system for use within the IVS: A precise independent set of coordinates must be derived over a sufficiently long period of time. The Intensives are not appropriate for this purpose. Both TTW1 and RTW participated in the Euro-130 experiment, and the coordinates derived for TTW1 were of good quality. A set of additional 24 h experiments is currently conducted in order to improve this time series.

Moreover, the TTW1 phase calibration system, manufactured at the Observatory, still has to be qualified for operational use, and adaptations have to be implemented for short baseline correlation.

References

- Niell A, Whitney A, Petrachenko B, Schlüter W, Vandenberg N, Hase H, Koyama Y, Ma C, Schuh H, Tuccari G (2006) VLBI2010: Current and Future Requirements for Geodetic VLBI Systems. IVS Memorandum 2006-008v01, Report of Working Group 3 to the IVS Directing Board, 16 September 2005, International VLBI Service for Geodesy and Astrometry, IVS Coordinating Center, NASA Goddard Space Flight Center, Code 697, Greenbelt, MD 20771, USA. <ftp://ivsc.gsfc.nasa.gov/pub/memos/ivs-2006-008v01.pdf>.
- Schüler T, Kronschnabl G, Plötz C, Neidhardt A, Bertarini A, Bernhart S, La Porta L, Halsig S, A. Nothnagel A (2015) Initial Results Obtained with the First TWIN VLBI Radio Telescope at the Geodetic Observatory Wettzell. *Sensors* 15(8), 18767–18800. doi: 10.3390/s150818767, <http://www.mdpi.com/1424-8220/15/8/18767>.
- López-Pérez J A, Tercero F, Serna J M, López-Fernández J A (2012) A Tri-Band Cryogenic Receiver for the RAEGE Project Antennas. In: D. Behrend, K. D. Baver (eds.), *Proc. IVS 2012 General Meeting*, NASA/CP-2012-217504, 66–70.
- Tercero F, López-Pérez J A, López-Fernández J A, Pérez O (2012) S/X/Ka Coaxial Feed for the Tri-Band of the RAEGE Antennas. In: D. Behrend, K. D. Baver (eds.), *Proc. IVS 2012 General Meeting*, NASA/CP-2012-217504, 61–65.
- Nothnagel A, Schnell D (2008) The impact of polar motion and nutation errors on UT1 determination from VLBI Intensive observations. *J. Geod.*, 82, 863–869.
- Tuccari G, Alef W, Bertarini A, Buttaccio S, Comoretto G, Graham D, Neidhardt A, Platania P R, Russo A, Roy A (2010) DBBC VLBI2010. In: D. Behrend, K. D. Baver (eds.), *Proc. IVS 2010 General Meeting*, NASA/CP-2010-215864, 28–30.
- Takefuji K, Takeuchi H, Tsutsumi M, Koyama Y (2010) Next-generation A/D Sampler ADS3000+ for VLBI2010. In: D. Behrend, K. D. Baver (eds.), *Proc. IVS 2010 General Meeting*, NASA/CP-2010-215864, 378–382.

The Yebes RAEGE telescope control, commissioning tests and first results

P. de Vicente, R. Bolaño, L. Barbas, A. Moreno, A. Díaz, S. García-Espada

Abstract The Yebes 13 m antenna is the first element of the Red Atlántica de Estaciones Geoespaciales (RAEGE) network. The telescope started regular operations in 2015, taking part regularly in some IVS programs. During 2014 the telescope was thoroughly tested and its control system debugged. The commissioning of the antenna included determining a pointing and a focus model and measuring the RFI and the aperture and forward efficiencies at the three receiving bands. VLBI observations were also performed to check the phase stability of the whole reception chain. In this article we present the results obtained.

Keywords RAEGE, telescope control

1 Introduction

The Red Atlántica de Estaciones Geoespaciales (RAEGE) is a VLBI network which will be composed of four 13.2 m telescopes located in Yebes (Spain), Santa María (Azores Islands, Portugal), Canary Islands (Spain), and Flores (Azores islands, Portugal). The telescopes in Yebes and Santa María have already been built but only the first one is already operative. All the telescopes have been designed by MT-Mechatronics and built by Asturfeito, a Spanish company.

The radiotelescope at Yebes is equipped with a three band receiver at 2, 8 and 30 GHz which will be re-

P. de Vicente, R. Bolaño, L. Barbas, A. Moreno, A. Díaz, S. García-Espada

Centro Nacional de Tecnologías Radioastronómicas y Aplicaciones Geoespaciales(CNTRAG), Observatorio de Yebes (IGN, Spain).

placed by a broadband one (2 to 14 GHz) by mid 2016. The antenna can move at speeds of 12 degrees per second in azimuth and 6 degrees per second in elevation to meet the specifications required for VGOS.

MT-Mechatronics has already built an identical antenna in Ishioka (Japan) and will probably deliver more antennas of this type in other observatories like Ny-Ålesund (Norway) and Onsala (Sweden). We believe that a description of the control system of the telescope installed in Yebes and of the results obtained from the commissioning phase and first VLBI observations may be useful for other institutes.

2 The control system

The control system for all the RAEGE telescopes will be the same and it has been derived from the work performed in the 40 m radiotelescope at Yebes (de Vicente et al., 2006).

The telescopes are equipped with an Antenna Control Unit, hereafter ACU, which is composed of two computers: one for the control of the main axes and a second one for the hexapod, where the secondary reflector is mounted. Both computers run a real time extension under Windows XP called TwinCAT (by Beckhoff). The antenna can be controlled manually, through a local control panel devised by MT-Mechatronics, and remotely.

The remote control and monitoring of the antenna is achieved using two TCP sockets: the first one is for commands and the second one for retrieving the status of the antenna. All commands are identified by a unique ID and provide an acknowledgement after being received. The status of the antenna is delivered

without any request every 200 ms. Both, the commands and the status format, are specified in a document called Interface Control Document (ICD) which was agreed by MT-Mechatronics and the Observatory of Yebes

Commands can be classified roughly in two main groups: those which set the antenna to a given mode and those related to tracking and performing superposition patterns on top of the tracking and movements of the secondary reflector as a function of time and elevation. The latter ones use tables. For example, tracking requires a table with three columns: modified julian day, and two coordinates: right ascension and declination or azimuth and elevation. In the first case the computation of azimuth and elevation is done by the ACU using DUT1 and the Greenwich sidereal time which have to be supplied everyday. It is possible to always append new tables to the one in use. The usage of these tables has determined the design of the control system. The superposition tables are used to create scans like calibration, on-offs or pointing drifts.

The remote control system developed by the Yebes Observatory staff, uses ALMA Common Software (ACS), as the communication infrastructure. All the code has been written in C++, Python and Java. The control system provides several monitoring tools, individual graphical applications and a command line shell which allows full control of the telescope for single dish observations.

The connection between the control system and the Field system is done using a client-server connection with TCP sockets. The client runs in the FS computer and the server in the control system. Both the client and the server, are written in C++, and transfer information using a structure composed of data and semaphores. A copy of such structure is also available in the station shared memory area of the Field System. Every time the Field System requires an operation from the telescope, like commanding the antenna or setting up the local oscillator of the receiver, the client enables a given semaphore in the local shared memory area, copies the local structure into the transfer structure and sends this one to the server via a socket. The remote control subsystem, acting as server, gets the structure, examines the active semaphore, performs the required operations, deactivates the semaphore and sends back the structure with updated content required by the Field System, like the weather parameters and the position of the antenna. This update is done every 250 ms even

if there are no commands from the Field System for the antenna. The data from the received structure are copied back to the shared memory area so that the Field System can use them. The IP address and port of the server are stored in a file in the control directory of the Field System. This design decouples the Field System computer from the telescope control system and allows to control two different antennas simultaneously. In fact a modification for the twin telescopes at Ny-Ålesund has been done and tested at Yebes, where the 13.2 m and the 40 m have been driven simultaneously from a single Field System instance.

Fig. 1 shows an overview of the architecture and of the interaction between the Field System and telescope control system.

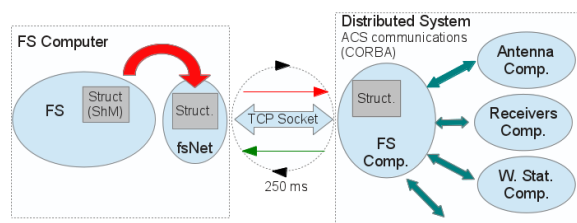


Fig. 1 Overview of the architecture and interaction between the Field System and the telescope control system. FS stands for Field System, Struct. for structure and ShM for Shared Memory. fsNet is a station program developed locally. The right side comprises the control system of the radiotelescope, composed of components that communicate among them using CORBA calls.

3 Signal transport

The Yebes radiotelescope is equipped with a dual polarization three band receiver whose bands range from 2.2 to 2.7 GHz, from 7.0 to 9.5 GHz and from 28 to 32 GHz. The downconverters generate IF signals in the baseband from 0.5 to 1 GHz at S and Ka band and between 0 and 1 GHz at X band. The receiver and the downconverters are installed in the elevation cabin and the 6 IF signals are fed into optical transceivers and sent through optical monomode fibers to the backends room, where they are converted back to analog signals which get injected into the backend. The distance between the antenna and the backends room is approximately 500 m and the cabling is laid underground.

For the moment the standard VLBI backend is one DBBC2 equipped with 4 IFs connected to one Mark5B+ whose largest writing rate is 2.048 Gb/s. For single dish observations either a Pocket Backend detector (de Vicente et al.) or a power meter with two sensors have been used. To characterize the spectrum of the receiving band we used one FFT backend with two modules 500 MHz bandwidth each.

The phase cal calibration is achieved with an updated traditional cable cal system composed of a ground unit and an antenna unit system, using a high speed logical gate, which provides pulses spaced 5 MHz in S, X and Ka band. The pulses at Ka band are achieved by mixing the tones from 0 to 5 GHz with a local oscillator. The ground unit is located at the pedestal of the antenna and hence measures cable variations along the cable wrap. It does not take into account variations in the optical fiber system up to the backends room. Cable length variations are measured using an HP 53131 counter with an ethernet to GPIB converter by Prologix. Since the current Field System does not support this device we developed some station code to manage and monitor it, allowing to have the readouts in the log files.

4 RFI across the band

We have checked the RFI across the band and compared it with the spectrum at the 40 m radiotelescope. Results are shown in Figs. 2 and 3. The RFI is in all cases much less important than for the 40 m telescope where encoders are suspect of being a major source of noise. In the 13.2 m, the receiver cabin is electrically isolated from the azimuth cabin where the main axes encoders are located. Additionally the ethernet switch that provides connectivity to all devices in the elevation cabin is enclosed in a shielded rack.

The RFI at X band and Ka band is negligible, and most of the RFI is present at low S band frequencies and gets worse towards the horizon and zenith (Fig. 2). The RFI is lower at intermediate elevations and is almost non-existent at the traditional IVS frequency intervals in S band (Fig. 3).

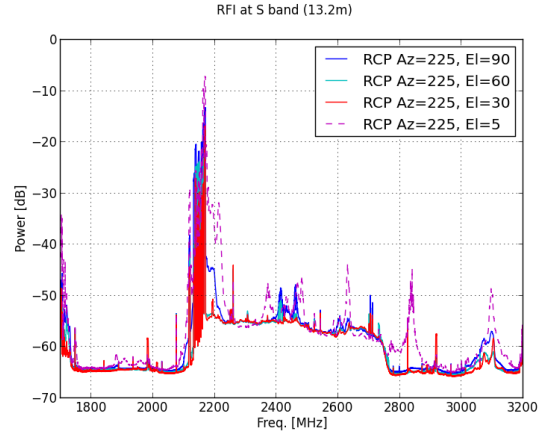


Fig. 2 RFI across the S band with four different elevations

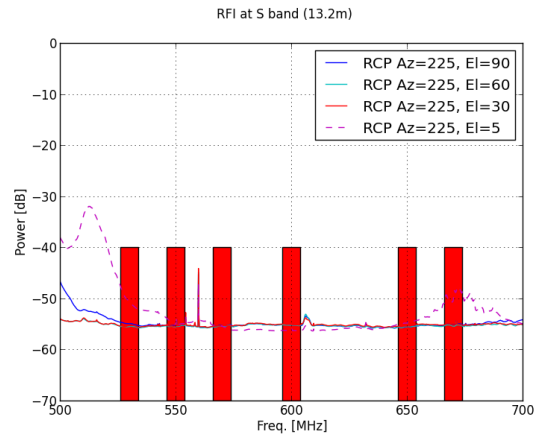


Fig. 3 RFI in the standard S band intervals used in IVS observations

5 Pointing and focus model

The 13.2 m uses a traditional 9 parameter pointing model which can be determined from continuous 24 hour observations at X band, using bright continuum sources to cover as much as sky as possible. Sources used were Taurus-A, OriIrc2, Virgo-A, Sagittarius-A, Cygnus-A and Cassiopea-A. Once the pointing model is implemented the pointing accuracy is 10 arcsecs and the pointing RMS across the whole sky 40 arcsecs. The Half Power Beam Width (HPBW) at X band is approximately 675 arcsecs.

Observations to obtain the optimum focus position as a function of elevation were also performed. Focus drifts along the Z axis while tracking the source were

not useful since the focus ring design and the subreflector close position to the secondary focus prevent a clear decrease in the detected intensity with defocusing (Fig. 4).

In order to obtain the best Z subreflector position, pointing drifts with different Z positions were performed. The optimum Z position was obtained from the intensity of the gaussians and the level of the secondary lobes. The model, which was obtained for X, Y and Z, and the tilts around the X and Y axes is only used for non-VLBI single dish observations. During VLBI observations the Z axis is kept at a fixed position, the optimum at 45 degrees, to prevent phase changes while allowing the movement of the Y and X axis to keep the gain as high as possible.

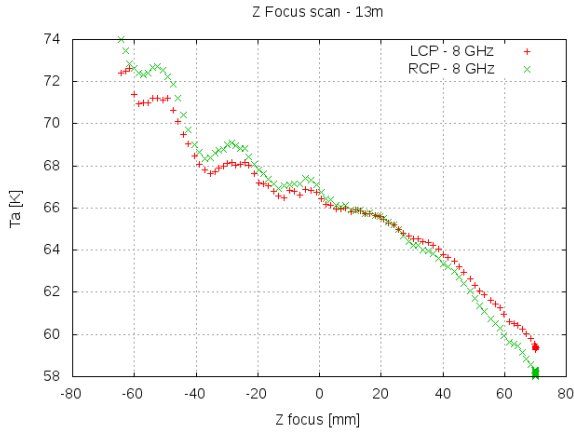


Fig. 4 Antenna temperature as a function of the Z position of the subreflector while tracking a source. The increasing slope towards negative Z hinders the determination of the maximum when doing focus drifts. An alternative strategy involving pointing drifts is required.

6 Efficiencies & SEFD

Calibration in the 13.2 m is achieved using a noise diode at the three receiving bands. The noise diode has been calibrated using a hot and a cold load in front of the horn. The hot load was an absorber placed in between the subreflector and the horn. The sky at 60 degrees elevation was used as cold load since a liquid nitrogen load in front of the horn was very big and difficult to manage. An atmospheric model based

on weather surface parameters was used to determine the opacity and emissivity of the atmosphere. The antenna temperature also depends on the forward efficiency, which we assumed to be 95 %. Skydips were performed to check the forward efficiency.

Table 1 summarizes the main characteristics of the antenna. System temperatures at S and X band are approximately 40 K, and 100 K at Ka band. Aperture efficiency is approximately 70 % at S and X band and close to 40 % at Ka band. Further work is required to check the efficiency at 30 GHz and determine if it can be improved.

Table 1 Main characteristics of the antenna. η_a stands for aperture efficiency and SEFD for Source Equivalent Flux Density.

Band	η_a	Tsys (K)	SEFD (Jy)	HPBW (arcsecs)
S band	70 %	40	1300	~ 2550
X band	70 %	40	1300	~ 675
Ka band	38 %	100	5400	~ 190

The aperture efficiency of the antenna was obtained by tracking sources of known flux and size. The efficiency at 8.4 GHz as obtained from pointing drifts towards Cas A and Tau A is depicted in Fig. 5. Efficiency is very flat in the elevation range between 15 degrees and 73 degrees.

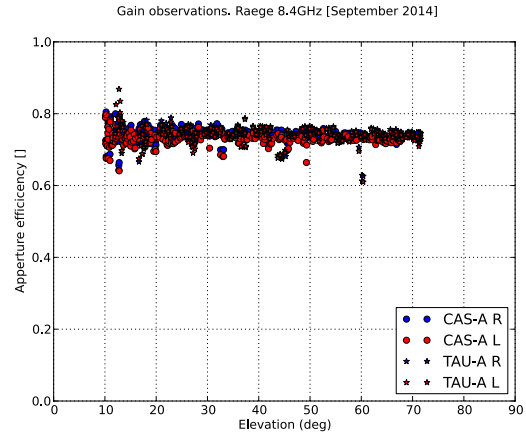


Fig. 5 Aperture efficiency at 8.4 GHz from observations towards Tau and Cas A

7 VLBI observations

First VLBI observations were performed in November 2014 and fringes at X band were obtained. They were followed by the participation in standard R1 and R4 IVS sessions starting on April 2015. Since May 2015 the telescope, identified as RAEGYEB, has been taking part in R1 and R4 observations once per week. By July 2015 all systems worked correctly, including the phase cal and cable measurement system.

Acknowledgments

We thank all the staff in Yebes Observatory for the generous help received. We acknowledge partial support from MINECO grants FIS2012-32096, and FIS2012-38160.

References

- de Vicente P, Bolaño R, Barbas L (2006) Development of the Control System for the 40m OAN Radiotelescope with the ALMA Common Software. In: C. Gabriel, C. Arviset, D. Ponz, E. Solano (eds.), *Astronomical Data Analysis Software and Systems XV*, ASP Conference Series, 351, 758–761.

Development of Multipurpose Digital Backend for "Quasar" network radio telescopes

E. Nosov

Abstract Multipurpose Digital Backend (MDBE) is a system intended to replace the currently used backend equipment of "Quasar" network radio telescopes. MDBE has a compact size and can be easily located inside the focal cabin of the antenna. MDBE digitizes up to 8 input signals with 512 MHz bandwidth or up to 4 signals with 1024 MHz bandwidth and processes the signals in FPGA. The system has several operating modes to perform all required types of observations. For VLBI observations, MDBE supports wide-band channel mode, digital downconverters (DDC) mode and polyphase filter bank mode. The output data stream is packed into 10G Ethernet frames and transferred through fiber optic lines. MDBE supports VDIF data format for all VLBI observation modes. For compatibility with existing data acquisition systems, the data in DDCs mode can also be packed in Mark5B data format. Besides VLBI observation modes, MDBE implements spectrometer and radiometric backend modes. The system implements a rich set of signal analysis features including PCAL extraction, 2-bits data statistics, input signals capture, power spectral density estimation and other. These features allow remote monitoring of the whole system condition and can greatly reduce fault lookup time. MDBE replaces a lot of equipment with one compact device and significantly simplifies overall system complexity.

Keywords Quasar network, RT-32, RT-13, MDBE, digital backend, data acquisition system, downconverter

Evgeny Nosov
Institute of Applied Astronomy, IAA RAS, 191187, Kutuzova nab. 10, Saint-Petersburg, Russia

1 Introduction

Institute of Applied Astronomy of RAS owns three 32-meters antennas (RT-32) and two recently constructed 13-meters antennas (RT-13) in (Ipatov et al., 2014). These antennas are equipped with various backend devices to provide different types of observations (see Table 1). For VLBI observations 32-m antennas are equipped with R1002 DAS which consists of 16 tunable downconverters (Nosov et al., 2010). The bandwidth of the channel is up to 32 MHz and the output data is intended to be recorded on Mark-5B recorder. The 13-m antennas are equipped with Broadband Acquisition System (BRAS), which consists of eight wide-band channels of 512 MHz each (Nosov et al., 2014). The output data packed into VDIF frames can be recorded by any recording system with 10GE interface and sufficient throughput. These systems are incompatible with each other and perform different processing algorithms. It is still possible to carry out joint observations, but the correlation processing is more sophisticated. To achieve more application flexibility it is desirable that each station could work both as downconverters and as wideband channels with direct sampling.

Most of 32-m antennas have various pieces of radiometric and spectrometric backend equipment. Most of it is rather old and has to be replaced because it is becoming difficult to keep its operability. Only Svetloe observatory has modern digital radiometric backend with wide bandwidth and interference rejecting in frequency domain (Grenkov et al., 2013). Another difficulty of the 32-m antennas signal chain (Fig. 1) is long coaxial cables used to transfer signals from the receivers to the backend equipment located in the main building. The cables affect frequency response and at-

Table 1 Backend equipment on "Quasar" network antennas. R1002M- data acquisition system based on downconverters, BRAS- broadband acquisition system, SSR- broadband digital radiometric backend with RFI suppression (Grenkov et al., 2013), PRM- radiometric backend based on analog detector (Ipatov et al., 2005), R3901/2- narrowband FFT-based spectrometers.

Operating mode	RT-32			RT-13	
	Svetloe	Zelenchuk.	Badary	Zelen.,	Badary
VLBI	R1002M DAS			BRAS	
Radiometric	SSR	PRM	PRM	No	
Spectrometric	R3902	No	R3901	No	

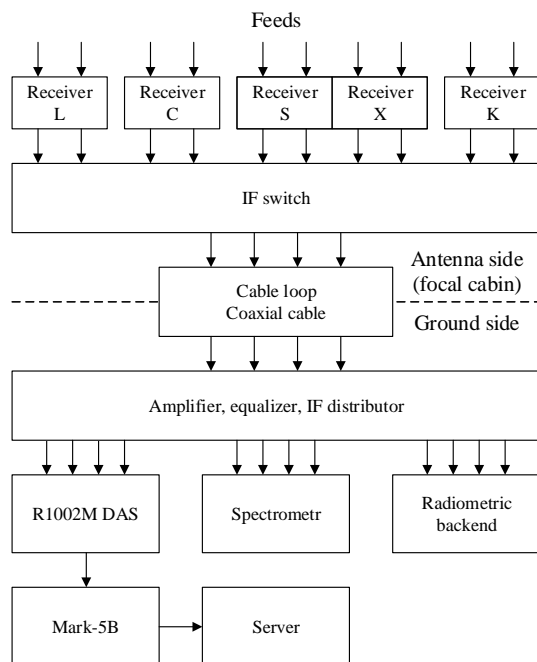


Fig. 1 Existing signal chain structure for RT-32 antennas

tenuate the signals. Some cables in the cable loop are rather worn out and their phase response fluctuates with antenna rotation. The intermediate equipment between the receivers and the backends introduces additional instability and noise. The signal chain is also sensible to strong RFI.

To eliminate the above listed problems it is necessary to minimize the equipment quantity between receivers and backends. The existing backend equipment cannot be placed in the focal cabin because of its size and weight. Modern technologies allow us to digitize wide-band signals by high-speed ADCs and perform complex processing of digital data in FPGAs.

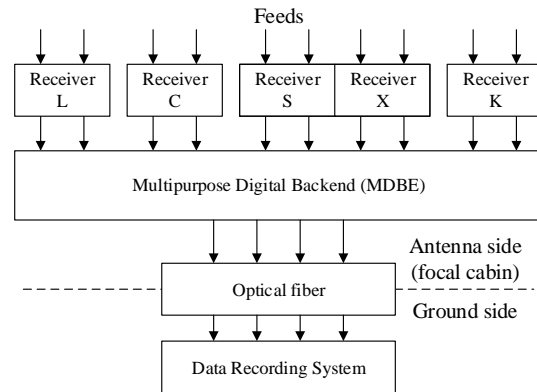


Fig. 2 Upgraded signal chain structure for RT-32 antennas

By using this IAA RAS is developing a Multipurpose Digital Backend (MDBE) able to perform all types of VLBI, radiometric and spectrometric observations. MDBE can be located in the focal cabin of the antennas near to receivers and the output data will be transmitted to recording system in digital form by fiber optics. It excludes the influence of signal transfer medium on the transmitted signals and protects them from RFI. The new structure of signal chain for RT-32 is presented on Fig. 2.

2 Requirements

To unify the equipment MDBE should be compatible with both RT-32 and RT-13 antennas. Thus it should support power level and intermediate frequency range of the receivers of RT-32 (0.1-1 GHz) and RT-13 (1-2 GHz, see Evstigneev et al. (2014)) antennas. The digitized signal bandwidth can be up to 1 GHz per channel. Also, MDBE should be able to use both 5 MHz (RT-32) and 100 MHz (RT-13) as a reference clock signals.

The basic output data format is VDIF, but to keep participating in international observations there is an option to pack data in Mark5B compatible format. To implement all required VLBI, radiometric and spectrometric observation modes MDBE has to support remote firmware reload. It allows to modify the system easily and to add new functions without direct access to the device.

MDBE placement near to receivers eliminates a lot of existing signal chain problems. However, in the same time it can produce new ones related to EMI emission from the noisy digital part of the system. Therefore, it is very important to keep it as low as possible. It is achieved by appropriate PCB design, using fiber optic channels instead of copper for control and data transfer and double shielding of the noisy parts.

As the system is located inside the focal cabin of the antenna there is no direct access to it for the staff while an observation is in progress. To compensate it MDBE provides full remote control of the system and signals. The control features include measuring PCB, FPGA and ADCs temperatures, power supplies voltages and currents, input signals power level, statistics of 2-bits output data and others. MDBE performs PCAL extraction, monitoring of phase and amplitude of its harmonics, input signal capturing for analysis in time and frequency domain.

3 MDBE structure

The structure of MDBE (Fig.3) is based on the listed requirements. Its main parameters are summarized in Table 2. Input signals are digitized by two 4-channels high-speed ADCs. MDBE can digitize up to 8 signals of 512 MHz each or up to 4 signals of 1024 MHz. The analog part of MDBE is implemented as a separate PCB. It contains switches to connect required input signals to ADCs, antialiasing filters, amplifiers and attenuators to adjust signal power to optimal level before digitizing. As the receivers of RT-13 and RT-32 antennas have different IF frequency ranges, power level and channel number, there are different analog parts for different antenna types.

Digitized data from ADCs are processed in FPGA chip. The analysis of required FPGA resources for the most demanding applications shows that it can be implemented in a single FPGA chip. The selected chip has an embedded dual-core ARM processor that greatly simplifies the implementation of control and communication functions. The processor "ecosystem" contains different types of memory for its appropriate operation and SD-card slot. Linux operation system runs on the first processor core and controls hardware parts through I2C and SPI bus and through dedicated GPIO lines. Firmware of FPGA and the second pro-

cessor core can be reloaded by Linux from embedded memory, SD-card or through the network. MDBE communicates with network through 1G Ethernet interface. There is also an USB/UART bridge for debugging purposes.

To transfer high-speed output data there are eight 10G Ethernet ports based on SFP+ modules connected with FPGA through embedded Multi-Gigabit Transceivers. Total theoretical throughput of MDBE outputs in case of raw Ethernet frames is close to 80 Gbit/s.

MDBE accepts 5, 10 and 100 MHz signals as reference clock. The system has two 1 PPS inputs for time stamps from H-maser and GNSS receiver and 1 PPS monitor output of local clock. FPGA measures time intervals between input 1 PPS signals and local clock with 1 ns accuracy.

Table 2 Basic parameters of MDBE.

Number of IF inputs	10
Number of digitizing wideband channels	8 channels @512MHz 4 channels @1024MHz
ADCs	2 ADCs, 10 bits, Fs=1024/2048 MHz
Automatic gain control	For each channel, 31 dB
Sync signals	5/10/100 MHz (autodetect), 1 PPS x 2
Control outputs for modulation	4 channels, independent frequency and phase adjustment
Control interface	10/100/1000 Ethernet
Output interface	8 x 10GE, SFP+ transceivers
Telemetry	Power circuits current and voltage, temperature of PCB, ADCs and FPGA
Signal analysis	PCAL extraction, Signal capturing for time and freq. domain analysis, signal power monitor etc.
Size	19 3U case, 483x132x314mm (WxHxD)

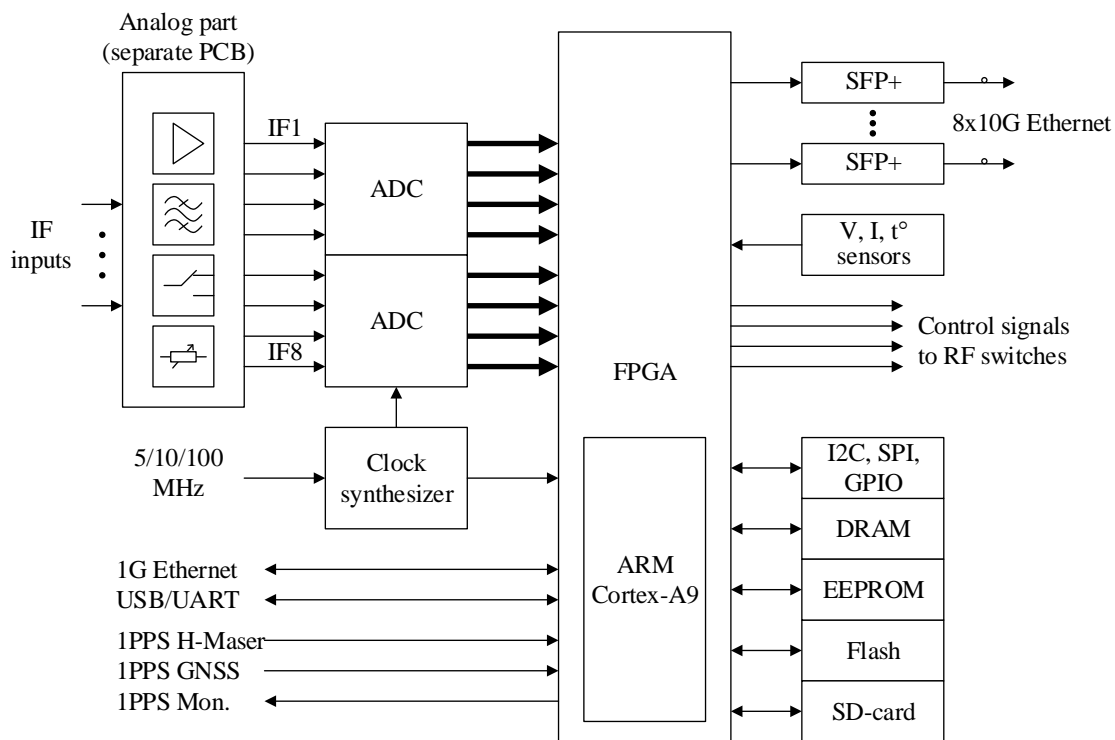


Fig. 3 MDBE structure

4 Operating modes

MDBE can be used for VLBI, radiometric and spectrometric observations. There are three operating modes for VLBI observations. The first one is wide-band channels mode. In this mode MDBE digitizes up to 8 input signals with 512 MHz or up to 4 signals with 1024 MHz bandwidth and re-quantize it to 2-bits using RMS value of the signals as a threshold. This mode is currently implemented in BRAS on RT-13 antennas. As RFI can significantly decrease signal-to-noise ratio in S-band, adaptive digital filtering based on FFT can be implemented.

Most of VLBI observations are currently performed with downconverter-based systems. Therefore, digital downconverter (DDC) mode is required to participate in international observations. MDBE supports up to 16 DDCs with 2/8/16/32 MHz bandwidth. DDC cuts out the narrow band in selected input signal and transfers it to baseband. Then the signals are re-quantized to 2-bits and packed into VDIF or Mark5B-compatible frames.

Another mode to be implemented is polyphase filter bank mode (PFB). It allows to cut out wide input band onto equally located narrow bands. 32 and 64 MHz bandwidth are supported.

There are two non-VLBI modes in MDBE. Radiometric backend mode provides signal power measurement with suppressing of pulse-like interference in time domain and narrow-band interference in frequency domain. The spectrometer mode allows high frequency resolution observations in narrow bands.

5 Conclusions

Implementation of all listed modes is a complex work that demands a lot of time. But the possibility to easily upgrade the firmware of MDBE through the network allows adding new functions and modes after the system is commissioned with the most basic features only. It also gives a possibility to implement the modes not listed above if necessary. MDBE significantly sim-

plifies the existing signal chain and eliminates its inherent disadvantages. The system provides all antennas of "Quasar" network with the same set of observation modes. The possibility to reload firmware remotely in conjunction with powerful and flexible hardware part allows MDBE to cover all needs of "Quasar"-network in backend equipment for years in advance.

References

- Ipatov A, Ivanov D, Ilin G, Smolentsev S, Varganov M, Gayazov I, Mardyshkin V, Fedotov L, Kajdanovsky M, Vytnov A, Salnikov A, Mikhailov A (2014) Russian VLBI System of New Generation. In: D. Behrend, K. D. Baver, K. L. Armstrong (eds.), *IVS 2014 General Meeting Proc.*, Science Press (Beijing), 25–29.
- Nosov E V, Grenkov S A, Fedotov L V, Koltsov N E (2010) A Digital Radio Interferometric Signal Conversion System. *Instrum Exp Tech*, 53(5), 675–681, ISSN 0020-4412, doi: 10.1134/S002044121005009X.
- Nosov E, Berdnikov A, Grenkov S, Marshalov D, Melnikov A, Fedotov L (2014) Current Development State of the Russian VLBI Broadband Acquisition System. In: D. Behrend, K. D. Baver, K. L. Armstrong (eds.), *IVS 2014 General Meeting Proc.*, Science Press (Beijing), 82–85.
- Ipatov A V, Koltsov N E, Krokhalev A V (2005) A Radiometric System for the RT-32 Radio Telescope. *Instrum Exp Tech*, 48(4), 482–490.
- Grenkov S A, Koltsov N E, Fedotov L V (2013) Spectral-Selective Radiometers with Bandwidths of up to 1 GHz. *Instrum Exp Tech*, 56(5), 555–559, ISSN 0020-4412.
- Evstigneev A, Ipatov A, Ipatova I, Mardyshkin V, Khvostov E, Lavrov A, Chernov V (2014) Tri-band System for the Russian Interferometer. In: D. Behrend, K. D. Baver, K. L. Armstrong (eds.), *IVS 2014 General Meeting Proc.*, Science Press (Beijing), 118–121.

Results from a test realization of a system monitoring for seamless auxiliary data

A. Neidhardt, J. Lovell, K. Kirschbauer, M. Schönberger, E. Himwich, J. McCallum, Ch. Plötz, J. Quick

Abstract During the analysis workshop, which was following the IVS General Meeting in Shanghai in the year 2014, a new IVS task force was formed to address the issue of seamless auxiliary data. The project has progressed to a stage where a formal proposal has been prepared and first test realizations are implemented at Wettzell. These developments are based on definitions in a vision for a Monitoring and Control Infrastructure (MCI). The current realization uses the Wettzell System Monitoring (SysMon) hardware and software but is also open for other monitoring environments, like MoniCA or the Haystack MCI. The paper presents the design of the system and the first realizations, and an initial demonstration of the results.

A. Neidhardt

Technische Universität München, Forschungseinrichtung Satellitengeodäsie, Geodetic Observatory Wettzell, Sackenrieder Str. 25, D-93444 Bad Kötzing, Germany

J. Lovell, J. McCallum

University of Tasmania, Sandy Bay Campus, Maths-Physics Building, Private Bag 86, HOBART TAS 7001, Tasmania/Australia

Ch. Plötz, M. Schönberger

Federal Agency for Cartography and Geodesy, Geodetic Observatory Wettzell, Sackenrieder Str. 25, D-93444 Bad Kötzing, Germany

K. Kirschbauer

Student, THD - Technische Hochschule Deggendorf, Edlmairstraße 6 und 8, D-94469 Deggendorf, Germany

E. Himwich

NASA(GSFC/NVI, Mail Code 698.2, Greenbelt, MD 20771, USA

J. Quick

Hartebeesthoek Radio Astronomy Observatory (HartRAO), P.O.Box 443, Krugersdorp 1740, South Africa

Keywords Seamless auxiliary data, system monitoring, infrastructure

1 Introduction and current situation

The Global Geodetic Observing System (GGOS) requires permanent monitoring systems (e.g. for the determination of the local-ties in sub-millimeter accuracy) to achieve the positioning precision goals (Rothacher, 2009). Beside the main products, several additional parameters might be worth to be monitored to improve the final geodetic solution. Some observatories and VLBI sites already collect parts of these seamless auxiliary data. Nevertheless they are often not publicly available. Correlation and analysis centers cannot directly use the data sets for their needs.

A simple example here are already the meteorological data, which are logged in the session log files. This means, that they are just available for the time intervals, while a session is observed. But it would be quite helpful, to have the data continuously for a uniformly available estimation of the meteorological situation. All times without observations must be interpolated or extrapolated from the existing data sets. This means, that meteorological data are also required for the times in between of the sessions. In most cases the observatories produce and store these data sets, but the data are not directly available for external usage, the access is restricted, or only current values are easily presented on Web interfaces.

The current situation can be characterized as follows:

- Auxiliary data are only available as log file entries (meteorology, time corrections).

- Auxiliary data are only available for session times.
- Additional data are often not publicly known (invar, local ties, etc.).
- Additional data are locally in proprietary formats at the observatory.
- Data can often just be requested directly from the observatories on demand.

Therefore the IVS Task Force for Seamless Auxiliary Data was founded during the Analysis Workshop in Shanghai 2014 to discuss and find solutions to improve the current situation.

2 A proposal for the IVS Task Force for Seamless Auxiliary Data

The IVS Task Force on Seamless Auxiliary Data should show possible realizations, make suggestions on what data should be provided and how observatories can contribute to the real-time data stream. It would have some positive effects on the accuracy of IVS data products if data were to be continuously available. Real-time ancillary data can also contribute in a dynamic observing scenario where scheduling decisions are automatically made.

Therefore the main goals are:

- Continuous, auxiliary data are of high interest
- Additional data might be interesting for research
- Centralized data repository
- Real-time overview of the observation network
- Preparations for dynamic observations

The realization plan follows two phases (see fig. 1). The first is a one year lasting proof-of-concept-section. The NASA Field System and the e-RemoteCtrl software (Ettl, 2012) should be extended with a sending functionality during this development section, so that currently available auxiliary data can be sent. This sending is possible at least for the times, when the Field System is running. To enable a centralized data repository, a server hardware with suitable RAID-sets of hard drives will be prepared at the Geodetic Observatory Wettzell. The current discussion follows a realization of several virtual servers for the Web presentation and data acquisition. Additionally the System Monitoring software "SysMon", which was developed in Wettzell, is extended to easily support the propagation of continuous data to that repository. Nevertheless the server

will be open enough to also support parallel existing system monitoring infrastructures, like the MoniCA-system in Australia (Brodrick, 2014) or the MIT Monitoring and Control Infrastructure for the new VGOS antennas in Haystack and Washington.

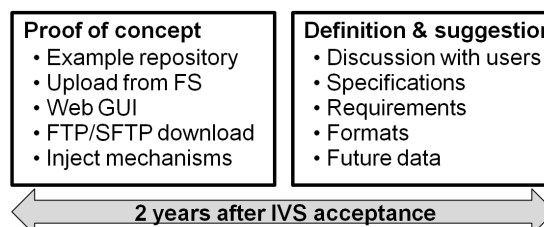


Fig. 1 The planned phases of the IVS Task Force on Seamless Auxiliary Data.

The second phase focuses on the discussions, developments and suggestions for future needs on seamless auxiliary data for the VGOS network. Feedback from users is required during this period and several teleconferences are planned. The goal is to meet future requirements and to define formats and prepare specifications. Another year is planned for this step.

The resulting work packages look like the follows:

Table 1 The work packages of the task force.

Main task	Result	Current status
Writing a test sender	NASA FS Streaming	Testing phase
SysMon, MCI, MoniCA access	Monitoring Node Box	In test use
Web server installation	Repository Web Server	Design phase
Telecons and meetings	Specification for VGOS-monitoring	Not yet started

3 Real-time streaming

The already existing streaming method of the e-RemoteCtrl (Neidhardt, 2014) should be used for the real-time streaming of currently already available auxiliary data. Even if this mode is still in the testing phase and still contains some problems according to the usage of stable and encrypted tunnels through the

Secure Shell (SSH), it is promising for such needs. Especially the general usage, also in other environments without the e-RemoteCtrl software, are a plus of this technique.

The principle is quite straight forward. The e-RemoteCtrl server or another reader takes already existing information (like meteorological data, clock offsets, etc.) from the shared memory of the Field System, creates a new file of a dedicated structure and format and sends it to a predefined server. Currently a server at the Technische Universität München is used. But for the auxiliary data a new target computer at the observatory will be used.

4 System Monitoring box

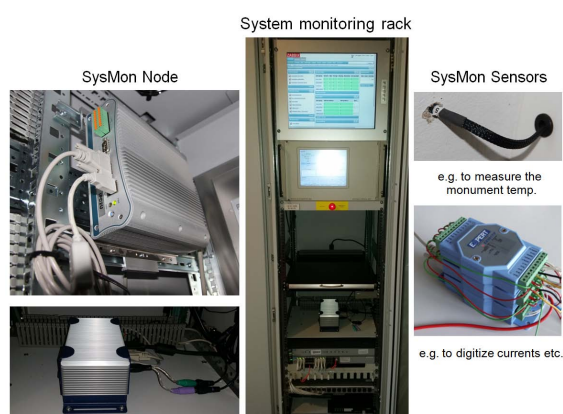


Fig. 2 The SysMon components in the test rack.

Parallel to the previously described real-time streaming from the NASA Field System, which can be supported by any antenna, while the Field System is active, also independent techniques should be realized. Because additional data are also required for the regular operation of the VLBI-antennas, the different modern realizations of new VGOS antennas also plan parallel monitoring systems. One is the "MoniCA" Monitoring Software from the CSIRO Australian Telescope National Facility (Brodrick, 2014). "MoniCA is a Java-based graphical application for viewing real-time and archival monitor data [...]" (Brodrick, 2014). Another development was made at the MIT Haystack observatory: the Monitoring and Control

Infrastructure (MCI). Originally it started with group meetings to define a generalized MCI interface and arbitrary MCI system architectures (Beaudoin, 2015). A first realization however focuses on the direct needs and setups of the GGAO, and Westford/Haystack antennas.

On the basis of the original definitions of the MCI, the Wettzell team started to extend the System Monitoring Software "SysMon", which was originally developed in Wettzell and is already used for several use cases (see Fig. 2), like a human protection system in the laser ranging instruments (Ettl, 2010). Within student projects all interfaces are now realized to offer a suitable and simple computer MCI architecture as monitoring node. The whole hardware system is composed of four layers: the sensors layer, the data collimating and safety layer, the data acquisition and storage layer, and the application and user interface layer (Ettl, 2010).

Several already existing modules are available to build up own sensors in the sensors layer. All parts are commercial off-the-shelf products. The data collimating and safety layer is optional. It uses data gathering hardware and special safety-proofed programmable logic arrays or controllers to realize human protections. The data acquisition and storage layer consists of a regular PC, usually as a fanless and robust architecture. And the application layer might be populated by the NASA Field System or by presentation tools.

The new, extended realization consists of an elementary application interface (SysMon API) on the basis of C/C++. Using this Sysmon API, each program can register new sensors. The registration is handled with a configuration file, which was originally defined by the MCI group. After the registration the program can inject data to the system.

The system itself consists of a database, which is automatically generated and uses sensor tables for historic data and also a separate table with the latest data set. Each sensor value is identified by a sensor identification and is tagged with a time-stamp. This SysMon core database is combined with Zabbix.

Zabbix is designed for real-time monitoring of metrics collected from different servers, virtual machines and network devices. It is an Open Source software (Zabbix, 2015). Also different other sensor data can be injected by using a special sender program. Zabbix allows to create containers for the metrics, called items. Each item can be combined with different triggers to rise further activities. For an ideal presentation,

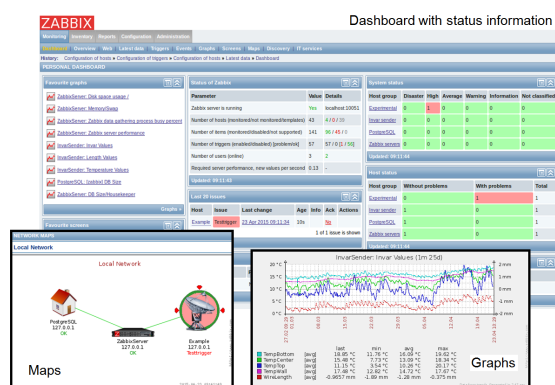


Fig. 3 The Zabbix frontend of the SysMon software from Wettzell.

Zabbix allows to create graphs of different styles. A monitoring dashboard allows to combine the system status information, using green, yellow and red status bars. User-defined maps combine symbols with network structures and allow to offer a graphical representation of the dependencies between the data collectors and devices. They also show error and alarm states in combination with the sensor symbols (see Fig. 3). In the current realization each registered sensor automatically produces a completely prepared template file for the registration to Zabbix, which then must be loaded to the Zabbix system.

Additionally all sensors can be realized as separate servers with the standardized interface, defined by "idl2rpc.pl". This is an interface generator, reading an interface definition file and creating a communication system with client and server modules on the basis of Remote Procedure Calls (RPC). Such an interface can also be used to transfer the latest data sets to the central repository, each time a new value is registered or within dedicated time intervals.

5 Ideas for a data repository at Wettzell

The repository as centralized data collector at Wettzell will take all incoming data sets from the NASA Field System or from the SysMon, MCI, and MoniCA boxes. In principle it will be nothing more than a more powerful system monitoring node. In Wettzell it will be realized in the same style as the previously described SysMon node. It will realize the SysMon core database, the

standardized interface, and the Zabbix frontend. Additionally it will offer a simple Web archive in the style of the VTC document repository, hosted at the Technische Universität München (see (VTCDoc (2015))). Historic data can also be fetched via Secure File Transfer Protocol (SFTP).

6 Conclusion and outlook

The work of the task force focuses on the realization of first usable implementations. On the basis of these discussions can be started to change, improve, and plan future monitoring ideas. Therefore the released IVS proposal describes the desired outcomes in the following way (Neidhardt, 2015):

1. A first standardization of an interface for a central data repository to receive incoming data and to fetch selected data sets from a data acquisition server.
2. The hardware and realization of a central repository at the Geodetic Observatory Wettzell
3. An initial proof-of-concept implementation with software and hardware components at selected observatories, which are able to send auxiliary data (focused on meteorological data) to a central repository.
4. A list of data, which may be relevant for future VGOS observations.
5. A transition and realization plan for IVS telescopes.

In best case the discussion will lead in an integration of the data at the IVS data centers.

References

- Beaudoin C, Corey B, Niell A, Whitney A (2015) Haystack Observatory Technology Development Center. Web document <ftp://ivscc.gsfc.nasa.gov/pub/annual-report/2010/pdf/tdhstk.pdf>, Download 2015.
- Brodrick D (2015) "MoniCA" Monitoring Software. Web document <https://www.narrabri.atnf.csiro.au/monitor/monica/>, Download 2015.
- Ettl M, Neidhardt A, Plötz C, Mühlbauer M, Dassing R, Hase H, Beaudoin C, Himwich E (2010) SysMon - a robust and flexible remote monitoring system for VLBI and more. In: *Proceedings of Science (PoS) - 10th European VLBI Network*

- Symposium and EVN Users Meeting: VLBI and the new generation of radio arrays, EID PoS(10th EVN Symposium)025*, Scuola Internazionale Superiore di Studi Avanzati (SISSA).
- Ettl M, Neidhardt A, Schönberger M, Alef W, Himwich E, Beaudoin C, Plötz C, Lovell J, Hase H (2012) e-RemoteCtrl: Concepts for VLBI Station Control as Part of NEXPRoS. In: D. Behrend, K. D. Baver (eds.), *IVS 2012 General Meeting Proc.*, NASA/CP-2012-217504, 128–132.
- Neidhardt A, Collioud A (2014) Real-time data streams from "e-RemoteCtrl" to central VLBI network status monitoring services like "IVS Live". In: D. Behrend, K Baver, K Armstrong (eds.), *IVS 2014 General Meeting Proc.*, Science Press (Beijing), 262–266.
- Neidhardt A, Lovell J (2015) *IVS Task Force for Seamless Auxiliary Data*. IVS Proposal, IVS.
- Rothacher M, Beutler G, Bosch W, Donnellan A, Gross R, Hinderer J, Ma C, Pearlman M, Plag H-P, Richter B, Ries J, Schuh H, Seitz F, Shum C K, Smith D, Thomas M, Velacogna E, Wahr J, Willis P, Woodworth P (2009) The future Global Geodetic Observing System (GGOS). In: H.-P. Plag, M. Pearlman (eds.), *The Global Geodetic Observing System. Meeting the Requirements of a Global Society on a Changing Planet in 2020*, Springer-Verlag.
- IVS VTC: IVS VTC Document Repository. Web <http://vtcdoc.iapg.bgu.tum.de/>, Download 2015.
- Zabbix: The Ultimate Enterprise-class Monitoring Platform. Web document <http://www.zabbix.com/>, Download 2015.

Current Operations of the Bonn Correlator and Preparations for VGOS

W. Alef, T. Schüler, A. Müskens, A. Nothnagel, A. Bertarini, H. Rottmann, L. La Porta, S. Bernhart, G. Bruni

Abstract We present the status of the Bonn Correlator Center (2013/2014) with emphasis on the geodetic correlation. The correlator center has been operated jointly by the Max Planck Institute for Radio Astronomy (MPIfR) in Bonn, the Federal Agency for Cartography and Geodesy (BKG) in Frankfurt with support from the Institute of Geodesy and Geoinformation (IGG) in Bonn. Correlation has been done exclusively with the DiFX software correlator. We will give a brief summary of our experience with correlating the CONT14 session, the first CONT to be correlated with DiFX. We will also discuss our plans for upgrading/renewing the HPC cluster in preparation for the expected impact of the future VGOS observations on the available computing and playback resources.

Keywords CONT14, VLBI correlation, DiFX correlator, VGOS

Walter Alef, Helge Rottmann, Alessandra Bertarini, Gabriele Bruni

Max-Planck-Institut für Radioastronomie, Auf dem Hügel 69, D-53121 Bonn, Germany

Torben Schüler

Bundesamt für Kartographie und Geodäsie, Geodätisches Observatorium Wettzell, Sackenrieder Str. 25, D-93444 Bad Kötzing, Germany

Arno Müskens, Axel Nothnagel, Alessandra Bertarini, Laura La Porta, Simone Bernhart

Rheinische Friedrich-Wilhelms Universität Bonn, IGG, Nußallee 17, D-53115 Bonn, Germany

1 Introduction

The MPIfR has been hosting five generations of VLBI correlators since 1978 – Mark II, Mark III, Mark IIIA, Mark IV (Whitney et al. 2004) and the DiFX software correlator (Deller et al. 2011). MPIfR and BKG have been jointly operating the Mark IV correlator from January 2000 to December 2012 and the DiFX correlator since 2007 on a fifty-fifty basis.

Highlights since the last meeting are the correlation of the CONT14 campaign with DiFX, which went smoothly and faster than previous CONT sessions with the Mark IV correlators, the correlation of RadioAstron satellite data, and of 1mm VLBI sessions. The plans to enlarge the correlator cluster for VGOS were delayed in accordance with the delays in VGOS observing. As a first important step the correlator room has been rebuilt to make space for additional Mark 6 playback units, while the new cluster will be installed in Q4/2015.

2 Correlator status

DiFX 2.0 (Deller et al. 2011) was the first version of this software correlator which could be used for geodesy. The Bonn correlator was the first to change all geodetic correlation to DiFX in 11/2010. At present the latest stable version DiFX 2.4 is installed as well as a number of older or “local” versions for special purposes, most notably a version to correlate RadioAstron (Kardashev et al. 2012) data (working title DRA-DiFX).

DRA-DiFX (Bruni et al. 2014) has been developed from DiFX version 2.01 by J. Anderson at MPIfR who is now working for the GFZ in Potsdam. It has re-

cently been merged back to the “trunk” which is the development version of DiFX 2.4 and will be part of the next official DiFX release. In particular to aid post-correlation fringe search for RadioAstron data the PIMA¹ software has been installed with help from L. Petrov and the Astro Space Center, Moscow.

Other enhancements since the last report are the implementation of a data-base for experiment status and disks, and archiving of the raw correlated data together with their FITS-IDI² or HOPS³ exports on the new MPIfR archive server.

Immediate enhancements planned are native playback from Mark 6 recorders for data from VGOS and the Event Horizon Telescope (EHT). The most challenging part is the implementation of multiple data streams per station. For instance an EHT observation at 64 Gbps would deliver the data spread over 4 Mark 6 recorders with extension chassis, resulting in 16 disk modules to be played into the correlator.

Experiment preparation and post-processing are handled separately for geodetic and astronomical observations

- geodesy: A. Bertarini, L. La Porta, S. Bernhart. Scheduling of IVS-Euro, INT3, and T2 sessions: A. Müskens
- astronomy: A. Bertarini, H. Rottmann, G. Bruni

H. Fuchs, H. Sturm, H. Rottmann, W. Alef, R. Märten (all MPIfR) are in charge of the correlation proper, cluster OS, cluster hardware, and correlation software. General computing services and the archive server are provided by the MPIfR computer division.

The HPC cluster used for correlation (see Fig. 1) was erected in 2007/2008. Of the original 60 compute nodes 58 are still operational which results in 464 compute cores. The disk space realised in fast RAIDs has grown from initial 40 TB to now 484 TB plus 10 TB for storage of the correlation results. In addition 20 TB were added for backup of the most important disk areas. 20 Gbps Infiniband is used as cluster interconnect. All 15 Mark 5 units can play back all flavours of Mark 5 data formats (5A, 5B, 5C). Four Mark 6 playbacks have been installed in early 2015, one of which has already been used for testing together with the DiFX correlator

¹ <http://astrogeo.org/pima>

² <ftp://ftp.aoc.nrao.edu/pub/software/aips/TEXT/PUBL/AIPSMEMO102.PS>

³ <http://www.haystack.mit.edu/tech/vlbi/hops.html>

using the VDIFuse software written and maintained by MIT Haystack.



Fig. 1 Photo of the MPIfR HPC cluster. The 2 racks on the right house the compute nodes, head nodes, and network switches. In the 2 racks on the left are the RAID systems.

3 Correlator usage 2013/2014

The Bonn correlator is the only VLBI correlator worldwide which is operated on a fifty-fifty basis by astronomers and geodesists, which means that the correlator usage is roughly 50% for geodesy and 50% for astronomy.

The load and throughput of the Bonn correlator has stayed about the same for geodetic observations with

- 94 R1
- 12 EURO
- 6 T2
- 10 OHIG
- 81 INT3 (in eVLBI mode)

except for the first CONT (CONT14) to be processed with the DiFX correlator (see section 4).

All the tests for the DBBC development have also been correlated in Bonn. Testing of the DBBCs is no longer limited to short observations with On, Wz and Ys, but it usually consists of parallel observations (whenever possible) of some geodetic session with both analogue and digital backends. In addition we support every station when new software or hardware for recording or transferring data are introduced like flexbuff, vdif format, jive5ab etc.

It should be noted that most geodetic observatories do not send disk modules any more, but transfer the data via the Internet

One part of the astronomy load of the correlator is data from the Global MM VLBI Array (GMVA), which observes two sessions per year of up to five days duration at 3 mm wavelength. Up to 15 antennas participate in GMVA observations. For the last two years the data-rate has been increased to 2 Gbps which results in about 500 TB of total disk space recorded in each session.

Correlation of RadioAstron observations has been a big load since 2013. It requires an additional very time consuming pass, as the RadioAstron clock has to be searched for every scan. As the orbit of RadioAstron is only known to about 500 m the changes in delay and delay-rate can be quite large, so that an additional acceleration term has to be taken into account. So far nine observations with up to 20 antennas at 128/256 Mbps, full track on the source, have been correlated. Sometimes even a third correlation pass with an improved satellite orbit has been necessary.

Very experimental work is done at 1 mm and 0.85 mm wavelength with the EHT which now records 16 Gbps on Mark 6 units. Part of the session from March 2015 will be correlated in summer.

4 Correlation of CONT14

CONT14 is a campaign of continuous VLBI sessions, scheduled to be observed in early May 2014 (6-MAY-2014 00:00 UT through 20-MAY-2014 24:00 UT)⁴. 16 stations with 17 antennas granted observing time for the 15 session days of the CONT14 campaign. The stations are: Badary, Fortaleza, Hobart 12m, Hobart 26m, Hartebeesthoek 15m, Katherine, Kokee, Matera, Ny-Ålesund, Onsala, Tsukuba, Westford, Warkworth, Wettzell, Yarragadee, Yebes, Zelenchuk-skaya. Observed frequency bands were the standard S- and X-band, with the classical setup of 16 channels, each with 8 MHz bandwidth and 2-bit sampling, thus resulting in a data-rate of 512 Mbps.

USNO had been the dedicated correlator for CONT14, but due to delays in the changeover to the DiFX software correlator, on March 20, 2014 USNO

⁴ For more information see <http://ivscc.bkg.bund.de/program/cont14/>

officially announced that the WACO DiFX correlator would not be ready for correlation of CONT14. Bonn volunteered to help out, and the IVS requested Bonn to correlate CONT14. On March 21 the first planning meeting to prepare the correlation was held at the MPIfR in Bonn. Items to organise:

- storage space on RAIDSS in Bonn? How many TB will be needed?
- How to make best use of the available bandwidth for e-transfers?
- which stations will have to resort to shipment of modules for data transfer?
- the correlator schedule had to be defined: CONT14 vs. other production correlation, and astronomy.
- Mark 5 units had to be upgraded to SDK 9.3a, as more than 1024 scans had to be recorded on the bigger modules.
- allocate scans and time for near real-time fringe tests at the beginning of CONT14.
- define the correlator setup.
- specify the requirements for post-processing.

It was determined that nine eVLBI stations require a total disk space of $\lesssim 260$ TB, while the total geodetic storage space at the correlator is only ~ 138 TB. Additional storage was organised from the astronomical users of the cluster, the MPIfR computing centre, and even the BKG in Frankfurt. The latter two only as a fallback strategy as the connection to the cluster is limited to 1 Gbps. The final total amount of disk space was ~ 590 TB. Two weeks before the start of the CONT14 all other e-transfers to Bonn were suspended. A great deal of effort went into defining and optimising the schedule for e-transfers as many different boundary conditions had to be taken into account.

All previous CONT observations had been correlated with the MarkIV Korrelator. Due to its limitations correlation had to be done in several passes. CONT14 was the first of the CONT series to be correlated with the DiFX software correlator which does not have a limitation on the number of simultaneously correlated antennas. Therefore CONT14 was the first to be correlated in one pass. The correlation parameters were quite standard with 32 spectral channels, and integration time of 1 s. The clocks and clock drifts were obtained by linearly fitting the clock values in station logs over several days taking clock jumps into account.

The first trial correlation started on May 9. A problem was encountered when reading data from modules

with large directories (> 1024 scans). On May 15, 2014 W. Brisken flew to Bonn and fixed the problem in one day. Another significant obstacle was that Mark 5 units would often hang. It was found that this was mostly due to not up-to-date firmware of the recording Mark 5 units at the stations. As a consequence the correlation could not run unattended as is usually done at Bonn. The geodetic team covered night shifts and shifts on weekends. Technical support was given by MPIfR staff.

All routine activities at Bonn correlator were suspended for about two months for processing CONT14 as quickly as possible. About 200 TB of data were e-transferred to Bonn, so that not all the allocated disk space had to be used. For correlating “1 day” of the CONT14 approximately 24 hours were needed in case that no problems occurred, which was rare. On average about 48 hours were needed, and sometimes even more.

A first version of the databases was delivered within roughly two months. Routine correlation was resumed on July 7, 2014. The post-processing operations were completed in mid July 2014. At the end the modules were shipped back, space on the RAID's on loan was released, the correlated data was archived. From September 2014 to January 2015 we re-fringe fitted the data using multi-tone phase-cal extraction. All in all the first correlation of a CONT session with DiFX was a big success for the team in Bonn.

5 VGOS readiness

As is mentioned in section 2 the HPC cluster which runs the correlator software has to be replaced because of its age. The next cluster should be matched to the requirements of VGOS and 1 mm-VLBI, both of which require much higher CPU and I/O power as well as Mark 6 playbacks.

In 2014 we wrote a proposal to the MPG for renewal of the cluster and were awarded a grant of 400 k€ plus VAT. In addition the BKG has allocated 190 k€ plus VAT to be spent in 2015. The call for tender should be issued in summer 2015 with an installation date in about November 2015. We expect a cluster to be delivered with 1000 to 1500 compute cores, two RAID's with nearly 300 TB, two head nodes, and 56 Gbps (FDR) Infiniband interconnect. Some

parts of the old cluster should be retained like for instance the 15 Mark 5s, the racks, most of the existing storage (~ 500 TB), and the cooling.



Fig. 2 Photo of the new chamber for the Mark5 and Mark6 units. The first Mark 6s are in the two racks on the left.

As additional racks are needed for the Mark 6 playbacks the correlator room has been rebuilt. The racks with the Mark 5s and the Mark 6s are now in a separate cooled chamber (see Fig. 2) similar to the cluster which reduces the energy needed for cooling and the noise level for the operators.

It is expected that this cluster will be powerful enough for the requirements of VGOS for the next five years, in particular as the present estimates of the readiness of VGOS antennas seem to be a bit optimistic.

The present Internet connection to the MPIfR is a 1 Gbps dedicated line to the GÉANT node in Frankfurt. A 10 year contract with the German NREN DFN, which was signed in 2007 when eVLBI was very much in vogue in Europe, allows us to use this connection at a very reasonable annual fee. Unfortunately the present “normal” prices for Internet connections are still much higher and unaffordable for our budget. Here is an excerpt of the DFN price list w/o VAT which can be found on the Internet:

Speed	Cost per year
1 Gbps	41.5 k€
2 Gbps	83.0 k€
4 Gbps	134.9 k€
10 Gbps	249.1 k€

So in that aspect the Bonn correlator is not VGOS-ready, and we will have to transfer data mostly by shipping Mark 6 modules. But prices for Internet connec-

tivity have halved roughly every two years, so that we might be able to accommodate the needs for VGOS with respect to e-transfer in the course of the next few years.

References

- Whitney A R, Cappallo R, Aldrich W, Anderson B, Bos A, Casse J, Goodman J, Parsley S, Pogrebenko S, Schilizzi R, Smythe D (2004) Mark 4 VLBI correlator: Architecture and algorithms. *Radio Sci*, 39, 1007
- Deller A T, Brisken W F, Phillips C S, Morgan J, Alef W, Cappallo R, Middelberg E, Romney J D, Rottmann H, Tingay S J, Wayth R (2011) DiFX-2: A More Flexible, Efficient, Robust, and Powerful Software Correlator. *Publ Astron Soc Pac*, 123, 275–287.
- Kardashev N S, Kovalev Y Y, Kellermann K I (2012) *The Radio Science Bulletin*, 343, 22–29.
- Bruni G, Anderson J, Alef W, Lobanov A, Zensus A J (2014) Space-VLBI with RadioAstron: new correlator capabilities at MPIfR. In: *Proc. 12th European VLBI Network Symposium and Users Meeting*, Cagliari, Italy, 2014, ID: 119

IAA VGOS GPU-based Software Correlator: current status and broadband processing

V. Ken, I. Surkis, Y. Kurdubova, A. Melnikov, N. Mishina, V. Mishin, V. Shantyr

Abstract The VGOS FX-type software correlator was designed in the IAA RAS. The correlator is able to process VDIF data from up to 6 stations simultaneously at a maximum rate of 16 Gb/s from each station in a near-real time mode. The correlator hardware is based on a hybrid blade server cluster. At present, the correlator cluster and the cooling system are assembled in the IAA. In order to test the six-station correlator in a maximal mode, an experiment was carried out with the following setup: 4 frequency channels each of 512 MHz bandwidth at 2 polarizations, 2-bit sampling. The first results of comparison of the DiFX correlator and the IAA VGOS correlator were obtained. The correlator control system and graphical user interface are close to be completed.

Keywords VLBI, VGOS, correlator, HPC, GPU

1 IAA correlator specifications

The VGOS FX-type software correlator design was started in 2012 and the 2-station prototype was constructed in 2013 in IAA RAS. The 6-station correlator was developed and assembled by the end of 2014. The correlator is able to process VDIF data from up to 6 stations simultaneously at a maximum rate of 16 Gb/s from each station in a near-real time mode. Table 1 presents the main correlator's specifications.

The main design feature is the use of graphical processing units (GPU) for the main computations such

Voytsekh Ken, Igor Surkis, Yana Kurdubova, Alexey Melnikov, Nadezda Mishina, Vladimir Mishin, Violet Shantyr
Institute of Applied Astronomy of RAS

as fringe stopping, bits repacking, Fourier transformation, spectra multiplication, and phase calibration signal extraction. All interblocks streams are transferred in a bit mode, and type conversion into float type is produced only in the GPU memory. It allows sufficiently decrease the data rate between correlator modules (Ken et al., 2014).

The correlator hardware is based on a hybrid blade server cluster. The present hardware contains 32 hybrid blade servers, which are inserted into 7 chassis, and 8 19-inch cache servers. Each blade server contains 2 Intel CPU, and 2 Nvidia Tesla K20 GPUs, and 64 GB RAM. These servers are used for FX data processing algorithms (fringe stopping, FFT and spectra multiplication) computing. The 19-inch server also contains 2 CPUs and 2 GPUs, 2x10 Gb fiber optic input, but RAM is increased up to 256 GB. Each of them provides data receiving operation, pcal extraction, delay tracking and bit repacking. The 256 GB memory allows to cache VGOS data due to any delays during data transmission. Data storage is based on PANASAS system with the 80 TB capacity. The interblocks data communication is provided by infiniband network. The cluster components are mounted in 4 racks. The air condition system is mounted in 3 racks. The correlator's front view is shown in Fig. 1.

2 Benchmark test

In order to test six-station correlator in near-realtime mode we used session which was carried out with the following setup: 1 frequency channel of 512 MHz bandwidth with 2-bit sampling and 1 polarization with 2 Gbps data rate. Then these one band scans were du-

Table 1 Correlator specifications

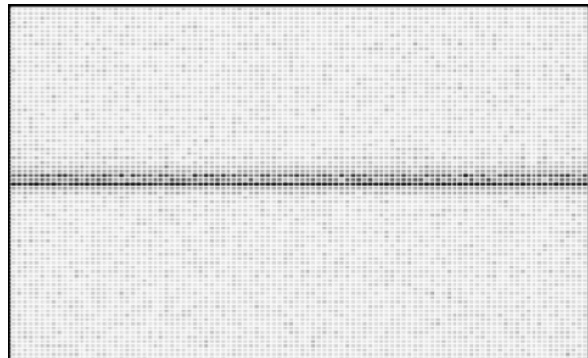
Input data format	VDIF
Sampling	1/2 bit
VGOS station	up to 6
Spectra channels	up to 4096
Input data stream	up to 16 Gb/s
Frequency bands	4
Polarization	1/2
Pcal tones	up to 32
Delay (RMS)	< 10 ps

**Fig. 1** High-performance computing cluster

plicated to get 8-channel scans to simulate 6-station 4 frequency bands 2 polarizations mode, so input data stream rate from one station was 16 Gbps. These scans were copied into RAM directly to simulate e-VLBI mode, so the data storage access lag was excluded. On December, 4 this benchmark test was done, 78 cross-spectra with 4096 spectra channels resolution were obtained. Figure 2 shows the top view of fringe delay vs time distribution (accumulation period is 1/16 s). The 30 s scan was processed for the 32 s, including initialization operations. During this test 6 cache and 28 blade servers were involved.

3 Comparison DiFX and IAA correlator

We used the previous broadband session to compare the output processed data of IAA correlator and DiFX. Also we used the same ephemeris data, so the differences of the output spectra and fringes may be caused

**Fig. 2** Fringe delay vs time

only by difference of the correlators. The output files analysis was implemented with MATLAB. We found that the IAA correlator fringe amplitude is less about 5 %. Also we found that the IAA fringe phase inclination had the rate about 0.7 ps/s, and this bug was fixed immediately. After fixing the fringes corresponded well.

At present both correlators are involved in the data processing of Ru-TEST session for UT determination on Zelenchukskaya-Badary baseline. More than 20 of these 1 hour S/X broadband sessions were carried out.

4 Correlator Control System

The Correlator Control System (CCS) is one of software parts of the IAA correlator. The CCS main purposes are:

- provide complete status and errors information for the whole system to the operator;
- provide all in one GUI and console tools for data processing and transfer control.

The CCS consists of 5 main modules: control, log parser, ephemeris software, schedule software, and GUI. These modules generates the task file, ephemeris data, parses station log files, and distributes all commands and data between correlator' modules and to the operator. The CCS is shown in the Fig. 3.

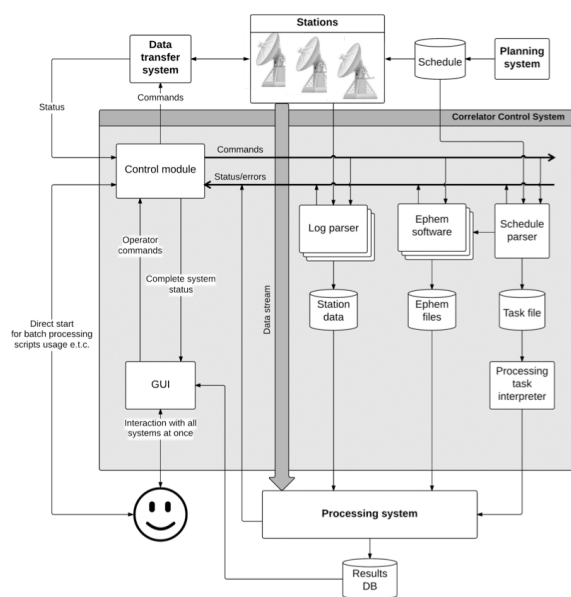


Fig. 3 Correlator Control System diagram

5 Russian VGOS network inauguration

On 16 April 2015 the first broadband session Ru-TEST119 was carried out with the new VGOS telescopes RT-13 (Ipatov et al., 2015) on Zelenchukskaya-Badary baseline in S and X bands in 2 polarization. As a result fringes were detected and polarization was found. Fig. 4 and Fig. 5 show the fringes in S and X band, respectively.

On 19 May the inauguration of the geodetic VLBI station in Zelenchukskaya was held during the EVGA-2015 meeting. Also the joint radio observations with a 13-m VGOS radio telescopes in Badary, Wettzell and Yebees observatories were carried out. The session were e-transferred to Bonn and to Saint Petersburg. The fringe on the Zelenchukskaya-Badary baseline was obtained 1.5 hour after observation.

6 Conclusions

At present the hardware of 6-station VGOS correlator is assembled and mounted in the IAA RAS. The main software modules are developed and the benchmark test was successfully passed. The graphical user interface is close to be done. The IAA VGOS corre-

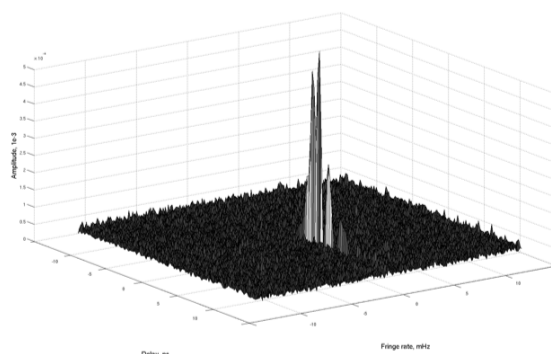


Fig. 4 Fringe in the S band, source 0212+735

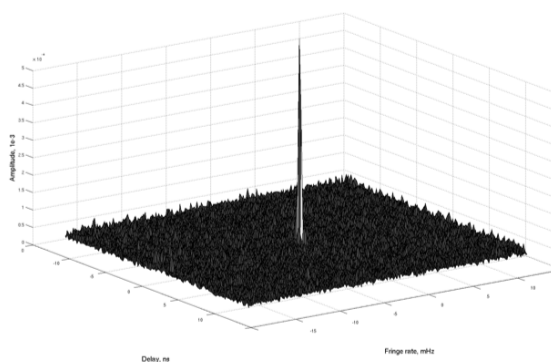


Fig. 5 Fringe in the X band, source 0212+735

lator is mainly used in the domestic intensive routine processing.

References

- Ken V, Mishin V, Pavlov D, Sokolova N, Surkis I (2014) Design of a VGOS Software Correlator Based on GPUs. In: D. Behrend, K. D. Baver, K. L. Armstrong (eds.), *IVS 2014 General Meeting Proc.*, Science Press (Beijing), 183–187.
- Ipatov A, Ivanov D, Ilin G, Olifirov V, Mardyshev V, Surkis I, Fedotov L, Gayazov I, Stempkovsky V, Bondarenko Yu (2015) Russian Radio Interferometer of New Generation. In: R. Haas, F. Colomer (eds.), *Proc. 22nd EVGA Working Meeting*, 75–79.

Wideband Cryogenic Feed Receivers for VLBI

R. Rayet, S. Rawson, T. Bonhoure, M. Sevrin, A. Martellosio, M. Pasian

Abstract Callisto has over 20 years experience producing cryogenic Low Noise Amplifiers for satellite ground stations. Callisto has produced more than 50 cryogenic receivers for worldwide renowned customers such as the European Space Agency (ESA), the Indian Space Agency (ISRO), the French Space Agency (CNES), the BKG (Wetzell Observatory) and several other institutional or private operators. Callisto has designed a wideband cryogenic receiver optimized for VLBI applications and using the Caltech designed QRFH feed (Quad-Ridged Flared Horn). This receiver has been specified to meet the VGOS (VLBI 2010) specifications and has a maximum target noise temperature below 40 K over the full continuous band 2.3–14 GHz. A prototype has been built and is currently being evaluated. Callisto will commercialize the receiver in two models:

- the "Compact" QRFH cryogenic receiver features zero maintenance and a very low cost of ownership for a cryogenic receiver;
- the "Ultra" QRFH cryogenic receiver features ultimate noise temperature performance (< 20 K) with low maintenance constraints thanks to a patented sleeve system used for the cryocooler maintenance.

The paper will present more in details the technologies and the performance of each receiver version. Laboratory test results of the prototype "Compact" receiver will be presented.

Rémi Rayet, Steve Rawson, Thomas Bonhoure, Maxime Sevrin
Callisto, 12 Avenue de Borde blanche, 31290 Villefranche-de-Lauragais, France.

Andrea Martellosio, Marco Pasian

Dipartimento di Ingegneria Industriale e dell'Informazione, Università degli Studi di Pavia, Via Ferrata, 5, 27100 Pavia, Italy.

Keywords VGOS, Wideband feeds

1 QRFH feed

The Quad-Ridged Flared Horn (QRFH) is a Caltech designed wideband RF feed family (Akgiray, 2013; Akgiray et al., 2013). It is a compact design made from aluminum (the feed used by Callisto has diameter below 210 mm and height < 160 mm), it is robust to cryogenic cooling and requires only two LNAs (Low Noise Amplifier) for linear polarization outputs. The standard QRFH feed delivered by Callisto fits on Patriot or Intertronic Solutions 12 m antenna optics. However, it is possible to adapt the feed design to other antennas such as the MT Mechatronics or the Vertex ring focus antennas, for instance. Akgiray (2013) and Akgiray et al. (2013) describe in detail the possible configurations of QRFH feed depending on gain, aperture angle and several other parameters. Figure 1 illustrates the QRFH

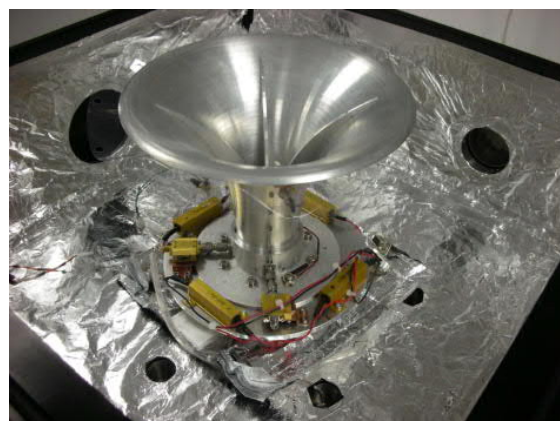


Fig. 1 QRFH feed inside Callisto cryogenic test Dewar.

feed used by Callisto and Fig. 2 is an example of its normalized radiation pattern (Co-Pol).

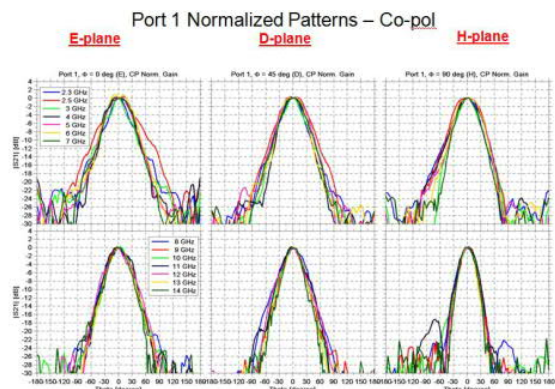


Fig. 2 QRFH feed model 45-6-2-2P3 normalized radiation pattern (Co-Pol).

2 Cryogenic receivers

2.1 Feed Integration

Callisto has developed a unique, patented thermal insulation system Callisto (2011, 2012) for cryogenic RF receivers based on a solid thermal insulation rather than vacuum insulation. The main benefit is that there is no need for high vacuum pumping before starting the cooldown of the receiver.

- The "Compact" cryogenic receiver is sealed at the factory and never requires a vacuum pump for operations (even after a warmup of the system).
- The "Ultra" cryogenic receiver requires only a rough vacuum (~ 1 mbar) after each cold head replacement for service, such vacuum level being processed with a simple scroll vacuum pump operating for few minutes (no need for turbomolecular high vacuum pump).

The thermal insulation system prevents liquid water condensation inside the sealed enclosure which will be harmful for the electronic components cooled inside.

For both receivers the QRFH feed and the two LNAs are assembled on a thermal isolative support structure ensuring the precise positioning of the QRFH feed centre focal point with respect to the mechanical interface to the antenna structure (see Fig. 6). They are also thermally anchored to the cold tip of a cryogenic cooler. These thermal links are carefully designed in

order to ensure proper cooling of the feed and of the LNAs to minimize the Noise Temperature (NT) of the system while minimizing the heat load on the cryogenic cooler.

The RF input of the receiver is a critical element of the design. On one hand it must be transparent and very low loss to the Radio-Frequencies between 2 and 14 GHz in order to minimize the degradation of the NT and to avoid modifying the QRFH beam pattern which could lead to a degradation of the antenna efficiency. On the other hand it must support a large mechanical load applied by the atmospheric pressure when the enclosure is under vacuum (estimated around 700 kg!). In addition:

- It must also be hermetic in order to ensure the gas isolation between the outer atmosphere and the internal vacuum while limiting as far as possible moisture condensation and permeation.
- It also has to thermally isolate the internal cooled components from the infrared (IR) heat loads coming from the warmer surrounding parts and possible direct solar radiation.
- It has to be resistant to weather effects (rain, wind, dusts, hail...), UltraViolet (UV) radiation, and even birds attack.

For this particular protection purpose (weather/UV...) Callisto has included a special radome material on top of the receiver which is transparent over the wideband 2–14 GHz.

The solution found is a two layer window with polymeric vacuum window, foam backing, external radome and dry gas between the two.

The final concern on feed integration is to reduce as far as possible the shadowing of the receiver on the antenna optics. This is achieved with a very compact design of the enclosure, with a compromise found on the design requirements from the thermal, mechanical and RF sections. Computer-aided simulations have also been used to optimise the thermal and RF (three dimensional electromagnetics, 3DEM) designs of the receiver enclosure.

2.2 RF simulations for optimization of the receiver input interface and noise injection antenna

RF simulations have been fundamental to design the input interface (i.e. the part of the enclosure above the

feed aperture). In particular, the internal dimensions (height and width) of the input interface and the dimension (height) and material of the radome have been engineered to provide a minimal impact on the QRFH radiation patterns, while achieving the best compromise in terms of thermal performance and mechanical robustness. To this aim, the system composed by the QRFH and the enclosure has been modelled using a

full-wave solver (HFSS), calculating the radiation patterns as modified by the presence of the enclosure.

These radiation patterns have been used as input for a GRASP model of the entire 12 m antenna (see Fig. 3) to evaluate the performance impact at antenna level. The results are shown in Table 1. It is observed that the degradation due to the enclosure can be considered acceptable along the entire frequency range. However, additional analysis is planned to optimise the design further.

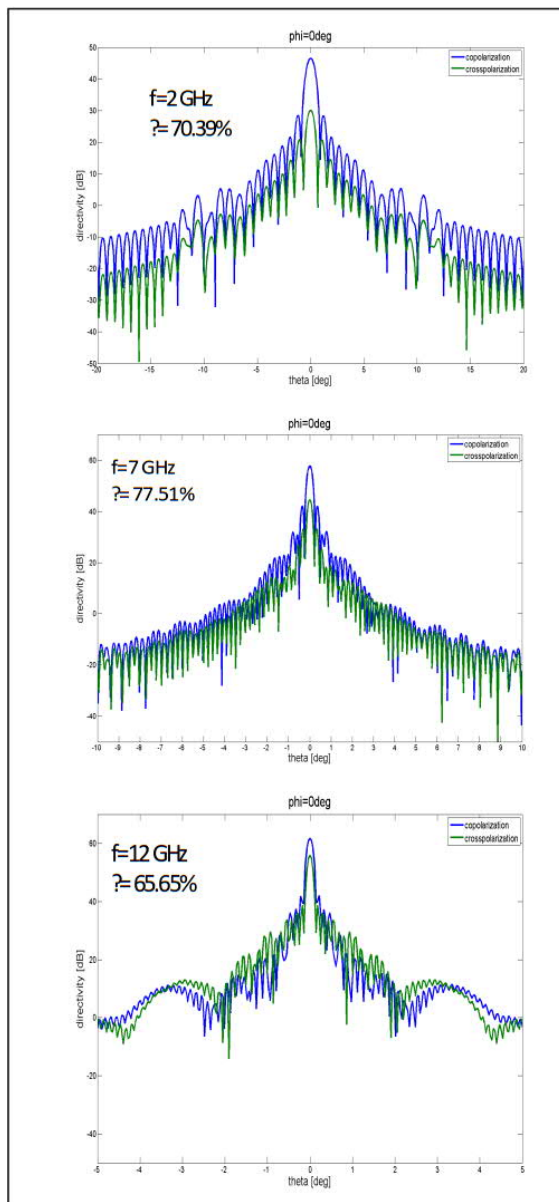


Fig. 3 Co-polar and Cross-polar radiations patterns of 12 m VLBI antenna with QRFH inside enclosure.

Table 1 Antenna performance degradation due to the input interface for different parameters, n.d. standing for no degradation.

Antenna parameter	Enclosure degradation		
	2 GHz	7 GHz	12 GHz
efficiency	n.d.	< 9 %	< 6 %
cross-polar discrimination	2.5 dB	1.4 dB	0.4 dB
first sidelobe	n.d.	n.d.	1 dB

RF simulations have been also used to optimise the coupling between the noise injection antenna probe and the QRFH. In this case, a wide-band patch antenna has been included into the HFSS model of the system composed by the QRFH and the enclosure. The position of the noise injection antenna probe has been optimised to achieve a minimum coupling of -35 dB from 2.5 GHz to 14 GHz and from 3.2 GHz to 14 GHz for the two QRFH input ports.

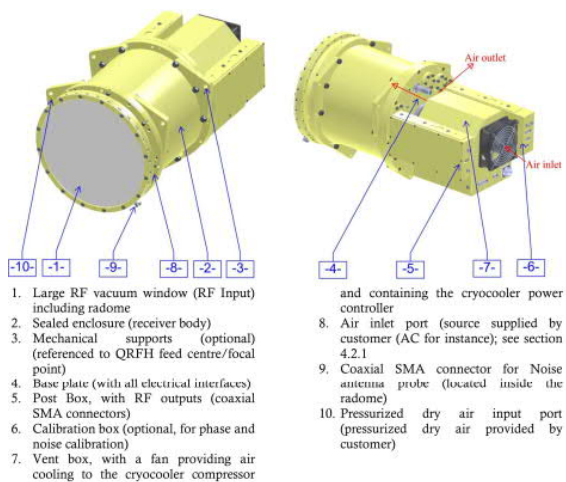


Fig. 4 Compact QRFH cryogenic receiver overview.

2.3 Compact QRFH cryogenic receiver description

This is a state-of-the-art piece of equipment for telescopes all over the world but with particular interest for those operated in remote locations where energy costs are high and maintenance logistics is particularly complex and expensive. The key features of the Compact QRFH cryogenic receiver are:

- NT < 40 K (From prototype results, at Dewar window, excluding external noise contributions (T_{sky} , T_g , T_{ant}).
- Very compact: L. 612 mm x \varnothing 311 mm < 25 kg (all included! receiver, cold head, compressor, heat exchanger)
- Very low power consumption (< 350 W, 20 times less than a conventional cryogenic receiver)
- No maintenance (for at least 5 years of continuous operation).

The patented thermal insulation system Callisto (2011, 2012) used by Callisto allows for continuous cryogenic operations without any routine maintenance required, even in the event of a power break that will warm-up the system. In such situation the Compact QRFH cryogenic receiver restarts automatically after the power is back to recover the cryogenic base temperature without the need for processing high vacuum in the enclosure as usually required on standard cryogenic receivers. So there is no need for vacuum pump connected to the receiver, at any time. The thermal insulation system is setup at factory and the enclosure is sealed, ready for operations.

The Compact QRFH cryogenic receiver includes a QRFH feed which can be model 45-6-2-2P3 (for classic Cassegrain antenna) or model 60-6-2P3 (optimized for ring focus antenna). The same enclosure is used for both models however the input window is adapted to each feed. So the overall dimensions of the receiver are the same for both configurations (see Fig. 5). Figure 5 also shows the feed phase centre position for the feed model 45. The feed phase centre is co-aligned with the central geometric axis of the Dewar with an accuracy of ± 1 mm in X and Y and $\pm 1^\circ$ of tilt.

The Compact QRFH cryogenic receiver uses a Stirling, single stage cryocooler. This type of cryogenic cooler is much more energy efficient than a classical Gifford-McMahon (GM) cooler however it cannot go as low in temperature. For this reason the Compact ver-

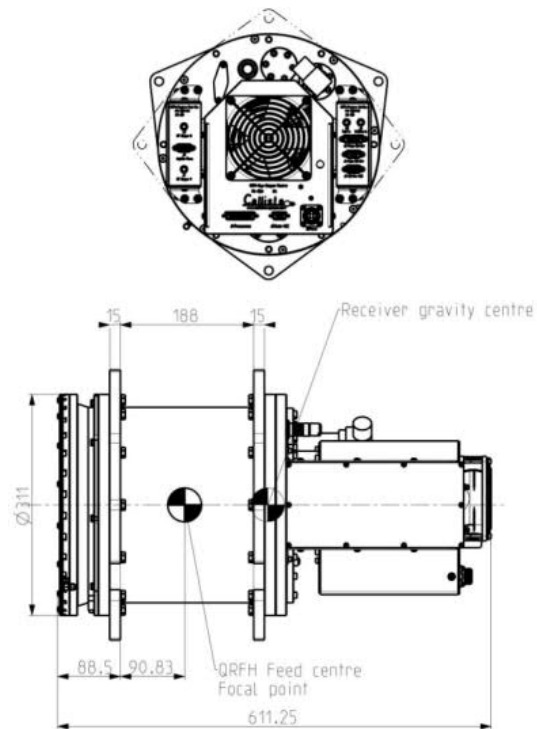


Fig. 5 Compact QRFH cryogenic receiver dimensions.

sion is limited to a base temperature between 80 K and 100 K but the entire system consumes a maximum of 350 W only, compared to several kilowatts for the GM version.

Moreover, this type of cryocooler does not require regular maintenance, compared to a standard GM cooler which has to be warmed-up for servicing roughly every year, which incurs cost and results in operational downtime. The typical Mean Time To Failure (MTTF) of the Stirling cooler used by Callisto for the Compact receiver is 200,000 hours.

Figure 6 shows a typical cooldown of the prototype Compact receiver. Both cold tip (cryocooler) and LNAs temperatures are shown; the most critical for the NT being the LNAs temperature. Cooldown time to reach NT specification is around 3 hours and takes around 5 hours to the base temperature; the temperature is then stable within ± 1 K over a period of 24 hours.

The Compact receiver has been designed to meet the VGOS receiver NT specification Corey (2012) of 40 K at a base temperature of 90 K.

Noise Temperature measurements have been done on the two polarization ports of the prototype receiver

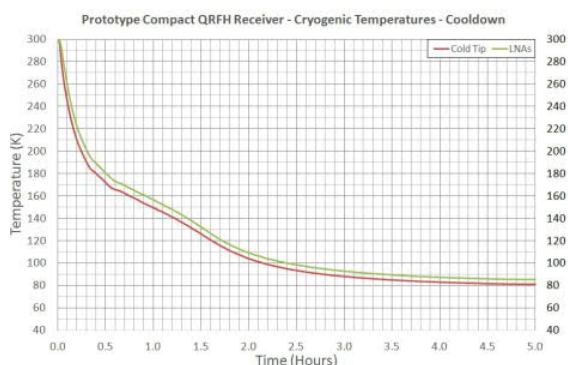


Fig. 6 Compact QRFH receiver - Cooldown.

(including large vacuum window, QRFH feed and LNAs). The NT measurement is done outside using the hot/cold method and the sky as a cold reference. Figure 7 presents these results. The X port is better than the specification for most of the band, and as expected there is a small degradation as the frequency increases above 11 GHz. The second port (named Y) is a bit worse but still well around the specification, with the same tendency as port X with the increasing frequency.

So the prototype performs well as expected and further tests will be conducted in operational conditions on a VLBI telescope. The University of Tasmania (UTAS, Dr. J. Lovell) has a 12 m Patriot telescope near Hobart and will test the integration, operation and performance of the prototype Compact receiver during August 2015.

From the work on the prototype unit, optimizations have been identified on the thermal design in order to further reduce the NT and improve the temperature

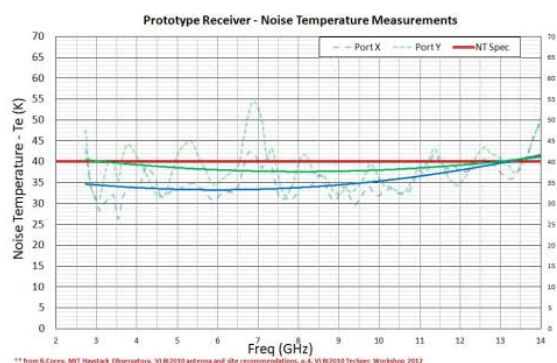


Fig. 7 Prototype Compact QRFH cryogenic receiver Noise Temperature measurements.

level and stability. The modifications will be implemented on the prototype after the testing on the UTAS antenna.

3 Conclusion

Callisto has developed a cryogenic receiver including the Caltech designed QRFH feed. A temperature stabilise phase and noise calibration unit has also been designed which is compatible with the receiver. The receiver can be fitted with either Stirling or GM cryocoolers, which are called, respectively, the "Compact" and the "Ultra" QRFH cryogenic receiver version. Key features of the two versions are as follows:

- The "Compact" achieves a NT of < 40 K over the 2–14 GHz band and is "zero-maintenance" (no service for at least 5 years), with low power consumption and a lightweight and compact size design. It is thus perfectly adapted for telescope and stations in remote locations where cost of electricity and maintenance is high.
- The "Ultra" achieves a NT < 20 K over the 2–14 GHz band but requires annual service and several kilowatts of operating power due to the GM cooling system. This receiver can be fitted with a "sleeve" system which allows for removing a GM cold head from the receiver without dismantling the receiver from the antenna. It is thus not required to realign the receiver to the focus of the antenna after the cold head service among other advantages.

References

- Akgiray A H (2013) Quad-Ridged Flared Horn and Compound-Semiconductor LNAs. PhD Thesis, Caltech
- Akgiray A H, Weinreb S, Imbriale W A, Beaudoin C (2013) Circular Quadruple-Ridged Flared Horn Achieving Near-Contant Beamwidth Over Multioctave Bandwidth: Design and Measurements. *IEEE Trans Antennas Propag*, 61(3), 1099–1108.
- Callisto (2011) Patent no WO 2011/003929 A1 "Dual Performance Low Noise Amplifier for Satellite-Based Radio Frequency communications".
- Callisto (2012) Patent no WO 2012/038400 A1 "Cryogenic Low Noise Amplifier".
- Corey B (2012) In: Presentations of the VLBI2010 TecSpec Workshop 2012, *VLBI2010 Antenna and Site Recommendations*, p.4, http://www.fs.wettzell.de/veranstaltungen/vlbi/tecspec2012/Session5/01_antenna_recommendations.pdf.

Ultra Wide-Band HTS filter for new geodetic VLBI front-ends

A. Caddemi, E. Cardillo, G. Tuccari

Abstract In this paper, an original and flexible CAD methodology is presented for the design of an UWB HTS filter equipped, if needed, with a notch at a desired frequency. The structure is designed in planar microstrip technology and it is capable of covering up to 150 % of fractional bandwidth. This design methodology is applied to an high-temperature superconductors substrate for reducing losses at a minimum level either showing good performance. In order to cut the strong radio interferences occurring in the low frequency band, as reported in the specifications, ad-hoc precautions have been performed. Furthermore the component has been designed with the aim of easily tailoring the notch frequency as a function of a single geometrical parameter. The procedures steps and relevant design results are shown.

Keywords UWB filter, notch, radioastronomy, HTS high temperature superconductor, microstrip filter.

1 Introduction

In recent years, the demand in high speed communication has led to the development and the design of very large bandwidth filters, extending from S-band even to low Ku-band, to support various demanding applications, particularly radioastronomy receivers for

Alina Caddemi, Emanuele Cardillo
DICIEAMA Engineering Dept., University of Messina, Messina, Italy
Gino Tuccari
Italian National Astrophysical Institute Radio Astronomy Institute, Italy

geodetic VLBI observations (Shaman and Hong, 2007; Mokhtari and Bornemann, 2012; Yang et al., 2008). Wide bandpass and rejection bandwidth, in-band low-losses, sharp rejection at cut-off frequency and maximally flat group delay are the most important features of a bandpass filter to be employed in advanced communication systems. Besides, strong unwanted interferences occurring within the basic ultra-wide band may need selective blocking sub-bands (notches) to be created ad hoc for a given application. This filter has been designed for the INAF - Institute of Radioastronomy (Noto - Italy) working actively in Very-long-baseline interferometry(VLBI) investigation because, within the typical operating frequency ranges, strong radio interferences occur in the low frequency band as reported in the specifications (2.095–2.185 GHz). This work presents a CAD methodology for the design of a microstrip UWB filter, with a FBW of 150 %, equipped (if needed) with a notch at a desired frequency. In addition, an abrupt rejection at lower cut-off frequency has been requested in order to eliminate the interferences occurring in the low frequency band, as reported in the specifications (2.095–2.185 GHz).

In order to satisfy the requisite of very low insertion loss, a superconductor material has been chosen for its very low resistance at moderate cryogenic temperatures. The dimensions obtained for the basic bandpass filter are 26.36 mm x 6.4 mm thus leading to a very compact structure. The effectiveness of the method and its good performance are outlined and a simple relationship between notch frequency and a single geometrical parameter is derived. In the scientific literature, it has been shown that structures depicted as UWB filters with multiple notches are very straightforward to achieve. Nevertheless, it is hard to find fil-

ters with a bandwidth greater than 100 % and, above all, to find a structure with a single notch, instead of multiple blocking sub-bands. It is indeed a critical issue the insertion of a single notch avoiding the appearance of multiple ones as typical of distributed structures with such a wide band (Zhao et al., 2013; Tu and Chang, 2006). Therefore, in a preliminary analysis step, classical structures as Stepped-Impedance, End-Coupled, Parallel Coupled Lines, Hairpin, Interdigital and Compline have shown to be unsuitable because they do not allow to achieve the desired results or because the required impedance values are often not physically realizable in a microstrip technology, i.e. leading to excessively small microstrip width or gap space. As a final choice to meet the constraint of such a wide bandwidth, the Stub Synthesis technique has been chosen for the filter design (Pozar, 1998). Afterward, the methodology has been adjusted to improve the performances and to insert a simple-to-shift notch. An electromagnetic (EM) analysis of the layout has then been performed for a more reliable and accurate prediction of the component behaviour. After the final optimization of the circuit, a lookup table is extracted to easily and quickly re-design part of the structure to obtain the desired notch frequency. The design has been carried out employing Microwave Office by NI AWR Design Environment. This paper is organized as follows. The technical specifications are described in Section II, the filter design methodology of the UWB filter and the integration of the notch are presented in Section III and IV respectively and the conclusive remarks are drawn in the Section V.

2 Technical specifications

The filter has been designed to fulfill the following specifications:

- Superconductor microstrip technology;
- Response bandwidth from 2.2 to 14 GHz;
- In-band Insertion Loss less than 0.6 dB;
- Out-of-band Insertion Loss higher than -14 dB;
- In-band maximally flat Group Delay;
- Out-of-band Insertion Loss higher than -15 dB, especially in the range 2.095–2.185 GHz;

In order to satisfy the requisite of very low insertion loss, a superconductor material has been chosen

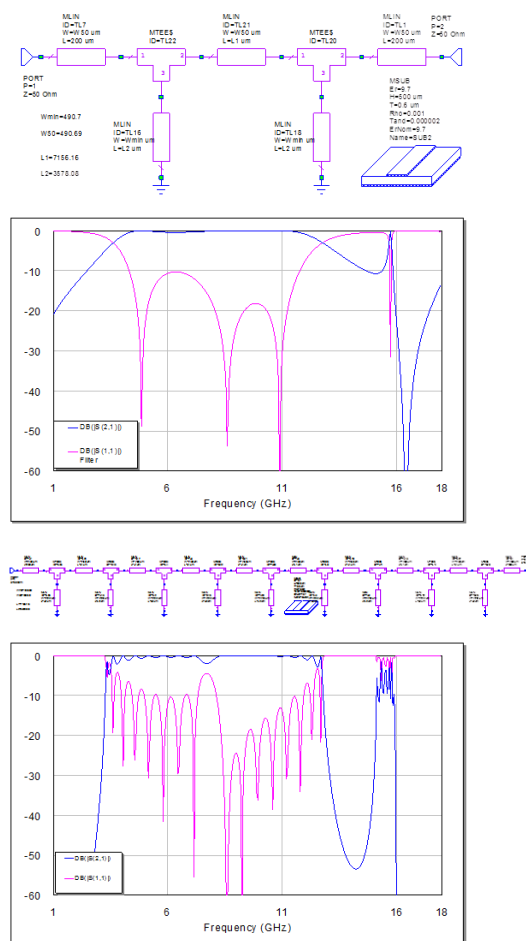


Fig. 1 Layout, S21 (blue) and S11 (fuchsia) of UWB filter before (a) - (b) and after (c) - (d) first enhancement.

for its very low resistance at moderate cryogenic temperatures. The selected substrate is a Magnesium Oxide (MgO) substrate, whereas the conductor film is Yttrium Barium Copper Oxide (YBCO).

3 Filter design methodology

The basic concept of this circuit is to create a path from the input to the output of the filter without modifying the signal at the centre frequency (Shaman and Hong, 2007; Pozar, 1998): for this reason the length of the path is chosen to be one wavelength at the centre frequency of 8.1 GHz. Moreover, the length of the path to ground is chosen to be one-quarter wavelength at the

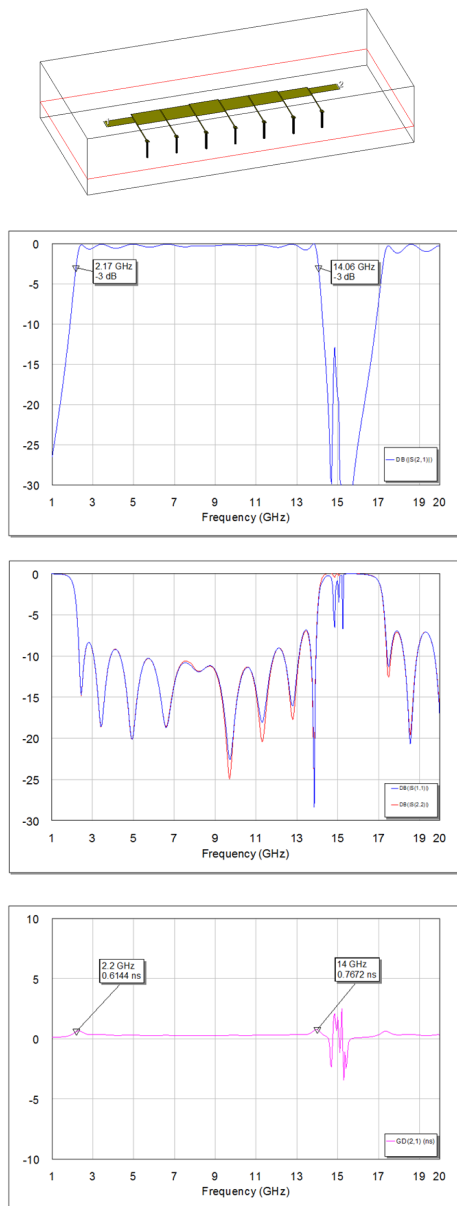


Fig. 2 Layout (a), S21 (b), Input (blue) and Output Return Loss (red) (c) and group delay (d) of final UWB filter. All graphs are EM simulations.

same frequency. The impedance values of the transmission lines are 50Ω . Modelling of the via holes has been accomplished by means of the resident cylindrical via model VIA.

Unfortunately the obtained scattering parameters showed that the band-pass needed to be widened and the transition at the edges to be more abrupt, therefore

the basic structure was repeated to obtain the requested performance.

Following the initial design, some adjustments were required to improve the filter performance. First of all, the width of the short-circuited stubs was set to a minimum value complying with reasonable fabrication constraints, to stretch out the bandwidth. Then, the lengths of either the main section and the short-circuited stub sections were adjusted to shift the bandwidth. The dimensions of the main transmission line section, from input to output, were slightly modified in order to reach the best performances, by means of Microwave Office Optimizer tool.

An electromagnetic (EM) analysis of the layout was then performed and a tuning of the line dimensions was made with the aim of obtaining a more reliable and accurate prediction of the real component behaviour, indeed, the EM simulation exhibited a frequency shift of the filter -3 dB cut-off frequencies which needed to be corrected. In Fig. 2 the final filter 3D layout, the group delay and the scattering parameters are shown.

4 Notch integration

The in-band notch frequency insertion needs to fulfill two main features:

- shifting the notch frequency without modifying the edge of the filter bandwidth;
- obtaining a simple relationship between the frequency and the lines dimensions

To accomplish these requirements an open-circuit stub has been introduced. Some simulations have been made in order to keep the notch bandwidth narrower.

As it can be observed, the notch centre frequency can be easily shifted only by varying the stub length,

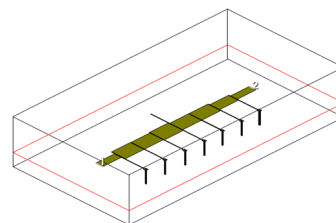


Fig. 3 Final filter layout.

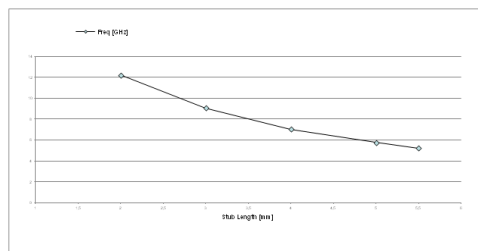


Fig. 4 Open-stub length vs frequency.

which is an interesting feature in order to obtain a simple correspondence between notch frequency and line

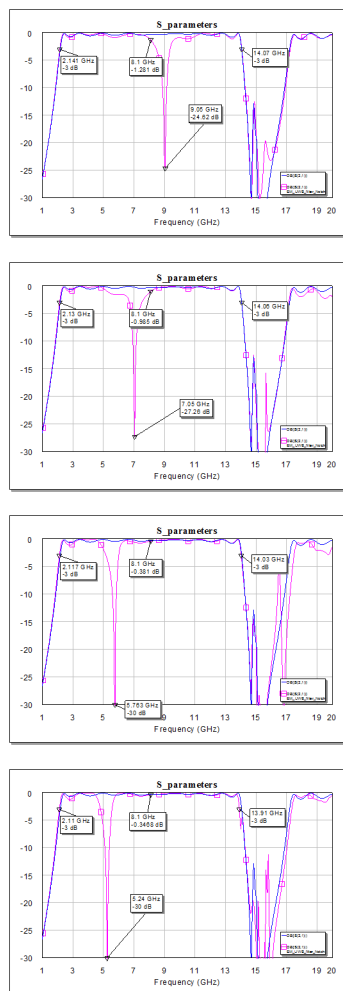


Fig. 5 S21 (blue) and S11 (fuchsia) for a stub length of 3.00 mm (a), 4.00 mm (b), 5.00 mm (c), 5.50 mm (d).

dimensions. In Fig. 4 the open-stub length versus frequency correspondence is reported.

In Fig. 5 the shifting notches are shown, clearly exhibiting a fixed notch narrow band and stable band-pass cut-off frequencies.

5 Conclusions

In this paper, an original and flexible CAD methodology, is presented for the design of an UWB HTS filter equipped, if needed, with a notch at a desired frequency. The structure is designed in planar microstrip technology and it is capable of covering a fractional bandwidth up to 150 %, showing good performances. Furthermore the components have been designed with the aim of easily tailoring the notch frequency as a function of a single geometrical parameter.

References

- Shaman H, Hong J S (2007) Ultra-Wideband (UWB) Bandpass Filter With Embedded Band Notch Structures. *IEEE Microw Compon Lett*, 17, 193–195.
- Marjan Mokhtaari J B, Bornemann J (2012) Microstrip Ultra-Wideband Filter with Flexible Notch Characteristics. *Wireless Engineering and Technology*, 3, 12–17.
- Yang G-M, Jin R, Vittoria C, Harris V G, Sun N X (2008) Small ultra-wideband (UWB) bandpass filter with notched band. *IEEE Microw Compon Lett*, 18, 176–178.
- Zhao J, Wang J, Li J-L (2013) Compact Microstrip UWB Bandpass filter with triple-notched bands. *Progress In Electromagnetics Research C*, 44, 13–26.
- Tu W-H, Chang K (2006) Compact Second Harmonic-Suppressed Bandstop and Bandpass Filters Using Open Stubs. *IEEE Trans Microw Theory Techn* 54(6).
- Pozar D M (1998) *Microwave Engineering*, John Wiley & Sons, Inc.

The German Antarctic Receiving Station O'Higgins - upgrades of the VLBI-capabilities for future challenges

Ch. Plötz, A. Neidhardt, T. Klügel, R. Wojdziak, J. Serna-Puente, B. Vaquero-Jiménez, T. Schüller, VLBI Team Wettzell, DFD Team DLR

Abstract The German Antarctic Receiving Station (GARS) O'Higgins started in the early 1990th with regular VLBI operations. Because of its remote position on the Antarctic Peninsula, the VLBI observations are mostly restricted to the Antarctic summer months. New equipment, a continuous operation by the German Aerospace Center (DLR), and new realizations of observation schedules may open the door for regular observations over the whole year. The paper shows the upgrades carried out in hard- and software and discusses ideas to realize more regular observations in a planned test phase.



Fig. 1 9 m radiotelescope O'Higgins.

Keywords Antarctica, O'Higgins, GARS

1 Introduction: GARS O'Higgins at a glance

The German Antarctic Receiving Station (GARS) is jointly operated by the German Aerospace Center

Ch. Plötz, T. Klügel, T. Schüller
Federal Agency for Cartography and Geodesy, Geodetic Observatory Wettzell, Sackenrieder Str. 25, D-93444 Bad Kötzing, Germany

R. Wojdziak
Federal Agency for Cartography and Geodesy, Karl-Rothe-Strae 10, 04105 Leipzig, Germany

A. Neidhardt
Technische Universität München, Forschungseinrichtung Satellitengeodäsie, Geodetic Observatory Wettzell, Sackenrieder Str. 25, D-93444 Bad Kötzing, Germany

J. Serna Puente, B. Vaquero Jiménez
Instituto Geográfico Nacional, Observatorio Astronómico de Yebes, Cerro de la Palera, 19080 Yebes, Guadalajara, Spain

(DLR) and the Federal Agency for Cartography and Geodesy (BKG, Geodetic Observatory Wettzell). The Institute for Antarctic Research Chile (INACH) coordinates the activities and logistics. The 9 m radio telescope at O'Higgins is mainly used for downloading of remote sensing data from radar satellites and for the commanding and monitoring of spacecraft telemetry. During dedicated campaigns it is also used for geodetic VLBI in the Antarctic summer.

Over the last few years, special flights using "C-130 Hercules"-aircrafts and small "DHC-6 Twin Otter"-aircrafts as well as transportation by ship were organized by INACH in order to transport staff, technical material and food for the entire stay from Punta Arenas via Base Frei on King George Island to O'Higgins. The conditions for transport and landing are strongly weather dependent and involve an increasing, challenging task.

The site is also equipped with other geodetic instruments:

- different time receivers in combination with a H-maser and Cs-standard
- several GNSS receivers
- a meteorological station
- a radar tide gauge and an underwater sea level gauge

2 Upgrades in the years 2013 to 2015

2.1 New receiver frontend



Fig. 2 New S-/X-Band VLBI Receiver at O'Higgins.

The VLBI receiver was renewed because of failures of the cryogenic system. This new receiver for both receiving frequency ranges in S- and X-band for standard dual band and right hand circular polarization was designed and built in the labs of the Observatory Yebes, Spain. New high performance cryogenic low noise amplifiers are used for first stage amplification of the incoming noise signal from the quasars. This improves the SEFD of the entire receiving chain. The down-converters were also renewed to simplify the maintenance.

The monitoring of the VLBI receiver is Ethernet-based. This gives more flexibility for remote control and supervision from Wettzell.

2.2 New data acquisition backend

To complete the receiving chain with new, stable equipment a new data acquisition rack was populated with state-of-the-art components in parallel to the existing VLBA4 rack.

The focus was on digital sampling components. Therefore a very stable and flexibly configurable ADS3000+ baseband converter is installed in combination with a Mark5B+ data recording system. A new Field System PC is available with one of the latest NASA Field System versions to control all the equipment.



Fig. 3 Newly installed data acquisition systems for VLBI.

A new maser EFOS-50 builds the basis for a stable frequency and timing. The UTC-connection is managed with a new GPS time receiver with NTP.

2.3 New control room

To enable a flexible control of satellite missions as well as of VLBI sessions, a new combined control room was build together with the DLR. The tasks can be controlled there an two operator desks.

First plans were discussed to integrate VLBI schedules into the scheduling system RPS and the control software SMCS of the DLR to enable a flexible scheduling of observations of satellite passages and intermediate VLBI sessions.

The VLBI sessions can also be controlled from remote at the new control room of the TWIN radio



Fig. 4 New combined satellite tracking and VLBI control room.

telescopes in Wettzell, using the software e- RemoteCtrl. This should extend the possibilities for VLBI-observations.

3 Integration tests in January and February 2015

The integration of the new receiver frontend and the data acquisition backend was done during the VLBI campaign from January to February 2015. The new VLBI receiver was successfully installed into the antennas elevation cabin. The VLBI sampler ADS3000+ and the Mark5B+ were mounted into an existing and available rack in the DLR control room in parallel to the old and still working VLBA4 rack with the Mark5A VLBI data recorder.

The new system was tested in parallel to the existing equipment during four VLBI sessions:

- OHIG94
- OHIG95
- OHIG96
- T2102

The OHIG sessions are dedicated to measure the southern reference frame. The T2 session is used to determine the terrestrial reference frame. Sample data scans were copied and sent to the Bonn correlator already during the ongoing sessions to evaluate the data quality of the new VLBI instrumentation. The first feedback from the correlator showed good data quality and performance.

4 Conclusion and outlook

Goals for the upgrades are an increase of times without maintenance and a higher automation. The idea behind is to enable one geodetic VLBI session per month in a more frequently used southern VLBI network (see Fig. 5¹). The VLBI sessions should be scheduled as intermediate observations within the satellite tracking and control sessions of the DLR. Parts of the VLBI sites may be operated from remote in such a scenario.

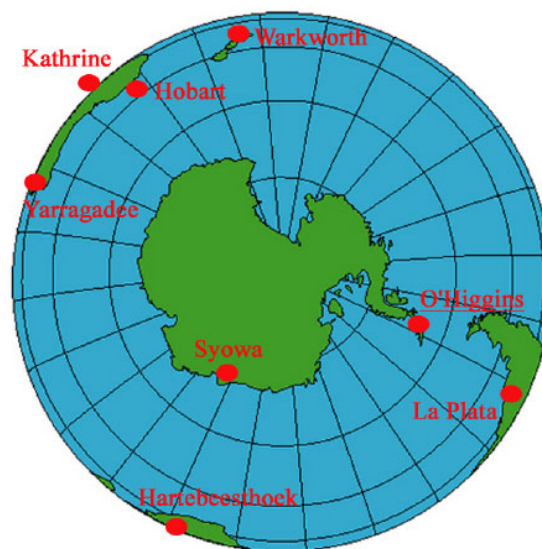


Fig. 5 A possible southern VLBI network for geodesy.

References

- Bundesamt für Kartographie und Geodäsie (2015) Geodätischen Observatorium O'Higgins/Antarktis. Web document <http://ivs.bkg.bund.de/vlbi/ohiggins/>, Download 2015.

¹ Maps are courtesy of Bruce Jones Design Inc. and FreeUSand-WorldMaps.com

Status of the Spanish-Portuguese RAEGE project

J. Gómez–González, L. Santos, J. A. López–Fernández, F. Colomer

Abstract The Spanish/Portuguese RAEGE project (“Atlantic Network of Geodynamical and Space Stations”) is being deployed. The status of the RAEGE project will be presented. Commissioning of the radio telescope at Yebes is ongoing, and the construction of the station in Santa María site is very advanced. Site works for a new station in Tenerife (Canary Islands) have started.

Keywords VGOS, RAEGE

1 Introduction

The National Geographic Institute of Spain (Instituto Geográfico Nacional, Ministerio de Fomento), runs geodetic VLBI programs at Yebes Observatory since 1995, and nowadays operates a 40-m radio telescope which is a network station for IVS. Yebes Observatory is also the reference station for the Spanish GNSS network and holds permanent facilities for gravimetry. Since March 2014, IGN Yebes Observatory is a Technology Development Center for IVS.

A new VGOS-type antenna has been built in Yebes as part of the RAEGE project (the acronym RAEGE stands for “Red Atlántica hispano-portuguesa de Esta-

Jesús Gómez-González, Francisco Colomer
Instituto Geográfico Nacional (IGN), Calle General Ibañez de Ibero 3, E-28003 Madrid, Spain
Luis R. Santos
DROPC/SRTT, Rua Conselheiro Dr. Luis Bettencourt 16, 9500-058 Ponta Delgada, Azores, Portugal
José Antonio López–Fernández
Yebes Observatory, IGN, Cerro de la Palera s/n, E-19141 Yebes, Spain



Fig. 1 Location of the RAEGE stations.



Fig. 2 The RAEGE station in Yebes (Spain).

ciones Geodinámicas y Espaciales”). This first antenna has seen its first VLBI fringes in November 2014 at Yebes Observatory. The construction of a second antenna, in Santa María (Azores, Portugal), is complete, and commissioning is ongoing. The construction of a control building is very advanced (see Fig. 3). The official inauguration took place on May 20th 2015, as a follow up of the 22nd meeting of the European VLBI Group for Astrometry and Geodesy (EVGA, see <http://evga2015.raege.net/>).

Detailed information on RAEGE is available on the Web at <http://www.raege.net/>.

2 Recent developments

First VLBI fringes with the RAEGE 13-m antenna in Yebeas were obtained in November 2014 at X-band using the triband (S/X/Ka) receiver, developed at the Yebeas laboratories. A new broadband receiver is being developed for VGOS, to be installed in 2016. This receiver may include a ultra-wideband Dyson conical quad-spiral array feed system, DYQSA, being developed in Yebeas and the University Carlos III Segovia-Vargas et al. (2015).

A local-tie between different geodetic techniques is also being established at Yebeas Observatory.

The most important development now is the continuation of the establishment of the RAEGE station in Santa María (Azores), in particular, the installation of the equipment at the radio telescope in order to start the commissioning phase.

Finally, preliminary works in Flores (Azores) are being conducted after the site of the station has been selected, in order to characterize the presence of radiofrequency interferences at the selected site for the RAEGE station there.

2.1 The RAEGE station in Santa María (Azores)

The station in Santa María is one of the two RAEGE stations in Azores islands, this one is located in the African tectonic plate (the same as the RAEGE station in Canary Islands), while the station in Flores will be located in the American tectonic plate.

In recent months, the station has been very busy with the construction of the control building and the erection of the antenna. Participants in the EVGA conference in May 2015 were able to check the status of the developments. There is however a lot of work still to do, mostly related to the instrumentation (receiver, backends, etc) and some infrastructure (access to high-speed internet). The station is expected to be operational in 2016 with a triband (S/X/Ka) receiver, to be upgraded to broadband as soon as possible.

2.2 VGOS Broadband receiver

A VGOS broadband receiver is being developed at the laboratories of Yebeas Observatory. The system allows observations in the 2–14 GHz band, dual polarization, where four channels of 1 GHz per polarization can be selected. One important aspect of this receiver is the design and construction of a ultra-wideband Dyson conical quad-spiral array feed system (DYQSA), however a Quadruple Ridged Flared Horn (QRFH) may also be used. For more information, read the contribution by López-Fernández et al. (2015).

2.3 Yebeas Observatory local tie

A network of 24 monuments (concrete pillars) have been built at Yebeas Observatory in order to relate the measurements taken by our two VLBI radio telescopes (40-m and 13-m) and two GNSS antennas (IGS code “YEBE”, on the roof of the office building, and “YEB1”, on the roof of the gravimeter building). The process is described in Córdoba and López-Ramasco (2015) and in Córdoba et al. (2015).

We have also investigated the possibility to measure the invariant reference point (IRP) of the new 13-m radio telescope with a robotic total station, installed on the central pillar of the concrete tower. A tripod with an optical plummet is placed on the marked centered screw of the pillar. Then it is possible to measure the position of a corner cube reflector with a manufacturing precision of 0.0001 mm, which is attached magnetically to the inner sides of both antenna counterweights. The operation can be done even when a regular VLBI session is ongoing.

2.4 The RAEGE station in Flores (Azores)

The RAEGE station in Flores will be located in the south of the island. The site has been selected (see Fig. 5) and preliminary works are being conducted, in particular to identify and characterize radiofrequency interferences. Located in the American tectonic plate, this station is expected to be operational in 2017.



Fig. 3 RAEGE station in Santa María (Azores islands, Portugal).



Fig. 4 Official inauguration of the RAEGE station in Santa María (Azores islands, Portugal).

3 Summary

The RAEGE station in Santa María, after the official inauguration on May 20th 2015 (during the events of the 22nd EVGA meeting), commissioning will be performed for an expected start of observations in 2016.

The infrastructure works for the RAEGE station near the city of Tegueste (Tenerife, Canary Islands) will



Fig. 5 Site selected for the construction of the RAEGE station in Flores island (Azores).

start in 2015, followed by the erection of the antenna, built by MT Mechatronics GmbH.

Preliminary works in Flores (Azores) are being conducted to characterize the presence of radiofrequency interferences at the site selected for the RAEGE station there.

In order to comply with the VGOS specifications, a new broadband receiver is being developed at Yebes and should be available for observations there in 2016, and later in the other RAEGE stations.

References

- Segovia-Vargas D, García-Muñoz L, Llorente-Romano S, Herraiz-Martínez F J, Salazar-Palma M, García-Lampérez A, Tercero F, Serna J M, López-Fernández J A, López-Pérez J A, Colomer F (2015) Dyson Conical Quad-Spiral Array as Ultrawideband Feed System. In: *2015 Loughborough Antennas & Propagation Conference (LAPC)*.
- Córdoba B, López-Ramasco J (2015) Cálculo del punto invariante de una antena. Método de ajuste clásico por círculos. Aplicación al radiotelescopio RAEGE del Observatorio de Yebes. IGN Yebes Observatory technical report CDT 2015-2.
- Córdoba B, López-Ramasco J, García-Espada S (2015) Local Tie Works in Yebes Observatory. In: R. Haas, F. Colomer (eds.), *Proc. 22nd EVGA Working Meeting*, 130–134.
- López-Fernández J A (2015) In: R. Haas, F. Colomer (eds.), *Proc. 22nd EVGA Working Meeting*, 11–14.

The southern hemisphere AUSTRAL program: A pathway to VGOS

J. Lovell, J. McCallum, L. Plank, E. Rastorgueva-Foi, S. Shabala, D. Mayer, J. Böhm, O. Titov, J. Quick, S. Weston, S. Gulyaev, T. Natusch, C. Reynolds, H. Bignall, J. Sun, A. Neidhardt

Abstract The AuScope VLBI array participated in 210 IVS sessions in the 12 months from July 2014. More than half of these were dedicated to the southern hemisphere AUSTRAL program together with antennas at Hartebeesthoek (South Africa) and Warkworth (New Zealand). AUSTRAL has three main streams: astrometry to monitor and enhance the southern hemisphere celestial reference frame; geodesy to improve the southern hemisphere terrestrial reference frame and the baseline time series; and 15-day CONT-like sessions to densify the time series and investigate a range of observing strategies. The high observing rate is pro-

viding new insight into some of the challenges of a 24/7 VGOS observing program and is allowing us to trial new scheduling and observing strategies such as Dynamic Observing. All AUSTRAL sessions are being scheduled with VieVS, observations are carried out remotely using the eRemoteCtrl software, data are processed at the Curtin University AuScope correlator and analysis is carried out in Hobart and at Geoscience Australia. We present some results from the AUSTRAL program and describe the steps we have taken and have planned to approach VGOS-like operations.

Jim Lovell, Jamie McCallum, Lucia Plank, Elizaveta Rastorgueva-Foi, Stas Shabala
University of Tasmania, Private Bag 37, 7001 Hobart, Australia
David Mayer and Johannes Böhm
Technische Universität Wien, Gußhausstraße 27-29, 1040 Vienna, Austria
Oleg Titov
Geoscience Australia, P.O. Box 378, Canberra, ACT 2601, Australia
Jonathan Quick
Hartebeesthoek Radio Astronomy Observatory (HartRAO), P.O.Box 443, Krugersdorp 1740, South Africa
Stuart Weston, Sergei Gulyaev, Tim Natusch
Institute for Radio Astronomy and Space Research, School of Computing and Mathematical Sciences, Auckland University of Technology, Private Bag 92006, Auckland 1142, New Zealand
Cormac Reynolds and Hayley Bignall
International Centre for Radio Astronomy Research, Curtin University, GPO Box U1987, Perth, WA 6845, Australia
Jing Sun
Shanghai Astronomical Observatory, Chinese Academy of Sciences, 80 Nandan Road Shanghai 200030, China
Alexander Neidhardt
Technische Universität München, Forschungseinrichtung Satellitengeodäsie, Geodetic Observatory Wettzell, Sackenrieder Str. 25, D-93444 Bad Kötzing, Germany

Keywords Geodesy, Astrometry, VLBI, VGOS

1 Introduction: The Challenges of VGOS

The move toward the VLBI Global Observing System (VGOS) presents some significant technical and organisational challenges to the geodetic VLBI community. Operations will move from approximately 150 24-hour sessions per year to continuous observations. Broader bandwidths, higher data recording rates and the need for fast turnaround of products will stress data network and storage resources. It is likely that economies will have to be found to keep the cost of operations down and this may require centralised, remote operations centres and more automation. Streamlining the connections between scheduling, observing, data processing and analysis will be required and real-time adaptation of schedules during an observation to react to unforeseen events will also improve data quality. Further, the improved accuracy and precision of solutions in the

VGOS era will only be possible if sources of error that are currently insignificant, such as quasar structure, are mitigated against. There is also the prospect of developing new observing modes involving twin and sibling telescopes.

In this paper we describe the work that has been undertaken in the southern hemisphere in recent years to address some of these challenges. In Section 2 we briefly describe the AuScope VLBI array and how it functions as a VGOS pathfinder. In Section 3 we outline the southern hemisphere focused AUSTRAL observing program and in Section 4 we show how it is helping to address some of the VGOS challenges. Lastly, in Section 5 we describe our plans to upgrade the AuScope network to full VGOS compatibility.

2 The AuScope VLBI Array

In 2007 the Australian Federal Government through the National Collaborative Research Infrastructure Strategy (NCRIS) funded Capability 5.13: "Structure and Evolution of the Australian Continent" from which AuScope was established (www.auscope.org.au). Part of the AuScope initiative was to upgrade Australian geospatial infrastructure, including VLBI. This involved the construction of three new 12 m diameter radio telescopes across the continent, in Hobart (Tasmania) co-located with the existing 26 m telescope and HOB2 GNSS antenna, at Yarragadee (Western Australia) co-located with the MOBLAS-5 SLR station, GNSS and DORIS facilities, and a new site in Katherine (Northern Territory) where a GNSS facility has also been established. The Hobart antenna (Hb) commenced operations in 2010 with the Katherine (Ke) and Yarragadee (Yg) sites following in 2011. The telescopes were built to match the VGOS requirements as closely as possible or to allow for future upgrades to VGOS compatibility where it was not possible to do so at the time. At present, all three telescopes operate with room-temperature S/X systems although an upgrade to cooled, broadband systems is now funded.

All three telescopes are controlled and monitored remotely from the operations centre at the University of Tasmania. Observations are coordinated through the IVS with most experiments correlated at Bonn, Washington, or the AuScope correlation facility at Curtin University in Western Australia. A detailed description

of the AuScope VLBI infrastructure and characteristics of the array has been presented by Lovell et al. (2013).

3 The AUSTRAL Observing Program

The AUSTRAL observing program is a series of sessions additional to the usual IVS program, dedicated to observations with the AuScope array, Hartebeesthoek and Warkworth (Figure 1) and focused on specific areas of priority in the southern hemisphere:

1. One session per month of astrometry to monitor and enhance the southern hemisphere reference frame. Some of these sessions have also included the Parkes 64 m antenna to improve sensitivity to weak sources,
2. About two 15-day CONT-like sessions per year to densify the geodetic time series and trial and evaluate a range of different observing strategies
3. The remainder (and vast majority) of sessions were geodetic and aimed at improving the terrestrial reference frame and baseline time series in the southern hemisphere

In the 12 months commencing 2014 July 1, the AuScope array was the busiest geodetic VLBI facility in the world, participating in 210 days of observations. Of these, 118 days were dedicated to the AUSTRAL program. The AuScope telescopes participated in all sessions while the Hartebeesthoek 15 m and Warkworth 12 m contributed to ~ 50% of the AUSTRAL days.

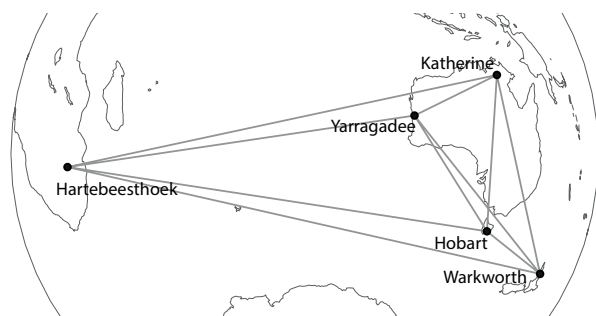


Fig. 1 The AUSTRAL network.

Scheduling for the AUSTRAL sessions is carried out in VieVS (Böhm et al., 2012), observations are made at 1 Gbps recording rates (16×16 MHz IFs and 2-bit digitisation), data correlated at Curtin University

and data analysis carried out at the University of Tasmania and Geoscience Australia.

4 Addressing VGOS Challenges with the AUSTRAL Program

The southern hemisphere network involved in the AUSTRAL program is not fully compliant with VGOS because it does not yet have broadband systems, fast internet connections to all sites or enough operational funding to support continuous observations. However, the array is capable of addressing some of the challenges of VGOS. We have small, fast slewing antennas and a higher than standard data recording rate which allows us to trial and investigate VGOS scheduling strategies that involve many more scans per day than typical IVS Rapid observations. Our ability to observe for 210 days over 12 months from a central operations centre also allows us to work on improving and streamlining operational procedures

4.1 Continuous Remote Operations

At its inception the model for operation of the AuScope array was to make it as automated as possible and remote controllable. To do this, we used our experience in remotely operating the University of Tasmania Ceduna 30 m antenna (in South Australia), adopted software that allows for remote operation and monitoring such as eRemoteCtrl (Ett et al., 2012) and MONICA (Brodrick, 2015) and also developed our own interfaces. The observatories are equipped with cameras to provide real-time visual monitoring of equipment, back-up power generators and internet connections, internet power switches and environmental monitors. In this way it is possible to operate the sites entirely remotely for long periods of time with the only required local support being management of recording media. Our experience with this mode of operations has provided feedback to the eRemoterCtrl software developers and has led to several improvements. At the Hobart observatory we operate a small PC cluster running the DiFX software correlator (Deller et al., 2007) and this is used regularly to run brief automated fringe checks on the AuScope baselines.

The high observing cadence in 2014/2015 combined with four non-stop 15-day CONT-like sessions between December 2013 and the end of June 2015 allowed us to experience VGOS-like operations and develop methods to handle a continuous stream of data.

In Figure 2 we show the baseline time series for Katherine-Yarragadee which demonstrates the benefits of a higher sampling rate since July 2013. Systematic effects become much more apparent as do the true uncertainties in the data.

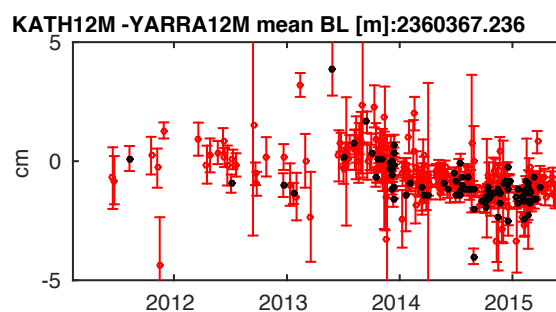


Fig. 2 The baseline time series for Katherine-Yarragadee from mid-2011 until June 2015. AUSTRAL sessions are indicated by the black points. This clearly shows the benefits of a higher sampling rate and its ability to clearly reveal systematic effects.

4.2 Scheduling Strategies

The complete management of the AUSTRAL sessions from scheduling through to analysis is carried out within our collaboration and this allows us to test and improve scheduling strategies (Mayer et al., 2015). In Figure 3 we show baseline length repeatabilities (weighted rms) as a function of baseline length for the AUST sessions. The data are divided into three time periods. The first period, until July 2014 shows the results for observations with the source catalogue comprising all common VLBI sources stronger than 0.5 Jy. The second period covers approximately the next six months after a reduction was made to the list of target sources and shows a significant improvement. Lastly, the third period, from the beginning of 2015 shows a further improvement following a revision of target SEFD levels and an increase in the minimum acceptable source flux density to 0.8 Jy, leading to more

scans per day. These continuous improvements over time have lead to almost a factor of two improvement in repeatability over the course of the AUST program.

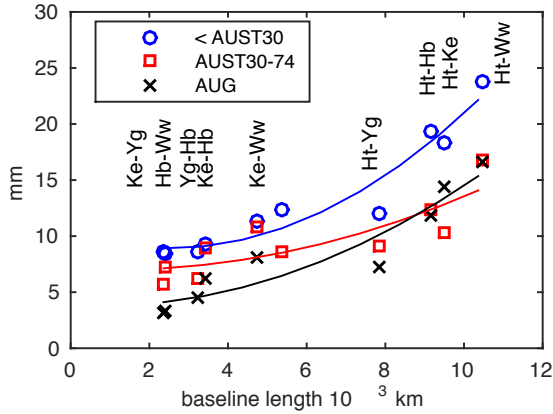


Fig. 3 A factor of ~ 2 improvement in baseline length repeatabilities (wrms) as a result of revision and optimisation of scheduling strategies. The blue circles cover the initial 12 months of the AUSTRAL program, the red squares cover six months following a revision of the source catalogue and the black crosses show results from the first six months of 2015 after SEFD target levels and catalogue flux density limits were revised.

4.3 Feedback and Dynamic Observing

We have commenced work on improving our observing and scheduling strategies through intra-session optimisations, or Dynamic Observing (Lovell et al., 2014). The main concept here is to use monitoring of antenna performance, local conditions (e.g. wind stows) to provide feedback to a central operations centre so that the observing schedule can be modified in real-time to optimise the data quality. Simulations of scenarios such as poorer than expected sensitivity have shown that a vast majority of scans can be recovered to an affected antenna if real-time adaptation is adopted. Further simulations are required and test observations should be planned.

4.4 Variability and Source Structure

While the troposphere is currently the dominant source of error in geodetic VLBI measurements, it is expected that in the VGOS era other effects will also become a significant contributor. One of these is source structure and this has been a significant focus of research at the University of Tasmania in recent years (Shabala et al., 2015). In Figure 4 we show the evolution in total flux density of the quasar 0059+581. There is a strong anticorrelation with group delay. When the quasar undergoes a flare in flux density a new jet component is ejected by the central engine and the source is 'core' dominated and compact and therefore a good target for geodesy. However, as the new component moves down the jet, the source becomes extended at VLBI resolution, group delay increases and the geodetic solution is degraded.

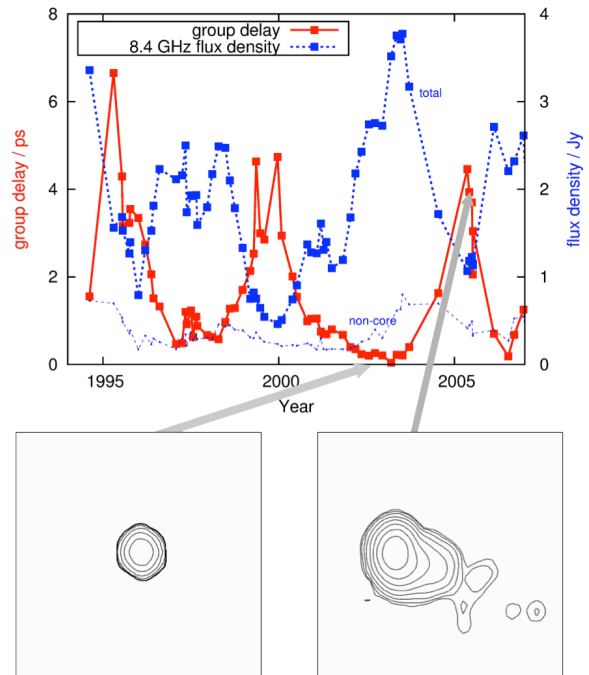


Fig. 4 Top panel: variability in total flux density in the quasar 0059+581 (blue) and a corresponding anti-correlation with group delay (red). Lower panel: VLBI images of the source during and after a flare (left and right respectively). The source is a good target for geodetic observations when it is bright and compact after a new jet component has just been emitted, but its usefulness for geodesy is degraded once the component propagates along the jet.

This work clearly demonstrates that an understanding of the parsec-scale astrophysics of AGN is important in mitigating against source structure effects. In the VGOS era it will be important to monitor the total flux density of the target sources and regularly update catalogues so that sources are scheduled only when they are predicted to be dominated by an unresolved component near the nucleus.

4.5 Twins and Siblings

At Hobart and Hartebeesthoek, we can work on understanding and developing the twin telescope concept by co-observing with the legacy 26 m telescopes. This is discussed in detail elsewhere by Plank et al (these proceedings). New Zealand's 12 m and 30 m telescopes at Warkworth can potentially be used for this program as well (Woodburn et al., 2015).

5 Next Steps

Our priorities during the ramp-up to VGOS operations are to upgrade the AuScope network to broadband receivers and recorders covering 3–14 GHz by the end of 2016. We will also continue to develop and trial some dynamic observing and source structure mitigation techniques, further develop observing software to improve reliability and automation, and use the Hobart 12 m and 26 m telescopes to investigate and assess various sibling/twin telescope observing strategies.

6 Acknowledgments

This work was supported by the AuScope Initiative, funded under the National Collaborative Research Infrastructure Strategy (NCRIS), an Australian Commonwealth Government Programme. The authors are grateful to the Australian Research Council for Fellowships FS1000100037 and FS110200045 and to the Austrian Science Fund (FWF) for Fellowship J3699-N29.

References

- Böhm J, Böhm S, Nilsson T, Pany A, Plank L, Spicakova H, Teke K, Schuh H (2012) The new Vienna VLBI software. In: S. Kenyon, M. C. Pacino, U. Marti (eds.), *Proc. IAG Scientific Assembly 2009*, IAG Symposia Series 136, 1007–1011, doi: 10.1007/978-3-642-20338-1_126.
- Brodrick D (2015) MoniCA Monitoring Software. Web document <https://www.narrabri.atnf.csiro.au/monitor/monica/>
- Deller A T, Tingay S J, Bailes M, West C (2007) DiFX: A Software Correlator for Very Long Baseline Interferometry Using Multiprocessor Computing Environments. *Publ Astron Soc Pac*, 119, 318–336.
- Ettl M, Neidhardt A, Schönberger M, Alef W, Himwich E, Beaudoin C, Plötz C, Lovell J, Hase H (2012) e-RemoteCtrl: Concepts for VLBI Station Control as Part of NEXPReS. In: D. Behrend, K. D. Baver (eds.), *IVS 2012 General Meeting Proc.*, NASA/CP-2012-217504, 128–132.
- Lovell J E J, McCallum J N, Reid P B, McCulloch P M, Baynes B E, Dickey J M, Shabala S S, Watson C S, Titov O, Ruddick R, Twilley R, Reynolds C, Tingay S J, Shield P, Adada R, Ellingsen SP, Morgan JS, Bignall HE (2013) The AuScope geodetic VLBI array. *J Geod*, 87, 527–538.
- Lovell J, McCallum J, Shabala S, Plank L, Böhm J, Mayer D, Sun J (2014) Dynamic Observing in the VGOS Era. In: D. Behrend, K. D. Baver, K. L. Armstrong (eds.), *IVS 2014 General Meeting Proc.*, ISBN 978-7-03-042974-2,
- Mayer D, Böhm J, Lovell J, Plank L, Sun J, Titov O (2015) Scheduling Strategies for the AuScope VLBI network. *Vermessung & Geoinformation*, 2+3/2015, 162–168, http://www.ovg.at/fileadmin/download/vgi2015_0203/Mayer.pdf.
- Shabala S, McCallum J, Plank L, Böhm J (2015) Simulating the effect of quasar structure on parameters from geodetic VLBI. *J Geod*, 98(9), 873–886.
- Woodburn L, Natusch T, Weston S, Thomasson P, Godwin M, Granet C, Gulyaev S (2015) Conversion of a New Zealand 30-Metre Telecommunications Antenna into a Radio Telescope. *Publ Astron Soc Aust*, 32, 14.

GSI's regional stations and AOV activities

R. Kawabata, T. Wakasugi

Abstract The Geospatial Information Authority of Japan (GSI) has been operating three regional VLBI telescopes in domestic sites, i.e. Aira 10-m, Chichijima 10-m, and Shintotsukawa 3.8-m telescopes. These telescopes have observed many IVS regular sessions including Japanese domestic sessions (JADE sessions). However, GSI decided to stop the VLBI observation at Shintotsukawa site in December 2013 and at Aira and Chichijima sites in March 2015. Therefore there is no regular JADE session from April 2015. Instead, GSI is now devoting their effort to the newly established Asia-Oceania VLBI Group for Geodesy and Astrometry (AOV) in scheduling, operation, and correlation.

Keywords GSI, JADE, AOV

1 Introduction

The Geospatial Information Authority of Japan (GSI) has been operating geodetic VLBI since 1980s. From 1986 to 1993 a transportable VLBI instrument with a 5-m telescope was used in conjunction with the Kashima 26-m telescope to perform VLBI observations at a number of locations in Japan. In the late 1990s, after the Great Hanshin-Awaji Earthquake, GSI installed four stationary VLBI telescopes in Japan: Shintotsukawa 3.8-m (1995), Aira 10-m (1997), Chichijima 10-m (1997), and Tsukuba 32-m (1998). These telescopes formed a domestic VLBI network

Ryoji Kawabata, Takahiro Wakasugi
Geospatial Information Authority of Japan, Kitasato-1, Tsukuba,
Ibaraki, Japan

in Japan called GARNET (GSI Advanced Radio telescope NETwork, see Fig. 1).

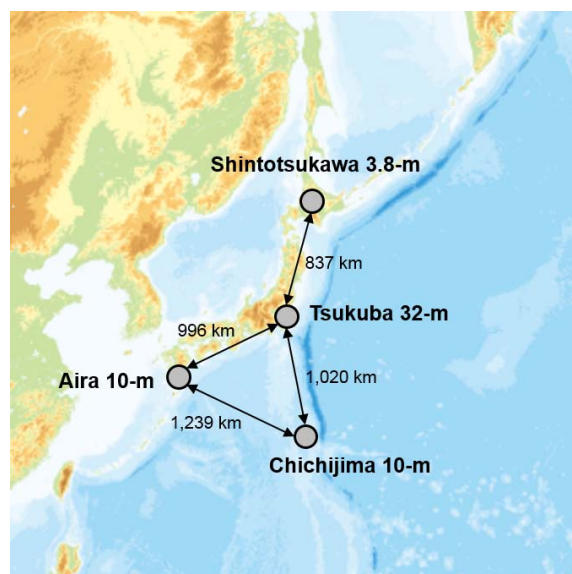


Fig. 1 Map of the GARNET stations. Tsukuba 32-m is the main telescope, and the other regional telescopes are located about 1,000 km away from Tsukuba.

2 GSI's VLBI Telescopes

The 32-m telescope at Tsukuba, about 50 km northeast of Tokyo, has been observing many IVS sessions owing to its high sensitivity and fast slewing rate (Tab. 1). Tsukuba 32-m has now become one of the fundamental VLBI telescopes among IVS Network Stations.



Fig. 2 Photos of GSI's regional telescopes: Shintotsukawa 3.8-m (left), Aira 10-m (middle), Chichijima 10-m (right).

Table 1 Specifications of the GARNET telescopes.

Station	Diameter	Slew rate (Az/El)	Typical SEFD (X/S)
Tsukuba	32 m	3 / 3 deg/s	300 / 400 Jy
Aira	10 m	3 / 3 deg/s	12,000/ 8,000 Jy
Chichijima	10 m	3 / 3 deg/s	12,000/ 8,000 Jy
Shintotsukawa	3.8 m	2 / 1 deg/s	140,000/ 100,000 Jy

The smaller telescopes initially participated only in the Japanese domestic VLBI sessions named JADE (Japanese Dynamic Earth observation by VLBI) together with the Tsukuba 32-m telescope (Fig. 2). The JADE sessions, whose purpose is to monitor the plate motions around Japan, have been scheduled, correlated, and analyzed by GSI.

From 2008 onward, the three regional telescopes have been added to other IVS sessions with global network such as IVS-T2s and APSGs. Thus, the smaller telescopes have also contributed well to the IVS. These telescopes observed IVS sessions almost on monthly basis, except that Shintotsukawa stopped observation in winter due to heavy snow. Between 1995 and 2015, Shintotsukawa observed in 110 IVS sessions, Aira in 213 sessions, and Chichijima in 196 sessions.

GSI basically operated these telescopes in unmanned operation by using Field System remotely controlled from Tsukuba. Since the network bandwidths at the sites were very limited, i.e., only 128 kbps, the observed data were shipped in media by janitors. Then the data were transferred via Tsukuba to correlators other than GSI.

Operation of the regional telescopes were very beneficial to GSI not only for monitoring of the plate motions around Japan. One important aspect was that GSI could maintain the operational technique of VLBI through regional stations and JADE sessions, that is, GSI could operate the telescopes and carry out scheduling, correlation, and analysis of JADE sessions by itself.

Another point worth mentioning for regional stations is that Aira observed IVS-R1 sessions for about six months in 2013 replacing Tsukuba which was down for rail track repair. For this we used a new sampler and recorders: ADS3000+ and K5/VSI system developed by the National Institute of Information and Communications Technology (NICT) because the ordinary recording system of Aira station could not observe wide bandwidth of IVS-R1 sessions (Wakasugi and Kawabata (2014)). This is the first time for us to operate this recording system on regular basis, and this experience is now utilized for the operation of the Ishioka 13-m telescope in legacy S/X observations (Fukuzaki et al. (2014)).

In addition, we have performed co-location surveys at the regional sites in order to measure the local ties between VLBI and GNSS. These results have already been submitted to the IERS in order to contribute to the construction of the ITRF.

3 Retirement of Regional Stations

In 2012, however, GSI started to discuss the continuation of the regional telescopes, because the maintenance and repair costs were getting higher due to aging systems. Another factor was the need to secure funds for the operation and maintenance of a new VGOS telescope in Ishioka. Furthermore, the dense GNSS network of GSI (GEONET), composed of about 1,300 GNSS antennas covering Japan, had become able to monitor the crustal movement of Japan instead of VLBI.

Considering above, GSI decided first to stop the operations of the Shintotsukawa 3.8 m in December 2013, since it was the smallest of the GSI's telescopes and not operational in winter. We then finally decided to retire the telescopes at Aira and Chichijima in March 2015. The hydrogen masers have already been stopped at all sites. Moreover, the main reflector of Chichijima 10-m was dismantled in order to ensure the safety for severe weather at the site.

As a consequence, no regular JADE session was scheduled after April 2015 except for some sessions dedicated for Tsukuba-Ishioka tie named also as "JADE". This means that GSI lost opportunities for correlation of the regular IVS sessions except for weekend 1-hour Intensive sessions as well as the stations.

4 GSI and AOV

At about the same time when we stopped operation at all regional sites, a new project started in the Asia-Oceania region: the activities of the Asia-Oceania VLBI Group for Geodesy and Astrometry (AOV). The AOV is a subgroup of IVS, established in 2014 to foster and encourage closer collaboration in the science, technology, and education aspects of VLBI in the region (Lovell et al. (2015)). As the first step for the AOV activities, AOV members discussed and decided to schedule six regional sessions in 2015.

This was actually a good opportunity for GSI to continue VLBI activities. GSI is now actively involved in the AOV; Tsukuba 32-m and Ishioka 13-m are scheduled to observe all AOV sessions in 2015. GSI is also assigned to a scheduler and a correlator for two AOV sessions respectively. This means that we are still

able to maintain our operational technique of VLBI through the AOV activities. GSI is going to devote its effort to AOV.

5 Summary

GSI had been operating three regional VLBI telescopes. However we decided to stop operations of these telescopes by March 2015. Instead GSI is now actively involved in the AOV activities by using Tsukuba 32-m and Ishioka 13-m telescopes.

References

- Fukuzaki Y, Tanabe T, Kuroda J, Kurihara S, Kawabata R, Wakasugi T (2014) Construction of a VGOS Station in Japan. In: D. Behrend, K. D. Baver, K. L. Armstrong (eds.), *IVS 2014 General Meeting Proc.*, Science Press (Beijing), 32–35.
- Lovell J, Kawabata R, Kurihara S, Cho J, Shu F, Gulyaev S (2015) The Birth of the Asia-Oceania VLBI Group for Geodesy and Astrometry. *IVS Newsletter*, Issue 41, April 2015, 5.
- Wakasugi T, Kawabata R (2014) Regular Geodetic VLBI Observation with a Wide-band Recording System. *IVS NICT Technology Development Center News*, ISSN 1882-3432, No. 34, 11–13.

First Geodetic Result of Ishioka VGOS Station

Y. Fukuzaki, K. Wada, R. Kawabata, M. Ishimoto, T. Wakasugi

Abstract The Geospatial Information Authority of Japan (GSI) started a new project for constructing a VGOS station in Japan. The construction of the antenna (radio telescope) has been completed and the necessary equipment (Front-end, Back-end, H-maser, and so on) has also been delivered. The name of the new site is Ishioka, which is located 16.6 km away from Tsukuba 32-m antenna. We briefly report the initial receiving performance of the Ishioka antenna, and the first geodetic results of VLBI observations carried out after February 2015.

Keywords VGOS antenna, receiving performance, geodetic VLBI observation

1 Introduction

The Geospatial Information Authority of Japan (GSI) has carried out VLBI observations since 1981. In the first period from 1981 to 1994, we developed transportable VLBI systems with a 5-m antenna and a 2.4-m antenna, and carried out domestic observations by using them. As a result, 8 sites in Japan were observed and precise positions determined. In addition, Japan-Korea VLBI observations were carried out by using a transportable 3.8-m antenna in 1995. In these observations, the Kashima 26-m antenna, which was removed in 2002, was used as a main station. Next, in the second period from 1994 to 1998, GSI established four

Yoshihiro Fukuzaki, Kozin Wada, Ryoji Kawabata, Masayoshi Ishimoto, Takahiro Wakasugi
Geospatial Information Authority of Japan, Kitasato-1, Tsukuba, Ibaraki, Japan

permanent stations: Tsukuba 32-m, Sintotsukawa 3.8-m, Chichijima 10-m and Aira 10-m antennas. Up to the present, regular VLBI observations by using the four stations have been carried out. Especially, Tsukuba 32-m antenna is a main station for not only domestic but also international VLBI observations now.

In 2011, GSI started a project for constructing a new antenna following the VLBI2010 concept, which is recommended by the International VLBI Service for Geodesy and Astrometry (IVS) as the next-generation VLBI system.

This paper gives the outline of the project, the initial receiving performance of the new antenna, and the first geodetic results of VLBI observations that have been carried out since February 2015.

2 Observing Facilities

In the new project, observing facilities are now being constructed. The conceptual design consisting of the six components is depicted in Figure 1. At present temporary operation rooms are installed instead of the Operation Building, and it will be completed by the end of February 2016.

The site name is Ishioka, which is located near Tsukuba (about 16.6 km NE from Tsukuba 32-m antenna).

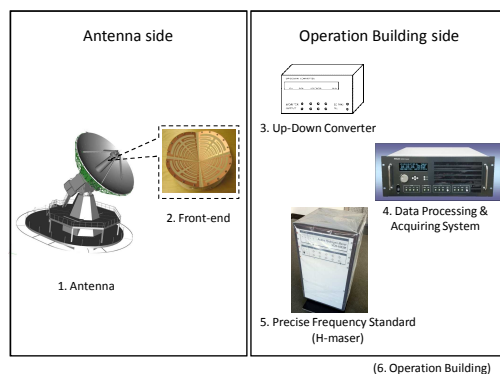


Fig. 1 Conceptual design of the new observing facilities

3 Antenna and Front-end

3.1 Antenna

The antenna (radio telescope) is the main part of the observing system (Figure 2). Since a single antenna is employed, very high slew rates are specified in order to be compliant with the VLBI2010 concept. In addition, Ring Focus optics was applied for the antenna design in order to match the beam pattern of the broadband feed. The specifications of the antenna are listed in Table 1.



Fig. 2 Photo of the new antenna.

Table 1 Specifications of the new antenna.

Parameter	Value
Diameter	13.2 m
RF frequency range	2–14 GHz
Optics	Ring Focus
Surface accuracy	≤ 0.1 mm (rms)
AZ maximum slew rate	12°/sec
EL maximum slew rate	6°/sec
AZ maximum acceleration rate	3°/sec ²
EL maximum acceleration rate	3°/sec ²
Special feature	Reference point can be measured directly from the ground for co-location.

3.2 Front-end

According to the VLBI2010 concept, a broadband feed is necessary to achieve high aperture efficiency over 2–14 GHz. At present the Eleven feed, which has been developed at Chalmers University of Technology in Sweden, and Quadruple-Ridged Flared Horn (QRFH), which is developed at California Institute of Technology (Caltech), are the practical as a broadband feed, so both feed systems are purchased. The employment of the feed will be determined after the evaluation of the antenna receiving performance with these two feeds.

In the both cases, the feeds and Low Noise Amplifiers (LNAs) are integrated into the each cryogenic system, whose physical temperature is less than 20 K.

In addition, in order to achieve the compatibility with the legacy S/X band observation, tri-band feed system is also purchased. By using the tri-band feed system the measurement of the initial receiving performance was performed. (See the following section.)

The phase and cable calibration system is also installed. A new type of P-cal unit, which was designed by Haystack observatory, is developed and employed. In addition, instead of the present D-cal unit a new cable calibration system developed by National Institute of Information and Communications Technology (NICT) is also employed. The specifications of the front-end are shown in Table 2.

Table 2 Specifications of the front-end.

Parameter	Value
RF frequency range	2–14 GHz
Polarization	Dual linear polarization
Feed	Eleven feed or QRFH
Dewar	Feed, LNAs, and other devices should be included and cooled by cryogenic system.
Physical temperature	≤ 20 K
Receiver noise temperature	≤ 30 K
Total gain	≥ 45 dB
Output frequency range	2–14 GHz
Number of output	2 (for dual linear polarization)
Phase and delay calibration	New-type P-cal unit designed by Haystack Observatory New cable calibration system developed by NICT
Injection of P-cal/noise-source	pre-feed (Eleven feed) or pre-LNA (QRFH)

4 Receiving Performance

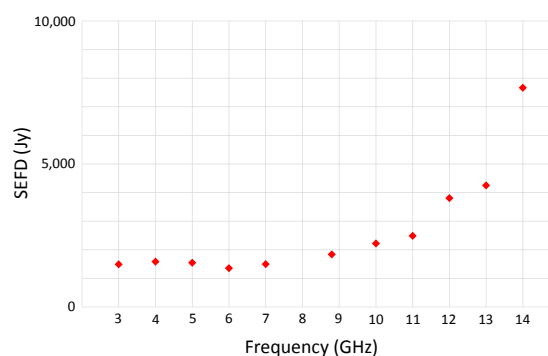
The receiving performance of the new antenna with tri-band feed system was measured by receiving some strong radio stars (Cas-A, Taurus-A, Virgo-A). As a result, the SEFD values for X and S band were approximately 1,250 Jy and 1,700 Jy, respectively. This means that the aperture efficiencies for X and S band are 77 % and 59 %, respectively, if the system noise temperature is assumed as 50 K. High receiving performance for X band was confirmed as the feature of the Ring Focus optics. (The measurement of the receiving performance for Ka band is not performed yet.)

As a next step QRFH system was installed on the antenna, and the receiving performance was measured. Unfortunately only Sun was detectable, and it was realized that the modification of the cryogenic dewar would be necessary to improve the sensitivity of QRFH. We have a plan to improve the cryogenic dewar by the end of March 2016.

Finally, Eleven feed system was installed on the antenna, and the receiving performance was measured by receiving the radio signal from some strong radio stars (Cas-A, Taurus-A, Cygnus-A). The SEFD values in the frequency range from 3 to 14 GHz are shown in Figure 3. The SEFD values less than 9 GHz are acceptable (less than 2,000 Jy), but unfortunately the SEFD val-

ues more than 10 GHz are getting worse and reaching 7,500 Jy at 14 GHz.

On the other hand, RFI is more serious than expected because of the feature of Ring Focus optics. In the case of Ring Focus optics, the aperture efficiency is better but the artificial radio signal can reach the feed more easily than the usually-used optics like Cassegrain. In the new station, the RFIs caused by the radio signal for cellular phone are so strong in the frequency range less than 2.1 GHz that the saturation of the amplifiers for S band occurs. In order to avoid the saturation of the S band amplifiers some filters (High Pass Filter (cut less than 2.2 GHz), Notch Filter (cut 2.1 GHz), and Band Pass Filter (pass 2.2–2.4 GHz) are installed in the signal chain of the antenna, and VLBI observation can be carried out normally at present.

**Fig. 3** SEFD values of Ishioka VGOS antenna with Eleven feed

5 First Geodetic Results

First geodetic VLBI observation was carried out in February 2015 in the Japanese domestic network including GSI's VLBI stations (Tsukuba 32-m, Aira 10-m, Chichijima 10-m antenna). Until the middle of June 2015 Ishioka station has participated in two types of VLBI sessions. One is Japanese domestic session JADE and another is AOV (Asia-Oceania VLBI group for Geodesy and Astrometry) session, which newly started in 2015 for Asia-Oceania region. Totally ten 24-h VLBI sessions were observed at

Ishioka station, and the precise geodetic results were successfully obtained for JADE sessions, which were analyzed by GSI quickly. The results of baseline lengths between Ishioka and Tsukuba 32-m antenna are listed in the Table 3. The standard deviation for each session is the range 1–2 mm, which is reasonable for Ishioka-Tsukuba baseline.

Table 3 Geodetic results of JADE sessions that were carried out at Ishioka station

Session	Date	Baseline Length (Ishioka-Tsukuba)
JD1502	Feb. 19	16,606,288.71 +- 1.58 mm
JD1503	Mar. 05	16,606,290.88 +- 1.04 mm
JD1504	Mar. 12	16,606,285.38 +- 1.39 mm
JD1505	Apr. 23	16,606,291.41 +- 1.31 mm
JD1506	May. 14	16,606,293.14 +- 1.50 mm
JD1507	Jun. 04	16,606,290.03 +- 1.27 mm
JD1508	Jun. 11	16,606,291.17 +- 1.34 mm

6 Summary

A new project for constructing a new antenna in Japan has started. The new station will be fully compliant with the VLBI2010 concept. The construction of the antenna was completed by the end of March 2014. The measurement of the receiving performance of the antenna was performed, and high aperture efficiency for X band was confirmed.

First geodetic VLBI observation was carried out in February 2015, and ten VLBI observations were performed till June 2015. As a result, precise coordinates of the new antenna are obtained successfully.

This station will play an important role as a main station in the Asian region instead of Tsukuba 32-m station in the near future.

On the Role of Tianma Radio Telescope for Improving Celestial Reference Frames

F. Shu, J. Wang, W. Jiang, G. Wang, Z. Shen

Abstract The Tianma 65-m radio telescope is newly built in Shanghai. By taking advantage of its high sensitivity, Tianma65 is able to improve detection of astrometric sources and increase the total number of observations in VLBI astrometry, which is of importance for connection of radio-optical frames and densification of the ICRF. We will briefly describe the characteristics of this new antenna, introduce its performance in recent observing sessions, present current status and discuss the future observations optimized for improving celestial reference frames.

Keywords Radio astrometry, Tianma radio telescope, Sensitivity

1 Introduction

The Tianma 65-m radio telescope, located in Shanghai and approximately 6 km west of the station Seshan25, has been operated by Shanghai Astronomical Observatory since its inauguration in 2012 (Xia et al., 2015). Tianma65 can be used as a single-dish or a powerful VLBI element for a variety of research on radio astronomy, geodesy as well as space science. Equipped with S/X dual band receiver and CDAS (Chinese VLBI Data Acquisition System), Tianma65 has been operational in CVN (Chinese VLBI Network) and then IVS sessions since 2013. It will be also equipped with X/Ka dual band receiver by the end of 2015.

Fengchun Shu, Jinqing Wang, Wu Jiang, Guangli Wang, Zhiqiang Shen
Shanghai Astronomical Observatory, Chinese Academy of Sciences, 80 Nandan Road Shanghai 200030, China

The original idea proposed in middle 1990's is to build a 64-m radio telescope in Shanghai, but it became true only after the VLBI technique was successfully applied for the navigation of the first Chinese Lunar satellite Chang'E-1 in 2007. With the great support of Shanghai local government, the project was jointly funded in 2008 altogether with Chinese Academy of Sciences and Chinese Lunar Exploration Project.

2 General informaton

The Tianma radio telescope is a fully steerable radio telescope. It is comprised of a 65-meter diameter main reflector and a 6.5-meter diameter sub-reflector. The main reflector is made up of 14 rings of 1008 high-precision solid panels, each having an area of 2.66-4.90 square meters. The sub-reflector is comprised of 3 rings of 25 aluminum honeycomb sandwich panels. The accuracies of the panels in the primary and sub-reflectors are better than 0.1 mm (rms) and 0.05 mm (rms), respectively. The total weight of the radio telescope is about 2640 tons so it can be regarded as a reduced size of Green Bank Telescope.

A novel technology known as active surface control was adopted for assembling the main reflector. A total of 1104 actuators were installed at the locations where the panels join the antenna backup structure so as to compensate for gravity deformation of the reflecting surface. This can greatly improve the observing efficiency at high frequencies. The whole supporting track employed seamless welding technique, by which 30 precision-machined 6-ton segments were all-welded together to be a single track with an overall unevenness of 0.5 mm (rms). This technique has laid the foundation

Table 1 Technical parameters of the Tianma radio telescope.

Name	Tianma Radio Telescope
Database name	Tianma65
2-letter name	T6
owner and operating agency	SHAO-CAS
year of construction	2012
antenna type	Cassegrain type
antenna mount	Az-El
receiving feed	primary focus
diameter of main reflector	65 m
focal length	20.8 m
f/d	0.32
surface contour of reflector	0.6 mm (without active surface)
latitude	31°05'31.57" N
longitude	121°08'09.63" E
altitude	49.57 m
DOMES number	21618S001
CDP monument number	7379
azimuth range	-80° - 440°
azimuth velocity	0.5°/s
azimuth acceleration	0.25°/s ²
elevation range	5° - 88°
elevation velocity	0.25°/s
elevation acceleration	0.15°/s ²
S/X dual band	2.2 - 2.4 GHz
frequency coverage	8.2 - 9.0 GHz
X/Ka dual band	8.2 - 9.0 GHz
frequency coverage	30 - 34 GHz
VLBI backend	CDAS, DBBC2
VLBI recorder	Mark5B
VLBI control	Field System

for assuring the precision of the antennas axial system. The telescope is equipped with receivers for L, S/X, C, Ku, K, X/Ka and Q bands which are corresponding to an observing wavelength coverage from 7 mm to 21 cm. The frequency switch can be accomplished within one minute.

The cross scan method has been used to measure antenna pointing error, and the least square fit was applied to estimate 8 coefficients in the antenna pointing correction model. The RMS error of antenna pointing is about 8.2 arc-seconds. The similar results have been obtained at different frequency bands. A set of antenna holography measurements show that aperture surface RMS error is better than 0.6 mm at certain elevations. The main technical parameters relevant to geodetic and astrometric VLBI are listed in Table 1. The S/X dual band has been operational while the X/Ka dual band will be tested by the end of 2015.

3 Performance of the Tianma radio telescope

An important scientific goal of Tianma65 is to improve celestial reference frames by VLBI method. According to the original proposal for the Tianma65 project, this goal can be reached through the following work.

- Densification of radio reference frames: Tianma65 is able to largely improve array sensitivity which open a window for VLBI astrometry of more weak sources at different frequency bands.
- Connection of radio-optical reference frames: the array sensitivity is still very critical for VLBI astrometry of radio counterpart of optically bright quasi stellar objects.
- Connection of radio-planetary dynamic reference frames: differential VLBI observations of a planetary spacecraft and nearby reference radio sources are required to measure their position offset with very high accuracy.

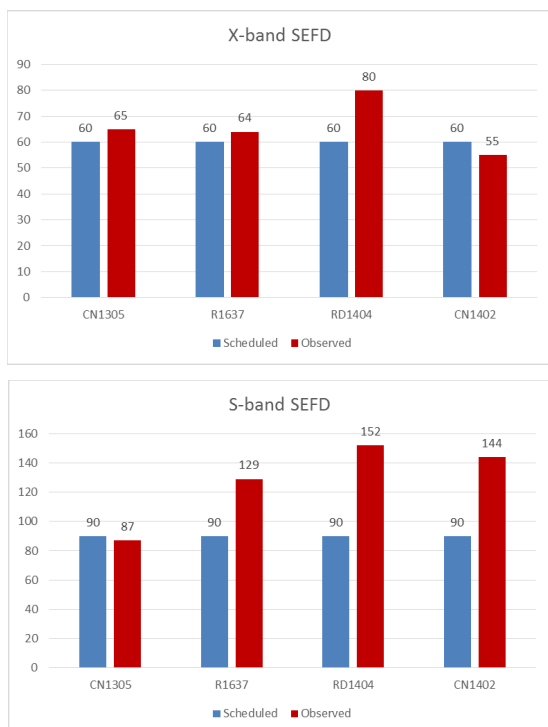
It should be figured out that for differential VLBI observations of spacecrafts, such as phase referencing observations and Δ DOR (Delta Differential One-way Ranging) observations, accurate station coordinates are required. As a result, all these work are relying on geodetic/astrometric VLBI technique.

In 2013, we began to make a number of fringe tests for Tianma65 at S/X dual band. The first geodetic session using Tianma65 was successfully performed in November 2013. After that, additional fringe tests were focused on wide X band (8200–9000 MHz) and S band frequency setup, and finally we got fringes of all IF channels in April 2014, hence Tianma65 was tagged along to its first IVS session R1637 in May 2013. Since then, 2 more sessions have been carried out. Details about these sessions are summarized in Table 2.

The Chinese domestic sessions CN1305 and CN1402 were processed at Shanghai correlator, and the other sessions were processed by other IVS correlators. The SEFD estimations were derived from observed baseline SNR. Fig. 1 shows the observed SEFDs compared to scheduled SEFDs at X and S bands. According to the original design goal, the SEFD should be 48 Jy at X-band and 46 Jy at S-band. Considering the effect of antenna gain curve and S-band RFI, the estimated results look reasonable and reflect the antenna performance. As a comparison,

Table 2 Summary of 4 geodetic sessions using Tianma65.

Session	Date (yyyy-mm-dd)	Start UT (hh:mm)	Stations	Data rate (Mbps)	Channels	Sampling (bits)
CN1305	2013-11-21	13:00	ShKmUrT6	256	16	1
R1637	2014-05-27	17:00	FtHbHtKeKkNyShT6TcTsWfWzYg	256	16	1
RD1404	2014-06-11	18:00	HtKbKkMaNyT6Wz	512	16	2
CN1402	2014-10-18	07:00	ShKmUrT6	256	16	1

**Fig. 1** Scheduled and estimated SEFDs of Tianma65 in the first 4 geodetic sessions.

from the IVS website we can find the SEFD is about 25 Jy at X-band and 100 Jy at S-band for Effelsberg 100-m radio telescope, while the SEFD is about 150 Jy at both of X and S bands for Parkes 64-m radio telescope.

There is one session RD1404 dedicated to the observation of 24 GAIA transfer sources in category 4 (Le Bail et al., 2015). These sources are mostly weak sources with large position uncertainties. As shown in Fig. 2, there are 13 sources with estimated flux lower than 0.1 Jy, and only one source 2135-184 was not detected. It exhibited the advantage of high sensitivity antennas, compared with lower detection rate in any other similar R&D sessions without Tianma65. As shown

Table 3 Statistics on the total number of successful observations.

	Source number	Total obs. without T6	Total obs. with T6	Rate of increase
GAIA4 sources	24	560	891	59%
Other sources	18	402	465	16%

in Table 3, Tianma65 (T6) can also increase the total number of observations of weak sources. In RD1404, the total number of successful observations of GAIA4 sources was increased 59% with addition of Tianma65.

4 Discussion

There was an unexpected maintenance for Tianma65 from November 2014 due to antenna elevation driving problem, and it lasted up to 6 months. After that, the first astrometric session participated by Tianma65 is AOV003 in May 2015 which also includes Parkes 64-m radio telescope. The following 5 sessions in 2015 are IVS-R&D and IVS-CRF series which are dedicated to VLBI astrometry of GAIA transfer sources and regular monitoring of astrometric sources respectively.

One important factor to limit the use of Tianma65 is the percentage of antenna slew time. There is a strong concern that the frequent slew in a wide range will shorten the lifetime of the big antenna. Table 4 is a list of antenna slew time for Tianma65. It is not typical in R1637 because Tianma65 is in tag-along mode. The SNR threshold was increased and the maximum angle between consecutive scans was reduced for Tianma65 in RD1504 so that its slew time was controlled to be less than 40%, while the total scan number was decreased and observing time was increased. This is a tradeoff between observing efficiency and antenna slew time.

In recent years, more and more stations began to install digital backend for data acquisition. Compared with the aged analog system, the new digital system

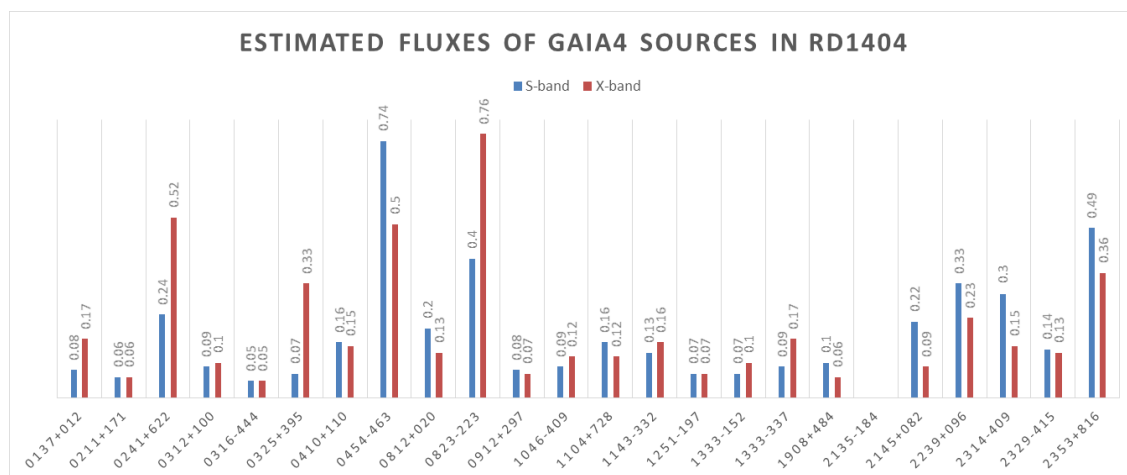


Fig. 2 Estimated fluxes of 24 GAIA4 sources in RD1404 session

Table 4 Statistics on the antenna slew time percentage of Tianma65.

Session	Scan No.	Observing time	Slew time
CN1305	290	51%	31%
R1637	143	5%	27%
RD1404	299	16%	63%
CN1402	373	26%	51%
AOV003	277	20%	48%
RD1504	235	30%	39%

has better bandpass and wider bandwidth which allow more weak sources to be detected and measured by a VLBI network with improved sensitivity. Recognizing this opportunity, we are observing 7016 objects which are brighter than 50 mJy at the 5 GHz from the PMN and GB6 catalogues that have not yet been observed with VLBI. The observing program is performed at X-band and 2 Gbps data rate, with participation of Chinese VLBI stations: Seshan25, Kunming and Urumqi, and several international stations that join on ad hoc basis. Since we are observing in the survey mode at the 3–4 station network, the position accuracy is only 3–7 mas. The next step is to improve position accuracy of those detected sources down to 0.3 mas level which require observations at S/X dual band with a much larger network. Hence Tianma65 can play an important role for improving the array sensitivity.

5 Conclusions

Tianma65 has been operational for absolute astrometric VLBI with expected performance. The 1 or 2 Gbps data rate recording mode provided by digital backends can help to form a more sensitive network than before. With participation of Tianma65, such a network will contribute more to improving celestial reference frames. However, Tianma65 is not suitable for frequent slew intensively due to its huge weight, and its observing time will be limited due to many competitive scientific proposals. How to best use of Tianma65 for VLBI astrometry is still a topic of discussion.

Acknowledgements

The work is supported by the National Natural Science Foundation of China (U1331205).

References

- Bail K, Gordon D, Gipson J, MacMillan D (2015) Observing Gaia transfer sources in R&D and RDV sessions. In: R. Haas, F. Colomer (eds.), *Proc. 22nd EVGA Working Meeting*, 277–280.
- Xia B, Shen Z, Liu Q (2015) Shanghai Station Report for 2014. In: K. D. Baver, D. Behrend, K. L. Armstrong (eds.), *IVS 2014 Annual Report*, NASA/TP-2015-217532, 106–108.

Russian Radio Interferometer of New Generation

A. Ipatov, D. Ivanov, G. Ilin, V. Olifirov, V. Mardyshkin, I. Surkis, L. Fedotov, I. Gayazov, V. Stempkovsky, Y. Bondarenko

Abstract The Radio Interferometer of new generation, created in the Institute of Applied Astronomy at the stations of "Quasar" VLBI network is considered. Currently this new Radio Interferometer consists of two antennas with a mirror diameter of 13.2-m installed at the Badary and Zelenchukskaya observatories. All installation works of the antenna systems were finished by the end of 2014. Antenna control system and sub-reflector were successfully tested. Tri-band Receiving System was installed on the antennas of the Radio Interferometer. The first observations of calibration radio sources were carried out. Processing and analysis of newly obtained data showed that the Radio Interferometer of new generation allows to operate as a part of the International and European VLBI networks.

Keywords VLBI, VGOS, Radio Telescope, EOP

1 "Quasar" VLBI Network

Radio Interferometer of new generation was created on the basis of the "Quasar" VLBI network. The network consists of three radio astronomical observatories: Svetloe near St. Petersburg, Badary in Eastern Siberia and Zelenchukskaya in the North Caucasus connected with the Data Processing Center in St. Petersburg by optical fiber lines with 1 Gbps average data transfer rate. Each observatory equipped with at least three co-located instruments of different techniques:

Alexander Ipatov, Dmitry Ivanov, Gennady Ilin, Valery Olifirov, Vyacheslav Mardyshkin, Igor Surkis, Leonid Fedotov, Iskandar Gayazov, Viktor Stempkovsky, Yuri Bondarenko
Institute of Applied Astronomy of RAS

VLBI, SLR, combined GNSS receivers and DORIS system (Ipatov et al., 2014). The main instrument in each of three observatories is a 32-m radio telescope, which provides a completely automatic process of observing the radio sources and satellites. Observations can be carried out both in radiometric and in radio interferometric mode. Satellite laser ranging systems have been installed in 2011 to obtain high-precision range and angular coordinates of geodetic and navigation satellites. All of the observatories are equipped with the identical hydrogen Time Standards, Water Vapor Radiometers and meteorological stations which are used when carrying out all types of observations.

State program of "Quasar" VLBI network modernization started in 2012. The aim of modernization was to develop a multi-band fast rotating 13.2-m Antenna System (RT-13) for determination the Earth rotation parameters (ERP), to improve the accuracy, reliability and efficiency of providing the ERP data to consumers in the Russian Federation and abroad. The Antenna System is designed to operate as a part of "Quasar" and international VLBI networks. Installation of two RT-13 Radio Telescopes in Zelenchukskaya and Badary observatories has been successfully completed in 2015.

2 Antenna System of RT-13

Table 1 presents some specifications of the RT-13 Antenna System, which meet all requirements of the VGOS program. The manufacturer of the antenna is the German company Vertex Antennentechnik GmbH. The mirror system is based on the paraboloid scheme with the shifted focal axis (Ringfocus). The support-rotary mechanism is constructed according to

Table 1 Specifications of RT-13.

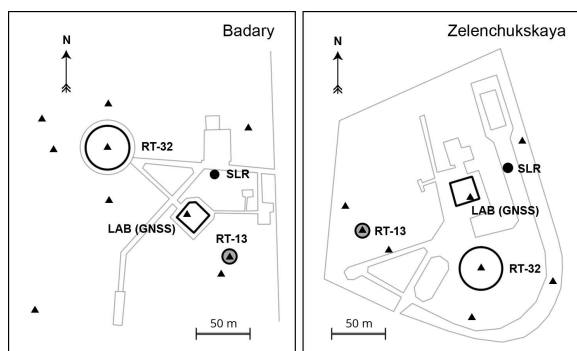
Main mirror diameter	13.2 m
Mount	alt-azimuth
Subreflector scheme	Ringfocus
Subreflector Mount	Hexapod
Azimuth speed	12 °/s
Elevation speed	6 °/s
Limits by Az	±270°
Limits by El	0° – 110°
Operation	24 h/7d
Tracking accuracy	±15 arcsec
Surface accuracy (RMS)	0.3 – 0.1 mm
Frequency range	2-40 GHz
The surface efficiency	> 0.7
Polarization	LCP + RCP
Ambient temperature	–20 °C to +35 °C
Humidity	up to 100 %
Snow load	100 kg/m ²
Wind velocity	50 m/s

the classical two-axial scheme with the vertical axis of azimuth and horizontal axis of elevation (alt-azimuth mount). The RT-13 Antenna System should operate and maintain all of its characteristics when the ambient temperature changes from –20 °C to +35 °C.

3 Location of RT-13

Figure 1 depicts the location of the new RT-13 Antenna System at the Badary and Zelenchukskaya observatories relative to other objects such as the GNSS receiver on the laboratory building, the 32-m radio telescope (RT-32), the satellite laser ranging system (SLR) and the local geodetic network markers. The location of RT-13 was chosen with a number of requirements:

- Minimum elevation angles;
- Convenient connection to the existing engineering networks;
- Cross-sections of local geodetic networks;
- Availability of sufficient areas for the construction of access roads and platforms (for installation work);
- The minimal impact on the instruments and landscaping of the observatory;
- Schedule of observations.

**Fig. 1** Badary and Zelenchukskaya observatories' site maps.

4 Construction Stages

The construction of the antenna tower began in July 2013 at the Badary and Zelenchukskaya observatories simultaneously. Concrete pouring into the prepared formwork of the RT-13 tower in Badary is shown in Fig. 2. At the same time the metal components of radio telescopes such as frames, aluminum reflecting panels and receiver cabins were created, assembled, tested and disassembled at the factory in Italy.

The parts of radio telescope have been delivered from Italy by sea to Novorossiysk (Russian's main port on the Black Sea), and then by trucks to the Eastern Siberia and North Caucasus. The delivery began in the winter 2014. This time of year was chosen on purpose. The problem was that in the Eastern part of Russia there are no special roads for transportation of such huge objects, and in that case we use so-called "win-

**Fig. 2** Antenna tower construction.



Fig. 3 On-site installation works.

ter road” (road on the snow). Another problem was the existing bridge on the nearby to the Badary observatory river. Its maximum load is not suitable for the trucks, so we built the ice bridge in a hundred meters from the existing.

Figure 3 depicts the final assembling of the RT-13 in the Badary observatory in February 2014. The installation of the Antenna System in Zelenchukskaya observatory has been finished two months later.

Photogrammetric measurements of the reflective surface were carried out after all installation works (see Fig. 4). The obtained values of the main mirror accuracy are shown in Tab. 2.



Fig. 4 Photogrammetric measurement of reflective surface.

Table 2 Photogrammetric measurement results.

Elevation (°)	RMS (μm)	
	Badary	Zelenchukskaya
58	57	53
0	151	142
90	132	130

5 Tri-band Receiving System

The tri-band Receiving System provides signal amplification in S, X and Ka frequency bands in both circular polarizations. All receiver units are placed in the focal container which is installed in the secondary focus of the RT-13. The tri-band feed and low-noise-amplifiers are installed inside the cryogenic module and cooled to the temperature of liquid hydrogen (20 K). Figure 5 shows the installation of noise load for calibration of Receiving System. First results of Receiving System on-site measurements at Badary observatory at 60° elevation are listed in Tab. 3.



Fig. 5 Calibration of Receiving System.

Table 3 Receiving System parameters at 60°.

Band	S (13 cm)	X (3.5 cm)	Ka (1 cm)
Frequency (GHz)	2.2 - 2.6	7.0 - 9.5	28.0 - 34.0
Polarization	RCP + LCP		
T _{sys} (K)	35	25	70
SEFD (Jy)	1000	670	2100
Surface efficiency	0.7	0.8	0.7

6 Digital Backend System

The Broadband data Acquisition System (BRAS) is the digital backend of the RT-13 installed in the telescope focal cabin (see Fig. 6). BRAS consist of eight 512 MHz channels. Each channel has a separate 10 G Ethernet fiber link for transmitting the output two-bit (or 8-bit) data stream of international VDIF format. The total data rate for the 2-bit sample at the system output is 16 Gbps (see Tab. 4). The system has built-in controls and diagnostics (Nosov et al., 2014).



Fig. 6 The Broadband data Acquisition System.

Table 4 BRAS specifications.

Number of channel	8
Intermediate frequency	1024 - 1536 MHz
Channel bandwidth	512 MHz
ADC	8 bits, $F_s=1024$ MHz
Output samples width	2/8 bits
Data frames format	VDIF
Total output data rate	16 Gbps
Location	Focal cabin

7 Time and Frequency Synchronization System

The Time and Frequency Synchronization System provides transmission of high stable reference time and

frequency signals to the focal cabin of the RT-13. The Reference 100 MHz frequency generator transfers the reference frequency to the radio telescope by optical fiber lines. A phase stabilization scheme is used for compensation of phase fluctuations due to the antenna rotation. The time synchronization unit provides time delay measurement and compensation in transmission lines. All components of the system are placed into thermostabilized boxes.

8 Data Recording and Transmitting System

Table 5 outlines parameters of Data Recording System which is installed on each RT-13 Antenna System in Badary and Zelenchukskaya observatories. The system is able to register eight streams with the total data rate of up to 16 Gbps. It transfer data to Data Processing Center in St. Petersburg with up to 2 Gbps data rate. It is able to buffer data from up to 5 hour session.

Table 5 Data Recording System parameters.

Number of data streams	8
Total data recording rate	16 Gbps
Data transfer rate to DPC	0,4 - 2 Gbps
Data storage	20 TB (4-5 1h sessions)
Data format	VDIF

9 Software Correlator

Figure 7 shows the new Software Correlator which was developed at the Institute of Applied Astronomy and installed in Data Processing Center in St. Petersburg (Ken et al., 2015). The near-real time correlator can process up to 16 Gb/s data stream from each of up to 6 VGOS stations. VLBI data are recorded from 4 frequency bands with bandwidth of up to 1024 MHz in one circular polarization or up to 512 MHz in two linear polarizations using 2-bit sampling. The input data format is VDIF. The correlator computes cross-spectra with resolution of 4096 spectral channels and extracts 32 phase calibration tones in each frequency band of each station in near-real time (see Tab. 6).



Fig. 7 High-performance computing cluster in St. Petersburg.

Table 6 Software Correlator parameters.

Number of stations	up to 6
Input data stream	up to 16 Gbps (from each station)
Number of bands	4
Bandwidth	up to 1024 MHz
Input data format	VDIF
Delay (RMS)	10 ps

The correlator's hardware is based on High-performance computing cluster with hybrid blade server technology. It contains 40 blade servers with 2 CPUs Intel E6-5-2670 8-core, 2.6 GHz and 2 GPUs Nvidia Tesla K20. The cluster also includes power supply and power distribution units, 8 cache servers (which are similar to blade servers but having 256 GB RAM and 16x10 GbE optic input), one head (master) server and data storage with capacity of 75 TB, as seen from Tab. 7.

Table 7 High-Performance Computing Cluster parameters.

Hybrid-blade server	40
CPU	2×(Intel E5-2670, 8-core, 2.6 GHz)
GPU	2×(NVIDIA Tesla K20)
RAM	64 - 256 GB
Data storage	75 TB
Ethernet	16*10 Gbps

10 Conclusions

The inauguration of the new Russian Radio Interferometer was held during the EVGA-2015 meeting. After the inauguration joint radio observations with a 13-m VGOS radio telescopes in Wettzell and Yebes observatories were carried out in real-time. A few hours after the experiment the fringes in S/X bands were obtained.



Fig. 8 RT-13 in "Zelenchukskaya" and "Badary" observatories.

References

- Ipatov A, Gayazov I, Smolentsev S, Ivanov D, Ilin G, Shuygina N, Bondarenko Y (2014) Co-location of Space Geodetic Techniques at the "Quasar" VLBI Network Observatories. In: D. Behrend, K. D. Baver, K. L. Armstrong (eds.), *IVS 2014 General Meeting Proc.*, Science Press (Beijing), 173–177.
- Nosov E, Berdnikov A, Grenkov S, Marshalov D, Melnikov A, Fedotov L (2014) Current Development State of the Russian VLBI Broadband Acquisition System. In: D. Behrend, K. D. Baver, K. L. Armstrong (eds.), *IVS 2014 General Meeting Proc.*, Science Press (Beijing), 82–85.
- Ken V, Kurdubova Y, Mishina N, Mishin V, Shantyr V, Surkis I (2015) IAA VGOS GPU-based software correlator: current status and broadband processing. In: R. Haas, F. Colomer (eds.), *Proc. 22nd EVGA Working Meeting*, 40–42.

Status report on the GGAO-Westford VGOS systems

A. E. Niell

Abstract In this article we describe the VGOS broadband signal chain as installed on the GGAO 12m and Westford 18m antennas and present a preliminary analysis of a set of approximately bi-weekly observations, called the VGOS Demonstration Series.

Keywords VGOS, VLBI2010, VLBI, Geodesy

1 Introduction

The broadband instrumentation for the next generation geodetic VLBI system, previously called VLBI2010 but now referred to as VGOS (for VLBI2010 Global Observing System), has been implemented on a new 12m antenna at Goddard Space Flight Center near Washington, D.C., and on the Westford 18m antenna at Haystack Observatory near Boston, Massachusetts, USA. In 2012 October the first geodetic observing sessions were conducted using the broadband system, and in 2013 May a twenty-four hour session yielded measurements of correlated flux densities as well as estimation of geodetic parameters. Results from these sessions were described in IVS Annual Reports (Niell et al., 2012, 2014).

The features of the VGOS system as implemented on the GGAO12M and Westford antennas are repeated here for reference:

- four bands of 512 MHz each, rather than the two (S and X) for the Mark4 systems

Arthur E. Niell
MIT Haystack Observatory, Off Route 40, Westford, MA, 01886,
USA

- dual linear polarization in all bands
- multitone phasecal delay for every channel in both polarizations
- group delay estimation from the full spanned bandwidth (3.0 GHz to approximately 10.5 GHz)
- simultaneous estimation of the group delay and the total electron content difference (dTEC) between sites using the phases across all four bands.

In late 2014 a series of bi-weekly one-hour sessions, called VGOS Demonstration Series (VDS), was initiated in order to bring the observations to operational capability. The emphasis has been on completion of Field System control of all equipment, evaluation of the equipment for sustained operation, and development of the procedures for minimum personnel interaction. Each of these leads toward the goal of unattended operation.

A major difference between the broadband systems and the legacy S/X systems is the use of both linear polarizations rather than one circular polarization. The method for accounting for differences between the electrical paths of the two linear polarizations was improved as a result of obtaining a series of observations.

In the following sections the current status of the broadband signal chain and data analysis are described and preliminary results from the VDS sessions are discussed.

2 Broadband instrumentation and configuration

Several improvements were made to the instrumentation in 2013 and 2014. In the Westford front end (De-

war and post-Dewar electronics) the Monitor and Control instrumentation was rebuilt to provide more reliable and versatile functionality. However, the most significant changes were the upgrade of the digital backends from RDBE-H (real samples, Mark5B format) to the RDBE-G (complex samples, vdif format). Internally the RDBEs were improved by the replacement of both the NRAO synthesizer and the attenuator assembly with, respectively, a much simpler Haystack-designed synthesizer and with commercial attenuators. The RDBE-G also has a new personality (fpga3.0) that incorporates noise diode control; internal time-comparison of the GPS, maser, and RDBE 1 pps ticks; and pulse cal extraction. Equally significant, recording is now to a single Mark6 instead of to four Mark5Cs.

The current configuration of the broadband signal chain is shown in Figure 1.

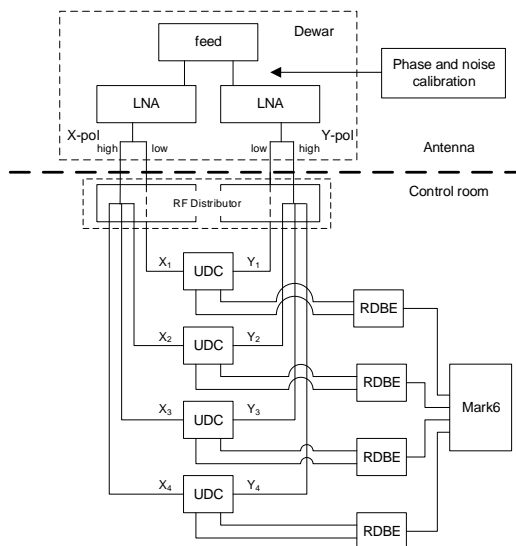


Fig. 1 Broadband signal chain configuration for GGAO 12m and Westford antennas.

One goal of the broadband design is simultaneous observation with the legacy S/X systems at 2.3 GHz and 8-9 GHz. However, it was anticipated that the radio frequency interference (RFI) at S-band can severely degrade the sensitivity of the systems, and this has been confirmed. As a result, for these observations, and perhaps for future VGOS-only sessions, the lower frequency bound was chosen to be 3 GHz. Also, while the goal for the upper frequency of the VGOS ob-

servations is 14 GHz, the GGAO and Westford systems, which are prototypes, are limited by the down-conversion hardware (UDC in Figure 1) to an upper bound of 11 GHz. Taking into account the need to estimate the line-of-sight charged particle dispersion, the optimum band frequencies were calculated by Bill Petrachenko to be centered on approximately 3.3 GHz, 5.5 GHz, 6.6 GHz, and 10.5 GHz.

Each band is approximately 512 MHz wide, set by the firmware capability of the RDBEs. In the RDBE the signal is digitized a polyphase filter bank provides sixteen 32-MHz channels of complex samples which are then quantized to two bits and output in VDIF format. If all channels were recorded, the data rate from each RDBE would be 4 gigabits per second (Gbps) for a total of 16 Gbps from each antenna. However, when the broadband systems were first implemented, each RDBE was fed to a separate Mark5C recorder, and in order to keep the number of recorders down to four, only half of the channels from each RDBE were recorded. (Even though the Mark6 recorder that is now being used is capable of 16 Gbps and the RDBEs are capable of that output, the data rate was maintained at 8 Gbps for the observations reported here.) Initially only the odd channels from each RDBE were selected, but, prior to the beginning of the VDS, the frequency sequence, or ‘frequency’, within each band was changed to using a minimum redundancy sequence, thus improving the delay sensitivity and reducing the sidelobes in the delay resolution function (Rogers, 1970). This is illustrated in Figure 2

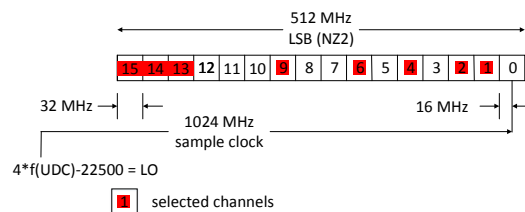


Fig. 2 The frequency configuration and channel selection for the output from one polarization of the RDBE. The sixteen 32-MHz channels generated by the PFB are numbered 0 to 15. The (same) selected channels from each polarization are combined in one VDIF packet for output to the Mark6. Channel 0 is not usable due to the algorithm in the PFB.

3 Broadband observing, correlation, and analysis

The steps for broadband observing and data analysis are a) create the session schedule using *sked*; b) *drudg* the *sked* output at each station and do the observations; c) correlate the data; d) extract the delay and other relevant observables from the correlator output; e) estimate the geodetic parameters. These are the same as for the legacy S/X observations, but modifications or compensation have been required for each step.

a) Scheduling the session

A new section was added to *sked* to allow for the higher data rates of the broadband systems going into a single recorder. Also, since the maximum record rate to a module in the Mark6 is only about 7 Gbps, the use of only one module for 8 Gbps is accomplished by buffering the data. Thus, additional time over the length of a scan is required to empty the buffer, and *sked* was modified to allow for this. This limitation could be alleviated by recording to two modules.

sked uses information at S- and X-band for both the radio sources and each antenna to calculate the minimum scan length to achieve the minimum SNR specified for each band. *sked* has not yet been modified to allow information from all four bands to be used for this objective, so the antenna characteristics at 3 GHz and 10 GHz were used as surrogates for S and X.

b) Observing

For S/X observations the Field System controls the session by setting equipment values, controlling antenna movement, executing calibration procedures, starting and stopping the recorder, and logging all of the relevant actions, queries for status or system values, and calibration data. For the early VDS sessions the Field System controlled only the antenna and the Mark6 and logged a subset of the metadata. Throughout the progression of the sessions this increased to almost full capability.

c) Correlation

During this period it was not possible to play directly from the Mark6 modules into the DiFX correlator. Instead the data were read off of the module and rewritten as four files, one for each band. Initially, each band was then correlated separately, but after the development of a different program to re-format the data, it became possible to correlate all four bands simultaneously. The native output of DiFX must be converted

to another format for ingestion by the following analysis. For geodesy this is done in *difx2mark4*, thus allowing direct input to the HOPS package that was developed for the Mark4 correlator and is used for post-correlation processing of geodetic S/X observations.

d) Post-correlation observable extraction

The program *fourfit* was used to estimate the delay, amplitude, and dTEC for all scans. For the broadband data the application of one existing feature of *fourfit* (multitone phasecal) and two new features (dTEC estimation and coherent polarization combination) are required.

Multitone phasecal: For some time it has been possible to calculate a delay from the multiple phasecal tones present in each channel, but this has not become standard for S/X observations. However, for the broadband data it greatly simplifies resolution of the group delay in each band.

dTEC estimation: The ‘ionosphere correction’ for S/X observations is calculated from the S- and X-band group delays. A modification to *fourfit* has enabled simultaneous estimation of the group delay and dTEC from the broadband phases. (Subsequent to this presentation at the EVGA a further addition was made to *fourfit* to correctly evaluate the uncertainties of the group delay and the dTEC value by taking into account the correlation of the two terms.)

Polarization: After applying this multitone phasecal delay and estimating the dTEC for each polarization for a strong source, the delay and phase differences between the two polarization paths are calculated for each antenna. The differences are thought to arise primarily from the uncalibrated signal path from the feed to the phasecal injection point. These values are then applied to each scan of the session using a recent enhancement of *fourfit* to coherently combine all of the cross-correlation products, HH, VV, HV, and VH, to obtain the amplitude, group delay, and dTEC in order to make use of all of the data (Corey, 2006). From the sessions to date it appears that these polarization differences are constant to a few picoseconds in delay and a few degrees in phase within all sessions and between sessions when no hardware changes are made. (*fourfit* documentation can be found at <http://www.haystack.mit.edu/tech/vlbi/hops.html>.)

After *fourfit* was applied to all scans, the output was transferred to GSFC for creation of a database and incorporation of the meteorological data recorded at each station. The program *dbedit* required modification

to accommodate the delay observable that is already ‘ionosphere corrected’. The calibrated databases were returned to Haystack for geodetic analysis.

e) Geodetic analysis

The geodetic analysis was done for each session separately using the new program *nuSolve* from GSFC. It is being used primarily as a pre-solve filter to determine the parameterization needed for a session when incorporated in a global solution. However, it provides all of the needed operations and modeling useful for inspection, evaluation, and parameterization of the VDS sessions.

For the *nuSolve* analysis, since these were only one-hour sessions, the model parameterization was relatively simple. Only the clock behavior at GGAO, the position of GGAO, and the atmosphere zenith delays and gradients at both stations were estimated. The clocks and atmospheres were modeled as piecewise-linear (PWL) functions using the default constraints from *nuSolve*. The uncertainties for the position components of GGAO are sensitive to the length of the segments of the clocks, zenith wet delays, and gradients. For example, with four segments for the clocks and zenith wet delays (ZWDs) and two segments of atmosphere delay gradient within the one hour session, the uncertainties of GGAO in Up, East, and North are 6.1, 2.5, and 1.6 mm after re-weighting to bring the chi-square per degree of freedom of the delays to 1.0. While the median formal uncertainty for the group delay for the VDS sessions is less than one picosecond (without accounting for the correlation of the group delay and dTEC, which multiplies the uncertainty by a factor of ~ 2.6), the actual scatter is much larger, probably due primarily to un-modeled atmosphere fluctuations. To achieve a chi-square p.d.o.f. of ~ 1 , an additional delay of 5-10 picoseconds must be added quadratically to the formal uncertainty. The post-fit delay residuals for the first VDS session is shown in Figure 3.

The length of the baseline between the two antennas is 601 km, oriented approximately northeast-southwest. The uncertainties for the position of GGAO with 1-1.5 hours of data are 3-7 mm for Up and 1-2 mm for East and North. The RMS scatters in the components are 4, 2, and 2 mm for Up, East, and North, respectively, and in length approximately 2 mm. The residuals of the length estimates for the first eleven sessions are shown in Figure 4.

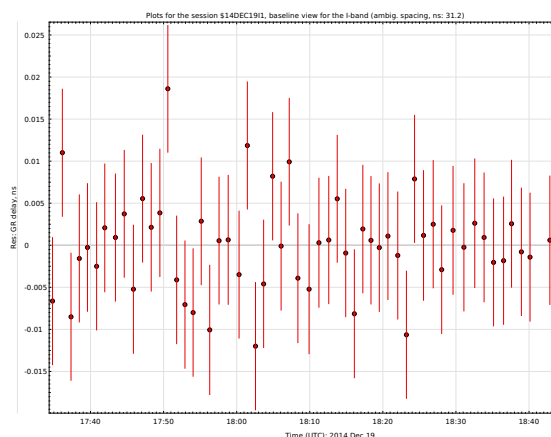


Fig. 3 Group delay residuals for V14353 after re-weighting. The weighted RMS value is 5.6 psec.

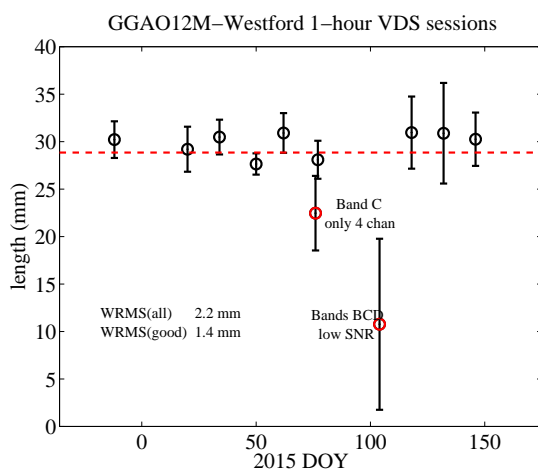


Fig. 4 Length residuals of the first 11 VDS sessions.

4 Needed developments

A shortcoming in the instrumentation at both sites is the lack of delay measurement instrumentation for the cable carrying the 5 MHz reference signal from the maser to the phase calibration generator in the front end. Any variation of delay in this cable would produce an uncorrected variation in the observed delay. If this variation is correlated with antenna position, it may result in an error in the estimated position. The most common problem is for the delay to vary due to cable stretching with motion in elevation or in azimuth (or both). In order to assess the possible magnitude of this effect the multitone phasecal delay was measured while moving each antenna in azimuth and elevation.

The magnitude of this delay was less than 5 picoseconds. For a simple model of delay change with position the resulting error in height due to elevation error or in horizontal position due to azimuth error is likely to be less than 1 mm. Nevertheless this capability will be added as soon as feasible and will be included as part of the signal chain in any future developments.

While not shown in this paper, there is a systematic frequency-dependent distortion of the phase residuals for one polarization, while for the other polarization any such distortion is much smaller. This should have been removed by the phasecal correction. Since the signature remains, and is persistent across sessions, it is likely that the problem is either introduced prior to the phasecal injection or is an artifact in the phasecal phases themselves, perhaps due to reflections in the signal path.

Even with application of the multitone phasecal delay the low-band residual delay differs from the three high-bands by 200 nsec, which corresponds to the ambiguity of the 5 MHz spacing of the phasecal tones. This is thought to be associated with the required *a priori* values for the electrical signal path lengths from the phase cal injection point to the digital back end but has not been resolved.

5 Plans

The plans for observation at the time of this meeting were to continue with the one-hour sessions until the operations were completing successfully under Field System control, and then to increase the duration to six then to 24 hours. Following demonstration of satisfactory performance for 24 hours the observations would migrate to regularly scheduled IVS sessions, incorporating new VGOS-capable stations as they become available.

During this time it is expected that a Mark 3 cable delay measurement system (CDMS) will be installed on Westford, and a new CDMS styled after that for the Kokee 12m will be constructed for GGAO.

6 Acknowledgements

I am reporting the status of the GGAO-Westford VGOS system, but the success is due to the entire Broadband Development group whom I thank for their efforts in constructing, implementing, and operating the systems at GGAO and at Westford and for participating in the testing and observations (in order from funding to building and checkout to observing to correlation to analysis).

- Chopo Ma and John Labrecque of NASA for funding the Proof of Concept development and the GGAO-Westford systems
- Chris Beaudoin, Chris Eckert, Mark Derome for broadband signal chain design and implementation
- Chet Rusczyk, Jason Soohoo, Mike Poirier, Katie Pazamikas, Jay Redmond, Russ McWhirter for observing session setup and operation
- Ed Himwich for antenna checkout for GGAO12M and Westford; Field Station modifications needed for the Broadband system
- John Gipson for *sked* modification
- Mike Titus for correlation
- Brian Corey for station performance analysis and amplitude calibration
- Roger Cappallo for *difx*, *fourfit*, and HOPS modifications
- David Gordon for data base creation
- Sergei Bolotin for *nuSolve* creation and for processing assistance

and special thanks to Bill Petrachenko for his creative ideas and contributions and for his continued encouragement.

References

- Niell A et al. (2012) First Broadband Results with a VLBI2010 System. In: D. Behrend, K. D. Baver (eds.), *IVS 2012 General Meeting Proc.*, NASA/CP-2012-217504, 13–17.
- Niell A E et al. (2014) VGOS Operations and Geodetic Results. In: D. Behrend, K. D. Baver, K. L. Armstrong (eds.), *IVS 2014 General Meeting Proc.*, Science Press (Beijing),
- Rogers A E E (1970) Effective Bandwidth for Phase Delay Measurements. *Radio Sci.*, 1239–1247.
- Corey B E (2006) Notes on antenna polarization and VLBI observables (Prepared for 2006 September 15 VLBI2010 workshop; revised 2012 Jan 11)

Contributions of HartRAO to Space Geodesy, Astrometry and related disciplines

L. Combrinck, R. Botha, P. Mey, A. de Witt, J. Quick

Abstract The Hartebeesthoek Radio Astronomy Observatory (HartRAO), located in South Africa, has been active for several decades in the various fields of space geodesy and astrometry. Within the framework of the VLBI Global Observing System (VGOS), HartRAO has commenced with a project to install a VGOS antenna, which will supplement the existing 26-m and 15-m antennas. We have added geophysical instruments on site and are expanding our activities on Marion Island, Gough Island and Antarctica. In support of the African VLBI Network (AVN), we are part of an international team that will provide training, equipment upgrade and new installations in Africa in support of the AVN and Square Kilometre Array (SKA). We will also increase our support for the RadioAstron VLBI satellite, by including ground control and data downlink capacity. Here we report on progress to date and sketch our plans for the next 3 years.

Keywords AVN, VLBI, SLR, LLR, astrometry, RadioAstron, Marion Island, Gough Island

1 Introduction

The Hartebeesthoek Radio Astronomy Observatory functions as a multidisciplinary scientific node on the southern part of the African continent. It operates within several global international radio astronomy, space geodetic and geophysical networks. The obser-

vatory is geographically strategically placed, therefore plays a significant role in instrumentation and scientific capacity in a region sparsely equipped when compared to other continents; it has also extended its instrumentation to Marion Island, Gough Island and Antarctica and has commenced with the preparation of an observational site at Matjiesfontein. A site for mm radio astronomy is being evaluated in Lesotho; such a site will bring unique observational advantages and collaborative opportunities with Lesotho. The facility participates in a number of internationally driven astronomical and space geodetic experiments within the European VLBI Network (EVN) and the International VLBI Service for Geodesy and Astrometry (IVS) respectively each year, fulfilling an important role in the global science value chain. HartRAO is in the process of increasing its international value through appropriate research infrastructure upgrades and installations in both astrophysics and fundamental astronomy; the facility also actively supports value chain synergistical sciences which feed into Earth and space sciences, effectively taking the products of astronomy to a level where practical spin-offs add societal and economic value. Continued efforts towards international relevance supports the South Africa's strategic objectives of knowledge generation and exploitation, the creation of a globally relevant knowledge infrastructure and through its strategy of combining astronomy, space geodesy and Earth-sciences, creates enabling opportunities which support bridging of research results and socioeconomic issues.

Ludwig Combrinck, Roelf Botha, Philip Mey, Alet de Witt and Jonathan Quick
Hartebeesthoek Radio Astronomy Observatory, PO Box 443, Krugersdorp, 1740, South Africa.

2 Research Infrastructure

Currently the 26 m antenna is available for single dish surveys/monitoring (astrophysical masers, pulsars and active galactic nuclei) and astrometric and astronomical VLBI experiments (EVN, JIVE, IVS); the 15 m antenna is utilized for Earth Orientation Parameters (EOP, within the IVS and IERS) work. A new antenna is being constructed (VLBI for the Global Geodetic Observing System; VGOS) with expected completion during 2017/18. A network of Global Navigation Satellite Systems (GNSS) receivers produces data available for access at HartRAO and global data centres; in addition tide gauge data from Gough Island and Marion Island are available. A collaborative network of seismometers, accelerometers and gravity sensors are also being installed to facilitate research on the interaction of the reference frames and the Earth. HartRAO hosts the NASA Satellite Laser Ranging (SLR) MOBLAS-6, the satellite tracking schedule is set by the International Laser Ranging Service (ILRS) and data are available at global data centres. To support Lunar Laser Ranging (LLR) and deep space laser ranging experiments, HartRAO is developing an LLR in collaboration with NASA and the Observatoire de la Côte d'Azur (OCA) (Combrinck, 2011). Completion of the LLR is expected during 2017, whereupon it will be moved to Matjiesfontein, where HartRAO is developing an outstation. New developments include negotiations with the Russian Federation towards the installation of a modern SLR system at HartRAO, which will allow accurate orbit determination of Glonass satellites as well as participate in ILRS targets. HartRAO has also started the process of refurbishing an 18-m diameter dish at the adjacent Telkom site in collaboration with Roscosmos (Russian Space Agency). This antenna will be used for command and control purposes of RadioAstron. HartRAO already participates in the VLBI science component of the RadioAstron mission.

3 Research Platforms

The research platforms (different instruments) and their development, upgrades, diversity (multi-wavelength, multidisciplinary) and expansion (increased numbers, geographical distribution) are

closely linked to our strategic objectives. In general the combination of all activities has as objective the provision of an international standard research platform which supports internal and external researchers (including students) in radio astronomy, fundamental astronomy (astrometry) and space geodesy. These research platforms are synergistically interlinked, fulfil an important geographic role, as network geometry (and the science output) is improved markedly (cf. Mayer et al. (2014)). Related engineering and technical development as well as niche areas linked into geophysics, atmosphere, are synergistically linked where appropriate. The objectives are to conduct and support observational research with the radio telescopes and other instruments, including:

1. Astronomical VLBI with international VLBI networks for high resolution imaging of radio sources.
2. Astrometric VLBI to maintain and extend the International Celestial Reference Frame (ICRF); establish precise location of sources in multi-wavelength astronomy, annual parallax determination for distance determination, proper motion measurement and phase referencing sources for VLBI.
3. Geodetic VLBI to measure the changing position of the antenna as it responds to effects such as crustal dynamics, International Terrestrial Reference Frame (ITRF) purposes; EOP (precession, nutation, UT1); to provide absolute reference points and ties between collocated geodetic instruments to act as constraints in global solutions using different techniques and as control point for the geodetic survey system of SA (Hartebeesthoek94 datum).
4. Planetary Radio Interferometric and Doppler Experiments (PRIDE) of spacecraft within the solar system in support of various space missions investigating both the gravitational pull on and other accelerations of the spacecraft and the plasma variations of the interplanetary medium along the line of sight towards it.
5. Single-dish radio astronomical observing using the techniques of radiometry, spectroscopy and pulsar timing.
6. Assist with the development of other radio telescopes for research, including C-Band All Sky Survey (C-BASS) South, Karoo Array Telescope-7 (KAT-7), MeerKAT and the AVN.

7. Collaborate in or support multi-wavelength astronomy e.g. observations relating to the High Energy Stereoscopic System (HESS) II gamma-ray telescope in Namibia, Fermi-LAT Large Area Telescope orbiting gamma-ray telescope, the Southern African Large Telescope (SALT) and others.
8. Range to selected satellites for the ILRS, using the NASA MOBILE LASER RANGER (MOBLAS-6) Satellite Laser Ranger (SLR). These satellites are used for precise positioning and navigation, determining Earth's gravity field, the height above sea level of the Earth's topography and sea surface and its changes (e.g. global warming).
9. Install and operate GNSS receivers and geophysical equipment at various locations across Southern Africa, islands off Africa, and Antarctica, for the IGS, in support of the International Terrestrial Reference Frame (ITRF), African Geodetic Reference Frame (AFREF) development and for other research purposes.
10. Install and operate tide gauges co-located with GNSS receivers for research into sea-level change and for tsunami warning.
11. Support local and international research in all the above fields.
12. Support science advancement and human capital development through tertiary level student training, study for higher degrees, projects, practicals, in-service training and outreach to school level learners, educators and the public at large.
13. The establishment of a multi-technique (geodetic VLBI, SLR, GPS) analysis and correlator centre at HartRAO in collaboration with UCT is in progress. A Dell cluster has been made available by the Centre for High Performance Computing (CHPC) to facilitate this initiative.

4 Astrometric VLBI

Our long-term strategy (to 2019+) includes densifying the Southern Hemisphere sky with reference sources for VLBI (Basu et al., 2015), the realization of the next generation ICRF (ICRF-3) and accurately matching the radio positions of Active Galactic Nuclei (AGN) radio reference sources, especially in the south, to future optical catalogues such as those to be produced by the

GAIA optical astrometry satellite that was launched in 2013. Astrometric VLBI Projects include:

1. HartRAO has taken part in the LBA calibrator survey (LCS), an ongoing VLBI project to observe a list of candidate AGN reference sources in the south at 8.4 GHz.
2. Multi-epoch imaging of southern AGN reference sources observed through existing astrometric sessions of the CRDS (Celestial Reference Frame Deep South) campaign of the IVS. These images will be used to monitor source structure of southern ICRF sources and to correct observations for source structure thereby allowing improved astrometric and geodetic results.
3. HartRAO is part of an international collaboration to observe Southern Hemisphere extra-galactic radio sources at 22 GHz. The aim of this project is to densify the ICRF at that frequency and to provide calibrators for astronomy. Both imaging and astrometric observations are in progress using the LBA in the south and the VLBA in the north.
4. A search for suitable calibrator sources at lower frequencies (1.4 -1.7 GHz) in the Southern Hemisphere. Calibrator sources will be needed for astrometric VLBI at lower frequencies, which is a requirement for a number of high-priority science goals, e.g. obtaining trigonometric parallax distances to pulsars and circumstellar OH (1665 and 1667 MHz) masers and in preparation for the SKA.
5. For consistency between optical and radio positions it will be essential to align the Gaia and VLBI frames with the highest accuracy. A dedicated program has been developed towards finding the most compact sources on VLBI scales that are also bright at optical wavelengths in the North and we are extending these efforts to the south.
6. HartRAO is involved in a collaborative project with a group at the University of Tasmania to study the effect of AGN source structure and core-shift on astrometric and geodetic observations.
7. The use of small optical telescopes (<1 m) for optical astrometry is being investigated as a tool to increase the number of astrometric observations of asteroids, planets (and their moons) and comets for precise ephemeris purposes. Accurate and long-term time series are important for high accuracy ephemerides, this project will link into our ICRF, LLR and planetary orbital integrator projects. The

1 m optical telescope in development for LLR purposes will be considered for certain astrometric work, although a dedicated refractor telescope is part of a longer term plan.

5 Geodetic VLBI

Participation in the IVS networks for Astrometry and EOP will be increased to 30 (on the 26 m) and 100+ (on the 15 m) sessions per year, with emphasis on Southern Hemisphere sources in collaboration with the Australian 'AuScope' array. The 15 m antenna is used for EOP observations. Eventually, the VGOS and 15 m antennas will be used to observe separate sources simultaneously; this will increase the number of sources observed. These networks maintain and improve the ICRF and ITRF and products of the IVS Geodetic networks are essential for modern astronomy. Availability of an additional instrument for geodesy will allow access to niche areas of research, through scheduling the telescope into specific networks. A research group on geodetic VLBI has been established for local processing of geodetic VLBI data. Setting up an IVS analysis centre has started, which will incorporate correlator capacity, with a view towards correlation of the African VLBI Network (AVN) (Loots and Gaylard, 2014) and as a node of the proposed distributed correlator network for VGOS. Geodetic VLBI Projects include:

1. Testing the accuracy of EOP using a 4 station strategic network compared to the full geodetic VLBI network.
2. Continued measurements of the antenna axis offsets and intersections (invariant points) of the HartRAO telescopes using geodetic VLBI data processed with VieVS.
3. A special reference pier has been built to conduct inter-system ties automatically, and to provide offsets between the different antennas, GNSS, SLR and LLR systems. These offsets are required to the 1 mm level for global multi-techniques solutions and combinations, and are important for ITRF maintenance. These solutions are used to determine system dependent scale problems (e.g. VLBI vs. SLR).
4. Special projects e.g. to determine HartRAO antenna positions after the 2014 earthquake, tropospheric measurements at the HartRAO site

from VLBI measurements (compared to GPS data), and investigations of seasonal variations in antenna axis-offset.

5. Investigations to discard references from being scheduled into geodetic VLBI observations, based on source structure as determined from VLBI imaging observations.

6 GNSS and Geophysical equipment

Two additional GNSS stations have been installed (Sept 2015) at Walvisbay and Luderitz (Namibia), in collaboration with the University of Luxembourg. These are collocated with existing tide gauges, and will support long term studies of ocean level changes within the framework of the IGS (TIGA project) and the Permanent Service for Mean Sea Level (PSMSL). Future upgrades to Marion Island and the South African National Antarctica Expedition base (SANAE IV) will include the addition of geophysical equipment; a seismometer has been installed on Marion Island and one is planned for Gough Island. The radar reflector network in Antarctica will be expanded to include the Norwegian Troll base in collaboration with the SA Navy, tide gauges and GNSS units will be installed to improve ocean level monitoring. A GNSS receiver will be collocated with the Ghanian AVN telescope during 2016/17 as part of the AVN collocation programme.

7 International collaboration

Most of HartRAO's scientific projects fall within the sphere of large international networks. These experiments typically resort under the EVN, AT-LBA and the Global Array, and also under the Russian Quasar VLBI network and Korean VLBI Network (KVN). HartRAO operates within the International Association for Geodesy (IAG) services; the IVS, IGS, ILRS, International DORIS Service (IDS) and International Earth Rotation and Reference Systems Service (IERS). Formal collaborative agreements of HartRAO:

1. Member of the European VLBI Network (EVN) since 2011, having been an associate member for the previous ten years; the EVN provides a high

- sensitivity astronomical VLBI platform and access to VLBI expertise.
2. Member of the Board of the Joint Institute for VLBI in Europe (JIVE), who processes EVN VLBI data and provide expertise and support in VLBI research and technology development (now JIVE/ERIC).
 3. HartRAO radio telescopes operate as part of the Australia Telescope Long Baseline Array (AT-LBA) to provide a Southern Hemisphere astronomical VLBI platform.
 4. We provide observing time to the IVS; HartRAO's geographic location in Southern Africa makes it of great value for these functions, and it is a key fiducial station in the global geodetic network, as well as the absolute reference point for the country's survey system.
 5. HartRAO, with the DST and SKA-SA comprise the team developing the African VLBI Network (AVN) with funding from the African Renaissance Fund (ARF) of the Department of International Relations and Cooperation (DIRCO).
 6. We are involved in the training component of the AVN, during 2015-2017, several training sessions in basic astrophysics will be held in targeted countries (Zambia, Kenya, Namibia) utilising a grant from the Newton Fund (UK) and the NRF.
 7. We participate in the ILRS for precise orbit determination of selected satellites through its operation of the NASA MOBLAS-6 SLR.
 8. HartRAO is a contributing organization of the IGS as it supplies data from geodetic-quality GNSS receivers to the IGS, which make the data and derived products freely available.
 9. Continuing support for test satellite receivers for the embryonic European Galileo GNSS constellation will be provided in collaboration with the Deutsches Zentrum für Luft- und Raumfahrt (DLR).
 10. Formal agreements with NASA GSFC and the Jet Propulsion Laboratory (JPL) to host equipment used for space geodesy will continue to be honoured. Our long-term collaboration with NASA GSFC has led to a collaborative development of the LLR laser, with facilitation by NASA to collaborate with the NASA SLR network contractor.
 11. Discussion with Russian collaborators concerning the installation of a Russian SLR system at HartRAO during 2016 is in progress as well as possi-

ble support for an optical space debris and asteroid tracking system.

8 Conclusions

Expansion, modernization and global compatibility as well as relevance will remain key features of our strategy for the foreseeable future. Our activities will be aligned with core objectives of the IVS, JIVE, EVN, IGS, ILRS and other global scientific institutions to assure our international involvement in astronomy, astrometry and space geodesy at an appropriate level. The value of collocated astronomical and geodetic instruments provide unique products for astronomy, astrometry, geodesy and geophysics, with valuable and tangible benefits to society. This synergistic, multidisciplinary approach is undervalued globally and often poorly understood due to the complexity of the integrated networks, instruments and the large number of scientific products. These range from the ICRF to the ITRF via the EOP and a plethora of practical uses within the Earth sciences, astronomy (optical and radio), space sciences, geophysics, global change management, troposphere and ionosphere and fundamental physics to mention but some. It is time for funding and government agencies, scientific review panels and research institutions to break away from the lethargy into which they force science by pretending that the universe is bracketed and demarcated into small blocks of knowledge; it is time to embrace multi-disciplinary instrumentation and techniques, and to exploit the vast richness which comes from synergistic collocation and scientific investigations.

References

- Basu S, De Witt A, Quick J, Bertarini A, Leeuw L (2015) Imaging and study of VLBI reference frame sources in the Southern Hemisphere. *Proc. SAIP2014*, 302–307.
- Combrinck L (2011) Development of a Satellite and Lunar Laser Ranger and its future applications. *Proc. IAC 2011*, IAC-11-A2.1.1, 471–477.
- Loots A, Gaylard M J (2014) Africa prepares for SKA: the African VLBI Network. *Quest*, 10(2), 16–20.
- Mayer D, Böhm J, Combrinck W L, Botai J, Böhm S (2014) Importance of the Hartebeesthoek Radio Astronomy Observatory for the VLBI network. *Acta Geod Geophys*, 49(2), 1–13.

Geodetic Italian VLBI: first tests

M. Stagni, M. Negusini

Abstract First experiments of the Italian VLBI network (VITA) correlated in Bologna have involved the Medicina, Noto and Matera antennas. Although the scientific validity of these tests are yet to be proven, these experiments have served as a benchmark to verify a full, in-house, correlation pipeline, from the scheduling through the software correlation using DiFX to finally generating a geodetic database. A future inclusion of the Sardinia Radio Telescope, when geodetic receivers will be installed, will enhance the capability to plan *ad hoc* observations and strengthen the VITA network to become a basis for the definition of the national datum.

Keywords Italian VLBI network, software correlation.

1 Introduction

Since the installation of the DiFX software correlator by Deller et al. (2011) in 2012 there has been a growing interest in correlating and processing geodetic experiments in Italy. The pipeline for processing this kind of data has not been straightforward, particularly in the preparation of an observing schedule using the GSFC SKED Package (http://vlbi.gsfc.nasa.gov/software/_sked.htm) and gaining the skills to post-process data using the tools provided by the Haystack Observatory HOPS software (<http://www.haystack.mit.edu/tech/vlbi/hops.html>).

Matteo Stagni, Monia Negusini
IRA - INAF, Via Gobetti 101, 40129 Bologna, Italy



Fig. 1 Italian baselines - shortest 500 km - longest 900 km.

At present, the antennas involved in the experiments are Medicina, Noto and Matera. Each of them has different setup and available backends (see Table 1), including the newly acquired dBBC backends, which require manual editing of the vex files to ensure that the recorded data could be correlated. The fourth Italian antenna, the Sardinia Radio Telescope (SRT),

Table 1 VLBI setup for Italian stations.

Station	Backend	Recorder	Network
Medicina	dBBC	Mark5C	10 Gbit
Noto	dBBC	Mark5B	10 Gbit
Matera	VLBA	Mark5B	512 Mbit
SRT	dBBC	Mark5C	-

which owns state-of-the-art receivers and backends, including an active surface, has not planned to acquire standard geodetic S/X receivers yet, so it was not involved in this series of preliminary tests.

2 Correlation pipeline

All correlations were performed with DiFX correlation software installed in Bologna. The cluster architecture chosen to perform the correlation duties is composed of three storage and computational machines, and a software dedicated node. All the three aforementioned machines have the storage capacity of 50 TB composed by a 20 TB SATA disks RAID5 array and 30 TB SAS disks RAID5 array (see Table 2). Moreover, each node has a 10 Gbit network card and a dedicated 40 Gbit InfiniBand board for local interconnect. The aim of this architecture is to use each node for recording capabilities when not correlating data, avoiding the use and shipping of disk packs from the stations. The newly acquired dBBC backends have the possibility to stream data through the network at a peak velocity of 4 Gbit/s when coupled with a Fila10 G board, that acts as a formatter which encapsulates the data samples either in Mark5B mode or in VDIF mode. In these tests all the data were recoded using Mark5B or Mark5C at the stations, for safety, and subsequently sent through network connections to Bologna but, as numerous tests have proven, there is the possibility to directly stream and record data at the correlation facilities, in Bologna. Once data have been sent to the correlator, it was a matter of hours to perform fringe finding tasks and start the correlation process. For a classical 24-hours experiment, involving three antennas, it takes approximately 10 hours to process all the data. To make available database products for analysis some more time is required to process the correlation raw output into MarkIV file format and then finally to MarkIII database files getting rid of RFIs and correcting phase calibra-

Table 2 Correlator architecture.

Machine	Cores	Storage	Connectivity
tank-mc	8	50 TB	10 Gbit network + 40 Gbit InfiniBand
tank-nt	8	50 TB	10 Gbit network + 40 Gbit InfiniBand
tank-srt	8	50 TB	10 Gbit network + 40 Gbit InfiniBand

tion in affected channels. The data is then ready to be processed by Calc/Solve software (http://vlbi.gsfc.nasa.gov/software/_calc/_solve.htm).

3 Italian VLBI network tests

In November 2013 there was a first short run of test involving the antennas of Medicina, Noto and Matera. It was unsuccessful due to a schedule problem happened in Matera, so it was only possible to correlate Medicina and Noto in this instance. Fringes were found but with no scientific use for a single baseline.

A second test was tried a month later, but this time the first half of the experiment was lost at Noto due to a failure at the recording system. Again a single correlated baseline was not enough to claim any valid scientific results.

The third trial has proven to be successful only in late 2015, though performed in March 2014. The main issue, lastly discovered, was a wrongly described setup in Noto. In fact, the schedule prepared with a not-up-to-date version of SKED still listed Noto as having a VLBA backend, whereas at the station it was decided to switch to the dBBC backend for that test. Retrieving the key information from the field system log, a new correlation process was set up to finally gather valid data for the three baselines.

4 First scientific outputs

The March 2014 experiment (called VI001) was shaped as an IVS standard EUROPE. Starting from the correlator output, the classical analysis steps have been performed: creation of the database with Dbedit, adding *a priori* information regarding sites, sources, models with Calc11, adding weather and cable information with Dbcab and performing group and phase delay ambiguities resolution and data editing with Solve. At the end, a typical solution of

a small network, with 516 used observations for the 24-hours, was achieved with ≈ 60 ps WRMS.

We have planned new observations in 2016, involving the three Italian geodetic antennas, that should be the beginning of a possible routine activity, creating a data set that can be combined with GNSS observations to contribute to the National Geodetic Reference Datum, to the ITRF and to study geophysical phenomena occurring in the Mediterranean area.

Particular care should be taken in the scheduling of the new experiments in order to optimize the number of the usable observations.

These observations will be used to study and plan future experiments in which the time and frequency standards can be given by an optical fiber link, so having a common clock at different VLBI stations.

5 Conclusions

The March 2014 geodetic VLBI test experiment (VI001), which involved the Medicina, Noto and Matera antennas, has proved the feasibility of a successful, in-house, correlation and analysis procedure.

The first tests marked the beginning of a progressive series of experiments planned to verify the validity of distributed time at the stations and the integration with the national GNSS network to contribute to the Geodetic Reference Datum.

A deeper integration of the correlation facilities could be forecasted, as the new VGOS system begins to be deployed and distributed correlation becomes a mean to ease the duties of the principal IVS correlators.

References

- Deller A T, Brisken W F, Phillips C F, Morgan J, Alef W, Cappallo R, Middelberg E, Romney J, Rottmann H, Tingay S J, Wayth R (2011) DiFX-2: A More Flexible, Efficient, Robust, and Powerful Software Correlator. *Pub Astron Soc Pac*, 123(901), 275–287, doi: 10.1086/658907.

A Vision for VGOS Observations and Analysis in 2020

H. Hase, D. Behrend, A. Nothnagel, H. Schuh

Abstract With the VGOS program, the IVS continues to improve its service. In the coming years a modern network of very fast radio telescopes will become available. The prospects of the ambitious VGOS plans lead to a new vision on how the VLBI infrastructure may be used by 2020. In order to take advantage of the new possibilities that the increased data volumes constitute, a new scenario for scheduling, observing, and analyzing VLBI data may shift the VLBI operations from being session-based to being scan-based. Depending on possible upgrades of data transfer and correlation infrastructure, we anticipate to move from an analysis session-by-session to other scenarios which depend on latency requirements of the products. One such scenario is a continuously running analysis, in which new scans are added to filtered solutions one-by-one as soon as they become available in the continuous transfer and correlation process. The utilization of near real-time VLBI data signifies a change of paradigm in the creation of VLBI products.

Keywords VGOS, analysis, continuous VLBI, data stream

Hayo Hase
Bundesamt für Kartographie und Geodäsie
Sackenrieder Str. 25, D-93444 Bad Kötzing, Germany
Dirk Behrend
NVI, Inc.
7257D Hanover Parkway, Greenbelt, MD 20770, USA
Axel Nothnagel
Rheinische Friedrich-Wilhelms Universität Bonn, IGG
Nußallee 17, D-53115 Bonn, Germany
Harald Schuh
GeoForschungsZentrum Potsdam
Telegrafenberg, D-14473 Potsdam, Germany

1 Introduction

For more than four decades of geodetic/astrometric VLBI operation, operators and data analysts got used to think of ‘VLBI sessions.’ A *VLBI session* is a collection of ‘VLBI scans’ over a given time interval (typically 1 hour or 24 hours). A *VLBI scan* is the time period during which a network of stations observes the same source simultaneously. A scan typically consists of several ‘VLBI observables.’ A *VLBI observable* refers to the time delay measurement by a pair of stations forming a single baseline. Hence, a 3-station scan has three observables, while a 4-station scan has six observables.

The current geodetic/astrometric VLBI operation is session-based. The IVS products result from product-tailored VLBI sessions (i.e., R1, R4, T2, CRF, OHIG). Even the Continuous VLBI campaigns (CONTs) were scheduled with daily sessions (to ease the data handling).

With the introduction of the VLBI Global Observing System (VGOS), the new VGOS radio telescope infrastructure is specified to realize continuous VLBI observations, that is 24 hours per day and seven days per week (Tab. 1), with a number of observables finally a factor 10 to 30 higher than currently. To take full advantage of the VGOS concept, there should be a continuous generation of IVS products following the continuous observation (Petrachenko et al. (2014)). In particular the Earth orientation parameters (EOP), and here especially the unique IVS product the Earth’s phase of rotation (represented as $dUT1 = UT1 - UTC$) will benefit from continuous observations. This challenges us on (a) how to organize the future VGOS observations, and (b) how to conduct VGOS data analysis.

This paper develops a vision for changing from ‘VLBI sessions’ to ‘continuous VLBI data streams’,

Table 1 Comparison of legacy VLBI with VGOS observations. Although the first VGOS observations will be session-based, the final goal could be to produce continuous data streams for producing EOP and especially UT1–UTC in a continuous mode.

Legacy system	VGOS system
two bands: X-band (8.1–8.9 GHz) and S-band (2.2–2.35 GHz)	broadband: four bands in the 2.0–14.0 GHz range
session-based	continuous
400 scans/24 h	$\geq 2,880$ scans/24 h

for which scheduling, observing, analysis, and product dissemination may need modifications.

2 Analysis of continuous data streams

VLBI data are traditionally analyzed in a session-based approach. The VLBI session is only correlated when the entire data set is available and then analyzed. The parameter estimation is carried out by several IVS Analysis Centers independently and their results are based on one or more sessions being aggregated. Eventually several independently produced solutions are combined into the official IVS solution.

Using instead a constant stream of VLBI data, i.e., correlating each scan as soon as completed and making the observables available instantly, the analysis concept needs to be adjusted to fully exploit the possibilities of the continuous availability of data. Time critical products could be delivered in increments continuously and as soon as possible. For this to work, an ongoing data processing of continuous data streams has to be envisioned.

For instance, a set of the most recent VLBI observables $s(t)$ from the correlator output data base (vgosDB) will be used for the estimation of time-dependent parameters $p(t)$, most probably together with a large number of prior observables $s(0)$. It is easily understandable that the volume of necessary observations $s(t)$ depends on the lowest possible time resolution of the parameters. As soon as a sufficiently long new set of observables becomes available, a new estimate can be carried out and more recent parameters (e.g., for UT1–UTC) can be disseminated. Depending on the analysis scheme used, the length of the incremental set of observables can be as short as a single scan, e.g., applying Kalman Filter techniques. This analysis technique is comparable to a ‘sliding window’

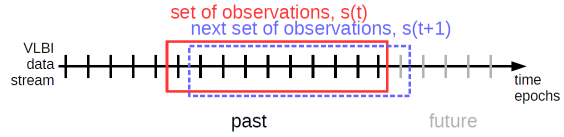


Fig. 1 Sliding window: Example of processing VLBI data streams instead of VLBI sessions. A number of observations (set $s(t)$) is used continuously for parameter estimation, delivering continuously updates of the IVS-products at certain epochs $t, t + 1, \dots, t + n$. The window size can be adjusted to the performance and combined with Kalman-filtering techniques.

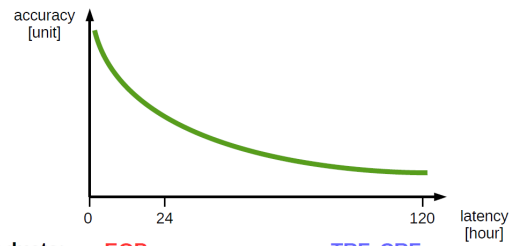


Fig. 2 Relationship latency vs. accuracy. Short latency is important for some EOP users, high accuracy is important for TRF and CRF.

(Fig. 1), although this expression does not explicitly incorporate all the observations to be included from beforehand for establishing the necessary geometric stability of the solution. Application of Kalman filter for VLBI data analysis was suggested by Herring et al. (1990) already three decades ago. A successful realization of a Kalman filter solution as part of the GFZ version of the Vienna VLBI Software (VieVS) was very recently reported by Nilsson et al. (2015) and Soja et al. (2015).

The analysis of VLBI data streams requires a lot of resources. Therefore a closer look at different IVS products shows that different users require different product accuracies, which in itself is related to their latency. Latency is the time interval between the availability of VLBI observables and the availability of the IVS product. Some products like the EOP are requested to be delivered with a short latency, while the TRF or CRF coordinates do not change rapidly and therefore the latency can be larger. This, of course, excludes rapid changes caused by earthquakes. Common practice shows that the accuracy of the products can be improved by allowing some time for the analysts to look into the data and/or using a combination of solutions. These aspects are more complicated to automate and require more time.

In Fig. 2 an approximate relationship between latency and accuracy is depicted for VLBI product creation. In an attempt to discretize this relationship, we foresee new product classes as a function of the latency. Such classes will better satisfy the users' demands and extend the product catalog of the IVS. Up to four classes could be introduced for (1) ultra-rapid, (2) rapid, (3) intermediate, and (4) final products. The first two classes might be of particular importance for any kind of positioning and navigation in near real-time but also with respect to the needs of the EOP Prediction Center at USNO (McCarthy and Luzum, 1991). The expected accuracy is increasing (standard deviations decreasing) with extended latencies (see Tab. 2). Currently, the listed latency periods are only rough estimates and need to be discussed and finalized within the IVS. The feasibility of ultra-rapid result generation for UT1–UTC has already been demonstrated by Haas et al. (2013) and should, thus, not pose any difficulties.

The latency of 5 s or 5 min for time critical EOP products such as UT1–UTC and polar motion mandates that only **one** automated analysis center can provide the official IVS product at a time because there will be no time for the combination of results of multiple analysis centers. However, a constellation of several ACs with a primary and at least one backup and one validation/monitoring analysis center will be needed and should be set up. The latter one should be able to identify gross errors and should intervene and restart the process within a few minutes. Such a constellation needs to be finalized prior to setting up the full VGOS operations.

3 Scheduling of continuous VLBI data streams

The traditional way of scheduling a VLBI session is a semi-automated process, in which sets of stations define the observing network, sets of radio sources define the observing catalog, and optimization tools prospect for the most accurate determination of a set of estimated parameters. The optimization depends on the network constellation and the target of the session. In general, regional networks like the European, the AuScope or the Japanese networks have always been scheduled for precise coordinate determination. Except for the purpose of special-application astrometry and ra-

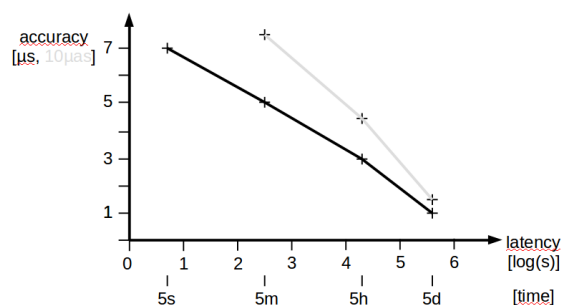


Fig. 3 Accuracy versus latency in IVS EOP products for UT1–UTC (black) and pole and nutation (grey). Low latency products require one reliable automated analysis center.

dio source monitoring, large networks with baselines of more than 4,000 km (or even of global extension) always serve the purpose of determining Earth orientation parameters, station coordinates, and source positions at the same time. All VLBI sessions are scheduled often more than one week prior to the actual observing.

In the context of VGOS with its continuous VLBI observations over twenty-four hours seven days per week, we will mostly run intercontinental networks producing the highest sensitivity for EOP determinations. Here, we will encounter a new scenario for scheduling the observations. The reason for this is that the networks will not run in a fixed constellation for several days, because the workload has to be distributed evenly among the participants and maintenance slots have to be planned for. For this reason, we envisage changes in the networks from day to day or even more frequently.

It is conceivable that the network constellations and the daily schedules could be organized all well in advance. However, considering that the condition for continuous observations is fast data transfer by communication lines to the correlators, we can take advantage of closing instantaneously the feedback loop between station performance (or readiness) and react accordingly by modifying the observing schedules. So, the scheduler will have to operate a changing network configuration depending on the target performance in near real-time. For this purpose, Lovell et al. (2014) proposed a dynamic scheduling in the VGOS era.

Currently the correlation process of one VLBI session is assigned to one correlator. If VLBI data streams become a reality, each individual scan could also be assigned to another correlator. The scheduler will have to take care of the data flow and can react to the traffic

Table 2 Introduction of product classes as a function of latency. The availability of continuous data and near real-time processing allows to satisfy different user needs already before the final solution is being delivered.

Product class	Product epoch	Update interval	Epochs to be updated	Latency	Sub-product	expected accuracy (WRMS)
Ultra-rapid	every 10'	every 10'	$t, t - 10' \dots 50'$	5 s	UT1-UTC	7 μ s
Rapid	every 1h	every 1h	$t, t - 1h \dots 5h$	5 min	UT1-UTC	5 μ s
					x_P, y_P	75 μ as
					nutations offsets	75 μ as
Intermediate	every 6h	every 6h	$t, t - 6h \dots 18h$	5 h	UT1-UTC	3 μ s
					x_P, y_P	45 μ as
					nutations offsets	45 μ as
Final	every 12h UT	every 24h	t	5 days	UT1-UTC	1 μ s
					x_P, y_P	15 μ as
					nutations offsets	15 μ as
					station coordinates	3 mm
					source positions	15 μ as

congestion on the network and at the correlators by assigning the VLBI data stream to an alternative correlator. This will guarantee that no observation will be lost. Therefore, redundancy in the availability of VLBI data correlators should also be foreseen for the processing of VLBI data streams. However, this will be one of the later steps to be realized in the VGOS operations.

4 Conclusions

Continuous VLBI observations may require a change of paradigm how we conduct our VLBI operation. VLBI sessions will be replaced by a never-ending sequence of VLBI observations, which are broadcast by stations that may fade in and out of the VLBI network. The subsequent correlation of individual scans may take place at several correlators (correlator multiplexing). The communication network and correlation loads are limiting factors which may be monitored and controlled by the scheduler, who operates the observing network on the fly and manages the data streams.

At the same time, the analysis of the data may be changed from session-wise products to more frequent product updates, especially for the UT1-UTC parameter. Here, the latency requirements of the users play an important role and need to be identified. To start the discussion, we have devised four different product categories for ultra-rapid, rapid, intermediate, and final products. To make this scenario happen, all impediments need to be identified and removed by good organizational planning. Nearly full automation of schedul-

ing, observing, correlation, and data analysis will become an essential requirement in the future.

References

- Haas R, Kurihara S, Nozawa K, Hobiger T, Lovell J, McCallum J, Quick J (2013) Ultra-rapid EOP determination with VLBI. *Geophys Res Abstr*, 15, EGU2013-8438, EGU General Assembly 2013.
- Herring T, Davis J, Shapiro I (1990) Geodesy by radio interferometry: the application of Kalman Filtering to the analysis of very long baseline interferometry data. *J Geophys Res*, 95 (B8):12561–12581, doi: 10.1029/JB095iB08p12561.
- Lovell J, McCallum J, Shabala S, Planck L, Böhm J, Mayer D, Sun J (2014) Dynamic Observing in the VGOS Era. In D. Behrend, K. D. Baver, and K. L. Armstrong (eds.), *IVS 2014 General Meeting Proc.*, Science Press (Beijing), 43–47.
- McCarthy D, Luzum B (1991) Combination of precise observations of the orientation of the Earth. *Bull Géod*, 65(1):22–27, doi: 10.1007/BF00806339.
- Nilsson T, Soja B, Karbon M, Heinkelmann R, Schuh H (2015) Application of Kalman filtering in VLBI data analysis. *Earth Planets Space*, 67(136), doi: 10.1186/s40623-015-0307-y.
- Petrachenko B, Bertarini A, Alef W, Behrend D, Cappallo R, Hase H, Ma C, Niell A, Nothnagel A, Zhang X (2014) VGOS Data Transmission and Correlation Plan (Version: November 18, 2014). Internal Report, *VGOS Project Executive Group (VPEG)*. ivsc.gsfc.nasa.gov/technology/vgos-docs/VGOS{_}DataTransmissionCorrelation{_}Plan{_}141118.pdf
- Soja B, Nilsson T, Karbon M, Zus F, Dick G, Deng Z, Wickert J, Heinkelmann R, Schuh H (2015). Tropospheric delay determination by Kalman filtering VLBI data. *Earth Planets Space*, 67(144), doi: 10.1186/s40623-015-0293-0.

Practical Uses of VGOSDB Format

J. Gipson

Abstract I demonstrate that using the vgosDB format you can easily answer questions that are difficult or impossible using Mark3DB format. What is the effect of using default values for meteorological data at some station? What is the effect of not applying cable-calibration at some station? Why do Mark3 databases of the same session produced by different institutions give different answers? All of these examples highlight the flexibility of the vgosDB format.

Keywords vgosDB

1 Introduction

The Mark3 database (MK3-DB) format has been used to store VLBI data since the 1970s, and is the default format in use by the IVS since its inception. It has many advantages, but it also has disadvantages, chief among them being that it was designed over 40 years, and much has changed since then. Because of this IVS Working Group IV on Data Structures was formed to design a new data structure. The new way of organizing and storing data is called the vgosDB format, see Gipson et al. (2013).

A key difference between MK3-DB and vgosDB is the file structure. A MK3-DB is unitary—all information is contained in a single file. A typical MK3-DB has around 250 distinct kinds of VLBI data, ranging from source-names and positions, to observables, to editing criteria, to solution setup—that is what calibrations to

apply, and what the default constraint levels are. Each MK3-DB file has associated with it a version number. Anytime *any* data is added, subtracted or modified a new MK3-DB is created and the version number is incremented. Within the context of *solve* this means that it is not easy to test the effect of changes in the data, or of using different models, since it requires either making a new version of the MK3-DB, or changing the code for *solve*, or both. Another issue is that it is difficult to isolate the differences between MK3-DBs produced for the same session by different groups.

In contrast, the vgosDB data storage is very granular. Data is split into many small files written in netCDF format, each typically containing a few closely related items. For example, all of the met-data from a site is in one file, station a priori information is in another file, group delay and sigma in a third, etc. This collection of files is organized by an ASCII file called a wrapper that contains pointers to the data for a given session, see Figures 1 and 2. To add or modify data, you make the corresponding file and create a new wrapper pointing to the new data. This is the analog of making a new MK3-DB version. This greater granularity allows you to answer questions which are difficult or impossible with the MK3-DB, and we demonstrate this with a few examples ranging from the simple to the complex.

2 Missing Met Data

Meteorological ('met' for short) data is used in VLBI processing in two different roles: 1) Pressure is used to calculate the a priori hydrostatic delay; 2) Temperature is used to model the effects of thermal deformation. Many sites have no met sensors, and sometimes sensors

John Gipson
NVI, Inc., 7257D Hanover Parkway, Greenbelt Maryland,
20770, USA

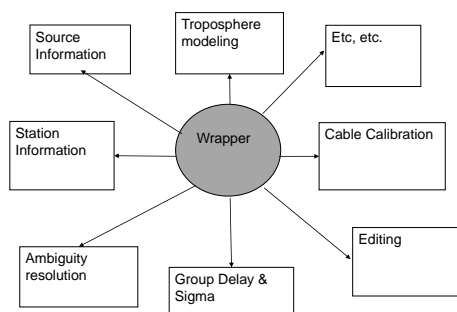


Fig. 1 The vgosDB wrapper organizes the data.

```

Begin History
CreateTimeTag 2015Jan20-12:22:22
Createdby JohnGipson
End History
! This is a comment.
Begin Description
This is a simple wrapper file for the data in NGS cards.
End Description
! ----another comment.
Begin Session
Session C1404
Head.nc
Default_Dir Solve
...
End Session
! ***start the station sections.
Begin Station KOKEE
! KOKEE must be one of the station names in Head.nc
Default_dir KOKEE
AzEl.nc
Met.nc
Cal-Cable.nc
End Station KOKEE
.... OMIT other stations
! **** Start the observation section
Begin Observation
Default_Dir Obs
ObsIndex.nc
GroupDelay_bX.nc
GroupDelay_bS.nc
Default_Dir ObsEdit
Edit_bX.nc
Ambig_bX.nc
Ambig_bS.nc
Cal-SlantIono_bX.nc
End Observation

```

Fig. 2 The wrapper is a readable and editable ASCII file.

fail. If met-data is unavailable for a site *solve* uses a default site-dependent value. How large an error does this introduce? Using MK3-DBs and *solve* there is no easy way to answer this question. Juhl et al. (2012) studied this issue by modifying *solve* and found that the effects can be significant. We show how to solve this problem using the vgosDB format. As illustrated in Figure 3, to remove the met-data you just ‘comment-out’ a line in the wrapper file.

```

...
Begin Station KOKEE
Default_dir KOKEE
TimeUTC.nc
AzEl.nc
!Adding a "!" makes the line a comment.
!Met.nc
Cal-Cable.nc
End Station KOKEE
...

```

Fig. 3 Commenting out a met line in the wrapper removes it from the vgosDB.

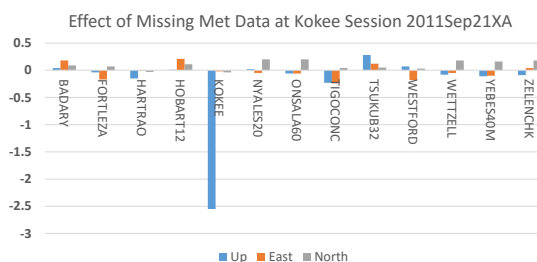


Fig. 4 The difference in estimates of station position from two solutions, with and without met data at Kokee.

Figure 4 plots the difference between two *solve* solutions, one done normally, and one without using Kokee met-data. The effect is concentrated at Kokee, with a 2.5mm change in Kokee’s Up position, which is large compared to our stated goal of 1mm accuracy. This illustrates the importance of having good met-data available for all IVS stations. The effect on other station parameters is under 0.25mm, and can be ignored.

3 Effect of Cable Cal

In November of 2014 analysts at GSFC discovered a problem with NyAlesund’s cable-cal. Including it degraded the fit of the VLBI solution. Ultimately this problem was traced to a bad cable at NyAlesund. Until the cable was replaced in January 2015, cable-cal at NyAlesund was not used in the GSFC VLBI analysis. This was done by ‘turning it off’ in the Version 4 MK3-DB. This also means that NGS cards for those sessions did not use cable-cal at NyAlesund.

What is the effect of turning off cable-cal at a given station on the estimated parameters? Using *solve* and MK3-DBs, you can answer this for a particular session by analyzing the data interactively. However, there is no way to answer this question for many sessions

```

...
Begin Station NYALSUND
Default_dir NYALSUND
TimeUTC.nc
AzEl.nc
Met.nc
!Adding a "!" makes the line a comment.
!Cal-Cable.nc
End Station NYALSUND
...
    
```

Fig. 5 Commenting out the cable-cal in a wrapper for a station prevents it from being applied.

in batch-mode without modifying the software. Fortunately if the session is in vgosDB format, there is a simple way of turning off cable-cal. As with met-data, all we need to do is ‘comment out’ (see Figure 5) the cable-cal line in the wrapper to prevent it being used.

Figure 6 shows the difference between two solutions for a single CONT14 session which differ only in that cable-cal is, or is not, applied at NyAlesund. This effect is small at most stations with the exception of NyAlesund, where the Up changes by 23mm.

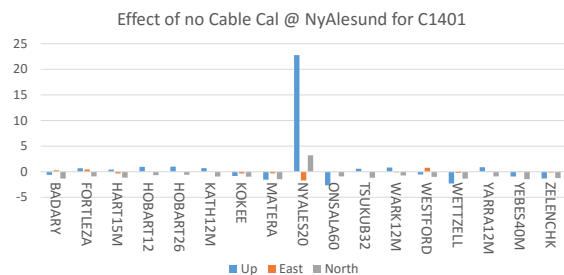


Fig. 6 Turning off cable-cal at NyAlesund predominately effects NyAlesunds Up, with a lesser effect on the East and North.

Figure 7 plots the difference in baseline length for baselines involving NyAlesund between two sets of solutions for the 2014: the default solution, where cable-cal was applied at NyAlesund (except for in November and December) and another solution where it was not. If the effect of cable-cal were systematic, this plot would not exhibit any scatter: for each baseline there would be a single point. The scatter implies that the affect of cable-cal is not systematic – making it difficult to model.

NyAlesund is a very important station and appears in many IVS sessions, including the R1 and R4 sessions which are designed to provide rapid, precise measurements of EOP. Figure 8 shows the difference between two solutions on the estimate of UT1. These so-

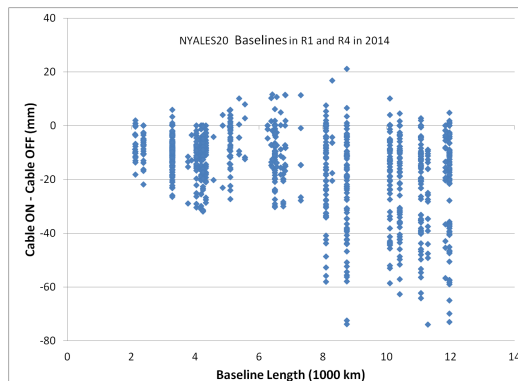


Fig. 7 The difference between solutions with, and without, cable-cal at NyAlesund.

lutions are the default solution, and one where cable-cal is turned off. The difference can be upto 8 μ s in UT1, many times the formal error $\sim 2\mu$ s. The points scatter around the horizontal axis, meaning that the effect is not systematic. The reason there is no scatter at the end of 2015 is that the default solution had cable-cal turned off at NyAlesund.

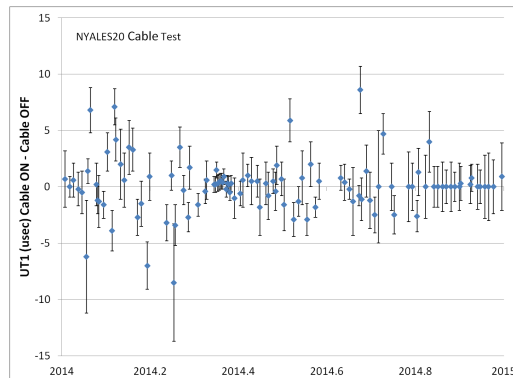


Fig. 8 Effect of turning-off cable-cal at NyAlesund on estimates of UT1. Sessions with no difference did not include NyAlesund.

4 Differences in VLBI Analysis

When different analysis groups process the same VLBI session they get different answers. Colloquially these differences are referred to as ‘analysis noise’. Usually the differences are small, on the order of a sigma or less, but occasionally they are much larger. Different software packages implement the various physical and geophysical models differently, resulting in small differences in the a priori delay. These differences are very small, resulting in changes in the a priori delay of 1 ps or less, which causes differences in the estimated quantities well under one sigma. Another cause for differences is due to the choices analysts make in analyzing the data. As I show below, these can result in large differences. In this section I use the vgosDB format to sort out the cause of one of these differences for one session.

The BKG VLBI group provided me with their MK3-DBs for CONT11. BKG is one of the few VLBI groups that processes all of the VLBI sessions starting from the version 1 MK3-DB, which is the common starting point of all VLBI analysis. BKG uses the *calc/solve* analysis software. Since their processing is independent of GSFC, and they use the same analysis package, any difference in the results are due only to differences in how they analyze the data.

Figure 9 shows the difference in WRMS repeatability of the Up, East and North components averaged over the CONT11 sessions. For most stations components, the agreement of the WRMS scatter between BKG and GSFC is good (a few mm) or excellent (under 1mm) with two notable exceptions: For Tsukuba Up the scatter is 20 mm (11 mm) for BKG (GSFC). For Hobart12M Up it is 18mm (23mm) for BKG (GSFC).

To determine if these difference were due to one or two ‘bad’ sessions, I looked at Tsukuba’s Up position on a session-by-session basis, see Figure 10. For most days the difference is small and within the error bars. September 21 is an exception– the difference is 58mm. The formal errors for Tsukuba in this session are also large, indicating that there might be a problem with the data. Tsukuba observed for only part of the day because of a typhoon. I looked at September 21 in detail to see if the differences were confined to Tsukuba. Figure 11 displays the difference in BKG and GSFC estimates for all components and all stations. The differences are



Fig. 9 WRMS position repeatability from BKG and GSFC. Apart from Hobart12M and Tsukuba Up there is good agreement.

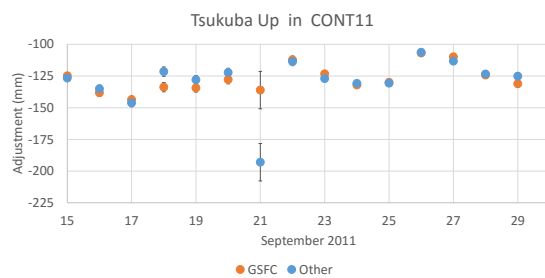


Fig. 10 Tsukuba’s Up adjustment for the CONT11 sessions as estimated using databases provided by BKG and GSFC.

small with the exception of Tsukuba Up (58mm) and Hobart12M Up (-15mm).

The above was done using the MK3-DB format. To proceed further I converted the 11SEP21XA session to vgosDB format. My approach to unraveling the cause of the differences was to start with the GSFC vgosDB, and then gradually, step-by-step, convert it

Scheduling of VLBI observations to satellites with the Vienna VLBI Software (VieVS)

A. Hellerschmied, J. Böhm, R. Haas, J. Kodet, A. Neidhardt, L. Plank

Abstract The observation of satellites with VLBI is an auspicious approach, providing a variety of new possibilities. Promising applications can be found, among others, in the field of inter-technique frame ties. Although several test observations to GNSS satellites have been carried out in recent years, this approach is still far away from being applied routinely. Difficulties already start during observation planning, with the standard geodetic scheduling software not being prepared to include satellites as observation targets in the required control files. The new satellite scheduling module of the Vienna VLBI Software (Böhm et al., 2012) offers a solution to this. It allows the user to prepare schedules for observations of selected satellites, also in combination with standard observations to natural radio sources. The schedule files in the current VEX format created this way provide the possibility to conduct actual VLBI satellite experiments. The next step is to evaluate suitable scheduling strategies for satellite observations, which will allow to implement an automatic source selection approach. The development of a convenient scheduling software in the form of the new VieVS module is important to support further research and development in this field.

Andreas Hellerschmied, Johannes Böhm
Technische Universität Wien, Department of Geodesy and
Geoinformation, Gußhausstraße 27-29, A-1040 Vienna, Austria
Alexander Neidhardt, Jan Kodet
Technische Universität München, Geodetic Observatory
Wetzell, Germany
Rüdiger Haas
Chalmers University of Technology, Onsala Space Observatory,
SE-439 92 Onsala, Sweden
Lucia Plank
University of Tasmania, Australia

Keywords VLBI, satellite observations, scheduling

1 Introduction

Observations of anthropogenic space objects with radio telescopes is not new for the VLBI in general. There have been numerous of those observations in the last decades, mainly for the navigation of (deep) space missions, e.g. carried out by the NASA Deep Space Network (e.g. Border, 2009). However, the observation of spacecrafts, in particular of Earth-orbiting satellites, is new for the geodetic VLBI system. The basic idea is to apply standard VLBI data acquisition and analysis schemes to direct observations of satellite signals, similar to those used for operational observations of natural radio sources (mostly quasars). This will offer a variety of new possibilities for the geodetic community, where probably the most promising ones can be found in the field of inter-technique ties, see e.g. Plank et al. (2014).

For successful VLBI data acquisition, suitable observation plans, referred to as schedules, are required to define the timing of a VLBI session and to configure the receiver equipment. The scheduling of geodetic VLBI sessions is a critical task and is usually done by dedicated software, such as SKED (Gipson, 2012), or VIE_SCHED (Sun et al., 2014), the standard scheduling module in VieVS. In case of VLBI satellite observations the problem was that those commonly used geodetic scheduling programs did not support satellites as radio sources routinely. Hence, lots of manual interactions were needed for previous experiments, to carefully prepare the required observation plans and the related interchange files. To close this gap a dedicated Satellite Scheduling Module was developed for VieVS (Hellerschmied et al., 2015), which enables the cre-

ation of realistic schedules for satellite observation for upcoming test and research campaigns in a simple and convenient way. The observation plans are saved in a standardized file format and can be applied to control real observations.

2 VLBI satellite observations

2.1 Basic observables

The choice of the basic observables in the data analysis affects how the data have to be taken, both in frequency setup and in the sequence of scans. In geodesy typically measurements of signal delays derived from phase slopes of wide frequency ranges are used. The available bandwidth of satellite signals is small compared to quasar signals. On the other hand, the signal strength is usually much higher, which is assumed to compensate the negative effects of the narrow bandwidth on the accuracy of the derived delay observables.

Alternatively, phase referencing could be used between satellite and a nearby target, e.g. a well defined natural radio source of known position. This scheme has been used for most astronomical applications, as well as for near-field VLBI observations of space probes, e.g. of the ESA Venus Express Spacecraft (Duev et al., 2012). A big complication for this approach for Earth orbiting satellites emerges due to the very short distance between target and observer: A quasar that is close to a satellite seen from one site is likely to be far from this satellite as seen from another site.

2.2 Combined schedules

The combination of satellite and quasar scans in one session and a common treatment in the data analysis offers various interesting possibilities, such as:

- Determine satellite positions directly in the CRF
- Reveal local-tie discrepancies between the VLBI frame and reference frames of other techniques, e.g. as shown for VLBI and GNSS in the simulation study by Plank et al. (2014)
- Establish a direct link between the geometric VLBI reference frame and the geocenter (Dickey, 2010)

However, there are severe observation restrictions on the station level, mainly due to limited receiver capabilities. Standard geodetic VLBI is done routinely in the S- and X-band, while satellite signals are not restricted to those bands. GNSS satellites, which are particularly interesting for VLBI observations, transmit radio signals in the L-band, which is generally not observable with the standard geodetic antenna equipment without changes in the hardware. Only a few antennas provide the possibility to combine S/X-band observations and L-band observations, either by automatically switching the receiver (e.g. Medicina¹), which has the drawback that those adaptations take some time and may change internal signal delays, or by using dedicated S/X/L-band receivers as developed at the station Wettzell by Kodet et al. (2014).

2.3 Future scheduling strategies

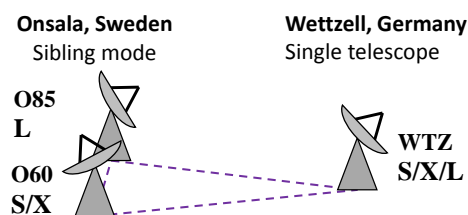


Fig. 1 Possible constellation for combined S/X/L-band observations. Wettzell is able to observe all bands. In Onsala sibling antennas are used to cover all three frequency bands.

One major task for the near future is the implementation of an automatic source-selection approach for satellites and combined sessions, respectively. Current geodetic scheduling software implement automatic source selection approaches, which usually optimize the sky coverage at the stations. This is required to determine accurate tropospheric corrections and to beat down atmospheric errors.

However, there are still several open questions: One question is how to combine satellite and quasar scans reasonably within one session (in terms of scan sequence, ratio between satellite and quasar scans, spatial source distribution, etc.) to improve the desired target estimates. Another important point is how to han-

¹ <http://www.med.ira.inaf.it/ManualeMedicina/>

dle station-dependent restrictions in the observable frequency bands, as discussed in Sec. 2.2. One possibility is to take advantage of twin or sibling telescopes: One telescope for satellites, e.g. in L-band, and the other one for classical S/X-band observations, as outlined in Fig. 1 for the baseline Onsala-Wettzell.

3 VieVS Satellite Scheduling Module

The Satellite Scheduling Module is integrated into the Graphical User Interface (GUI) of VieVS. In addition to the function range of the standard scheduling module VIE_SCHED it provides the following features:

Orbit prediction: Satellite positions and velocities are required for two tasks: (a) For the observation planning to check the conditions for a valid scan (see Sec. 3.2) and to determine whether a satellite is observable at a certain epoch. (b) For the calculation of the tracking data which are included in the final schedule files to enable a stepwise satellite tracking (see Sec. 3.3). The applied orbit determination approach has to provide the possibility to predict satellite positions at least a few days to the future with sufficient accuracy, because the scheduling is usually done several days before the actual sessions are carried out. In VieVS the orbit determination is based on Two-Line Element (TLE) datasets. The great advantage of TLE data is their wide availability for thousands of space objects on a daily basis and free of charge². The calculations are based on analytical Simplified General Perturbation models (SGP; Hoots and Roehrich, 1980), without the requirement of CPU-intensive interpolations. The accuracy of those orbit predictions is not sufficient to be used for the correlation. Therefore, the satellite positions have to be obtained from other sources, e.g. from GNSS final orbits provided by the IGS.

Interactive user interface: The scheduling is controlled via a text-based user interface. Several interactive plots visualize the current satellite-station constellation, observation restrictions and summarize the available observation times of

potential targets. Useful auxiliary information are also provided, e.g. cable wrap positions, etc.

Satellite scans: Satellite scans can be added scan by scan, just by selecting the target. The scan start time is calculated automatically, but the on-source has to be defined manually.

Combined schedules: Quasar and satellite scans can be mixed in one schedule, where blocks of quasars scans can be added automatically using the station-based scheduling strategy of VIE_SCHED (Sun et al., 2014). Individual station networks can be defined for both observation types, including antennas in twin/sibling mode.

3.1 Program overview and workflow

A program overview is outlined in Fig. 2:

1. **Input data:** On program start, different kinds of input data are loaded. Catalog files provide all required information about VLBI stations, e.g. coordinates, equipment and antenna parameters. Configuration files are used to define the receiver configuration for specific observation scenarios and TLE data are needed for orbit predictions.
2. **VieVS GUI:** The basic observation setup can be defined in the GUI. The user selects the station network, session start time and duration, and further observation parameters, e.g. the cut-off elevation. Via mouse-click the internal TLE library can be updated automatically over a web service. Furthermore, a pre-selection of satellites has to be made.
3. **User interface:** After setting all required parameters, the program calculates the available observation periods for all selected satellites and provides this information to the user in terms of text and graphics. Via the provided interface, the user is able to compile an observation plan by assembling satellite and quasar scans manually in the desired order. After selecting a target source, the program calculates the required slew times and suggests a scan start time automatically. For quasar scans, also the optimal scan duration (on-source time) is calculated. For satellites the determination of the on-source time is still a subject of research, because several required parameters (e.g. flux density, receiver efficiency, etc.) are still unknown. There is also the possibility to combine satellite

² For more information visit: <http://www.celestrak.com/NORAD/elements/>

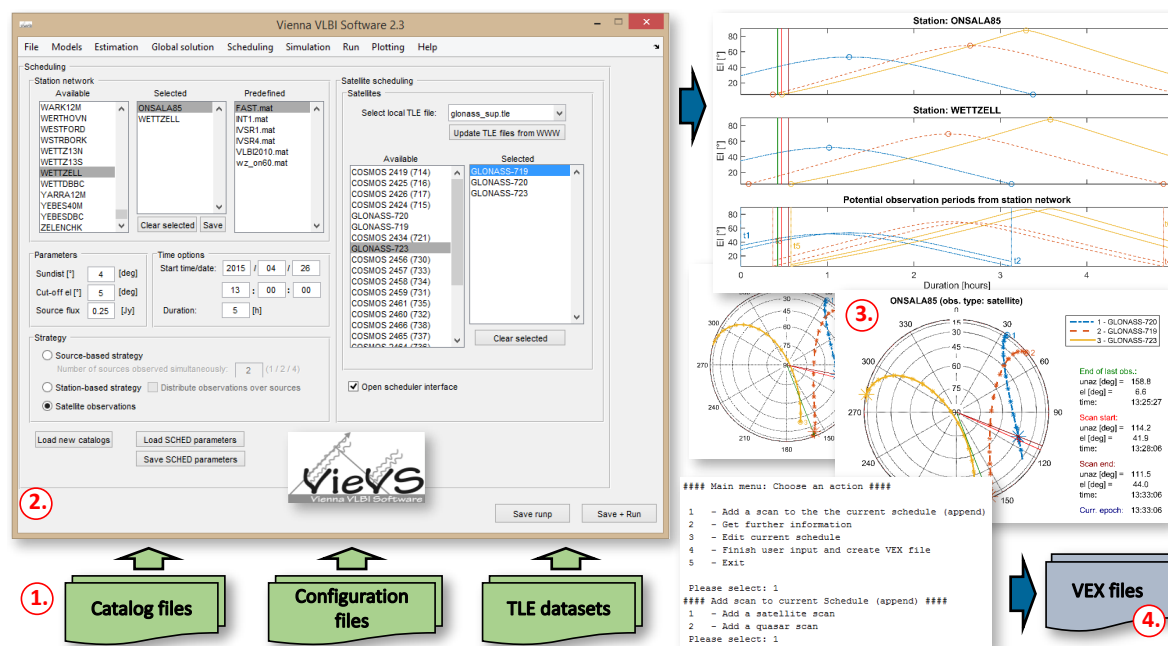


Fig. 2 Overview of the VieVS Satellite Scheduling Module: (1.) Input data, (2.) GUI, (3.) user interface and (4.) output.

scans in sequence with classical geodetic schedules of quasar scans, computed by the station-based scheduling approach of VIE.SCHED (Sun et al., 2014).

4. **VEX files:** The final observation plans are saved as VEX-formatted files (see Sec. 3.3).

3.2 Observation conditions

To determine whether an observation target is observable at a certain epoch, several visibility conditions and limitations in the antenna hardware are considered:

Common visibility: A satellite has to be visible simultaneously from all antennas of the defined station network. Therefore, the visibility is examined separately for each site, considering the defined cut-off elevation and a horizon mask, if available. By combining these data, the common visibility from the network is examined. Although it would be required for large (up to global) station networks, sub-netting is not supported so far. For delay time calculations a target has to be visible simultaneously from at least two stations forming one baseline. However, single station observations,

e.g. for signal acquisition tests, can also be scheduled.

Slew rates: Contrary to quasars, satellites can move quite fast relative to the Earth's surface, depending on their orbit height. Hence, it has to be ensured, that the antenna slew rates are sufficiently high, so that the antennas are able to keep track of the satellite during data acquisition.

Axis limits and cable wrap: Axis limits of individual antennas are checked. Furthermore, the cable wrap of AzEl-mounted antennas has to be tracked to calculate slew times between consecutive scans unambiguously.

Sun distance: A certain distance between the Sun and the observation target has to be kept to prevent signal degradation.

3.3 Schedule files

The final observation plans are saved in VEX-formatted schedule files. VEX (Whitney et al., 2002) is a standard file format for VLBI schedules. Those files comprise all required information to carry out a VLBI session. Additionally to the scan sequence, all setup

parameters for the receiver equipment are defined there, e.g. sample rates, frequencies and bandwidths.

To enable satellite tracking without the requirement of dedicated satellite tracking modes, a so-called *stepwise tracking* (e.g. Hellerschmied et al., 2015) is implemented in the issued VEX files. Satellite orbits are fragmented and approximated by discrete positions in the VEX files, defined by topocentric Ra/Dec similarly to the source definition of quasars. Satellites are tracked by repositioning the antennas in a defined time interval to the defined tracking points. Individual VEX files are generated for each station, because the topocentric satellite positions differ between sites.

The testing period for a revised VEX format (VEX 2.0) already started in December 2014³. This is quite important for VLBI satellite tracking, because the new format will provide the possibility to include TLE orbit data directly to the control files. In combination with dedicated satellite tracking features of the VLBI Field System this will enable continuous and smooth tracking (Himwich and Gipson, 2013).

4 Summary and outlook

The VieVS Satellite Scheduling Module provides a flexible tool for the scheduling of real VLBI satellite observations, also in combination with classical quasars scans. The final observation plans are saved in VEX-formatted schedule files, which are able to control real experiments by applying a stepwise tracking approach for satellites. This module was initially applied for successful test observations of GLONASS satellites in January 2014 on the baseline Onsala-Wetzell (Haas et al., 2015).

The implementation of a suitable scheduling optimization approach, which is a prerequisite for an automatic selection of satellites, requires further research. Therefore, it is planned to combine the simulation tools for satellites (Plank et al., 2014) with the new scheduling module in VieVS, to investigate scheduling strategies for satellites based on realistic schedules.

³ <https://safe.nrao.edu/wiki/bin/view/VLBA/Vex2>

References

- Böhm J, Böhm S, Nilsson T, Pany A, Plank L, Spicakova H, Teke K, Schuh H (2012) The new Vienna VLBI software. In: S. Kenyon, M. C. Pacino, U. Marti (eds.), *Proc. IAG Scientific Assembly 2009*, IAG Symposia Series 136, 1007–1011.
- Border J S (2009) Innovations in delta differential one - way range: from Viking to Mars Science Laboratory. In: *Proc. 21st Int. Sym. Space Flight Dynamics*, Toulouse, France
- Dickey J M (2010) How and Why do VLBI on GPS. In: D. Behrend and K. Baver (eds.), *IVS 2010 General Meeting Proc.*, NASA/CP 2010-215864, 65–59.
- Duev D A, Molera Calvés G, Pogrebenko S V, Gurvits L I, Cimó G, Bocanegra Bahamon T (2012) Spacecraft VLBI and Doppler tracking: algorithms and implementation. *Astron Astrophys*, 541:A43+
- Gipson J (2012) Sked - VLBI Scheduling Software. NASA Goddard Space Flight Center, ftp://gemini.gsfc.nasa.gov/pub/sked/sked_Manual_v2012May09.pdf
- Haas R, Hobiger T, Hellerschmied A, Neidhardt A, Kodet J (2015) GLONASS-VLBI: Onsala-Wetzell test observations. In: R. Haas, F. Colomer (eds.), *Proc. 22nd EVGA Working Meeting*, 107–111.
- Hellerschmied A, Böhm J, Neidhardt A, Kodet J, Haas R, Plank L (2015) Scheduling VLBI Observations to Satellites with VieVS. In: C. Rizos and P. Willis (eds.), *Proc. IAG Commission 1 Symposium 2014: Reference Frames for Applications in Geosciences (REFAG2014)*, Springer Berlin Heidelberg, IAG Symposia, DOI 10.1007/1345_2015_183, accepted.
- Himwich E, Gipson J (2013) GSFC Technology Development Center Report. In: K. D. Baver, D. Behrend, K. Armstrong (eds.) *IVS 2012 Annual Report*, NASA/TP-2013-217511, 280–282.
- Hoots F, Roehrich R (1980) Spacetrack Report No.3: Models for Propagation of NORAD Element Sets. Tech. rep., US Airforce Aerospace Defense Command, Colorado Springs, CO.
- Kodet J, Schreiber K, Plötz C, Neidhardt A, Kronschnabl G, Haas R, Molera Calvés G, Pogrebenko S, Rothacher M, Maennel B, Plank L, Hellerschmied A (2014) Co-locations of Space Geodetic Techniques on Ground and in Space. In: D. Behrend, K. D. Baver, K. L. Armstrong (eds.) *IVS 2014 General Meeting Proc.*, Science Press (Beijing), 446–450.
- Plank L, Böhm J, Schuh H (2014) Precise station positions from VLBI observations to satellites: a simulation study. *J Geod*, 88(7), 659–673.
- Sun J, Böhm J, Nilsson T, Krásná H, Böhm S, Schuh H (2014) New VLBI2010 scheduling strategies and implications on the terrestrial reference frames. *J Geod*, 88(5), 449–461.
- Whitney A, Lonsdale C, Himwich E, Vandenberg N, van Langevelde H, Mujunen A, Walker C (2002) VEX File Definition/Example, Rev. 1.5b1. <http://www.vlbi.org/vex/docs/vex>

GLONASS-VLBI: Onsala-Wetzell test observations

R. Haas, T. Hobiger, A. Hellerschmied, A. Neidhardt, J. Kodet

Abstract A series of VLBI observations of GLONASS signals were performed in January 2014 on the baseline Onsala–Wetzell. Several GLONASS satellites were observed in alternating mode, the resulting data were correlated and fringes were successfully found. The results prove that signal-to-noise-ratio (SNR) on the order of 50 can be achieved with just 2 s of observations already. It appears however important to choose appropriate attenuation at the stations to receive the strong satellite signals. Furthermore, the rather simple a priori delay model used for the correlation needs to be improved in order to be able to derive phase delays.

Keywords GLONASS, VLBI, DiFX, Fourfit

1 Introduction

Since several years the question of how to connect the reference frames of the various space geodetic techniques is a topic of continual discussion. Currently, the production of the International Terrestrial reference Frame (ITRF) (Altamimi et al., 2011) depends heav-

Rüdiger Haas, Thomas Hobiger,
Chalmers University of Technology, Department of Earth and Space Sciences, Onsala Space Observatory, SE-439 92 Onsala, Sweden
Andreas Hellerschmied,
Technische Universität Wien, Department of Geodesy and Geoinformation, Karlsplatz 13, AT-1040 Wien, Austria
Alexander Neidhardt, Jan Kodet,
Technische Universität München, Forschungseinrichtung Satellitengeodäsie, Geodetic Observatory Wettzell, Sackenrieder Str. 25, DE-93444 Bad Kötzing, Germany

ily on so-called co-location stations that are equipped with instruments for several space geodetic techniques. Accurate information on the so-called local-tie vectors between the reference points of the instruments is needed in order to be able to connect the different space geodetic techniques. For various reasons the quality of the local-tie vectors appears not to be equal at all co-location stations and in some cases is heavily debated (Ray and Altamimi, 2005). Thus, to improve the connection of the different space geodetic techniques, ideas have been developed to achieve co-location in space as a complement to co-location on the ground.

One idea is to launch low earth orbiting (LEO) satellites that are equipped with receiving instruments for GNSS signals, retro-reflectors for Satellite Laser Ranging (SLR), and transmitters for artificial VLBI signals (Bar-Sever et al., 2014). A first satellite following this approach has been launched recently (Geshi, 2015) and it is to be expected that first VLBI observations of this satellite will be done soon.

Another idea is to observe GNSS signals directly with VLBI telescopes (e.g. Tornatore et al. (2011)). However, since GNSS signals are in the L-band, radio telescopes with L-band receivers are needed for such observations while today's normal geodetic VLBI observations use S- and X-band. To realize the observation of GNSS signals with radio telescopes used for geodetic VLBI, an L-band system has been developed at the Wettzell Geodetic Observatory for its 20 m radio telescope (Kodet et al., 2014). This new system extracts the L-band signals through the S-band signal chain. In early 2013 first successful tests have been performed (Haas et al., 2014) together with the Onsala 25 m radio telescope in Sweden, which is equipped with a dedicated L-band system for astronomical VLBI observations. At that time one GLONASS satellite was ob-



Fig. 1 The 20 m radio telescope at Wettzell (left) and the 25 m radio telescope at Onsala (right).

served for about 45 minutes and fringes were found successfully. Further test observations were performed in early 2014, again using the Onsala–Wettzell baseline. Figure 1 depicts photos of the involved telescopes. In the following we present first results of the 2014 observations.

2 GLONASS-VLBI observations 2014

In January 2014 a series of GLONASS VLBI-observations was scheduled for the Onsala–Wettzell baseline. These observations involved the 25 m radio telescope at Onsala with its dedicated L-band receiving system, and the 20 m radio telescope at Wettzell with its L-band via S-band system (Kodet et al., 2014). The scheduling was done with the satellite-scheduling module of the VieVs software (Hellerschmied et al., 2014) which produced the necessary telescope control files. The observations were planned for several hours on January 16 and 21. In total eight GLONASS satellites were observed in an alternating mode, i.e. switching between the satellites, with observations of several minutes, see Table 1. Since the satellite signals are much stronger than the signals of natural radio sources, at Onsala additional attenuation had to be added in order to avoid saturation of the L-band receiving system. For the observations on Jan. 16 additional attenuation of 10 dB was used, while for the observations on Jan. 21 even 30 dB were used. In contrast to that, at Wettzell, the weak L-band signal that passes through the S-band horn needed to be amplified by about 30 dB.

Table 1 Overview of the GLONASS-VLBI observations in January 2014. Given are the observing times, the GLONASS, NORAD and PR numbers of the satellites.

Date	UT-Time	GLONASS	NORAD	PR
2014-01-16	12:30-12:45	743	37869	PR08
	12:50-13:05	723	32395	PR11
	13:10-13:25	730	36111	PR01
	14:00-14:15	730	36111	PR01
	14:20-14:35	737	37138	PR12
	14:40-15:00	747	39155	PR02
	2014-01-21	13:30-13:35	743	37869
13:37-13:42		732	36402	PR23
13:44-13:49		743	37869	PR08
13:51-13:56		732	36402	PR23
13:59-14:04		743	37869	PR08
14:08-14:13		735	36401	PR24
14:14-14:19		''	''	''
14:25-14:30		732	36402	PR23
15:00-15:04		735	36401	PR24
15:05-15:09		''	''	''
15:10-15:14		''	''	''
15:20-15:24		746	37938	PR17
15:25-15:29		''	''	''
15:30-15:34		''	''	''
15:45-15:49		723	32395	PR11
15:50-15:54		''	''	''
15:55-16:00		''	''	''

3 Data processing

The correlation of the observed data was done with Version 2.3 of the software correlator DiFX (Deller et al., 2011), which is installed at the Onsala Space Observatory. The necessary a priori delay values were externally calculated with a simple model following Moyer (2000). Every 15 s the a priori delays were expressed as coefficients of a polynomial model and inserted in the control files for the DiFX correlation. Each scan of 15 s length was correlated individually, with 256 lags and 0.16 s accumulation period.

After correlation the resulting files were processed with Fourfit¹. Examples of fringe plots for all eight GLONASS satellites that were observed are presented in Fig. 2 and Fig. 3. It becomes clear that the higher attenuation used at Onsala on Jan. 21 caused worse correlation results compared to the Jan. 16 observations. For example, the SNR values are lower and the correlation amplitudes and phases are more noisy than for the Jan. 16 observations.

¹ <http://www.haystack.mit.edu/tech/vlbi/hops/fourfit.txt>

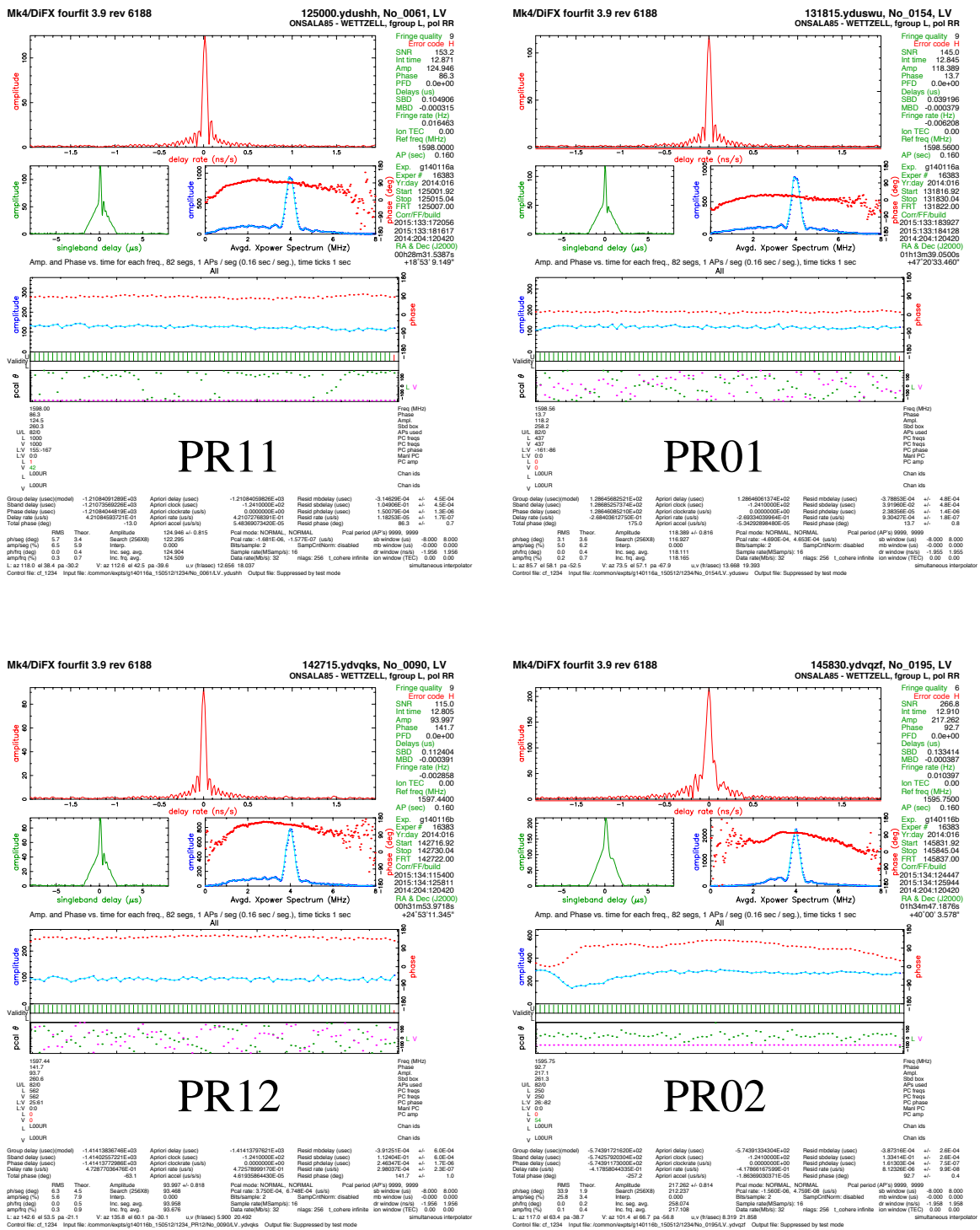


Fig. 2 Examples of fringe plots for GLONASS PR11 (top left), PR01 (top right), PR12 (bottom left) and PR02 (bottom right), observed on January 16, 2014, on the Onsala–Wetzell baseline.

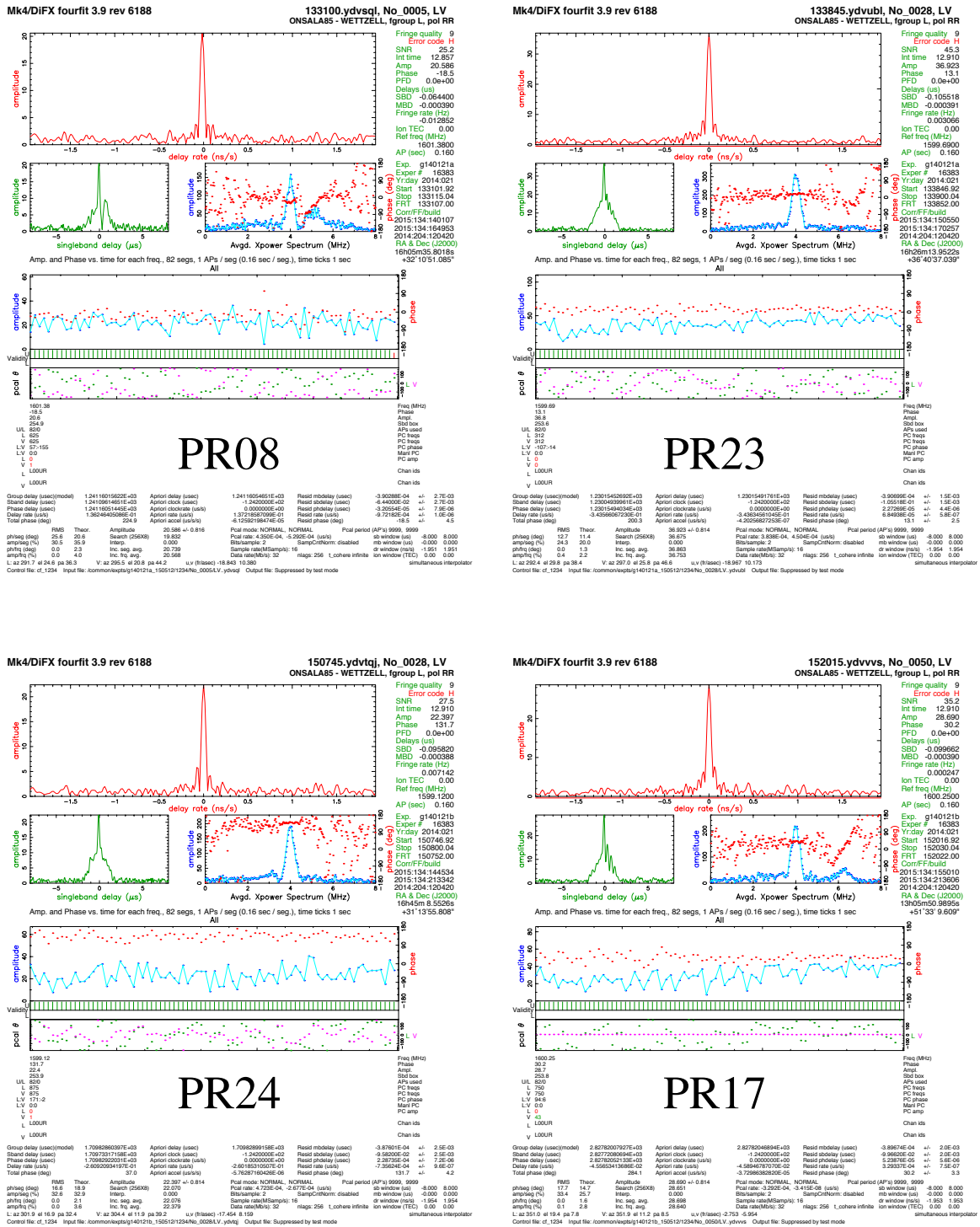


Fig. 3 Examples of fringe plots for GLONASS PR08 (top left), PR23 (top right), PR24 (bottom left) and PR17 (bottom right), observed on January 21, 2014, on the Onsala–Wetzell baseline.

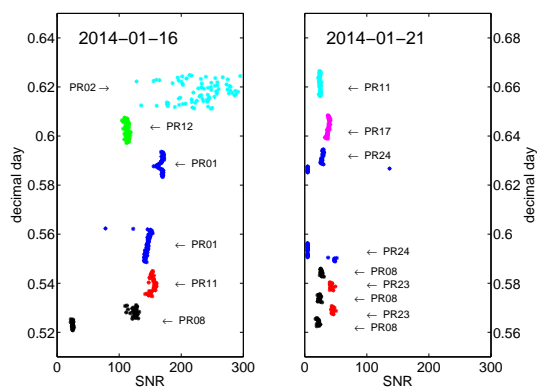


Fig. 4 Signal-to-noise (SNR) values obtained for the observation of Jan. 16 (left plot) and Jan. 21 (right plot).

Figure 4 depicts as an example the SNR values for both days. The data of Jan. 16 consistently gave higher SNR than the data of Jan. 21. Some of the observations did not perform very well, e.g. in the beginning of Jan. 16 with PR08 when one of the telescopes probably was not tracking correctly yet, and about in the middle of Jan. 21 with PR24. The problems on Jan. 21 were due to an operator mistake at Onsala that caused the disconnection of the backend and led to problems with PR24 and a complete loss of the PR23 observations planned directly afterwards (see Table 1).

Additionally, tests were performed with the Jan. 16 data using different scan lengths in Fourfit, between 2 s and 300 s. The results show that SNR of about 50 can already be achieved with 2 s of observed data. Scan length of 15 s give SNR on the order of 150 to 200, while scan length of 300 s give SNR of more than 500.

4 Conclusions and outlook

The GLONASS-VLBI tests performed in January 2014 were successful. The satellite-scheduling module in VieVs was successfully used to plan the observations and to prepare the necessary telescope control files. Several GLONASS satellites could be observed in alternating mode and fringes were successfully found for all satellites. SNR values of 50 could be achieved with scan lengths as short as 2 s. However, the simple a priori delay model used for the correlation turned out to be not sufficiently accurate enough. The observed

phases could not be unwrapped successfully and thus it was not possible yet to determine phase delays. A refinement and improvement of this simple delay model is planned for the near future. Furthermore, additional GLONASS-VLBI observations are planned, also using more than just one baseline.

References

- Altamimi Z, Collilieux X, Metivier L (2011) ITRF2008: an improved solution of the international terrestrial reference frame. *J Geod*, 85, 457–473, doi: 40410.1007/s00190-011-0444-4.
- Bar-Sever Y, Haines B, Nerem S, Biancale R (2014) Revisiting the Geodetic Reference Antenna in Space (GRASP) Mission Concept. *IDS workshop 2014*, Konstanz, Germany.
- Deller A T, Brisken W F, Phillips C F, Morgan J, Alef W, Cappallo R, Middelberg E, Romney J, Rottmann H, Tingay S J, Wayth R (2011) DiFX-2: A More Flexible, Efficient, Robust, and Powerful Software Correlator. *Pub Astron Soc Pac*, 123(901), 275–287.
- Geshi T (2015) personal communication.
- Haas R, Neidhardt A, Kodet J, Plötz Ch, Schreiber K-U, Kronschnabl G, Pogrebenko S, Duev D, Casey S, Marti-Vidal I, Yang J, Plank L (2014) The Wettzell-Onsala G130128 experiment – VLBI-observations of a GLONASS satellite. In: D. Behrend, K. D. Baver, K. L. Armstrong (eds.), *IVS 2014 General Meeting Proc.*, Science Press (Beijing), 451–455.
- Hellerschmied A, Plank L, Neidhardt A, Haas R, Böhm J, Plötz Ch, Kodet J (2014) Observing satellites with VLBI radio telescopes – practical realization at Wettzell. In: D. Behrend, K. D. Baver, K. L. Armstrong (eds.), *IVS 2014 General Meeting Proc.*, Science Press (Beijing), 441–445.
- Kodet J, Schreiber K U, Plötz Ch, Neidhardt A, Kronschnabl G, Haas R, Molera Calvés G, Pogrebenko S, Rothacher M, Maennel B, Plank L, Hellerschmied A (2014) Co-location of space geodetic techniques in space and on the ground. In: D. Behrend, K. D. Baver, K. L. Armstrong (eds.), *IVS 2014 General Meeting Proc.*, Science Press (Beijing), 446–450.
- Moyer T D (2000) Formulation for Observed and Computed Values of Deep Space Network Data Types for Navigation. *Deep Space Communications and Navigation Series, Monograph 2*, JPL Publication 00-7, Jet Propulsion Laboratory, California Institute of Technology.
- Ray J, Altamimi Z (2005) Evaluation of co-location ties relating the VLBI and GPS reference frames. *J Geod*, 79, 189–195.
- Tornatore V, Haas R, Duev D, Pogrebenko S, Casey S, Molera Calvés G, Keimpema A (2011) Single baseline GLONASS observations with VLBI: data processing and first results. In: W. Alef, S. Bernhart, A. Nothnagel (eds.), *Proc. 20th EVGA Working Meeting*, 162–165.

Hb-Ho: Observations with the sibling telescope in Hobart

L. Plank, J. Lovell, J. McCallum, J. Böhm, D. Mayer

Abstract With the transition to VGOS, co-located radio telescopes will be common at many sites. This can be as a sibling telescope, when a VGOS antenna is built next to a legacy one or as the concept of a twin telescope, with two identical VGOS antennas. Besides a number of new observing possibilities in a network, such a configuration also allows for the investigation of local effects or antenna-specific systematics. This is for example the measurement of the local baseline with VLBI and the subsequent comparison with the local tie as determined with classical surveying. The comparison of redundant observations to other antennas can be used as independent verification and identify systematic delays specific to each antenna. Lastly, co-location offers new possibilities in analysis, by combining common parameters like station positions, tropospheric conditions or clock modelling. The two telescopes in Hobart, (12m-Hb, 26m-Ho) have observed in more than 70 common IVS sessions, offering a great dataset for studying the performance of a sibling telescope. In addition, dedicated Hb-Ho experiments were performed in 2014. We report on differences found in redundant observations, compare common parameters, determine the local baseline and its variations, and report on newly applied scheduling and analysis strategies.

Keywords Sibling Telescope, Analysis, Twin Telescope

Lucia Plank, Jim Lovell, Jamie McCallum
University of Tasmania, Private Bag 37, 7001 Hobart, Australia
Johannes Böhm and David Mayer
Technische Universität Wien, Gußhausstraße 27-29, A-1040 Vienna, Austria

1 Introduction

With the erection of the AuScope VLBI network (Lovell et al., 2013) in 2010, the Mt. Pleasant observatory in Hobart, Australia, can be operated as a sibling telescope. This consists of the 26m legacy antenna (Ho), contributing to IVS sessions since 1989, and the 12m Hb dish, designed to become part of the future VGOS network and one of the busiest antennas within the IVS at the moment.

During the initialization phase of the Hb antenna (in 2010-2012) both telescopes observed regularly together in IVS (R-) experiments. Later on, the major workload was transferred to the Hb antenna and today the legacy Ho antenna only contributes to special CRF- or R&D-sessions.

In Figure 1 we show the results for the estimated baseline between the two co-located telescopes in Hobart, as determined from 72 common sessions. We find a mean length of 295.914 m and a wrms of 9 mm. This result differs 4 mm from the local tie measured in two surveying campaigns performed by Geoscience Australia in 2009 and 2014. Also, the distribution of the data points might indicate some systematic signal of about ± 1.5 cm, especially for the time before 2013. Unfortunately the common sessions are very sparse after that and are mostly CRDS sessions where the results for station positions are less accurate. It is worth mentioning that since the beginning of 2014 both Hobart telescopes are connected to the identical frequency maser, while they were running on different clocks before. Very promising are the results of the 15-day *CONT14* campaign in May 2014, revealing a baseline wrms of 2 mm for the sibling telescope.

This large dataset of Hb-Ho experiments offers a great opportunity for a more comprehensive study

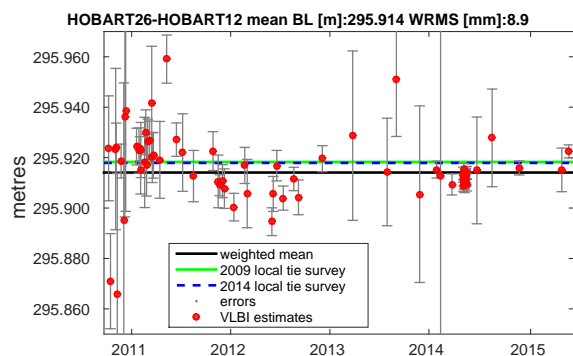


Fig. 1 The Hobart-Hobart baseline determined of 72 common VLBI sessions. The black line shows the mean calculated baseline length of 295.914 m, which is 4 mm off from the baseline determined in two local tie surveys.

of the performance of a sibling telescope. With the prospect of the transition to VGOS in the next years, co-located telescopes will be common: either as a sibling telescope consisting of a legacy and a new antenna or as the new twin telescope concept with two identical antennas. For an optimal combination of the observables, the determination of the local tie between the co-located telescopes will be of major importance, as will be any systematic effects. The configuration of a sibling (twin) telescope offers new ways in the analysis, which need to be implemented and tested. This is introduced in Section 2. In order to better understand the differences we found in redundant observations of the sibling telescope we performed a dedicated Hb-Ho experiment, *AUST65*. A session description, including the scheduling and the analysis is given in Section 3. We end this report with the introduction of our new project *Sibling Telescopes* in Section 4, which will concentrate on a thorough investigation of the optimal use of co-located VLBI antennas.

2 Improved analysis

As illustrated in Figure 2, observations of the sibling telescope in Hobart pass through the (quasi-) identical atmosphere, large-scale station motions are expected to be the same for both telescopes and a single clock is used at the station. These parameters can be combined

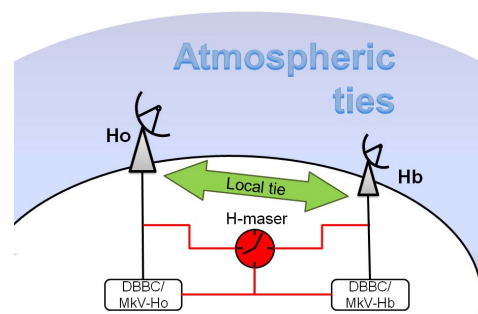


Fig. 2 The Hb-Ho sibling telescope offers new possibilities in the analysis: a combination of the parameters for the atmosphere, station coordinates and the identical clock.

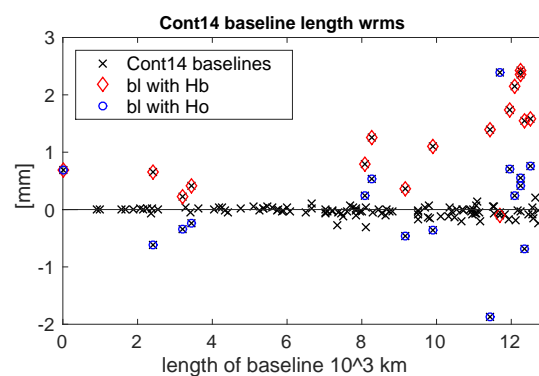


Fig. 3 Differences in baseline length wrms between a classical solution of the *CONT14* data and applying additional constraints for common parameters in the analysis. Positive values indicate an improvement for the new analysis. Differences are mainly found for baselines to one of the co-located antennas marked with red diamonds (Hb) and blue circles (Ho).

in the analysis (e.g. Nilsson et al., 2015; Hobiger and Otsubo, 2014).

Using the Vienna VLBI Software (Böhm et al., 2012) we introduced additional constraints in the estimation part between site positions, zenith wet delays, and atmospheric gradients of the two Hobart antennas. Applied to the data of *CONT14* (a 15-day continuous global VLBI campaign comprising 17 antennas), we find improved results in the wrms of daily determined baseline lengths. This is shown in Figure 3: For baselines to one of the Hobart antennas (marked with larger red and blue symbols) we largely find improvements, up to 3 mm compared to the classical solution. This improvement is larger for baselines to the Hb antenna than for baseline to the Ho antenna. A reason for this is that

in the classical solution the repeatabilities for Ho are slightly better than for Hb. Through the combination of the station coordinates, the total results are approximately equal, meaning an improvement for Hb and a slight worsening for the Ho antenna. However, the combination of the tropospheric parameters adds an additional significant improvement. The results for other baselines are only marginally different, at the tenth of a millimetre level.

Despite this promising result, there are still things to work on: in a careful study the optimal weights for the combination of the parameters have to be determined. How strong should the common parameters be forced to be identical? Next, rather than combining the parameters of the two antennas by additional constraints, the ultimate goal would be to actually only estimate one parameter for both antennas, where all observations contribute. Further, our results for combined clocks are not convincing so far, revealing worse results than without a combination. A possible reason for this is the fact that, besides the pure clock drifts themselves, the estimated clock terms often include other (instrumental) delays which may be different for the two antennas.

This is also evident when studying the ionospheric delays. Due to its dispersive behavior the effect of the ionosphere can be *removed* from the data by combining the X-band group delays with the measurements done in S-band. In VieVS we use the data provided via the so-called *NGS-files*, which are based on the level 4 database files and explicitly give the determined ionospheric delay. At this stage the data has been also adjusted for ambiguities and for closures within the network.

In theory (also see Section 3) we do not expect any ($\ll 1$ mm) delay due to the ionosphere on the Hb-Ho baseline. Neither should there be differences between the ionospheric delays on identical observations to a third antenna, e.g. between the ionospheric contribution for the same scan on the Hb-Katherine and the Ho-Katherine baseline. The fact is, however, that in the *CONT14* data we find (a) huge offsets in the ionospheric correction between the Hb and the Ho antenna of up to 10 ns (≈ 30 m) and (b) an rms difference of ≈ 1 cm after removal of these offsets. This is also true for observations on the Hb-Ho baseline.

We therefore conclude that the ionospheric delay as given in the *NGS-files* (resp. database level 4) has to include other effects than solely those of the iono-

sphere. To first order, these are large ambiguities. But also other effects, e.g. of instrumental origin, may be the reason for these differences (e.g. Alizadeh et al., 2013, Sec. 4.2.4). In order to get more insight into these discrepancies we performed a dedicated experiment (*AUST65*) which, after correlation, was fully processed in-house.

3 AUST65

On November 29 2014, *AUST65* was performed with the antennas in Katherine (Ke), Yarragadee (Yg), Warkworth (Ww) and the sibling telescope in Hobart. Hereby, Hb and Ho did redundant observations, i.e. they observed the identical sources at identical epochs. To realise this in the scheduling, the sensitivity in terms of antenna target sensitivity (in terms of the system equivalent flux density - SEFD) of the large 26m dish was set to the lower values of the 12m antenna. Without the need to adjust the slew speeds or schedule one antenna as tag-along, we got 456 common observations using the scheduling module of the VieVS software. In total, Hb had 463 scheduled observations over 24 hours and Ho 458, using the *AUSTRAL* observing mode with 1 Gbps recording.

After correlation (at Curtin University) we ran four-fit and created a database. Using *vSolve*, the ionospheric correction was added to the level 4 *NGS-files*. The subsequent analysis was done with VieVS.

First thing to notice are problems with the ionospheric delays. We find that almost all observations on the Hb-Ho baseline have extremely high ionospheric delays of up to ± 4 ns, most likely a result of the strong local RFI in S-band. This causes troubles in the analysis. The simplest solution is to exclude all observations on the Hb-Ho baseline. Another possibility is to simply set the contribution of the ionosphere on the local baseline to zero. In Figure 4 we compare the estimated 3D station position offsets for Hb and Ho during *AUST65*. Without taking care of the huge ionospheric delay on the Hb-Ho baseline, we find station position offsets of about 15 ± 3 cm for the two stations (not shown). Excluding observations on the Hb-Ho baselines we find offsets of 3 and 1.5 cm for the Hb and Ho antenna respectively. These estimates improve marginally when we choose to keep the observations on the local baselines and set the ionospheric contribution to zero. Due

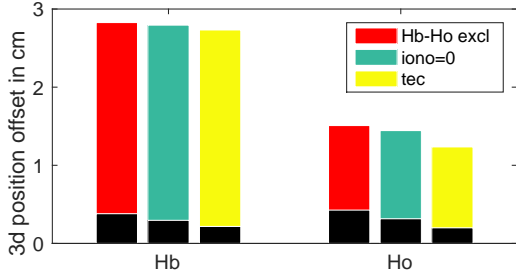


Fig. 4 Estimated 3D station position offsets in *AUST65* using different ionospheric corrections. The black bars indicate the corresponding nominal 3D position errors.

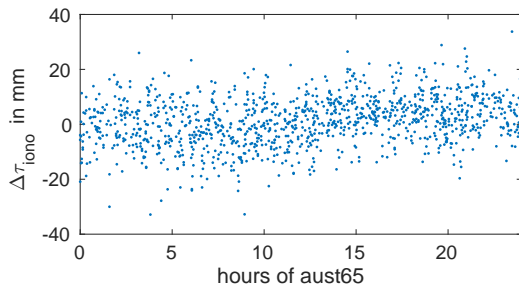


Fig. 5 Difference in the ionospheric delay of redundant observations of the Hobart sibling telescope in *AUST65*.

to the additional observations, the formal uncertainties (shown with the black bars) of the estimates could also be improved.

Having resolved the ionospheric differences on the local baseline, we now have a look at the baselines to third antennas. With this we mean comparing observations within the same scan, Hb-antenna_x to Ho-antenna_x. We call these *redundant observations*. For the data of *AUST65*, we find significant differences in the ionospheric corrections of these redundant observations, with an rms of 1.2 cm or 40 ps (Figure 5). At this stage it is not clear whether these differences are purely the precision of the measurements or whether they occur due to other (systematic) differences between the two Hobart antennas. A comparison of these differences versus elevation or azimuth did not reveal any clear correlation either. In theory (calculated using ionospheric TEC maps), however, the difference in the ionospheric delay should not exceed the 30 μm (10 fs) level on these redundant observations. Accounting for this, we ran a new solution using the ionospheric delays as calculated from GNSS-derived iono-

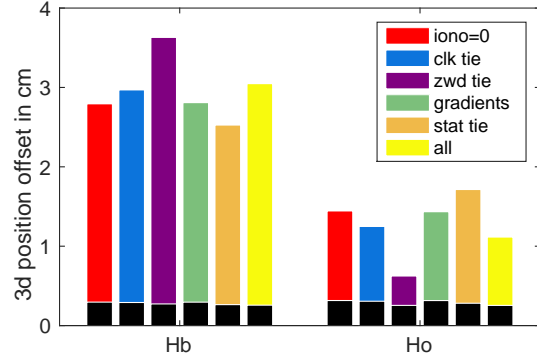


Fig. 6 Estimated 3D station position offsets in *AUST65* using different analysis options for combining common parameters of the sibling telescope. The black bars indicate the corresponding nominal 3D position errors.

spheric TEC maps (Tierno Ros et al., 2011) instead of the ones created by the combination of the S-band and X-band data. Comparing the results to our previous two solutions, we find a further slight improvement in the estimated station position offsets for the sibling telescope in *AUST65* (Figure 4). However, the use of TEC-maps does not seem to be sufficient for longer baselines, as we find considerably larger (additional 1-2 cm) offsets for the other three antennas in *AUST65*. Hence, we keep the second solution with setting the ionospheric delays on the Hb-Ho baseline to zero as our default solution.

In a final investigation we applied the new analysis options of combining common parameters of the sibling telescope to *AUST65*. The results in terms of 3D station position offsets are presented in Figure 6. On the very left the results for the reference solution are shown. We then applied a combination of a single parameter in the analysis, namely clocks, zenith wet delays, atmospheric gradients, and station coordinates. The bars on the right indicate our results when combining all four parameters in the solution. We find that additional constraints for the clocks and the zenith wet delays can significantly change the results in terms of station positions. However, for one station to the better and for the other to the worse. At the moment, constraining the clocks does not have a big influence and we do not find any changes for combining the atmospheric gradients in the analysis. One reason for this could be that both antennas observe (almost) identical scans, so that there is no additional information through

observations in a different azimuthal direction. We conclude from this initial experiment that the various combination strategies do change the results; but they have to be tested carefully and the right values for the constraints need to be found.

4 Outlook

Studying previous and more recent observations with the Hobart twin telescope do raise some questions which need further investigation. In July 2015, the new project *Sibling Telescope* was started, funded by the Austrian Science Fund (FWF). In the upcoming three years, dedicated research will be performed on the topics of:

- Local tie discrepancy: in order to tackle the present discrepancy between the baseline measured by VLBI and the local survey, we have multiple plans; first, we intend to add the Ho antenna more frequently to the standard IVS experiments, in order to extend the baseline observations shown in Figure 1. We further investigate the option of local single-baseline VLBI sessions to derive the local tie, with *hob001* and *hob002* already under analysis at the moment. Lastly, a combination between VLBI and GPS observations within the AuScope network also revealed to be promising for this purpose (Plank et al., 2015).
- Improved analysis: a first step is done by implementing additional constraints in the VieVS software. Now the new options can be tested thoroughly and further refinements will be done. For the single baseline *hob* experiments, we also plan to do a phase delay solution.
- Scheduling strategies: In combination with the new analysis options, new scheduling options will also be developed. The scheduling and simulation tools integrated in VieVS are perfectly suitable for this work.

Acknowledgments

This work was supported by the AuScope Initiative, funded under the National Collaborative Research Infrastructure Strategy (NCRIS), an Australian Commonwealth Government Pro-

gramme. The authors are grateful to the Australian Research Council for Fellowships FS1000100037 and FS110200045 and to the Austrian Science Fund (FWF) for Fellowship J3699-N29.

References

- Alizadeh M M, Wijaya D D, Hobiger T, Weber R, Schuh H (2013) Ionospheric Effects on Microwave Signals. In: J. Böhm, H. Schuh (eds.), *Atmospheric Effects in Space Geodesy*, Springer Atmospheric Sciences.
- Böhm J, Böhm S, Nilsson T, Pany A, Plank L, Spicakova H, Teke K, Schuh H (2012) The new Vienna VLBI software. In: S. Kenyon, M. C. Pacino, U. Marti (eds.), *Proc. IAG Scientific Assembly 2009*, IAG Symposia Series 136, 1007–1011, doi: 10.1007/978-3-642-20338-1_126.
- Hobiger T, Otsubo T (2014) Combination of GPS and VLBI on the observation level during CONT11 – common parameters, ties and inter-technique biases. *J Geod*, 88, 1017–1028, doi: 10.1007/s00190-014-0740-x.
- Lovell J E J, McCallum J N, Reid P B, McCulloch P M, Baynes B E, Dickey J M, Shabala S S, Watson C S, Titov O, Ruddick R, Twilley R, Reynolds C, Tingay S J, Shield P, Adada R, Ellingsen S P, Morgan J S, Bignall H E (2013) The AuScope geodetic VLBI array. *J Geod*, 87, 527–538.
- Nilsson T, Karbon M, Soja B, Heinkelmann R, Lu C, Schuh H (2015) Atmospheric modeling for co-located VLBI antennas and twin telescopes. *J Geod*, 89, 655–665, doi: 10.1007/s00190-015-0804-6.
- Plank L, Santamaría-Gómez A, Lovell J (2015) Comparison of AuScope VLBI and GPS geodetic data. *Geophys Res Abstr*, 17, EGU2015-7343, EGU General Assembly 2015.
- Tierno Ros C, Böhm J, Schuh H (2011) Use of GNSS-derived TEC maps for VLBI observations. In: W. Alef, S. Bernhart, A. Nothnagel (eds.), *Proc. 20th EVGA Working Meeting*, 114–117.

The Asia-Oceania VLBI Group for Geodesy and Astrometry

J. Lovell, R. Kawabata, S. Kurihara, F. Shu, J. Cho

Abstract The Asia-Oceania VLBI Group for Geodesy and Astrometry (AOV) is a recently-formed organisation of scientists supporting geodetic and astrometric VLBI in the Asia-Oceania region and is a sub-group of the International VLBI Service. The purpose of the AOV is to foster and encourage closer collaboration in the science, technology and education aspects of VLBI in the region. There is a focus on the challenges that are particular to Asia-Oceania. We present a brief history of the formation of the AOV, describe its aims, outline our initial observing program and plans for the future.

Keywords Geodesy, Astrometry, VLBI

1 Introduction

Over the past decade, the Asia-Oceania region has seen a significant increase in representation within the IVS. Several organisations from Australia, New Zealand and South Korea have become IVS Member Organisations and the number of geodetic and astrometric facilities in the region has increased with new telescopes at

Jim Lovell

University of Tasmania, Private Bag 37, 7001 Hobart, Australia
Ryoji Kawabata and Shinobu Kurihara

Geospatial Information Authority of Japan, 1, Kitasato, Tsukuba
305-0811, Japan

Fengchun Shu

Shanghai Astronomical Observatory, Chinese Academy of
Sciences, 80 Nandan Road Shanghai 200030, China

Jungho Cho

Korea Astronomy and Space Science Institute, 776,
Daedeokdae-ro, Yuseong-gu, Daejeon, Republic of Korea
(34055)

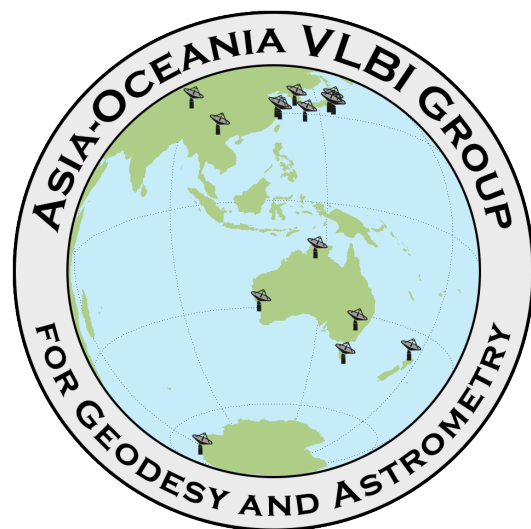


Fig. 1 The logo of the Asia-Oceania VLBI Group for Geodesy and Astrometry (AOV).

Warkworth, Sejong, Ishioka, Kunming, Tianma, Hobart, Katherine and Yarragadee. Many telescopes are planning or are undergoing upgrades to the new VGOS standard and new correlation and analysis centres are also coming on-line.

Countries in Asia-Oceania are also linked by challenges particular to the region, which is highly dynamic in geophysics and climate, with a large number of destructive earthquakes, tsunamis, typhoons and cyclones. Asia-Oceania will experience the effects of climate change much sooner or to a greater degree than other regions, due to more frequent extreme weather events and rising sea levels for example. In order to better understand the risks and reduce the effects of these phenomena, VLBI has an important role to play

through measurement of tectonic plate motions, atmospheric variations and determination of the Geodetic Reference Frame for the region.

As a consequence of these challenges and the increased involvement in VLBI geodesy and astrometry in the region, the Asia-Oceania VLBI Group for Geodesy and Astrometry (AOV) has been formed. Figure 1 depicts the official logo of the AOV. At present it includes members and facilities from five countries in the Asia-Oceania region: Australia, Japan, South Korea, China and New Zealand (Table 1). The purpose of the AOV is to foster and encourage closer collaboration in the science, technology and education aspects of VLBI in the region, to establish an observing program and to meet regularly to facilitate these activities.

Table 1 AOV member organisations.

Organisation	Country
Geoscience Australia	Australia
University of Tasmania (UTAS)	Australia
Commonwealth Scientific and Industrial Research Organisation (CSIRO)	Australia
Shanghai Astronomical Observatory (SHAO)	China
Xinjiang Astronomical Observatory (XAO)	China
Geospatial Information Authority of Japan (GSI)	Japan
National Astronomical Observatory of Japan (NAO)	Japan
National Institute of Information and Communications Technology (NICT)	Japan
National Institute of Polar Research (NIPR)	Japan
Auckland University of Technology (AUT)	New Zealand
Korea Astronomy and Space Science Institute (KASI)	South Korea
National Geographic Information Institute (NGII)	South Korea

2 The Beginning

Informal discussions on the need for the AOV began with Cho Jungho, Fengchun Shu, and Shinobu Kurihara over dinner at the 21st EVGA Meeting in Finland in 2013. Following a positive and enthusiastic response at their home institutions, the discussions were expanded to include colleagues from other organisations in the region with another informal meeting at

the IAG Scientific Assembly in Potsdam in September 2013. A name and acronym for the new group was tentatively agreed and work began on the Terms of Reference. Support for the establishment of the AOV was received from the IVS Directing Board at their meeting on September 7.

Work continued over the following months, culminating in the first meeting of the AOV prior to the 8th IVS General Meeting in Shanghai in March 2014. More than 30 people attended the inaugural meeting. The final draft of the Terms of Reference was agreed shortly after and the process of electing a Chair and Secretary was put in place. Voting in the election was institute based and was managed by the AOV Election Committee comprising Shinobu Kurihara, Stas Shabala, Fengchun Shu, Sergei Gulyaev, and Jungho Cho. Jim Lovell (University of Tasmania) was subsequently elected as Chair and, in accordance with the Terms of Reference, he appointed Ryoji Kawabata (GSI) as Secretary.

3 The 2015 AOV Observing Program

The highest priority within the AOV is to establish an observing program focussed on the region and where member organisations manage all aspects of the program from scheduling through to analysis, research and publication.

Until 2015, the only IVS observing program optimised for the Asia-Oceania region was the Asia-Pacific Space Geodynamics program (APSG), scheduled for 2 days per year. Following consultation with the AOV Membership, we have arranged for 6 more sessions in 2015 (Table 2) for which scheduling will be carried out at the University of Tasmania, GSI or SHAO, and correlation will be shared (two sessions each) between SHAO, GSI and NGII. 18 telescopes are participating in AOV observations in 2015 (Fig. 2). The observed data will be e-transferred to the correlators as much as possible and, during the observations, the data from Hobart and Tsukuba will be transferred in real-time to the Tsukuba Correlator for near-real-time processing.

The correlated data from AOV sessions will be analysed and compared by two or more analysis centres in the region. Results will be used to help improve the schedules for future AOV sessions and consequently the quality of the final data products. Most



Fig. 2 The AOV Network.

Table 2 A summary of the 2015 AOV observing program.

Session	Date	Stations	Schedule	Correlator
AOV001	March 21	Ai Hb Is K1 Ke Km Sh Ts Ur Ww Yg	UTAS	SHAO
AOV002	April 30	Hb Is Ke Kv Sy Ts Vm Ww Yg	GSI	GSI
AOV003	May 17	Hb Ho Is K1 Ke Kg Km Pa T6 Ts Ww Yg	UTAS	GSI
AOV004	August 26	Hb Is Kb Ke Kv Sh Ts Ww Yg	SHAO	NGII
AOV005	September 26	Is K1 Kb Ke Kg Ts Vm Ww Yg	GSI	NGII
AOV006	December 16	Hb Is Kb Ke Km Kv Sh Ts Ur Ww Yg	SHAO	SHAO

of the sessions will be geodetic with attention given to improving measurements of the terrestrial reference frame in the region, but one session (AOV003) will include the large sensitive telescopes at Tianma (65 m) and Parkes (64 m) and this will be focussed on improving the celestial reference frame.

3.1 AOV Meetings

Another high priority within the AOV is to establish a program of regular scientific and working meetings along similar lines to the EVGA. A meeting is planned in Hobart in November 2015 to discuss research programs, technical developments (particularly in connection with VGOS), compare results from the 2015 ob-

servicing campaign and plan future activities. Importantly, this and other meetings will help strengthen collaborations within the region and, because they will be held in Asia-Oceania, the travel distances are shorter and we hope many members will be able to attend.

4 Conclusions

Further information on the AOV, including Terms of Reference, news and information on the observing program is available on the AOV web pages at <http://www.spacegeodesy.go.jp/vlbi/AOV>.

Twin Telescopes at Onsala and Wettzell and their contribution to the VGOS System

C. Schönberger, P. Gnilsen, J. Böhm, R. Haas

Abstract During the last years the International VLBI Service for Geodesy and Astrometry (IVS) spent efforts to improve the accuracy of the geodetic Very Long Baseline Interferometry (VLBI) system to 1 mm for station positions and 0.1 mm/yr for station velocities. To achieve these ambitious goals the VLBI2010 Global Observing System (VGOS) concept was developed, which includes broadband observations with fast-slewing antennas and suggests twin telescopes to reduce the source switching interval and increase the number of observations. Wettzell in Germany has already installed a twin telescope and further twin telescopes will be built in the coming years at Onsala (Sweden) and Ny-Ålesund (Spitsbergen, Norway). In this study, the Vienna VLBI Software (VieVS) is used to schedule and simulate a global VLBI network using the sites that participated in the CONT11 campaign. We compare schedules using the legacy telescopes at Onsala and Wettzell with schedules where either one or both legacy telescopes are replaced by VGOS twin telescopes. The scheduling was done with the source based strategy with four sources at a time, and multidirectional mode for the twin telescopes. The evaluation concerns the numbers of observations and scans, as well as baseline length repeatability and atmospheric parameters.

A higher number of observations and scans can be seen at all sites for the schedules including twin telescopes. Especially at the sites with twin telescopes the number of scans and observations nearly doubles. Also the

Caroline Schönberger, Paul Gnilsen, Johannes Böhm
Technische Universität Wien, Karlsplatz 13, A-1040 Wien, Austria
Rüdiger Haas
Chalmers University of Technology, Onsala Space Observatory,
SE-439 92 Onsala, Sweden

zenith wet delay (ZWD) estimation improves at sites with twin telescopes. However, so far no significant improvement was found for baseline length repeatabilities and further investigations are ongoing.

Keywords VLBI, VLBI2010, VGOS, Radio Telescope, Twin Telescope

1 Introduction

Geodetic Very Long Baseline Interferometry (VLBI) is essential in providing high-precision geodetic data. It is the only technique to derive Universal Time 1 (UT1), the International Celestial Reference Frame (ICRF), and nutation over longer time spans. Beyond that VLBI plays a very important role for deriving the International Terrestrial Reference Frame (ITRF), in particular concerning its scale (Schuh and Böhm, 2013).

When the VLBI technique was developed in the 1970's, the accuracy was on the order of about one meter. Nowadays, VLBI has an accuracy of about 5 mm (Schlüter and Behrend, 2007).

This accuracy shall be improved to 1 mm in station position and 0.1 mm/yr in station velocity with the realization of the VLBI2010 Global Observing System (VGOS) concept, developed by the International VLBI Service for Geodesy and Astrometry (IVS). It includes broadband observations with fast-slewing telescopes and changes in the data management.

Also twin telescopes are suggested in the VLBI2010 design (Petrachenko et al., 2009) in order to improve the handling of atmospheric turbulence that has been identified as the limiting factor

for geodetic VLBI (Nilsson and Haas, 2010). A twin telescope is a pair of identical VLBI telescopes in max 100 m distance, connected to the same frequency standard and with an accurately known local tie vector between the telescopes. Due to the short distance between the twin telescopes, the atmosphere above the telescopes can be assumed to be identical.

The first twin telescope was built at the Wettzell Geodetic Observatory, Germany, in 2011–2013. Additional twin telescopes will be installed in the coming years at the Onsala Space Observatory (Sweden) and the Ny-Ålesund Geodetic Observatory (Spitsbergen, Norway). In this study we focus on the twin telescopes at Onsala and Wettzell.

The Onsala Space Observatory is operated by the Department of Earth and Space Sciences at the Chalmers University of Technology and currently uses a 20 m radio telescope for geodetic VLBI, known as ONSALA60 telescope. A proposal to build the Onsala Twin Telescope (OTT) was submitted in 2011 to the 'Knut and Alice Wallenberg Foundation' and was accepted in 2012. The process of getting building permit was delayed due to issues concerning local wild life and archeological findings (Haas, 2013). Finally, in late 2014 two 13.2 m radio telescopes were ordered. Since these details were not known at the time when the simulations for this work were done, the simulation assumed a smaller telescope diameter of just 12 m for the OTT. The necessary infrastructure work for the OTT will be done in 2015 and installation of the twin telescopes will start in spring 2016. It is expected that OTT will be fully operational in 2017 and gradually take over the regular observations of the legacy telescope.

The Wettzell Geodetic Observatory in Germany is operated by the Bundesamt für Kartographie und Geodäsie (BKG) and the Forschungseinrichtung Satellitengeodäsie (FESG) of the Technische Universität München. It is equipped with a legacy 20 m radio telescope and since 2013 with two 13.2 m radio telescopes, the Twin Telescope Wettzell (WTT) (Kronshnabl et al., 2014).

This work compares the results that can be achieved if the 20 m legacy telescopes at Onsala and Wettzell were replaced by twin telescopes following the VGOS concept.

For this work existing telescopes used in the CONT11 campaign were used, since this is a network that has produced results which can be used as a



Fig. 1 The stations participating in the CONT11 campaign. The station WARK12M in New Zealand had to cancel its participation because of technical problems (<http://ivscc.gsfc.nasa.gov/program/cont11/cont11.jpg>)

reference. A map of the CONT11 network is presented in Figure 1. The station WARK12M in New Zealand had to cancel its participation because of technical problems and it is thus not included in this study. Details on each station are given in Table 1.

The scheduling, simulation and analysis for this study was done using the Vienna VLBI Software (VieVS) (Böhm et al., 2013).

The scheduling was done with the `vie_sched` module (Sun, 2014) using a source-based strategy. In this approach the scheduling program selects two or four sources at a time (SAAT) in a way to achieve the

Table 1 Stations participating in the CONT11 campaign with information on the telescope diameter, d , and the slewing velocity in azimuth and elevation, v_α and v_ϵ , respectively. The corresponding information for the twin telescopes is given, too.

Station	d [m]	v_α [°/min]	v_ϵ [°/min]
BADARY	32.0	72	48
FORTLEZA	14.2	40	20
HOBART12	12.0	300	75
HARTRAO	26.0	240	120
KOKEE	20.0	117	117
NYALES20	20.0	120	120
ONSALA60	20.0	144	60
OTT	12.0	720	360
TIGOCONC	6.0	360	180
TSUKUB32	32.0	180	180
WESTFORD	18.0	200	120
WETTZELL	20.0	180	90
WTT	13.2	720	360
YEBES40M	40.0	60	60
ZELENCHK	32.0	72	48

best distribution of sources on the celestial sphere. The sources are selected without considering any effects on individual stations. In the 2-SAAT approach the two selected sources are as far apart as possible and for the 4-SAAT approach the sources form a regular tetrahedron (Sun, 2013). For this study we used the 4-SAAT approach.

A twin telescope allows two additional observing modes, namely the multidirectional mode and the continuous mode. In the multidirectional mode, the two telescopes are part of different subnets at the same time by observing separately different sources in different directions. To operate a twin telescope in the multidirectional observing mode the 4-SAAT strategy has to be chosen, because for the 2-SAAT approach one of the two sources will be blocked by the Earth. In the continuous mode one telescope observes while the other one slews to the next radio source. This leads to continuous observations without temporal gaps (Sun, 2013). However, since previous studies showed that the multidirectional mode gave better results than the continuous mode, we focussed in this study on the multidirectional mode.

All schedules were finalized with the fill-in mode and a cut off elevation angle of 5° was applied. Sources with a minimum source flux density of 0.5 Jansky (Jy) were included in the scheduling and the minimum Sun distance chosen was 4° .

With the `vie_sim` (Pany et al., 2011) module the observations of the first day of the CONT11 campaign were simulated 25 times, artificially generating a wet troposphere using the turbulence parameter listed in Table 2, clock errors corresponding to an Allan Standard Deviation (ASD) of $1e-14$ @ 50 min, and white noise with 32 ps standard deviation.

The parameters listed in Table 3 were estimated in a least-squares adjustment using the `vie_lsm` module.

The four schedules listed in Table 4 are compared to each other in Section 2. The comparison parameters are the numbers of observations, the number of scans, as well as the baseline length repeatabilities, and zenith wet delay estimates. Sky plots are presented in Fig. 4.

2 Results

The figures in this section depict results for the schedules listed in Table 4.

Table 2 Turbulence parameters C_n (assumed constant up to 2 km) in $10^{-7} \text{ m}^{-1/3}$ and wind velocities in north and east direction v_n and v_e in m/s for all sites participating in the CONT11 campaign (Nilsson and Haas, 2010).

Station	C_n	v_n	v_e
BADARY	1.37	0.24	4.74
FORTLEZA	2.46	2.93	-7.11
HOBART12	1.60	3.03	11.14
HARTRAO	1.34	2.03	-2.84
KOKEE	1.39	4.38	-3.35
NYALES20	0.65	7.46	0.53
ONSALA	2.19	7.46	0.53
TIGOCONC	2.08	1.21	4.96
TSUKUB32	3.45	1.03	10.49
WESTFORD	2.30	5.39	11.88
WETTZELL	1.50	7.75	4.22
YEBES40M	1.48	7.75	4.22
ZELECHK	1.86	4.66	4.15

Table 3 Estimated parameters in the least-squares adjustment. The time interval is given in column 2. Column 3 states constraints using the same unit as the parameter. ZWD: zenith wet delay; NGR/EGR: north/east gradients; EOP: earth orientation parameters.

Parameter [Unit]	interval	constraint
ZWD [cm]	10 min	1.5
NGR [cm]	15 min	0.05
EGR [cm]	15 min	0.05
Station coord.[cm]	24 h	NNT/NNR
EOP [mas/ms]	24 h	$1.0 \text{ e-}4$
Clock offset [cm]	1 h	1.3

Table 4 The four different schedules that were compared in this study. All four were scheduled using the 4-SAAT strategy and the twin telescopes used the multidirectional observing mode.

Schedule	explanation
CONT11	original CONT11 network
OTT	OTT replacing ONSALA60 in CONT11
WTT	WTT replacing WETTZELL in CONT11
OTT & WTT	OTT and WTT replacing ONSALA60 and WETTZELL in CONT11

Figures 2 and 3 depict the number of observations and scans for Onsala and Wettzell, and the average number of the other stations. The number of observations declares how often baselines are formed during a session.

The number of observations for this session varies between 700 and 20100 per site with 5000 observations on average. With a VGOS twin telescope, nearly twice as many observations can be carried out at that site, compared to using a 20 m legacy telescope, and also the average value for the other sites increases. The

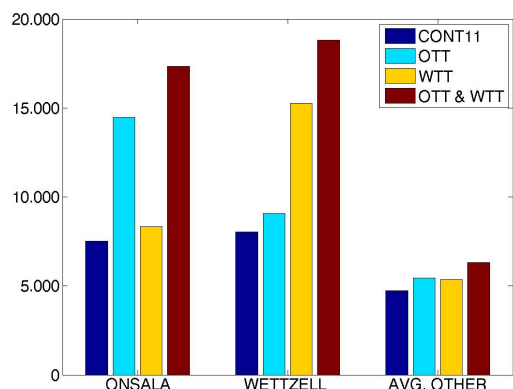


Fig. 2 Number of observations at Onsala and Wettzell and the average number over all other sites. The value for Onsala and Wettzell is the sum of the two single telescopes. With a VGOS twin telescope, nearly twice as many observations can be carried out at that site than with a 20 m legacy telescope.

largest number of observations is achieved with both twin telescopes in the network.

The number of scans varies between 150 and 900 per day with an average value of around 400. This result is in accordance with the number of observations with a high increase at the site using a twin telescope and the highest increase with both twin telescopes in the network.

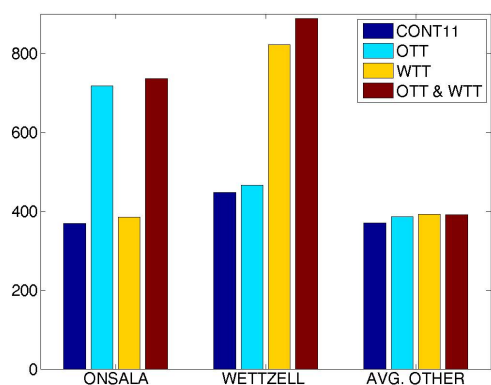


Fig. 3 Number of scans at Onsala and Wettzell and the average over all other sites. The value for Onsala and Wettzell is the sum of the two single telescopes. With a VGOS twin telescope, nearly twice as many scans can be carried out at that site than with a 20 m legacy telescope.

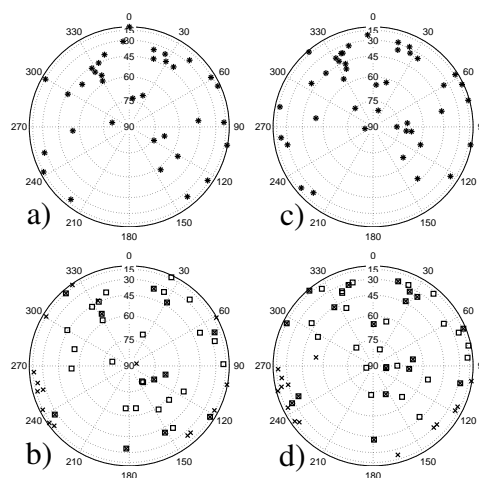


Fig. 4 Sky plot of the first 2 hours for Onsala (left column) and Wettzell (right column). Shown are the sky plots for the CONT11 schedule (upper row) with asterisks (*) and the schedules OTT and WTT (lower row) with crosses (x) and squares (□) for each twin telescope. When both telescopes observe the same source simultaneously the symbols are plotted on top of each other and create crossed box (⊠). With the twin-telescope schedules (OTT Fig. 4b, WTT Fig. 4d) more sources are observed in different elevation and azimuth angles, which leads to an improved sky coverage and furthermore to improved ZWD estimations.

Figure 4 depict the sky plot of the first 2 hours for stations Onsala and Wettzell with the legacy 20 m antenna or the corresponding VGOS twin telescopes. Since the baseline between the two stations is less than 1000 km and they are mainly part of the same subnets.

The increased number of scans with the VGOS twin telescopes is clearly visible and the sky coverage is obviously improved, which leads to a better zenith wet delay (ZWD) estimation, as shown in Fig. 5. However there is still room for improving the sky coverage with twin telescopes.

The RMS values of the ZWD are calculated between the estimated ZWD compared to the simulated ZWD shortly after the estimation time, and varies between 4 mm and 14 mm, with an average value of 9 mm. As seen in Fig. 5, the use of a VGOS twin telescope improves the ZWD estimation at that site. As stated in Section 1, the main goal for twin telescopes is the improved handling of the atmospheric turbulence, which can be seen as achieved.

The results for baseline length repeatability show no significant improvement yet. Further investigations are ongoing.

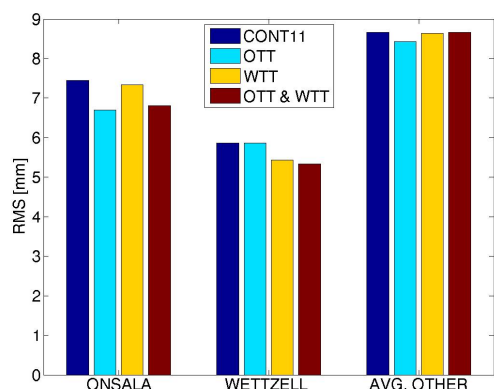


Fig. 5 RMS between estimated ZWD and simulated ZWD for Onsala and Wettzell and the average of the other stations in mm. An improvement with twin telescopes is clearly visible.

3 Conclusions

Replacing the legacy 20 m telescopes at Onsala and/or Wettzell by VGOS twin telescopes has significant effects on the investigated parameters.

The analysis of the schedules shows that more scans and observations are obtained for all stations in the investigated network if the legacy telescopes at Onsala and/or Wettzell are replaced by VGOS twin telescopes. Especially the stations with twin telescopes benefit from an increase in the number of scans and observations by almost a factor of two. This is an important goal in the VGOS concept and yields improved sky coverage and improved zenith wet delay estimation.

The presented results are based on the current version of VieVS. However, the scheduling for twin telescopes needs to be optimized in the next years. Besides that, the continuous realization of the VGOS concept with the introduction of broadband observations and more antennas on the southern hemisphere will point out advantages of twin telescopes clearer.

References

Böhm J, Böhm S, Nilsson T, Pany A, Plank L, Krásná H, Teke K, Schuh H (2013) The new Vienna VLBI software. In: S. Kenyon, M. C. Pacino, U. Marti (eds.), *Proc. IAG Scientific Assembly 2009*, IAG Symposia Series 136, 1007–1011,

doi: 10.1007/978-3-642-20338-1.126.

- Haas R (2013) The Onsala Twin Telescope Project. In: N. Zubko, M. Poutanen (eds.) *Proc. 21st EVGA Working Meeting*, 61–65.
- Kronshnabl G, Schüler T, Neidhardt A, Plötz C, Klügel T, Kodet J (2014) Status of the Wettzell Radio Telescope Triple and the O’Higgins VLBI System at Antarctica. In: D. Behrend, K. D. Baver, K. L. Armstrong (eds.), *IVS 2014 General Meeting Proc.*, Science Press (Beijing), 145–149.
- Nilsson T, Haas R (2010) Impact of atmospheric turbulence on geodetic very long baseline interferometry. *J Geophys Res*, 115, doi: 10.1029/2009JB006579.
- Pany A, Böhm J, MacMillan D, Schuh H, Nilsson T, Wresnik J (2011) Monte Carlo simulations of the impact of troposphere, clock and measurement errors on the repeatability of VLBI positions. *J Geod*, 85, 39–50.
- Petrachenko B, Niell A, Behrend D, Corey B, Böhm J, Charlot P, Collioud A, Gipson J, Haas R, Hobiger T, Koyama Y, MacMillan D, Malkin Z, Nilsson T, Pany A, Tuccari G, Whitney A, Wresnik J (2009) Design aspects of the VLBI2010 system. *Progress report of the IVS VLBI2010 Committee*, NASA/TM-2009-214180.
- Schlüter W, Behrend D (2007) The International VLBI Service for Geodesy and Astrometry (IVS): Current Capabilities and Future Prospects. *J Geod*, 81(6-8), 379–387.
- Schuh H, Böhm J (2013) Very Long Baseline Interferometry for Geodesy and Astrometry. In: G. Xu (ed.) *Sciences of Geodesy II, Innovations and Future Developments*, 339–376.
- Sun J (2013) VLBI scheduling strategies with respect to VLBI2010. *Geowissenschaftliche Mitteilungen*, 92, ISSN 1811-8380.
- Sun J, Böhm J, Nilsson T, Krásná H, Böhm S, Schuh H (2014) New VLBI2010 scheduling strategies and implications on the terrestrial reference frames. *J Geod*, 88, 449–461.

Contributions of Onsala Space Observatory to GGOS

R. Haas, G. Elgered, T. Hobiger, H.-G. Scherneck, J. Johansson

Abstract The Onsala Space Observatory (OSO) on the Swedish west coast is the fundamental geodetic station of Sweden and operates several co-located geodetic and geophysical infrastructures that contribute to the GGOS. Currently, work is ongoing to establish a twin telescope to be part of the VGOS network.

Keywords GGOS, VLBI, GNSS, tide gauges, gravimetry, atmospheric measurements, time and frequency

1 Introduction

The Onsala Space Observatory (OSO) is the National Facility for Radioastronomy in Sweden and has the task to provide equipment and expertise in radio astronomy and geosciences to the Swedish as well as the international scientific community. In this role it is also the fundamental geodetic station of Sweden.

Already since the 1960ies radio telescopes are operated at OSO for geodetic Very Long Baseline Interferometry. Since the 1990ies, also equipment for GNSS is operated at OSO. A number of geodetic and geophysical research instruments have been installed during the last decades, including microwave radiometers for atmospheric research, a superconducting gravimeter, a seismometer, and several tide

Rüdiger Haas, Gunnar Elgered, Thomas Hobiger, Hans-Georg Scherneck, Jan Johansson
Chalmers University of Technology, Department of Earth and Space Sciences, Onsala Space Observatory, SE-439 92 Onsala, Sweden

gauges. With its variety of co-located instrumentation used for geoscience observations, OSO contributes to several of the services of the International Association for Geodesy (IAG), such as the International VLBI Service for Geodesy and Astrometry (IVS), the International GNSS Service (IGS), and the Global Geodynamics Program (GGP), and thus to the Global Geodetic Observing System (GGOS). Figure 1 depicts an aerial photo of OSO and indicates the location of the different instruments.

2 VLBI

OSO has the longest VLBI observational record in Europe, going back to April 1968 (Scherneck et al., 1998; Elgered and Haas, 2000). Currently, about 40 to 50 sessions per year are observed in IVS programs. OSO participated successfully in all CONT campaigns and performed CONT11 and CONT14 in ultra-rapid mode together with the Tsukuba station in Japan. During these continuous campaigns UT1-UTC was derived in near real-time. The left photo in Fig. 2 shows the radome-enclosed 20 m radio telescope that currently is used for geodetic VLBI observations. The right photo in Fig. 2 shows the 25 m radio telescope that occasionally is used to do VLBI with GNSS signals, see e.g. Haas et al. (2014, 2015).

In 2012 we received funding for a twin telescope (Haas, 2013), to be part of the VGOS network. Two VGOS-type telescopes with 13.2 m diameter have been ordered in late 2014 from the company MT Mechatronics. Currently the necessary infrastructure work at OSO is ongoing, including the construction of two concrete towers. As an example, Fig. 3 depicts the form for the



Fig. 1 Aerial photo of OSO: (1) the radome-enclosed 20 m radio telescope, (2) the microwave radiometer "Konrad", (3) the GNSS-station ONSA, (4) the microwave radiometer "Astrid", (5) the location of the northern telescope of the future Onsala Twin Telescope, (6) the location of the southern telescope of the future Onsala Twin Telescope, (7) the tide gauge station, (8) the 25 m radio telescope, (9) the GNSS-R based tide gauge, (10) the seismometer, (11) the six-station GNSS-array around the OTT, (12) the GNSS-station ONS1, (13) the gravimeter laboratory with the superconducting gravimeter, (14) the time and frequency laboratory.



Fig. 2 Left: The radome-enclosed 20 m radio telescope at OSO that is used for VLBI observations in the IVS programs. Right: The 25 m radio telescope that is used primarily for astronomy VLBI but occasionally also to track GNSS satellites.

concrete pouring of the northern tower. The telescopes themselves will be delivered in early 2016 and installed during the summer of 2016. The signal chain will be installed in late 2016. It is expected that first test observations with the Onsala Twin Telescope (OTT) can be started in early 2017, and that OTT becomes fully

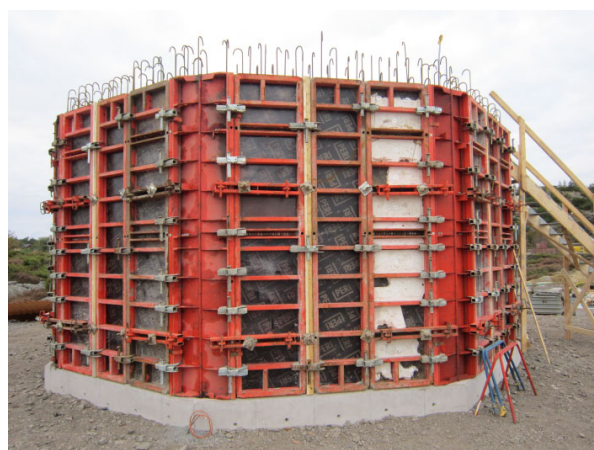


Fig. 3 The form for the concrete pouring of the bottom floor of the northern OTT tower.

operational 1–2 years later. Figure 4 depicts an artist's view on the future OTT.

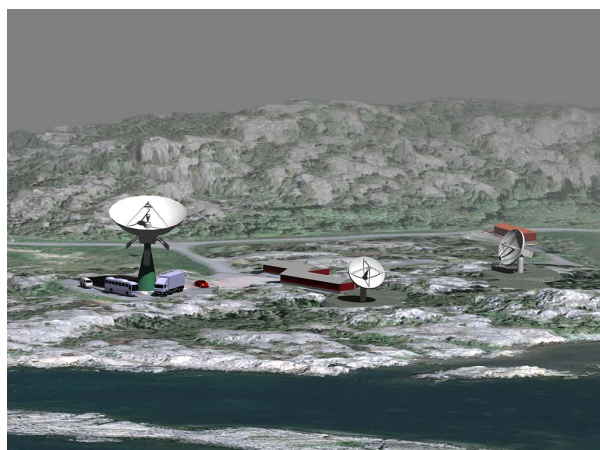


Fig. 4 An artist's view on the future OTT.

3 GNSS

In collaboration with Lantmäteriet, the Swedish Mapping, Cadastral and Land Registration Authority, OSO operates the IGS stations ONSA and ONS1, see Fig. 5. Data of ONSA are used for both geodynamical research, e.g. Johansson et al. (2002), and atmospheric research, e.g. Ning et al. (2012). A new GNSS array consisting of six additional stations is under construction in the area around the OTT. Its baselines are of the order of hundreds of metres, and this network will also be operated together with Lantmäteriet. Currently we are in discussion with ESA to investigate the possibility to include one of these array stations in ESA's ionospheric monitoring network.



Fig. 5 The pillar and antenna of the IGS station ONSA (left), and the mast and antenna of the IGS station ONS1 (right).

4 Gravimetry

Since 2009 OSO operates a gravimeter laboratory for relative and absolute gravity measurements which is equipped with a superconducting gravimeter. It has been operated continuously since then with a reliability well above 99 %. Data are available via a webpage and are sent to the archive of the Global Geodynamics Project (GGP). In collaboration with the University of Uppsala, a seismometer is operated that is part of the Swedish National Seismic Network (SNSN). A screen-shot of the webpage presenting near real-time results from the superconducting gravimeter is shown in Fig. 6. The OSO superconducting gravimeter also supports studies with visiting absolute gravimeters, e.g. Timmen et al. (2015).

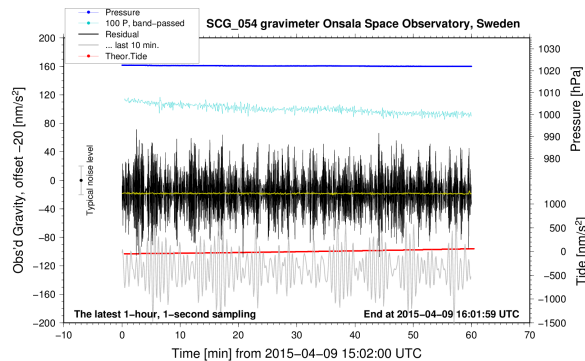


Fig. 6 An example of near real-time data results from observations of the superconducting gravimeter.

5 Tide gauges

Since 2011 GNSS-R tide gauge is operated at OSO, utilizing reflected signals from multiple GNSS, see Fig. 7 right. Signals of several GNSS are used to determine time series of sea level, e.g. Löfgren and Haas (2014); Hobiger et al. (2014). Additionally, in 2013 and 2014 several pneumatic and bubbler sensors and a radar-based sensor have been installed in a dedicated tide gauge well, see Fig. 7 left. The latter installation was inaugurated officially in September 2015 and is operated together with the Swedish Meteorological and Hydrological Institute (SMHI). It is now an official site in the national sea level monitoring network.

Figure 8 depicts a comparison of sea level time series derived from GNSS-R and the traditional tide gauge.



Fig. 7 The traditional tide gauge (left) equipped with a radar and several bubbler sensors in the well, and the GNSS-R based tide gauge (right).

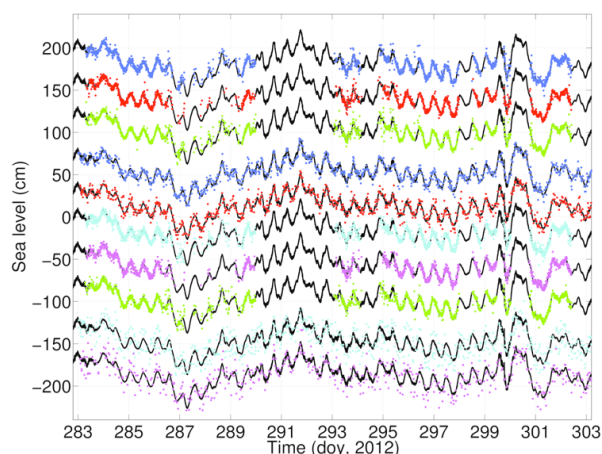


Fig. 8 Sea level derived from the GNSS-R tide gauge at OSO during 20 days in 2012 (Oct. 9 to 29). From top to bottom the sea level times series are derived from: GPS phase (L1), GLONASS phase (L1), GPS and GLONASS phase (L1), GPS SNR (L1), GLONASS SNR (L1), GPS phase (L2), GLONASS phase (L2), GPS and GLONASS phase (L2), GPS SNR (L2) and GLONASS SNR (L2). Each time series is paired with the independent sea level observations from the co-located tide gauge (black line). A mean is removed from each time series and the pairs are displayed with an offset of 40 cm to improve visibility.

6 Atmospheric measurements

Several ground-based microwave radiometers for atmospheric research are operated at OSO. The two microwave radiometers "Astrid" and "Konrad" are shown in Fig. 9. They are used to infer the time delay caused

by atmospheric water vapour. This information is used to validate atmospheric parameters estimated from the space geodetic techniques, i.e. VLBI and GNSS, see e.g. Teke et al. (2013), but is also used for in meteorological studies, e.g. Elgered and Jarlemark (1998). A new microwave radiometer is currently under development and will be installed in the near future in the OTT area.



Fig. 9 The microwave radiometers Konrad (left) and Astrid (right).

7 Time and frequency

In collaboration with SP Technical Research Institute of Sweden, OSO operates a time and frequency laboratory with two H-masers, a cesium clock, and several GNSS time receivers. These instruments are used for the local time and frequency distribution for the scientific equipment at OSO, and to support the Swedish UTC realization. Based on VLBI and GNSS observations, we perform intercontinental frequency-transfer between OSO's time laboratory and international partner institutions, see Hobiger et al. (2015).

References

- Elgered G, Haas R (2000) VLBI in the service of geodesy 19682000: An Onsala perspective. In: J. E. Conway, A. G. Polatidis, R. S. Booth, Y. Pihlström (eds.), *Proc. 5th European VLBI Network Symposium*, 209-216.
- Elgered G, Jarlemark P O J (1988) Ground-based microwave radiometry and long-term observations of atmospheric water vapor. *Radio Sci*, 33(3), 707-717.
- Haas R (2013) The Onsala Twin Telescope Project. In: N. Zubko, M. Poutanen (eds.) *Proc. 21st EVGA Working Meeting*, 61-65.

- Haas R, Neidhardt A, Kodet J, Plötz Ch, Schreiber K-U, Kron-schnabl G, Pogrebenko S, Duev D, Casey S, Marti-Vidal I, Yang J, Plank L (2014) The Wettzell-Onsala G130128 experiment – VLBI-observations of a GLONASS satellite. In: D. Behrend, K. D. Baver, K. L. Armstrong (eds.), *IVS 2014 General Meeting Proc.*, Science Press (Beijing), 451–455.
- Haas R, Neidhardt A, Kodet J, Plötz Ch, Schreiber K-U, Kron-schnabl G, Pogrebenko S, Duev D, Casey S, Marti-Vidal I, Yang J, Plank L (2014) The Wettzell-Onsala G130128 experiment – VLBI-observations of a GLONASS satellite. In: R. Haas, F. Colomer (eds.), *Proc. 22nd EVGA Working Meeting*, 107–111.
- Hobiger T, Haas R, Löfgren J S (2014) GLONASS-R: GNSS reflectometry with a Frequency Division Multiple Access-based satellite navigation system. *Radio Sci*, 49, doi: 10.1002/2013RS005359.
- Hobiger T, Rieck C, Haas R, Koyama Y (2015) Combining GPS and VLBI for inter-continental frequency transfer. *Metrologia*, 52, 251–261, doi: 10.1088/0026-1394/52/2/251.
- Johansson J M, Davis J L, Scherneck H-G, Milne G A, Vermeer M, Mitrovica J X, Bennett R A, Jonsson B, Elgered G, Elosegui P, Koivula H, Poutanen M, Roännäng B O, Shapiro I I (2002) Continuous GPS measurements of post-glacial adjustment in Fennoscandia 1. Geodetic results. *J Geophys Res*, 107(B8), 2157, doi: 10.1029/2001JB000400.
- Löfgren J S, Haas R (2014) Sea level measurements using multi-frequency GPS and GLONASS observations. *EURASIP Journal on Advances in Signal Processing*, 2014, 50.
- Ning T, Haas R, Elgered G, Willén U (2012) Multi-technique comparisons of 10 years of wet delay estimates. *J Geod*, 86, 565–575 doi: 10.1007/s00190-011-0527-2.
- Scherneck H-G, Elgered G, Johansson J M, Rönnäng B O (1998) Space geodetic activities at the Onsala Space Observatory: 25 years in the service of plate tectonics. *Phys ChemEarth*, 23(7–8), 811–823.
- Timmen L, Engfeldt A, Scherneck H-G (2015) Observed secular gravity trend at Onsala station with the FG5 gravimeter from Hannover. *J Geod Sci*, 5, 1–8, doi: 10.1515/jogs-2015-0001.
- Teke K, Nilsson T, Böhm J, Hobiger T, Steigenberger P, García-Espada S, Haas R, Willis P (2013) Troposphere delays from space geodetic techniques, water vapor radiometers, and numerical weather models over a series of continuous VLBI campaigns. *J Geod*, 87(10–12), 981–1001, doi: 10.1007/s00190-013-0662-z.

Local Tie Works in Yebes Observatory

B. Córdoba, J. López–Ramasco, S. García–Espada

Abstract An important requirement to convert the RAEGE station in Yebes (Spain) into a Fundamental Geodetic Station is to accurately relate all the different geodetic techniques, which is known as the Local Tie. We have investigated the possibility to measure the invariant reference point (IRP) of the 13-m radio telescope. In our case, there is a big advantage since the measurements can be performed inside the telescope cabin with a robotic total station, located on a central pillar built inside the radio telescope tower. The methodology used is based in the adjustment from measurements points on the radio telescope frame of circles in 3D constrictions, taken with a robotic total station, installed on a tripod with an optical plummet placed on the marked centered screw of this central pillar. A network of 20 monuments (concrete pillars) has also been built in the area of Yebes Observatory in order to relate the measurements taken by our two VLBI radio telescopes (40-m and 13-m) and two GNSS antennas (IGS code YEBE, on the roof of the office building, and YEB1, on the roof of the gravimetry building).

Keywords Local Tie, Invariant Reference Point

Beatriz Córdoba, Javier López–Ramasco
Observatorio de Yebes, IGN
Cerro de la Palera s/n, 19141 Yebes, Guadalajara, Spain
Susana García–Espada
RAEGE Santa Maria, IGN
Rua Teófilo Braga n28, 9580-535 Vila do Porto, Santa Maria,
Azores. Portugal

1 Introduction

Yebes Observatory is located 70 kilometers far from Madrid, in the center of the Iberian Peninsula, a strategic place in the limit of the European Tectonic Plate. It is provided with two VLBI antennas (40 meter radio telescope (Fig. 1a) and 13 meters radio telescope (Fig. 1b)), two GNSS antennas, (YEBE (Fig. 1c), on the roof of the office building and YEB1 (Fig. 1d), on the roof of the gravimetry building) and a superconducting gravimeter inside the gravity building. There is also some complementary instrumentation which can be useful as for example a LAMBRECHT rain gauge, a SENTEK ENVIROMENT humidity sensor with five heights and a UNIK piezometric sensor to measure the water level.

Our main goal is to relate 40 meters and 13 meters radio telescopes with one of the GNSS antennas, YEBE, which belongs to the EUREF Permanent Network. In Figure 2 a map of the Observatory with the different techniques is shown. Yellow vectors point out the required local ties.

To perform this task we show here some first works as the calculation of the invariant reference point of the 13-m radio telescope and the design of a pillar network to relate the different techniques with the required accuracy.

2 RAEGE 13M-Radio telescope Invariant Reference Point determination

The Invariant Reference Point (IRP) of a radio telescope is defined as the intersection between its azimuth and elevation axis if this intersection exists. Otherwise

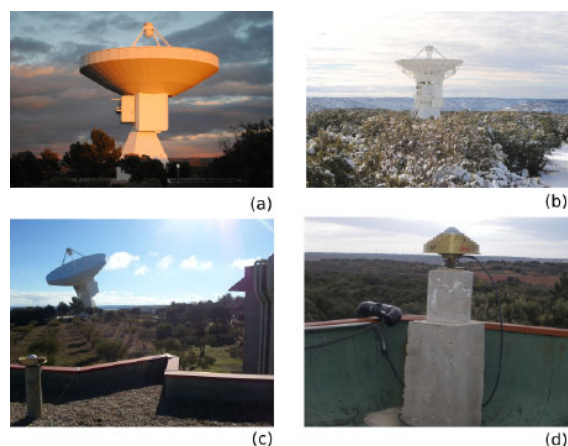


Fig. 1 Yebes Observatory is provided with (a) VLBI 40m Antenna, (b) VLBI 13m Antenna (RAEGE), (c) YEBE GNSS Antenna and (d) YEB1 GNSS Antenna.

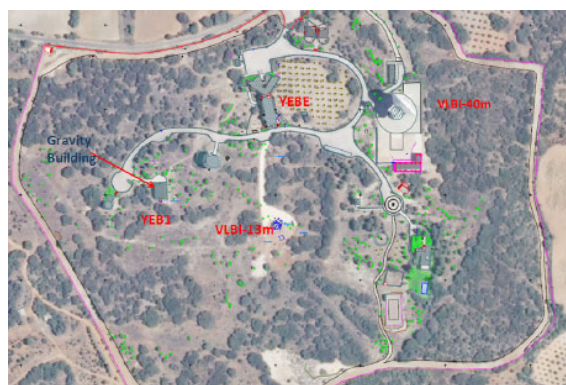


Fig. 2 Aerial view of Yebes Observatory and the location of the different geodetic techniques.

it is defined as the projection of the elevation axis on the azimuth axis. Usually this point is inaccessible or it is not materialized. There are several methodologies to calculate it. A big advantage of the new 13 meters RAEGE radio telescope in the Observatory is that measurements can be performed inside the cabin with a robotic total station, located on the central pillar of the radio telescope during the measurement campaign.

For this purpose a Leica TS50 total station with an angular and distance accuracy of $0.5''$ and 0.6 mm respectively, located on the central pillar of the radio telescope has been used. For it, a tribranch tripod with optical plummet was established over the marked centered screw of the pillar (Fig. 3a). Using the total station was measured the position of a corner cube reflector RRR Hexagon, which was attached magneti-

cally to the inner sides of both antenna counterweights (Fig. 3b) with a manufacturing precision of 0.0001 mm. Measurements of the reflector (CCR) were taken every 30 seconds for right counterweight by moving the antenna around the elevation and azimuth axis. Movements of the antenna were performed in increments of 20° for both the azimuth and elevation axis. The sequence of measured movements were carried out by fixing one azimuth of 18 possible and moving the telescope at five different elevation positions (7° , 27° , 47° , 67° , 87°). Then the azimuth angle was increased 20° and the procedure was done again but this time by decreasing the elevation angle from 87° to 7° . This measurements were carried out for all azimuth and elevation combinations. Afterwards the previous steps were repeated but placing the CCR at the left counterweight. Therefore a total of 180 ($18 \cdot 5 \cdot 2$) points were measured every 30 seconds using an automated observation of 90 minutes of duration. A total of 5 azimuth circles and 18 elevation arcs were adjusted for each counterweight. There were a total of 10 azimuth circles and 36 elevations arcs for both counterweights from which the 18 elevations axes were calculated.

The TS50 station was controlled by a laptop connected via Bluetooth running an own software that handles the tasks of orientating, targeting, measuring, recording and synchronization with the control center of the antenna.

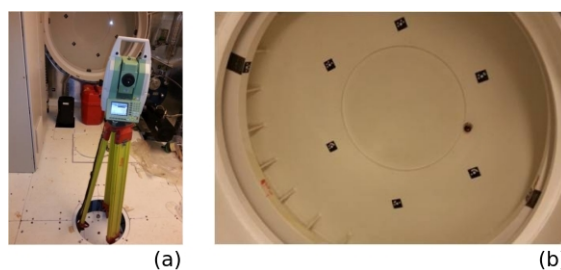


Fig. 3 (a) Leica TS50 total station and (b) corner cube reflectors attached to the counterweights inner side.

The determination of the IRP both the azimuth and elevation axis have been estimated adjusting the observation data with a Mixed Model Least Squares with constraints.

For the estimation of the azimuth axis, observations to the targets during the rotation of the radio telescope around the azimuth axis for different elevations have been measured. Observations have been adjusted to cir-

cles in space, this is, the intersection of a sphere and a plane. Also, the center of the sphere must satisfy the plane equation. In this adjustment the parameters for each sphere (center and radio) and for each plane have been determined.

For the estimation of the elevation axes, observations during the targets on the rotation of the radio telescope around the elevation axes for different azimuths have been measured. Observations must be adjusted to circles arcs in space. Measurements have been performed in both counterweights for each azimuth position. Centers from both circle arcs generate the elevation axes.

The Equations for the sphere (Eq. 1), plane (Eq. 2) and the constraints (Eq. 3) used in the Mixed Model Least Squares are:

$$F(L, X) = (x_i - a)^2 + (y_i - b)^2 + (z_i - c)^2 - r^2 = 0 \quad (1)$$

$$G(L, X) = A \cdot x_i + B \cdot y_i + C - z_i = 0 \quad (2)$$

$$H(L, X) = A \cdot a + B \cdot b + C - c = 0 \quad (3)$$

where $(a, b, c), r$ are the center and the radio of the sphere and A, B, C are the plane parameters.

Measured circles for the azimuth axis estimation and circles arcs for the elevation axis estimations are shown in Figure 4 and Figure 5 respectively.

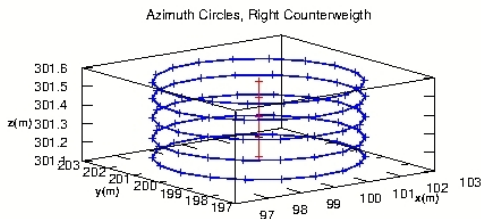


Fig. 4 A total of 5 circles for each Counterweight (10 in total) were adjusted. Each circle is adjusted from 18 observed points. 52 parameters have been adjusted from 360 observation equations.

Results from the adjustment are shown in Table 1.

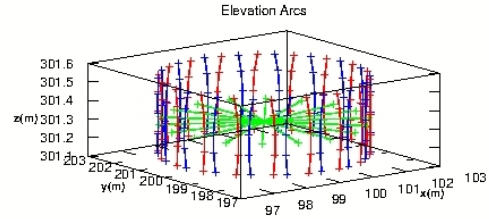


Fig. 5 A total of 18 circle arcs for each Counterweight (36 circle arcs in total) and 18 elevation axes have been adjusted.

Table 1 Results from the adjustment for the Radiotelescope geometric parameters.

Radiotelescope geometric parameters		
	Value	Standard deviation
Invariant Reference Point (m)	X	99.99774
	Y	199.99226
	Z	301.314795
Eccentricity (m)	0.00013	0.00007
Azimuth axis inclination from the vertical (°)	-8.3	0.3
Non-orthogonality angle between azimuth and elevation axes (°)	5.6	0.9

3 Feasibility and design of the Geodetic Network of pillar in the Yebes Observatory

Different studies of different networks configurations have been done before the construction of the pillar network. From a least square adjustment point of view, it has been concluded that the best configuration, which allow to us to get accuracy below 1 mm, has 24 vertex. Included on this network are the four available geodetic techniques (Fig. 6). Each geodetic technique is surrounded by pillars that are in the line of sight and so that there is a connection between all the techniques.

The design and construction of the network was not very easy because of the vegetation, trees and low bushes, in the Observatory. It was tried to create base-lines with approximately the same length and triangles the most equilateral possible.

To simulate the network some distances and angles measurements have been generated with random errors from the Box-Muller method with an error of

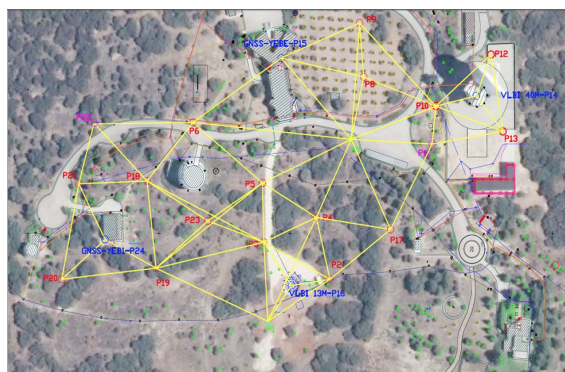


Fig. 6 Pillar network at the Yebees Observatory.

0.6 mm in distances plus the parts per million and 2.5'' in angles. For now, the adjustment of the network has been done just in planimetry without taking into account heights. It has been used the variation of coordinate methodology using two kinds of observation equations: azimuth and distances equations. Due to it is a free network, it is necessary to add some constrains to the problem to obtain a solution. We have included an internal constrain matrix which has the property that the estimated solutions has a minimum variance. In the near future we will introduce also heights in the adjustment.

The results of the precision of the adjusted coordinates using azimuth and distances equations are represented through error ellipses in Fig. 7.

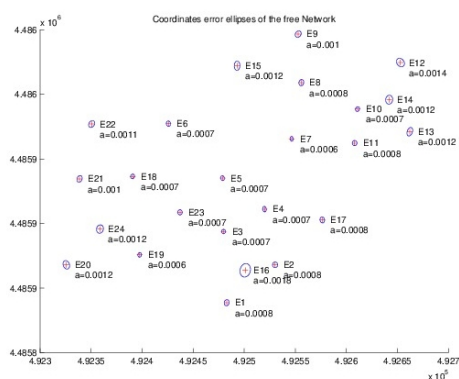


Fig. 7 Results of the precision of the adjustment coordinates using azimuth and distances equations.

In Table 2 it is shown the local tie accuracy that could be achieved between the different techniques.

Table 2 Local tie accuracy between different techniques at Yebees Observatory.

Local tie	Accuracy (m)
VLBI13 - GNSS(YEBE) (~ 159 m)	0.0008
VLBI40 - GNSS(YEBE) (~ 151 m)	0.0007

4 Building pillars

After the design of the network, pillars were built. They are made of concrete and iron and they are a 30 cm diameter and 1.30 m height cylinder covered by a protecting tube. Between the cylinder pillar and the protecting tube there is a free space of 5 cm to isolate the interior pillar. At the top of the exterior protecting tube, it has a metal lid to prevent the entry of water, and a drainage hole at the bottom of pillar. Fixed to the top of the interior pillar, there is a stainless steel plate of 5 mm thickness, in which center there is a 5/8'' standard screw for fixing total station or prism reflector tribrach, see Fig. 8.

The observation methodology of the network will be done with the resection with all possible angles and distances. Currently the leveling will be done using the trigonometric methodology until we will get a level for more accurate slopes. We will use the Leica TS50 station with an accuracy of 0.5'' and 0.6 mm for angles and distances respectively.



Fig. 8 Built pillars at Yebees Observatory.

5 Conclusions

We have presented here the first works performed in the Yebes Observatory to calculate the local tie between the different geodetic techniques. The invariant reference point of the 13 meters radio telescope has been estimated with a very high accuracy (below a tenth of a millimeter) and the design of a pillar network to get the required accuracy (1 mm) have been realized. For the near future there are still many tasks to work as for example the calculation of the 40 meters radio telescope and GNSS antennas invariant reference points and the compensation of the network.

References

- Camacho A G, Martín M D (1986) Constreñimientos internos en la compensación de estaciones. 13, 42-46.
- Dawson J, Sarti P, Johnston G M, Vittuari L (2007) Indirect approach to invariant point determination for SLR and VLBI systems: an assessment. *J Geodyn*, 81, 433-441.
- Fancher K, Smith D, Breidenbach S, Olsen J, Paudel N (2010) Recent IERS Site Survey of Multiple Co-located Geodetic Techniques by NGS. *FIG Congress 2010, Facing the challenges- Building the Capacity*
- Ghilani C D (2010) Adjustment computation spatial data analysis.
- Henneberg H (1986) Redes geodésicas de alta precisión. *III Curso de Geodesia Superior 2*, 123-196.
- Linkwitz, H., (1986). Compensación de grandes redes geodésicas. *III Curso de Geodesia Superior, 2*, 72-121.
- Martín F (1990). Geodesia y cartografía matemática.
- Santamaría-Gómez A, García-Espada S (2011) Simulating the estimation of the 40m radio-telescope Invariant Reference Point at the Yebes observatory. *Informe técnico, IT-OAN 2011-9*.
- Sevilla M J (1986) Formulación de modelos matemáticos en la compensación de redes geodésicas. *III Curso de Geodesia Superior, 2*, 2-69.
- Sevilla M J (1987) Colocación Mínimos Cuadrados. *IV Curso de Geodesia Superior, 2*, 97-141,
- Sevilla M J (2003) Ajuste con Constreñimientos. *Seminario de Geodesia Superior*
- Sevilla M J (2005) Ajuste de redes libres. Modelos matemáticos singulares.
- Sarti P, Sillard P, Vittuari L (2004) Surveying co-located space-geodetic instrument for ITRF computation. *J Geod*, 78, 210-222.

Coordinate-Based Bundle Adjustment – Advanced Network Adjustment Model for Polar Measurement Systems

M. Lösler, C. Eschelbach, R. Haas

Abstract To fulfill the requirements on local-ties formulated by GGOS, high precision instruments and rigorous uncertainty propagation are necessary. To evaluate the results of e.g. high performance total stations or laser trackers, the accuracy-limiting parameters of the measurement process have to be quantified and projected onto an uncertainty model. Using the generally across disciplines accepted *Guide to the Expression of Uncertainty in Measurement* (GUM) a transparent and traceable stochastic model can be derived. A Cartesian coordinate-based bundle adjustment is suggested, to integrate the local measurements into a global context avoiding gravitational influences. The included comprehensive uncertainty model is based on a specific geometric model of a polar measurement system and takes instrument specific and target dependent error parameters into account.

Keywords Laser Tracker, Total Station, Guide to the Expression of Uncertainty in Measurement, Local Tie, Network Adjustment, Uncertainty

1 Introduction

An interdisciplinary collaboration requires standard notations and terminologies as well as the acceptance

Michael Lösler, Cornelia Eschelbach
Frankfurt University of Applied Sciences, Laboratory for Industrial Metrology, Nibelungenplatz 1, DE-60318 Frankfurt am Main, Germany
Rüdiger Haas
Chalmers University of Technology, Onsala Space Observatory, SE-439 92 Onsala, Sweden

of analytical procedures. An analysis must be transparent and traceable. In the field of metrology, the *Guide to the Expression of Uncertainty in Measurement* (GUM) was introduced in 1995 and supplemented in 1999 (cf. GUM (2008a), GUM (2008b)). The GUM specifies two distinct types of uncertainty classes called type-A and type-B. Whereas uncertainties of type-A are based on methods of evaluation of uncertainty by statistical analysis of multiple readings of the same measurement, type-B uncertainties make use of non-statistical approaches. The application of statistical analysis like the method of least-squares or the usage of Monte-Carlo techniques is well known in geodesy and are counted among type-A uncertainties. In the easiest case, the result is given by the sample mean, and the corresponding type-A uncertainty is represented by the experimental standard deviation called standard uncertainty. Type-B uncertainties are evaluated by scientific knowledge or experiences about the measurement process, calibration reports or manufacturer specifications, and cannot be obtained from repeated measurements. The combined standard uncertainty that contains type-A as well as type-B uncertainties is derived by the propagation of uncertainties (cf. GUM (2008a)). Although modern instruments like GNSS antennas, total stations, laser scanners and high precision laser trackers provide the coordinates of an observed position at the push of a button, complex background processes and the amount of parameters influencing and limiting the accuracy have to be kept in mind.

The following sections describe several effects that restrict the accuracy of a polar measurement. By assigning the identified error parameters and their corresponding uncertainties to the measurement process, type-A as well as type-B uncertainties of an observed

position can be estimated and introduced during the network adjustment.

2 Coordinate-based network adjustment

In classical geodesy, the observed polar observations are combined during a network adjustment to derive spatial coordinates and corresponding uncertainties. Depending on the extent of the local network and the accuracy requirements, the influence of the curvature of the earth cannot be neglected. To overcome the influence of the inclination, different analysis strategies are developed (e.g. Schwarz (1994), Awange and Grafarend (2005)).

2.1 Functional model

In metrology, the influence of the curvature of the earth is mostly disregarded, because instruments like coordinate measuring machines and laser trackers are unrelated to the gravity field. Fig. 1 depicts a local tie measurement at the Onsala Space Observatory with a laser tracker LTD840, which is not related to the gravity field. To combine several stations, coordinate-based algorithms are developed in metrology (e.g. Calkins (2002), Lösler and Eschelbach (2012)).



Fig. 1 Local Tie Measurement at Onsala Space Observatory with Leica Laser Tracker LTD840.

For this purpose, the polar observations of the i th point \mathbf{p} of the j th station are converted into Cartesian spatial coordinates

$$\mathbf{p}_{i,j}(\Theta, \Phi, d) = \begin{pmatrix} x \\ y \\ z \end{pmatrix}_{i,j} = \begin{pmatrix} d \sin \Phi \cos \Theta \\ d \sin \Phi \sin \Theta \\ d \cos \Phi \end{pmatrix}_{i,j}. \quad (1)$$

Here, the slope distance is denoted by d , and Θ and Φ are the yaw and pitch angle w.r.t. the local station coordinate system, respectively. The usage of Eq. 1 assumes a perfect instrument. Fig. 2 shows possible deviations from the ideal case, e.g. an axis-offset or misalignment of the distance measurement unit. Most of these

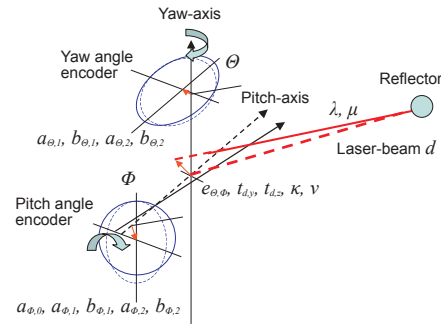


Fig. 2 Irregularities of a Polar Measurement Instrument (Hughes et al., 2011).

errors are compensated by the manufactures firmware and only a few errors can be rechecked by the instrument operator. Based on the work of Muralikrishnan (2009), a compensation model for mobile laser trackers is suggested by Hughes et al. (2011). The corrected slope distance \hat{d} results by adding the distance dependent scaling factor μ and the displacement offset λ .

$$\hat{d} = (1 + \mu)d + \lambda \quad (2)$$

The angle encoder errors are parameterized as Fourier series.

$$\hat{\Theta} = \Theta + \sum_{q=1}^{n_q} (a_{\theta,q} \cos q\Theta + b_{\theta,q} \sin q\Theta) \quad (3)$$

$$\hat{\Phi} = \Phi + a_{\phi,0} + \sum_{q=1}^{n_q} (a_{\phi,q} \cos q\Phi + b_{\phi,q} \sin q\Phi) \quad (4)$$

where a_q and b_q represents the Fourier coefficients. The harmonic order of the Fourier series can be restricted to the order of $n_q = 2$ (Lewis et al., 2011).

The conversion of the polar observations into their Cartesian representation w.r.t. the irregularities of the observation instrument can be expressed by

$$\mathbf{p}_{i,j}(\hat{\theta}, \hat{\phi}, \hat{d}) = \mathbf{p}_0 + \mathbf{b}(\hat{\theta}, \hat{\phi}) + \hat{d}\mathbf{n}(\hat{\theta}, \hat{\phi}) \quad (5)$$

with

$$\mathbf{b}(\hat{\theta}, \hat{\phi}) = \mathbf{R}_{\hat{\theta}}^z \begin{pmatrix} e_{\theta, \phi} \\ 0 \\ 0 \end{pmatrix} + \mathbf{R}_{\hat{\theta}}^z \mathbf{R}_{\hat{\phi}}^x \mathbf{R}_{\hat{\phi}-\frac{\pi}{2}}^y \mathbf{R}_{\hat{\phi}}^z \begin{pmatrix} t_{d,x} - e_{\theta, \phi} \\ t_{d,y} \\ t_{d,z} \end{pmatrix} \quad (6)$$

and

$$\mathbf{n}(\hat{\theta}, \hat{\phi}) = \mathbf{R}_{\hat{\theta}}^z \mathbf{R}_{\hat{\phi}}^x \mathbf{R}_{\hat{\phi}-\frac{\pi}{2}}^y \mathbf{R}_{\hat{\phi}}^z \begin{pmatrix} 1 \\ 0 \\ 0 \end{pmatrix}. \quad (7)$$

The vector \mathbf{p}_0 summarizes the coordinates of the station and \mathbf{b} considers the axis-offset $e_{\theta, \phi}$ and the centering error of the distance measurement unit $t_d = (t_{d,x} \ t_{d,y} \ t_{d,z})^T$. The trunnion axis error κ and the horizontal collimation error ν are compensated by the vector \mathbf{n} . Even if the model was derived for laser trackers, it is also valid for total stations and laser scanners.

A conformal spatial seven-parameters transformation is used to combine the observed coordinates $\mathbf{p}_{i,j}$ of the j th station with the global coordinate system \mathbf{P}_i . The global datum can be defined as (local) topocentric coordinate system or as a global geocentric one like the ITRF.

$$\mathbf{p}_{i,j} = \mathbf{T}_j + m_j \mathbf{R}_j \mathbf{P}_i \quad (8)$$

Here, \mathbf{T} denotes the translation vector, m is the scaling parameter, which is applied uniformly to all axes, and \mathbf{R} represents the rotation matrix. A common Gauß-Markov model can be used (e.g. Mikhail and Ackerman (1976), Koch (1999)) to derive the global coordinates \mathbf{P}_i and the unknown transformation parameters of each station.

$$\mathbf{Ax} = \mathbf{l} + \mathbf{v} \quad (9)$$

The Jacobi matrix \mathbf{A} can be divided by column-sorting in a coordinate part \mathbf{A}_P and a part \mathbf{A}_T , which contains the transformation parameters of each station. The local coordinates of each station are given by the (reduced) observation vector \mathbf{l} , the vector \mathbf{v} contains the observational errors, and the unknown parameters are denoted by $\mathbf{x} = (\mathbf{x}_P \ \mathbf{x}_{T,1} \ \mathbf{x}_{T,j} \ \mathbf{x}_{T,k})^T$.

$$\begin{pmatrix} \mathbf{A}_{P,1} & \mathbf{A}_{T,1} & 0 & 0 \\ \mathbf{A}_{P,j} & 0 & \mathbf{A}_{T,j} & 0 \\ \mathbf{A}_{P,k} & 0 & 0 & \mathbf{A}_{T,k} \end{pmatrix} \begin{pmatrix} \mathbf{x}_P \\ \mathbf{x}_{T,1} \\ \mathbf{x}_{T,j} \\ \mathbf{x}_{T,k} \end{pmatrix} = \begin{pmatrix} \mathbf{l}_{p,1} \\ \mathbf{l}_{p,j} \\ \mathbf{l}_{p,k} \end{pmatrix} + \begin{pmatrix} \mathbf{v}_{p,1} \\ \mathbf{v}_{p,j} \\ \mathbf{v}_{p,k} \end{pmatrix} \quad (10)$$

If available, prior results or additional GNSS observations \mathbf{x}_{GNSS} can be introduced to define the geodetic datum of the network.

$$\begin{pmatrix} \mathbf{A}_P & \mathbf{A}_T \\ \mathbf{E} & \mathbf{0} \end{pmatrix} \begin{pmatrix} \mathbf{x}_P \\ \mathbf{x}_T \end{pmatrix} = \begin{pmatrix} \mathbf{l}_P \\ \mathbf{l}_{\text{GNSS}} \end{pmatrix} + \begin{pmatrix} \mathbf{v}_P \\ \mathbf{v}_{\text{GNSS}} \end{pmatrix} \quad (11)$$

The stochastic model of this extended model reads

$$\begin{pmatrix} \mathbf{Q}_P & \mathbf{0} \\ \mathbf{0} & \mathbf{Q}_{\text{GNSS}} \end{pmatrix}. \quad (12)$$

To restrict the number of estimated transformation parameters, e.g. to fix the scale parameter to $m = 1$ or to rectify the defect of the normal equation matrix in case of a free network adjustment, additional restrictions $\mathbf{C}^T \mathbf{x} = \mathbf{c}$ can be applied (cf. Lösler and Eschelbach (2012))

$$\begin{pmatrix} \mathbf{N} & \mathbf{C} \\ \mathbf{C}^T & \mathbf{0} \end{pmatrix}^{-1} \begin{pmatrix} \mathbf{n} \\ \mathbf{c} \end{pmatrix} = \begin{pmatrix} \mathbf{x} \\ \mathbf{k} \end{pmatrix}, \quad (13)$$

where $\mathbf{N} = \mathbf{A}^T \mathbf{Q}_{\Pi}^{-1} \mathbf{A}$ and $\mathbf{n} = \mathbf{A}^T \mathbf{Q}_{\Pi}^{-1} \mathbf{l}$ are substitutions, and \mathbf{k} contains the Lagrange multipliers (e.g. Koch (1999)). With $\mathbf{Q}_{\mathbf{kk}} = (\mathbf{C}^T \mathbf{N}^{-1} \mathbf{C})^{-1}$ the variance-covariance matrix $\mathbf{Q}_{\mathbf{xx}}$ of the unknown parameters \mathbf{x} are given by

$$\mathbf{Q}_{\mathbf{xx}} = \mathbf{N}^{-1} - \mathbf{N}^{-1} \mathbf{C} \mathbf{Q}_{\mathbf{kk}} \mathbf{C}^T \mathbf{N}^{-1} \quad (14)$$

2.2 Stochastic model

The stochastic model describes the a-prior uncertainties of the measurement process and allows for combining different types of observations w.r.t. their uncertainties. In general, the uncertainties are a composition of various parameters and distributions (e.g. GUM (2008a), GUM (2008b)).

The geometrically related parameters of the instrument shown in Eq. 5 are equivalent for all observations. In addition, each measurement can be considered as a realization of a random experiment. Therefore, a target centering error ζ , a resolution limiting error of the digital output ξ , and a random error τ should be introduced. Eqs. 2, 3 and 4 become

$$\hat{d} = (1 + \mu + \tau_d)d + \lambda + \zeta_d + \xi_d, \quad (15)$$

$$\hat{\theta} = \theta + \tau_\theta + \xi_\theta + \frac{\zeta_\theta}{d}\rho + a_{\theta,0} + \sum_{q=1}^{n_q} (a_{\theta,q} \cos q\theta + b_{\theta,q} \sin q\theta), \quad (16)$$

$$\hat{\phi} = \phi + \tau_\phi + \xi_\phi + \frac{\zeta_\phi}{d}\rho + a_{\phi,0} + \sum_{q=1}^{n_q} (a_{\phi,q} \cos q\phi + b_{\phi,q} \sin q\phi), \quad (17)$$

where $\rho = \frac{\pi}{200 \text{ gon}}$ denotes the angle conversion factor between radian and gon.

If forced centering or wooden tripods are used, the uncertainties of the station \mathbf{Q}_{p_0} have to be taken into account (Lösler and Eschelbach, 2012). The a-priori variance-covariance matrix \mathbf{Q}_p of statically observed coordinates \mathbf{p} results by substituting Eq. 15, 16 and 17 in Eq. 5 and applying the propagation of uncertainty.

2.3 Systematic effects

During a measurement process several effects limit the accuracy. Most of these effects are of random nature but there are also systematic effects that distort the results unilaterally. For example, the laser beam of the distance measurement unit is effected by meteorology and a non-representative survey of the meteorological parameters yields in systematic errors. Whereas this effect is well-known, the influence of misaligned glass body reflectors is not. To avoid systematic lateral $\varepsilon_{\text{lateral}}$ and radial $\varepsilon_{\text{radial}}$ errors, it is important to align the normal of the reflector surface to the line of sight (e.g. Pauli (1969), Rüeger (1990)). The magnitude of the errors caused by a misaligned reflector depends on the reflector type, size and on the angle of incidence δ .

$$\varepsilon_{\text{radial}} = d(n_r - \sqrt{n_r^2 - \sin^2 \delta}) - e(1 - \cos \delta) \quad (18)$$

$$\varepsilon_{\text{lateral}} = (d - e) \sin \delta - d \sec \delta_G \sin(\delta - \delta_G) \quad (19)$$

where $\delta_G = \arcsin \frac{\sin \delta}{n_r}$. The distance between the front surface of the prism and the center-symmetric point is denoted by e , while d is the distance between the front surface of the prism and the corner point of the triple prism, and $n_r \approx 1.52$ represents the ratio of the group refractive indices of glass and air (Rüeger (1990)).

The systematic errors depend on the angle of incidence δ . Fig. 3 depicts the resulting systematic errors for various reflector sizes. Even if small size glass body reflectors yield in lower errors, these kind of reflectors reflect only a small part of the instrument's laser beam. Due to the small spot size, the likelihood for measurement failure is increased.

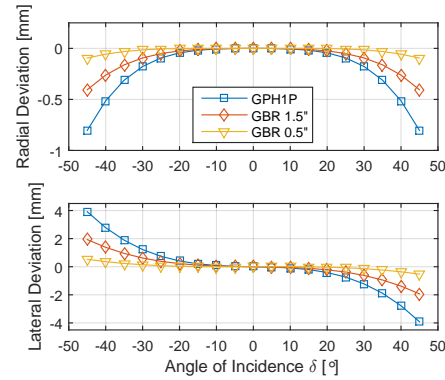


Fig. 3 Radial and Lateral Deviations caused by Reflector Misalignment for Precision Reflector GPH1P, Glass Ball Reflector 1.5'' and 0.5''.

During reference point determination, a misalignment of the reflectors is unavoidable, because of the rotation characteristic of the radio telescope. As shown by (Lösler et al., 2013) the systematic errors can be corrected for all radio telescope orientations. The remaining residual uncertainty is similar to the centering error ζ and can be taken into account in the network adjustment process (Lösler et al., 2015). Fig. 4 shows a comparison of corrected and uncorrected spatial positions.

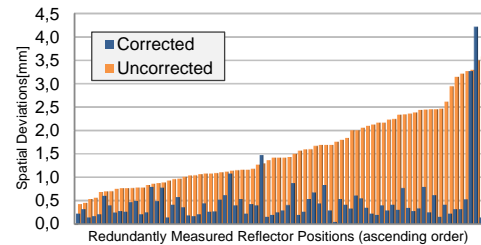


Fig. 4 Comparison of Corrected and Uncorrected Spatial Positions (Lösler et al., 2015).

3 Conclusion

A proper and traceable uncertainty budgeting is important in order to archive reliable results. An incomplete stochastic model or an unrepresentative sample of the population effects the estimated uncertainties (cf. Hennes (2007), Xu (2013)). In most cases the results are too optimistic and the derived confidence intervals do not reflect the true uncertainties. By using common network adjustment tools, only a few uncertainties can be taken into account. Following the *Guide to the Expression of Uncertainty in Measurement* (GUM) a coordinate-based network adjustment is developed that includes a comprehensive uncertainty budgeting.

Moreover, the use of spatial similarity transformations paves a simple way to provide local observations in a global context like the ITRF. Whereas in conventional approaches the ITRF-transformation process is carried out as a final step, in our approach the transformation into the global reference frame takes place right in the beginning of the bundle adjustment.

References

- Awange J L, Grafarend E W (2005) *Solving Algebraic Computational Problems in Geodesy and Geoinformatics*, Springer, Heidelberg/Berlin.
- Calkins JM (2002) *Quantifying Coordinate Uncertainty Fields in Coupled Spatial Measurement systems*. Dissertation, Faculty of the Virginia Polytechnic Institute and State University, Virginia.
- GUM (2008a) *Evaluation of measurement data – Guide to the expression of uncertainty in measurement*. JCGM 100:2008, GUM 1995 with minor corrections, <http://www.bipm.org/en/publications/guides/gum.html>, retrieved: 2015-06-04.
- GUM (2008b) *Evaluation of measurement data – Supplement 1 to the "Guide to the expression of uncertainty in measurement" – Propagation of distributions using a Monte Carlo method*. JCGM 101:2008, <http://www.bipm.org/en/publications/guides/gum.html>, retrieved: 2015-06-04.
- Hennes M (2007) Konkurrierende Genauigkeitsmaße Potential und Schwächen aus der Sicht des Anwenders. *Allgemeine Vermessungs-Nachrichten*, 7, 136–146.
- Hughes B, Forbes A, Lewis A, Sun W, Veal D, Nasr K (2011) Laser Tracker Error Determination Using a Network Measurement. *Meas Sci Technol*, 22, 1–12.
- Koch K R (1999) *Parameter Estimation and Hypothesis Testing in Linear Models*. Springer, Heidelberg/Berlin, 2nd edn.
- Lewis A, Hughes B, Forbes A, Sun W, Veal D, Nasr K (2011) Determination of misalignment and angular scale errors of a laser tracker using a new geometric model and a multi-target network approach. In: *Proc. MacroScale 2011 – Recent developments in traceable dimensional measurements*, Federal Office of Metrology METAS, Wabern, Switzerland, doi: 10.7795/810.20130620S.
- Lösler M, Eschelbach C (2012) Concept of a Realisation of a Prototype for Adequate Evaluation of Polar Measurements (in German). *Allgemeine Vermessungs-Nachrichten*, 119, 249–258.
- Lösler M, Haas R, Eschelbach C (2013) Automated and continual determination of radio telescope reference points with sub-mm accuracy: results from a campaign at the Onsala Space Observatory. *J Geod*, 87, 791–804, doi: 10.1007/s00190-013-0647-y.
- Lösler M, Eschelbach C, Haas R (2015) Zum Einfluss variierender Reflektorausrichtungen auf polare Messsysteme – Analytische Korrektur systematischer Zentrierabweichungen beim Messen auf bewegte Objekte. *GeoNews*, 3, 6–7.
- Mikhail E M, Ackerman F (1976) *Observations and Least Squares*, University Press of America, Lanham/Ney York/London.
- Muralikrishnan B, Sawyer D S, Blackburn C J, Phillips S D, Borchardt B R, Estler W T (2009) ASME B89.4.19 Performance Evaluation Tests and Geometric Misalignments in Laser Trackers. *J Res Natl Inst Stan* 114, 21–35.
- Pauli W (1969) Vorteile eines kippbaren Reflektors bei der elektrooptischen Streckenmessung. *Vermessungstechnik*, 412–415.
- Rüeger J M (1990) *Electronic Distance Measurement - An Introduction*, Springer, Heidelberg/Berlin, 3rd edn.
- Schwarz W (1994) Zur Reduktion der Messungen bei räumlichen Punktbestimmungen. *Allgemeine Vermessungs-Nachrichten*, 101, 207–218.
- Xu P (2013) The effect of incorrect weights on estimating the variance of unit weight. *Stud Geophys Geod*, 57, 339–352, doi: 10.1007/s11200-012-0665-x.

Determining HartRAO antenna parameters with VieVS

M. Nickola, A. de Witt, H. Krásná, W. L. Combrinck, J. Böhm

Abstract Geodetic VLBI sessions are analysed using the Vienna VLBI Software (VieVS) to estimate the antenna axis offsets (AOs) of both the Hartebeesthoek Radio Astronomy Observatory's (HartRAO) 26m and 15m radio telescopes and also to determine the local tie between the telescopes. Possible seasonal variations in AO as well as baseline length between the 26m and 15m are investigated.

Keywords axis offset, local tie, HartRAO

1 Introduction

The HartRAO 26m and 15m radio telescopes regularly participate in astrometric and geodetic VLBI sessions. The HartRAO 26m radio telescope suffered a critical bearing failure in 2008 and returned to operations in 2010 after repair. The 15m was built as SKA prototype during 2007 and converted to an operational geodetic VLBI antenna during 2012. It officially joined geodetic VLBI operations in 2013.

In 2014, antenna axis offset (AO) values of both the 26m and 15m were estimated using the Vienna VLBI Software (VieVS) (Böhm et al. (2012)) from geodetic VLBI sessions before and after bearing repair Krásná et al. (2014). A discrepancy was found to exist between the VieVS estimated AO values for the 26m before and

Marisa Nickola, Aletha de Witt, Ludwig Combrinck
Hartebeesthoek Radio Astronomy Observatory, PO Box 443,
Krugersdorp 1740, South Africa
Hana Krásná, Johannes Böhm
Vienna University of Technology, Department of Geodesy and
Geoinformation, A-1040 Vienna, Austria

after bearing repair and values previously determined for before bearing repair by other methods, such as ground surveys (which are taken to be the more accurate), as well as from analysis with other VLBI analysis software packages.

Additional geodetic VLBI sessions are analysed using VieVS to estimate the AO of both the 26m and 15m antennas, to investigate possible seasonal variations in AO as well as to determine the local tie between the two telescopes.

2 HartRAO 26m and 15m radio telescopes

The HartRAO 26m is an equatorially mounted Cassegrain radio telescope built by Blaw Knox in 1961. The VLBI reference point is the intersection of the fixed Hour Angle (HA) axis with the perpendicular plane containing the moving Declination (Dec) axis (see Fig. 1 and Fig. 2). It serves as the reference point for the co-location of the Satellite Laser Ranging (SLR) and Global Navigation Satellite System (GNSS) stations on-site and as reference datum for South Africa's surveying system. On the 3rd of October 2008, the 26m suffered a critical failure of its south polar bearing. On the 11th of August 2010, the first post repair geodetic VLBI session was run. Post-repair position time series solutions indicated no noticeable shift in position.

The HartRAO 15m is an alt-az radio telescope built as SKA prototype during 2007. The VLBI reference point is the intersection of the fixed azimuth axis with the perpendicular plane containing the moving elevation axis (see Fig. 3 and Fig. 4). The 15m was con-

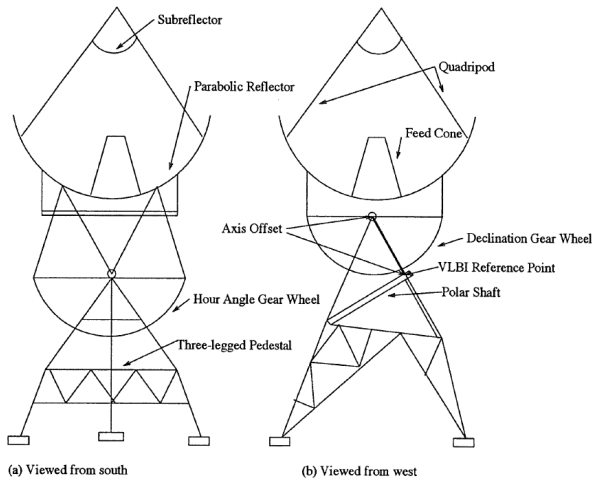


Fig. 1 Main structural components of HartRAO 26m radio telescope (Combrinck and Merry, 1997).



Fig. 2 Ludwig Combrinck surveying the 26m's polar shaft during bearing repair (Credit: Mike Gaylard).

verted to an operational geodetic VLBI antenna during 2012. On 11 October 2012, the first geodetic session was run as part of the 15m's commissioning. Regular geodetic VLBI sessions have since been off-loaded to the quick-slewing, all-sky seeing 15m.

3 Axis offset comparison

When a telescope's rotation axes do not intersect, an antenna axis offset (AO) exists. The VLBI reference point is then the point represented by the intersection of the fixed axis with the perpendicular plane contain-

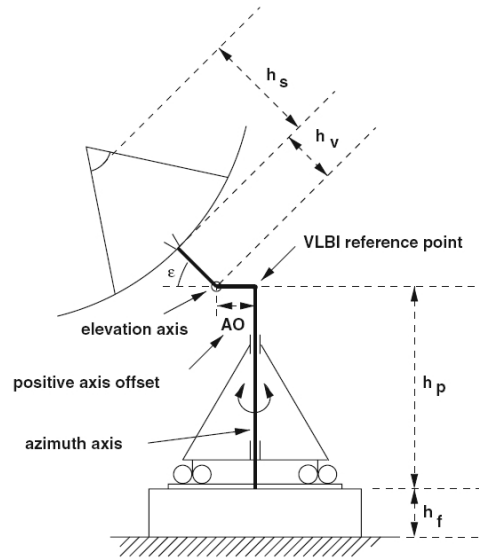


Fig. 3 Alt-azimuth telescope mount with positive axis offset (Nothnagel, 2008).



Fig. 4 HartRAO 15m telescope mount with offset elevation axis (Credit: Mike Gaylard).

ing the moving axis. An antenna axis offset (AO) affects the geometrical and tropospheric components of the delay model. The accuracy with which the AO is determined therefore influences the accuracy of VLBI results (Combrinck and Merry, 1997).

Antenna axis offset (AO) values for the 26m as determined by ground survey and estimated by VLBI solution are displayed in Tab. 1. AO values before bearing repair, obtained by using either method, are given in the top section of the table, while the middle section provides the VieVS estimates obtained by Krásná et al. (2014) for before and after bearing repair as well as from the start of the 26m's operation in 1986 until the end of 2013. The value obtained in the current study, using VieVS to estimate the AO after antenna repair until the end of November 2014, are given in the bottom section of the table. This value of (6707.9 ± 0.7 mm) agrees within the formal error with the estimate of (6707.3 ± 0.8 mm) by Krásná et al. (2014). Both VieVS estimates of AO after bearing repair differ considerably from the IVS recommended value, taken from ground survey before the bearing repair, of 6695.3 mm.

Table 1 HartRAO 26m antenna axis offset determined by independent techniques (a priori value = 6695.3 mm).

Method	Determined by	Value (mm)
Standard value	JPL (1961)	6706
Conventional survey	Newling (1993)	6695 ± 3
VLBI solution	Ma (1995)	6693.6 ± 2.5
VLBI solution	Eubanks (1995)	6692.5 ± 1.5
HartRAO GPS	Combrinck (1995)	6695.6 ± 2.3
VLBI solution	Ma (1996)	6688.8 ± 1.8
Local tie survey	Michel et al. (2005)	6695 ± 2.5
VieVS solutions: Before repair (1986-2008.8)	Krásná et al. (2014)	6699.2 ± 0.5
After repair (2010.8-2014.0)		6707.3 ± 0.8
1986-2014.0		6707.1 ± 0.5
VieVS solution: After repair (2010.8-2014.11) (180 sessions)	Current study	6707.9 ± 0.7

Antenna axis offset (AO) values for the 15m as determined by ground survey and estimated by VLBI solution are displayed in Tab. 2. Both the value for the AO from Dan MacMillan's VLBI solution of 2014 of (1494.1 ± 2.6 mm) and the VieVS estimate of (1495.0 ± 2.6 mm) obtained by Krásná et al. (2014) for the period covering the start of the 15m's operation until the end of 2013, agree within the formal error with the AO value obtained by a preliminary GPS survey by Atie Combrinck in 2007 of 1495 mm (the IVS recommended value). The value obtained in the current study, using VieVS to estimate the AO for the period from

start of operations until the end of November 2014, of (1499.8 ± 1.1 mm) differs by 4.8 mm from the IVS recommended value.

Table 2 HartRAO 15m antenna axis offset determined by independent techniques (a priori value = 1495.0 mm).

Method	Determined by	Value (mm)
GPS survey	Combrinck (2007)	1495
VLBI solution (from 1st IVS sessions)	GSFC, Gordon and Bolotin (2012)	1464
VLBI solution	MacMillan (2014)	1494.1 ± 2.6
VieVS solution (2012.10-2014.0)	Krásná et al. (2014)	1495.0 ± 3.4
VieVS solution (2012.10-2014.11) (134 sessions)	Current study	1499.8 ± 1.1

4 Seasonal variation in 26m and 15m AO

Sessions after bearing repair until the end of November 2014 for the 26m, and sessions for the entire period of the 15m's operation until the end of November 2014, were divided into seasonal groupings as well as into two six monthly periods to investigate the possibility of seasonal variations in antenna axis offset (AO).

The differences in AO for the 26m and 15m between their respective a priori AO values and the VieVS estimated values for the particular season are displayed in Tab. 3. For both the 26m and 15m, the smallest deviation is for sessions taking place during the autumn months (MarAprMay), while the largest deviation is for sessions taking place during the summer months (DecJanFeb).

The differences in AO for the 26m and 15m between their respective a priori AO values and the VieVS estimated values for the particular six monthly period are displayed in Tab. 4. For both the 26m and 15m, the smaller deviation is for sessions taking place during the autumn and winter months (Mar-Aug), while the larger deviation is for sessions taking place during the spring and summer months (Sep-Feb).

Table 3 HartRAO 26m and 15m difference in antenna axis offset between a priori value and VieVS estimated value for specified months/seasons a priori values - 26m = 6695.3 mm; 15m = 1495.0 mm).

Month/Season	26m dAO (mm)	15m dAO (mm)
DecJanFeb (Summer)	17.30 ± 1.67 (46 sessions)	7.09 ± 2.12 (42 sessions)
MarAprMay (Autumn)	5.77 ± 1.97 (31 sessions)	1.41 ± 2.22 (27 sessions)
JunJulAug (Winter)	13.25 ± 1.56 (44 sessions)	6.67 ± 2.37 (27 sessions)
SepOctNov (Spring)	12.03 ± 1.06 (59 sessions)	6.02 ± 2.47 (38 sessions)

Table 4 HartRAO 26m and 15m difference in antenna axis offset between a priori value and VieVS estimated value for specified six monthly period a (a priori values - 26m = 6695.3 mm; 15m = 1495.0 mm).

Month/Season	26m dAO (mm)	15m dAO (mm)
Sep - Feb (Spring and Summer)	13.14 ± 0.91 (105 sessions)	7.11 ± 3.78 (80 sessions)
Mar - Aug (Autumn and Winter)	9.75 ± 1.23 (75 sessions)	3.74 ± 1.64 (54 sessions)

5 Baseline between 26m and 15m

The baseline length between the 26m and 15m radio telescopes was estimated with VieVS for sessions in which both the telescopes participated from the start of the 15m's operation until the end of November 2014 in order to determine the local tie between the two telescopes. Values for baseline length as estimated with VieVS for eleven dual sessions taking place during 2013 and 2014 are displayed in Fig. 5. An average value of 113.0924 m agrees within the formal error with the a priori value of 113.0953 m. It was intended to compare the estimated values with the value obtained by a co-location survey, which took place at HartRAO during March 2014, but the survey results are not available yet.

Baseline lengths according to the BKG Combination Centre between the 26m and 15m for five dual sessions during 2013 and 2014 are displayed in Fig. 6. The average value of 113.0924 m obtained with VieVS compares within the formal error with the average value of 113.0938 m obtained from the five BKG baseline lengths.

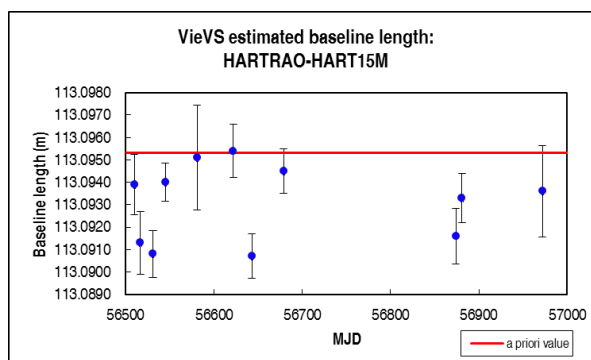


Fig. 5 Baseline lengths between 26m and 15m for 11 dual sessions during 2013 and 2014 estimated using VieVS (a priori = 113.0953 m).

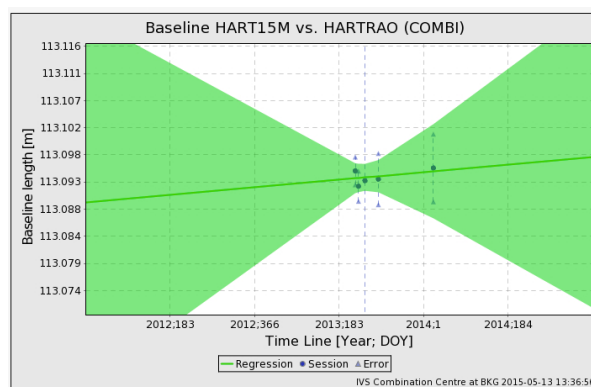


Fig. 6 Baseline lengths between 26m and 15m for 5 dual sessions during 2013 and 2014 according to BKG Combination Centre IVS.

6 Conclusions

The difference in AO value for the 26m between the local survey value before bearing repair and the VieVS estimated value after bearing repair may be ascribed to a change in station position due to the bearing failure and replacement, propagating into the axis offset estimation (Krásná et al., 2014). We are awaiting values from a local site tie, which was performed during the early part of 2014, for comparison. The local site tie value for the 15m's AO will also be compared with the VieVS estimated and IVS recommended values.

Regarding possible seasonal variations in the AO - as a construction value, the AO value is supposed to remain constant over the entire year. If seasonal variations seem to occur, seasonal mismodelled and unmodelled effects, such as troposphere delay and atmosphere

and hydrology loading, are possibly propagating into the AO estimates in the VLBI analysis. Seasonal variations in antenna axis offset values will be further investigated as additional sessions become available. For the 26m, sessions from before the bearing repair could also be included in the analysis.

The baseline length between the 26m and 15m estimated with VieVS will also be compared with the value obtained by the 2014 local tie survey. As indicated by Plank (2014), by comparing these values, instrumental or systematic effects causing variation in the VLBI reference points may be revealed thus. Possible seasonal variations in baseline length will be investigated as more dual sessions become available for analysis.

During 2016, an automated total station for continuous monitoring of vector ties will become operational at HartRAO. This will contribute significantly to improving the local ties between the various techniques on site.

References

- Böhm J, Böhm S, Nilsson T, Pany A, Plank L, Spicakova H, Teke K, Schuh H (2012) The new Vienna VLBI software. In: S. Kenyon, M. C. Pacino, U. Marti (eds.), *Proc. IAG Scientific Assembly 2009*, IAG Symposia Series 136, 1007–1011, doi: 10.1007/978-3-642-20338-1_126.
- Combrinck W L, Merry C L (1997) Very long baseline interferometry antenna axis offset and intersection determination using GPS. *J Geophys Res*, 102(B11), 24741–24744.
- Krásná H, Nickola M, Böhm J (2014) Axis offset estimation of VLBI telescopes. In: D. Behrend, K.D. Baver, K. Armstrong (eds.), *IVS 2014 General Meeting Proc.*, Science Press (Beijing), 339–343.
- Nothnagel A (2008) Conventions on thermal expansion modelling of radio telescopes for geodetic and astrometric VLBI. *J Geod*, doi: 10.1007/s00190-008-0284-z.
- Plank L (2014) Sibling radio telescopes for geodesy: Optimising the use of co-located VLBI telescopes in the southern hemisphere. Proposal, September 10, 2014.

Continuous VLBI Scheduling: The CONT14 Example

D. Behrend

Abstract One of the main goals of the Continuous VLBI Campaign 2014 (CONT14) was to collect VLBI observations over 15 contiguous days without interruptions. In order to achieve this continuity some aspects of the standard, session-wise scheduling procedure had to be modified. These modifications mostly pertained to the day boundaries but also to the station check times of one or two hour lengths. The driving factor was the retention and continuation of the cable-wrap across boundaries, which is not taken into account with session-wise schedule writing. Carrying forward the cable-wrap information for each station had to be implemented into *sked* and the script file controlling *sked*, respectively. Further, as CONT14 was still organized as individual days, three-minute gaps were incorporated at the end of each observing day so that each station was able to change schedules before continuing with observing the subsequent day. Similar procedures may need to be implemented in the VGOS system.

Keywords CONT14, continuous scheduling, *sked*

1 Introduction

The Continuous VLBI Campaign 2014 (CONT14) was observed during May 6–20, 2014 on an observing network of 17 stations at 16 sites. One of the main goals of the campaign was to collect VLBI observations over a time period of 15 days without interruptions (e.g., Behrend et al. (2014)). Given its network size and the

Dirk Behrend
NVI, Inc., 7257D Hanover Parkway
Greenbelt, MD 20770, USA

continuous observing, this campaign approximated the operational workload anticipated for the VLBI Global Observing System (VGOS) reasonably well. While the recording rate of 512 Mbps with the legacy S/X system was not as high as the 8 Gbps (or higher) expected for the broadband system, the 24/7 recording with 17 stations was an excellent testbed for the initial full operations of VGOS foreseen for 2017 (e.g., Petrachenko et al. (2014)). Hence, in this paper we focus on the scheduling aspect of CONT14.

To achieve the observational continuity in CONT14, the standard session-wise scheduling procedure was modified. For a better understanding of these modifications we first describe the session-wise scheduling as currently done with regular IVS sessions. Then we introduce some of the special characteristics of the CONT campaigns including the station check and schedule changeover times in concert with the continuance of the cable-wrap information. Finally, we discuss the implementation using the VLBI scheduling software *sked* (Gipson, 2012) and take a look at the implications for VGOS.

2 Session-wise Scheduling

Following the recommendations of Working Group 2, the IVS observing program for the legacy S/X system is organized into 24-hour sessions (e.g., R1, T2, EURO, CRF, RDV, R4) and 1-hour Intensive sessions (Schlüter and Behrend, 2007). In order to optimize the shipment time from the stations to the correlator, the observing week for 24-hour sessions starts on Monday at 17:00 UT and ends on Friday at 18:30 UT (Figure 1). The additional 1.5 hours at the end comes into being, be-

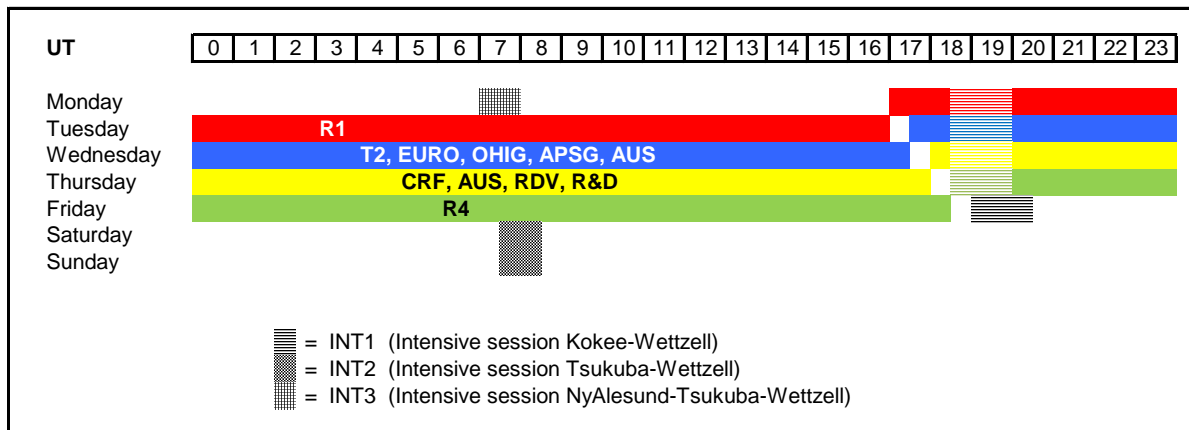


Fig. 1 The typical IVS observing week with the legacy S/X system consists of three to four 24-hour sessions and at least one 1-hour Intensive session every day. In order to optimize data transport and to avoid weekend operations with 24-hour sessions, the observing week commences on Monday at 17:00 UT with an R1 session, with most of the R1 observing actually occurring on Tuesday. Following each 24-hour session during the work week, there is a 30-min break before the subsequent 24-hour session starts. The concluding R4 session terminates the week on Friday at 18:30 UT. Hence, there are “only” four full days of 24-hour observing during the week. The Intensive sessions are observed by a small number of stations either in parallel to the 24-hour sessions or take place during the (extended) weekend time.

cause after each 24-hour session there is a break of 30 minutes to allow for schedule changes at the stations. The Intensive sessions either overlap the 24-hour sessions (Int1), are observed over the weekend (Int2), or run prior to the start of the 24-hour observing sessions (Int3). “Overlapping Intensives” have a cushion of 15 minutes at each end to allow the Intensive stations to make the necessary schedule changes.

The schedules for the individual sessions are thus completely independent of each other: no information needs to be carried over from one schedule to the next. This also allows different Operations Centers to write the observing schedules for their supported sessions without additional information.

3 Scheduling of Earlier CONT Campaigns

In earlier CONT campaigns (e.g., CONT02 and CONT05) the same session-wise organization was applied to writing the schedules: each day was treated independently and there was a gap of 30 minutes between days to allow for schedule changes and station checks. However, the observational gaps between days resulted in unrealistic artifacts in the sub-daily EOP time series derived from the CONT data. Hence,

starting with CONT08, staggered station check times were introduced (e.g., Behrend (2009)). The daily station checks (e.g., pointing) were decoupled from the change of schedules and were instead introduced at convenient and well coordinated times for the stations (i.e., different daily check times for each station). In this way, it was possible to avoid longer observational gaps. The time for changes between schedules was reduced to three minutes.

In CONT08, with the reduction of the time between schedules to three minutes while still writing the schedule for each CONT day individually, there was the possibility of a cable-wrap conflict at the changeover to the new schedule. As a result, all day transitions had to be checked for conflicts for all antennas individually and for some antennas a wrap change needed to be forced manually during observation at the station. The system checks were performed in two-hour slots, which were staggered over the 24-hour period of the session. The station was scheduled in tag-along mode during the two-hour slot allowing the station to leave and re-enter the session at any given moment of the slot.

With CONT11 the scheduling technique was altered to writing first one single schedule for the entire CONT period and then subsequently breaking it up into individual UT days. This procedure ensured having continuous cable-wrap information and thus avoided con-



Fig. 2 The observational network of the CONT14 campaign with 17 stations at 16 sites. At Hobart, both the 26-m and the 12-m radio telescopes participated in the campaign.

flicts at day boundaries. The staggered station check times were reduced to one hour in length; they were again filled using tag-along mode. As these gaps were filled after the actual scheduling run, cable-wrap conflicts were possible at the end of the check time slot.

4 Scheduling CONT14

Many of the general features of the previous CONT campaigns were continued with CONT14:

- global network: 17 stations at 16 sites (Figure 2);
- continuous VLBI: 15 consecutive days with three minutes between days for schedule changes;
- UT-day observing: the observing days ran from 0 UT to 24 UT;
- station check times: 1-hour and 2-hour slots in staggered fashion for days 2 through 14.

The continuous scheduling was basically realized as in CONT11 by writing a 15-day schedule file that then was broken up into individual days. In order to obtain complete continuity also through the 1-hour (or 2-hour) slots of the station check times, the process of filling in observations into these slots was changed with respect to CONT08 and CONT11. In those two

campaigns the slots were filled by making use of the ‘tagalong’ command at the very end of the scheduling procedure. The disadvantages of this were that the cable-wrap information was not carried forward across the “downtime gaps” and that the tag-along procedure resulted in possible conflicting cable-wrap settings at the end of the check time slot requiring manual editing at times. In CONT14, the scheduling was done in hourly steps using subnets and tag-along, always retaining the cable-wrap information.

The station check times (Figure 3) were organized in the usual staggered fashion, so that they were scheduled during regular working hours and never coinciding (except for Intensive stations). Thus, at any given time there was a network of at least twelve stations available for observing.

The actual schedule files for CONT14 were created by running *sked* in batch mode with the necessary parameters being input from a text file at the shell level. Using interactive mode would have been too error prone and tedious. The main focus was on retaining and continuing the cable-wrap information across boundaries. The scheduling procedure can be summarized as follows:

1. Prepare a ‘seed’ schedule file with the proper setup for the stations and observing mode (e.g., recording mode, target SNRs).

2. Using the seed schedule file, create one complete schedule for all 15 UT days:
 - use ‘downtime’ command to keep the last 3 min of each UT day free of observations (except the final CONT day);
 - schedule scans in hourly blocks for the predefined subnets and immediately tag along the non-subnet stations (i.e., Intensive stations, stations performing station checks).
3. Save the 15-day schedule file.
4. Divide the 15-day schedule into 15 single UT days:
 - load the 15-day schedule file;
 - remove the scans prior to and after the individual day boundaries for each individual day using *sked*’s ‘delete’ command;
 - save the individual schedule files, write schedule summary and cable-wrap information files.
5. Check to see if scans were inadvertently omitted during step 4 and restore if needed.
6. Check the cable-wrap setting at day boundaries to uncover any problems and rectify.

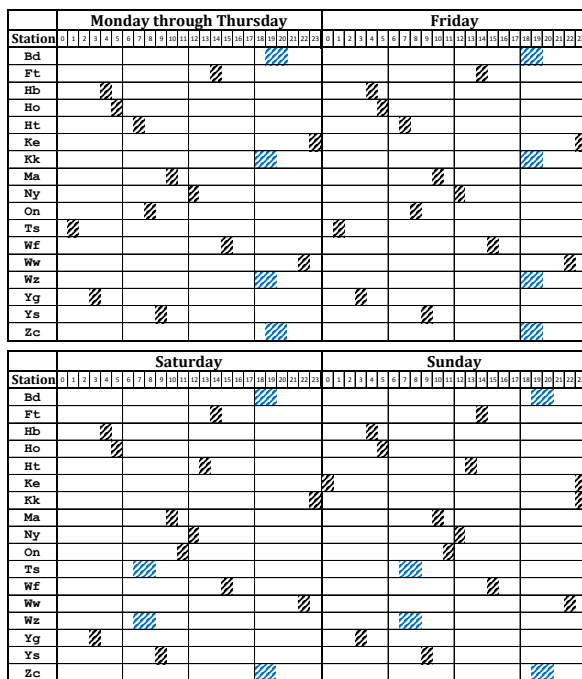


Fig. 3 Allotted station check times for the CONT14 stations for specific week days. The Intensive stations (Bd, Kk, Ts, Wz, and Zc) had 2-hour slots (blue) and first ran their respective Intensive sessions (Int1, Int2, or Ru-U) before performing their checks. All other stations had 1-hour check times (black).

The number of *sked* commands used in the input file amounted to 1,445. A full scheduling run (without manual control at the end) took about 20 min to execute.

5 Implications for VGOS

A major feature of VGOS will be continuous observing. Although it has not been fully decided yet, it is very likely that for operational purposes VGOS data will be organized in 24-hour periods by UT days. This setup will align the VGOS data to the way the other space-geodetic techniques organize their data. In contrast to, for instance, GPS where data can be taken (passively) and broken down into analysis blocks later in the processing chain, VLBI data needs to be organized at the scheduling level. Scans across boundaries cannot simply be broken into two pieces; hence, scans need to be planned and completed for a specific period.

To allow for complete continuity of VLBI data across day boundaries, antenna state information needs to be maintained for the scheduling process. That is, when writing the schedule for a subsequent day, the antenna state (such as cable-wrap) at the end of the previous schedule must be known. Assuming that the schedules for VGOS will be written by a given number of Operations Centers, storing antenna state information will have to become part of a general bookkeeping effort.

In CONT14, a changeover time of three minutes was allowed to change from one schedule to the next (basically resulting in observing days of 23 hours and 57 minutes length). This was the amount of time a station operator needed to perform the necessary steps involved in the process. The changeover time could be reduced, ideally to virtually instantaneous; however, as long as a change of modules is involved, it will not drop below a couple of minutes.

As VGOS antennas slew faster than the legacy antennas, it may be acceptable to neglect the information about the antenna state and risk the possible loss of a small number of scans (or rather observations) due to cable-wrap conflicts. Then the need for a bookkeeping process of the antenna state is eliminated with only adding no more than 15–30 seconds to the three minutes of time reserved for schedule changes.

6 Conclusions

For scheduling continuous VLBI observations using individual schedule files for subsequent observing days, it is essential to maintain information about the antenna state across (day) boundaries. In particular, the cable-wrap information needs to be carried forward. To satisfy the needs of scheduling the recent CONT campaigns, the *sked* program was altered to retain the cable-wrap setting for a longer time period (in an earlier version it forgot about the cable-wrap after about 10 min). For VGOS it may become necessary to include information about the antenna state in the general bookkeeping for scheduling purposes. This may be a challenge, as unlike with CONT14 observing schedules will probably be written by various Operations Centers.

In order to facilitate a change of schedules, a three-minute changeover time was needed in CONT14. For VGOS a similar setup may be implemented. A bookkeeping of the antenna state could be dropped if a small loss of scans (or observations) is tolerable.

References

- Behrend D (2009) Coordinating Center Report. In: D. Behrend and K. D. Baver(eds.), *IVS 2008 Annual Report*, NASA/TP-2009-214183, 77–79.
- Behrend D, Thomas C, Himwich E, MacMillan D (2014) CONT14: Preparation and Prospects. In: D. Behrend, K. D. Baver, K. L. Armstrong (eds.), *IVS 2014 General Meeting Proc.*, Science Press (Beijing), 196–200.
- Petrachenko B, Behrend D, Gipson J, Hase H, Ma C, MacMillan D, Niell A, Nothnagel A, Zhang X (2014) VGOS Observing Plan. In D. Behrend, K. D. Baver, K. L. Armstrong (eds.), *IVS 2014 General Meeting Proc.*, Science Press (Beijing), 16–19.
- Gipson J (2012) Sked. VLBI Scheduling Software. http://lupus.gsfc.nasa.gov/files/_user/_manuals/sked/sked.pdf.
- Schlüter, Behrend D (2007) The International VLBI Service for Geodesy and Astrometry (IVS): current capabilities and future prospects. *J Geod*, 81(6–8), 379–387, doi: 10.1007/s00190-006-0131-z.

Implementation of the vgosDb format

S. Bolotin, K. Baver, J. Gipson, D. Gordon, D. MacMillan

Abstract The IVS Working Group 4 developed a new format to store and exchange data obtained from geodetic VLBI observations. The new data format, vgosDb, will replace existing Mk3 databases in the forthcoming year. At GSFC we are working on software that will implement the vgosDb format and will be used routinely to convert correlator output to the new data storage format.

Keywords VLBI data analysis software, vgosDb

1 Introduction

Data produced at a correlator are subject to various changes before they become available to an end user. Historically, the results of the correlation of a VLBI session are stored in a special self-descriptive file called a *database*. Each modification or introduction of new information leads to a new version of the database. Fig. 1 shows the traditional data flow of the geodetic VLBI observations.

Typically, the version numbers correspond to the following modifications of the content of a database:

database_V001: data from correlator output are extracted and organized in the database format via the utility `dbedit`;

Sergei Bolotin, Karen Baver, John M. Gipson, David Gordon and Daniel S. MacMillan
NVI, Inc., NASA GSFC Code 698.2, 8800 Greenbelt Road, Greenbelt, Maryland 20771 USA

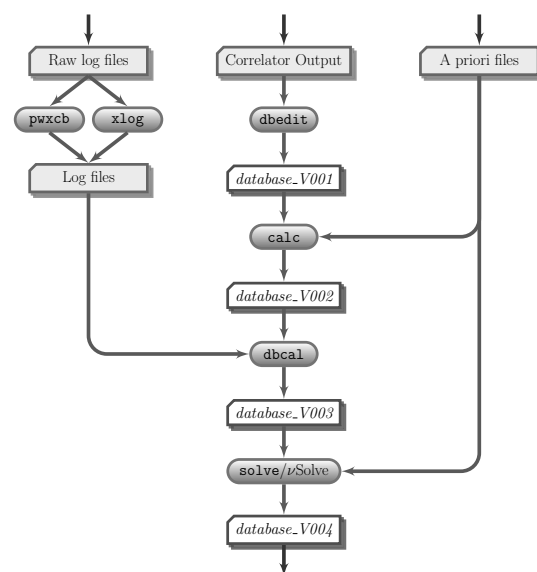


Fig. 1 Traditional dataflow of geodetic VLBI observations.

database_V002: the software `calc` reads the observations as well as a priori files and adds calculated theoretical values and partials into the database;

database_V003: meteorological data and cable calibration readings are extracted from station log files (via the utility `pwxcb`) and added into the database (with the utility `dbcal`);

database_V004: all necessary editing (e.g., ambiguity resolution, outlier determination, clock breaks, etc.) is performed for the session. Ionospheric corrections are evaluated and stored in the database. All of these modifications are performed with the software `solve` or its modern replacement, `vSolve`.

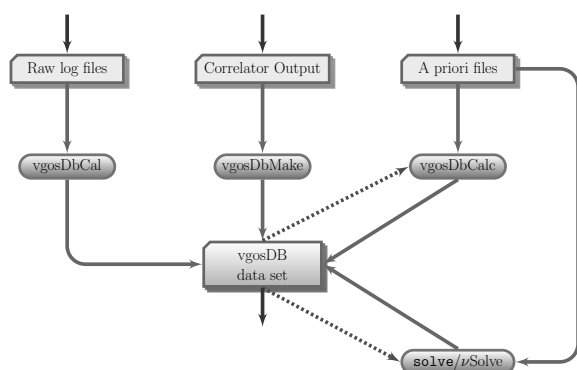


Fig. 2 New vgosDb dataflow of geodetic VLBI observations.

It is assumed that databases with version number 4 and higher are suitable for batch data processing. Databases with version numbers 1 and 4, as a rule, are available on the IVS public ftp sites.

Because, by definition, every update or modification of database content results in a new database file with an incremented version number, there is undesired redundancy of the data.

Other drawbacks of the current geodetic VLBI data format are missing documentation on the Mk3 database format and a lack of support of its realization. The library that implements these input/output operations, Mk3 database handler (Mk3 DBH), was created more than 30 years ago.

2 New vgosDb Format

The new VLBI data format removes unnecessary redundancy. It keeps data in netCDF binary files. This implementation allows flexible, platform independent access and is well documented. The interaction between various utilities and VLBI data is shown in the Fig. 2.

In accordance with the vgosDb format, the VLBI data are stored in various files in the form of $\{key \Rightarrow value\}$. Each file represents an atomic piece of data, e.g., observables with their standard deviations or station coordinates. An additional feature is that it is possible to keep alternative models or approaches to the editing of observations in the same data tree. The set of data files a user should use is specified in a special file

called a *wrapper file*. It is possible to have more than one wrapper file for one VLBI session.

Such an approach to organization of the VLBI data departs from the traditional meaning of version.

The new geodetic VLBI data format is a result of activity of the IVS Working Group 4, (Gipson, 2012).

The work on implementation of the vgosDb format by the GSFC VLBI group started in mid 2013. The ν Solve software as well as global solve are now ready to use VLBI data in the vgosDb format. The traditional utilities `dbedit` and `dbcal` will be replaced by a completely new software. The software `calc` will be extended to use the vgosDb format.

3 Design of the New Software

The new utilities, `vgosDbMake` and `vgosDbCal`, are parts of the new VLBI data analysis software developed at NASA GSFC (Bolotin et al., 2010) and currently distributed under the name `nuSolve`. The utilities have the same design as ν Solve software. The same software development environment is also used.

The utilities are designed to operate on any POSIX compatible OS. We use C++ as the programming language due to its power, flexibility and portability. GNU Build System is used to make the software distribution portable.

The software consists of two parts:

- Space geodesy library, a library where data structures and algorithms are implemented (about 90% of the total source code).
- Executables `vgosDbMake` and `vgosDbCal`, drivers that call library functions and organize work with an end user (about 10% of the total source code).

Such organization of the software allows us to reuse the source code in other applications.

The software has a modular structure that makes it flexible and scalable. A module is a logical block of code that is loosely tied with other parts of the software. Fig. 3 displays the general modular structure of the whole software package, including ν Solve.

Several modules in the figure (e.g., HOPS, netCDF, Qt) represent external libraries. The sizes of the modules can vary.

Obviously, not all the modules will be used by `vgosDbMake` and `vgosDbCal`. On the other hand, the

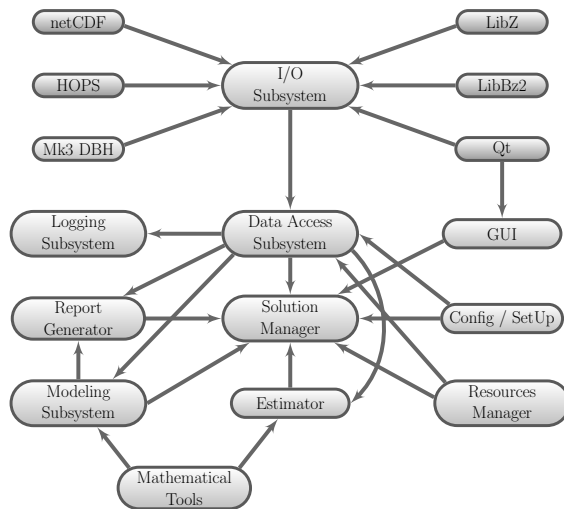


Fig. 3 The modular structure of the new VLBI data analysis software.

modular design of the software makes it easy to add the functionality of the utilities to the interactive VLBI data editor, *vSolve*.

Modification of the software *calc* will be done in a different way. A library that mimics the Mk3 DBH programming interface will be created. The library will replace database functions with *vgosDb* I/O operations. In this case we do not need to modify *calc* source code at all, but just need to link the software with the new library.

4 Conclusions

Our group will switch to the new VLBI data format at the beginning of 2016. The work on *vgosDbMake* is at the final stage. At the time of writing we are performing extensive testing of the software. The utility *vgosDbCa1* will be available in November. Also, we expect to prepare *vgosDbCa1c* in December. Starting in December we will perform tests of the whole VLBI data flow using the *vgosDb* format and then start to release VLBI sessions in the new format routinely.

We strongly encourage all VLBI data analysis centers to switch to the new VLBI data format.

References

- Bolotin S, Gipson J M, MacMillan D (2010) *Development of a New VLBI Data Analysis Software*. In: D. Behrend, K. D. Baver (eds.), *IVS 2010 General Meeting Proc.*, NASA/CP-2010-215864, 197–201.
- Gipson J M (2012) *IVS Working Group 4: VLBI Data Structures*. In: D. Behrend, K. D. Baver (eds.), *IVS 2012 General Meeting Proc.*, NASA/CP-2012-217504, 212–221.

Observing GNSS L-band Signals: Ionospheric Corrections by co-located GNSS Measurements

B. Männel, M. Rothacher

Abstract In recent years a few experimental sessions were carried out to observe the L-band signals transmitted by Global Satellite Navigation System (GNSS) satellites using radio telescopes. This observation concept, called G-VLBI, allows Very Long Baseline Interferometry (VLBI) to participate in a geodetic co-location in space. Therefore, G-VLBI needs radio telescopes participating regularly in geodetic VLBI sessions which can observe in the L-band signal domain. As a number of these telescopes, and the observations available so far, are not sensitive to GNSS signals at both frequencies, high-quality ionospheric delay corrections are necessary. These corrections can be derived from the geometry-free linear combination of co-located GNSS observations by the L4R method (Männel et al., 2014; Männel and Rothacher, 2015). In this paper G-VLBI as a way to reach a co-location in space is highlighted, and current limitations and potential applications of the L4R approach are discussed.

Keywords G-VLBI, Ionosphere, GNSS, VLBI satellite-tracking

1 Introduction

Co-location in space as a possibility to combine geodetic space techniques was introduced by several authors in recent years (Rothacher, 2003; Plag and Pearlman, 2009; Thaller et al., 2011; Tornatore et al., 2014). However, VLBI, designed to observe quasars (or far distant

space-probes), could not participate in this combination so far. By tracking GNSS satellites with VLBI radio telescopes (Tornatore et al., 2014; Haas et al., 2014) a new world for co-location in space opens. In this paper we will discuss the idea and the potential of G-VLBI in Section 2. As the available G-VLBI observations are limited to single-frequency, high-quality ionospheric delay corrections are crucial. Therefore, in Section 3 the L4R approach, as introduced by Männel et al. (2014) to derive ionospheric delay corrections from co-located GNSS receivers, is reviewed. Further possibilities to improve these corrections and potential applications are discussed in Section 4. The paper is summarized with some conclusions in Section 5.

2 The Potential of G-VLBI Observations

Figure 1 shows the idea of G-VLBI and co-location in space. The inclusion of VLBI into a combination on-board a GNSS satellite is achieved by tracking the L-band signals transmitted by this satellites. Therefore, the connection between GNSS and VLBI and between the Terrestrial Reference Frame (ITRF) and the Celestial Reference Frame (ICRF) becomes available directly at the radio telescopes. As part of this idea it is obvious that telescopes which participate regularly in geodetic sessions and with a co-located Satellite Laser Ranging (SLR) telescope are desirable for G-VLBI observations. From EVN (2015) one can only find a small number of telescopes, able to track GNSS L-band signals, which meets the above mentioned requirements. According to the nominal bandwidths none of these telescopes is sensitive to both GNSS frequencies (L_1

Benjamin Männel, Markus Rothacher
ETH Zürich, Institute of Geodesy and Photogrammetry, Robert-Gnehm-Weg 15, CH-8093 Zürich, Switzerland

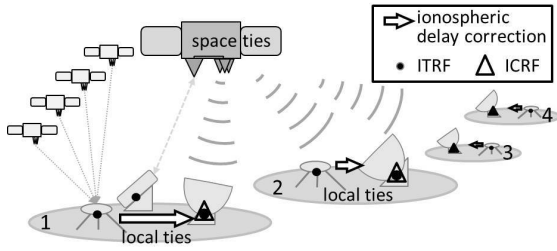


Fig. 1 Observing a GNSS satellite for co-location in space by GNSS, SLR and G-VLBI.

$= 1.598\dots 1.605 \text{ GHz}$, $L_2 = 1.242\dots 1.248 \text{ GHz}$ ¹). In addition some radio telescopes are sensitive to L-band signals via the S-band channels (Kodet et al., 2014). However, one can say that the majority of telescopes participating regularly in geodetic VLBI sessions are not able to track both GNSS L-band signals. Therefore, the ionospheric error will be the most important error source and high-quality ionospheric delay corrections are essential for single-frequency G-VLBI observations.

With the progress of dedicated co-location satellite missions like GRASP (Bar-Sever et al., 2009), some questions concerning the purpose of G-VLBI arose. Beyond the unique possibility to get prepared for GRASP, we see the following advantages of G-VLBI. Firstly, receivers for all techniques are co-located at a fundamental site, exposed to the same environmental conditions, instead of combining observations tracked in space (GNSS) and on ground (VLBI, SLR) for GRASP-type missions. Secondly, tracking the same signal with GNSS and VLBI might be helpful for combining common parameters like tropospheric delays and clock parameters. And, thirdly, the bigger altitude of GNSS satellites allows the observation of baselines up to the Earth's diameter. Figure 2 shows the relation between baseline length, orbital height of the satellite and the chosen cut-off angle. As in this figure the observation time is not considered, one has to keep in mind that successful G-VLBI observations will require a certain time of visibility, at least a couple of minutes. The requirement of a sufficient observation window will reduce the geometrically-derived maximum baseline length significantly. Therefore, we believe that G-VLBI observations are seminal and

¹ in this work we only considered GPS and GLONASS

more investigations on this observation concept should be done.

These conclusions lead us to study approaches to correct the critical ionospheric delay. In the following sections we will discuss some basic aspects when using co-located GNSS observations to derive these corrections.

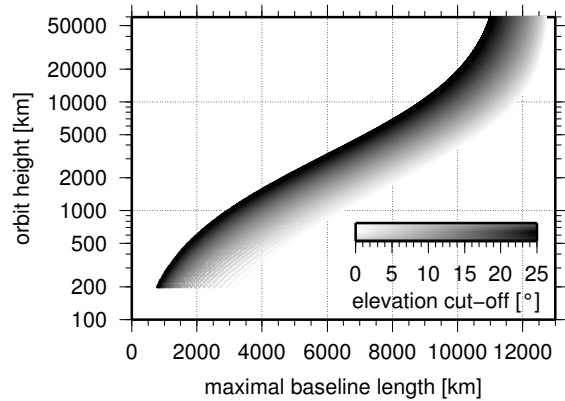


Fig. 2 Maximal baseline length for different orbital heights and different cut-off angles.

3 A Short Review on the L4R Approach

Apart from the possibility of deriving ionospheric corrections from GNSS-based TEC maps, calibrator sources, or deterministic models, such corrections can also be derived from co-located observations. This is done by the L4R approach, where the ionospheric delay in the G-VLBI observation is determined from co-located GNSS measurements. The corrections derived are based on the residuals of a least squares adjustment of double-differenced GNSS phase observations in a geometry-free linear combination L_4 . This linear combination can be written in metric units as

$$L_{rs,4}^{ij} = -\left(1 - \frac{f_1^2}{f_2^2}\right) I_{rs,4}^{ij} + \lambda_1 N_{rs,1}^{ij} - \lambda_2 N_{rs,2}^{ij}. \quad (1)$$

Where i, j and r, s are two satellites and two receivers, respectively, f_1, f_2 are the frequencies of the L_1 and L_2 signal with the wavelengths λ_1, λ_2 . The ionospheric delay is represented by $I_{rs,4}^{ij}$, the phase ambiguities by $N_{rs,1}^{ij}, N_{rs,2}^{ij}$. After fixing the ambiguities to integer

values by using the SIGMA-dependent (e. g. Dach et al., 2007) and the quasi-ionospheric free (QIF, Mercant, 1995) algorithms residuals are obtained from a least-squares adjustment, where only unresolved ambiguities as parameters remain. To derive baseline- or station-satellite-specific corrections from these double-differenced residuals a zero-mean condition has to be introduced. Therefore, only relative ionospheric delays are obtained. An external ionospheric model is needed to account for the absolute part of the ionosphere. We used the Global Ionospheric Maps from CODE (Schaer, 1999) for this purpose. The accuracy level of the L4R corrections is assumed to be below two TECU for short and medium-range baselines (up to 5000 km). The necessary processing steps have been implemented in a project version of the Bernese GNSS Software (Dach et al., 2013).

As shown by Männel and Rothacher (2015) the derived corrections can be validated by applying them to a GNSS L_1 processing and by analyzing the coordinate repeatability, i. e. the variations of daily results with respect to a multi-day solution. We computed three different solutions for the baselines Medicina-Wetzell, and Ny-Ålesund-Wetzell. Firstly, an L_3 solution (V_{L3}) was derived, which is assumed to be free from ionospheric effects. Secondly, an L_1 solution (V_M) using GIMs to account for the ionosphere were computed. The third solution is also an L_1 solution (V_{L4R}), but with ionospheric corrections derived by L4R. To avoid too optimistic results by using the same baseline for the L4R and the L_1 processing we formed the baselines using the WTZZ receiver, whereas the L4R processing was done with WTZR. In Figure 3 the daily height repeatabilities derived from 30-s GNSS data are shown. The usage of L4R leads to a significant decrease of the repeatabilities in V_{L4R} compared to V_M . However, the accuracy of the L4R corrections is limited by the baseline length due to reasons, which are discussed in the next session.

4 The L4R Approach Limitations, Improvements and Possible Applications

According to Männel and Rothacher (2015) the major limitations are the (1) unresolved ambiguities especially for longer baselines (5000 km and more), (2) the

accuracy of the external ionosphere model, and, to a smaller extent, (3) the zero-mean condition.

Concerning limitation (1), regarding the ambiguities, Männel and Rothacher (2015) concluded that, for baselines longer than 5000 km, the ionospheric delay is partly absorbed by unresolved ambiguities. To reduce the impact of this limitation, either (a) a more suitable ambiguity resolution approach, (b) unambiguous observations, or (c) directly a zero-difference strategy can be used. Improving the ambiguity resolution, option (a), might be very difficult as long baselines have fewer observations and shorter observation periods for a certain satellite compared to short or medium-range baselines. Option (b), the processing of unambiguous observations, namely pseudo-range or code observations, has two major advantages, the ionospheric delay corrections are not biased by unresolved ambiguities and a zero-difference processing is possible. In that case the geometry-free linear combination reads as

$$P_{rs,4}^{ij} = \left(1 - \frac{f_1^2}{f_2^2}\right) I_{rs,4}^{ij} + c(\Delta b^i - \Delta b_r). \quad (2)$$

Here c represents the speed of light, whereas $\Delta b^i, \Delta b_r$ are the Differential Code Biases (DCB). During the processing these biases must be determined or very good a priori values are needed for them. In addition code observations (and the ionospheric corrections derived thereof), suffer from a higher level of measurement noise, decimeters instead of millimeters for the phase, and multipath effects, which can reach several meters. Hernandez et al. (2011) estimate the uncertainty of corresponding ionospheric corrections to amount to up to 20 TECU. Therefore, we decide to use phase observations, where the potential to reach millimeter accuracy is given (even though we are currently not able to reach this accuracy).

A processing of GNSS phase observations at the zero-difference level, as option (c), might benefit from the quality of phase observations and the avoidance of ambiguity-fixing over long baselines. Furthermore, as in the zero-difference mode, only the satellite-baseline pair of interest has to be considered. However, in the zero-difference processing receiver and transmitter hardware delays cannot be eliminated and have to be estimated. Zero-difference phase ambiguity solutions are presented in the literature based on the hardware delay calibration (Laurichesse et al., 2009) or the wide-lane and phase bias information (Bertinger et

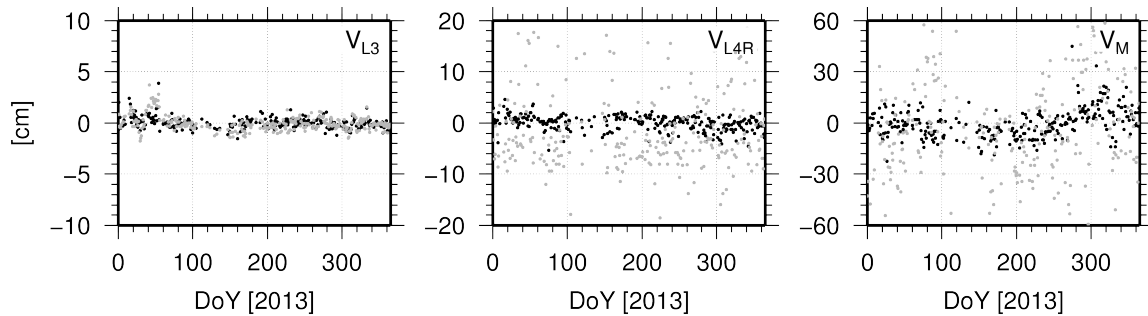


Fig. 3 Daily height coordinate repeatability for Medicina-Wetzell (*black*) and Ny-Ålesund-Wetzell (*darkgrey*).

al., 2010). As the zero-difference ambiguity-fixing is currently not implemented in the Bernese GNSS Software, we did not use a zero-difference phase approach.

Concerning limitation (2), regarding external ionospheric models, a higher spatial and temporal resolution could improve the corrections. For example there are TEC maps with a higher resolution, like the IGS TEC maps with a spatial $5^\circ \times 2.5^\circ$ and a 2 h temporal resolution. Also the use of physical models like the International Reference Ionosphere (IRI, (Bilitza, 2001) or the Global Assimilative Ionospheric Models (GAIMs, JPL, 2015) are possible. However, we believe that the impact on the derived corrections will be rather small.

Limitation (3), regarding the zero-mean condition, can simply be avoided by omitting the forming of double-differences. Alternatively, as we are forced to form double-differences for ambiguity fixing, we can introduce the zero-mean condition over several epochs. As a consequence, jumps caused by a constellation change should be removed. However, based on the findings by Männel and Rothacher (2015) the possible improvement will be rather small. Applying a weighting function, as it is possible in the zero-mean condition, will degrade the derived corrections as the L4R approach is based directly on equal-weighted residuals.

It is clear that the L4R approach has been developed for G-VLBI observation, where the same signal and the same signal path are observed with the GNSS receiver and the radio telescope. Whereas the previous G-VLBI sessions were single-baseline observations we hope that in the near future a first network will track GNSS-satellite L-band signals together. Using a network will improve the number of observations and the

derived results. As the ionospheric error of one station is visible in all baselines containing this station, the ionospheric correction can be derived from the shortest of these baselines. Therefore, we expect also a benefit for the ionospheric corrections derived by the L4R approach, as the disturbing influence of the ambiguity resolution will be reduced.

Beyond G-VLBI, the application of the L4R method in tracking other spacecrafts or in single-frequency astrometry is conceivable. However, the basic requirement is a close distance between the observed radio source in VLBI and a GNSS satellite. This must be considered during the VLBI scheduling process. Figure 4 shows the probability of finding a GNSS satellite within a certain time window and spherical distance as seen from one ground station (zero-difference mode). Assuming a suitably small separation angle it will be rather difficult to ensure that for each observed source a GNSS satellite will be within the specified distance. However, in Figure 4, only GPS and GLONASS were considered. With the increasing number of satellites due to the upcoming systems Galileo and BeiDou the scheduling process will become easier.

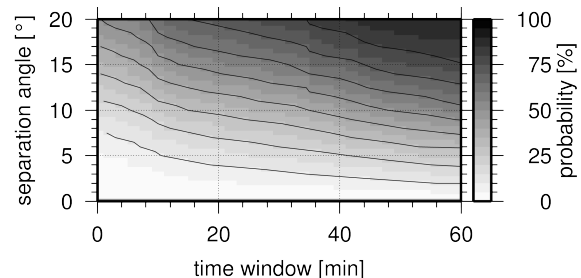


Fig. 4 Probability of finding a GNSS satellite (GPS or GLONASS) within a certain time window and spherical distance around a fictitious source.

5 Conclusions

We discussed the tracking of GNSS L-band signals with radio telescopes for a geodetic co-location in space. Compared to the planned co-location satellite mission GRASP, G-VLBI benefits from the higher altitude of the GNSS satellites resulting in longer baselines and longer observation times. As the major limitation of the currently available G-VLBI observations is the restriction to one frequency, we discussed the L4R approach based on the geometry-free linear combination of co-located GNSS phase data. From the discussion concerning the problems of the ambiguity resolution for long baselines we conclude that the usage of zero-difference phase observations might be beneficial if the ambiguities can be fixed on this level. Additionally we discussed a potential application in classical VLBI. However, scheduling the VLBI observation based on the GNSS satellite constellation will be a difficult task.

Acknowledgements The authors want to thank IVS and IGS for providing the necessary observations allowing a suitable processing. This work was done within the project "Co-location of Space Geodetic Techniques on Ground and in Space" which is part of the DFG funded Research Unit "Space-Time Reference Systems for Monitoring Global Change and for Precise Navigation in Space" (FOR 1503).

References

- Bar-Sever Y E, Haines B, Wu S, F. Lemoine F, Willis P (2009) Geodetic Reference Antenna in Space (GRASP): A Mission to Enhance the Terrestrial Reference Frame. *COSPAR colloquium: scientific and fundamental aspects of the Galileo program*, Padua.
- Bertiger W, Desai SD, Haines B, Harvey N, Moore AW, Owen S, Weiss JP (2010) Single receiver phase ambiguity resolution with GPS data. *J Geod*, 84(5), 327–337, doi: 10.1007/s00190-010-0371-9
- Bilitza D (2001) International Reference Ionosphere 2000. *Radio Sci*, 36, 261–275.
- Dach R, Fridez P, Hugentobler U, Meindl M (2007) Bernese GPS Software 5.0.
- Dach R (2013) Bernese GNSS Software: New features in version 5.2.
- Haas R, Neidhardt A, Kodet J, Plötz C, Schreiber U, Kronschnabl G, Pogrobenko S, Duev D, Casey S, Marti-Vidal I, Yang J, Plank L (2014) The Wettzell-Onsala G130128 Experiment - VLBI observation of a GLONASS satellite. In: D. Behrend, K. Baver, K. Armstrong (eds.), *IVS 2014 General Meeting Proc.*, Science Press (Beijing), 451–455.
- Hernández-Pajares M, Juan J M, Sanz J, Aragón-Àngel À, García-Rigo A, Salazar D, Escudero M (2011) The ionosphere: effects, GPS modeling and the benefits for space geodetic techniques. *J Geod*, 85(12), 887–907.
- Kodet J, Schreiber U, Plötz C, Neidhardt A, Kronschnabl G, Haas R, Molera Calvés G, Pogrebenko S, Rothacher M, Männel B, Plank L, Hellerschmied A (2014) Co-locations of Space Geodetic Techniques on Ground and in Space. In: D. Behrend, K. Baver, K. Armstrong (eds.), *IVS 2014 General Meeting Proc.*, Science Press (Beijing), 446–450.
- Laurichesse D, Mercier F, Berthias J P, Broca P, Cerri L (2009) Integer Ambiguity Resolution on Undifferenced GPS Phase Measurements and its Application to PPP and satellite Precise Orbit Determination. *Nav*, 56(2), 135–149.
- Männel B, Rothacher M, Kodet J, Schreiber U, Schmid R (2014) GLONASS Satellites Simultaneously Observed by VLBI, GNSS and SLR. In: D. Behrend, K. Baver, K. Armstrong (eds.), *IVS 2014 General Meeting Proc.*, Science Press (Beijing), 461–465.
- Männel B, Rothacher M (2015) Ionospheric corrections for single-frequency tracking of GNSS satellites by VLBI based on co-located GNSS. *J Geod*, submitted.
- Mervant L (1995) Ambiguity Resolution Techniques in Geodetic and Geodynamic Applications of the Global Positioning System. PhD thesis, Universität Bern
- Plag H-P, Pearlman M (2009) Global Geodetic Observing System, Meeting the Requirements of a Global Society on a Changing Planet in 2020. Springer Verlag.
- Rothacher M (2003) Towards a rigorous combination of space geodetic techniques. In: B. Richter, W. Schwegmann, W. R. Dick (eds.), *Proc. IERS Workshop on combination research and global geophysical fluids*, IERS Technical Note 30, 7–18.
- Schaer S (1999) Mapping and predicting the Earth's ionosphere using the Global Positioning System. PhD thesis, *Geod.-Geophys. Arb. Schweiz*, 59, Universität Bern.
- Thaller D, Dach R, Seitz M, Beutler G, Mareyen M, Richter B (2011) Combination of GNSS and SLR observations using satellite co-locations. *J Geod*, 85(5), 257–272.
- Tornatore V, Haas R, Duev D, Pegrebenko S, Casey S, Molera Calvés G (2014) Direct VLBI Observations of Global Navigation Satellite System Signals. In: C. Rizos, P. Willis (eds.), *Proc. IAG General Assembly 2011*, IAG Symposia 139, 274–252, doi: 10.1007/978-3-642-37222-3_32.
- EVN (2015) EVN Status Tables. http://www.evlnbi.org/user_guide/EVNstatus.txt, accessed 03 August 2015.
- JPL (2015) Introduction to GAIM. <http://iono.jpl.nasa.gov/gaim/intro.html>, accessed 03 August 2015.

VLBI-like GNSS delays in the analysis of CONT11

Y. Kwak, J. Böhm, T. Hobiger, L. Plank

Abstract During CONT11, seven VLBI sites had co-located GNSS antennas sharing the identical clocks. We build VLBI-like GNSS delays between the ranges from two stations to a GNSS satellite by using post-processed phase measurements from a precise point positioning (PPP) solution with the c5++ software and analyze those delays together with VLBI observations with the Vienna VLBI Software. We estimate station coordinates, common parameters at the sites, i.e. zenith wet delays, troposphere gradients and clocks. For combination, zenith wet delays, troposphere gradients and local ties are constrained between two techniques, VLBI and GNSS. We compare the combination solutions with single technique solutions and discuss the impact of the combination at the observation level.

Keywords CONT11, GNSS-VLBI hybrid system, Combination at the observation level

1 Introduction

The GNSS-VLBI (GV) hybrid system, where co-located VLBI antennas and GNSS antennas si-

Younghee Kwak, Johannes Böhm
Technische Universität Wien, Gußhausstraße 27-29, 1040 Vienna, Austria
Thomas Hobiger
Department of Earth and Space Science, Chalmers University of Technology, Onsala Space Observatory, SE-439 92 Onsala, Sweden
Lucia Plank
University of Tasmania, Private Bag 37, Hobart 7001, Australia

multaneously receive signals from quasars and GNSS satellites, respectively, and both signals are processed in the VLBI system, is a concept of combination for space geodetic techniques at the observation level. The pilot GV hybrid experiment was conducted on a short and single baseline between Kashima and Koganei inside Japanese territory (Kwak et al, 2011); however, the estimation of a full set of parameters was not possible due to the small network size. In this paper, we extend the network of the GV hybrid system to the IVS CONT11 network which has a reasonably balanced geographical distribution globally and co-located International GNSS Service (IGS) stations. In particular, we adopted seven CONT11 sites (Fig. 1) as a test bed in which both techniques, VLBI and GNSS, are connected to the identical frequency standard, i.e. the hydrogen maser atomic clocks.

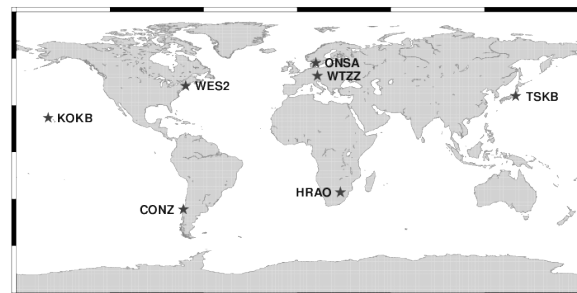


Fig. 1 A global network of co-located CONT11 sites using the same clock for both VLBI and GNSS. The station codes are written following IGS station code names.

2 Generation of VLBI-like GNSS Delays

In order to perform a realistic test for combination, we generated VLBI-like GNSS observations, i.e. single differenced GNSS data, based on real GNSS phase measurements. Later on, those VLBI-like GNSS observations were merged with VLBI CONT11 data and analyzed together in the Vienna VLBI Software (VieVS). In the followings, we provide the detailed procedure to generate the data (Kwak et al, 2015).

- We processed general GNSS data (phase measurements) using precise point positioning (PPP) technique with the c5++ software. In the c5++ software, the ionospheric delays were cancelled out using linear combination of dual frequencies and the estimated phase ambiguities, phase center variations (PCV) and phase wind-up effects were subtracted from the original phase measurements.
- We took the differences of the corrected phase measurements between two stations which are receiving the same satellite signals like as single difference of the GNSS processing technique.
- Those difference values (hereafter “VLBI-like GNSS delays”) are the input data in VieVS. To make the test faster, we sampled the data with a 5-minute interval.

Two baselines (CONZ-TSKB and HRAO-KOKB) do not have any common observations at all since the lengths of baselines are too long to observe common GNSS satellites.

3 Combination of VLBI and GNSS at the Observation Level

We created the merged data files, i.e. VLBI CONT11 data plus VLBI-like GNSS delay data, in which the data are sorted by order of time regardless of data type (Fig. 2). In the combination, we did not combine products nor normal equations but constructed a combined design matrix which contains the partial derivatives of VLBI and GNSS according to the merged data.

For both data, all geophysical models, e.g. atmospheric and tidal models, are the same except for geometric models. The constraints for parameters are also the same. We estimated all parameters separately and

```

:
2011 9 15 0 5 15.00 WTZZGNSS WES2GNSS PG10 sc -0.00193562711807780 ...
2011 9 15 0 5 15.00 WTZZGNSS WES2GNSS PG13 sc 0.01079601557621570 ...
2011 9 15 0 6 50.00 KOKEE TSUKUBS2 1144-379 qb 0.00732405933076071 ...
2011 9 15 0 6 50.00 KOKEE TIGOCONC 1144-379 qb 0.00542015727254934 ...
:

```

Fig. 2 The merged data file which consists of both VLBI CONT11 data and VLBI-like GNSS delay data.

gave additional constraints for site-wise common parameters, i.e. zenith wet delays (ZWDs) and troposphere gradients.

Troposphere gradients can be assumed to be identical if the horizontal distances between the reference points of the co-located techniques are close enough, i.e. within a few kilometers (Hobiger and Otsubo, 2014). We gave rather loose constraints (2 cm) on the troposphere gradients.

ZWDs are the vertical delay values when radio signals pass through wet troposphere and thus it highly depends on height. Therefore, we need to take the ZWD corrections due to height differences between the reference points of the co-located techniques into account. We applied mean ZWD correction values according to Teke et al (2011) and used 1 cm constraints.

We also introduce the local tie vectors between two reference points at the co-located site. Usually the formal errors of the local tie measurement are too optimistic and thus we applied 3 cm for the constraints.

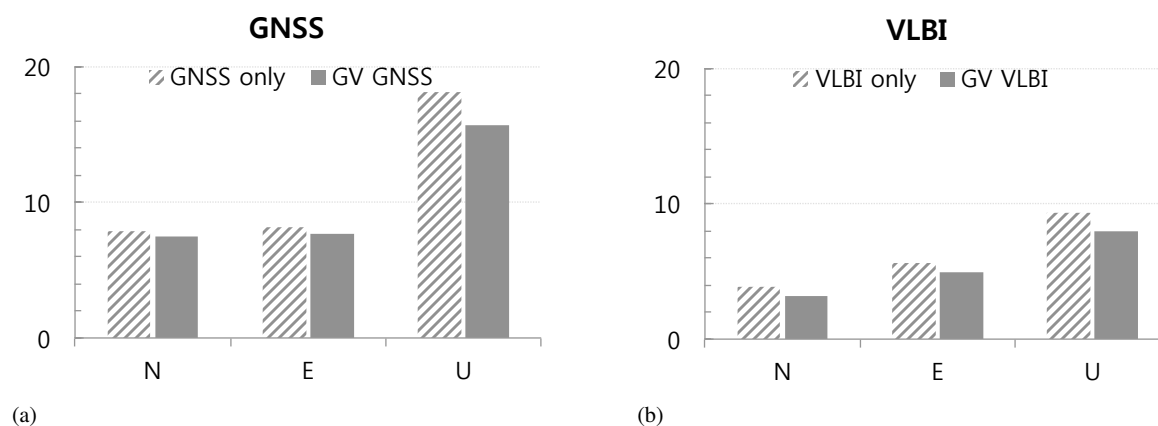
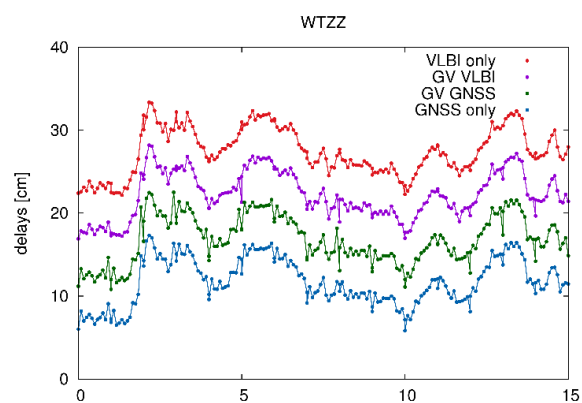
The overview of general analysis strategies is shown in Table 1. Since the partial derivatives of EOP were not introduced in the GNSS part, we fixed EOP values to IERS 08 C04. In this paper, we check how the constrained ZWDs and troposphere gradients to each other improve geodetic results, i.e. station coordinate repeatabilities. We applied NNR/NNT constraints to respective frames, i.e. Vienna TRF for VLBI and PPP solutions from c5++ for GNSS to avoid unexpected distortion in the frames.

4 Results

In order to check the combination performance, we compare mean station position repeatabilities with single solutions. Fig. 3(a) shows the comparison of GNSS solutions and Fig. 3(b) the comparison of VLBI solutions (single versus combination solutions). Since we are still in the test phase to process GNSS data using VieVS, the accuracy of the model involved for GNSS

Table 1 Models and a priori used in this study.

Sources (VLBI / GNSS)	ICRF2 / IGS final orbit
Station coordinates (VLBI / GNSS)	Vienna TRF / PPP solutions from c5++
Solid Earth tide	IERS 2010 Conventions (Petit and Luzum, 2010)
Ocean loading	FES2004 (Lyard et al, 2006)
Earth orientation parameters	IERS 08 C04
Troposphere delay	Zenith hydrostatic delays from GPT (Böhm et al, 2007) VMF (Böhm et al, 2006)
Ionosphere	No a priori for troposphere gradient Corrected by using ionosphere-free linear combination in the PPP processing

**Fig. 3** Mean station position repeatabilities of single solutions (box with a pattern of diagonal lines) and combination solutions (solid box) for north, east and up components. Plot (a) shows the results of GNSS stations and plot (b) the results of VLBI stations. The unit is mm.**Fig. 4** ZWDs at Wettzell (WTZZ) from single solutions and combination solutions during 15-day CONT11 period. For readability, the lines are shifted by 5, 10 and 15 cm. They agree with each other (VLBI only versus GV VLBI and GNSS only versus GV GNSS) within 1 cm. The order of the lines follows the order of the legends

data is at the cm-level and thus the station position repeatability of GNSS stations is larger than the repeatability of usual GNSS solutions (not shown here). For more details, see Kwak et al (2015). Nevertheless, one can see that the combination solutions are improved compared to single solutions. While the GNSS solutions are improved by 5, 6 and 13 % for north, east and up components, the VLBI solutions are improved by 17, 12 and 14 % for each component. This means that both techniques gain the same level of benefits in vertical components but VLBI benefits more in horizontal components than GNSS. Better sky coverage of GNSS data due to multiple radio sources at one epoch would be the strong candidate for these improvements. Fig. 4 shows the estimated ZWD values at Wettzell (WTZZ) from single solutions and combination solutions as an example of estimated parameters. The agreements of ZWD values throughout 15 days are within 1 cm (root mean squared value) for each reference point (each technique) even though there are a few spikes which look like outliers.

5 Conclusions

In this paper, we merged VLBI CONT11 data and VLBI-like GNSS delay data for seven co-located sites and analyzed them in VieVS as well as single technique data. For combination, ZWDs, troposphere gradients and local ties were constrained between two techniques, VLBI and GNSS. Finally, the combination solutions improve station position repeatability in comparison with single solutions. Additional constraints for clock parameters will be added for the combination in the next stage since both techniques shared the atomic clocks at the co-location sites.

6 Acknowledgements

This work has been supported by project Hybrid GPS-VLBI (M1592) which is funded by the Austrian Science Fund (FWF) and the Australian Research Council for Fellowship FS1000100037.

References

- Böhm J, Werl B, Schuh H (2006) Troposphere mapping functions for GPS and very long baseline interferometry from European Centre for Medium-Range Weather Forecasts operational analysis data. *J Geophys Res*, 111(B2), doi: 10.1029/2005JB003629.
- Böhm J, Heinkelmann R, Schuh H (2007) Short Note: A global model of pressure and temperature for geodetic applications. *J Geod*, 81(10), 679–683, doi: 10.1007/s00190-007-0135-3.
- Hobiger T, Otsubo T (2014) Combination of GPS and VLBI on the observation level during CONT11 - common parameters, ties and inter-technique biases. *J Geod*, 88(11), 1017–1028, doi: 10.1007/s00190-014-0740-x.
- Kwak Y, Kondo T, Gotoh T, Amagai J, Takiguchi H, Sekido M, Ichikawa R, Sasao T, Cho J, Kim T (2011) Validation Experiment of the GPS-VLBI hybrid system. In: W. Alef, S. Bernhart, A. Nothnagel (eds.), *Proc. 20th EVGA Working Meeting*, 154–157.
- Kwak Y, Böhm J, Hobiger T, Plank L (2015) The Processing of Single Differenced GNSS Data with VLBI Software. In: *Proc. IAG Commission 1 Symposium 2014*, under revision.
- Lyard F, Lefevre F, Letellier T, Francis O (2006) Modelling the global ocean tides: modern insights from FES2004. *Ocean Dynam*, 56(5-6), 394–415, doi: 10.1007/s10236-006-0086-x.
- Petit G, Luzum B (2010) (eds.) IERS Conventions (2010). *IERS Technical Note 36*, Verlag des Bundesamtes für Kartographie und Geodäsie.
- Teke K, Böhm J, Nilsson T, Schuh H, Steigenberger P, Dach R, Heinkelmann R, Willis P, Haas R, Garcia Espada S, Hobiger T, Ichikawa R, Shimizu S (2011) Multi-technique comparison of troposphere zenith delays and gradients during CONT08. *J Geod*, 85(7), 395–413, doi: 10.1007/s00190-010-0434-y.

Influence of the horizontal resolution of numerical weather models on ray-traced delays for VLBI analysis

A. Hofmeister, D. Landskron, J. Böhm

Abstract Ray-traced delays offer the opportunity to correct the influences of the troposphere on observations of space geodetic applications such as Very Long Baseline Interferometry (VLBI). As the Numerical Weather Model (NWM) builds the data base for the ray-tracing through providing the needed meteorological data, the selection of an appropriate NWM is of major concern. In this respect also the horizontal resolution of the NWM may have significant impact on the resulting ray-traced slant delays. So, directly on the ray-traced delays the horizontal resolution of the NWM shows an increasing impact with decreasing elevation angle. In case of using horizontal resolutions of either $0.125^\circ \times 0.125^\circ$ or $1^\circ \times 1^\circ$, real significance in terms of differences in the resulting ray-traced delays is only given at elevation angles smaller than 10° , as the differences start to exceed the cm-level at lower elevations. If the ray-traced delays are applied to the VLBI analysis of the CONT11 campaign, the horizontal resolution of the NWM has in general a very small influence with respect to Baseline Length Repeatability (*BLR*) and Station Coordinate Repeatability (*SCR*). Depending on the general parameterization of the analysis, the influence of the horizontal resolution of the NWM may even be negligible.

Keywords Ray-tracing, Troposphere, Numerical weather model, VLBI

Armin Hofmeister, Daniel Landskron, Johannes Böhm
Technische Universität Wien, Department of Geodesy and
Geoinformation, Gußhausstraße 27-29, A-1040 Vienna, Austria

1 Introduction

The application of ray-tracing for the calculation of tropospheric slant delays serves as a promising alternative for the correction of the influences of the troposphere on the observations of space geodetic techniques such as the Very Long Baseline Interferometry (VLBI). Compared to the standard approach, where the slant delays for the tropospheric correction are determined via estimating zenith delays and applying mapping functions, the ray-tracing approach estimates the slant delays directly for the actual ray paths of the observations.

In order to determine these ray paths and the delays along these paths, meteorological data are needed as main input for the ray-tracing approach. These data are usually taken from a Numerical Weather Model (NWM). Nowadays there are many different NWMs available, which can be used for the ray-tracing. But besides the general selection of a specific NWM it is also necessary to choose its horizontal resolution, which may have significant impact on the resulting ray-traced delays. Concerns why not to use the highest available horizontal resolution of a NWM may be driven by the fact that a higher resolution also means increased amount of data to download and to process per needed epoch of the NWM data.

2 The ray-tracing approach

This chapter gives a short introduction to the ray-tracing method for the application in geodetic VLBI. The calculation of the ray-traced slant delays for each VLBI observation consists of two parts.

The first part is the ray-tracing itself. Here the real signal path is reconstructed within an iterative process using the so-called outgoing elevation angle of the signal, which represents the elevation angle in the vacuum. For this task different approaches exist that in principle differ in complexity and therefore also in accuracy, but basically all of these approaches have in common that they need refractivity values in order to determine the signal path. These refractivity values can be derived from the meteorological data that are provided by the NWM.

In the second part the gained knowledge of the actual signal path is needed as the refractivity values along the reconstructed path are used to calculate the tropospheric slant delay of the observation.

3 Impact of the horizontal resolution of the NWM

On the one hand it is possible that the use of a horizontally higher resolved NWM may lead to improved accuracy of the ray-traced delays, but on the other hand it is certain that a horizontally higher resolved NWM leads to an increased demand for storage space and processing time. If a calculation of ray-traced delays for geodetic VLBI sessions that cover a broad time span is considered, many epochs of NWM data are needed. Thus, using a NWM with a high horizontal resolution leads to high amounts of data that need to be processed. Therefore the research on how the horizontal resolution of the NWM affects the ray-traced delay results should reveal a quantification of the need of a horizontally highly resolved NWM for ray-tracing.

3.1 Methodology of the research

In order to assess the effect of the horizontal resolution of the NWM on the ray-traced delays, we carry out two different main fields of investigation. The first part covers the assessment of the direct effects on the ray-traced delays if the same NWM, but with different horizontal resolutions, is used to calculate the delays. In the second part we apply these differently determined ray-traced delays to the VLBI analysis in order to see the effects on the results with respect to Baseline Length Repeatability (*BLR*) and Station Coordinate Repeatability (*SCR*).

3.2 Data for the research

As observational data input for the ray-tracing and the VLBI analysis we use the CONT11 campaign of the International VLBI Service for Geodesy and Astrometry (IVS), covering 15 days of continuous VLBI observations.

As meteorological data input for the ray-tracing we utilize the operational NWM from the European Centre for Medium-Range Weather Forecasts (ECMWF). This global NWM delivers the meteorological data via 25 pressure levels with a temporal resolution of 6 hours. For our research we use two different horizontal resolutions of the NWM: $0.125^\circ \times 0.125^\circ$ and $1^\circ \times 1^\circ$.

For the calculation of the ray-traced delays we utilize our program RADIATE, which is developed within project RADIATE VLBI (Ray-traced Delays in the Atmosphere for geodetic VLBI), funded by the Austrian Science Fund (FWF). Within the processing the vertical resolution of the NWM is increased by interpolation at discrete height levels. As ray-tracing method the piecewise-linear approach is used. In order to receive the delay for each observation at the exact observation time, a linear interpolation of the delays calculated at the two adjacent epochs of the NWM, that directly surround the observation time, is carried out. More detailed information on the ray-tracing program RADIATE can be found in Hofmeister and Böhm (2014).

Now, with the use of the program RADIATE ray-traced delays for the CONT11 observations of all participating stations are calculated twice. Once using the NWM(0.125°) with a horizontal resolution of $0.125^\circ \times 0.125^\circ$ and once using the NWM(1°) with a horizontal resolution of $1^\circ \times 1^\circ$. These two sets of ray-traced delays, which will be called RD(0.125°) and RD(1°) from now on, are used for the following comparisons.

3.3 Direct effect on the ray-traced delays

For assessing the impact of the different horizontal resolutions directly on the ray-traced delays, a comparison of the differences in the domain of the Slant Total Delay (*STD*) is carried out. Besides the comparison of the direct *STD* differences (ΔSTD), also the

ΔSTD_{mf} are compared, which denote the differences in the STD calculated from the mapping factors (mf). Equations (1) to (3) show the formalism of the calculations. ZTD refers to the Zenith Total Delay. The subscripts describe the ray-tracing solution, i.e. the horizontal resolution of the NWM used for its calculation. The calculation of the ΔSTD_{mf} using the mf together with the $ZTD_{RD(0.125^\circ)}$ as the reference ZTD leads to a kind of scaled result compared to the ΔSTD .

$$\Delta STD = STD_{RD(0.125^\circ)} - STD_{RD(1^\circ)} \quad (1)$$

$$\Delta STD_{mf} = STD_{RD(0.125^\circ)} - mf_{RD(1^\circ)} \cdot ZTD_{RD(0.125^\circ)} \quad (2)$$

with

$$mf_{RD(1^\circ)} = \frac{STD_{RD(1^\circ)}}{ZTD_{RD(1^\circ)}} \quad (3)$$

Figure 1 shows the ΔSTD and Figure 2 shows the ΔSTD_{mf} for the station KOKEE.

Concerning the results of ΔSTD for all CONT11 stations, the differences for elevation angles larger than 10° reach up to only a few cm for the majority of stations and remain mainly at a level of 1-2 cm. At elevation angles smaller than 10° the differences rise significantly and can even reach a few dm at 1° elevation as we have seen in our studies with simulated observations. The general size of the differences is mainly caused by the differences in the wet delay.

Looking at the domain of STD_{mf} , again for all CONT11 stations, the differences in general are, as expected, scaled in the sense of reduced compared to the ΔSTD . So, only very small differences of mostly below 1 cm are visible at elevation angles larger than 10° . At smaller elevation angles the differences start to rise and some outliers can be found. A few stations, but especially KOKEE (see Figure 2) and TSUKUB32, show a kind of special behaviour. At these stations the ΔSTD_{mf} are significantly increased at low elevations compared to the quite small and homogeneous differences at higher elevations.

In general, the influence of the horizontal resolution of the NWM directly on the ray-traced delay is increasing with decreasing elevation angle. Nevertheless, a really significant effect is only given at low elevations.

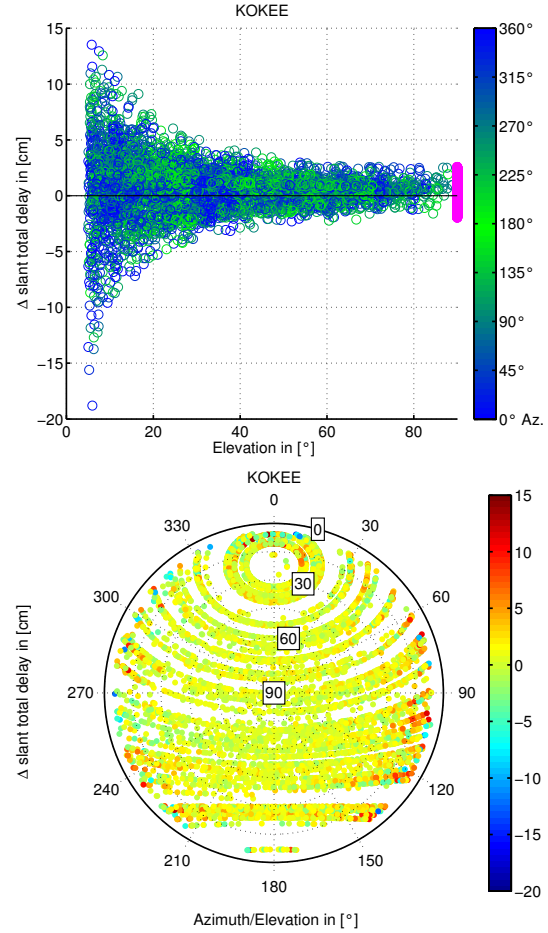


Fig. 1 ΔSTD for the station KOKEE. Upper plot: ΔSTD w.r.t. to the elevation angles, the respective azimuths are shown via colour-coding. Lower plot: skyplot of the observations with colour-coded ΔSTD . Please refer to the web version of the proceedings to see the plots in colour.

3.4 Effect on VLBI analysis results

In order to assess the influence of the horizontal resolution of the NWM on the VLBI results, the ray-traced delays $RD(0.125^\circ)$ and $RD(1^\circ)$ are applied to the VLBI analysis of CONT11. As parameters for the quantification of the impact on the VLBI results, the weighted BLR and the weighted SCR are used. The weights for the calculation of the BLR are the inverse formal baseline length errors. These are derived using the covariances of the baseline-forming stations. For the SCR the weights are calculated using the inverse formal coordinate errors. The VLBI analysis is carried out with the

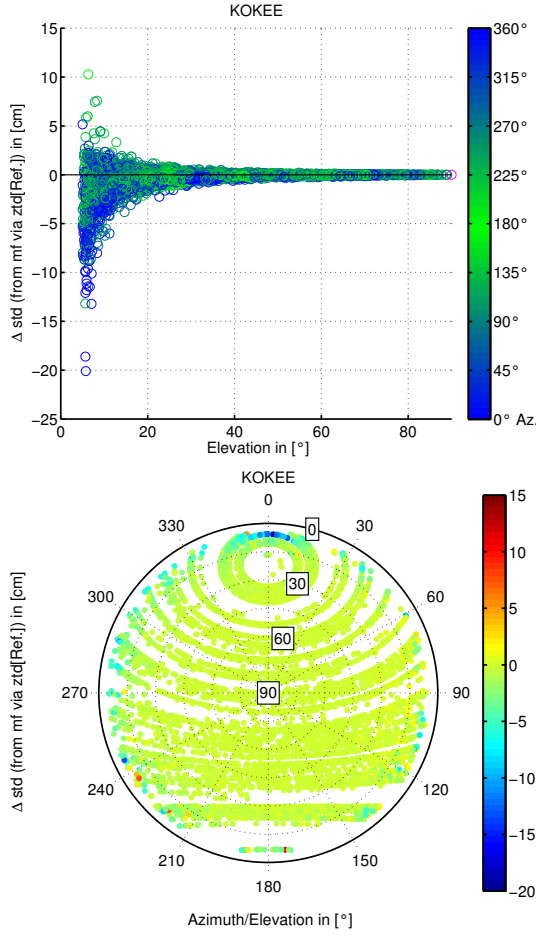


Fig. 2 ΔSTD_{mf} for the station KOKEE. Upper plot: ΔSTD_{mf} w.r.t. to the elevation angles, the respective azimuths are shown via colour-coding. Lower plot: skyplot of the observations with colour-coded ΔSTD_{mf} . Please refer to the web version of the proceedings to see the plots in colour.

software VieVS (Böhm et al., 2012) using two different parameterizations:

1. Ray-tracing only

- Ray-traced slant delays used as a priori input.
- No estimation of Zenith Wet Delays (ZWD) or tropospheric gradients.

2. Ray-tracing, est. ZWD 1h, est. gradients 6h

- Ray-traced slant delays used as a priori input.
- Estimation of ZWD every hour with a relative constraint of 1.5 cm after 1 hour.

- Estimation of tropospheric North- and East-gradients every 6 hours with a relative constraint of 0.05 cm after 6 hours for both.

In the analysis of CONT11 the stations WARK12M and ZELENCHK are not considered.

The following comparisons investigate the differences Δ in BLR and SCR resulting from the use of the ray-traced delays $RD(0.125^\circ)$ or $RD(1^\circ)$ in the VLBI analysis. Equations (4) and (5) show how the Δ are calculated. Each subscript describes which ray-tracing solution has been applied to the analysis.

$$\Delta BLR = BLR_{RD(0.125^\circ)} - BLR_{RD(1^\circ)} \quad (4)$$

$$\Delta SCR = SCR_{RD(0.125^\circ)} - SCR_{RD(1^\circ)} \quad (5)$$

The ΔBLR and ΔSCR derived from the analysis with parameterization 1 can be seen in Figure 3. The BLR differs on average only by -0.5 mm. No clear trend of an improvement can be derived in case the horizontally higher resolved NWM(0.125°) has been used for the delay calculation, as only 34 of the 66 baselines are improved. The baselines formed by the station KOKEE are influenced the most on average. The ΔSCR are at a very low mm-level. The stations KOKEE, TSUKUB32 and YEBES40M show increased Δ in the up-direction. This effect may come from their significantly increased ΔSTD_{mf} at low elevations, described in Section 3.3. Interestingly, this effect is inverse for the station TSUKUB32. The North-components seem to be improved by the usage of the horizontally higher resolved NWM(0.125°), but concerning the small amounts, this trend is not really significant.

Figure 4 shows the ΔBLR and ΔSCR derived from the analysis with parameterization 2. The BLR differs on average only by +0.2 mm. There is no clear trend for the impact of the horizontal resolution of the NWM derivable. For the most baselines the ΔBLR is in between ± 1 mm. The baselines for the station KOKEE are again influenced the most on average, but this time oppositely compared to the results of the first analysis parameterization. Also in the domain of the SCR no trend for the impact of the horizontal resolution of the NWM can be derived. Parameterization 2 reduces the Δ in the North- and East-direction to sub-mm-level. Only the Δ in the up-direction is again a bit increased at some stations. In general, the impact on the SCR is too small to be significant.

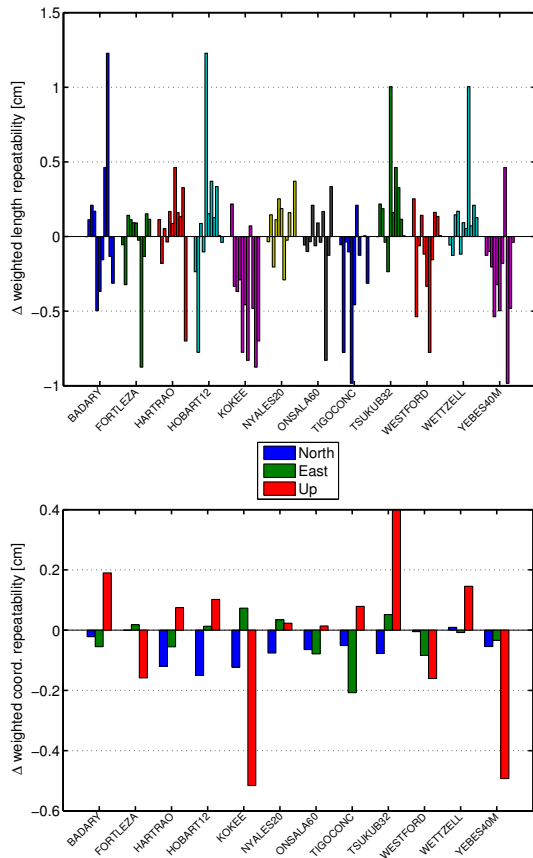


Fig. 3 Δ in analysis results from parameterization 1. Upper plot: Δ of weighted *BLR* for each station sorted by mean baseline length. Lower plot: Δ of weighted *SCR*. Negative Δ indicate that the horizontally higher resolved NWM(0.125°) would improve the solution. Please refer to the web version for coloured plots.

4 Conclusions

The impact of the horizontal resolution of the NWM directly on the ray-traced delays is increasing with decreasing elevation angle, but a really significant influence is only given at small elevation angles. If the ray-traced delays are applied to the VLBI analysis, there is only a quite small impact as seen with respect to *BLR* and *SCR* and no clear trend of an improvement can be derived in case of using a horizontally higher resolved NWM. Furthermore the size of the influence is depending on the parameterization of the VLBI analysis. If ZWD and tropospheric gradients are estimated in the analysis, the influence of the horizontal resolution of the NWM, as investigated here for resolutions of 0.125° x 0.125° and 1° x 1°, is negligible.

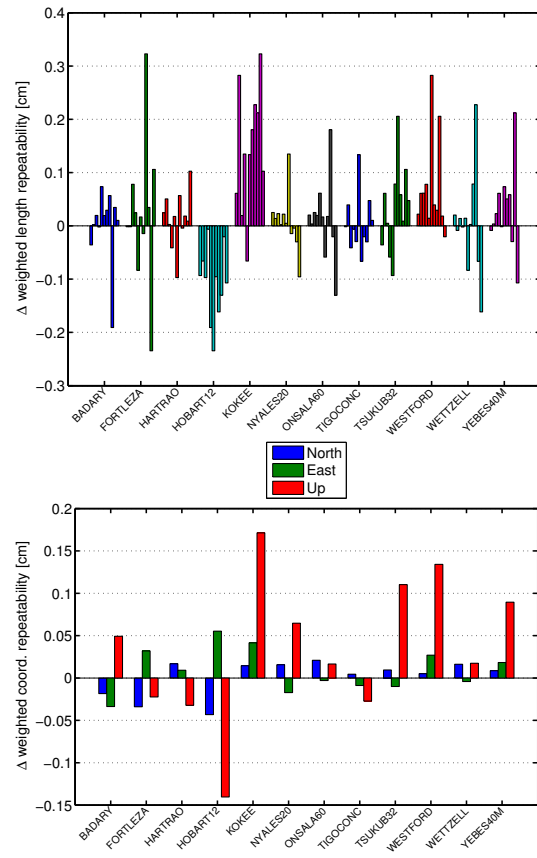


Fig. 4 Δ in analysis results from parameterization 2. Upper plot: Δ of weighted *BLR* for each station sorted by mean baseline length. Lower plot: Δ of weighted *SCR*. Negative Δ indicate that the horizontally higher resolved NWM(0.125°) would improve the solution. Please refer to the web version for coloured plots.

Acknowledgements The authors are very grateful to the Austrian Science Fund (FWF) for the financial support of the project RADIATE VLBI (P25320) and would like to thank the IVS for providing the observational data of CONT11.

References

- Hofmeister A, Böhm J (2014) Ray-traced Delays in the Atmosphere for Geodetic VLBI. In: D. Behrend, K.D. Bayer, K. Armstrong (eds.), *IVS 2014 General Meeting Proc.*, Science Press (Beijing), 283–287.
- Böhm J, Böhm S, Nilsson T, Pany A, Plank L, Spicakova H, Teke K, Schuh H (2012) The new Vienna VLBI Software VieVS. In: S. Kenyon, M. C. Pacino, U. Marti (eds.), *Proc. 2009 IAG Symposium*, IAG Symposia Series, 136, 1007–1011, doi: 10.1007/978-3-642-20338-1(_)126.

Augmenting the stochastic model in VLBI data analysis by correlations from atmospheric turbulence models

S. Halsig, T. Artz, A. Iddink, A. Nothnagel

Abstract Dynamic processes in the neutral atmosphere contribute considerably to the error budget of Very Long Baseline Interferometry (VLBI). In particular, micro-scale fluctuations in refractivity lead to elevation-dependent uncertainties and induce physical correlations between the observations. However, up to now such physical correlations are typically disregarded in the stochastic model of geodetic VLBI data analysis. Contrary, only the uncertainties from the VLBI correlation process are used. Thus, the formal errors of, e.g., station coordinates or Earth orientation parameters, are too optimistic. In this study, the standard stochastic model is augmented by correlations induced by atmospheric turbulence. Thus, dependencies of the observations in time and space are introduced. For this purpose, turbulence-based models following the principles of the widely accepted Kolmogorov turbulence theory are used to represent turbulence behaviour. Such a turbulence model is applied to the continuous VLBI campaign 2002 in order to validate the new stochastic model and to investigate the performance compared to other stochastic model refinement strategies.

Keywords VLBI, Stochastic model, Atmosphere, Turbulence

1 Introduction

Temporal and spatial refractivity variations in the neutral atmosphere represent the limiting factor in fur-

S. Halsig, T. Artz, A. Iddink, A. Nothnagel
Institute of Geodesy and Geoinformation, University of Bonn,
Nußallee 17, 53115 Bonn, Germany

ther improving the quality of space-geodetic observations for monitoring the Earth's rotation and determining antenna positions. However, variability issues have been widely ignored in the traditional data analysis of Very Long Baseline Interferometry (VLBI) as well as other space-geodetic techniques, e.g., Global Navigation Satellite Systems (GNSS). In fact, only spatial and long-term effects are taken into account.

In the routine data analysis of the International VLBI Service for Geodesy and Astrometry (IVS Schuh and Behrend, 2012), the total excess path length $\Delta L_t(\epsilon)$ is considered by using an adequate model (e.g., the modified Saastamoinen model, see Davis et al., 1985) for the hydrostatic component $\Delta L_h(\epsilon)$, and additionally estimating model correction parameters in the VLBI adjustment process for the wet component $\Delta L_w(\epsilon)$. Both components are modeled or estimated in zenith direction and are transformed from zenith to an arbitrary elevation angle ϵ using mapping functions ($m_h(\epsilon)$ and $m_w(\epsilon)$, respectively). Additionally, gradients in North-South (G_{ns}) and East-West (G_{ew}) direction are introduced as a further model component with respect to the azimuth α to incorporate azimuthal asymmetries (MacMillan and Ma, 1997). This leads to

$$\Delta L_t(\epsilon) = m_f_h(\epsilon)\Delta L_h(\epsilon) + m_f_w(\epsilon)\Delta L_w(\epsilon) \quad (1)$$

$$+ m_f_g(\epsilon)[G_{ns} \cos(\alpha) + G_{ew} \sin(\epsilon)]. \quad (2)$$

However, in addition to such purely lateral considerations, also small-scale refractivity fluctuations, both in space and time, due to turbulent eddies in the neutral atmosphere affect VLBI observations and lead to spatial and temporal correlations between the observations. In the routine data analysis of the IVS, correlations between observations are not taken into account and the stochastic model of the observations is limited to the

uncertainties of the VLBI correlation process and an additional noise term (cf. Sec. 6). This automatically leads to incorrect formal errors of the derived target parameters, which are too optimistic.

To overcome this issue, an external turbulence model is customized for VLBI in this study to deal with small-scale refractivity fluctuations. This is then incorporated in the stochastic model as an additional variance-covariance matrix for the observations.

In the last decades, a few approaches have been proposed using atmospheric turbulence models in the data analysis of either VLBI or GNSS observations. Treuhaf and Lanyi (1987) first introduced a turbulence model based on the widely known Kolmogorov turbulence theory (Kolmogorov, 1941) and the frozen-flow hypothesis of Taylor (1938). Further applications have been made using this model for real data analyses (e.g., Romero-Wolf et al., 2012) or simulation studies (e.g., Nilsson and Haas, 2010). Moreover, Schön and Brunner (2008) developed the SIGMA-C model, a turbulence model based on a 3D spectrum (e.g., the von Karman spectrum) for GPS carrier phase observations, which was modified for VLBI observations by Halsig et al. (2014). The SIGMA-C model was extended by Kermarrec and Schön (2014) in order to overcome the issue, that most other turbulence models depend on a double integral which has to be solved numerically leading to an enormous computational effort. This becomes important in case of a routine use of correlations due to atmospheric dynamics in the stochastic model. Further, except for the SIGMA-C model, the concept of Kermarrec and Schön (2014) is the only application which allows to omit the condition of assuming the atmosphere to be a homogeneous and isotropic random medium, which is hardly true in reality.

Besides direct turbulence modeling, there have been other applications to deal with the underestimation of the formal errors in VLBI data analysis. For instance, Gipson et al. (2008) added additional station-dependent noise to the data analysis leading to an increase of the standard deviations and introducing correlations between observations. For this purpose, a distinction is made between a constant term of station-dependent noise to deal with clock variations and elevation-dependent components to deal with the atmospheric behaviour.

In contrast to this, we embark to introduce more realistic correlations which are also interpretable in a physical sense. To be independent of any assumptions

concerning inhomogeneity and anisotropy, we make use of a modified and VLBI-adapted version of the Kermarrec and Schön (2014) turbulence model.

2 Turbulence Description

Turbulent motions are generally considered as a medium randomly varying in space and time, and thus, can be best described stochastically following the widely spread turbulence theory of Kolmogorov (1941). Usually, the stochastic properties are expressed by structure functions or a power law expression yielding spatial covariance information. Temporal correlations mainly depend on the wind field and are considered by the frozen flow hypothesis of Taylor (1938). Assuming the entirety of turbulent air masses to be frozen and transported by the wind field \mathbf{v} , the resulting temporal covariance is equivalent to the spatial correlation with a separation distance $\mathbf{d} = \mathbf{v}\tau$. Following Wheelon (2004) and based on the so-called von Karman spectrum for the refractivity fluctuations and the Wiener-Khinchine-theorem, Kermarrec and Schön (2014) proposed a power spectral density representation for the temporal covariance. Further, they found, that this covariance is a so-called Matérn covariance function, expressed as

$$C(t, t + \tau) = 0.7772 \frac{k^2 H C_n^2 c \kappa_0^{-\frac{3}{5}}}{\sin(\epsilon_i(t)) \sin(\epsilon_j(t + \tau))} \quad (3)$$

$$\times \left(\frac{\kappa_0 v \Delta \tau}{a} \right)^\nu K_\nu \left(\frac{\kappa_0 v \Delta \tau}{a} \right), \quad (4)$$

with a smoothness parameter $\nu = \frac{5}{6}$ and a Matérn correlation time $\mathcal{T}_M = \frac{1}{\alpha_M}$, where $\alpha_M = \frac{\kappa_0 v}{a}$. K_ν is the modified Bessel function of second kind (Abramowitz and Segun, 1972). The so-called structure constant is denoted as C_n^2 and characterizes the strength of the turbulence (see, e.g., Nilsson and Haas, 2010). H is the effective tropospheric height, and a, b, c are horizontal and vertical stretching parameters describing the different elongations of the turbulent eddies. The wave number for the outer scale length L_0 is given by $\kappa_0 = \frac{2\pi}{L_0}$. Further, ϵ describes the elevation angle of the corresponding observation and k is the electromagnetic wave number. Note that Eq. (4) does implicitly depend on the separation distance $d_{\tau, H}$ at troposphere height H and time τ as well as the wind velocity v . Similarly, we

receive an expression for the temporal variances,

$$C(t, t) = 0.782 \frac{k^2 H C_n^2 c \kappa_0^{-\frac{3}{5}}}{\sin^2(\epsilon_i(t))}. \quad (5)$$

For more details, see Kermarrec and Schön (2014), Schön and Brunner (2008) or Wheelon (2004).

3 Data Analysis Setup

To validate the new stochastic model for the VLBI observations, the turbulence model is applied to the continuous VLBI campaign 2002 provided by the IVS. The geodetic data analysis is performed following the conventions of the International Earth Rotation and Reference Systems Service (IERS, Petit and Luzum, 2010). The modeling and estimation process settings used in this study are described in Artz et al. (2010).

4 Results

Traditionally, the stochastic model of VLBI observations consists of the uncertainties of the correlation process and an additional noise term. The easiest approach is to add the same constant noise term for all stations and sessions, referred to as reference solution in the following. Two further solution types have been processed following the model of Gipson et al. (2008), who added station-dependent noise to the data analysis, which then leads to an increase of the standard deviations and induces correlations between the observations. While the first of these solutions only consists of the variances and, therefore, has a diagonal structure, the second solution considers the full variance-covariance information including correlations between the observations. For both solutions, we added a constant and an elevation-dependent noise term to the standard deviations, whose order of magnitude is related to the analyses in Gipson et al. (2008). Finally, a solution is set up including the fully populated variance-covariance matrix due to turbulent fluctuations, in which no further additional noise is used in the data analysis. However, concerning the turbulence description, we used the same turbulence parametrization for all stations, i.e., a constant structure constant $C_n^2 \approx 1$, effective tropospheric height $H \approx 2km$ and a

Table 1 Solution types including a reference solution and different strategies to refine the stochastic model of VLBI observations. The mean χ^2 and the WRMS values over the CONT02 period are illustrated for all solution setups.

Solution type	χ^2 [-]	WRMS [ps]
reference solution (constant additional noise)	2.50	25.7
additional noise, diagonal (Gipson et al., 2008)	1.13	28.4
additional noise, correlated (Gipson et al., 2008)	1.67	29.7
turbulence model (Kermarrec and Schön, 2014)	0.87	24.4

constant horizontal wind velocity of $v = 8 \frac{m}{s^2}$ is assumed.

Table 1 gives an overview over the different solution setups and shows the weighted root mean squared (WRMS) post-fit residuals of the delay observables as well as the χ^2 values over the CONT02 period. Both are statistical criteria for the validation of a VLBI adjustment.

First, the χ^2 value indicates whether the global test for an adjustment is fulfilled (which would be the case if $\chi^2 \approx 1$) or not, and is defined as the quotient between the a priori σ_0^2 and a posteriori variance factor $\tilde{\sigma}$,

$$\chi^2 = \frac{\tilde{\sigma}^2}{\sigma_0^2}. \quad (6)$$

Given the Jacobian matrix \mathbf{A} , the observed-minus-computed vector \mathbf{b} with the corresponding variance-covariance matrix of observations Σ_{bb} , the vector of parameters \mathbf{x} and the degrees of freedom f , the a posteriori variance factor can be written as

$$\tilde{\sigma}^2 = \frac{\langle \mathbf{A}^T \mathbf{x} - \mathbf{b} \rangle_{\Sigma_{bb}^{-1}}}{f}. \quad (7)$$

Figure 1 shows the χ^2 values for all solution types. It is obvious, that the solutions, in which a station-dependent reweighting is used, lead to an χ^2 value closer to one and, therefore, to a more realistic adjustment. In particular, the application of the turbulence model leads to a χ^2 of approximately 0.9, which is only slightly too low. This can be explained by the fact, that the turbulence parametrization is not quite as realistic, which has to be investigated in the near future. Surprisingly, the χ^2 value is increasing for the Gipson et al.

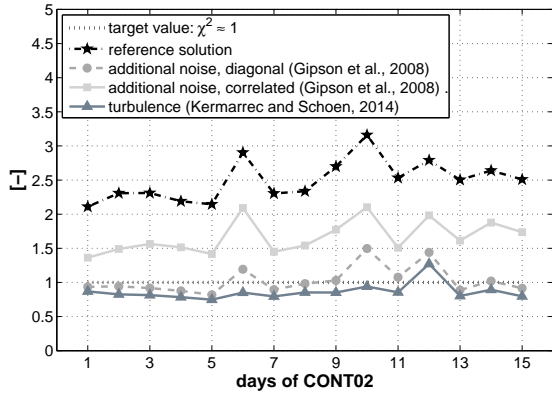


Fig. 1 χ^2 values for the 15-day CONT02 period and different solution setups including a reference solution (black stars), two approaches following Gipson et al. (2008) with and without correlations between observations (dark gray circles and light gray squares, respectively), and a turbulence-based solution (dark slate gray triangles).

(2008) approach using correlations between the observations compared to the same model without correlations. The second statistical criterion, the WRMS scatter per solution is based on the post-fit residuals and is computed by

$$WRMS = \sqrt{\frac{\langle \mathbf{A}^T \mathbf{x} - \mathbf{b} \rangle_{\Sigma_{bb}^{-1}}}{tr(\Sigma_{bb})}}. \quad (8)$$

Considering the WRMS mean values (cf. Tab. 1), there are significant differences, particularly between the reference solution and the turbulence-based approach, which is improved by about 9 ps in quadrature.

Furthermore, the accuracy of baseline length determinations is measured in terms of their repeatabilities (Fig. 2). First, it is obvious that in comparison to the reference solution the baseline length repeatabilities improve for all solutions, in which station-dependent additional noise is used in any form. The different turbulence models as well as the two approaches according to Gipson et al. (2008) are approximately in the same range. This could be due to the short time period covered by CONT02 and has to be investigated in future using a more sufficient time interval over several years. However, this is not part of this study.

Regarding Fig. 2, the influence of a modified stochastic model of the observations is dramatically. The baseline length repeatabilities of the solution with additional correlations due to turbulent dynamics

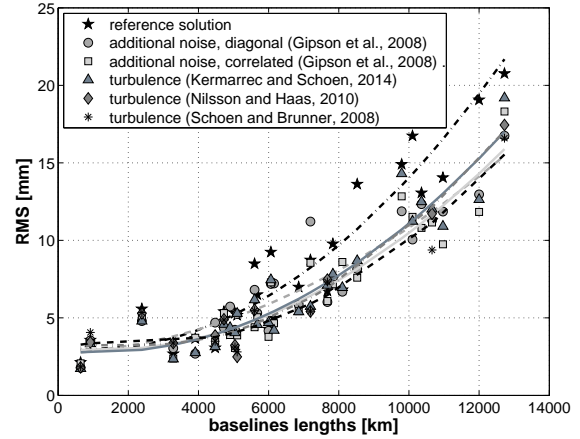


Fig. 2 Baseline length repeatabilities for the 15-day CONT02 period and different solution setups including a reference solution (black stars), two approaches following Gipson et al. (2008) with and without correlations between observations (dark gray circles and light gray squares, respectively), and three turbulence-based solutions (dark slate gray triangles for the Kerमारrec and Schön (2014) adapted model, gray diamonds for the Nilsson and Haas (2010) approach and black asterisks for the Schön and Brunner (2008) model).

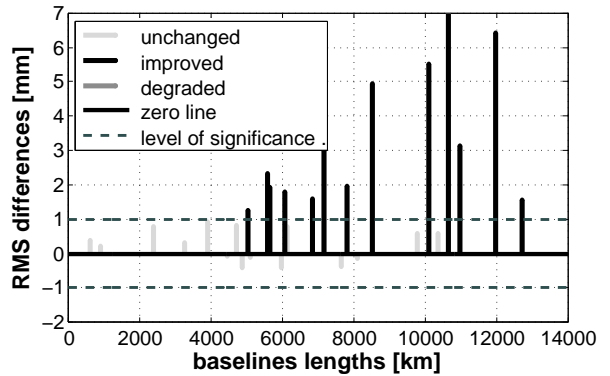


Fig. 3 RMS differences between the reference solution (black stars in Fig. 2) and the turbulence-based approach (dark slate gray triangles in Fig. 2). Black bars show an improvement, dark gray bars denote a degradation and light gray bars indicate an unchanged situation.

decreases sharply compared to the reference solution, in which only additional noise is added in the data analysis. Fig. fig:diff shows the difference in RMS for the same situation. While black bars indicate an improvement, light gray bars represent an unchanged situation and dark gray bars denote a degradation. In this comparison, about 46 % of the baselines are

improved by at least 1 mm (level of significance), about 54 % of the baseline remain unchanged and hardly any baseline gets worse by at least 1 mm.

Of course, it would be possible to simply increase the magnitude of these additional noise term in order to decrease the χ^2 value to approximately one (cf. Fig. 1). However, this would not be valid for all databases. Thus, that the turbulence-based approach leads to a more realistic stochastic model of the observations without reweighting the observations in a traditional sense and without a loss of physical interpretability.

5 Conclusions

The stochastic model of VLBI observations was augmented by correlations due to refractivity fluctuations induced by atmospheric turbulence. For comparison reasons, a reference solution was defined, in which a constant noise term is added to the standard deviations. Further, two solutions following the Gipson et al. (2008) approach, i.e., introducing station-dependent noise to the observations, have been set up for the validation of the turbulence-based modified version of the Kermarrec and Schön (2014) model. It becomes obvious that a modified stochastic model is really important for the VLBI data analysis, since the χ^2 values converge to one for all solutions with station-dependent noise in any form. Further, the turbulence-based solution allows for a physical interpretability without using an arbitrary additional noise term. Whereas the WRMS post-fit residuals remain nearly unchanged, the baseline length repeatabilities decrease sharply (for $\approx 45\%$ of the baselines for CONT02) when introducing turbulence-based correlations.

Further work needs to be done concerning the turbulence parametrization and other errors sources in addition to the effects of the neutral atmosphere. Here, common values for the state of the troposphere have been used for all stations. This has to be improved by in-situ measurements or sophisticated models to represent the actual correlations.

Acknowledgements

S. Halsig thanks the German Research Foundation (Deutsche Forschungsgemeinschaft, DFG) for its financial support (Project NO 318/10-1).

References

- Abramowitz M, Segun I A (1972) Handbook of mathematical functions. *Dover Publications*, New York.
- Artz T, Böckmann S, Nothnagel A, Steigenberger P (2010) Subdiurnal variations in the Earth's rotation from continuous Very Long Baseline Interferometry campaigns. *J Geophys Res*, 115, B05404, doi: 10.1029/2009JB006834.
- Davis J L, Herring T A, Shapiro I I, Rogers A E E, Elgered G (1985) Geodesy by radio interferometry: Effects of atmospheric modeling errors on estimates of baseline length. *Radio Sci*, 20(6), 1593–1607.
- Gipson J, MacMillan D, Petrov L (2008) Improved Estimation in VLBI through Better Modeling and Analysis. In: A. Finkelstein, D. Behrend (eds.), *IVS 2008 General Meeting Proc.*, 157–162.
- Halsig S, Artz T, Leek J, Nothnagel A (2014) VLBI analyses using covariance information from turbulence models. In: D. Behrend, K. D. Baver, K. L. Armstrong (eds.), *IVS 2014 General Meeting Proc.*, Science Press (Beijing), 272–276.
- Kermarrec G, Schön S (2014) On the Matern covariance family: a proposal for modeling temporal correlations based on turbulence theory. *J Geod*, 88, 1061–1079, doi: 10.1007/s00190-014-0743-7.
- Kolmogorov A N (1941) The local structure of turbulence in incompressible viscous fluid for very large Reynolds numbers. *Dokl Akad Nauk SSSR*, 30(4), 301–305.
- MacMillan D S, Ma C (1997) Atmospheric gradients and the VLBI terrestrial and celestial reference frames. *Geophys Res Lett*, 24(4), 453–456.
- Nilsson T, Haas R (2010) Impact of atmospheric turbulence on geodetic very long baseline interferometry. *J Geophys Res*, 115, B03407, doi: 10.1029/2009JB006579.
- Petit G, Luzum B (2010) (eds.) IERS Conventions 2010. *IERS Technical Note*, 35, ISSN: 1019-4568.
- Romero-Wolf A, Jacobs C S, Ratcliff J T (2012) Effects of Tropospheric Spatio-temporal Correlated Noise on the Analysis of Space Geodetic Data. In: D. Behrend, K. D. Baver (eds.), *IVS 2012 General Meeting Proc.*, NASA/CP-2012-217504, 231–235.
- Schön S, Brunner F K (2008) Atmospheric turbulence theory applied to GPS carrier-phase data. *J Geod*, 82, 47–57, doi: 10.1007/s00190-007-0156-y.
- Schuh H, Behrend D (2012) VLBI: A fascinating technique for geodesy and astrometry. *J Geodyn*, 61, 68–80, doi: 10.1016/j.jog.2012.07.007.
- Taylor G I (1938) The spectrum of turbulence. *Proc R Soc London*, Ser. A., 164(919), 476–490.
- Treuhaft R N, Lanyi G E (1987) The effect of the dynamic wet troposphere on radio interferometric measurements. *Radio Sci*, 22(2), 251–265.
- Wheelon A D (2004) Electromagnetic Scintillation - I. Geometrical Optics. *Cambridge University Press*, Cambridge.

Short-term station coordinate variations from Kalman filtering VLBI data

B. Soja, M. Karbon, T. Nilsson, K. Balidakis, S. Glaser, R. Heinkelmann, H. Schuh

Abstract Station coordinates are one of the most important parameters in geodetic VLBI analysis as they are necessary for global terrestrial reference system realization. Several models are essential to account for station coordinate variations on shorter time scales, e.g. solid Earth tides, ocean and atmospheric pressure loading. Here, we investigate whether Kalman filtering can be used to recover unmodeled effects on station coordinates. Only for solid Earth tides, however, a significant part of the signal shows up in the Kalman filter time series. Tidal ocean loading is barely detectable, and atmospheric pressure loading effects are too small to be recovered by the Kalman filter.

Keywords Kalman filter, station coordinates, loading, CONT14

1 Introduction

In the analysis of space geodetic techniques like VLBI, the estimation of station coordinates is an important task, for instance serving as input for terrestrial reference frames. Station coordinates are affected by secular changes, e.g. due to continental plate motion, seasonal signals, and effects on shorter time scales, e.g. few hours to several days. The latter include coordinate variations due to solid Earth tides, tidal and non-tidal loading effects, pole tides, and thermal expansion (IERS Conventions, 2010).

By using a Kalman filter for VLBI analysis, it is possible to model station coordinates as stochastic processes. In this study, we assess the extent to which the Kalman filter is capable of capturing unaccounted station position variations. Previous investigations in Nilsson et al. (2015) focused on solid Earth tides, and found that the Kalman filter is able to recover a significant part of the signal if not corrected for. In this study, we extend

Benedikt Soja, Maria Karbon, Tobias Nilsson, Robert Heinkelmann, Harald Schuh
GFZ German Research Centre for Geosciences, Telegrafenberg,
D-14473 Potsdam, Germany
Kyriakos Balidakis, Susanne Glaser, Harald Schuh
Technische Universität Berlin, Straße des 17. Juni, 135,
D-10623 Berlin, Germany

these investigations, also including tidal ocean loading, as well as tidal and non-tidal atmospheric pressure loading. Results for solid Earth tides are provided as well, providing more details and using slightly different analysis options compared to Nilsson et al. (2015).

2 Data and Methodology

We used the VLBI data collected during the CONT14 campaign, as observed, correlated and provided by the IVS. The data set comprises continuous observations by 17 VLBI stations over 15 days. Using the Kalman filter and smoother (which we from here on simply designate as *Kalman filter*) module VIE.KAL of the software VieVS@GFZ, a fork from the Vienna VLBI Software VieVS (Böhm et al., 2012), a reference solution was derived abiding by the IERS Conventions (2010). All unknown parameters (station and radio source coordinates, tropospheric delays and gradients, clock offsets, and Earth orientation parameters) were modeled as random walk processes. All state parameters were updated for every observational epoch, i.e. every few minutes. More details about the parametrization can be found in Soja et al. (2015), although no station-dependent noise for zenith wet delays was used. The station coordinate process noise was set to $\Phi = 0.1 \text{ cm}^2/\text{day}$, so that the Kalman filter can follow small coordinate variations due to unmodeled effects or due to potential errors in the geophysical models. Following the IERS Conventions (2010), non-tidal ocean or continental water storage loading deformations were not modeled and were therefore absorbed by the process noise, but we did apply non-tidal atmospheric pressure loading corrections as it is usually done in VLBI analysis (Wijaya et al., 2013).

Additional solutions were computed without correcting for a certain effect at a time, e.g. solid Earth tides, for selected stations. Compared to the models used in the reference solution, every solution had a certain model switched off. In order to guarantee a stable datum definition, the ten VLBI stations included in the ITRF2008 (Altamimi et al., 2011) were used for the no-net-translation and -rotation (NNT+NNR) conditions and were treated the same way as in the reference solution. The particular model (e.g. solid Earth tides) was only switched off for non-

datum stations. Furthermore, to examine a specific station, e.g. Fortaleza or Badary, it was also excluded from the datum and could therefore be used for the investigations without tight constraints. For the stations with neglected models, the process noise for the station coordinates was strongly increased compared to the datum stations to values between 10 and 1000 cm^2/day .

To test, to what extent the Kalman filtered time series can recover unmodeled station coordinate variations, the coordinate difference between the solution without modeling a certain effect $X_{unmodeled}$ and the reference solution X_{ref} was compared to the model itself X_{model} :

$$\Delta = X_{unmodeled} - X_{ref} - X_{model} \quad (1)$$

The uncertainty of the quantity Δ was computed by propagating the uncertainties of the coordinates from the Kalman filter solutions. The geophysical models were assumed to be perfectly known as an assessment of their uncertainty is beyond the intended scope of this study. By subtracting the reference solution, the offsets to the a priori coordinates, which can reach several decimeters for the non-datum stations, and in theory all other sub-diurnal effects were eliminated. However, due to correlations with other parameters, the latter cannot be taken as granted.

3 Solid Earth tides

In the case of solid Earth tides, the signal amounts to a few decimeters at the investigated stations. Figure 1 depicts the time series of the quantities in Eq. 1 for station Fortaleza. The Kalman filter follows the model reasonably well and the difference is smaller than the initial signal for all three components. Table 1 provides the numerical values for station Yebes (best performance in this test), Hartebeesthoek (worst), and averaged over all non-datum stations including Fortaleza. The average difference Δ is usually at the millimeter level, but can reach 1 cm for some stations. The WRMS of Δ is largest for the height component, which also exhibits the largest tidal signal. (In this study, (W)RMS values have to be interpreted as a measure of signal power and not as a measure of error or uncertainty.) Bringing the WRMS in relation to the RMS of the model time series, it becomes evident that a large portion of the signal can be recovered. For the solution using process noise $\Phi = 100 \text{ cm}^2/\text{day}$, this recovery on average amounts to about 80 % for the vertical component and 70 % for the horizontal components. While the 300 cm^2/day noise has better recovery for the radial component, the horizontal coordinates deteriorate marginally. The worst performance is given by the 1000 cm^2/day solution with a recovery of the horizontal signals of only about 60 %. The vertical component is not that much affected, with a difference of only about 5 % compared to the other two solutions.

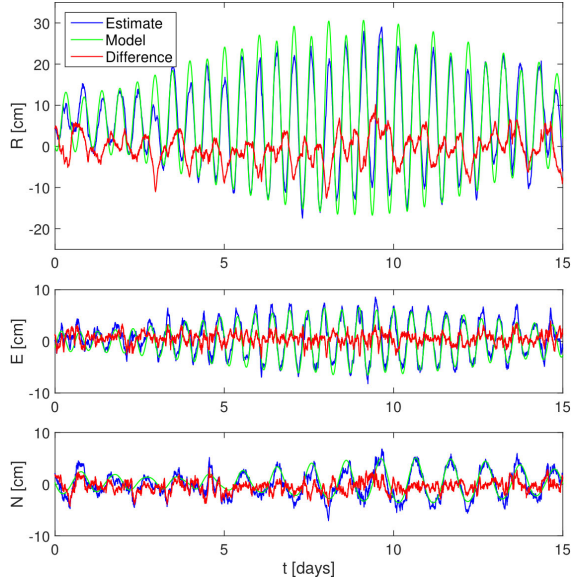


Fig. 1 For station Fortaleza, the terms $X_{unmodeled} - X_{ref}$ (estimate), X_{model} (model), and Δ (difference) are plotted for solid Earth tides. In the Kalman filter, a station coordinate process noise of 100 cm^2/day was used.

4 Ocean and atmospheric pressure loading

In the case of tidal ocean loading, only a solution with station coordinate process noise of 30 cm^2/day was tested. The Kalman filter estimates were compared to the FES2004 model, which is based on the assimilation of TOPEX/POSEIDON altimetry data into a hydrodynamic tide model (Lyard et al., 2006). Again, the non-datum stations including Fortaleza (see Fig. 2) were used for the investigations. Numerical values are tabulated in Table 2. The amplitude of the effects is much smaller than in the case of solid Earth tides (i.e., a few cm), and for the horizontal components, no loading signals can be recovered. Even for the vertical component, only for two stations (Warkworth and Fortaleza, see Table 2), the WRMS of the difference between Kalman filter and model time series is smaller than the RMS of the model time series (28 % and 17 % recovered, respectively). As can be deduced from Fig. 1, the Kalman filter is able to capture the phase of the signal reasonably well, while the amplitudes are off in several occasions, which is also the case for the other stations.

In the case of tidal and non-tidal atmospheric pressure loading, the effects are even smaller, usually at the millimeter level for vertical and sub-millimeter level for horizontal components. A station coordinate process noise of 10 cm^2/day and the models provided by NASA GSFC (Petrov and Boy, 2004) were used in both cases. Figures 3 and 4 show the Kalman filter time series for stations Fortaleza and Badary together with tidal and non-tidal atmospheric pressure loading models, respectively. Badary was chosen here because of its relatively large non-tidal atmospheric pressure loading signals, due to the high seasonal variability of

Table 1 Recovery of solid Earth tidal signals. The weighted mean and weighted RMS of the difference Δ are given for two selected stations and averaged over all non-datum stations (including Fortaleza). Additionally, the RMS of the model time series is depicted. All values are given in units of cm.

Station/Solution	Radial	East	North	Radial	East	North	Radial	East	North
YEBES40M	WMEAN(Δ)			WRMS(Δ)			RMS(X_{model})		
$\Phi = 100 \text{ cm}^2/\text{day}$	-0.01	-0.01	0.09	1.79	0.47	0.41			
$\Phi = 300 \text{ cm}^2/\text{day}$	-0.06	-0.02	-0.18	1.81	0.59	0.70	9.87	2.92	3.16
$\Phi = 1000 \text{ cm}^2/\text{day}$	-0.13	-0.03	-0.35	2.36	0.74	0.54			
HART15M	WMEAN(Δ)			WRMS(Δ)			RMS(X_{model})		
$\Phi = 100 \text{ cm}^2/\text{day}$	-0.10	0.03	-0.07	3.29	1.02	1.17			
$\Phi = 300 \text{ cm}^2/\text{day}$	-0.13	-0.83	-0.06	3.06	1.47	1.26	11.36	3.12	2.82
$\Phi = 1000 \text{ cm}^2/\text{day}$	-0.14	1.33	-0.03	3.59	1.89	1.45			
Average	WMEAN(Δ)			WRMS(Δ)			RMS(X_{model})		
$\Phi = 100 \text{ cm}^2/\text{day}$	0.08	0.03	0.01	2.46	0.83	0.89			
$\Phi = 300 \text{ cm}^2/\text{day}$	-0.09	-0.06	-0.05	2.19	0.97	1.02	11.13	3.07	2.87
$\Phi = 1000 \text{ cm}^2/\text{day}$	0.51	0.19	-0.07	3.05	1.20	1.13			

Table 2 Recovery of loading signals. The same information as in Table 1 is given, here for tidal ocean and atmospheric pressure loading. All values are given in units of cm.

Station/Model	Radial	East	North	Radial	East	North	Radial	East	North
Tidal ocean loading	WMEAN(Δ)			WRMS(Δ)			RMS(X_{model})		
WARK12M	-0.04	-0.04	0.18	1.32	0.55	0.63	1.83	0.62	0.44
FORTLEZA	-0.39	0.54	-0.39	2.28	0.96	0.94	2.75	0.37	0.43
Average	-0.16	0.07	-0.08	1.52	0.61	0.65	1.29	0.31	0.24
Tidal atmospheric pressure loading	WMEAN(Δ)			WRMS(Δ)			RMS(X_{model})		
FORTLEZA	-0.36	0.54	-0.41	1.47	0.78	0.75	0.11	0.03	0.01
Average	0.01	0.08	-0.07	1.01	0.48	0.51	0.08	0.03	0.01
Non-tidal atmosphere loading	WMEAN(Δ)			WRMS(Δ)			RMS(X_{model})		
BADARY	0.31	-0.46	0.19	1.15	0.61	0.50	0.31	0.06	0.07
Average	0.10	-0.05	0.00	0.97	0.46	0.48	0.16	0.06	0.08

atmospheric pressure and the large distance to oceans. It was, like Fortaleza for the other models, excluded from the datum. As evident in Table 2, the model amplitudes are too small for any recovery. In the case of tidal atmospheric pressure loading, the WRMS of the difference Δ in radial direction is on average 10 times larger than the RMS of the model time series. For non-tidal atmospheric pressure loading the factor of this relation is about 5, and much larger for the horizontal components.

5 Conclusions

In this study, we investigated whether short-term station coordinate variations that are not corrected for can be recovered by using a Kalman filter with appropriately large process noise for station coordinates. In the case of solid Earth tides, up to 80 % of the vertical and 70 % of the horizontal coordinate changes are found in the Kalman filter time series. For tidal ocean loading, only signals at two stations were recovered. While the time series of the estimates and model agreed well in terms of phase, the amplitudes showed large deviations. The effects due to tidal and non-tidal atmospheric pressure loading were too small to be recovered.

The main reason for the inability of the Kalman filter to estimate coordinate time series sensitive to small loading displacements is that once the station coordinate process noise is increased, clock offsets and tropospheric parameters may leak into the station coordinate time series. Even for CONT14, with its geometrically strong network and large number of observations (in terms of VLBI standards), these correlations are contaminating the station position estimates to a large extent. By external calibration of the tropospheric parameters, the correlations could possibly be reduced. Furthermore, the assumption of a random walk process is certainly not ideal for pronounced diurnal and semi-diurnal signals. In such cases, a stochastic oscillator (e.g., Chin et al., 2009; Wu et al., 2015), would be more appropriate.

It has to be emphasized that by no means does this study want to discourage the use of the models discussed in favor of simply estimating highly resolved and loosely constrained station coordinate time series in the Kalman filter. The aim is to find the boundaries of what signals are possibly detectable in the Kalman filter. For general VLBI analysis using Kalman filtering, the best option would be to apply all models discussed here at the observational level and allow for small variations due to un- or mismodeled effects in the estimated station coordinate time series (as it is done in the reference solution of this study).

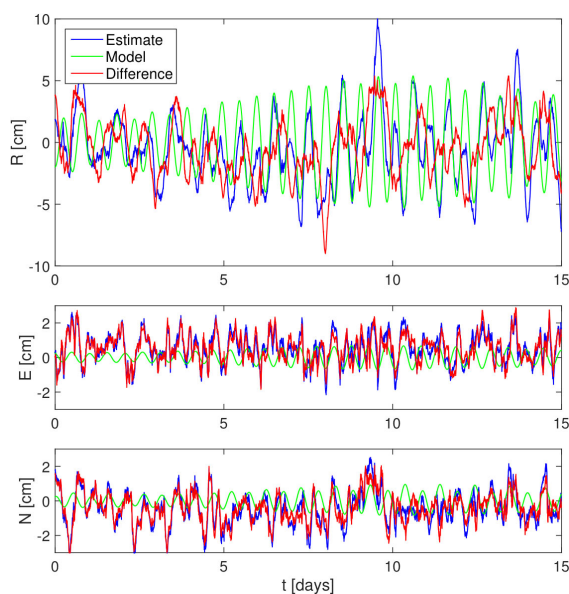


Fig. 2 For station Fortaleza, the same quantities as in Fig. 1 are shown, although for tidal ocean loading.

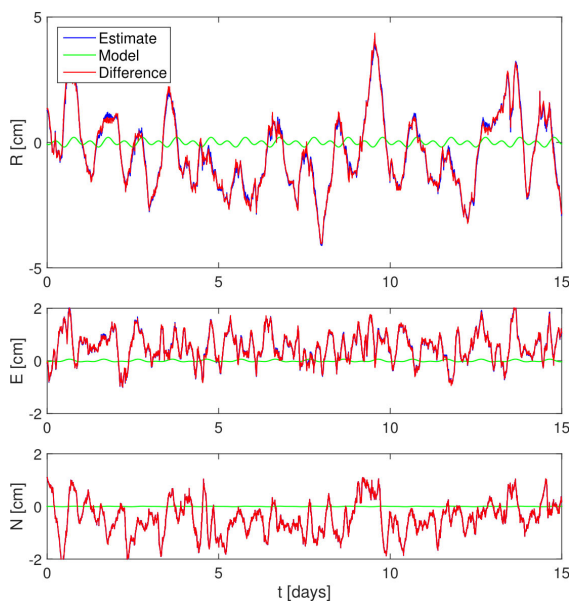


Fig. 3 For station Fortaleza, the same quantities as in Fig. 1 are shown, although for tidal atmospheric pressure loading.

References

Altamimi Z, Collilieux X, Métivier L (2011) ITRF2008: an improved solution of the international terrestrial reference frame. *J Geod*, 85(8), 457–473, doi: 10.1007/s00190-011-0444-4, <http://dx.doi.org/10.1007/s00190-011-0444-4>

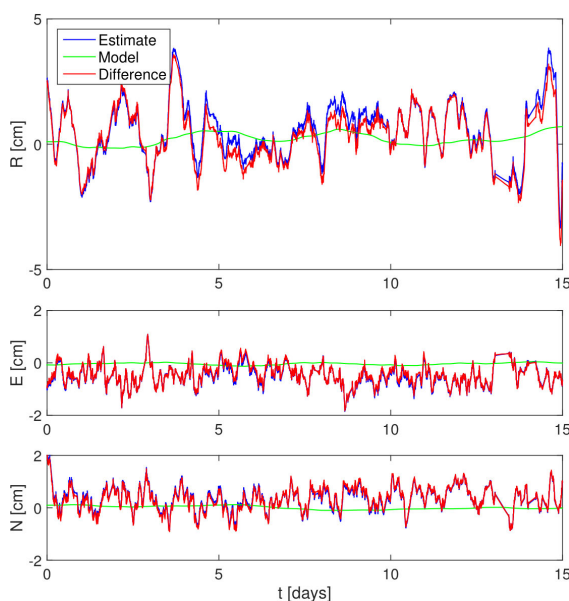


Fig. 4 For station Badary, the same quantities as in Fig. 1 are shown, although for non-tidal atmospheric pressure loading.

- Böhm J, Böhm S, Nilsson T, Pany A, Plank L, Spicakova H, Teke K, Schuh H (2012) The new Vienna VLBI software. In: S. Kenyon, M. C. Pacino, U. Marti (eds.), *Proc. IAG Scientific Assembly 2009*, IAG Symposia Series 136, 1007–1011, doi: 10.1007/978-3-642-20338-1-126.
- Chin T M, Gross R S, Boggs D H, Ratcliff J T (2009) Dynamical and Observation Models in the Kalman Earth Orientation Filter. *IPN Progress Report* 42(176), 24 pp.
- IERS Conventions (2010) G. Petit and B. Luzum (eds.), *IERS Technical Note 36*, Frankfurt am Main: Verlag des Bundesamtes für Kartographie und Geodäsie.
- Lyard F, Lefevre F, Letellier T, Francis O (2006) Modelling the global ocean tides: modern insights from fes2004. *Ocean Dynam*, 56(5-6), 394–415, doi: 10.1007/s10236-006-0086-x, <http://dx.doi.org/10.1007/s10236-006-0086-x>
- Nilsson T, Soja B, Karbon M, Heinkelmann R, Schuh H (2015) Application of Kalman filtering in VLBI data analysis. *Earth Planets Space*, 67(1), 136, doi: 10.1186/s40623-015-0307-y, <http://www.earth-planets-space.com/content/67/1/136>
- Petrov L, Boy J P (2004) Study of the atmospheric pressure loading signal in very long baseline interferometry observations. *J Geophys Res: Solid Earth*, 109, B03405, doi: 10.1029/2003JB002500, <http://dx.doi.org/10.1029/2003JB002500>.
- Soja B, Nilsson T, Karbon M, Zus F, Dick G, Deng Z, Wickert J, Heinkelmann R, Schuh H (2015) Tropospheric delay determination by Kalman filtering VLBI data. *Earth Planets Space*, 67(1), 144, doi: 10.1186/s40623-015-0293-0, <http://www.earth-planets-space.com/content/67/1/144>

- Wijaya D, Böhm J, Karbon M, Krásná H, Schuh H (2013) Atmospheric Pressure Loading. In: J. Böhm, H. Schuh (eds.) *Atmospheric Effects in Space Geodesy*, Springer Atmospheric Sciences, Springer Berlin Heidelberg, 137–157, doi: 10.1007/978-3-642-36932-2_4, http://dx.doi.org/10.1007/978-3-642-36932-2_4
- Wu X, Abbondanza C, Altamimi Z, Chin T M, Collilieux X, Gross R S, Heflin M B, Jiang Y, Parker J W (2015) KALREF – A Kalman filter and time series approach to the International Terrestrial Reference Frame realization. *J Geophys Res: Solid Earth*, 3775–3802, doi: 10.1002/2014JB011622, <http://dx.doi.org/10.1002/2014JB011622>

Antenna axis offsets estimated in VLBI data analysis

T. Nilsson, M. Karbon, J. A. Mora-Diaz, V. Raposo-Pulido, B. Soja, R. Heinkelmann, H. Schuh

Abstract We estimate antenna axis offsets for the VLBI telescopes in the IVS network using data from 1980–2013. We find that the estimated axis offsets differ from those measured in local surveys in some cases by several millimeters, what is larger than could be expected based on the formal errors. Possible reasons for this discrepancy are investigated, e.g., modeling of the station coordinates and the tropospheric delays. It is found that these error sources can occasionally affect the estimated axis offsets by several millimeters. Furthermore, it is found that the axis offsets can change due to, e.g., antenna repairs.

Keywords VLBI, radio telescope, axis offsets

1 Introduction

The reference point of a VLBI radio telescope should be the intersection of the two rotation axes of the telescope (e.g., the azimuth and elevation axes). However, the problem with this definition is that in reality the axes do not intersect. Some telescopes are designed with an offset between the axes, which can be several meters. Even if the design does not contain any axis offset, no telescope is constructed perfectly, hence there will, in general, still be an axis offset of some millimeters or more. Thus the reference point is normally defined as the point on the primary axis that is closest to the secondary axis. The distance between the reference point and the secondary axis, the axis offset, then needs to be taken into account in the VLBI analysis.

Since the axis offset affects the measured delay, it should be known precisely in the data analysis. Nilsson et al. (2015a) showed that an error of 1 cm in the axis offset of an azimuth-elevation mount telescope causes an error in the estimated vertical coordinate of about 1.3 cm. Thus, in order to reach the VGOS goal of 1 mm accuracy in the station coordinates, we need to

Tobias Nilsson, Maria Karbon, Julian A. Mora-Diaz, Virginia Raposo-Pulido, Benedikt Soja, Robert Heinkelmann, Harald Schuh

GFZ German Research Centre for Geosciences, Telegrafenberg A17, D-14473 Potsdam, Germany

know the axis offsets with sub-millimeter accuracy. There are mainly two ways of obtaining the axis offset of a VLBI radio telescope. One way is to measure it in a local survey. This is normally the most accurate method, however it has not been done at most stations. The other way is to estimate the axis offsets in the VLBI data analysis. Due to the high correlation with other parameters, like station positions, this requires a lot of data. Hence, this should ideally be done in a global solution using many VLBI sessions. However, even if data from many years are used, there might still be systematic errors in the estimates. When comparing the values from a global VLBI solution and local surveys, we can find differences of several millimeters (Nilsson et al., 2015a). This is much larger than what could be expected based on the formal errors. The reason could be errors in the models used in the data analysis. Hence, in order to get accurate axis offsets we need to identify these errors and correct them. In this work, we investigate a number of possible error sources in the VLBI data analysis which could systematically affect the axis offsets, like the tropospheric mapping functions, pressure measurements, and unmodeled station motions.

2 Effect of axis offset on the delay

The effect of an axis offset on the delay, τ_{axis} , can be calculated with the following formula (Nothnagel, 2009):

$$\tau_{axis} = AO \sqrt{1 - (\mathbf{s} \cdot \mathbf{f})^2} \quad (1)$$

where AO is the length of the axis offset, \mathbf{s} a unit vector in the direction of the radio source, and \mathbf{f} a unit vector in the direction of the primary axis. Thus this effect will be different for different antenna mounts. For the most common mount, azimuth-elevation (AZEL), τ_{axis} is:

$$\tau_{axis} = AO \cos \epsilon \quad (2)$$

where ϵ is the elevation angle. For expressions for other antenna mounts, e.g., X-Y and equatorial (EQUA), see Nothnagel (2009).

3 Data analysis

In this work, we used the observations from 4241 VLBI sessions observed in the period 1980–2013. These are all included in the GFZ contribution to ITRF2014 (Heinkelmann et al., 2014), and fulfill the following criteria: (i) at least 4 stations with more than 100 observations, and (ii) the station network spanning a polyhedron with volume larger than 10^{15} m^3 . The sessions were analyzed with the GFZ version of the Vienna VLBI Software (Böhm et al., 2012), VieVS@GFZ (Nilsson et al., 2015b). The normal equations of all single sessions were combined and inverted using the global solution module of VieVS@GFZ, VIE_GLOB. In the global solution, we estimated station coordinates and velocities, radio source coordinates, and axis offsets. The terrestrial datum was realized by applying No-Net-Translation (NNT) and No-Net-Rotation (NNR) conditions relative to ITRF2008 (Altamimi et al., 2011), and the celestial datum was realized by NNR conditions relative to ICRF2 (Fey et al., 2015). Positions were estimated for all stations and velocities for all stations with an observing period spanning at least one week; for the other stations we fixed the velocities to their ITRF2008 values. Radio source coordinates were estimated as global parameters for all radio sources except the special handling sources, which were session-wise reduced. The tropospheric delays were modeled in the standard way, calculating the zenith hydrostatic delay (ZHD) from surface pressure measurements and estimating the zenith wet delay (ZWD) and gradients, and using the Vienna Mapping Function 1 (VMF1, Böhm et al. 2006).

4 Results

4.1 Estimated axis offsets

Table 1 lists the estimated axis offsets. In total, there were 143 stations in our solution and we estimated axis offsets for all of them; however, here we only present the results for the 21 station which participated in more than 300 sessions. As comparison the IVS recommended values (<http://vlbi.geod.uni-bonn.de/Analysis/Thermal/antenna-info.txt>, Nothnagel 2009) are shown. We can note that our estimates often differ from the IVS values by a few millimeters. Especially, several of our estimates differ from the values measured in local surveys by several millimeters.

4.2 Modeling of station coordinates

Since the errors in the axis offsets affect the station position estimates, it is also likely that errors in the modeling of the station coordinates affect the axis offset estimates. For example, it could happen that there are non-linear variations at some stations which are not described well with an offset and a velocity. To test this,

Table 1 Axis offsets and their formal errors for the stations which have participated in more than 300 sessions. Shown are the axis offsets from the solution presented in this work, the IVS recommended values (Nothnagel 2009), as well as the difference between them (our estimates-IVS). Values from local survey are marked in boldface. All values are in millimeters.

Station	Mount	Estimates		IVS values		Diff.
		Value	Sigma	Value	Sigma	
ALGOPARK	AZEL	4.7	0.5	3.3	0.4	1.4
FORTLEZA	AZEL	4.7	0.5	3.5	0.5	1.2
KOKEE	AZEL	521.6	0.3	518.0	0.3	3.6
MATERA	AZEL	-1.6	0.4	-2.0	0.3	0.4
MEDICINA	AZEL	1828.0	0.4	1830.1	-	-2.1
NRAO20	AZEL	510.2	0.5	509.1	0.4	1.1
NYALES20	AZEL	521.2	0.2	524.2	0.2	-3.0
ONSALA60	AZEL	-9.6	0.4	-6.0	0.4	-3.6
SVETLOE	AZEL	-7.3	0.5	-7.5	5.0	0.2
TIGOCONC	AZEL	-6.8	0.9	0.0	0.3	-6.8
TSUKUB32	AZEL	5.3	0.3	4.9	0.3	0.4
WESTFORD	AZEL	318.6	0.2	318.2	0.2	0.4
WETTZELL	AZEL	1.3	0.2	-0.1	0.04	1.4
ZELENCHK	AZEL	-3.3	0.7	-11.5	-	8.2
GILCREEK	XYNS	7289.5	0.1	7284.6	0.1	4.9
HOBART26	XYEW	8195.3	0.4	8191.3	1.5	4.0
MOJAVE12	XYNS	-2.7	0.3	-2.5	0.3	-0.2
HARTRAO	EQUA	6670.0	0.4	6695.3	1.9	4.7
HRAS 085	EQUA	6704.2	0.8	6701.8	0.6	2.4
NRAO85 3	EQUA	6711.4	0.5	6706.5	0.4	4.9
RICHMOND	RICH	5182.2	0.6	5180.1	0.6	2.1

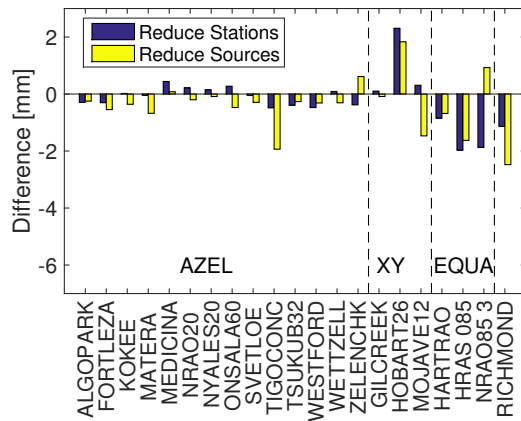


Fig. 1 Effect on the axis offset estimates when session-wise reducing the station coordinates or the radio source coordinates. Shown are the differences relative to the standard solution presented in this work (Table 1).

we made a solution where the station coordinates were session-wise reduced before stacking the normal equation (i.e., the station coordinates were estimated session-wise). The difference in the axis offset estimates relative to the original solution is shown in Fig. 1. In this figure, the case when the radio source coordi-

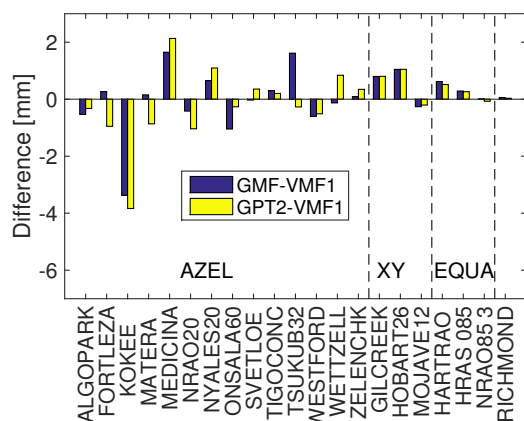


Fig. 2 Effect on the axis offset estimates when using the GMF or the GPT2 mapping functions instead of VMF1. Shown are the differences relative to the standard solution presented in this work (Table 1).

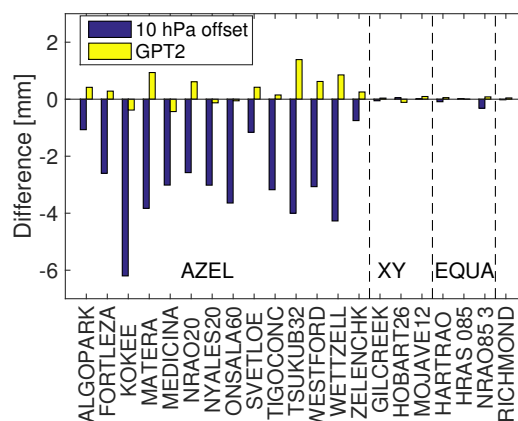


Fig. 3 Effect on the axis offset estimates caused by a 10 hPa pressure offset or by using pressure from the GPT2 model. Shown are the differences relative to the standard solution presented in this work (Table 1).

nates are session-wise reduced is also shown. Normally, the radio sources should not move, however, there might be effects related to, e.g., source structure that cause apparent motions over time.

As seen in Fig. 1 the effect of reducing station or radio source coordinates is below 1 mm for most stations. However, for some stations it can reach a few millimeters. For example, the effect of session-wise reduction of radio source coordinates is significant at some southern stations (TIGOCONC, HOBART26) and stations which mainly observed in the 80ies and early 90ies (MOJAVE12, HRAS 085, RICHMOND). Since the ICRF2 is less dense in the southern hemisphere than in the northern, it is possible that there are some southern sources commonly observed which have noticeable source structure. Furthermore, in the early days of VLBI, stronger sources, which often have more significant structure, were commonly observed.

4.3 Tropospheric mapping function

Another possible error source are the tropospheric mapping functions. To test how large this error source could be, we applied the GMF (Böhm et al., 2006) and the GPT2 (Lagler et al., 2013) mapping functions instead of VMF1. The results are shown in Fig. 2. For most stations the effect is 1 mm or smaller, however, for some stations the effect is up to several millimeters, for example at KOKEE.

4.4 Pressure measurements

Pressure measurements are needed for the calculation of the ZHD. Normally, pressure measured at the VLBI sites is used for

this purpose. If there is an offset in the pressure measurement, and consequently in the ZHD, this will mostly affect the ZWD estimates. However, there will also be effects on other parameters, such as station coordinates and the axis offsets.

Fig. 3 shows the effect on the axis offset estimates when we artificially introduce an error of 10 hPa in the pressure measurements. We can note that the effect is quite significant for antennas with azimuth-elevation mounts where the effect is around 3 mm. However, for other mounts the effect is small. The figure also shows the effect of using pressure values from the GPT2 model (Lagler et al., 2013) instead of measured values. For a few antennas, this effect reaches about 1 mm.

4.5 Effects of antenna repairs

In the analysis we have assumed that the axis offsets are constant in time. However, this is not necessarily true. It is possible that they have changed due to, e.g., major antenna repairs. We made a test where we allowed for changes in the axis offsets at antenna repairs. Fig. 4 shows the results before and after the repairs, as well as the results when as single offset is estimated for the whole period. Shown are the differences between the estimated values and the values estimated in local surveys. The local surveys were all performed before respective repair, and we can see that the values before the repairs generally agree better with the survey measurements than the values after the repair.

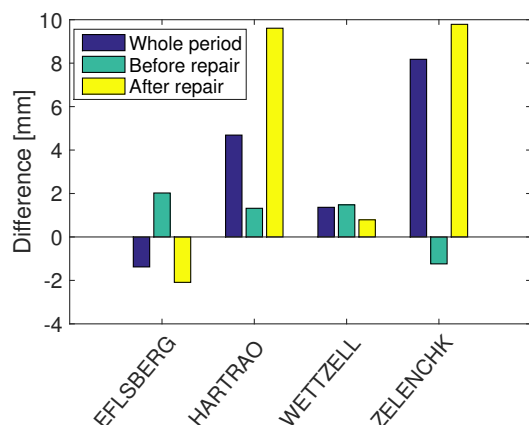


Fig. 4 Effect on the axis offsets of estimating different values before and after antenna repairs. Shown are the estimates before and after the repairs, as well as the results when estimating one value for the whole period. All values are relative to the values obtained in local surveys performed before the repairs.

5 Conclusions

We have seen that the modeling of station coordinates, radio source coordinates, and tropospheric delays could affect the estimated axis offsets by several millimeters. Thus, accurate models are crucial if sub-millimeter accuracy is needed. The best mapping functions are generally considered to be VMF1, and the most accurate pressure is normally that obtained from the pressure sensors at the stations (provided that they are well calibrated). Thus we are presently unable to recommend any improvements in the modeling. What, however, can be recommended, is to consider that the axis offsets can change in time. As seen in Section 4.5, antenna repairs can change the axis offsets by about 1 cm in some cases.

References

- Altamimi Z, Collilieux X, Métivier L (2011) ITRF2008: an improved solution of the international terrestrial reference frame. *J Geod*, 85(8), 457–473, doi: 10.1007/s00190-011-0444-4.
- Böhm J, Niell A, Tregoning P, Schuh H (2006) Global mapping function (GMF): a new empirical mapping function based on numerical weather model data. *Geophys Res Lett*, 33, L07304, doi: 10.1029/2005GL025546.
- Böhm J, Werl B, Schuh H (2006) Troposphere mapping functions for GPS and very long baseline interferometry from european centre for medium-range weather forecasts operational analysis data. *J Geophys Res*, 111, B02406, doi: 10.1029/2005JB003629.
- Böhm J, Böhm S, Nilsson T, Pany A, Plank L, Spicakova H, Teke K, Schuh H (2012) The new Vienna VLBI software. In S. Kenyon, M. C. Pacino, and U. Marti, (eds.), *Proc. 2009 IAG Symposium*, IAG Symposia 136, 1007–1011, doi: 10.1007/978-3-642-20338-1_126.
- Fey A L, Gordon D, Jacobs C S, Ma C, Gaumel R A, Arias E F, Bianco G, Boboltz D A, Böckmann S, Bolotin S, Charlot P, Collioud A, Engelhardt G, Gipson J, Gontier A M, Heinkelmann R, Kurdubov S, Lambert S, Lytvyn S, MacMillan D S, Malkin Z, Nothnagel A, Ojha R, Skurikhina E, Sokolova J, Souchay J, Sovers O J, Tesmer V, Titov O, Wang G, Zharov V (2015) The second realization of the international celestial reference frame by very long baseline interferometry. *Astron J*, 150(58), 1–16, doi: 10.1088/0004-6256/150/2/58.
- Heinkelmann R, Nilsson T, Karbon M, Liu L, Lu C, Mora-Diaz J A, Parselia E, Raposo-Pulido V, Soja B, Xu M, Schuh H (2014) The GFZ VLBI solution - characteristics and first results. In: D. Behrend, K. D. Baver, K. L. Armstrong (eds.), *IVS 2014 General Meeting Proc.*, Science Press (Beijing), 330–334, ftp://ivscc.gsfc.nasa.gov/pub/general-meeting/2014/pdf/071_Heinkelmann_etal.pdf.
- Lagler K, Schindelegger M, Böhm J, Krásná H, Nilsson T (2013) GPT2: Empirical slant delay model for radio space geodetic techniques. *Geophys Res Lett*, 40(6), 1069–1073, doi: 10.1002/grl.50288.
- Nilsson T, Mora-Diaz J A, Raposo-Pulido V, Heinkelmann R, Karbon M, Liu L, Lu C, Soja B, Xu M, Schuh H (2015) Antenna axis offsets and their impact on VLBI derived reference frames. *IAG Symposia* Springer, doi: 10.1007/1345_2015_126, in press.
- Nilsson T, Soja B, Karbon M, Heinkelmann R, Schuh H (2015) Application of Kalman filtering in VLBI data analysis. *Earth Planets Space*, 67(136), 1–9, doi: 10.1186/s40623-015-0307-y.
- Nothnagel A (2009) Conventions on thermal expansion modelling of radio telescopes for geodetic and astrometric VLBI. *J Geod*, 83, 787–792, doi: 10.1007/s00190-008-0284-z.

Numerical Issues of VLBI Data Analysis

T. Artz, S. Halsig, A. Iddink, A. Nothnagel

Abstract Very Long Baseline Interferometry (VLBI) observations are used to provide fundamental scientific products like the terrestrial and celestial reference frame or the Earth orientation parameters. These parameters are typically determined in a least squares adjustment. Within this process, numerical issues play an important role. Thus, conditioning as well as stability of the solution have to be investigated. While conditioning refers to numerical problems and has no connection to the solution strategy, numerical stability refers to the algorithms which are used. This paper focuses on the impact of numerical conditioning. For VLBI, the equation system of the least squares adjustment is apparently ill-conditioned. Thus, errors of the observations would be amplified during the adjustment process. However, we reveal that the conditioning is not that bad as it highly depends on the set-up.

Keywords Least Squares Adjustment, Conditioning, Singular Value Decomposition

1 Introduction

Very Long Baseline Interferometry (VLBI) is a fundamental geodetic space technique. The products which are derived from VLBI observations are entering into a wide area of Earth and Space sciences. Some of them like the celestial reference frame and nutation as well as Universal Time (UT1) are uniquely observed by VLBI, while VLBI contributes to the terrestrial reference frame and polar motion in a similar way like other geodetic space techniques (e.g., Altamimi et al., 2011).

All of these parameters are derived from VLBI observations via linearized observation equations. These equations represent the functional dependences between the observations and the parameters. As this equation system is overdetermined, i.e., more observations than parameters are present, the parameters are typ-

Thomas Artz, Sebastian Halsig, Andreas Iddink, Axel Nothnagel
Rheinische Friedrich-Wilhelms Universität Bonn,
Institut für Geodäsie und Geoinformation, Nußallee 17,
D-53115 Bonn, Germany

ically estimated in a least squares adjustment. To judge the precision and the reliability of this process, the covariance matrices of the parameters as well as of the residuals are analyzed.

As computers can calculate only with a limited number of digits, several algebraically equivalent approaches might lead to different results. The reason is that (1) the problem to be solved is ill-conditioned, and (2) the algorithms which are used provide different numerical stabilities. Thus, the parameters as well as the above mentioned covariance matrices might be more or less corrupted by the errors of the input data.

Within this paper, we aim at describing the conditioning in VLBI data analysis and its dependence on the solution set-up. We show how to optimize conditioning and present the implications of set-up changes.

2 Least Squares and Conditioning

2.1 Least Squares Adjustment

When a VLBI session is analyzed, the observations of typically 24 h are used to estimate a set of parameters given the known functional relationship

$$\mathbf{x} = \varphi(\mathbf{b}) \quad (1)$$

with the parameter vector \mathbf{x} and the vector of the observations \mathbf{b} . This leads to the linearized equation system

$$\mathbf{A}\mathbf{x} = \mathbf{b} \quad (2)$$

with the functional or Jacobian matrix

$$\mathbf{A} = \frac{\partial \varphi(\mathbf{b})}{\partial \mathbf{x}}. \quad (3)$$

As there are typically more observations than parameters, there is no unique solution for Eq. (2) and the equation system is extended by the post-fit residuals \mathbf{r}

$$\mathbf{A}\mathbf{x} = \mathbf{b} + \mathbf{r}. \quad (4)$$

Thus, we try to find the optimal solution in the sense of a least squares adjustment, where the gradient of the squared residual

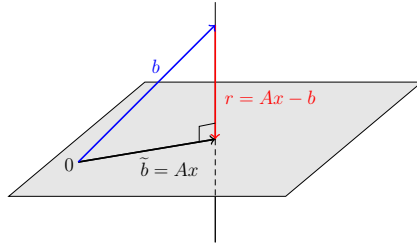


Fig. 1 Geometrical representation of the least squares adjustment.

function Φ vanishes

$$\begin{aligned} \Phi &= \|\mathbf{r}\|_2^2 = \|\mathbf{Ax} - \mathbf{b}\|_2^2 \\ \nabla\Phi &= 0, \end{aligned} \quad (5)$$

where $\|\cdot\|_2$ represents the L_2 -norm. The geometrical interpretation of this least squares procedure is shown in Fig. 1. The observations are projected into the column space of the Jacobian matrix. Thus, the adjusted observations $\tilde{\mathbf{b}} = \mathbf{Ax}$ are the linear combination of the parameters and the columns of the Jacobian matrix which have minimal distance to the observations. Here, the residuals have only components in the orthogonal range of the Jacobian matrix.

To solve the equation system, several approaches can be used. Equation 5 directly leads to the normal equation approach

$$\begin{aligned} \mathbf{0} &= \mathbf{A}^T (\mathbf{Ax} - \mathbf{b}) = \mathbf{A}^T \mathbf{Ax} - \mathbf{A}^T \mathbf{b} \\ \Rightarrow \mathbf{A}^T \mathbf{Ax} &= \mathbf{A}^T \mathbf{b} \quad \Leftrightarrow \quad \mathbf{Nx} = \mathbf{n} \end{aligned} \quad (6)$$

where \mathbf{N} is the normal matrix and \mathbf{n} the normal vector. The normal equations might be solved by a Cholesky decomposition of the normal matrix and subsequent forward and backward substitution. Equivalently, a QR-decomposition or a singular value decomposition (SVD, Eq. (7)) of the Jacobian matrix could be used. In case of the SVD approach, the solution is

$$\mathbf{A} = \mathbf{USV}^T \quad (7)$$

$$\mathbf{x} = \mathbf{VS}^{-1}\mathbf{U}^T\mathbf{b} \quad (8)$$

where \mathbf{U} and \mathbf{V} are matrices with the left and the right singular vectors, and \mathbf{S} is a diagonal matrix containing the singular values ($\mathbf{S} = \text{diag}(s_i)$). Thus, its inverse is simply made up of the reciprocal singular values.

Algebraically, these three approaches should lead to identical results. However, while the normal equation approach is the fastest, its numerical stability is relatively poor in comparison to the approaches via QR-decomposition or SVD (Demmel, 1997). As this stability of the algorithms is not in the focus of this paper, this issue will not be discussed in more detail.

To achieve a relative weighting of the observations, a weight matrix \mathbf{W} , which depends on the stochastic properties of the observations (expressed by their variance-covariance matrix Σ_{bb}), has to be applied

$$\mathbf{W} = \Sigma_{bb}^{-1}, \quad (9)$$

$$\mathbf{A}^T \mathbf{W} \mathbf{Ax} = \mathbf{A}^T \mathbf{W} \mathbf{b}. \quad (10)$$

To use algorithms different to the normal equation approach, a de-correlation has to be performed via Cholesky decomposition of the weight matrix into a lower triangular matrix \mathbf{L}

$$\mathbf{W} = \mathbf{L}^T \mathbf{L}, \quad (11)$$

$$\tilde{\mathbf{A}} = \mathbf{LA}. \quad (12)$$

Subsequently, the matrix $\tilde{\mathbf{A}}$ can replace \mathbf{A} and then the weight matrix is the identity matrix.

2.2 Conditioning of the Problem

Conditioning of the problem describes whether input errors are magnified during the adjustment procedure. As a measure, the condition of the Jacobian matrix

$$\kappa(\tilde{\mathbf{A}}) = \frac{s_{max}}{s_{min}} \quad (13)$$

can be expressed by the singular values. The optimal condition number is one, indicating that the problem is well conditioned, and a small perturbation of the input data leads to small variations of the results. Contrary, in an ill-conditioned case, even a small perturbation of the input data might lead to large errors of the output (Meyer, 2000). In other words, in an ill-conditioned case we are not entirely aware of the column space of the Jacobian matrix which means that the orientation of the plane depicted in Fig. 1 is not well known. Thus, the least squares solution might not be optimal due to an insufficient solution set-up.

Furthermore, not all errors are magnified in the same way. Re-formulating Eq. (8) to

$$\mathbf{x} = \sum_{i=1}^n \frac{\mathbf{u}_i^T \mathbf{b}}{s_i} \mathbf{v}_i \quad (14)$$

leads to a different view on the least squares problem. Obviously, especially the observational errors in direction of the small singular values are magnified the most. Thus, a problem can be considered as not ill-conditioned if the so-called discrete Picard condition is fulfilled. In this case, the singular values decrease not faster to zero than the SVD coefficients $|\mathbf{u}_i^T \mathbf{b}|$ (e.g., Hansen, 1990). Otherwise, a regularization can be used where filter factors are used to dampen the small singular values (e.g., Tikhonov, 1963).

Finally, one has to distinguish between singularities and ill-conditioning. As depicted in Fig. 2, a worse condition number might result from various situations. On the one hand, the majority of the singular values are on the same level, and others are on a different, significantly lower level. This jump in the spectrum of the singular values indicates a singularity due to non-estimatable parameters. On the other hand, constantly but significantly decreasing singular values indicate an ill-conditioned problem. In this case, it can also be noted that the discrete Picard condition is only fulfilled for the first parameters, indicating that the only

Table 1 Solution set-up for one 24 h session. CPWLF denotes continuous piece-wise linear functions, clock parameters are estimated for all but one site, as the solution is singular without selecting a reference clock.

Parameter	set-up	unit
clocks	2nd deg. polynomial	$s, s/d, s^2/d$
	+ hourly CPWLF	s
ZWDs	hourly CPWLF	s
trop. gradients	daily CPWLF	mm
X-/Y-pole	offset + rate	$rad, rad/d$
UT1-TAI	offset + rate	$ms, ms/d$
nutiation	offset	rad

unperturbed right-hand side (corresponding to large singular values) satisfies the discrete Picard condition.

3 Impact of Parameterization

To demonstrate the numerical issues within VLBI data analysis, we analyze the observations of the continuous VLBI campaign 2002 (CONT02). The data is fairly old, however, this has no impact on the characteristics of the equation system. Furthermore, the number of observations and parameters is nice for processing and visualization. Every day of the CONT02 is analyzed separately. The estimated parameters are clocks, zenith wet delays (ZWDs), tropospheric gradients in North-South and East-West direction as well as the EOPs (X-/Y-pole, UT1-TAI, and nutiation). The details of the parametrization are listed in Tab. 1. Numerical values are only given for the first session of CONT02 as they are representative for the other sessions.

The solution set-up leads to a condition number of the Jacobian matrix of $\kappa(\tilde{\mathbf{A}}) \approx 10^{16}$ which indicates singularities or a highly ill-conditioned problem. In Fig. 3, the corresponding singular values are depicted. Obviously, there are several critical points. First of all there is a singularity which is related to the estimation of the clocks. Estimating the clock polynomials together with the continuous piece-wise linear functions (CPWLF) leads to huge correlations and, thus, to un-resolvable parameters.

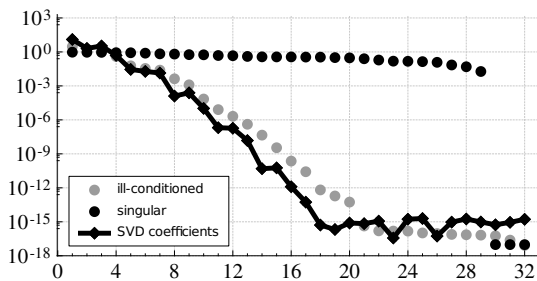


Fig. 2 Singular values for an ill-conditioned (gray circles) and a singular problem (black circles) together with SVD coefficients (diamonds connected by lines; identical for both set-ups).

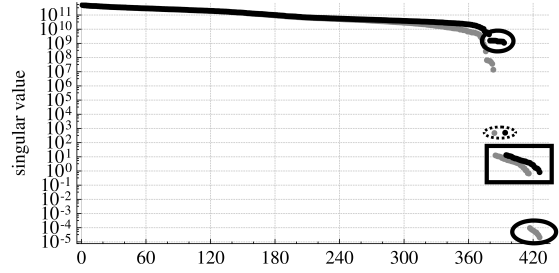


Fig. 3 Singular values of the unconstrained (gray) and constrained solution (black). The ellipses highlight parameters which are highly affected by the constraints (clocks). Within the rectangle, the gradients can be found, and within the dotted ellipse UT1-TAI.

Hence, prior information are added in form of pseudo observations fixing the rate between two subsequent clock parameters to zero with a given standard deviation (σ_{B_i})

$$\mathbf{B}_i = (0 \dots 0 \ 1 \ -1 \ 0 \ \dots \ 0), \quad (15)$$

$$\mathbf{W}_B = \text{diag}(1/\sigma_{B_i}^2), \quad (16)$$

$$\tilde{\mathbf{A}} = \begin{pmatrix} \tilde{\mathbf{A}} \\ \mathbf{B} \end{pmatrix}, \quad \mathbf{W} = \begin{pmatrix} \mathbf{W} & \mathbf{0} \\ \mathbf{0} & \mathbf{W}_B \end{pmatrix}. \quad (17)$$

The actual pseudo observations are set to zero. The effect on the singular values is shown in Fig. 3, where ZWDs and gradients are constrained in the same way. Here we used standard deviations of $\sigma_{cl} = 10^{-14}$ for clocks, $\sigma_{ZWD} = 40 \text{ ps/h}$ for ZWDs, and $\sigma_{grad} = 2 \text{ mm/d}$ for tropospheric gradients. It can be noticed, that the singularities concerning the clocks have been eliminated. Thus, the condition of the Jacobian matrix is now $\kappa(\tilde{\mathbf{A}}) \approx 6 \cdot 10^{11}$. This is still a bad value, which can be attributed to remaining jumps between the singular values. These correspond to the gradients and to UT1. As the gradients have already been constrained, the small singular values are due to the set-up which is discussed in Sec. 4.

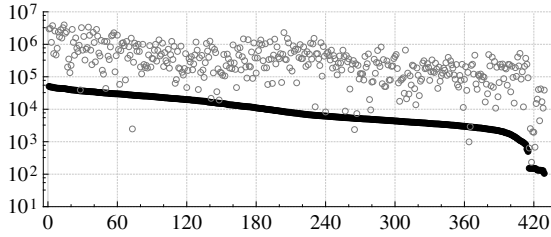
To demonstrate the consequences of the huge condition number, we analyze the quality of the re-construction of normal equation matrix from its Cholesky decomposition

$$\mathbf{0} \stackrel{!}{=} \mathbf{L}^T \mathbf{L} - \mathbf{N}. \quad (18)$$

Generally, the differences are zero, but, there are also some large differences which appear primarily on the main diagonal. Thus, the norm of the difference between the re-constructed and the original normal matrix is $\|\mathbf{L}^T \mathbf{L} - \mathbf{N}\|_2 \approx 10^8$, where major differences appear for elements corresponding to the ZWDs. However, the effect of these deviations on the estimates is below 1 ppm. Nevertheless, optimization of the conditioning is desired as the discrepancies are only due to the characteristics of the solution algorithm. Thus, the good agreement of the parameters results from identical input errors.

Table 2 Modified solution set-up implementing the new units.

Parameter	set-up	unit
clocks	2nd deg. polynomial	$\mu s, \mu s/d, \mu s^2/d$
	+ hourly CPWLF	μs
ZWDs	hourly CPWLF	μs
trop. gradients	daily CPWLF	m
X-/Y-pole	offset + rate	$\mu rad, \mu rad/d$
UT1-TAI	offset + rate	$\mu rad, \mu rad/d$
nutation	offset	μrad

**Fig. 4** Singular values of the modified solution implementing the new units; σ_i are represented by black dots, and the SVD coefficients $|\mathbf{u}_i^T \mathbf{b}|$ by gray circles, respectively.

4 Modifications of the solution set-up

To overcome the numerical problems discussed above, one feasible and typically used approach is to scale the Jacobian matrix. This is done in a way, that results in a normal matrix with only ones on its main diagonal

$$\mathbf{F} = \text{diag} \left(\frac{1}{\sqrt{\text{diag}(\tilde{\mathbf{A}}^T \tilde{\mathbf{A}})}} \right), \quad (19)$$

$$\hat{\mathbf{A}} = \tilde{\mathbf{A}} \mathbf{F}. \quad (20)$$

This significantly improves the condition from $\kappa(\tilde{\mathbf{A}}) \approx 6 \cdot 10^{11}$ to $\kappa(\hat{\mathbf{A}}) \approx 200$. However, to derive the scaling factors in \mathbf{F} , the matrix elements have to be summed squared and then the square root is taken. This might also lead to loss of precision.

As this pre-conditioning is equivalent to changing the parameter units arbitrarily, we tried to find the optimal units for a typical VLBI solution leading to reasonable condition numbers by trial and error. The new units which are found to be optimal are listed in Tab. 2 yielding $\kappa(\tilde{\mathbf{A}}) \approx 480$. The corresponding singular values are depicted in Fig. 4. With this set-up, the largest as well as the smallest singular values are attributed to clock parameters. For the smallest singular values there is a slight jump, which can be resolved by replacing the clock polynomials with CPWLF at finer intervals. However, this degrades the solution (not shown here). Thus, the clock parametrization might be refined for further improvements of the condition. Furthermore, Fig. 4 reveals, that the discrete Picard condition is more or less fulfilled. The SVD coefficients are fairly noisy, but, on average, they decrease similarly slowly as the singular values.

The impact of the new parameters on the re-construction of the normal matrix can again be evaluated based on Eq. (18). The norm of the difference between re-constructed and original normal matrix is now $\|\mathbf{L}^T \mathbf{L} - \mathbf{N}\|_2 \approx 2 \cdot 10^{-6}$, but the discrepancies between the parameters are still at the same level compared to the old set-up.

5 Conclusions and Outlook

The conditioning of the VLBI solution appears to be bad, which has been investigated by the analysis of the singular values. This ill-conditioning is forced by two aspects. On the one hand there are singularities due to unsolvable parameters, which are typically eliminated by adding pseudo information to the equation system. Nevertheless, jumps between the singular values remain. Thus, on the other hand, other groups of parameters are weakening the equation system. The reason is not due to a limited number of observations, but, due to large differences between the entries of the Jacobian matrix. Therefore, we introduced new units for the parameters which significantly improved the conditioning for the sessions of CONT02 which have been analyzed. All values presented throughout the paper are for the session on September 16th, 2002. However, they are representative for the whole campaign.

Although stabilization approaches like using a preconditioner which scales the main diagonal of the normal equation matrix to ones are feasible, the proposed unit change is useful. Even though the estimates are not changed significantly. It reduces computational load and leads to a reasonable conditioning of the problem. The effects are not directly assessable, as the input errors do not change. For further investigations, a Monte-Carlo simulation of the input errors will be used to gain better insights in the estimation mechanisms.

Obviously, the conditioning of the VLBI data analysis is not that bad if feasible units are used for the estimated parameters. However, the condition numbers are still not optimal. Furthermore, it has to be investigated why the improvements in terms of numerical stability do not lead to an improved estimation.

References

- Altamimi Z, Collilieux X, Métivier L (2011) ITRF2008: an improved solution of the international terrestrial reference frame. *J Geod*, 85(8), 457–473, doi: 10.1007/s00190-011-0444-4.
- Demmel J W (1997) Applied Numerical Linear Algebra, SIAM, Philadelphia.
- Hansen P C (1990) The Discrete Picard Condition for Discrete Ill-Posed Problems. *BIT*, 30, 4, 658–672, doi: 10.1007/BF01933214.
- Meyer C D (2000) Matrix Analysis and Applied Linear Algebra, SIAM, Philadelphia.
- Tikhonov A N (1963) Solution of Incurrectly Formulated Problems and the Regularization Method, *Doklady Akademi Nauk*, 151, 3, 501–504.

Sophistication in UT1-Intensive Scheduling by Using Impact Factors - First Results of Field Tests

A. Nothnagel, J. Leek, M. Beier, T. Artz, D. Ullrich

Abstract Since January 1, 2015, the observing schedules of the Int2 UT1-*Intensive* sessions being observed on Saturdays and Sundays on the Tsukuba – Wettzell baseline are produced on the basis of impact factors. This is a new procedure since previous schedules were solely based on optimal sky coverage criteria. After more than half a year of operating in this mode, a sufficiently long series of observations is now available to compare the results of the two approaches. Looking at the formal errors, the impact-factor-approach seems to be superior to the sky-coverage-approach. Considering the deviations from a mean UT1 path as defined by the results of regular 24h network sessions of the International VLBI Service for Geodesy and Astrometry (IVS), the scatter is the same before and after the date of change in scheduling strategy. There are, however, a few outliers which might originate from the interpolation process of the reference series. In the course of the analysis it appeared that the analysis strategies of individual IVS Analysis Centers is quite different in terms of the number of observations identified as outliers. The impact of this difference is on the order of $13.1 \mu\text{s}$ (Weighted Root Mean Squared, WRMS), thus, having a non-negligible effect on the final results.

Keywords IVS Intensives, scheduling with impact factors

1 Introduction

VLBI observations are carried out in a predefined sequence which has to be prepared centrally before the observing session can take place. The scheduling process mainly consists of a sequential selection of the next observation or observations. Most geodetic VLBI observing plans were created with the software

Axel Nothnagel, Judith Leek, Meike Beier, Thomas Artz
Rheinische Friedrich-Wilhelms-Universität Bonn, Institute of
Geodesy and Geoinformation, Nußallee 17, D-53115 Bonn, Germany
Dieter Ullrich
Bundesamt für Kartographie und Geodäsie, Karl-Rothe-
Straße 10–14, D-04105 Leipzig, Germany

package SKED (Vandenberg, 1999), which can be run with automated decision processes for different optimization criteria. In the classical approach, SKED uses a homogeneous sky coverage target to reach uniform sensitivity for all unknown parameters, although earlier on a covariance optimization was implemented by Steufmehl (1994). SKED is heavily used in the International VLBI Service for Geodesy and Astrometry (Schuh and Behrend, 2012) and is continually maintained and updated, e.g. Gipson (2012). Recently, a new source-based scheduling strategy was published, which starts with selecting radio sources from a pre-defined catalog without regard for their direct impact on individual stations as part of the Vienna VLBI Software (Sun et al., 2014).

For preparing observing schedules for the IVS *Intensive* sessions for short duration UT1-TAI determinations and here in particular the Int1 series, several publications appeared on optimizing strategies related to the SKED sky coverage option, e.g., (Baver and Gipson, 2013). In contrast to this, Leek et al. (2015) developed an approach for improving the scheduling process for *Intensive* sessions, where the next observation is selected on the basis of a new optimization criterion, the impact factor.

Impact factors are intermediate results of the least squares adjustment and can help to analyze the design or geometry of an experiment at every stage of the scheduling process. Starting point for the computation of one or more impact factors is the Jacobian matrix which contains information on the geometry of the design of an adjustment problem (Vennebusch et al., 2009). From this, the impact factor for each possible new observation can be computed (Leek et al., 2015). The next observation to be chosen is then the one with the biggest impact factor. For more details see Leek (2015).

This scheduling strategy has been applied to the Int2 UT1-TAI short duration VLBI sessions on the baseline Tsukuba (Japan) - Wettzell (Germany) (Nothnagel and Schnell, 2008) from January 1, 2015, onwards. The purpose of this paper is to show results of comparisons of the two approaches.

2 Scheduling

Until December 31, 2014, the observing schedules for the Int2 sessions were produced using the homogeneous sky coverage option of SKED. With this option, the software tries to fill the mutually visible sky with observations as homogeneously as possible (Gipson, 2012). This is done sequentially recomputing the geometrical parameters for each source in a list provided with the respective radiation intensities to compute the necessary duration of the observation to achieve a predefined signal-to-noise ratio. For scheduling each session, all available 92 geodetic VLBI radio sources above a certain flux density were made available to the automatic selection process. Thresholds for the signal-to-noise ratio were routinely set to 25 for X band and 20 for S band. Normally, about 40 scans composed the final schedules.

Since January 1, 2015, the scheduling method using impact factors has been applied regularly in preparing the Int2 observing sessions. The procedure itself is only different from the SKED scheduling in that the criterion for the selection of the next observation is the impact factor. This is determined by computing the impact factors of all possible candidate sources at a given instance and just selecting that with the biggest impact factor.

3 Results

The data used for the comparisons consists of analyses carried out operationally by the VLBI IVS Analysis Centers of the NASA Goddard Space Flight Center (GSFC) and the German Federal Agency for Cartography and Geodesy (BKG) (Thorandt et al., 2015). Both centers regularly analyze completely independently all IVS *Intensive* and all IVS 24 h R1 and R4 sessions for rapid EOP determinations. The results are reported in data files provided at the IVS Data Centers under the names `bkgint14.eopi` and `gsf2014a.eopi` for the *Intensives* and `bkg00014.eoxy` and `gsf2014a.eoxy` for the R1 and R4 sessions.

When looking at the analysis strategies of the two institutions for the *Intensives*, it became obvious that the BKG Analysis Center identified many more observations as outliers than the GSFC center. Considering that most sessions have only about 35 to 45 individual delay observations, the down-weighting or elimination of up to 10 observations means a severe difference in the overall geometrical consistency of the solutions (Fig. 1). The effect can be seen when forming the differences of the UT1-TAI results (Fig. 2). Besides an overall bias of $+7.6 \mu\text{s}$ two large values stick out as apparent outliers. The remaining noise level is $13.1 \mu\text{s}$ (WRMS).

3.1 Standard deviations

The standard deviations of both analyses are computed using additive noise to push the χ^2 to unity. The standard deviations of the results of the BKG Analysis Center (Fig. 3) show a general scatter between 4 and $17 \mu\text{s}$ with a noticeable increase in the middle of the year 2014. The difference in the scheduling procedures can

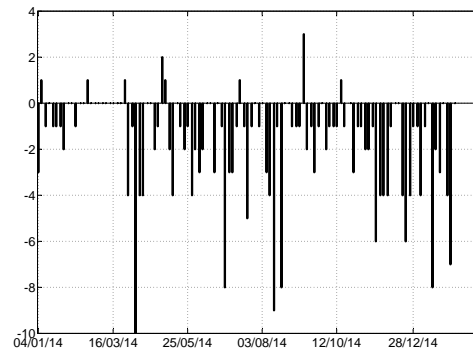


Fig. 1 Differences in number of observations (BKG - GSFC) used in the analysis of the Int2 sessions in 2014.

easily be discerned with the help of the vertical line separating the two periods. After January 1, 2015, the standard deviations belong to the smallest in the total sample. In the June/July period, an increase is visible again, however, not quite as high as in the 2014 northern summer. The visual impression of the scatter of the 2015 period seems to be originating only from very few data points.

Considering the fact that BKG had eliminated many more observations as outliers, it is no wonder that its standard deviations are generally smaller (Fig. 3) than those of GSFC (Fig. 4). In general, however, smaller standard deviations prevail after the change of scheduling strategy in the results of GSFC, with a larger scatter though. We should note that three sessions at the end of June/beginning of July 2015 show some larger standard deviations than all the other sessions. We had hoped that the results of 2015 are less prone to larger formal errors but these three sessions clearly stick out. The reason still needs to be investigated.

It should be noted that both series show a noticeable increase of the UT1-UTC standard deviations in the middle of 2014. This pattern seems to exist not only for this year but also for all VLBI sessions in general and most probably have to be attributed to the increased water vapor content in the atmosphere.

3.2 Absolute deviations

An evaluation of the quality of the absolute values is always difficult for UT1-TAI results from VLBI observations because no series of equal or superior accuracy from parallel VLBI measurements or of other techniques exists. For this reason, reference series are deduced from the results of the IVS R1 and R4 sessions as analyzed by the respective analysis center applying a cubic spline interpolation for the respective epochs of each *Intensive* session.

In an absolute sense, there are no great differences between the BKG and the GSFC solutions. As stated above, the WRMS

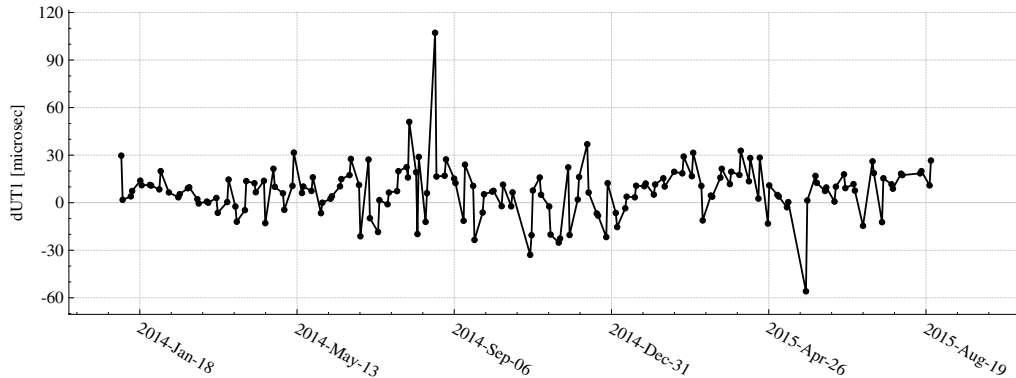


Fig. 2 Differences in UT1-TAI determinations (BKG - GSFC).

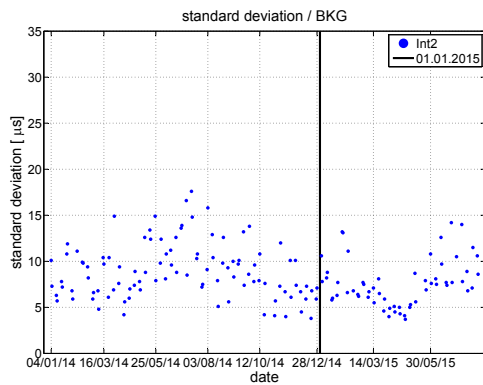


Fig. 3 Standard deviations of the Int2 sessions from the BKG solution.

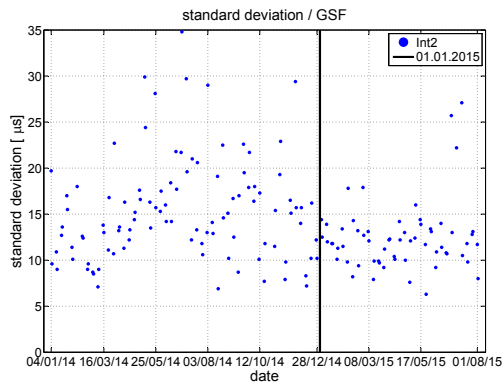


Fig. 4 Standard deviations of the Int2 sessions from the GSFC solution.

difference is $13.1 \mu\text{s}$ level which does not produce noticeable differences in the residual plots to be discussed here. For this reason, only the BKG series is contemplated below.

Fig. 5 shows the differences between the interpolated UT1-TAI values and the measured ones where the grey dots refer to a base series generated by the interpolation of the BKG R1/R4 results mentioned above. The black crosses are the differences w.r.t. the USNO *finals.data* series (Wooden et al., 2004). Overall, there is no noticeable change of the differences before and after the change of the scheduling procedure. The general noise level is on the order of $40 \mu\text{s}$ (RMS) with a few data points deviating by more than $\pm 80 \mu\text{s}$ in 2014 as well as in 2015. In 2015, a few more data points seem to show larger deviations up to $120 \mu\text{s}$ in the series relative to the R1/R4 results. In terms of RMS and WRMS the results of 2014 possess a scatter of $38.5/39.7 \mu\text{s}$ while in 2015 the numbers are higher ($49.3/46.0 \mu\text{s}$) due to the few larger values mentioned before. For the latter, we suspect that at least the two negative outliers in mid July 2015, if not also a few others, rather originate from an unfavorable undulation in the cubic spline interpolation than from bad UT1-TAI determinations but so far we were not able to identify the cause for this. Eliminating just the five worst data points, the RMS/WRMS values reduce to $34.7/36.2 \mu\text{s}$ respectively, which is insignificantly smaller than the 2014 differences.

The series relative to the base data tabulated in the USNO *finals* appears much smoother with $21.6/18.2$ and $18.8/17.2 \mu\text{s}$ for the RMS/WRMS of 2014 and 2015, respectively. Here, the differences are slightly smaller in 2015. However, this fact is not really conclusive because the generation of the USNO *finals* includes the results of the IVS *Intensives*, with a small weight, though (Stamatakos, priv. comm.).

Using as a reference for these interpretations the values of spline-interpolations from R1/R4 sessions, which are of a sufficiently high quality, cannot serve for a quantitative evaluation. Only a visual contemplation is possible because we can hardly model and subtract the natural variability of the UT1-TAI time series at any time with sufficient accuracy. Only a general impression of the roughness of the time series can be considered. In this respect, the 2015 data determined with the new scheduling strategy is similarly rough but shows a few more outliers.

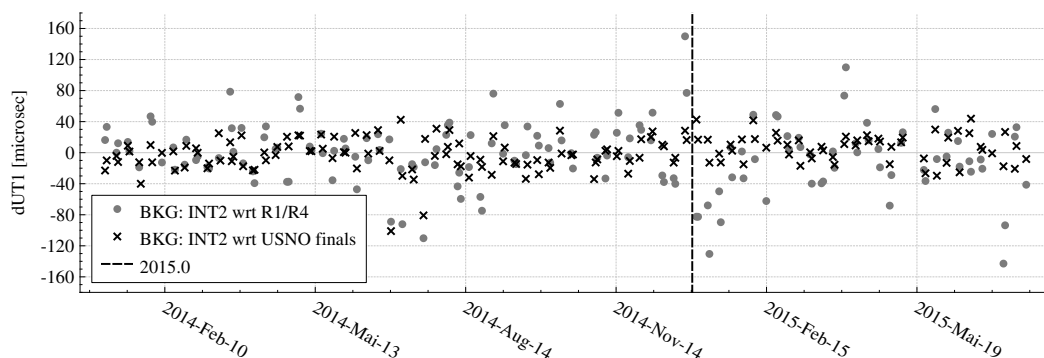


Fig. 5 Differences of the BKG solution w.r.t. spline interpolations of the R1/R4 reference series.

4 Conclusions

The new scheduling strategy for UT1-TAI *Intensive* sessions selecting the sequence of observations on the basis of impact factors has proven to produce similarly reliable time series as the standard scheduling procedure. However, it cannot be shown convincingly, that they are better than those where the standard approach is applied attempting to reach homogeneous sky coverage. From the current data volume, we must admit that a few rather large differences show up, a situation which should be avoided. Whether this is just a result of some technical problems during the observations on these specific days, whether it is an interpolation problem, or whether it is indeed a result of the scheduling still needs to be investigated. For this reason, this method will continue to be used for the Int2 Wettzell – Tsukuba sessions on Saturdays and Sundays for the time to come.

This study has also shown that there are severe differences in the treatment of outliers in the observations at least by two of the IVS Analysis Centers. Although both centers use the same suite of analysis software, this leads to notable differences in the results which go much beyond any tolerable levels. The analysis centers are urged to investigate this issue.

References

- Baver K, Gipson J (2013) Refining the Uniform Sky Strategy for IVS-INT01 Scheduling. In: N. Zubko, M. Poutanen (eds.), *Proc. 21th EVGA Working Meeting*, 205–209.
- Gipson J M (2012) Sked. VLBI Scheduling Software. NASA Goddard Spaceflight Center, May 2012, available electronically at http://lupus.gsfc.nasa.gov/files_user_manuals/sked/sked.pdf.
- Leek J (2015) The application of impact factors to scheduling VLBI Intensive sessions with twin telescopes. Dissertation, Landwirtschaftliche Fakultät, Rheinische Friedrich-Wilhelms-Universität Bonn, <http://hss.ulb.uni-bonn.de/2015/3905/3905.htm>.
- Leek J, Artz T, Nothnagel A (2015) Optimized scheduling of VLBI UT1 intensive sessions for twin telescopes employing impact factor analysis. *J Geod*, doi: 10.1007/s00190-015-0823-3
- Nothnagel A, Schnell D (2008) The impact of polar motion and nutation errors on UT1 determinations from VLBI Intensive observations. *J Geod*, 82(12), 863–869; doi: 10.1007/s00190-008-0212-2.
- Schuh H, Behrend D (2012) VLBI: A fascinating technique for geodesy and astrometry. *J Geodyn*, 61, 68–80, doi: 10.1016/j.jog.2012.07.007.
- Steuftmehl H-J (1994) Optimierung von Beobachtungsplänen in der Langbasisinterferometrie (VLBI). Dissertation, Rheinische Friedrich-Wilhelms-Universität Bonn, Frankfurt am Main, Deutsche Geodätische Kommission Bayer. Akad. Wiss., Reihe C, Vol. 406, ISSN 0071-9196.
- Sun J, Böhm , Nilsson T, Krsn H, Böhm S, Schuh H (2014) New VLBI2010 scheduling strategies and implications on the terrestrial reference frames. *J Geod*, 88(5), 449–461, doi: 10.1007/s00190-014-0697-9.
- Thorandt V, Engelhardt G, Ullrich D (2015) VLBI Analysis at BKG. In: R. Haas, F. Colomer (eds.), *Proc. 22nd EVGA Working Meeting*, 256–258.
- Vandenberg N (1999) Interactive/Automatic Scheduling Program. Program Reference Manual. NASA/Goddard Space Flight Center, NVI, Inc., 1999.
- Vennebusch M, Nothnagel A, Kutterer H (2009) Singular value decomposition and cluster analysis as regression diagnostics tools for geodetic applications. *J Geod*, 83, 877–891, doi: 10.1007/s00190-009-0306-5.
- Wooden W H, Johnson T J, Carter M S, Myers A E (2004) Near Real-Time IERS Products. In: A. Finkelstein, N. Capitaine (eds.), *Proc. Journées 2003 Systèmes de Référence Spatio-Temporels*, 160–163.

The CONT Campaigns as a Precursor to VGOS Observing

D. MacMillan

Abstract Continuous (CONT) VLBI campaigns have been carried out about every three years since 1994. The basic idea of these campaigns has been to acquire state-of-the-art VLBI data over a continuous time period of about two weeks to demonstrate the highest accuracy of which the current VLBI system is capable. In addition, these campaigns support scientific studies such as investigations of high resolution Earth rotation, reference frame stability, and daily to sub-daily site motions. The size of the CONT networks and the observing bandwidth has increased steadily since 1994. The performance (based on reference frame scale precision and polar motion/LOD comparison with GPS) of these networks has been substantially better than that of the weekly operational series of experiments. The CONT precision has improved by more than a factor of two since 2002. Polar motion precision of the most recent campaigns is comparable to that of GNNS. The CONT series are a natural precursor to the planned future VLBI observing networks. We compare the performance of the most recent CONT campaign with the expected performance of the future VGOS network using simulations. Simulations indicate the expected future precision of scale and EOP will be at least 3 times as good as the current CONT precision.

Keywords CONT, Earth Rotation, Terrestrial Reference Frame, Scale

1 Introduction

IVS has carried out five continuous observing campaigns since 2000, CONT02, CONT05, CONT08, CONT11, and CONT14. These experiments provide the opportunity for scientific studies such as investigations of high resolution Earth rotation variation, reference frame stability, and daily to sub-daily site motions. They are designed to obtain state-of-the-art VLBI data continuously over a period of 2 weeks and demonstrate the best ac-

Daniel MacMillan

NVI, Inc. at the Planetary Geodynamics Laboratory, Goddard Space Flight Center, Greenbelt, Maryland, USA

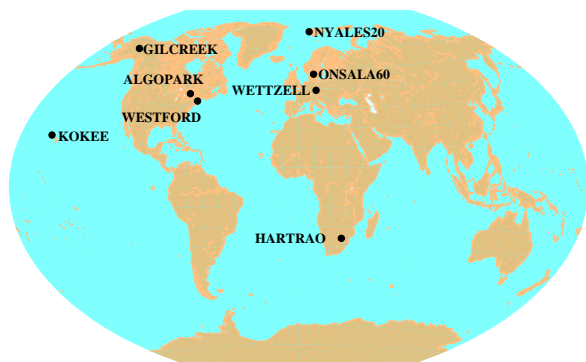


Fig. 1 CONT02 observing network.



Fig. 2 CONT14 observing network.

curacy that the current VLBI system is capable. An important contribution to the success of CONT sessions is the extensive testing and diagnosing of any possible station problems in the weeks before the experiment sessions begin. Generally the best performing stations are used in the observing network.

The continuous IVS observing sessions began with the campaign in 2002 that used an 8-station network shown in Fig. 1. Although the global distribution of sites has improved, even the latest campaign CONT14 with the 16-station network in Fig. 2 has limited observing on the three continents of North America, South America, and Africa. The predominance of Northern

hemisphere stations has always been problematic for VLBI; it does not allow sufficient observing of high declination sources in the Southern hemisphere, where there is a lack of mutual visibility between Northern and Southern hemisphere antennas. There was a significant loss of stations in North America after 2005 when ALGOPARK (Algonquin Park, Quebec, Canada) and GILCREEK (Fairbanks, Alaska) were closed.

It is expected that the IVS will observe continuously with large networks of broadband and fast-slewing antennas in the 5-10 year time frame. The CONT sessions are a natural precursor to the expected next-generation VGOS (VLBI Geodetic Observing System) network. The number of observations will increase dramatically and the large globally-distributed network of 17-28 stations will lead to significantly improved Earth orientation parameter precision as well as reference frame scale precision.

Section 2 summarizes the procedures involved in generating VLBI solutions using the Calc/Solve software. In Section 3, we discuss the precision of Earth orientation estimates and the scale determined from the series of CONT campaigns since 2000.0. In Section 4, we discuss the global networks of next generation VLBI stations that we expect to have in the next 5-10 years. We then analyze the performance of the current CONT sessions and future sessions by simulation to gauge the expected future improvement.

2 Data Analysis Procedure

The VLBI analysis reported in this paper used the Calc/Solve analysis system (Calc/Solve, 2008). Ma et al. (1990) gives a general description of the Solve least-squares estimation program and the theoretical models that are used. The models that are employed generally follow the recommendations of the IERS Conventions 2010 (Petit and Luzum, 2010). In this analysis, we applied other additional correction models including antenna thermal deformation (Nothnagel, 2008), VMF1 tropospheric mapping functions (Boehm et al., 2006), and atmospheric pressure loading (Petrov and Boy, 2004).

Solutions reported in this paper yield global or session parameter estimates that depend on the solution type: 1. Global parameters (based on the entire observing period of VLBI daily sessions in the solution: site positions and velocities, radio source positions; 2. Session parameters (based on observations within each VLBI 24-h session): site positions when estimating site position time series, pole coordinates and their rates, UT1 and UT1 rate, nutation, wet zenith delay, tropospheric gradient delay parameters, clock parameters.

3 Continuous VLBI Session Performance

3.1 EOP Precision

To evaluate the performance of the CONT sessions, we compared EOP estimates from these sessions with independent es-

timates from other geodetic techniques. The GNNS technique provides the most precise estimates of the geodetic techniques (VLBI, SLR, DORIS, GNNS) for polar motion, primarily because the IGS global network has hundreds of globally distributed stations and observing is continuous. Problems with specific GNNS receivers are averaged out in the estimates of global parameters like EOP. In geodetic combinations such as the ITRFs (e.g., ITRF2008 or ITRF2014) the stated precision of GNNS site and EOP estimates is so much smaller than for other techniques that it dominates the combination (Altamimi et al., 2011). Operationally the the IVS observes with the R1 and R4 VLBI networks every week, which each have 8-11 sites. Other networks observe less frequently. Although the R1 and R4 networks each have a core set of 4-5 sites, the remaining sites in the networks are not the same every week, which results in inhomogeneous observing.

The VLBI continuous sessions provide the opportunity to make comparisons with GNNS and to evaluate the EOP from both techniques. Characteristics of the CONT series are a) they use the same observing network during a two week period, 2) the observing is continuous, and 3) the networks are larger than the operational networks. Fig. 3 and Fig. 4 show the differences between VLBI and IGS polar motion for the CONT14 series. In the same figures are shown the differences for the operational R1 and R4 series for 2014. The obvious conclusion is that the precision (WRMS of the differences) relative to IGS is much smaller for the CONT14 series than for the two weekly operational series. Tab. 1 presents the EOP precision for each of the CONT series and for the R1 and R4 series in 2014. Based on this WRMS measure of precision, the polar motion precision of the CONT series has improved by about a factor of 2 since CONT02. GPS cannot accurately estimate UT1, but it can provide estimates of LOD along with the corresponding polar motion rate parameters. Polar motion rate precision has improved by a factor of 2-3 and LOD precision has improved by a factor of 3-4.

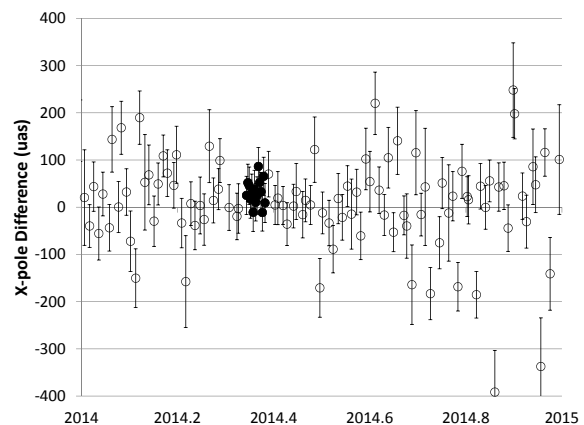


Fig. 3 Differences between estimates of the X component of polar motion from VLBI and IGS during 2014. The solid black circles are the CONT14 differences and the open black circles are the operational R1 and R4 session differences.

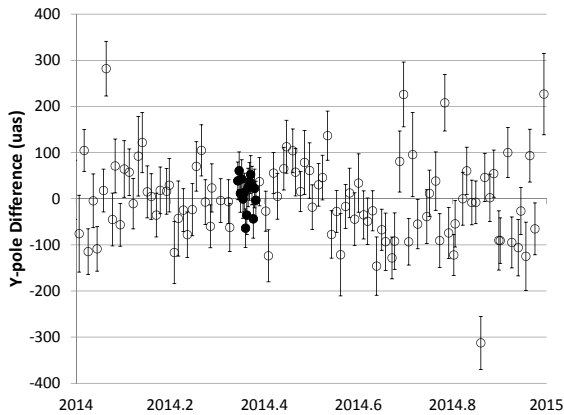


Fig. 4 Differences between estimates of the Y component of polar motion from VLBI and IGS during 2014. The solid black circles are the CONT14 differences and the open black circles are the operational R1 and R4 session differences.

One way of determining the precision of GNNS EOP is to perform tests internal to the GNNS technique. For example, there are several IGS EOP products with latencies ranging from 1 day (Ultra), 2 days (Rapid) and 1 week (Finals). Ray and Griffiths (2012) reported results of a 3-corner hat comparison of these series (P. Rebischung, IGS) that yielded a precision of 25.3 uas and 31.3 uas for the X and Y components of polar motion in the IGS Finals series. This level of precision is at the level of the wrms difference between CONT14 and IGS polar motion, which implies that the precision of the CONT14 series is also at this level or better.

3.2 Reference Frame Scale Precision

One of strengths of the VLBI technique is the determination of reference frame scale. For this reason, the scale of the ITRF combinations is determined by VLBI and SLR (Altamimi et al., 2011). Fig. 5 shows the scale time series for VLBI, where the scale was estimated for each R1, R4, and CONT14 24-hour observing session. The precision of the scale estimates given by the WRMS of the scale estimates is clearly smaller for the CONT14 sessions than for the series of R1 and R4 operational sessions in 2014. The likely reason for this is the inhomogeneity of station composition of the operational networks. It is likely that this inhomogeneity leads to systematic differences in the global scale estimates. Similar to the precision of EOP, the scale precision has improved by about a factor of 2 since 2002.

Table 1 Scale and EOP Precision

	Scale	Xpl	Ypl	Xpr	Ypr	LOD
	ppb	mm	uas	uas	uas/d	uas/d
CONT02	0.43	2.7	59	61	200	310
CONT05	0.31	2.0	64	40	240	150
CONT08	0.24	1.5	52	48	130	120
CONT11	0.23	1.5	37	31	120	120
CONT14	0.20	1.3	26	35	82	97
R1 2014	0.55	3.5	84	86	195	217
R4 2014	0.47	3.0	73	82	206	291

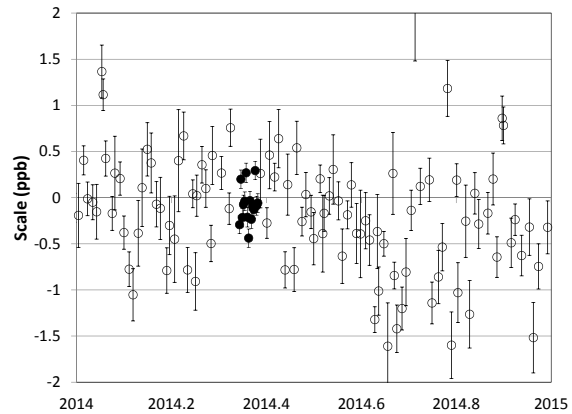


Fig. 5 Reference frame scale series. The solid black circles are for CONT14 and the open black circles are the operational R1 and R4 sessions.

Table 2 Observing Session Comparison

Session Type	Number of Stations	Site average scans/hr	Range scans/hr	Number of Observations
Weekly R1	8-10	15	12-21	5100
CONT11	14	16	12-20	10900
CONT14	17	19	14-24	20300
+5 Yr	17	79	58-97	141800
+10 Yr	27	76	61-86	274200

Table 3 EOP and Scale Precision From Simulation

Session Type	X	Y	UT1	LOD	Scale
	uas	uas	us	uas/d	ppb
CONT11	33.4	31.2	2.35	4.61	0.43
CONT14	26.7	28.5	1.86	5.16	0.30
+5 Yr	16.3	19.2	0.79	2.6	0.16
+10 Yr	12.8	11.5	0.74	2.1	0.11

4 Future Networks

Given the recent progress in the construction of new VLBI antennas, it is expected that in the +5 year to +10 year time frames, the number of stations in the global broadband network will grow to 17-27 stations. We envision that these broadband networks will operate continuously, making them the natural extension of the

CONT 2-week observing sessions. To investigate their performance, simulations were run for these networks, where it is assumed that all antennas have broadband (2-14 GHz receivers). There are several different manufacturers of the antennas that have been constructed thusfar, but the main differences that affect scheduling of observations are the slew rates of the antennas. All of the antennas have significantly faster slew rates than the average slew rates of current (legacy) X/S radio telescopes, which have an average azimuth slew rate of about 1.3 deg/sec. The new antennas have either slew rates of 12 deg/sec (in azimuth) and 6 deg/sec (in elevation) or 5–6 deg/sec (in azimuth) and 1–2 deg/sec (in elevation). Fig. 6 shows the locations of the projected broadband network in 5 years and 10 years. The global coverage is significantly improved in the +10 year network with the addition of sites in South America, Africa, and Tahiti.

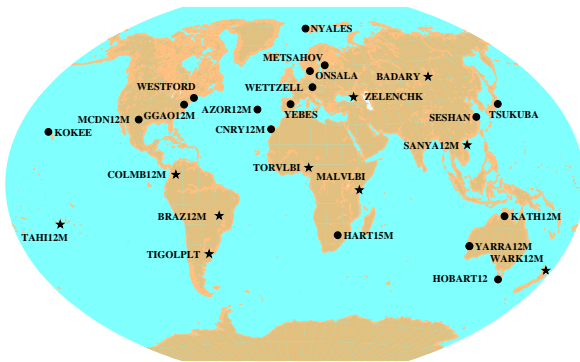


Fig. 6 Global distribution of future broadband stations. Stations expected in 5 years are indicated by solid black circles and in 10 years by black stars.

Tab. 2 summarizes statistics of the observing sessions ranging from current operational networks to the future envisioned networks. Progressing from the CONT networks to the future network (+5 years), it is clear that the faster antennas allow each antenna to make about four times as many scans/hour with the same number of antennas in the network. The number of observations increases by a factor of six. Going to the larger 27 site network in +10 years increases the number of network observations by about a factor of two due to the increase in the number of baselines.

We have performed simulations of different networks to assess the expected improvement with the future networks. Simulations were run for the CONT11 and CONT14 sessions in addition to simulations for the +5 year and +10 year networks. From these simulations the precision of EOP and scale were derived. Tab. 3 summarizes the results of the Monte Carlo simulations, showing the evolution of EOP and scale precision with the different networks. EOP and scale precision improves by a factor of 2-3 going from CONT14 to the +10 year network. Since the CONT14 simulated EOP and scale precision is about a factor of 1.4 larger than the observed precision, one could be more optimistic about the future expected precision by about 40 %.

5 Conclusions

We have seen the clear improvement of the CONT series as they have evolved since 2002. EOP and scale precision have improved by a factor of 2-3. The CONT11 and CONT14 EOP and scale precisions are more than twice as good as the precision of the weekly operational R1 and R4 network sessions. Given the predominance of GNSS precision in combination solutions like ITRF2008, it is striking that CONT11 and CONT14 polar motion precision is at the level of GNSS (based on IGS finals). The future implementation of the CONT campaign model is continuous VGOS network observing. Simulations of the expected +10 year networks yield EOP precision of $9 \mu\text{s}$ in polar motion, $0.5 \mu\text{s}$ for UT1, and 0.08 ppb for scale.

References

- Altamimi Z, Collilieux X, Metivier L (2011) ITRF2008: an improved solution of the international terrestrial reference frame. *J Geod*, 85, 457–473, doi: 10.1007/s00190-11-0444-4.
- Boehm J, Werl B, Schuh H (2006) Troposphere mapping functions for GPS and very long baseline interferometry from European Centre for Medium-Range Weather Forecasts operational analysis data. *J Geophys Res*, 111, B02406, doi: 10.1029/2005JB003629.
- Calc/Solve. Mark-5 vlbi analysis software calc/solve. Web document <http://gemini.gsfc.nasa.gov/solve/>, July 2008.
- Ma C, Sauber J M, Bell L J, Clark T A, Gordon D, Himwich W E, Ryan J W (1990) Measurement of horizontal motions in Alaska using very long baseline interferometry observations. *J Geophys Res*, 95(B13), 21,991–22,011.
- Nothnagel A (2008) Conventions on thermal expansion modelling of radio telescopes for geodetic and astrometric VLBI. *J Geod*, 83, 787–792. doi: 10.1007/s00190-008-0284-z.
- Petit G, Luzum B (eds.) (2010) IERS Conventions (2010). International Earth Rotation and Reference Systems Service (IERS). IERS Technical Note, No. 36, Frankfurt am Main, Germany: Verlag des Bundesamtes für Kartographie und Geodäsie, ISBN 978-3-89888-989-6, 179 pp.
- Petrov L, Boy J-P (2004) Study of the atmospheric pressure loading signal in very long baseline interferometry observations. *J Geophys Res (Solid Earth)*, 109:B03405, doi: 10.1029/2003JB002500.
- Ray J, Griffiths J (2012) High accuracy subdaily ERPs from the IGS. European Geophysical Union 2012, Session G5.1, Vienna.

Investigation of Earth Orientation Parameters for VLBA Calibrator Survey sessions

D. Mayer, J. Böhm, H. Krásná

Abstract About two thirds of the sources in the ICRF-2 catalog are estimated from VLBA Calibrator Survey (VCS) sessions. These sessions were carried out from 1994 to 2007 by a network of ten radio telescopes in North America with the densification of the celestial reference frame as the primary goal. A total of twenty-four VCS sessions, each with duration of 24 h, were observed in six campaigns. Coordinates estimated from these sessions have up to five times worse precision when compared to non-VCS sources from the ICRF catalog, which is to a great extent due to the limited number of observations. In the analysis of VCS sessions Earth Orientation Parameters (EOP) were estimated alongside source coordinates and other parameters. This, however, is not ideal, since the network is regional (only North American telescopes) and, therefore, not suitable for EOP estimation (EOP estimates w.r.t. IERS 08 C04 are up to 3 mas). We examine the effect of EOP estimation on source coordinates from VCS sessions and show that wrong EOP estimates generate systematic errors up to 1 mas. This is done by comparing solutions with EOP estimated in the analysis with solutions where EOP are fixed to IERS C04 08 combined series.

Keywords VLBA Calibrator Survey, Earth Orientation Parameters

1 Introduction

The ICRF2 (Ma et al., 2009) is to date the celestial catalog with the highest positional accuracy. It is derived from VLBI data up to early 2009 and consists of 3414 sources in total. The majority (2197) of the sources in the ICRF are observed by the so called VLBA Calibrator Survey (VCS) sessions. We will call sources observed only in these sessions VCS sources hereafter. The purpose of these sessions was to densify the consisting reference frame with as many sources as possible. Since observing time is limited these sources were only observed in a couple of, some

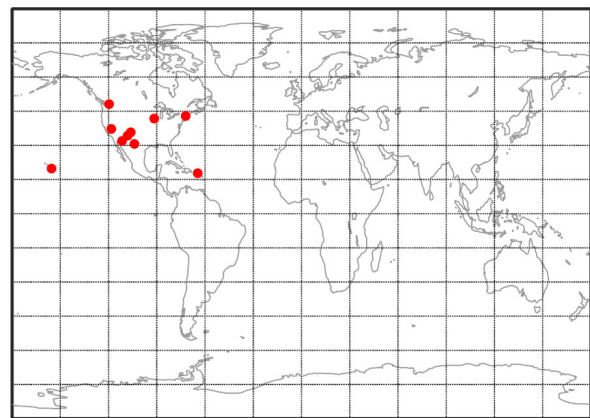


Fig. 1 Global distribution of the ten VLBA antennas.

only in one, sessions. This subsequently resulted in a low number of observations for these sources and, therefore, in lesser positional accuracy. Furthermore, the network used for the observations is the VLBA, see Fig. 1 for a plot of the station distribution. This network consists of ten stations across North America and is, therefore, regional in a global sense.

The VCS sessions (23 in total) were separated into 6 campaigns, named VCS1 - VCS6 (Beasley et al., 2002; Petrov et al., 2003, 2005, 2006; Kovalev et al., 2007; Petrov et al., 2008), which took place from 1994 to 2007. However, recently (from end of 2014 until beginning of 2015) a second VCS campaign was conducted, the VCSII. The main aim of these new sessions was to observe the VCS sources again and increase their accuracy. However, this investigation concentrates on the old VCS sessions. No results from the new sessions are presented here.

2 Scheduling of the VCS sessions

In this section we will discuss the different scheduling techniques used for the VCS sessions. Scheduling a VCS session is a complicated task. On the one hand, as many sources as possible

David Mayer, J. Böhm und H. Krásná
Technische Universität Wien, Department für Geodäsie und
Geoinformation, Gußhausstraße 27-29, A-1040 Wien, Austria

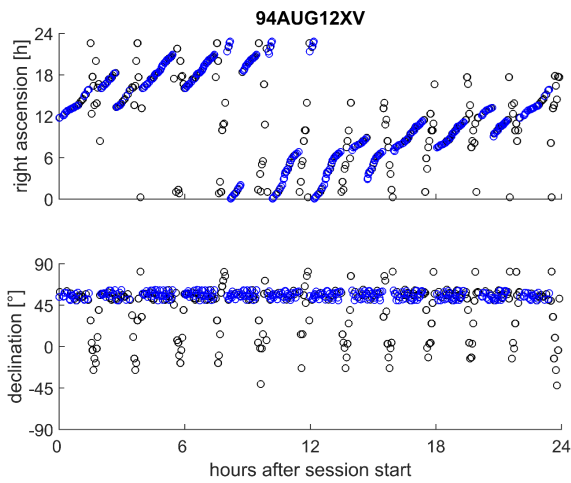


Fig. 2 Declination and right ascension of sources used in a typical schedule of the VCS1 sessions plotted from beginning to end of the session.

should be observed in one session, because observing time is a scarce resource. On the other hand, a good geodetic solution should be obtained in order to ensure high quality source coordinates. The problem with a geodetic solution is that many observations in different directions are needed to separate the height of the stations, clock and troposphere parameters. Therefore, a lot of time is spent on slewing. This is especially critical with the VLBA, since its telescopes have a very slow slew rate. Subsequently a compromise has to be found which provides as many observations as possible while still producing a good geodetic solution. The VCS sessions were scheduled using three different techniques.

In the first VCS sessions (VCS1) sources with a similar declination were observed on a meridian stripe, see Fig. 2 for an illustration of the schedule. This scheme was interrupted every 2 hours to observe non-VCS sources spread over right ascension and declination. This was done to ensure a good sky coverage and to observe sources which were later used to link the VCS sources to the ICRF.

For the VCS2 - VCS6 sessions the scheduling strategy was changed, see Figure 3 for an illustration of the schedule. The sources were also observed on a constant meridian but this time the declination was spread out over the whole observable sky (in this case up to approximately -45° declination). Another difference to the VCS1 schedule is that the non-VCS sources (for linking the catalog to the ICRF) are included in the general strategy.

The recent VCS sessions (VCSII) are scheduled in a similar manner as the VCS2 - VCS6 sessions with the difference that sources are observed in clusters in order to keep the time a telescope slews to a minimum. Figure 4 illustrates the schedule.

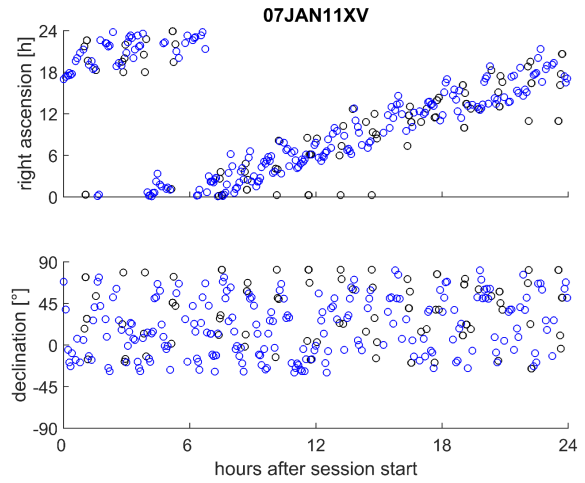


Fig. 3 Declination and right ascension of sources used in a typical schedule of the VCS2 - VCS6 sessions plotted from beginning to end of the session.

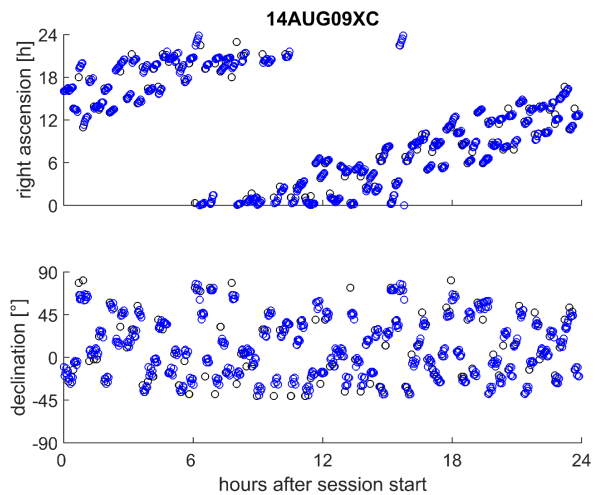


Fig. 4 Declination and right ascension of sources used in a typical schedule of the VCSII sessions plotted from beginning to end of the session.. (courtesy of David Gordon)

3 Estimating EOP from VCS sessions

When the ICRF2 was generated standard geodetic parameters, such as ZWD, clock parameters, EOP etc., were estimated alongside source coordinates. However, the quality of EOP is highly dependent on the size of the VLBI network. Therefore, EOP estimates of regional networks, such as the VLBA, are of questionable accuracy. Figure 5 depicts a series (all 23 VCS sessions in chronological order) of EOP estimates and formal errors w.r.t. the C04 08 time series (Bizouard et al., 2009; Gambis, 2004) which was used as a priori values. One can see that the estimates

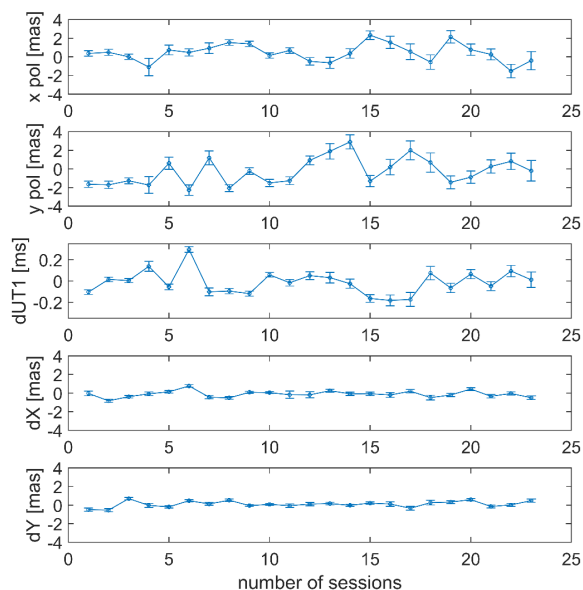


Fig. 5 EOP estimates and formal errors from 23 VCS sessions.

Table 1 RMS of the EOP estimates w.r.t. the C04 08 time series.

EOP	RMS
x-pole	0.95 mas
y-pole	1.31 mas
dUT1	0.11 ms
dX	0.34 mas
dY	0.31 mas

get quite large (up to 3mas) at some of the sessions. RMS values for each EOP are provided in Table 1. The C04 08 is the most accurate EOP time series available, it includes polar motion data from GNSS observations.

4 Estimating source coordinates from VCS sessions

We estimated source coordinates from the 23 VCS sessions with a general geodetic parametrization:

- Station coordinates (NNR + NNT w.r.t. VTRF2008) (Böckmann et al. (2010))
- Source coordinates (NNR w.r.t. ICRF2 non-VCS sources)
- Troposphere (ZWD + gradients)
- Clock parameters
- EOP offsets

A second analysis was conducted as well, with the difference that EOP were fixed to the a priori C04 08 values. The difference in source position from both analysis strategies for the session 06DEC18XV is depicted in Figure 6. One can see a clear

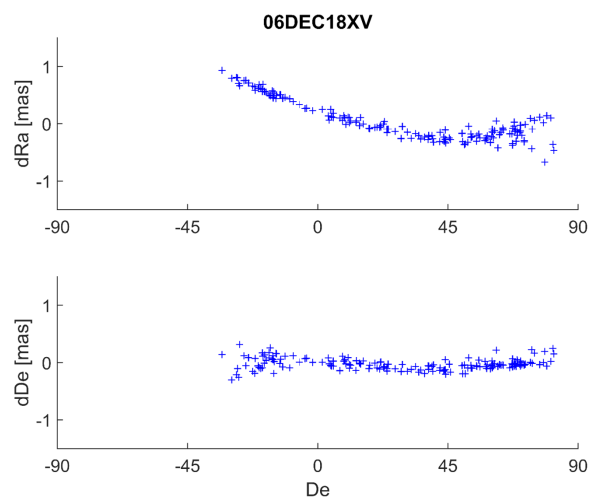


Fig. 6 Difference in source position from two analysis strategies estimated from session 06DEC18XV.

systematic effect which reaches up to 1 mas. This indicates that systematic errors might mitigate into the source coordinates.

4.1 Using different a priori EOP

Since the C04 08 EOP time series is estimated with data from different space geodetic techniques the estimates from VLBI might be a little larger due to technique dependent systematic. In order to investigate the magnitude of this effect we generated our own a priori EOP time series using interpolated EOP values from IVS-R1 and IVS-R4 sessions. These sessions were chosen because they are used to estimate EOP twice a week and are, therefore, perfectly suitable for the task. Figure 7 illustrates the interpolation for two (x-pole and y-pole) of the five EOP, with the IVS-R1 and IVS-R4 sessions being marked as 'R1' and 'R4' and the dots in between being the interpolated EOP values per day. For comparative reasons the C04 08 values (crosses) are also plotted.

In order to test the new a priori values the session 05JUN30XV was analyzed in a similar manner to Section 4. Once the interpolated a priori EOP values were used and once the C04 08 a priori EOP values were used. The comparison can be seen in Figure 8. On the left side the general approach with the C04 08 a priori EOP values is depicted. The systematics, here up to 1.8 mas, are clearly visible. The plot on the right side depicts the approach where a priori EOP values from IVS-R1 and IVS-R4 sessions were used. One can see that the systematic effect is reduced. However, the systematic effects do not disappear.

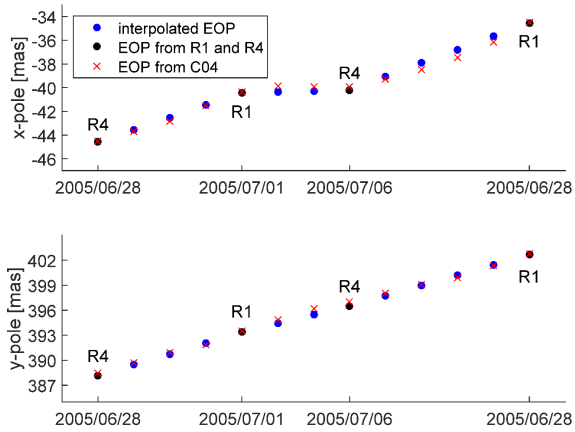


Fig. 7 Interpolation of EOP between solutions of IVS-R1 and IVS-R4 sessions.

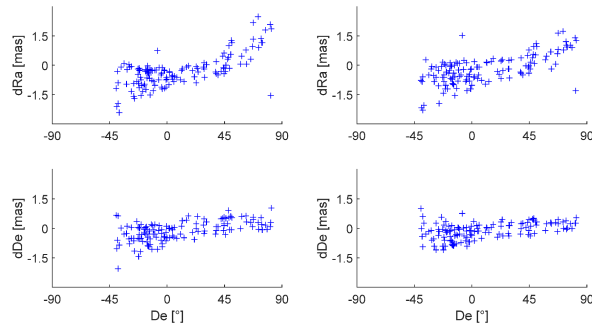


Fig. 8 Comparison of solutions with different a priori EOP. On the left the C04 05 time series was used as a priori and on the right the interpolates EOP from IVS-R1 and IVS-R4 sessions were used.

5 Difference in arc-length

In order to test if the systematic errors affect the relative position of sources, the difference in arc-length for each source with each other source was calculated for session 07JAN11XV, the result is illustrated in Figure 9. One can see that the distribution of differences is random. We can conclude that the errors are resulting in a rotation of the whole frame and have, therefore, no systematic effect on relative source position.

6 Conclusion

The VCS sources are observed by the VLBA network, which is located in North America, in only a couple of sessions. This network is not global but regional and, therefore, not suitable for high accuracy EOP estimation.

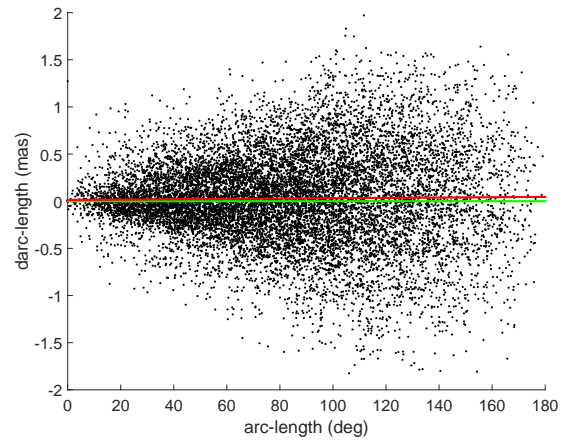


Fig. 9 Difference in arc-length of sources estimated from session 07JAN11XV.

When estimating EOP with these sessions, the offsets are larger than expected (up to approx. 3 mas). This offset is higher than one would expect for a precise a priori EOP time series such as C04 08 and is, therefore, an indication that the estimation process should be revised.

Systematic effects (up to 1 mas) can be found when comparing the source coordinates from a normal geodetic solution (estimated are: station coordinates, source coordinates, EOP, troposphere and clock parameters) to a geodetic solution where the EOP are fixed to the a priori values. Using EOP time series which are derived from VLBI observations only (EOP estimated from IVS-R1 and IVS-R4 sessions) as a priori values reduces the effect, but doesn't eliminate it. Since the arc-length is not affected systematically we can assume that the effect resembles a rotation of the whole frame which would leave the relative source position in tact.

References

- Beasley A J, Gordon D, Peck A B, Petrov L, MacMillan D S, Fomalont E B, Ma C (2002) The VLBA Calibrator Survey-VCS1. *Astrophys J Suppl*, 141, 13–21, doi: 10.1086/339806.
- Bizouard C, Gambis D (2009) The Combined Solution C04 for Earth Orientation Parameters Consistent with International Terrestrial Reference Frame 2005. In: H. Drewes (ed.) *Proc. IAG Symposium 2006*, IAG Symposia Series 134, 265–270, doi: 10.1007/978-3-642-00860-3_41.
- Böckmann S, Artz T, Nothnagel A (2010) VLBI terrestrial reference frame contributions to ITRF2008. *J Geod*, 84, 201–219, doi: 10.1007/s00190-009-0357-7.
- Fomalont E B, Petrov L, MacMillan D S, Gordon D, Ma C (2003) The Second VLBA Calibrator Survey: VCS2. *Astron J*, 126, 2562–2566, doi: 10.1086/378712.

- Gambis D (2004) Monitoring Earth orientation using space-geodetic techniques: state-of-the-art and prospective. *J Geod*, 78, 295–303, doi: 10.1007/s00190-004-0394-1.
- Kovalev Y Y, Petrov L, Fomalont E B, Gordon D (2007) The Fifth VLBA Calibrator Survey: VCS5. *Astron J*, 133, 1236–1242, doi: 10.1086/511157.
- Ma C, Arias E, Bianco G, Boboltz D, Bolotin S, Charlot P, Fey A, Gaume R, Gontier A, Heinkelmann R, Jacobs C, Kurdubov S, Lambert S, Malkin Z, Nothnagel A, Petrov L, Skurikhina E, Sokolova J, Souchay J, Titov O, Zharov V (2009) The Second Realization of the International Celestial Reference Frame by Very Long Baseline Interferometry. In: A. L. Fey, D. Gordon, C. S. Jacobs (eds.), *IERS Technical Note 35*, 1–204.
- Petrov L, Kovalev Y Y, Fomalont E, Gordon D (2005) The Third VLBA Calibrator Survey: VCS3. *Astron J*, 129, 1163–1170, doi: 10.1086/426920.
- Petrov L, Kovalev Y Y, Fomalont E B, Gordon D (2006) The Fourth VLBA Calibrator Survey: VCS4. *Astron J*, 131, 1872–1879, doi: 10.1086/499947.
- Petrov L, Kovalev Y Y, Fomalont E B, Gordon D (2008) The Sixth VLBA Calibrator Survey: VCS6. *Astron J*, 136, 580–585, doi: 10.1088/0004-6256/136/2/580.

Revisiting the VLBA Calibrator Surveys, VCS-II

D. Gordon

Abstract The 3414 sources in ICRF2 were divided into two categories, multi-epoch sources and 'VCS-only' sources. The 'VCS-only' group comprised $\sim 2/3$ of the sources, but their average formal errors were ~ 5 times greater than the other $1/3$. In order to reduce this two class distinction for the upcoming ICRF3, a second epoch VCS campaign was undertaken in 2014-2015 and most of these sources were re-observed. Very significant improvements are seen for 2063 re-observed sources and a large number of 'new' sources were also added to the S/X catalog.

Keywords VLBA Calibrator Surveys, ICRF2, ICRF3

1 Introduction

The original VLBA Calibrator Surveys (VCS) were a series of six VLBI campaigns at S/X bands made between 1994 and 2007 in order to compile a large list of compact radio sources with precise positions for use in phase-referencing VLBI [Beasley et al. (2002); Fomalont et al. (2003); Petrov et al. (2005, 2006, 2008); Kovalev et al. (2007)]. Approximately 2500 such sources were detected in the 24 individual 24-hr sessions. The precision goals were ~ 1 milli-arc-sec (mas) or better for their positions, something that could be accomplished for most of them with single epoch observations. The calibrator lists which resulted greatly enhanced the ability to do precise mapping and astrometry on the VLBA and other VLBI arrays.

In 2009, the VCS data, along with nearly 30 years of geodetic VLBI data, was used to construct the second revision of the International Celestial Reference Frame, ICRF2 [Fey et al. (2009, 2015)]. Use of the VCS data greatly expanded ICRF2, supplying $\sim 2/3$ of the 3414 sources. The downside was that the average position uncertainties of those $2/3$ were ~ 5 times larger than the other $1/3$. Some of these 'VCS-only' sources were re-observed in RDV sessions in the few years after ICRF2, but most remained single epoch sources. Therefore, it was decided to re-observe these sources for the upcoming ICRF3. A 'VCS-

II' team was formed and 8 days of observing time on the VLBA was requested, and later granted. Members of the VCS-II team are: D. Gordon/PI, C. Jacobs (JPL), A. Beasley (NRAO), A. Peck (NRAO/ALMA), R. Gaume (NSF), A. Fey (USNO), C. Ma (GSFC), O. Titov (Geosciences Australia), D. Boboltz (NSF), and P. Charlot (Bordeaux Observatory).

2 The VCS-II Sources

To compile the source list, we extracted all sources between $+90^\circ$ and -50° declination that were observed in only 1 or 2 sessions during the VCS1-6 period (1994-2007) and not re-observed after ICRF2. Approximately 2065 sources were obtained. The VLBA is much more sensitive now than during the VCS1-6 campaigns and we believed we could observe up to 300 sources in each of the 8 sessions, provided slewing times were kept to a reasonably small fraction of the total time. Therefore an additional ~ 335 sources were extracted from the list of sources observed but not detected in the original VCS1-6 analysis, for a total of 2400 sources. The sources were then divided into narrow declination zones and sorted by increasing RA. The zones were then split into 400 groups of 6 nearby sources, all within ~ 10 - 20° of each other. For each of the 8 24-hr sessions, 50 of these groups were picked, spread fairly evenly about the sky. The scheduling philosophy was to observe a troposphere/ICRF2 calibrator, then observe the 6 nearby sources in one of the 50 groups, then repeat with another calibrator and another group, etc. Slewing times between sources in a group were typically 10-20 seconds (as opposed to ~ 1 -2 minutes between sources in regular geodetic sessions). Thus we were able to make ~ 30 scans/hr and the observing time was ~ 65 - 70% of the total time.

3 The VCS-II Observations

The dual S/X VLBA system was used for consistency with the earlier VCS1-6 sessions and ICRF2 in general. We used the VLBA's new RDBE/Mark5C system which has 16 32-MHz

David Gordon
NVI Inc./GSFC, Greenbelt, Maryland, USA

channels and records at 2 Gbits/sec using 2-bit sampling. By contrast, most of the VCS1-6 sessions used 128 Mbits/sec with 1-bit sampling. Twelve of the 16 channels were used at X-band and 4 were used at S-band. Filters and RFI at S-band prevented using more channels there.

Schedules were made using the NRAO *SCHED* program. Each source was observed in two scans, several hours apart. Integration times were between 60 and 126 seconds for the target VCS-II sources. The troposphere calibrator scans were typically 20-30 seconds long. The schedules were made in the dynamic mode, which allowed them to be run at any time. The project was designated BG219. The sessions, observation times, and number of observations used are listed in Table 1.

Table 1 The VCS-II Sessions.

Session	Time Range	# Obs
VCS-II-A/BG219A	2014 01/04 10:04 - 01/05 10:02	9288
VCS-II-B/BG219B1	2014 05/31 17:12 - 06/01 17:05	25861
VCS-II-D/BG219D	2014 06/09 09:13 - 06/10 09:10	24955
VCS-II-C/BG219C	2014 08/05 13:03 - 08/06 13:00	23740
VCS-II-E/BG219E	2014 08/09 00:00 - 08/09 23:55	22920
VCS-II-F/BG219F	2014 12/20 01:18 - 12/21 01:14	27207
VCS-II-H/BG219H	2015 01/23 23:00 - 01/24 22:55	23355
VCS-II-I/BG219I	2015 03/17 07:57 - 03/18 07:57	25637

4 Data Processing

The VCS-II data was correlated using the VLBA's implementation of the *difx* software correlator [Deller et al. (2011)] at the NRAO Array Operations Center (AOC) in Socorro, New Mexico. The correlator output was converted to both FITS IDI format (using *difx2fits*) and Mark4 format (using *difx2mark4*). The Mark4 files were fringed with *hopsfourfit* in the usual manner. Geodetic style databases were then made and analyzed with the *Calc/Solve* system. The analyzed sessions were then included in large least squares *Solve* solutions using all the available Mk3 databases.

5 Results

For comparison, large global solutions were run with and without the 8 VCS-II sessions. The results for the 2400 VCS-II sources were then compared. A total of 2063 single epoch sources were re-observed. The average (unscaled) formal errors without the VCS-II sessions were 0.84 and 1.44 mas in RA and Dec. With the VCS-II sessions, the average formal errors drop to .22 and .38 mas, an improvement of 3.8 and 3.7 times. Also, 325 'new' sources were detected and added to the S/X catalog, with average formal errors of 1.2 and 2.0 mas in RA and Dec. These 'new'

sources are predominantly weaker and observed in only one session, and thus have larger formal errors. Only 12 sources were not detected, which is a failure rate of only 0.5%. Fluxes have also been calculated for these sources. The flux limit for these sessions appears to be ~15 mJy in X-band and ~28 mJy in S-band. Imaging of the sources is also being performed using the FITS IDI files, and the images will be used to compute structure indices.

6 Acknowledgements

The VLBA is operated by the National Radio Astronomy Observatory, which is a facility of the National Science Foundation, and operated under cooperative agreement by Associated Universities, Inc. This work made use of the Swinburne University of Technology software correlator, *difx*, developed as part of the Australian Major National Research Facilities Programme and operated under license. For a description of the *difx* correlator, see Deller et al. (2011).

References

- Beasley A J, Gordon D, Peck A B, Petrov L, McMillan D S, Fomalont E B, Ma C (2002) The VLBA Calibrator Survey - VCS1. *Ap J Supp*, 141, 13–21.
- Deller A T, Brisken W F, Phillips C J, Morgan J, Alef W, Cappallo R, Middelberg E, Romney J, Rottmann H, Tingay S J, Wayth R (2011) DiFX-2: A More Flexible, Efficient, Robust, and Powerful Software Correlator. *Pub Astron Soc Pac*, 123, 275–287, <http://www.jstor.org/stable/10.1086/658907>.
- Fey A, Gordon D, Jacobs C (eds.) (2009) The Second Realization of the International Celestial Reference Frame by Very Long Baseline Interferometry. *IERS Technical Note No. 35*, <http://www.iers.org/TN35>.
- Fey A L, Gordon D, Jacobs C S, Ma C, Gaume R A, Arias E F, Bianco G, Boboltz D A, Böckmann S, Bolotin S, Charlot P, Collioud A, Engelhardt G, Gipson J, Gontier A-M, Heinkelmann R, Kurdubov S, Lambert S, Lytvyn S, MacMillan D S, Malkin Z, Nothnagel A, Ojha R, Skurikhina E, Sokolova J, Sposchay J, Sovers O J, Tesmer V, Titov O, Wang G, Zharov V (2015) The Second Realization of the International Celestial Reference Frame by Very Long Baseline Interferometry. *Astron J*, 150, 58–73, doi: 10.1088/0004-6256/150/58.
- Fomalont E B, Petrov L, MacMillan D S, Gordon D, Ma C (2003) The Second VLBA Calibrator Survey: VCS2. *Astron J*, 126, 2562–2566, doi: 10.1086/378712.
- Kovalev Y Y, Petrov L, Fomalont E B, Gordon D (2007) The Fifth VLBA Calibrator Survey: VCS5. *Astron J*, 133, 1236–1242, doi: 10.1086/511157.

-
- Petrov L, Kovalev Y Y, Fomalont E, Gordon D (2005) The Third VLBA Calibrator Survey: VCS3. *Astron J*, 129, 1163–1170, doi: 10.1086/426920.
- Petrov L, Kovalev Y Y, Fomalont E B, Gordon D (2006) The Fourth VLBA Calibrator Survey: VCS4. *Astron J*, 131, 1872–1879, doi: 10.1086/499947.
- Petrov L, Kovalev Y Y, Fomalont E B, Gordon D (2008) The Sixth VLBA Calibrator Survey: VCS6. *Astron J*, 136, 580–585, doi: 10.1088/0004-6256/136/2/580.

Assessment of CRF Solutions from Session-wise Normal Equation Systems

A. Iddink, T. Artz, S. Halsig, A. Nothnagel

Abstract The International Celestial Reference Frame (ICRF) is one of the fundamental products of the International VLBI Service for Geodesy and Astrometry (IVS). Until now, two realizations were computed and the next one is under construction. Today, most of the IVS analysis centers routinely produce solutions as session-wise normal equation systems also including radio source positions. For this reason, a rigorous combination using datum-free normal equation systems is also feasible for the upcoming realization of the International Celestial Reference Frame 3 (ICRF3). However, various peculiarities have to be considered for the generation of a combined CRF. As a first step towards such a combined CRF, we focus on the achievable level of agreement by using data from a single analysis center. A source catalogue based on the official SINEX files submitted to the IVS is compared and validated to the source catalogue of a official global solution. We present our approach of stacking several thousand of datum-free normal equation systems in such a way, to be as similar as possible to the reference solution setup.

Keywords VLBI, ICRF3, Session-wise combination, Normal equation stacking

1 Introduction

Very Long Baseline Interferometry (VLBI) is the unique existing geodetic space technique for the generation of the International Celestial Reference Frame (ICRF), one of the fundamental products of the International VLBI Service for Geodesy and Astrometry (IVS, e.g. Schuh and Behrend (2012)). Until now, two realizations of the International Celestial Reference System (ICRS) were computed and the next one is under construction. The latest realization, the ICRF2 (IERS, 2009), consists of precise positions of 3414 sources, including 295 defining sources. Furthermore, 2197 out of the 3414 sources were observed only

Andreas Iddink, Thomas Artz, Sebastian Halsig, Axel Nothnagel

Rheinische Friedrich-Wilhelms Universität Bonn, IGG, Nußallee 17, D-53115 Bonn, Germany

in VLBA Calibrator Survey (VCS, e.g. Beasley et al. (2002)) sessions, which are special astrometric survey campaigns, optimized to observe a huge number of new radio sources. Both previous realizations were computed by a single analysis center, the VLBI group at the NASA Goddard Space Flight Center (GSFC), using a single software package.

While the benefit of the intra-technique combination of various analysis centers on the Terrestrial Reference Frame (TRF) and Earth Orientation Parameters (EOPs) is well known (Böckmann et al., 2010) and utilized for the official IVS products since many years, only comparisons between source catalogues of different analysis centers were made for the computation of the ICRF2. Due to the fact that today most of the IVS analysis centers routinely produce contributions containing radio source positions, an intra-technique combination is likewise feasible for the generation of a CRF. For this reason, a rigorous combination procedure for CRF determinations has been proposed in Iddink et al. (2014, 2015).

The developed approach is based on the combination at the level of datum-free normal equation systems (NEQs), which enables the rigorous transfer of the full variance-covariance information of all individual input contributions and all related parameters. Since high precision geodetic VLBI started operating in 1979 over 5000 sessions were observed and analysed by several analysis centers. These sessions are freely available on the server of the IVS and can be used for the combination on a session-by-session level. Furthermore, based on these NEQs generated by different analysis centers, individual CRFs can be computed and finally assessed.

Additionally to the single sessions provided in the Solution Independent Exchange Format (SINEX), analysis centers regularly provide global solutions, containing source positions in form of source catalogues, station coordinates and time series of EOPs. In general these results are supplied by the analysis centers and are freely accessible. An example for such a global solution is the latest gsf2014a solution. This leads to the opportunity to compare the individual CRFs, based on the session-wise NEQs, to the official source catalogue from the global solution, provided by the analysis centers. These comparisons are an essential step towards a reliable combined CRF based on contributions from different analysis centers. Furthermore, comparisons among the individual CRFs and to the official ICRF2 will help to

identify blunders while further investigations will help to distinguish systematics from stochastic deviations.

In this paper we focus on the level of agreement by using data from GSFC. Based on the achieved results further investigations can be performed by focussing on the combination of contributions from different analysis centers. For our first tests, we currently selected the data from GSFC because this analysis center computed the last two realizations of the ICRS and will be one of the major players for the realization of the upcoming ICRF3.

2 Methodology

In order to calculate a reliably combined CRF one initial aspect is to study the achievable level of agreement between the official SINEX files submitted to the IVS and the official global solution, in our case provided by GSFC. A sufficient level of agreement between these two different solution procedures is a mandatory prerequisite to move forward with investigations concerning the combination of contributions from different analysis centers.

In general the official contributions to the IVS combination centre relies on several thousand datum-free single session NEQ systems. By stacking these datum-free NEQs, we are able to generate one monolithic datum-free NEQ, containing CRF, TRF and all corresponding EOPs. In order to solve this monolithic datum-free system the rank deficiency needs to be eliminated by applying conditions to TRF and CRF. Finally, after solving the system, we obtain the individual CRF which can be compared to the CRF from the official global solution by means of Helmert transformation.

The monolithic datum-free NEQ system based on stacked NEQs need to be set up as similar as possible in comparison to the official solution from GSFC. Based on the information given from the latest solution gsf2014a, the stacking algorithm and solution setup need to be adjusted. The latest global solution gsf2014a is based on 5425 independent sessions. Not all of these sessions are available in the SINEX format on the official IVS data server. Hence, only 5276 sessions could be used and stacked together. In our first initial tests we weighted all sessions equally.

Before stacking on a session-by-session level, the parameterization of each session need to be adjusted. Stacking all these parameters, especially the EOPs, to one big monolithic NEQ system, leads to a huge system with thousands of parameters. This is due to the fact that EOPs need to be set up as local parameters and cannot be stacked together like station coordinates and source positions for a long period of time. In order to keep the system easily processable and to avoid such a big system, EOPs need to be reduced before stacking. Furthermore, based on information given from the gsf2014a solution, in some sessions the EOPs need to be fixed to their aprioris due to unsuitable network configurations. Reducing the EOPs leads to the circumstance that the EOPs are not explicitly estimable anymore. Due to the fact that we are currently focussing on CRF assessments we neglect this disadvantage.

The estimation of source positions in the latest solution gsf2014a was done in a manner similar to the generation of the ICRF2. This solution contains positions of 39 ICRF2 special handling sources, estimated as local parameter in each session individually. The positions of the remaining 1670 sources were estimated as global parameters. In order to keep the dimensions of our monolithic system as small as possible, we reduce the positions of the special handling sources in contrast to the official solution. All the other sources are set up as global parameters, stacked session-by-session. Hence, our upcoming CRF assessment will be based only on comparisons between the global estimated source positions.

As the station coordinates are not in focus of this paper, we just set up a single set of station coordinates for each site covering the whole time period, neglecting a parameterization of the site velocity and discontinuities. This simplification does not affect the estimation of the CRF. Finally we obtain a datum-free monolithic NEQ system only containing TRF and CRF components explicitly.

Stacking thousands of NEQ systems can lead to numerical issues due to inadequate units of different parameter groups. To avoid such effects we scaled the source parameters, which are typically parameterized in radian, to μs . Without scaling the systems, we were not able to solve the monolithic ill-conditioned system.

In the next step, in order to be able to solve the system we need to apply a datum to TRF and CRF. Considering the goal to be as similar as possible to the latest global solution gsf2014a we follow their datum definitions. The TRF is defined in such a manner that the positions of a subset of 33 strong stations have no net translation or rotation with respect to their positions reported in the ITRF2008 (Altamimi et al., 2011). The CRF is defined in such a way that the positions of the 295 ICRF2 defining sources do not have any net rotation with respect to their coordinates reported in ICRF2. Because all used NEQ systems are based on the same a priori, we do not need to perform any a priori transformations.

After applying conditions to the monolithic system we are able to solve the system and finally obtain an estimated source catalogue. As a next step, this catalogue need to be compared to the official catalogue of the latest gsf2014a solution.

3 Results and Catalogue Comparison

Our estimated catalogue illustrated in Fig. 1 contains 1691 global source positions. As might be expected, the sources in the southern sky are weaker and have a higher standard deviation in declination. The standard deviation in right ascension looks similar to Fig. 1 and is not illustrated explicitly. Despite all efforts, the number of estimated sources does not fit with the latest gsf2014a solution. This might be due to naming convention issues. It seems so far, that the used stacking procedure computes reliable and comprehensible results which can be used for further assessments.

In order to assess the level of agreement between both catalogues, we need to take a look at the residuals.

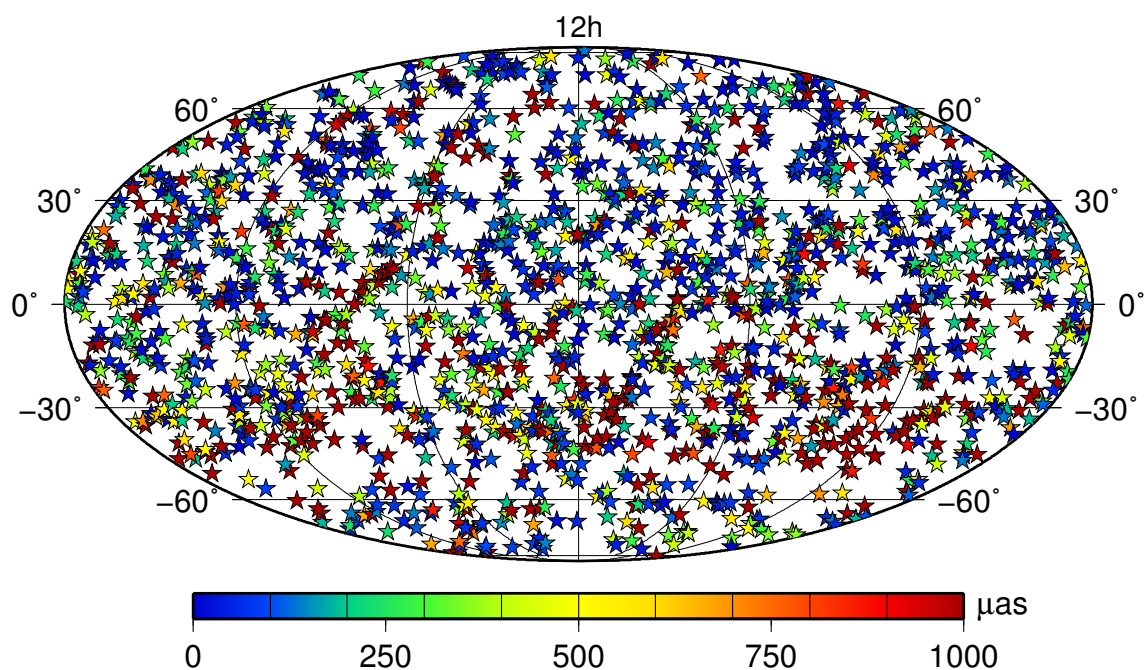


Fig. 1 Generated catalogue based on daily datum-free GSFC SINEX files. The colorbar illustrates the standard deviation in declination.

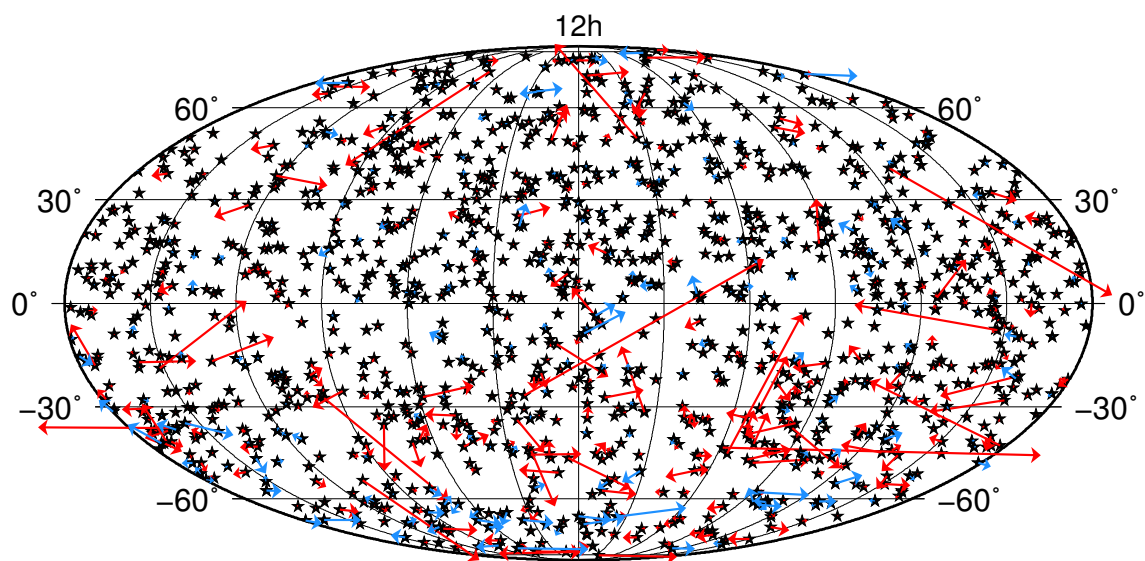


Fig. 2 Residuals between stacked solution and GSFC catalogue after transformation. Blue arrows indicate residuals of the defining sources while red arrows indicate non-defining sources. 1 cm arrow is equal to 1 mas.

For that reason we need to estimate the three rotation angles between both catalogues by means of Helmert transformation. The transformation is based on the 295 ICRF2 defining sources and the results are shown in Tab. 1. In general, the estimated rotation angles and their standard deviations match the expect-

tations. After rotating the catalogues on each other, the residuals between corresponding sources can be computed and visualized. The results are shown in Fig. 2. The residuals of the defining sources are illustrated in blue while the residuals of the non-defining sources are shown in red. As already mentioned,

Table 1 Rotation angles and their standard deviations between stacked catalogue and official gsf2014a catalogue.

x [mas]	y [mas]	z [mas]
-0.005 ± 0.003	0.007 ± 0.003	0.002 ± 0.001

the stacked solution and hence the residual plot does not contain special handling sources due to performance reasons.

Assessing the residuals shown in Fig. 2 we can see that most of the sources have quite small residuals which are not visible at this scale. Nevertheless, there are also many sources with big and even huge residuals up to several mas. It is obvious that the residuals of the defining sources (blue) are principally smaller in comparison to the residuals of the non-defining sources (red).

Comparing the northern and southern sky we can notice that most of the bigger discrepancies are in the southern sky where the weaker sources are located. There are several aspects which might influence the differences between both catalogues. As already mentioned we used less sessions than used in the latest gsf2014a solution. Furthermore, all sources which did not have at least 3 good observations in a single session are not stored in the SINEX files we are using. This leads to hidden constraints and singularity inconsistencies in the NEQ systems. It also might be possible that position parameters of different sources have been stacked mistakenly together due to naming convention issues.

Before moving forward to comparisons between our generated catalogue and the ICRF2 we have to investigate the reasons for these discrepancies in detail.

4 Conclusions and Outlook

We have shown, that we are able to generate a CRF based on session-wise NEQs, using a configuration setup best possible aligned to the gsf2014a solution. About 5000 single SINEX files were used and stacked together. The resulting system contained 1691 global source positions including all 295 ICRF2 defining sources. In general, the small rotation angles between the catalogues indicate, that the resulting CRF is comparable to the CRF of the official global solution.

Nevertheless, the occurring discrepancies need to be investigated in future. In order to generate a reliable combined CRF, investigations concerning the features and properties of a CRF combined from several VLBI solutions have to be made. More individual CRFs based on session-wise SINEX files generated by other analysis centers are planned. These CRFs need to be compared among themselves and to the official ICRF2. Furthermore, the effect of the additional data, which became available after the ICRF2 was computed, have to be investigated as well.

References

- Altamimi Z, Collilieux X, Métivier L (2011) ITRF2008: an improved solution of the International Terrestrial Reference Frame. *J Geod*, 85(8), 457–473, doi: 10.1007/s00190-011-0444-4.
- Beasley A J, Gordon D, Peck A B, Petrov L, MacMillan D S, Fomalont E B, Ma C (2002) The VLBA Calibrator Survey-VCS1. *APJS*, 141, 13–21, doi: 10.1086/339806.
- Böckmann S, Artz T, Nothnagel A, Tesmer V (2010) International VLBI Service for Geodesy and Astrometry: Earth orientation parameter combination methodology and quality of the combined products. *J Geophys Res*, 115, B04404, doi: 10.1029/2009JB006465.
- Iddink A, Nothnagel A, Artz T (2014) Rigorous VLBI Intra-Technique Combination For Upcoming CRF Realizations. In *Proc. Journées 2013 Systèmes de référence spatio-temporels*, Paris, France.
- Iddink A, Artz T, Nothnagel A (2015) Development of a Combination Procedure for Celestial Reference Frame Determination. *IAG Scientific Assembly, Potsdam*, doi: 10.1007/1345-2015-22.
- IERS (2009) The second realization of the international celestial reference frame by very long baseline interferometry. In: A. L. Fey, D. Gordon, C. S. Jacobs (eds.), *IERS Technical Note 35*, presented on behalf of the IERS/IVS Working Group, Verlag des Bundesamtes für Geodäsie und Kartographie, Frankfurt am Main.
- Schuh H, Behrend D (2012) VLBI: A fascinating technique for geodesy and astrometry. *J Geodyn*, 61, 68–80, doi: 10.1016/j.jog.2012.07.007.

Comparison of VLBI nutation time series

C. Gattano, S. Lambert, C. Bizouard

Abstract We carried out comparisons between nutation time series made available by different analysis centers of the IVS. We characterize differences between series in terms of amplitude and phase of prominent free and forced nutation components, as well as noise color.

Keywords VLBI, nutation

1 Introduction

Very long baseline interferometry (VLBI) is the only technique that determines the Earth's nutation at sub milliarcsecond (mas) accuracy. After 35 years of observations and about two sessions per week, it allows to estimate nutation over periods from 14 days up to almost 20 years. The quality of nutation estimates is fundamental for further use in geophysics for, e.g., inferring Earth's interior parameters relevant to the mantle, the core, and the inner core (Mathews et al., 1991, 1995, 2002).

Several VLBI analysis centers of the International VLBI Service for Geodesy and Astrometry (IVS) (Schuh et al., 2012), make available nutation time series covering the last 35 years. Although based on the same, or at least partly the same, observational data set, these nutation series are not exactly the same. Significant divergences show up, that are likely due to the different analysis strategies used by the analysis center. We propose here to quantify the differences.

2 Data sets

We carried out a comparison of several nutation time series provided by different analysis centers of the IVS: Bundesamt für Kartographie und Geodäsie (BKG00014, Germany), God-

César Gattano, Sébastien Lambert and Christian Bizouard
SYRTE, Observatoire de Paris, PSL Research University, CNRS,
Sorbonne Universités, UPMC Univ. Paris 06, LNE, Paris, France

dard Space Flight Center (GSF2014A, USA), Institute of Applied Astronomy (IAA2007A, Russia), Observatoire de Paris (OPA2014A, France), U. S. Naval Observatory (USN2014A, USA), and the IVS combined time series (IVS14Q2X) which is computed with the transformed and weighted normal equations of several operational analysis center solutions (Böckmann et al., 2010)

Solution technical descriptions are summarized in Table 1 where we display the analysis options that are connected to nutations. Globally, all series are obtained by similar analysis strategies except for some steps concerning

- the status of radio sources (are their positions locally or globally estimated, fixed, constrained?),
- the wet zenith troposphere delay a priori at the observing elevation (mapping function),
- the wet zenith troposphere delay and gradient estimation strategy and interval
- the clock offset estimation strategy and interval.

Concerning the first item, several works reported a non negligible influence of the instability of the targeted radio sources in Earth orientation parameter estimates (Dehant et al., 2003; Feissel-Vernier, 2003; Feissel-Vernier et al., 2005; Feissel-Vernier et al., 2006; Lambert et al., 2008). The use of the ICRF1 (Ma et al. 1998) or its extension (Fey et al., 2004), which axes stability was estimated around 0.25 mas in place of the current ICRF2 (Fey et al., 2015) which is more stable by a factor of 5 could lead to detectable perturbations in the nutation time series. Concerning the VLBI analysis software package, four analysis centers out of five use CALC/SOLVE. The remaining center (IAA) uses OCCAM.

3 Analysis and results

Figure 1 displays differences of each time series with respect to the IVS combined series. For each graph, we plot error bars of both center's solution and IVS combined's solution (bottom plot). We use the IVS combined time series as references purely for sake of clarity. At no time, we consider the IVS combined time series better than the others. A drift appears on the IAA

Table 1 Analysis strategies of different analysis centers. NNR: no-net rotation applied to the defining sources; NL: 39 sources called “non linear” in Fey et al. (2015); LS: linear spline; Q: quadratic polynomial; VMF/NMF = Vienna (Böhm et al., 2006)/(Niell, 1996) mapping function.

	BKG	GSF	IAA	OPA	USN
CRF	a priori	ICRF2	ICRF2	ICRF1-Ext. 2	ICRF2
	NNR	ICRF2	ICRF2	ICRF1	ICRF2
	global/local	all/0	1670/NL	not estimated	all-NL/NL
Nutation/precession a priori					
	IAU2006/2000A	IAU2006/2000A	IAU2000A	IAU2006/2000A	IAU2006/2000A
IERS Conventions					
	2010	2010	2003	2010	2010
mapping					
	VMF	VMF	VMF	VMF	NMF
Troposphere					
ZTD	1 h LS	20 min LS	random walk	20 min LS	20 min LS
gradients					
	24 h offset	6 h linear spline	-	6 h offset	6 h linear spline
Clock interval					
	1 h LS	1 h Q	random walk	1 h Q	1 h Q
Elevation cutoff					
	5°	5°	quality flag	5°	5°
Software package					
	CALC/SOLVE	CALC/SOLVE	OCCAM	CALC/SOLVE	CALC/SOLVE

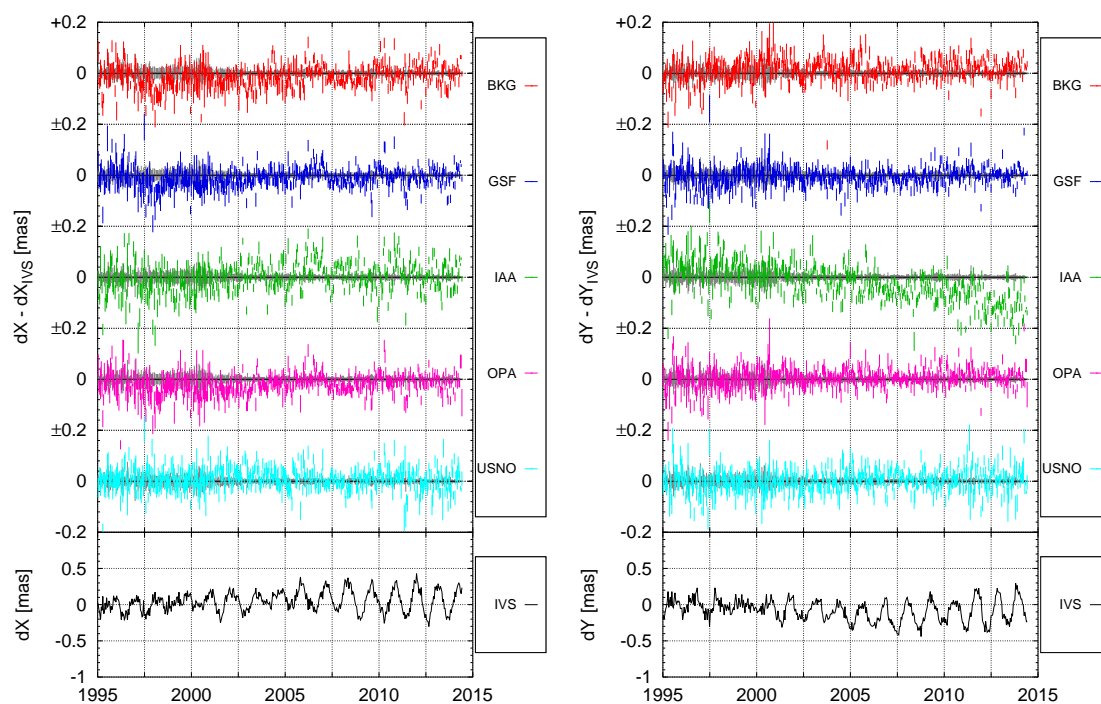


Fig. 1 Differences nutation time series with respect to the IVS combination. The reference IVS time series is shown on the bottom.

graph, likely due to the use of the IAU 2000 precession model as a priori precession, while other analysis centers used the IAU 2006 precession (Capitaine et al., 2005).

Even if, globally, time series are very similar at the level of 0.1 mas, we can see that they significantly diverge at some dates (in the sense that error bars do not account for the differences). Spectral analysis reveal that, from one solution to an-

other, the difference of amplitude for a given frequency do not exceed $10 \mu\text{s}$ for periods shorter than 2 years and $20 \mu\text{s}$ for longer periods. The free core nutation (FCN) and the annual retrograde nutation show small differences from one analysis center to another. In contrast, larger differences show up for larger periods, typically between 6 and 10 years.

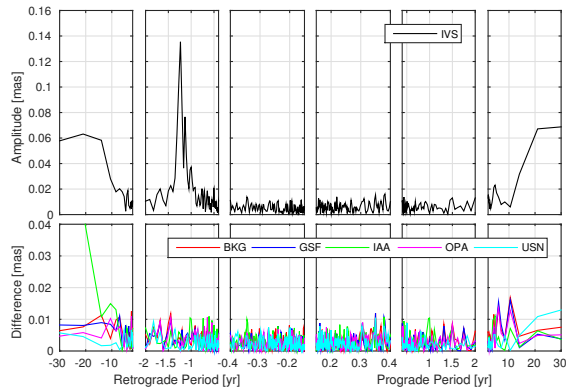


Fig. 2 Differences of analysis center nutation spectra with respect to the IVS.

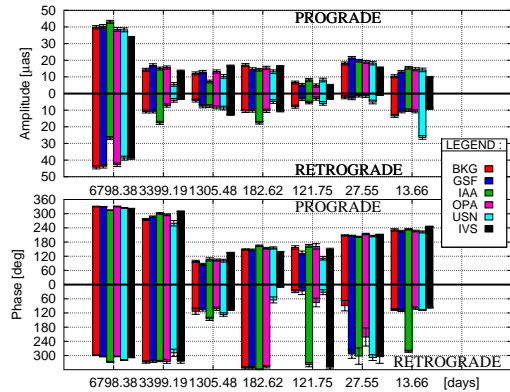


Fig. 4 Amplitude and phase of principal nutations.

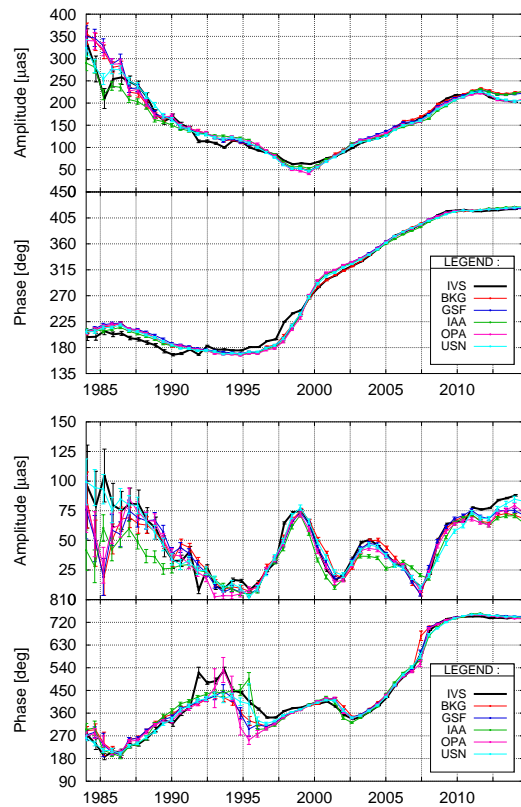


Fig. 3 Amplitude and phase of the free core nutation (FCN) and retrograde annual nutation.

Figure 3 displays the time-variable amplitude and phase of the FCN and the retrograde annual nutation, adjusted by least-squares every 0.6 years over a 7-yr sliding window. We can see that adjustments are consistent between different analysis centers at the order of $10 \mu\text{as}$. We also checked that the obtained FCN amplitudes were comparable with those raised by other filtering techniques based on least-squares, e.g. (Herring et al., 2002;

Vondrak et al., 2005; Krasna et al., 2013), wavelets (Malkin, 2004, 2014) or Pantelev filter (Zotov et al., 2015).

The IVS combination presents the largest deviation, for example between 1992 and 1994. It seems that the combination process creates artifacts that affect the precession-nutation components. The same remarks can be made for the annual nutation, with an additional period of phase instability between 1992 and 1997. We will not discuss features after 2011 because it could be a side effect. The excitation mechanism of both the FCN and the annual retrograde nutation should be investigated in the future, especially to understand their amplitude variability and the cancellation of the annual retrograde nutation amplitude in 1995 and 2007.5. This mechanism likely originates in external fluid layer mass exchanges but the difficulty in modeling high frequency behavior of the atmosphere prevents one from any verification (Lambert, 2006).

After subtracting the FCN and annual components to the time series, we adjusted amplitudes of other principal lunisolar nutations. These nutation components are those formerly used by Mathews et al. (2002): it consists of 21 prograde and retrograde waves of prominent amplitudes in the rigid Earth nutation theory of Souchay et al. (1999). They are almost completely uncorrelated over the current time span. We show the largest amplitudes in Fig. 4. The amplitudes are quite small, less than $40 \mu\text{as}$. IAA differs from the others for long periods, while USN shows a difference for the 14-day nutation, which can be a consequence of troposphere modeling (USN is the only center using NMF). Other nutations are consistent within $10 \mu\text{as}$.

4 Noise characterization

In the previous section, we adjusted a number of prominent nutation components and removed them from the time series, such that residuals can be considered as close to a noise. We computed Allan standard deviation σ_A defined for a time sampling interval τ as (Allan, 1966; Rutman, 1978)

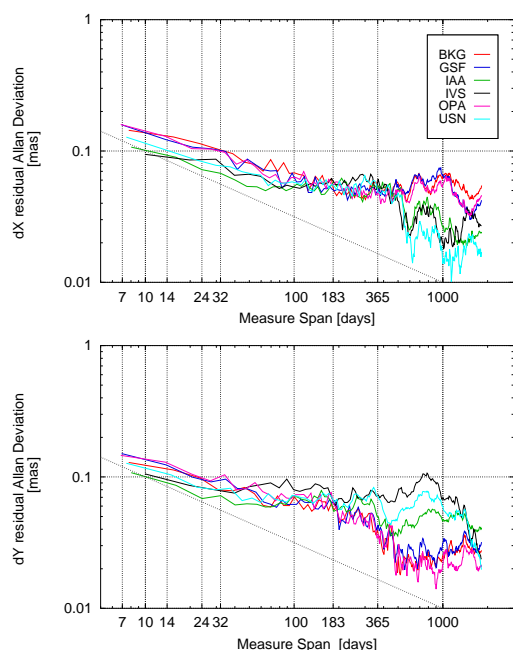


Fig. 5 Allan standard deviation of residual nutation time series.

$$\sigma_A^2(\tau) = \frac{1}{2} (\bar{y}_i + \bar{y}_{i+1})^2, \quad (1)$$

where y is a data set and \bar{y}_i is the weighted mean of data along the i -th τ -duration interval. The Allan standard deviation of the residual series are displayed in Fig. 5. We investigate noise on time scales up to about 5 years. In the figure, a slope of -0.5 indicates the presence of a white noise, while a slope between -0.25 and 0.25 reveals colored noise (including flicker noise and random walk).

At low time scales, residual nutation time series can be considered as a white noise. Colored noises appear around approximately 50 days. The difference of stability between each series does not exceed a factor of 2. We can see some bump on both X and Y components, which separate time series into two groups: (i) IAA, IVS and USN show in X a bump that stops around 2 years (and maybe a second one that stops around 3 years) and in Y a bump that stops around 5 years. (ii) For BKG, GSF and OPA, the features are reversed between X and Y . These features could be the signature of periodic residual components, not removed above, or the presence of a flicker noise due to, e.g., network effects (irregular addition or removal of antennas and target sources). This point is being currently investigated by the authors.

5 Conclusion

We compared the nutation time series obtained by different analysis centers using different VLBI analysis configurations. These

differences affect the nutation at the level of $20 \mu\text{s}$. No clear dependence in the software nor the analysis configuration shows up: more thorough analyses are needed to separate the effects due to delay modeling, constraints, and parameterization.

Although small compared to, e.g., the stability of the current celestial reference frame (Fey et al., 2015), differences between nutation series raise some questions about the observability of tiny phenomenon that are currently under investigation by the geophysical community. In particular, we can cite (i) the determination of the quality factor (damping factor) of the FCN which is linked to deformability of the core-mantle interface as well as possible topographic and electromagnetic couplings (Mathews et al., 2002; Koot et al., 2008, 2010) (ii) the determination of the period of the free inner core nutation (FICN) which is currently very uncertain (Rogister et al., 2009). In a work in preparation, we consider more nutation series and a more thorough spectral analysis to extract periodic components, so that the characterization of the internal noise of each series is more relevant.

References

- Allan D W (1966) Statistics of Atomic Frequency Standards. In: *Proc. of the IEEE*, 54, 2, 221–230.
- Böckmann S, Artz T, Nothnagel A, Tesmer V (2010) International VLBI Service for Geodesy and Astrometry: Earth orientation parameter combination methodology and quality of the combined products. *J Geophys Res*, 115, B04404, doi: 10.1029/2009JB006465
- Böhm J, Werl B, Schuh H (2006) Troposphere mapping functions for GPS and very long baseline interferometry from European Centre for Medium-Range Weather Forecasts operational analysis data. *J Geophys Res*, 111, B02406, doi: 10.1029/2005JB003629.
- Capitaine N, Wallace P T, Chapront (2005) Improvement of the IAU 2000 precession model. *Astron Astrophys*, 432, 355–367.
- Dehant V, Feissel-Vernier M, de Viron O, Ma C, Yseboodt M, Bizouard C (2003) Remaining error sources in the nutation at the submilliarc second level. *J Geophys Res*, 2275, doi: 10.1029/2002JB001763, B5.
- de Viron O, Schwarzbaum G, Lott F, Dehant V (2005) Diurnal and subdiurnal effects of the atmosphere on the Earth rotation and geocenter motion. *J Geophys Res*, 110, doi: 10.1029/2005JB003761.
- Feissel-Vernier M (2003) Selecting stable extragalactic compact radio sources from the permanent astrogeodetic VLBI program. *Astron Astrophys*, 403, 105.
- Feissel-Vernier M, Ma C, Gontier A-M, Barache C (2005) Sideral orientation of the Earth and stability of the VLBI celestial reference frame. *Astron Astrophys*, 438, 1141–1148.
- Feissel-Vernier M, Ma C, Gontier A-M, Barache C (2006) Analysis strategy issues for the maintenance of the ICRF axes *Astron Astrophys*, 452, 1107–1112.
- Fey A L, Ma C, Arias E F, Charlot P, Feissel-Vernier M, Gontier A-M, Jacobs C S, Li J, MacMillan D S (2004) The Second Extension of the International Celestial Reference

- Frame: ICRF-EXT.1. *Astron J*, 127, 3587–3608, doi: 10.1086/420998.
- Fey A F, D. Gordon D, Jacobs C S, Ma C, Gaume R A, Arias E F, Bianco G, Boboltz D A, Böckmann S, Bolotin S, Charlot P, Collioud A, Engelhardt G, Gipson J, Gontier A-M, Heinkelmann R, Kurdubov S, Lambert S, Lytvyn S, MacMillan D S, Malkin Z, Nothnagel A, Ojha R, Skurikhina E, Sokolova J, Souchay J, Sovers O J, Tesmer V, Titov O, Wang G, Zharov V (2015) The Second Realization of the International Celestial Reference Frame by Very Long Baseline Interferometry. *Astron J*, 150(58), doi: 10.1088/0004-6256/150/2/58.
- Herring T A, Mathews P M, Buffett B A (2002) Modeling of nutation and precession: Very long baseline interferometry results. *J Geophys Res*, 107(B4), doi: 10.1029/2001JB000165.
- Koot L, Rivoldini A, de Viron O, Dehant V (2008) Estimation of Earth interior parameters from a Bayesian inversion of very long baseline interferometry nutation time series. *J Geophys Res*, 113, doi: 10.1029/2007JB005409.
- Koot L, Dumberry M, Rivoldini A, de Viron O, Dehant V (2010) Constraints on the coupling at the core-mantle and inner core boundaries inferred from nutation observations. *Geophys J Int*, 182(3), 1279–1294, doi: 10.1111/j.1365-246X.2010.04711.x.
- Krásná H., Böhm J, Schuh H (2013), Free core nutation observed by VLBI. *Astron Astrophys*, 555, A29.
- Lambert S (2006) Atmospheric excitation of the Earth's free core nutation. *Astron Astrophys*, 457, 717–720.
- Lambert S, Dehant V, Gontier A-M (2008) Celestial frame instability in VLBI analysis and its impact on geophysics. *Astron Astrophys*, 481, 535–541.
- Ma C, Arias E F, Eubanks T M, Fey A L, Gontier A-M, Jacobs C S, Sovers O J, Archinal B A, Charlot P (1998) The International Celestial Reference Frame as Realized by Very Long Baseline Interferometry. *Astron J*, 116, 516, 1538–3881, doi: 10.1086/300408.
- Malkin Z (2004) A New Free Core Nutation Model with Variable Amplitude and Period. In: N. R. Vandenberg, K. D. Baver (eds.), *IVS 2004 General Meeting Proc.*, NASA/CP-2004-212255, 388–392.
- Malkin Z (2014) On the Accuracy of the Theory of Precession and Nutation. *Astr Rep*, 58(6), 415–425, doi: 10.1134/S1063772914060043.
- Mathews P M, Buffett B A, Herring T A, Shapiro I I (1991) Forced nutations of the Earth: Influence of inner core dynamics: 1. Theory. *J Geophys Res*, 96(B5), 8219–8242, doi: 10.1029/90JB01955.
- Mathews P M, Buffett B A, Shapiro I I (1995) Love numbers for diurnal tides: Relation to wobble admittances and resonance expansions. *J Geophys Res*, 100(B6), 9935–9948, doi: 10.1029/95JB00670.
- Mathews P M, Herring T A, Buffett B A (2002) Modeling of nutation and precession: New nutation series for nonrigid Earth and insights into the Earth's interior. *J Geophys Res*, 107, doi: 10.1029/2001JB000390.
- Niell A E (1996) Global mapping functions for the atmosphere delay at radio wavelengths. *J Geophys Res*, 101(B2), 3227–3246, doi: 10.1029/95JB03048.
- Rogister Y, Valette B (2009) Influence of liquid core dynamics on rotational modes. *Geophys J Int*, 176(2), 368–388.
- Rothacher M, Beutler G, Herring T A, Weber R (1999) Estimation of nutation using the Global Positioning System. *J Geophys Res*, 104(B3), 4835–4859.
- Roosbeek F, Defraigne P, Feissel M, Dehant V (1999) The free core nutation period stays between 431 and 434 sidereal days. *Geophys Res Lett*, 26, 131, doi: 10.1029/1998GL900225.
- Rutman J (1978) Characterization of phase and frequency instabilities in precision frequency sources: fifteen years of progress. In: *Proc. of the IEEE*, 66, 9, 1048–1075, IV
- Schuh H, Behrend D (2012) VLBI: A fascinating technique for geodesy and astrometry. *J Geodyn*, 61, 68–80, doi: 10.1016/j.jog.2012.07.007.
- Souchay J, Loysel B, Kinoshita H, Figueira M (1999) Corrections and new developments in rigid earth nutation theory. *Astron Astrophys Suppl Ser*, 135, 111–131.
- Vondrák J, Weber R, Ron C (2005) Free core nutation: direct observations and resonance effects. *Astron Astrophys*, 444, 297–303.
- Zotov L, Bizouard C (2015) Regional atmospheric influence on the Chandler wobble. *Adv Sp Res*, 55(5), 1300–1306, doi: 10.1016/j.asr.2014.12.013.

Estimating a Celestial Reference Frame in the Presence of Source Structure

L. Plank, S. Shabala, J. McCallum, H. Krásná, E. Rastorgueva-Foi, J. Lovell, B. Petrachenko

Abstract The presence of source structure has long been identified as providing a non-zero contribution to the group delay measured by VLBI. It has also been shown previously that the positions of sources with high structure show larger variability or even systematic apparent motion. Using simulations of the IVS rapid sessions schedules, we investigate the effects of simple two-component sources on globally estimated source positions. We find that sources with nominal structure indices 2, 3, and 4 can all cause systematic displacements of source positions at the level of tens to hundreds of microarcseconds, clearly above today's level of source position uncertainties. In a thorough simulation study we compare multiple source models with only slightly changed parameters, namely the relative brightness of the two components and their separation. We then investigate the characteristics of the effects, in particular the relationship between changes in apparent source position and the jet axis of the sources. Finally we present a new method for mitigating the effect of this dislocation in the analysis when estimating a celestial reference frame.

Keywords Source structure, Celestial Reference Frame, VieVS structure simulator

1 Introduction

It has long been known that quasars, our preferred target radio sources in geodetic/astrometric VLBI, are not ideal point sources. Structure of the innermost regions of synchrotron jets causes additional contribution to observed group delays and corrupts our measurements. These structure delays are dependent

Lucia Plank, Stas Shabala, Jamie McCallum, Elizaveta Rastorgueva-Foi, Jim Lovell

University of Tasmania, Private Bag 37, 7001 Hobart, Australia
Hana Krásná

Technische Universität Wien, Gußhausstraße 27-29, A-1040 Vienna, Austria

Bill Petrachenko

Natural Resources Canada, 588 Booth St, Ottawa, Canada

on the observing frequency, but also on the changing geometry between the observing baseline and the direction to the source. In addition, the evolution of quasars is changing on timescales of months to years, hence structure effects can be quite different for different observing epochs. In this contribution we investigate the effects of such additional structure delays as they can appear in real IVS observing sessions, applying standard geodetic/astrometric analysis. Any possible variations of sources with time are not taken into account and are not part of this study. This contribution summarises the most important findings of a thorough simulation study, described in more detail in Plank et al. (2015).

2 The basics of source structure

Radio-loud quasars often have structure, showing secondary or multiple components roughly aligned with the direction of the synchrotron jet in addition to a compact core. Charlot (1990) developed the formalism to model the effects of this additional structure in the VLBI group delays. A non-point source causes an additional (different) phase term in each of the eight observed frequency bands, resulting in an additional delay in the group delay which is defined as the slope of phase against frequency. The resulting structure delay is variable, changing with the observing frequencies as well as with the length and orientation of the baseline. In terms of the source itself, the important parameters are the location and strength of the individual components, described in the following as the separation (*sep*) along the jet direction and its relative brightness b_r , both with respect to the main component.

In this work we investigate structure in X-band only, using the standard eight frequency bands of 8213, 8252, 8353, 8513, 8733, 8853, 8913, 8933 MHz and the reference frequency of 8217 MHz.

In the structure simulator of the Vienna VLBI Software (Shabala et al., 2015), we can calculate the delay due to source structure based on multi-component source models. Fully incorporated in the software, this allows us to test the effects of real or mock source models for VLBI observations, in both standard analysis as well as in simulations. Once accurate source models

are available, the observations can be corrected for the effects of source structure.

Having reliable and up-to-date source models is difficult and as a result such corrections are not part of the standard analysis. The common solution today is a selective choice (usually $SI < 3$) of target sources, based on the structure index SI . The SI (Fey and Charlot, 1997) is a measure for the expected magnitude of structure delays, calculated as the median over all possible Earth-bound baselines.

3 Simulation study

In the presented simulation study we took the observation setup of all 104 IVS rapid turnaround sessions (R1, R4) of the year 2013. For these we ran multiple simulations, accounting for source structure effects and/or tropospheric turbulence, measurement noise and clock errors. The target of our investigation were source coordinates, which were estimated from all sessions in a global solution. Being interested in the effects of different source models, in each solution we assigned every source an identical source model, with only the direction of the jet varying randomly for each source. Once the jet direction was assigned to a particular source, it was kept constant for all investigated source models. Simulations were run for 19 different source models with nominal structure indices of 2, 3, and 4 (Table 1, col. 1 and 2). Two component models were chosen for the sake of simplicity, allowing a systematic comparison between them. This is representative of many observed sources. The range of relative brightnesses b_r and separations sep was also chosen on the basis of multiple images of real sources. We then created two-component models for 7 (5 for $SI = 4$) relative brightnesses from $b_r = 0.05$ to 0.35 (Table 1, col. 1 and 2). The separation is then a result of tuning the models to the nominal structure index of 2.0, 3.0 and 4.0. In general, sources with structure index 2 are less extended (≈ 1 mas). Sources of structure index 3 and 4 follow the principle of either having a stronger component close to the primary component or a fainter secondary component further away (up to 6 mas).

4 Results

Applying source structure to the selected sessions we find that source positions, estimated within a global solution, can be distorted significantly, at the level of a few tens of microarcseconds. In Table 1 the median offsets over all sources are given for the various source models. In the full simulations (col. 4), additionally accounting for errors due the troposphere, station clocks, and measurement noise, we see that source structure causes a systematic displacement of source positions, above the level of common error sources. The more random errors mainly due to tropospheric turbulence and measurement errors modelled as white noise vary for each session, however the median source position does not change significantly from the catalog position. Hence

we find the median source position offset, calculated as

$$d = \sqrt{(\delta RA \cdot \cos(Dec))^2 + \delta Dec^2}, \quad (1)$$

is at the same level as the nominal accuracy. On the other hand, source structure effects seem to have similar effects for all sessions and hence systematically displace the source. A similar result was found for station positions by Shabala et al. (2015).

Table 1 Simulated median source position offsets and formal uncertainties (cf. Equation 1) for an estimated CRF. We compare the results of different simulations, using no source structure and structure due to various source models. In the third column results of source structure-only simulations are shown and in the fourth column we give the numbers for the full simulations, additionally including simulated errors due to clocks, troposphere, and measurement noise.

b_r	sep	structure-only	full simulations
no structure			$49 \pm 44 \mu\text{as}$
$SI = 2.0$			
0.35	0.26 mas	$25 \pm 2 \mu\text{as}$	$58 \pm 44 \mu\text{as}$
0.30	0.35 mas	$33 \pm 4 \mu\text{as}$	$63 \pm 44 \mu\text{as}$
0.25	0.51 mas	$63 \pm 4 \mu\text{as}$	$82 \pm 45 \mu\text{as}$
0.20	0.53 mas	$50 \pm 3 \mu\text{as}$	$71 \pm 44 \mu\text{as}$
0.15	0.57 mas	$35 \pm 3 \mu\text{as}$	$62 \pm 44 \mu\text{as}$
0.10	0.67 mas	$15 \pm 2 \mu\text{as}$	$53 \pm 44 \mu\text{as}$
0.05	1.52 mas	$7 \pm 3 \mu\text{as}$	$52 \pm 44 \mu\text{as}$
$SI = 3.0$			
0.35	0.67 mas	$51 \pm 9 \mu\text{as}$	$81 \pm 45 \mu\text{as}$
0.30	0.70 mas	$39 \pm 8 \mu\text{as}$	$72 \pm 45 \mu\text{as}$
0.25	0.82 mas	$33 \pm 8 \mu\text{as}$	$65 \pm 45 \mu\text{as}$
0.20	1.01 mas	$26 \pm 8 \mu\text{as}$	$57 \pm 45 \mu\text{as}$
0.15	1.49 mas	$23 \pm 9 \mu\text{as}$	$57 \pm 45 \mu\text{as}$
0.10	2.45 mas	$24 \pm 9 \mu\text{as}$	$56 \pm 45 \mu\text{as}$
0.05	5.67 mas	$16 \pm 9 \mu\text{as}$	$57 \pm 45 \mu\text{as}$
$SI = 4.0$			
0.35	2.45 mas	$82 \pm 33 \mu\text{as}$	$102 \pm 55 \mu\text{as}$
0.30	2.75 mas	$60 \pm 31 \mu\text{as}$	$88 \pm 54 \mu\text{as}$
0.25	3.08 mas	$57 \pm 28 \mu\text{as}$	$82 \pm 52 \mu\text{as}$
0.20	3.93 mas	$47 \pm 27 \mu\text{as}$	$73 \pm 52 \mu\text{as}$
0.15	6.35 mas	$36 \pm 27 \mu\text{as}$	$66 \pm 52 \mu\text{as}$

Studying our results we find clear differences between the various source models. For the $SI = 3$ and $SI = 4$ models there are larger median source displacements for a strong component close by than when having a weaker component further away. This shows that the actual effects of structure in geodetic/astrometric VLBI observations are a result of the complex interplay between source structure, the observing network, and the observation schedule. Sources with the same structure index can have considerably different structures and hence a completely different effect on actual observations.

This becomes even more obvious with the results for the $SI = 2$ models. We find that for the models with a relative brightness of 0.15, 0.20 and 0.25 the median effects are about $40 - 60 \mu\text{as}$, at the same level as for the $SI = 4$ models. The reason for this can be found by studying the distribution of the structure delays amongst the various lengths and orientations of the observing baseline. This is illustrated in Figure 1. For four different structure models the structure delays are given as a function of length and orientation of the observing baseline, for all possible Earth-bound baselines. If one calculates the median over each of the circular graphs, one gets the SI for each of these models.

Most prominent is the fact that the maximal structure delays increase with higher SI , from $\pm 25\text{ps}$ for $SI = 2$, $\pm 50\text{ps}$ for $SI = 3$ to $\pm 150\text{ps}$ for $SI = 4$. However, more important than the magnitude of the structure delays seems to be how they are distributed amongst the individual observations. As visible in Figure 1 the *beating pattern* of the structure delays is much more rapid for the $SI = 3$ and 4 models than for $SI = 2$. This means that although we get much higher structure delays, they quickly change in the sign as the projected baseline to the source changes, and seem to largely cancel amongst all observations. On the other hand, in the $SI = 2$, $b_r = 0.25$ model we see broad areas of similar structure delays, meaning that all baselines in that area experience similar structure delays. These highly systematic delays do not cancel over the whole session resulting in relatively high source position offsets. A special case seems to be the model on the very left, $SI = 2$, $b_r = 0.35$. Here, most of the (projected) baselines experience a quite small structure delay of a few picoseconds only. The reasons that this model has the same structure index of 2.0 as the previous model are the two areas of higher structure delays on the left and right edges. However, in the real observations there are only few observations that are projected in these areas, hence the overall effects of this model on source positions are quite small.

5 Alignment to jet

Radio sources that are used in VLBI usually have one of the two relativistic jets pointing close to directly at Earth. The observed radio emission emerges from irregular mass outbursts moving along this jet. The direction of the jet in these quasars is generally thought to remain constant (e.g. Lister et al., 2009). It is known that (variable) source structure can manifest itself as observed proper motion (e.g. Ma et al., 1998; Fey and Charlot, 1997). Moór et al. (2011) further found a general correlation between the characteristic of observed proper motion and the direction of the source's jet.

The results of our study show that source structure indeed causes source displacements preferable along the jet direction. However, we also show that this effect is stronger for $SI = 2$ sources and weaker for source models of higher structure indices. In Figure 2 the globally estimated source position offsets of all sources in the investigated sessions are shown versus the alignment of this offset to the direction of the jet.

We find that the $SI = 2$ model tends to displace the sources into the direction of the jet (for this model, 90% of displace-

ments are within 30° of the jet direction) while the displacement due to the $SI = 3$ and $SI = 4$ models are more noise-like, i.e. there is no strong correlation between the directions of displacement and the jet. It is also evident that the simulated displacement for a few sources can be much higher than the median values given in Table 1, up to a few hundreds of microarcseconds. Once more we want to emphasize that the differences between the sources and between the different models are solely the effect of the observing geometry and the interplay with the source model. This strongly suggests that, assuming the source structure is well known, one might be able to influence a session's schedule accordingly to minimize the negative effects of source structure.

6 New modelling

The final idea investigated in this study builds on the relation between the estimated source position offset and the jet direction. For the determination of a CRF, MacMillan and Ma (2007) suggested to model the positions of unstable (e.g. due to source structure) sources as arc parameters (i.e. essentially unconstrained values determined on a session-by-session basis) rather than global positions over all sessions. Following this concept, we suggest that instead of the classical parameterisation of sources into right ascension and declination the sources are modelled as a component along the jet and one component perpendicular to the direction of the jet. In the global solution, we then only estimate the source's position in the component perpendicular to the jet (which should not be affected by source structure) and model the other component as arc parameter, allowing the source to *move* along the jet from session to session.

In simulations, we find that for the $SI = 2$ and $SI = 3$ models this new parameterisation successfully reduces the median effects on source positions down to the level of the tropospheric errors. Due to the fact that the $SI = 4$ models do not necessarily displace the sources into a direction along the jet, the new method is less successful for the more noise-like structure effects of the investigated $SI = 4$ sources. For more details we refer the interested reader to Plank et al. (2015).

7 Conclusions

In VieVS, we can apply source structure corrections (based on real or mock source models) in VLBI analysis and simulations. Testing mock source catalogs using classical IVS observations, we find that source structure can systematically displace source positions, clearly above the level of today's CRF accuracies and other (stochastic) error sources. Apparent variations in source positions occur simply due to the changing observation geometry and networks, even when the structure of a source does not change with time.

We find that the magnitude of the effect (as given by the median source position offset) does not scale straightforwardly

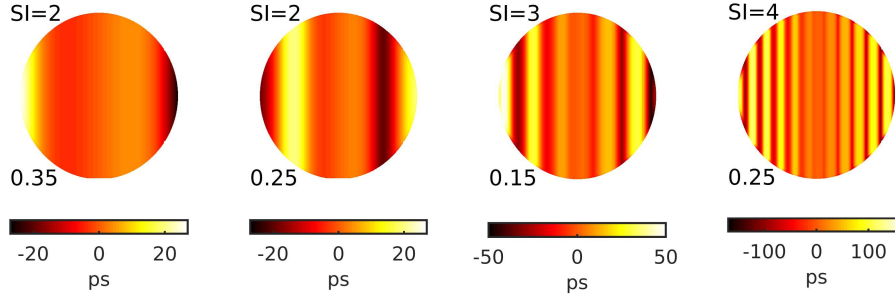


Fig. 1 Source structure delay in picoseconds as a function of observing the projected baseline in the direction of the source. One baseline represents one point in these graphs, with longest baselines up to the Earth’s diameter at the edge of the circle. Four different source models are shown. Note the different scales of the color coding between panels.

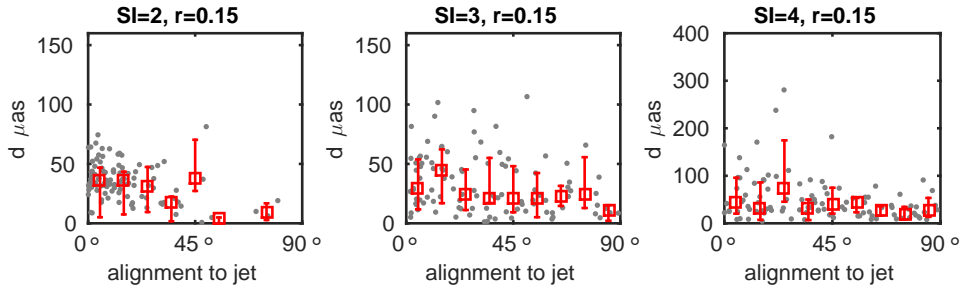


Fig. 2 Globally estimated source position offsets d versus the alignment of the offset to the direction of the jet. We show the results of three different source models, with a different scale for the very right ($SI = 4$) graph. The estimated offsets are binned by alignment with the jet in increments of 10° , with the red squares and the whiskers indicating the median source position offset as well as the 25th and 75th percentile. In the $SI = 2$ case most of the sources are *moved* along the jet direction while for the other models this relation is less clear.

with the nominal structure index (SI) of the source. Moreover, within a whole session sources of higher structure indices (3, 4) cause more noise-like structure delays which tend to cancel in the analysis. Sources of $SI = 2$ on the other hand act more systematically and can also significantly influence the results in terms of estimated source positions.

Our simulations confirm a relation between the estimated source position offset and the jet direction, which is stronger for lower structure indices and less evident for higher SI s. This information could be used in a newly presented analysis strategy for the estimation of a CRF, where source positions are modelled in components along and perpendicular to the direction of the jet.

It is important to account for source structure in today’s VLBI analysis. Care has to be taken with the commonly used structure index SI , which might not always mirror the level of the actual effects of source structure, as seen by real observations. Without the availability of accurate source images, the direction of a source’s jet may offer some new possibilities to account for source structure in the analysis.

We hope that our new source structure simulator enables further similar studies, e.g. for testing new frequencies (K, Ka-band), optimal selection of sub-bands, and of course the yet fairly unknown effects of source structure in VGOS.

Acknowledgments

This work was supported by the AuScope Initiative, funded under the National Collaborative Research Infrastructure Strategy (NCRIS), an Australian Commonwealth Government Programme. The authors are grateful to the Australian Research Council for Fellowships FS1000100037, FS110200045, and DE130101399, and to the Austrian Science Fund (FWF) for Fellowships J3699-N29 and T 697-N29.

References

- Charlot P (1990) Radio-source structure in astrometric and geodetic very long baseline interferometry. *Astron J*, 99 (4), 1309.
- Fey A L, Charlot P (1997) VLBA: observations of radio reference frame sources II. Astrometric suitability based on observed structure. *Astroph J Suppl Ser*, 111:95–142.
- Lister M, Cohen M, Homan D, Kadler M, Kellermann K, Kovalev Y, Ros E, Savolainen T, Zensus J (2009) MOJAVE: Monitoring of jets in active galactic nuclei with VLBI ex-

- periments. VI. Kinematics analysis of a complete sample of blazar jets. *Astron J*, 138, 1874.
- Ma C, Arias E F, Eubanks T M, Fey A L, Gontier A-M, Jacobs C S, Sovers O J, Archinal B A, Charlot P (1998) The international celestial reference frame as realized by very long baseline interferometry. *Astron J*, 116:1, 516.
- MacMillan D, Ma C (2007) Radio source instability in VLBI analysis. *J Geod*, 81, 443.
- Moór A, Frey S, Lambert S, Titov O, Bakos J (2011) On the connection of the apparent proper motion and the VLBI structure of compact radio sources. *Astron J*, 141, 178.
- Plank L, Shabala S, McCallum J, Krásná H, Petrachenko B, Rastorgueva-Foi E, Lovell J (2015) On the estimation of a celestial reference frame in the presence of source structure. *Mon Not R Astron Soc*, doi: 10.1093/mnras/stv2080.
- Shabala S, McCallum J, Plank L, Böhm J (2015) Simulating the effect of quasar structure on parameters from geodetic VLBI. *J Geod*, 98, 9:873–886.

Imaging the IYA09 VLBI Super-session

A. Collioud, P. Charlot

Abstract In the framework of the International Year of Astronomy (IYA2009), the IVS organized a dedicated 24-hour astrometric VLBI session with a large network of radiotelescopes in order to observe as many of the 295 ICRF2 defining sources as possible. This “super-session” took place on the 18th of November 2009. In all, 35 radiotelescopes observed 243 sources, which made the IYA09 session the largest VLBI session ever conducted. Although the session was primarily targeted to astrometry, the observations prove also to be useful to produce VLBI images of the sources due to the large network of telescopes that participated. In this paper, we present results of such imaging, including details about the data path and procedures. Overall, 228 sources were successfully imaged at X-band and 230 at S-band, corresponding to almost 95% of the scheduled sources. Taking an additional step, we derived structure indices from the resulting IYA09 images in order to assess the astrometric suitability of the sources. From the structure index distribution, we inferred that 80% of the IYA09 sources are compliant with the “ICRF2-defining” source definition.

Keywords IVS, International Year of Astronomy 2009, VLBI imaging, structure index

1 Introduction

Initiated by the United Nations Educational, Scientific and Cultural Organization (UNESCO) and the International Astronomical Union (IAU), the year 2009 was declared as the International Year of Astronomy (IYA2009), in order to make everyone realize the impact of astronomy on our daily lives. All around the world, IYA2009 activities, like astronomical observations, conferences, etc., took place from local to international levels.

In August 2009, the second realization of the International Celestial Reference Frame (ICRF2) was adopted. The ICRF2

Arnaud Collioud, Patrick Charlot
Laboratoire d’Astrophysique de Bordeaux, Université de Bordeaux – CNRS, 2 rue de l’Observatoire, BP89, 33271 Floirac Cedex, France

comprises precise positions of 3414 compact radio astronomical sources and its definition is made using a set of 295 sources selected on the basis of positional stability and the lack of extended source structure (Fey et al., 2015).

In order to celebrate these two events, the International VLBI Service for Geodesy and Astrometry (IVS) which supports research and operational activities for the Very Long Baseline Interferometry (VLBI) technique, decided to organize a special VLBI astrometric session, named “IYA09”. Its main goal was to observe in a single session as many ICRF2 defining sources as possible with the largest network of radiotelescopes. Although the session was primarily targeted to astrometry, the observations are also of interest for imaging the sources, which is the topic of the present paper. The IYA09 session was also accompanied with outreach activities, including setting up a Web page to follow the session in real-time¹.

Section 2 presents details about the IYA09 session. The data workflow, including post-processing and analysis, is described in Section 3. Finally, Section 4 presents the results of the analysis, i.e. the VLBI maps and the astrometric suitability of the IYA09 sources, as derived from the structure indices.

2 IYA09 session details

The IYA09 VLBI astrometric “super-session” took place on the 18th of November 2009 for a duration of 24 hours. The observing setup was the dual-frequency S/X (2.3/8.6 GHz) mode used for “classical” geodetic and astrometric sessions, with 4 intermediate frequencies (IF) per frequency band.

In all, 35 radiotelescopes were scheduled², making the IYA09 session the largest VLBI session ever conducted. The stations are heterogeneously distributed on Earth with a sparse coverage in the southern hemisphere (3 less-sensitive antennas)

¹ Available at <http://iya09-ivs.obs.u-bordeaux1.fr/>. The IYA09 session may be also accessed through the “IVS Live” Web site at <http://ivslive.obs.u-bordeaux1.fr/index.php?session=iya09>.

² The complete list of stations is available at <http://ivsc.gsfc.nasa.gov/program/iya09/> along with some additional details about the session.

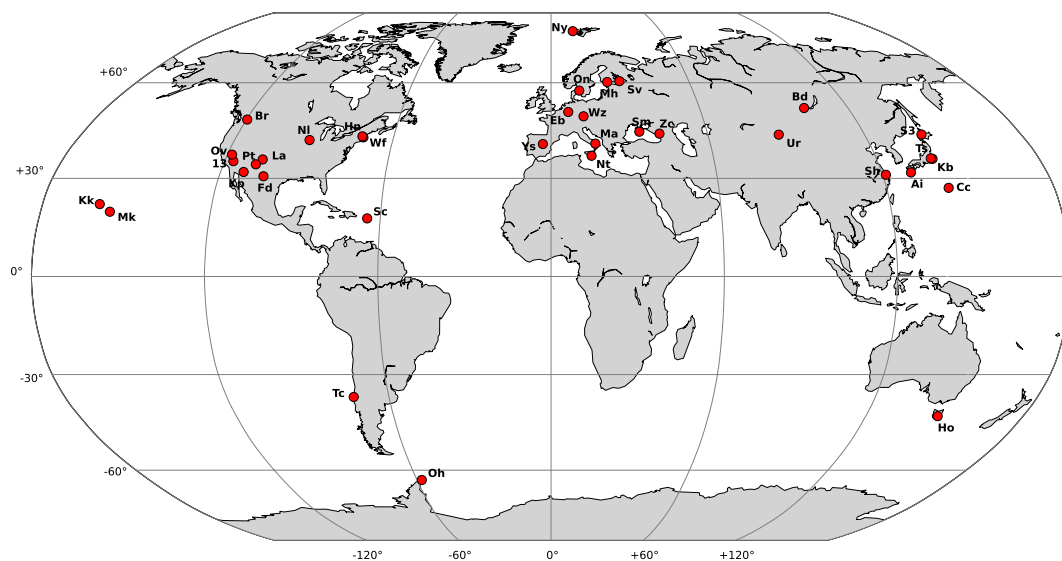


Fig. 1 The 35 radiotelescopes scheduled in the IYA09 session. The network is sparse in the southern hemisphere, and very heterogeneous in antenna size, which ranges from 3 m (Shintotsukawa, S3, Japan) to 100 m (Effelsberg, Eb, Germany).

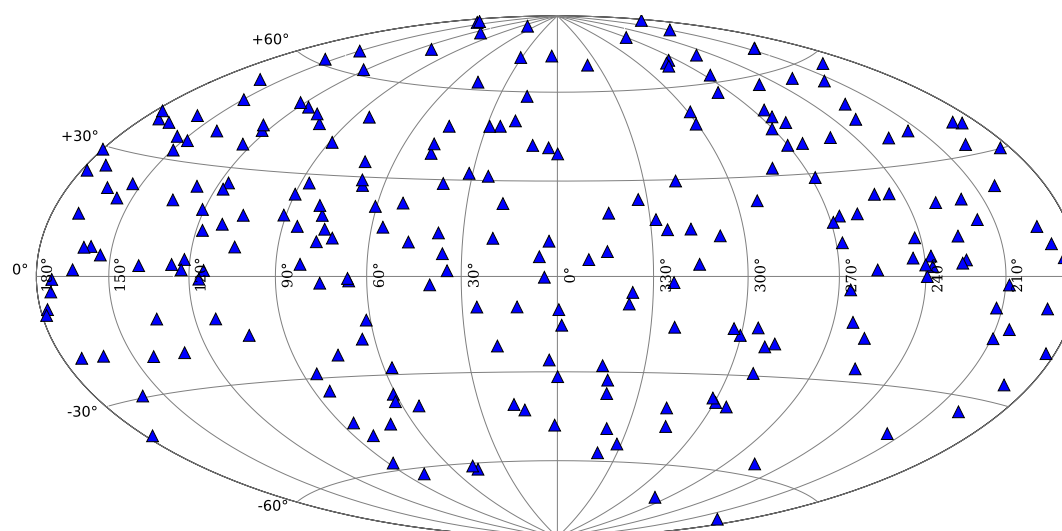


Fig. 2 Sky distribution of the 243 ICRF2 defining sources observed during the IYA09 session.

as shown in Fig. 1. This disparity has some impact on the resulting maps, especially for the most southern sources. Moreover, the IYA09 antennas exhibit a large diversity of dish size, which ranges from 3 m (Shintotsukawa, Japan) to 100 m (Effelsberg, Germany), implying a large range of sensitivity. At the processing stage, the data of only 33 stations was available because Svetloe (Russia) did not observe and DSS13 (USA) was not correlated.

The set of sources scheduled includes 243 of the 295 ICRF2 defining sources. Among the 52 missing sources (all with a negative declination), 4 were too close to the Sun to be observed, and the rest could not be optimally scheduled (essentially due to the

poor southern coverage of the observing network). Nevertheless, the distribution of sources on the sky is reasonably uniform, as shown in Fig. 2.

3 Data workflow

This section presents the complete data path, from the initial post-processing steps to the final products (maps and structure indices).

3.1 Post-processing

Once the IYA09 session was over, the data from each antenna was shipped (or e-transferred) to Haystack Observatory for correlation. The correlated data was fringed using Fourfit, a software which is part of the Haystack Observatory Postprocessing System (HOPS)³. The option “-X” was used in order to write the cross-power spectra of each baseline. Then, the fringed data was transferred to the Astronomical Image Processing System (AIPS) software using the “MK4IN” pseudo-AIPS task (Alef and Graham, 2002). One of the benefits of MK4IN is that it reads the phases, residual delays and delay rate corrections determined by Fourfit and stores them into an AIPS baseline correction table. At the end of this stage, we obtained one UVFITS file per band, each one containing about 4.9 million visibilities, to be further processed with AIPS.

3.2 Analysis

We used AIPS to calibrate the data. First, we applied the a priori amplitude calibration for each antenna using the gain information and the system temperatures extracted from the log files (along with the flagging information). Then, we used the AIPS task “BLAPP” to apply the Fourfit solutions to the data, instead of re-fringing it. After exporting one FITS file per source, we derived an “a posteriori” amplitude calibration based on the raw maps of 26 strong sources. It consists in determining an amplitude scaling factor for each IF of each antenna. The derived factors are typically within a 10% range, but are occasionally larger for some antennas. These scaling factors were then applied to the data, before re-exporting the FITS files for imaging. During the processing with AIPS, we encountered and solved some bugs and limitations, mainly because of the exceptional nature of the IYA09 session.

Imaging was achieved using the Difmap software package. The data was edited either manually (X-band) or automatically (S-band). Automatic editing was done using a self-developed Difmap command, called “smartedit”, which detects and edits the outliers within each scan for each IF and each antenna using the classical Tukey boxplot method (Frigge et al., 1989). After the editing, we averaged the data in time for homogenization. The selected averaging time for each source was almost exclusively dependent on the scan length for Effelsberg (the largest and slowest antenna), if present. After that, we used Difmap in an automatic mode to generate a fully self-calibrated and CLEANed naturally-weighted map for each source, as well as ancillary files (color and B&W maps, u-v plots, statistics, etc.). This procedure is similar to the one we extensively use to process the Research and Development with the VLBA (RDV) sessions. During the mapping process, we also did additional editing. For example, the short and less-sensitive intra-Japan baselines were not used. Likewise, TIGO (Chile) at X-band and Seshan (China) for the

³ See <http://www.haystack.mit.edu/tech/vlbi/hops.html> for further details.

most part of the S-band had to be removed. From the final images, we derived structure correction maps and structure indices in order to assess the astrometric suitability of the sources.

4 Results

4.1 Images

Overall, we successfully imaged 228 sources at X-band and 230 sources at S-band, which represents 94 % and 95 % of the 243 observed sources, respectively. Among the 15 sources that were not imaged, 14 of them have a declination below -40° . In order to evaluate the image quality, we calculated the dynamic range of each map which is defined as the CLEAN map peak brightness divided by the residual map RMS. For the X-band maps, the dynamic range is from 39 to 4047, with a median value of 781. This is a rather good value considering that

1. the IYA09 session was dedicated to astrometry, and thus its schedule was not optimized for imaging,
2. the large number of targets limited the number of scans per source and thus the number of observations

Additionally, high angular resolution was achieved (median beam size of 0.5×1 mas at X-band and 2×4 mas at S-band), thanks to the large observing network. The image quality and resolution are attenuated for the most southern sources where the network coverage is poorer.

The maps revealed a large variety of morphologies. Visually, roughly 70 % of the sources look point-like or almost point-like, 20 % exhibit some structure (jet with a limited extension) while the remaining 10 % show a more complex structure (double source, complex and/or extended jets). A sample of images from each such “categories” is shown in Fig. 3. The integrated flux density ranges from 0.14 Jy to 7 Jy (median value of 0.58 Jy) at X-band, and from 0.08 Jy to 6.75 Jy (median value of 0.48 Jy) at S-band.

4.2 Structure corrections

The structure corrections products, and especially the structure index (SI) (Fey and Charlot, 1997; Fey et al., 2015), which characterizes the astrometric quality of a source, were derived from the VLBI maps using the CLEAN model truncated to the level of the negative component with the highest absolute flux density. The distribution of the SI values for the 228 sources mapped at X-band is shown in Fig. 4. In all, 180 sources (80 % of them) have a SI value lower than 3.0 (equivalent to a median structural delay smaller than 10 ps), which was the threshold to select the ICRF2 defining sources. Several reasons may explain why not all sources match this criterion despite the initial selection.

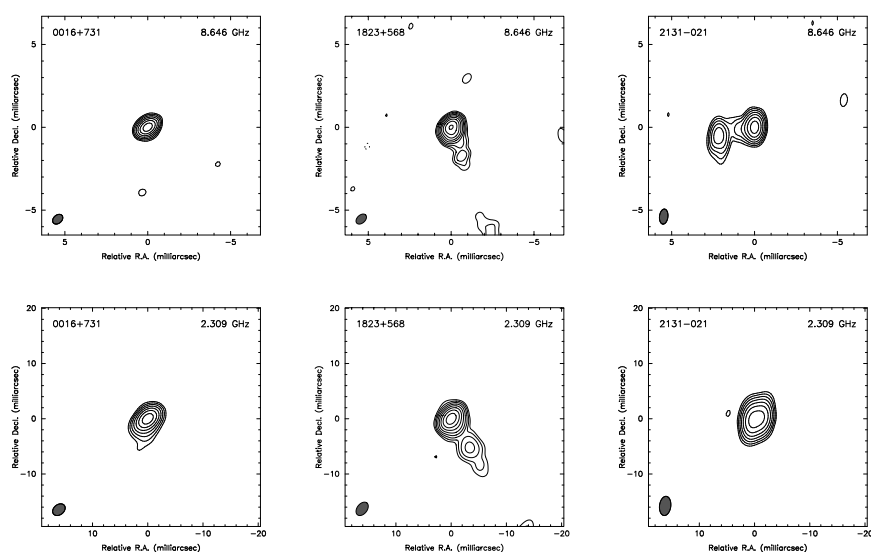


Fig. 3 Examples of IYA09 VLBI maps at X- (top panels) and S-band (bottom panels). Morphologies range from point-like (left-hand side panels) to more complex (right-hand side panels).

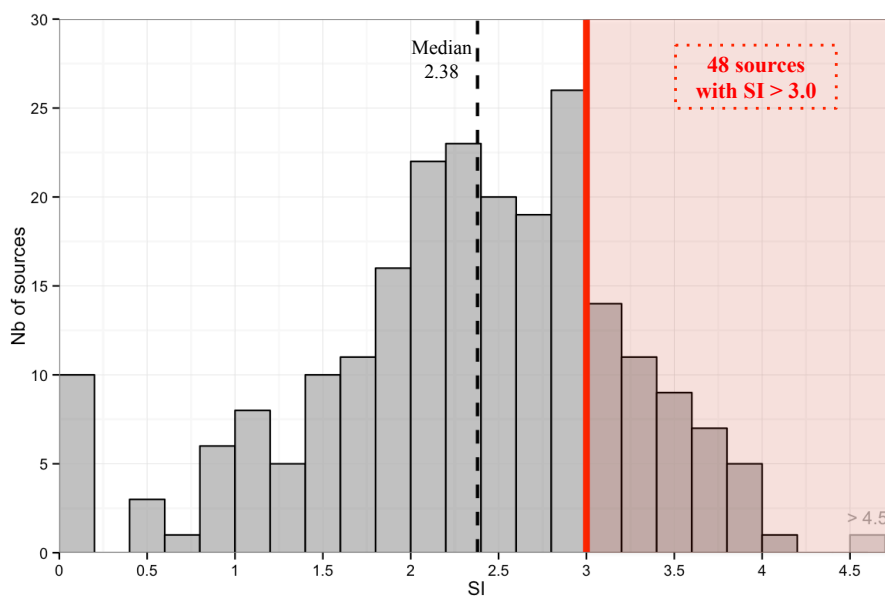


Fig. 4 Distribution of the IYA09 source structure index (SI) values at X-band. 48 sources have a SI larger than 3.0, which was the threshold to select the ICRF2 defining sources.

1. At the time the ICRF2 was built, some defining sources had no SI value available (Fey et al., 2015), hence it was not possible to check whether they comply with this criterion.
2. Source structure may evolve with time, and the SI values may vary too since they are closely tied to the structure.
3. The relevance of some of the SI values still need to be checked, especially when derived from low quality maps (which is the case for most of the southern sources).

Comparing with the sources that had a SI available in the ICRF2 Technical Note (Fey et al., 2009), we identified 24 sources, imaged in IYA09, which had no previous SI. These sources are not specifically southern sources nor weak sources (mean flux of 0.4 Jy).

5 Conclusion

The IYA09 session is the largest VLBI session ever conducted, with the participation of 35 stations observing 243 ICRF2-defining sources. Using these data, images were produced automatically for about 95 % of these 243 sources at X- and S-band. The sources exhibit various morphologies with about 70 % of them that could be visually classified as point-like sources. By deriving structure indices, we determined that more than 80 % of these sources have a X-band structure index strictly lower than 3.0, which was the criterion to qualify as defining sources. Moreover, the IYA09 session adds structure index values for an additional 24 sources, in comparison to those available at the time the ICRF2 was built. The maps and structure indices will be available in the near future through the Bordeaux VLBI Image Database (BVID)⁴.

Frigge M, Hoaglin D C, Iglewicz B (1989) Some Implementations of the Boxplot. *Am Stat*, 43(1), 50–54, doi: 10.2307/2685173.

Acknowledgement

The authors would like to thank Mike Titus at Haystack Observatory (USA), Walter Alef and Dave Graham at MPIfR (Germany), Eric Greisen and Amy Mioduszewski at NRAO (USA) for their support to this work.

References

- Alef W, Graham D A (2002) The New Bonn Mk IV-AIPS Data Export Path. In: E. Ros, E.W. Porcas, A.P. Lobanov, J.A. Zensus (eds.): *Proc. 6th European VLBI Network (EVN) Symposium*, Bonn (Germany), June 25th-28th 2002.
- Fey A, Charlot P (1997) VLBA Observations of Radio Reference Frame Sources. II. Astrometric Suitability Based on Observed Structure. *Astrophys J Suppl Ser*, 111(1), 95–142, doi: 10.1086/313017.
- Fey A, Gordon D, Jacobs C S (eds.) (2009) The Second Realization of the International Celestial Reference Frame by VLBI. In: *IERS Technical Note 35*, Frankfurt am Main: Verlag des BKG, ISBN 3-89888-918-6.
- Fey A L, Gordon D, Jacobs C S, Ma C, Gaume R A, Arias E F, Bianco G, Boboltz D A, Böckmann S, Bolotin S, Charlot P, Collioud A, Engelhardt G, Gipson J, Gontier A-M, Heinkelmann R, Kurdubov S, Lambert S, Lytvyn S, MacMillan D S, Malkin Z, Nothnagel A, Ojha R, Skurikhina E, Sokolova J, Spochay J, Sovers O J, Tesmer V, Titov O, Wang G, Zharov V (2015) The Second Realization of the International Celestial Reference Frame by Very Long Baseline Interferometry. *Astron J*, 150, 58–73, doi: 10.1088/0004-6256/150/58.

⁴ The BVID may be accessed at <http://www.obs.u-bordeaux1.fr/BVID/>.

Aligning VLBI and Gaia Extragalactic Celestial Reference Frames

G. Bourda, P. Charlot, A. Collioud

Abstract By 2020, two extragalactic celestial reference frames will coexist: the VLBI frame currently adopted by the IAU as the fundamental one and the Gaia frame determined from direct optical observations of quasars by this satellite. Aligning them with the highest accuracy will be important for consistency between optical and radio positions of any celestial targets. In this paper, we discuss the selection of the VLBI-Gaia transfer sources, present the various initiatives to reach this goal, review the status of the projects and draw plans for the future.

Keywords celestial frame, astrometry, quasars, Gaia

1 Context and motivations

At the beginning of the 21st century, the IAU (International Astronomical Union) fundamental celestial reference frame was the ICRF (International Celestial Reference Frame; Ma et al., 1998; Fey et al., 2004), composed of the VLBI (Very Long Baseline Interferometry) positions of 717 extragalactic radio sources, measured using dual-frequency S/X observations (2.3 and 8.4 GHz). Since 1 January 2010, the IAU fundamental celestial reference frame has been the ICRF2 (Fey et al., 2015), successor of the ICRF. It includes VLBI coordinates for 3 414 extragalactic radio sources, with a floor in position accuracy of 60 μ as and an axis stability of 10 μ as.

The European space astrometry mission Gaia, launched in December 2013, is surveying¹ all stars and QSOs (Quasi Stellar Objects) brighter than apparent optical magnitude 20. Using Gaia, optical positions will be determined with an unprecedented accuracy, ranging from a few tens of μ as at magnitude 15 to about 400 μ as at magnitude 20 (Lindgren et al., 2008; Mignard, 2014), considering the post-commissioning astrometric accuracy². Gaia

G. Bourda, P. Charlot & A. Collioud
Univ. Bordeaux, CNRS, LAB, UMR 5804, F-33270, Floirac, France.

¹ <https://www.youtube.com/watch?v=BnFyzZGWuYs>

² <http://www.cosmos.esa.int/web/gaia/science-performance>, or <http://arxiv.org/pdf/1502.00791v1.pdf>

will observe about 500 000 quasars, two third of them being new (Mignard, 2014), hence permitting the realization of the extragalactic celestial reference frame directly at optical bands, based on the QSOs that have the most accurate positions (probably 10 000–20 000 of these objects). On average, these extragalactic sources will be observed 80 times during the 5-year mission (between 45 and 150 times). The final version of the catalog is planned to be released by 2021.

In this context, aligning VLBI and Gaia frames will be crucial for ensuring consistency between the measured radio and optical positions. This alignment should allow one, for example, to pinpoint the relative location of the optical and radio emission in active galactic nuclei (AGN) to a few tens of μ as, placing constraints on the overall AGN geometry. Theoretical estimates of this optical-radio core shift indicate that it may amount to ~ 100 μ as on average at X-band (Kovalev et al., 2008), significantly larger than Gaia and VLBI position accuracies. It should thus be directly measurable.

In this paper, we discuss the selection of the VLBI–Gaia transfer sources, present the various initiatives to produce the best alignment, review the status of the projects and draw plans for the future.

2 Transfer sources

This alignment, to be determined with the highest accuracy, requires several hundreds of common sources, with a uniform sky coverage and very accurate radio and optical positions. Obtaining such accurate positions implies that the link sources must be brighter than optical magnitude 18 (Mignard, 2003), and must not show extended VLBI structures (Charlot, 1990).

In a previous study, we investigated the potential of the ICRF for this alignment and found that only 70 sources (10% of the catalog) were appropriate for this purpose (Bourda et al., 2008). This highlighted the need to identify additional suitable radio sources, which was the goal of a VLBI program that we initiated in 2007. This program has been devised to observe 447 optically-bright extragalactic radio sources, on average 20 times weaker than the ICRF sources, extracted

from the NRAO VLA Sky Survey (NVSS), a dense catalog of weak radio sources (Condon et al., 1998). The declination cut-off was set to -10° , because these observations were carried out with the EVN (European VLBI Network) and the VLBA (Very Long Baseline Array), which are northern arrays. The observing strategy to detect, image, and measure accurate VLBI positions for these sources is described in Bourda et al. (2010). About 90% of the sample could be detected and VLBI images were produced for about 60% of those detected sources, hence revealing point-like VLBI structures for half of them (Bourda et al., 2011, 2015a); 119 sources were selected for the final stage dedicated to astrometry (Bourda et al., 2015b). Figure 1 shows the sky distribution of these 119 sources (red points).

In the meantime, we investigated the potential of the ICRF2 catalog in terms of transfer sources (excluding the VCS sources; VLBA Calibrator Survey; see Petrov et al., 2008 and references therein), by cross-correlating it with the optical LQAC2 catalog (Souchay et al., 2012). By selecting only those sources brighter than optical magnitude 18 and with an X-band continuous structure index below 3 for ensuring a good astrometric accuracy (i.e. point-like structure on VLBI scales), we identified 195 ICRF2 transfer sources (Bourda & Charlot, 2012). Figure 1 shows the sky distribution of these sources (green points) and Figure 2 shows their total flux density at X-band, as determined from VLBI images (see Bordeaux VLBI Image Database; BVID³). They are relatively well distributed on the sky. Some of them are weaker than other ICRF2 sources observed more regularly by the IVS (i.e. X-band total flux density < 100 mJy). An observing proposal was submitted to the IVS for specifically maintaining these sources: recommendations were made to reach proper astrometric accuracy (i.e. below $200 \mu\text{as}$) and observing rate (i.e. once a month). Accordingly, since 2013, these ICRF2 transfer sources have been observed more intensively by the IVS, through a GSFC continuous effort (see K. Le Bail, this issue).

Concerning the southern hemisphere and higher frequencies, in the framework of the ICRF3 working group, various projects were launched considering the observation of suitable Gaia transfer sources:

- Based on the LBA (Long Baseline Array) Calibrator Survey (LCS; Petrov et al., 2011), 190 southern optically-bright VLBI sources were identified. About 20% of them were already observed for VLBI imaging at the beginning of this year, with a follow-up imaging experiment that should soon be carried out (PI: A. de Witt). Astrometry is under study for observations between South Africa and Australia.
- X/Ka observations of optically-bright VLBI sources are also regularly carried out with DSN (Deep Space Network) antennas:
- K-band observations of potential Gaia transfer sources might also be a goal within the next years (see A. de Witt, this issue).

³ <http://www.obs.u-bordeaux1.fr/BVID/>

3 Conclusion

To summarize, we can consider that the current number of VLBI–Gaia transfer sources available is of the order of ~ 400 (S/X-bands) : (i) the 195 ICRF2 transfer sources described above, as well as (ii) the 119 *weak* non-ICRF2 extragalactic radio sources observed with the EVN and the VLBA, and finally (iii) ~ 100 potential southern sources (if half of those identified as transfer sources candidates are really point-like on VLBI scales). In the future, this list might be adjusted, depending on what Gaia will effectively observe and detect.

Concerning the ICRF2 Gaia transfer sources, the VCS catalogue must be investigated. More than 2000 sources from ICRF2 have indeed been observed mostly only one time during such a VCS session and they had not been considered from our studies until now. For the optically bright sources, the structure index must be computed if possible (i.e. for those with VLBI images) in order to investigate their astrometric quality.

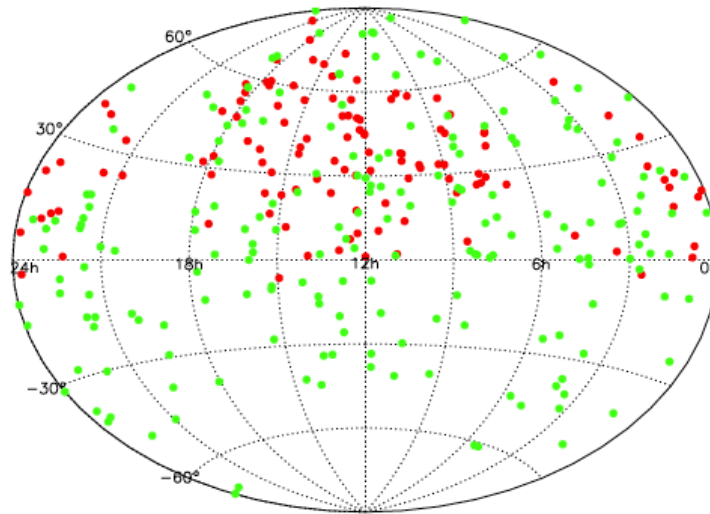


Fig. 1 Sky distribution for the Gaia transfer sources: red points are the 119 *weak* extragalactic radio sources from NVSS catalog; green points are the 195 ICRF2 transfer sources identified

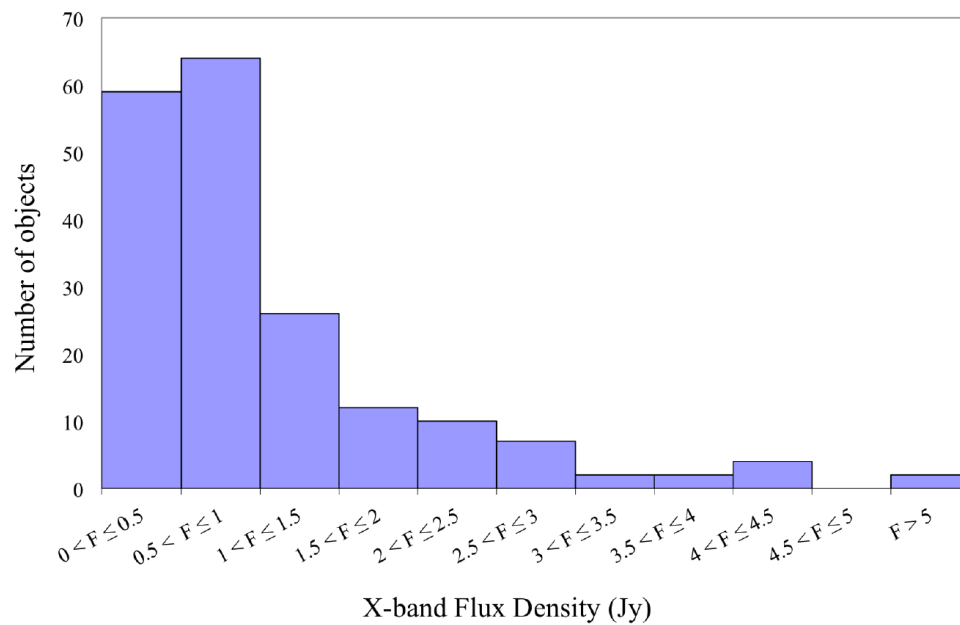


Fig. 2 Distribution of the X-band flux density for the 195 ICRF2 transfer sources suitable for the alignment with the Gaia frame (units in Jy). The values plotted here correspond to the integrated flux density over the VLBI images (as available from the BVID) and represent for each source the mean value of all measurements over the years.

References

- Bourda G, Charlot P, Le Campion J F (2008) Astrometric suitability of optically-bright ICRF sources for the alignment with the future Gaia celestial reference frame. *Astron Astrophys*, 490, 403–408.
- Bourda G, Charlot P, Porcas R, S. Garrington S (2010) VLBI observations of optically-bright extragalactic radio sources for the alignment of the radio frame with the future Gaia frame: I–Source detection. *Astron Astrophys*, 520, A113.
- Bourda G, Collioud A, Charlot P, Porcas R, Garrington S (2011) VLBI observations of optically-bright extragalactic radio sources for the alignment of the radio frame with the future Gaia frame: II–Imaging candidate sources. *Astron Astrophys*, 526, A102.
- Bourda G, Charlot P (2012) Observations of ICRF2 Sources to Improve the Astrometry of the Future Radio-optical Transfer Sources, In: *IVS Memorandum*, 2012-001v01 May 4, 2012.
- Bourda G, *et al.* (2015) VLBI observations of optically-bright extragalactic radio sources for the alignment of the radio frame with the future Gaia frame: III–Final Images of candidate sources. *Astron Astrophys*, (in prep.).
- Bourda G, *et al.* (2015) VLBI observations of optically-bright extragalactic radio sources for the alignment of the radio frame with the future Gaia frame: IV–Astrometry of candidate sources. *Astron Astrophys*, (in prep.).
- Charlot P (1990) Radio-source structure in astrometric and geodetic very long baseline interferometry. *Astron J* 99, 1309–1326.
- Condon J J, Cotton W D, Greisen E W, *et al.* (1998) The NRAO VLA Sky Survey. *Astron J*, 115, 1693–1716.
- de Witt A, Bertarini A, Jacobs C S, Quick J, Horiuchi S, Lovell J E J, McCallum J M, Jung T, Bourda G, Charlot P (2015) A Celestial Reference Frame at 22 GHz (K-band). In: R. Haas, F. Colomer (eds.) *EVGA 2015 Proc.*, 272–276.
- Fey A L, Ma C, Arias E F, Charlot P, Feissel-Vernier M, Gontier A-M, Jacobs C S, MacMillan D S (2004) The Second Extension of the International Celestial Reference Frame: ICRF-EXT.1. *Astron J*, 127, 3587–3608.
- Fey A F, D. Gordon D, Jacobs C S, Ma C, Gaume R A, Arias E F, Bianco G, Boboltz D A, Böckmann S, Bolotin S, Charlot P, Collioud A, Engelhardt G, Gipson J, Gontier A-M, Heinkelmann R, Kurdubov S, Lambert S, Lytvyn S, MacMillan D S, Malkin Z, Nothnagel A, Ojha R, Skurikhina E, Sokolova J, Souchay J, Sovers O J, Tesmer V, Titov O, Wang G, Zharov V (2015) The Second Realization of the International Celestial Reference Frame by Very Long Baseline Interferometry. *Astron J*, 150, 58.
- Kovalev Y Y, Lobanov A P, Pushkarev A B, Zensus J A (2008) Opacity in compact extragalactic radio sources and its effect on astrophysical and astrometric studies. *Astron Astrophys*, 483, 759–768.
- Le Bail K, Gordon D, Gipson J M, MacMillan D S (2015) Observing Gaia transfer sources in R&D and RDV sessions. In: R. Haas, F. Colomer (eds.) *EVGA 2015 Proc.*, 277–280.
- Lindgren L, Babusiaux C, Bailer-Jones C, *et al.* (2008) The Gaia mission: science, organization and present status. In: W. Wenjin, I. Platais & M. Perryman (eds.) *Proc. IAU Symposium 248, A Giant Step: from Milli- to Micro-arcsecond Astrometry*, Cambridge University Press, 217–223.
- Ma C, Arias E F, Eubanks T, Fey A L, Gontier A-M, Jacobs C S, Sovers O J, Archinal B A, Charlot P (1998) The International Celestial Reference Frame as Realized by Very Long Baseline Interferometry. *Astron J*, 116, 516–546.
- Mignard F (2003) Future Space-Based Celestial Reference Frame, R. Gaume, D. McCarthy & J. Souchay (eds.) In: *Proc IAU General Assembly XXV*, Joint Discussion 16: The International Celestial Reference System: Maintenance and Future Realization, 133–140.
- Mignard F (2014) *EGSG 2014 workshop*, Paris, France.
- Petrov L, Kovalev Y Y, Fomalont E, Gordon D (2008) The Sixth VLBA Calibrator Survey: VCS6, *Astron J*, 136, 580–585.
- Petrov L, Phillips C, Bertarini A, Murphy P, Sadler E M (2011) The LBA Calibrator Survey of southern compact extragalactic radio sources – LCS1. *Mon Not R Astron Soc*, 414, 2528–2539.
- Souchay J, Andrei A, Barache C, Bouquillon S, Suchet D, Taris F, Peralta R (2012) The second release of the Large Quasar Astrometric Catalog (LQAC-2). *Astron Astrophys*, 537, A99.

Estimating the velocity of the barycenter of the solar system from VLBI observations

M. H. Xu, J. Anderson, R. Heinkelmann, H. Schuh, G. L. Wang

Abstract The property of time independence of the International Celestial Reference Frame (ICRF) requires a careful contemplation for the aim of establishing and using the ICRF at the microarcseconds level. The proper motion of the radio sources, which has always been ignored in geodetic VLBI, is actually caused by the relative motion of the observed object and the observer. The motion field of radio sources with respect to the Cosmic Microwave Background (CMB) may be regarded as random over the sky, but the motion of the origin of the ICRF, the barycenter of the solar system (SSB), with respect to the CMB is identical for all the observed objects. Therefore, proper motions caused by the motion of the barycenter should manifest in systematic variations. Based on the current value of this motion from astrophysical research, around 400 km/s, the magnitude of this systematic variation would be 1 microarcsecond (μas) per year for a radio source with redshift of 0.02. We investigate the magnitude of the proper motion caused by the velocity of the SSB based on the ICRF2 radio sources with redshifts and a priori values for the velocity, and present the result of the estimation of the velocity from VLBI data.

Keywords Velocity of the barycenter of the Solar system, redshift, VLBI

1 Introduction

The ICRF realized by extragalactic radio sources is by definition time independent because the radio sources are extremely distant. It thus effectively circumvented the intricate difficulty of determining separately from the proper motions of the objects

Minghui Xu, Guangli Wang
Shanghai Astronomical Observatory (SHAO), Chinese Academy of Sciences, No. 80 Nandan Road, 200030, Shanghai, China
Minghui Xu, James Anderson, Robert Heinkelmann, Harald Schuh
DeutschesGeoForschungsZentrum (GFZ), Potsdam, Telegrafenberg, A17, 14473 Potsdam, Germany

the motions of the equator and the ecliptic, namely the precession, in constructing the stellar reference frame.

Obviously, this definition of time independence for the ICRF requires a careful investigation if the required level of accuracy for the celestial frame is at the level of μas . The typical astrometric and geodetic observation has four components: motion of the observed object, motion of the observer, light propagation and the process of observation. In this article we will focus on the first two components. Moreover, for the observation of an radio source, the motion of the observed object should take into account its interior motion, the effect of the intrinsic source structure. Therefore, four effects by the first two components can alter the apparent position of a radio source: the effect of source structure, the proper motion, the parallax caused by the velocity of the SSB in space, and the aberration drift caused by the acceleration of the SSB. It is of note that the summation of the proper motion and the parallax is actually caused by the relative motion of the observed object and the observer. The determination of the parallax caused by the motion of the observer with respect to the SSB is facilitated by the periodic character which it produces. However, since the motion of the SSB with respect to the CMB, probably steady constant during a few hundreds of years, is practically treated as part of the motion of the object, the parallax caused by this motion is modeled as the proper motion. However, the motion of each individual object should be random over the sky, but the motion of the SSB is identical for all objects.

If the effects of the intrinsic source structure and of the proper motion are random over the sky, there will be two effects causing systematic variations of source positions considering the desired level of accuracy of a few μas in astrometry: the aberration drift caused by the acceleration of the SSB with respect to the CMB, which has been determined and discussed in a series of papers (Xu et al., 2012; Titov and Lambert, 2013) and the proper motion caused by the velocity of the SSB that manifests in a secular change of the parallax.

In this study, we will investigate three questions: 1. how does the secular parallax caused by the motion of the barycenter in space affect the determination of the acceleration of the barycenter? 2. can VLBI observations detect the velocity of the barycenter with respect to radio sources? If yes, to what level? 3. Should we consider the systematic variation caused by the secular parallax in VLBI data analysis?

2 Method

Due to the secular aberration drift the direction of the radio source is a function of the barycenter's acceleration \mathbf{a} , given by

$$\mathbf{K}_t = \mathbf{K}_0 + \frac{(\mathbf{K}_0 \times \mathbf{a}) \times \mathbf{K}_0}{c} (t - t_0), \quad (1)$$

where \mathbf{K}_0 is the direction of the radio source in the BCRS at reference epoch t_0 (e.g. J2000.0), and c is the speed of light in vacuum. Since the change in the SSB's velocity is very small with respect to the speed of light, the classical formula of the aberration and the first order of the acceleration are sufficient here.

When the parallax caused by the velocity of the barycenter is considered, the direction of the radio source is expressed as follows

$$\mathbf{K}_t = \mathbf{K}_0 - \frac{(\mathbf{K}_0 \times \mathbf{V}) \times \mathbf{K}_0}{d} (t - t_0), \quad (2)$$

where \mathbf{V} is the velocity of the SSB, which is a constant at least in hundreds of years, and d is the distance to the object. According to astrophysical studies, the velocity of the Solar system with respect to the CMB is estimated to be 370 km/s towards the direction, $(\alpha, \delta) = (167^\circ.4, -6^\circ.7)$ (Fixsen et al., 1996).

According to the formula of the geometric delay given by IERS Conventions 2010, the partial derivative of the VLBI geometric delay τ with respect to the instant direction \mathbf{K}_t , accurate up to terms of order $O((\mathbf{V}_\oplus + \omega_2)^2/c^2)$, can be written as follows

$$\frac{\partial \tau}{\partial \mathbf{K}_t} = -\frac{\mathbf{b}}{c + \mathbf{K}_t(\mathbf{V}_\oplus + \omega_2)} + \frac{\mathbf{K}_t \cdot \mathbf{b}}{c^2} (\mathbf{V}_\oplus + \omega_2), \quad (3)$$

where \mathbf{b} is the geocentric baseline vector, and $\mathbf{V}_\oplus, \omega_2$ are the barycentric velocity of the geocenter and the geocentric velocity of the second receiver, respectively. In fact, when calculating the value of this partial derivative, it is accurate enough to apply \mathbf{K}_0 instead of the \mathbf{K}_t in the right hand of equation (3).

Upon these equations, the partial derivatives of the VLBI geometric delay τ with respect to the acceleration and the velocity are given by the expressions

$$\frac{\partial \tau}{\partial \mathbf{a}} = \frac{\partial \tau}{\partial \mathbf{K}_t} \cdot \frac{\partial \mathbf{K}_t}{\partial \mathbf{a}}, \quad (4)$$

$$\frac{\partial \tau}{\partial \mathbf{V}} = \frac{\partial \tau}{\partial \mathbf{K}_t} \cdot \frac{\partial \mathbf{K}_t}{\partial \mathbf{V}}, \quad (5)$$

where the partial derivatives of the direction of the object with respect to the acceleration and the velocity is readily calculated by equations (1) and (2), respectively.

We notice that, from equations (1) and (2), it is impossible to separate the acceleration and the velocity of the barycenter by using an individual object even though we exactly know the proper motion and the distance. And the velocity of the barycenter and of the object could not be separated, neither. The practical way that can achieve this is to use as many radio sources as possible with a good distribution over the sky and a sufficient wide range of redshift.

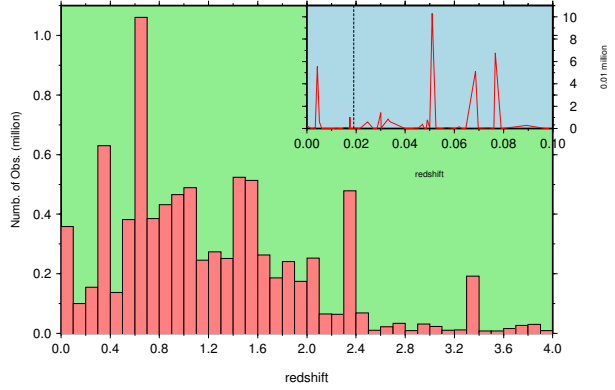


Fig. 1 The number of VLBI observations with respect to redshift. The inset plot in the upper right corner shows the number of observations as a function of redshift up to redshift 0.1.

3 Redshift

The only way at present to infer the distance of a radio source is based on the cosmological distance by using the redshift. There are 3414 radio sources in the ICRF2, 950 radio sources of which have available data of redshift (Andrei et al., 2009; Souchay et al., 2012). There are in total about 9 million VLBI group delay observables available from IVS archives, and more than 90 % of the observables refer to one of the 950 radio sources. Figure 1 shows the number of VLBI observations to radio sources with known redshift grouped by redshift. We see that radio sources with redshift from 0.3 to 2.4 serve as main targets for geodetic observations. According to the model of the angular size distance of a distant object, the source with the redshift at the level of 1 is located at about 1000 Mpc away. Based on the astrophysical estimation of the SSB's velocity, the proper motion caused by the SSB's velocity, for most of these sources, is actually less than $0.1 \mu\text{as/yr}$, far beyond the accuracy level of today's VLBI observations. The inset plot in the upper right corner shows the number of observations as a function of redshift up to redshift 0.1. The black dashed line at the redshift of 0.019 indicates that a closer radio source would have an expected proper motion at the level of $1 \mu\text{as/yr}$. The number of observations with redshift smaller than 0.019 is about 75,000 only.

Table 1 shows the statistics of the radio sources in the ICRF2 catalog, which have redshift less than 0.029. There are three radio sources that are still observed nowadays.

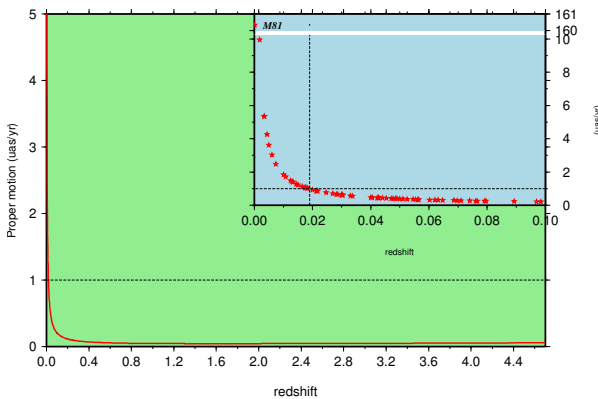
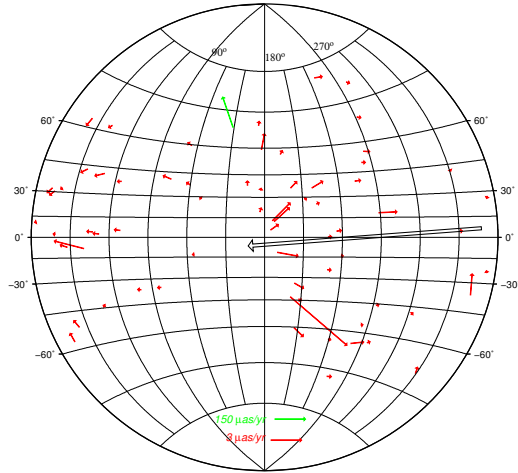
Based on the SSB's velocity and equation (2), the expected proper motion can be figured out (Fig. 2). When the redshift lies above 0.3, the proper motion becomes less than $0.1 \mu\text{as/yr}$. The inset plot in the upper right corner shows the proper motions of radio sources in the ICRF2 catalog with redshift less than 0.1. And the black dashed line corresponds to the proper motion of $1 \mu\text{as/yr}$. M81, with its extremely small redshift, should have a proper motion of about $156 \mu\text{as/yr}$ as shown in the inset plot.

Figure 3 shows the proper motions of 68 radio sources with redshift less than 0.1 caused by the velocity of the SSB. The big black vector illustrates the direction of the velocity of the Solar

Table 1 Statistics of the radio sources with red shift less than 0.03.

Source name	Num. of Obs. Sess.	First obs.	Last obs.	Redshift	
M81	2207	77	1993.06	2009.10	0.0001
CEN-A	72	8	1990.08	2002.05	0.0018
M84	667	28	1996.08	2009.10	0.0033
M104	40	14	1995.06	2005.06	0.0034
3C274	55681	1646	1986.03	2014.04	0.0042
NGC1052	5851	257	1988.01	2014.04	0.0050
2254-367	19	4	2002.01	2004.05	0.0060
NGC4261	79	3	1996.08	2007.01	0.0073
NGC6500	32	4	1996.08	2002.05	0.0100
NGC3894	120	7	1994.08	2000.08	0.0107
1333-337	189	5	2008.01	2013.12	0.0124
1343-601	22	4	2003.09	2004.05	0.0129
NGC5675	85	10	1996.08	2000.05	0.0132
1718-649	93	22	1990.08	2008.07	0.0144
NGC0262	981	26	1996.05	2010.04	0.0150
NGC0315	869	22	1996.05	2004.06	0.0164
NGC5141	8	2	1999.04	2004.05	0.0173
3C84	10208	282	1979.08	2013.07	0.0175
0147-076	18	8	1994.06	2005.06	0.0176
0056-572	36	8	1989.04	2003.10	0.0180
0125+628	81	1	2006.08	2006.08	0.0183
0131-522	417	66	1990.09	2014.04	0.0200
UG01841	45	2	1999.09	2004.03	0.0212
0651+410	230	7	1996.06	2004.06	0.0215
NGC3862	274	17	1996.10	2004.05	0.0217
NGC6251	5825	211	1997.08	2014.03	0.0247
2201+044	42	1	2007.06	2007.06	0.0270
2152-699	23	7	1990.08	2003.11	0.0282
NGC1218	1071	36	1996.08	2010.05	0.0286

system. The directions of this proper motion field have a dipole characteristic but the magnitude is random over the sky.

**Fig. 2** The proper motion field of radio sources in the ICRF2 catalog due the velocity of the Solar system as a function of redshift.**Fig. 3** The proper motion field of 68 radio sources in ICRF2 with redshift less than 0.1 due to the velocity of the Solar system.

4 Results from VLBI observations

The data we used in our solutions were taken from the International VLBI Service for Geodesy and Astrometry (IVS; Schuh and Behrend, 2012) data center. There were totally 8.1 million group delay observables from April 1980 to April 2013. The CALC/SOLVE software (Petrov, 2008) developed and maintained by NASA Goddard Space Flight Center was used for the VLBI data analysis. The USER_PARTIAL function, an external interface provided by this software, was utilized for the integration of the estimation models of the acceleration and the velocity into the VLBI data processing. The routine global solution, comparable to the ITRF solution, was applied and the common parameterization was divided into three groups including global, local, and segmented parameters, see Xu et al. (2012).

Two solutions were made to estimate the velocity. First, the acceleration of the SSB, obtained by Xu et al. (2012) with the magnitude of $8.45 \text{ mm} \cdot \text{s}^{-1} \cdot \text{yr}^{-1}$ towards the direction, $(\alpha, \delta) = (242^\circ.8, -11^\circ.5)$ was used as a priori value to correct the secular aberration drift, and then the velocity was estimated. Second, both the acceleration and the velocity were estimated simultaneously based on the models. Table 2 shows the results with the theoretical values for comparison.

The uncertainty of the estimated velocity, at the level of 10^4 km/s , is comparable to the magnitude of the velocity itself, which means that this parameter is not a significant signal in VLBI observations. And the uncertainty to this level is quite reasonable according to the previous discussion on the cosmological distances of radio sources. The magnitude of the estimated velocity is much larger than the one predicted by theory. This should tell us that, as one may expect, in VLBI observations till nowadays the effect of the proper motion caused by the SSB's velocity is not significant. And the result from the estimation differs from the theoretical value so much because VLBI data at present can only be sensible for this parameter to the level of 10^4 km/s .

Table 2 The estimated acceleration and velocity with their uncertainties from VLBI data in the equatorial coordinate system. The first line gives the theoretical values for the acceleration and the velocity of the SSB for comparison.

	Acceleration ($\text{mm} \cdot \text{s}^{-1} \cdot \text{yr}^{-1}$)			Velocity (10^3 km/s)		
	X	Y	Z	X	Y	Z
Theoretical values	-3.78	-7.37	-1.68	-0.36	0.08	-0.04
Est. velo. only	-	-	-	-7.5 ± 1.0	-9.1 ± 0.8	-11.4 ± 11.5
Est. simult.	-3.21 ± 0.45	-7.07 ± 0.42	1.05 ± 0.72	-5.1 ± 1.2	-3.9 ± 0.9	-12.2 ± 13.9

The last row in Table 2 shows the estimated results when the acceleration and the velocity were estimated simultaneously in the data analysis. The X and Y components of the estimated acceleration coincide with the theoretical values within the uncertainties, while the Z component differs significantly. The Z component is the most insensitive of the three components for the velocity as well as for the acceleration.

5 Conclusion and discussion

VLBI data covering about 34 years have the capacity to constrain the solar velocity to about 10^4 km/s , which is much larger than it is expected to be. Through the estimation we find that the systematic variation caused by the relative motion between radio source and barycenter is negligible for the determination of the barycentric acceleration. As one may expect, the proper motion caused by the SSB's velocity is not a significant effect. The variation in position of radio source should be dominantly caused by the source structure. Gaia (Lindegren et al., 2010) is observing and will observe many more quasars with a wide range of redshifts. If the expected accuracy of Gaia can be reached, the motion of the barycenter can be studied based on Gaia data. The relationship between the cosmological distance and the astrometric distance of an extragalactic object may then be studied as well.

References

- Andrei A H, Souchay J, Zacharias N, Smart R L, Vieira Martins R, da Silva Neto D N, Camargo J I B., Assafin M, Barache C, Bouquillon S, Penna J L, Taris F (2009) The large quasar reference frame (LQRF): An optical representation of the ICRS. *Astron Astrophys*, 505, 385-404.
- Fixsen D J, Cheng E S, Gales J M, Mather J C, Shafer R A, Wright E L (1996) The Cosmic Microwave Background Spectrum from the Full COBE FIRAS Data Set. *Astrophys J*, 473, 576.
- Lindegren L, Seidelmann P K, Soffel M H (2010) Gaia: Astrometric performance and current status of the project. Paper presented at the IAU Symposium. <http://adsabs.harvard.edu/abs/2010IAUS..261..296L>
- Petrov L (2008) Mark-5 vlbi analysis software calc/solve. Web document <http://gemini.gsfc.nasa.gov/solve/>, 02 2014.
- Schuh H, Behrend D (2012) VLBI: A fascinating technique for geodesy and astrometry. *J Geodyn*, 61, 68–80.
- Souchay J, Andrei A H, Barache C, Bouquillon S, Suchet D, Taris F, Peralta R (2012) The second release of the Large Quasar Astrometric Catalog (LQAC-2). *Astron Astrophys*, 537, 99.
- Titov O, Lambert S (2013) Improved VLBI measurement of the solar system acceleration. *Astron Astrophys*, 559, 95.
- Xu M H, Wang G L, Zhao M (2012) The solar acceleration obtained by VLBI observations. *Astron Astrophys*, 544, 135.

The CVN Geodetic Observation and its Result

G. Wang, M. Xu, Z. Zhang, S. Xu, L. Li, F. Shu

Abstract The China VLBI Network, CVN, has been developed to consist of five antennas, Seshan 25m, Urumq 25m, Kunming 30m, Miyun 50m and Tianma 65m. Since the year of 2006, more than 20 geodetic domestic observations have been carried out. In this report the observation and data result will be presented.

Keywords CVN, data analysis

1 Introduction

In the background of the Chinese lunar exploration project, Chang'E-1 and Chang'E-2, the CVN has been developed to have four antennas, Seshan 25m, Urumq 25m, Kunming 30m and Miyun 50m (see Fig. 1). A new antenna in Shanghai with aperture 65m has been built and will involved in observations of the CVN in the end of this year.

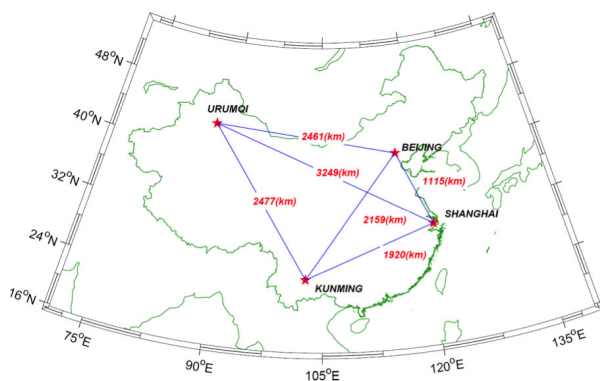


Fig. 1 Map of the CVN.

Guangli Wang, Minghui Xu, Zhibin Zhang, Shuangjing Xu, Liang Li, Fengchun Shu
Shanghai Astronomical Observatory

2 The geodetic experiments of CVN

The CVN experiments started since 2006, supporting by a project of crustal motion observation network and by lunar mission. There were about 25 experiments scheduled, 19 of them obtained results. These experiments are listed below in Table 1. The columns Sh, Bj, Km, Ur, Tm are Seshan25, Beijing, Kunming, Urumqi and Tianma65 station, respectively.

Table 1 Statistical information on the CVN experiments.

Exp.code	Date	Stations	Wrms D.res. (ps)	Nobs
s6602	2006.06.01	ShBjKmUr	30.27	187
r7404a	2007.04.04	ShBjKmUr	57.31	1561
r7620a	2007.06.20	ShBjKmUr	32.66	479
r8919a	2008.09.19	ShBjKmUr	36.11	282
g1003d	2010.06.22	ShKmUr	65.84	545
g1004a	2010.07.27	ShKmUr	48.49	368
g1005a	2010.08.10	ShKmUr	64.49	414
r0902a	2010.09.02	ShBjKmUr	45.97	1509
r1117a	2011.01.17	ShBjKmUr	34.3	2534
r1325a	2011.03.25	ShBjKmUr	53.79	1598
r1425a	2011.04.25	ShBjKmUr	55.67	902
r1524a	2011.05.24	ShKmUr	44.44	1136
r1720a	2011.07.20	ShKmUr	44.04	2248
r1a11a	2011.10.11	ShKmUr	112	641
r1b14a	2011.11.14	ShKmUr	100.1	1302
cn1304	2013.09.11	ShKmUr	46	446
cn1305	2013.11.21	ShKmUrTm	16.5	1323
cn1401	2014.09.28	ShBjKmUr	57.8	1097
cn1402	2014.10.18	ShKmUrTm	55.6	1082

3 Data reduction

There are two software systems used in data reduction:

1. SCORR+GAPS+OCCAM/VieVS
2. DiFX+HOPS+CALC/SOLVE

The first system can only produce NGS data file. Since last year (2014) we started work on the second system. We use the first

software system to do the data processing for CVM experiments. SCORR is software correlator, GAPS is post-correlation software, both developed by SHAO, the data production was written in NGS format through software gnss. Data analysis is done by OCCAM. We estimated the NGS data from IVS data containing CVN stations and CVN data from 2006.1 to 2014.10, reference frames are constraint to ICRF2/ITRF2008. Parameters estimated are stations positions, nutations, UT1 rate, piecewise clock/atm. 60/30min.

4 Results

The data we used here are totally 11 sessions of the CVN observations from Jun. 2006 to Oct. 2014. The results are shown in tables 2, 3 and 4. Time series of station positions are displayed in Fig. 2, while Fig. 3 depict the postfit WRMS residuals for experiment CN1305.

Table 2 CVN stations positions (Ref.Epoch 2010).

Station	X (mm)	Y (mm)	Z (mm)
BEIJING	-2201304677.55 ±8.75	4324789078.87 ±6.17	4125367778.93 ±6.59
KUNMING	-1281152740.24 ±12.16	5640864383.96 ±12.26	2682653476.02 ±8.06
SESHAN25	-2831687299.99 ±0.73	4675733525.17 ±0.66	3275327536.25 ±0.67
URUMQI	228310309.47 ±1.52	4631922766.55 ±1.52	4367064047.76 ±1.13

Table 3 CVN station velocities.

Station	Vx (mm/yr)	Vy (mm/yr)	Vz (mm/yr)
BEIJING	-26.62 ± 5.81	-6.32 ± 4.06	-11.44 ± 4.24
KUNMING	-36.33 ± 6.63	2.74 ± 5.78	-9.60 ± 4.28
SESHAN25	-29.87 ± 0.11	-11.35 ± 0.11	-11.93 ± 0.09
URUMQI	-32.12 ± 0.28	-0.97 ± 0.30	5.21 ± 0.18

Table 4 Tianma65s position from CVN experiments.

	X (mm)	Y (mm)	Z (mm)
CN1305	-2826708626.59	4679237079.15	3274667538.14
(2013.11.21)	±2.267	±3.961	±3.691
CN1402	-2826708609.64	4679237024.88	3274667446.25
(2014.10.18)	±9.124	±19.370	±12.286

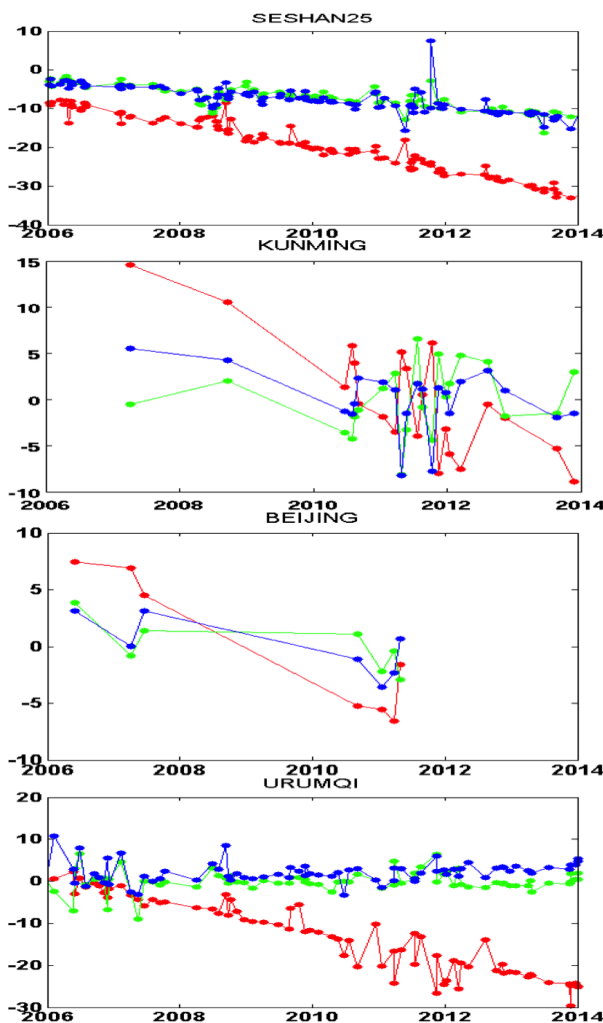


Fig. 2 The 4 stations positions time series.

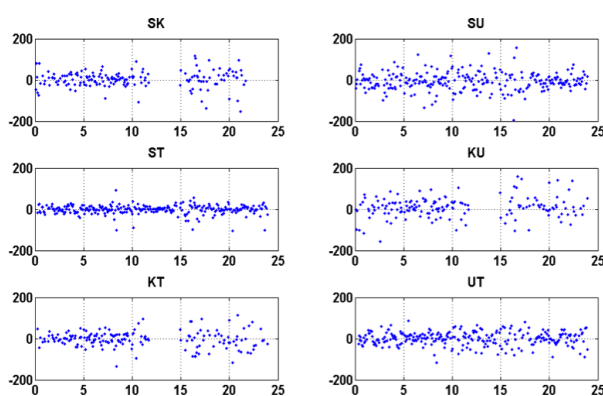


Fig. 3 CN1305 post-fit delay wrms residuals(ps).

Minimization of the UT1 Formal Error Through a Minimization Algorithm

J. Gipson, K. Baver

Abstract The purpose of the IVS-INT01 sessions is the estimation of UT1. Improving the accuracy and the precision of the UT1 estimates is an important goal in scheduling these sessions. We previously investigated reducing the UT1 formal error through the use of the *Sked* scheduling program (e.g., by using new source catalogs or by changing *Sked* parameters). Here we describe a new approach — using minimization algorithms to find the hypothetical observation set that minimizes the UT1 formal error. We report on our progress and on the application of our work to evaluating actual and possible Intensive schedules.

Keywords Minimization, UT1

1 Introduction

Suppose that we could put our observations anywhere. Where would we put them to minimize the UT1 formal error? Of course the resulting schedules would be unrealistic, but we might learn something that will help us in writing real schedules. In this paper we report on our approach to this question. First, we give background about the use of gradients in evaluating schedules. Then we describe our development of software that uses gradients to minimize the UT1 formal error. We present the results of using the minimization software and the insights we gained into scheduling. Finally, we create two new scheduling techniques suggested by the minimization results and test them on two sessions. We focus on the IVS INT01 Intensive series, which uses the Kokee-Wettzell (KK—WZ) baseline.

John Gipson and Karen Baver
NVI, Inc., 7257D Hanover Parkway, Greenbelt Maryland,
20770, USA

2 Using Gradients to Evaluate Intensive Schedules

Assume that the epochs and sigmas of the observations are fixed, but we can vary the location of the observations. Then we can consider σ_{UT1} as a function of the azimuths and the elevations of the observations. The gradient of σ_{UT1} tells us the sensitivity of the UT1 formal error to small changes in the position of the observations:

$$\sigma_{UT1}(\vec{az} + \delta\vec{az}, \vec{el} + \delta\vec{el}) \cong \sigma_{UT1}(\vec{az}, \vec{el}) + \frac{\partial\sigma_{UT1}(\vec{az}, \vec{el})}{\partial\vec{az}} \cdot \vec{\delta az} + \frac{\partial\sigma_{UT1}(\vec{az}, \vec{el})}{\partial\vec{el}} \cdot \vec{\delta el} \quad (1)$$

If the gradient is large, then small changes in position will result in large changes in the UT1 formal error. If the gradient is small, then small changes in position will have little effect.

The plots in Figure 1 show gradients for two IVS-INT01 sessions. In Figure 1a, σ_{UT1} is relatively insensitive to changes in the positions of the observations. Moving any of the observations a small amount will have a negligible effect on σ_{UT1} . A session's composite gradient average is the average of its observations' composite gradients, where each observation's composite gradient is calculated by squaring the observation's gradients with respect to azimuth and elevation, adding the two squares, and taking the square root of the sum. The composite gradient average for Figure 1a is 0.025 $\mu\text{s}/\text{degree}$ —that is, moving a single observation 1° would, on average, change the UT1 formal error by 0.025 μs . In contrast, in Figure 1b, σ_{UT1} is very sensitive to the changes in positions of a few of the observations. The session's composite gradient average is 0.436 $\mu\text{s}/\text{degree}$.

3 Our Approach to Minimization

We used the Fletcher-Reeves-Polak-Ribiere (FRPR) variant of the Conjugate Gradient method from Numerical Recipes (third edition) and its Fortran software package to minimize the UT1 formal error. The Conjugate Gradient method uses gradients to determine the direction of greatest change of a function in order

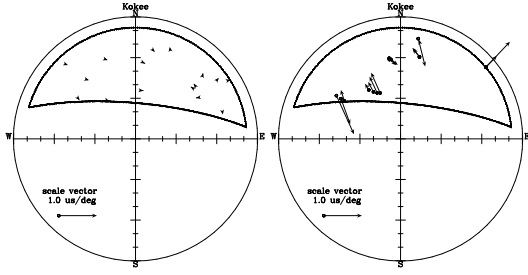


Fig. 1 a) Small initial gradients (\$14NOV14XU) and b) large initial gradients (\$14OCT16XU). The crescent shaped area denotes the area of mutual visibility for Kokee and Wettzell. Gradients were calculated using elevation dependent observation sigmas for \$14NOV14XU and constant (30 ps) observation sigmas for \$14OCT16XU.

to efficiently minimize it. In our case, the function is the UT1 formal error, and our variables are the positions of the observations. The FRPR algorithm begins by evaluating the gradient at the starting point. It then performs a 1-D minimization along the line determined by the gradient. At the minimum it evaluates the gradient again. But, unlike in the Steepest Descent method, the new direction chosen is orthogonal to the previous direction. This process is repeated until the change in function between iterations is below some threshold or some number of iterations is exceeded. In our case the threshold was $1e-7 \mu s$, and the number of iterations was 250. Use of this method required calculation of the UT1 formal error and its gradient.

We wrote a subroutine to calculate σ_{UT1} given the observations' epochs, positions in Az-El at Kokee, and uncertainties. This subroutine builds up the normal equation for the six parameters that we usually estimate for the INT01 Intensives (UT1, an atmosphere offset at Kokee and Wettzell, and a clock offset, clock rate and clock second order term at Wettzell). The normal matrix is inverted, and the UT1 formal error is extracted. We verified our results against the UT1 formal error calculated by *Sked* and by our Solve program.

We also wrote a subroutine to compute the gradient of UT1 with respect to the azimuth and elevation of the observations. The gradient was evaluated numerically. For example, for the azimuth partial we used:

$$\frac{\partial \sigma_{UT1}(az_j)}{\partial az_j} \cong \frac{\sigma_{UT1}(az_j + \frac{\delta az}{2}) - \sigma_{UT1}(az_j - \frac{\delta az}{2})}{\delta az} \quad (2)$$

where j labels the observation and δaz is 0.1 degree.

In our implementation of the FRPR algorithm, we made two simplifying assumptions: 1) the observation epochs do not change and 2) the observation errors are either a) 30 ps or b) elevation dependent, defined as follows:

$$\sigma_{obs}^2 = (30ps)^2 + \left(\frac{6ps}{\sin(el_{kk})} \right)^2 + \left(\frac{6ps}{\sin(el_{wz})} \right)^2 \quad (3)$$

The FRPR algorithm pushed the observations below the elevation limit. To prevent this, we added a "penalty term" to the

UT1 formal error which was proportional to $(el_{min} + 0.1 - el)^2$ for $el < el_{min} + 0.1$. This kept the elevation above $el_{min} + 0.1$.

4 Minimization Results

Figure 2 shows the results of applying the minimization algorithm using 30 ps observation sigmas. The top row shows gradients from a session with small initial gradients (\$14NOV14XU), with the left figure showing the gradients before minimization and the right figure showing the gradients after minimization. The bottom row shows gradients from a session with large initial gradients (\$14OCT16XU). The plot coordinates are azimuth and elevation. Similarly, Figure 3 shows the results of applying the minimization algorithm using elevation dependent sigmas to the same schedules. The minimization results shown in the plots are typical for the 2014 sessions. With minimization using 30 ps observation sigmas, the observations tend to move to the "corners" of the crescent shaped area of mutual visibility between Kokee and Wettzell, although imperfectly. The final gradients are very small. With minimization using elevation dependent observation sigmas, observations also move towards the mutual visibility "corners", but to a cluster at $\sim 20^\circ$ of elevation, in most cases totally, and always with at most a few outlying observations. The final gradients are even smaller than in the 30 ps case.

Table 1 shows the effect of minimization on the UT1 formal error. With constant 30 ps observation sigmas, the final UT1 formal errors are $\sim 3.6 \mu s$. With elevation dependent observation sigmas, the final UT1 formal errors are $\sim 5.1 \mu s$.

Table 2 shows the effect of minimization on each session's composite gradient average. With constant 30 ps observation sigmas, the final composite gradient averages are $\sim 0.005 \mu s/\text{degree}$. With elevation dependent observation sigmas, the final composite gradient averages are $\sim 0.002 \mu s/\text{degree}$. Although these numbers are small, they are not zero (which they would be at a true minimum), indicating that there may be room for further improvement.

Table 1 UT1 formal error changes due to minimization (μs).

	30 ps observation sigmas		elevation dependent observation sigmas	
	before	after	before	after
small initial gradients	6.92	3.54	9.12	4.98
large initial gradients	24.31	3.78	31.17	5.21

The results indicate that the observations in the IVS-INT01 sessions are not ideally placed to minimize the UT1 formal errors under the minimization algorithm used in this study. So a different distribution of observations, one that concentrates the observations near the corners of mutual visibility, should be considered during scheduling in order to minimize the UT1 formal errors. We investigate this type of scheduling in the next section.

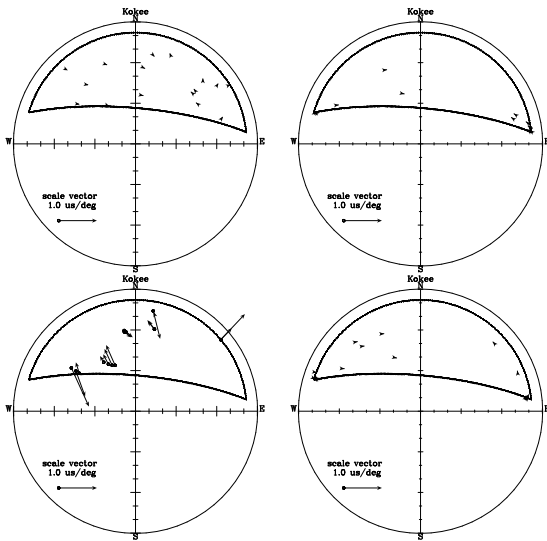


Fig. 2 Session gradients, before (left) and after (right) minimization of the sessions using 30 ps observation sigmas. Top row: a session with small initial gradients. Bottom row: a session with large initial gradients. The coordinate system is Az-El.

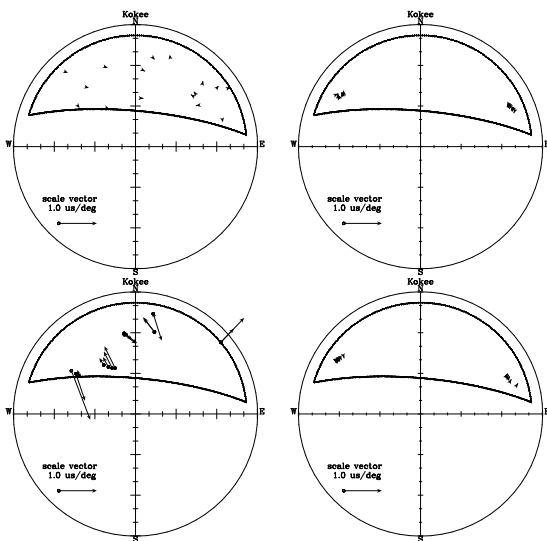


Fig. 3 Session gradients, before (left) and after (right) minimization of the sessions using elevation dependent observation sigmas. Top row: a session with small initial gradients. Bottom row: a session with large initial gradients.

5 Scheduling Application

Two alternating strategies that differ in their available sources are currently used to schedule operational IVS-INT01 sessions. The first strategy, which we call STN (for standard), draws on a small set of strong (but unevenly distributed) sources. Because of the uneven sky distribution, there are times when the STN strat-

Table 2 Composite gradient average changes due to minimization ($\mu\text{s}/\text{degree}$).

	30 ps observation sigmas		elevation dependent observation sigmas	
	before	after	before	after
small initial gradients	0.016	0.005	0.025	0.002
large initial gradients	0.436	0.004	0.508	0.003

egy performs poorly — particularly early October, which has few available sources. The second strategy draws on all geodetic sources that are mutually visible on the Kokee-Wetzell baseline. We call this strategy the Maximal Source Strategy (MSS), and it is described further in Bayer et al. (2012).

We used *Sked* to manually make two kinds of schedules suggested by the minimization results. We drew from the MSS source list and compare our results against MSS schedules. But whereas the MSS strategy may schedule any available source and tends to schedule widely distributed observations, our two test strategies were restricted to schedule within limited areas of the sky that the minimization results had suggested would minimize σ_{UT1} . Because our studies of the STN schedules indicate that early October can be problematic, we made two sets of schedules, one apiece for the source sets available on October 1 and on December 16, a time of the year with a normal number of available sources.

In the Cluster approach we tried to schedule observations at an elevation near 20° and in the regions $66\text{--}75^\circ$ and $301\text{--}310^\circ$ in azimuth. All angles refer to Kokee. This appeared to be the optimum region when we assumed elevation dependent noise. Figure 4 shows schedules made with the Cluster approach. The October 1 and December 16 schedules use four and six sources, respectively, which are low numbers; operational STN and MSS schedules use $\sim 6\text{--}10$ and $10\text{--}18$ sources, respectively. The targeted scheduling area is very small, and it is very hard to find sources near that area, especially using the limited source list that is available on October 1. Table 3 compares the UT1 formal errors and composite gradient averages from these schedules with those from the MSS, assuming elevation dependent noise in both cases. The Cluster formal error for October 1 is 2 to 2.5 times as large as the MSS formal error for October 1 and the Cluster formal error for December 16 (17.71 vs. 7.89 and 6.91 μs , respectively). The October 1 Cluster schedule also has a very large gradient average (0.905 $\mu\text{s}/\text{degree}$), indicating that we could lower the formal errors if we moved the observations, but we were not able to find any other sources to observe given our strategy's constraints. Due to the limited number of sources and the large UT1 formal error and composite gradient average for October 1, we conclude that the Cluster approach is not viable.

The Cone approach was suggested by the case where we used 30 ps of noise for all observations. Here we observed in the corners of the mutual visibility plot; we restricted our azimuths to $270\text{--}315^\circ$ and $45\text{--}90^\circ$, observing as close as possible to 270° and 90° , respectively. We did not restrict the elevations. Figure 5 shows schedules made with the Cone approach. Table 4 compares the UT1 formal errors and the composite gradient averages from the Cone schedules with those from the MSS schedules,

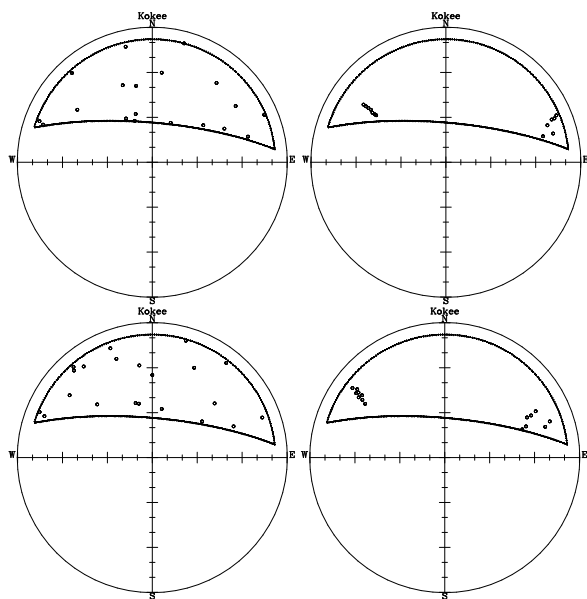


Fig. 4 Cluster and MSS (control) schedules. Top left: MSS Oct 1. Top right: Cluster Oct 1. Bottom left: MSS Dec 16. Bottom right: Cluster Dec 16.

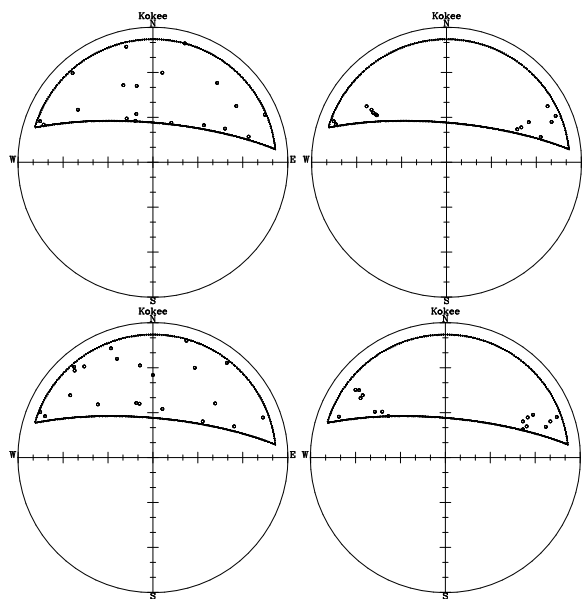


Fig. 5 Cone and MSS (control) schedules. Top left: MSS Oct 1. Top right: Cone Oct 1. Bottom left: MSS Dec 16. Bottom right: Cone Dec 16.

Table 3 UT1 formal errors (μs) and composite gradient averages ($\mu s/\text{degree}$) from hypothetical schedules using the Cluster approach or the MSS (control case). The sparse source list is the list of available sources on October 1. The normal source list is the list on December 16.

	UT1 Formal Error		Gradient Average	
	MSS	Cluster	MSS	Cluster
Sparse source list	7.89	17.71	.021	.905
Normal source list	8.18	6.91	.013	.059

assuming 30 ps noise in both cases. The targeted scheduling area is much larger than in the Cluster approach, and it is easier to find sources. This slightly lessens the source repetition. The October 1 and December 16 schedules use six and eight sources, respectively, which is better than the cluster schedules and within the range of STN schedules but less than the ~10–18 sources scheduled for operational MSS schedules. Both of the Cone schedules have UT1 formal errors ~ 4.1 μs , which are better than the corresponding MSS schedules’ errors of ~ 5.5 μs . Also, although the Cone composite gradient average for October 1 (0.030 $\mu s/\text{degree}$) is higher than the October 1 MSS average (0.014 $\mu s/\text{degree}$), it is much lower than the October 1 Cluster approach average (0.905 $\mu s/\text{degree}$), and the Cone average for December 16 (0.003 $\mu s/\text{degree}$) is lower than both the December 16 MSS and Cluster averages (0.008 and 0.059 $\mu s/\text{degree}$). We think that the Cone approach might be viable, depending on further testing.

6 Conclusions

We wanted to use gradients to identify observation positions that minimize the UT1 formal error. We implemented FRPR Conjugate Gradient minimization, and this implementation identified observation positions near the “corners” of mutual visibility between the Kokee and Wettzell stations as the best positions for minimizing σ_{UT1} . Using elevation dependent observation sigmas for minimization identified positions near a small area of the sky at ~ 20° elevation, and using 30 ps observation sigmas identified positions nearer the horizon and over a wider part of the sky.

We then used the suggested positions as a basis for creating realistic schedules using available sources at two times of the year. The Cluster approach used positions suggested by the minimization with elevation dependent observation sigmas, and the Cone approach used positions suggested by minimization with 30 ps observation sigmas. Due to limited source availability, the Cluster approach does not seem viable. The Cone approach may be viable, subject to further testing.

Table 4 UT1 formal errors (μs) and composite gradient averages ($\mu s/\text{degree}$) from hypothetical schedules using the Cone approach or the MSS (control case).

	UT1 Formal Error		Gradient Average	
	MSS	Cone	MSS	Cone
Sparse source list	5.20	4.37	.014	.030
Normal source list	5.90	3.93	.008	.003

Uunila et al. (2013) demonstrated that observations at the mutual visibility corners are important for obtaining small UT1 formal errors. We go one step further and suggest that corner observations may be not only necessary for obtaining small UT1 formal errors but also sufficient. But it should be noted that other scheduling goals and criteria could make it advisable to observe other areas of the sky.

References

- Bayer K, Gipson J, Carter M S, Kingham K (2012) Assessment of the First Use of the Uniform Sky Strategy in Scheduling the Operational IVS-INT01 Sessions. In D. Behrend, K. D. Bayer (eds.), *IVS 2012 General Meeting Proceedings*, NASA/CP-2012-217504, 251–255.
- Press W H, Teukolsky S A, Vetterling W T, Flannery B P (2007) *Numerical Recipes, The Art of Scientific Computing*, Third Edition: 515–519 and associated software, Cambridge University Press, New York, New York, USA.
- Uunila M, Nothnagel A, Leek J, Kareinen N (2013) Influence of Source Distribution on UT1 Derived from IVS INT1 Sessions. In N. Zubko and M. Poutanen (eds.), *Proc. 21st Meeting of the European VLBI Group for Geodesy and Astrometry*, Finnish Geodetic Institute, Masala, Finland, 111–115.

Automated analysis of Kokee–Wettzell intensive sessions

N. Kareinen, T. Hobiger, R. Haas

Abstract We present results from an automated analysis of IVS intensive sessions, carried out between 2001–2015 on the Kokee–Wettzell baseline. The analysis is based on the version 1 X- and S-band databases in Mark3 format, which means that ambiguity resolution and ionosphere correction need to be done within the automated analysis chain. We use the c5++ VLBI analysis software and process all available databases using several different analysis configurations and investigate the impact of a priori information on the obtained UT1-UTC estimates. We also assess whether external information, i.e. cable delay and weather data extracted from the station log files, is required in order to obtain highly accurate UT1-UTC products. This allows us to conclude whether the availability of external information is crucial for real-time analysis of intensive sessions, or if empirical models can be applied without a significant degradation of the target parameters.

Keywords VLBI, automated analysis, intensive sessions, Earth rotation, UT1

1 Introduction

The International VLBI Service for Geodesy and Astrometry (IVS) (Schuh and Behrend, 2012) conducts daily 1-hour Intensive sessions. These sessions are a crucial part for providing daily estimates of UT1, which are important for applications related to Earth- and space-based navigation. There are three types of Intensive sessions (hereafter called INT), which can be distinguished by the day of the week and the observing network. INT1 are observed from Monday to Friday 1730 UTC on the Kokee–Wettzell baseline, INT2 are on Saturdays and Sundays 0730 UTC on Wettzell–Tsukuba, and INT3 are carried out on Mondays 0700 with Wettzell, Tsukuba, and Ny-Ålesund. In our work we focus on a total of 1669 INT1 experiments on the

Niko Kareinen, Thomas Hobiger, Rüdiger Haas
Department of Earth and Space Sciences, Chalmers University of Technology, Onsala Space Observatory SE-439 92 Onsala, Sweden

Kokee–Wettzell baseline between 2001 and January of 2015. These sessions were processed with the c5++ VLBI analysis software (Hobiger et al., 2010) starting from version 1 databases for X- and S-band. Version 1 databases contain only the observed group delays and their formal errors. The databases were converted to National Geodetic Survey (NGS) cards (Gordon, 2007) to start the processing with c5++, which was first used to do ambiguity resolution and ionosphere calibration in automatic mode with GMF2 mapping function and pressure data from GPT2 (Lagler et al., 2013). The analysis process is shown schematically in Fig. 1. In c5++ the ambiguity resolution and ionosphere calibration is an iterative process, which yields ambiguity free databases. These ambiguity resolved and ionosphere corrected databases were then processed to derive UT1-UTC. Using different analysis setups, we address the following questions:

1. Do we need the local weather information from the station log files?
2. What is the impact of using different mapping functions?
3. What is the effect of the cable delay data?
4. How accurately do we need to know the a priori polar motion?
5. Can we simultaneously estimate UT1-UTC and the position of one of the stations?

We used several criteria to select the databases that were included in the analysis. Firstly, only the databases that had version 1 available on the IVS Data Centre file server¹ were downloaded for the analysis. From these databases we only included sessions where Kokee–Wettzell was the only available baseline and discarded sessions which had an additional observing station (e.g. Svetloe). We also required that station log files were available for both stations.

2 Analysis strategy

To address the questions posed in Section 1 we processed the sessions following the procedure depicted in Fig. 1 using different analysis strategies with different combinations of mapping functions and choice of applying/not applying station log files. The

¹ <ftp://cddis.gsfc.nasa.gov/pub/vlbi/ivsdata/db/>

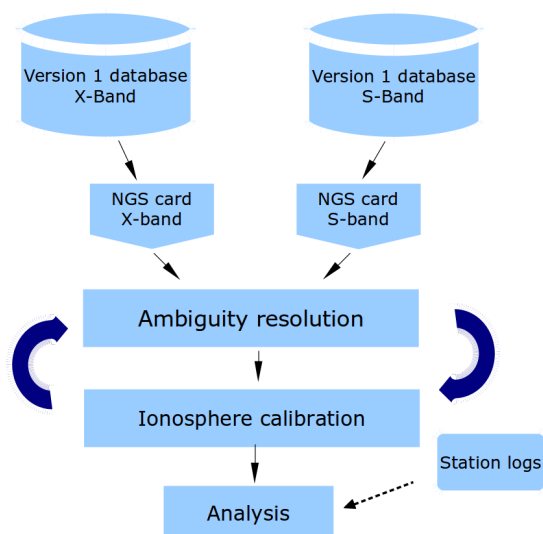


Fig. 1 Flowchart of the automated data analysis with c5++.

strategies, labelled as A, B, C, and D are shown in Table 1. The latest IERS 2010 conventions (Petit and Luzum, 2010) were used in the analysis. The parametrisation options and a priori information used with all strategies are listed in Table 2. C04 refers to the IERS EOP 08 C04 time series (Bizouard and Gambis, 2011). We processed the data with two mapping functions, VMF1 (Boehm et al., 2006) and GMF(GPT2).

Table 1 Overview of the four analysis strategies used.

Strategy	Mapping function	Cable delay data	Pressure data
A	VMF1	Not applied	GPT2
B	GMF(GPT2)	Not applied	GPT2
C	VMF1	Station log files	Station log files
D	GMF(GPT2)	Station log files	Station log files

In all tested analysis runs sessions which resulted in UT1-UTC residuals w.r.t. C04 over $1000 \mu\text{s}$ (in absolute value) or $50 \mu\text{s}$ for the formal errors were eliminated as crude outliers. Additionally, a number of sessions were excluded because the UT1-UTC could not be estimated due to insufficient number of good observations w.r.t. number of unknowns.

3 Results

The following subsections discuss the processing results from the different analysis strategies (A-D).

Table 2 Parametrisation and a priori values used in the analysis.

Parameter	Kokee	Wetzell
Station clock	Est. 2nd order polynomial	Reference
Station position	Fix to ITRF2008	Fix to ITRF2008
ZHD	Fix	Fix
ZWD	Solve 1 offset	Solve 1 offset
Source positions		Fix to ICRF2
UT1-UTC		Est. 1 offset w.r.t. C04
Polar motion		Fix to C04
Nutation/Precession		Fix to C04

3.1 Impact of mapping functions and log files

The results show that the choice of mapping function and the use of log files give differences smaller than $1 \mu\text{s}$. Table 3 summarizes statistical information for each solution type. Questions 1 and 2 are addressed in Figures 2 and 3, respectively. In order to make the comparison straightforward, only the sessions appearing in all of the four strategies after the outlier elimination are included in these two figures.

Table 3 Statistical information on individual analysis strategies: rejected sessions (out of 1669), WRMS and weighted bias w.r.t. C04.

Strategy	Rejected sessions	WRMS [μs]	Weighted bias [μs]
A	311	17.63	2.65
B	311	17.64	2.65
C	263	18.03	2.65
D	263	18.04	2.67

The results in Table 3 show that the Weighted Root Mean Square (WRMS) is slightly improved by using the data from the station log files. However, the use of log files also reduces the number of sessions that pass the session-wise outlier rejection criteria (absolute values of estimates $<1000 \mu$, formal errors $<50 \mu\text{s}$). There is practically no difference in the weighted biases between the processing strategies. Based on the small differences between the processing strategies GMF(GPT2) was chosen for all further investigations.

3.2 Impact of cable delay data

We can investigate the impact of cable delay on the UT1-UTC estimate w.r.t. C04 by differencing the two time series which use the same mapping function, but different station log file setup. As an example, the top graph in Figure 4 depicts the difference of the data in Figures 2B and 3D, respectively.

Shown in the bottom graph are the same data plotted against the de-trended RMS of cable delays for Kokee (left) and Wetzell

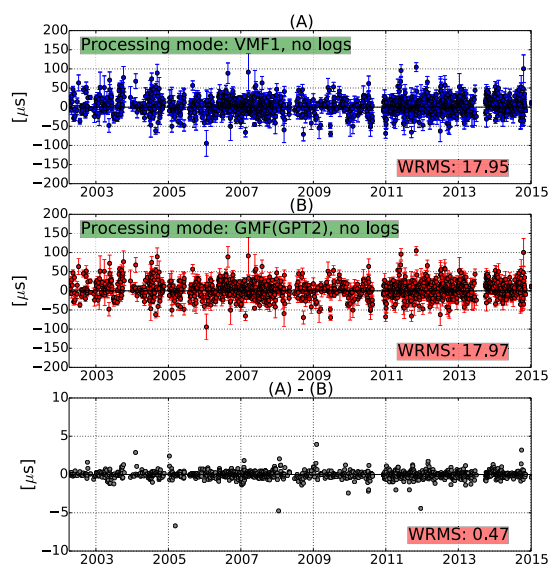


Fig. 2 Processing without log files: UT1-UTC residuals w.r.t. C04 processed with (A) VMF1 and (B) GMF(GPT2). The bottom row presents the difference of time series (A) and (B).

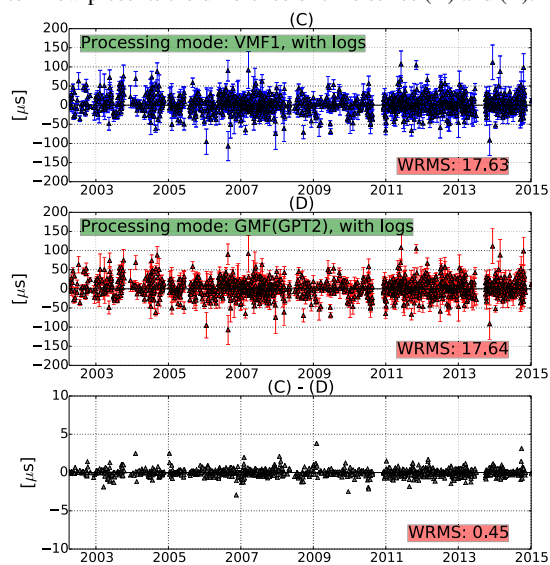


Fig. 3 Processing with log files: UT1-UTC residuals w.r.t. C04 processed with (C) VMF1 and (D) GMF(GPT2). The bottom row presents the difference of time series (C) and (D).

(right). A jump exceeding $5 \mu\text{s}$ is seen in the difference of the residuals in late 2013 to early 2014. From these station-wise plots we can see, that the jump points are correlated with high RMS values for the cable delay data at Wettzell.

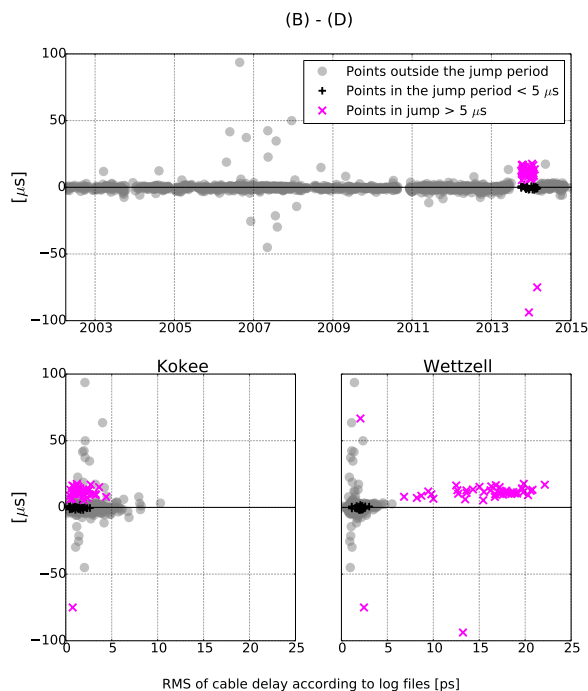


Fig. 4 Top: differences between results presented in Figures 2B and 3D. fig. A systematic behaviour is seen in the end of 2013. Bottom: scatter plots of the differences vs. RMS of de-trended cable delay values for Kokee (left) and Wettzell (right).

4 The impact of polar motion accuracy

According to the IERS Bulletin A² (IERS, 2015) (update frequency of one week) the accuracy of the predicted polar motion is

$$\sigma_{x_p, x_p} = 680 \cdot D^{0.80} [\mu\text{as}], \quad (1)$$

where D is the days elapsed since the Bulletin A epoch. The impact of the polar motion accuracy on the UT1-UTC estimation was studied by a Monte Carlo simulation. The simulation was carried out by adding a noise term to the a priori polar motion information. This noise term was drawn from a normal distribution with a standard deviation based on the estimated accuracy according to Equation (1). This was done in a Monte Carlo fashion 20 times for each of the 1669 sessions with a prediction interval of 0.25 to 6 days in 24 steps of 0.25 days. For each set of Monte Carlo calculations (1–20) within a noise level a weighted RMS was computed and then these 20 values were averaged over the respective noise level, and a standard deviation for the 20 values was computed as a measure of formal error. Figure 5 presents the result of the Monte Carlo simulation and a power function fit to the data. We can see that the mean WRMS of the UT1-UTC residuals depends strongly on the accuracy of the a priori pole

² <http://datacenter.iers.org/eop/-/somos/5Rgv/latest/6>

components. After 1 day the WRMS degrades from approximately $5 \mu\text{s}$ from $18 \mu\text{s}$ to $23 \mu\text{s}$.

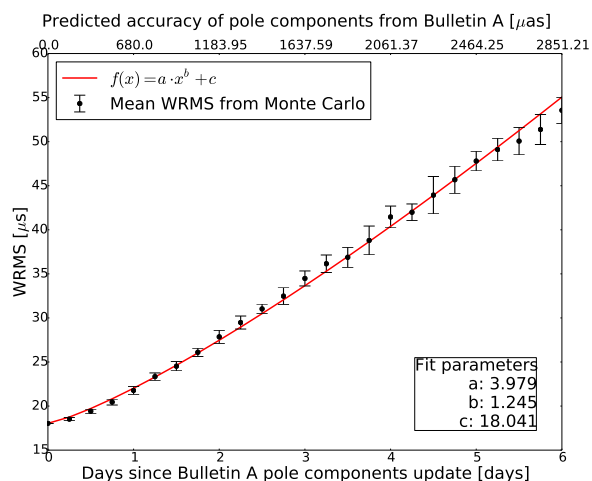


Fig. 5 Mean WRMS of UT1-UTC residuals w.r.t. C04 as a function of polar motion accuracy. The X-axis shows days elapsed since Bulletin A epoch (bottom) and polar motion accuracy (top).

4.1 Impact of estimating the station position

Wetzell was kept as the reference station, while the position of Kokee was estimated with constraints between 0.1 mm to 10 mm, with steps of 0.025 mm in a logarithmic scale. Figure 6 shows the effect of the constraint level on the WRMS of UT1-UTC residuals w.r.t. C04. Also shown is the number of sessions lost relative to the number of sessions. Sessions are lost because estimating the station position of Kokee with too loose constraints sometimes causes solutions to not converge. While the applied constraints remain on the millimetre level or tighter, there is no degradation in terms of WRMS of the UT1-UTC residuals w.r.t. C04. However, no improvement can be seen either. Beyond 1 millimetre constraint level the solution becomes unstable, causing both the accuracy of the UT1-UTC estimate to decrease as well as non-convergence in the least-squares adjustment.

5 Conclusions

Based on our results on the automated analysis of INT1 sessions we can conclude for the research questions posed in Section 1:

1. There is no clear advantage in using local weather data from the station log files compared to using GPT2.

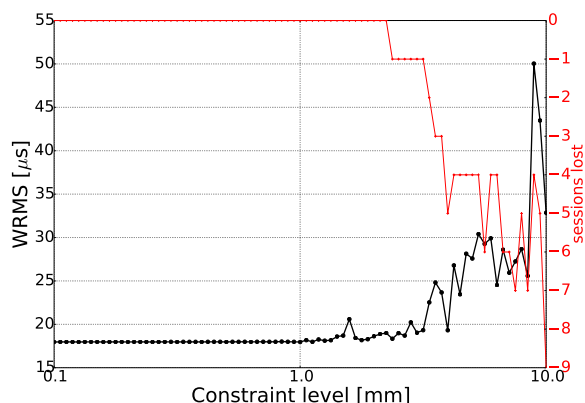


Fig. 6 Effect of constraint level for station position estimation on the WRMS of the UT1-UTC residuals w.r.t. C04 (left scale) and the number of sessions that failed when station position was estimated (right scale).

2. There is no significant difference in using VMF1 or GMF.
3. There is a benefit in using cable delay data, provided that it is reliable.
4. Outdated polar motion values have a significant impact on UT1-UTC estimates. Polar motion with sub-daily resolution is necessary to provide UT1-UTC with a mean accuracy of better than $20 \mu\text{s}$.
5. Station position estimation does not degrade UT1-UTC if tight constraints on the millimetre level are applied.

We can conclude from the results of the processing strategies with and without station log files that if the pressure and cable data are reliable the UT1-UTC accuracy is slightly improved. However, when station log data were used, 48 sessions were rejected based on our outlier exclusion criteria (see Section 2). In all instances the rejections were due to bad pressure data in the station log files. Compared to pressure, bad cable calibration data degraded the UT1-UTC estimates to a lesser extent. Rigorous automatic procedures to filter the bad station log data are needed to ensure that if the station log files are used they do not degrade the UT1-UTC estimate. Inaccuracy in a priori polar motion values remain the largest cause to degradation in the accuracy of UT1-UTC estimates. Further details of this study can be found in Kareinen et al. (2015).

References

- Bizouard C, Gambis D (2011) The combined solution C04 for Earth Orientation Parameters consistent with International Terrestrial Reference Frame 2008. https://hpiers.obspm.fr/iers/eop/eopc04/C04_guide.pdf. Accessed 17 Aug 2015
- Boehm J, Werl B, Schuh H (2006) Troposphere mapping functions for GPS and very long baseline interferometry from

- European Centre for Medium-Range Weather Forecasts operational analysis data. *J Geophys Res*, 111(B2). doi: 10.1029/2005JB003629
- Gordon D (2007) NGS Format for VLBI Data Transfer – Revised June 11, 2007. http://lacerta.gsfc.nasa.gov/mk5/help/dbngs_format.txt. Accessed 31 Aug 2015
- Hobiger T, Otsubo T, Sekido M, Gotoh T, Kubooka T, Takiguchi H (2010) Fully automated VLBI analysis with c5++ for ultra-rapid determination of UT1. *Earth Planets Space*, 62(12), 933–937.
- IERS Bulletin A (2015) IERS Rapid Service Prediction Centre. <http://hpiers.obspm.fr/eoppc/bul/bulb/explanatory.html>. Accessed 17 Aug 2015
- Kareinen N, Hobiger T, Haas R (2015) Automated analysis of Kokee–Wetzell Intensive VLBI sessions — algorithms, results, and recommendations. *Earth Planets Space*, 67:181, doi: 10.1186/s40623-015-0340-x.
- Lagler K, Schindelegger M, Boehm J, Krásná H, Nilsson T (2013) GPT2: Empirical slant delay model for radio space geodetic techniques. *Geophys Res Lett*, 40, 1069–1073. doi: 10.1002/grl.50288
- Petit G, Luzum B (2010) (eds.) IERS Conventions (2010). International Earth Rotation and Reference Systems Service (IERS). IERS Technical Note, No. 36, Frankfurt am Main, Germany: Verlag des Bundesamts für Kartographie und Geodäsie, 179 pp.
- Schuh H, Behrend D (2012) VLBI: A fascinating technique for geodesy and astrometry. *J Geodyn*, 61, 68–80. doi: 10.1016/j.jog.2012.07.007

Comparison of tropospheric delays from GPS and Kalman filtered VLBI data

B. Soja, T. Nilsson, M. Karbon, C. Lu, X. Li, K. Balidakis, J. Anderson, S. Glaser, L. Liu, J. Mora-Diaz, M. Xu, R. Heinkelmann, H. Schuh

Abstract The troposphere is the most critical error source in VLBI analysis. As the rapid variation of water vapor cannot be modeled with sufficient accuracy, it is necessary to estimate the resulting delays in the analysis process. Due to the turbulent nature of the atmosphere, parameters like zenith wet delays (ZWD) are best approximated stochastically. For this purpose, we have implemented a Kalman filter into the GFZ version of the Vienna VLBI Software (VieVS@GFZ). In this study, we compare ZWD estimated from VLBI data to results from GPS data. By using Kalman filtering instead of the classical least-squares method, we see an improvement of about 5 % concerning ZWD differences. By tuning the ZWD process noise depending on the individual stations, the Kalman filter solution can be further enhanced by 7 %. Furthermore, it is investigated whether a calibration of VLBI estimates by using GPS ZWD has a positive impact on station coordinate stability. Preliminary results show a positive effect on station coordinate repeatabilities.

Keywords Kalman filter, zenith wet delays, CONT campaigns, GPS

1 Introduction

A goal of the upcoming VLBI Global Observing System (VGOS) is the reduction of the time delay between observation and availability of products, e.g. station coordinates, Earth orientation parameters (EOP), and tropospheric delays. By using optical fiber links, the data from the telescopes could be transferred to the correlator in near real-time. In order to analyze the resulting observables in a similar time frame,

Benedikt Soja, Tobias Nilsson, Maria Karbon, Cuixian Lu, James Anderson, Li Liu, Julian Mora-Diaz, Minghui Xu, Robert Heinkelmann, Harald Schuh
GFZ German Research Centre for Geosciences, Telegrafenberg, D-14473 Potsdam, Germany
Kyriakos Balidakis, Susanne Glaser, Harald Schuh
Technische Universität Berlin, Straße des 17. Juni 135, D-10623 Berlin, Germany

real-time capable algorithms, such as Kalman filtering (KF), play an important role. This was the initial motivation for the implementation of a Kalman filter into the VLBI analysis software VieVS@GFZ (Nilsson et al, 2015).

Still, nowadays' VLBI analysis is mainly focusing on post-processing tasks. In this regard, Kalman filtering has the advantage that certain processes estimated in the analysis, such as tropospheric delays or clock offsets, are better approximated stochastically compared to the deterministic functional model of least-squares adjustments (Herring et al, 1990).

In recent studies, we investigated the advantages of using our implementation of a Kalman filter, module VIE_KAL in VieVS@GFZ, compared to the application of least-squares fitting, module VIE_LSM, to estimate geodetic parameters (Karbon et al, 2014; Nilsson et al, 2015; Soja et al, 2015; Heinkelmann et al., submitted). Improvements in baseline length, station and source coordinate repeatabilities were found, and comparisons with external data sets for EOP, zenith wet delays (ZWD) and tropospheric gradients were positive as well. In Soja et al. (2015), a station-based noise model for ZWD is described, which further improved the repeatabilities. Furthermore, ZWD derived by using VIE_KAL were compared with those from other techniques.

VIE_KAL outputs ZWD for every scan, i.e. every few minutes. In Soja et al. (2015), the GPS ZWD solutions for comparison had a temporal resolution of 1 h. By using filtering algorithms instead of least-squares adjustments, the resolution provided by GPS can be much higher. In this study, we show preliminary results of comparing VLBI ZWD from VIE_LSM and VIE_KAL to GPS ZWD of different temporal resolutions. Further, we incorporate the GPS ZWD into the VLBI analysis and investigate the effects on station coordinates.

2 Data and Methodology

For this study, the VLBI data from the CONT14 campaign was used. The Kalman filter and LSM solutions were derived consistently, i.e. based on the same models and observations. For both LSM and Kalman filter solutions, the zenith hydrostatic delays (ZHD) were calculated from in-situ pressure measurements, and VMF1 were used as mapping functions (Böhm et al, 2006). In

VIE.LSM, the temporal resolution of ZWD was set to 30 min. In the Kalman filter, ZWD were modeled as random walk processes. For one solution, we used a process noise of $19 \text{ cm}^2/\text{day}$, which is the average value derived from all data considered in Soja et al. (2015). For a second Kalman filter VLBI solution, the noise was tuned to fit the atmospheric conditions at each individual telescope, with process noise values derived from ZWD time series of the particular stations.

The GPS data was processed using precise point positioning, both in a sequential least-squares filter (Li et al, 2013) and in a classical least-squares adjustment (Gendt et al, 2004). In the former case, the temporal resolution of zenith total delays (ZTD) is 5 min, in the latter 1 h. The ZTD was converted to ZWD by subtracting ZHD calculated from the VLBI pressure measurements, which were in turn corrected for the height difference. More information about the filter solution can be found in Lu et al (2015). The other solution and the conversion to ZWD is described in more detail in Soja et al. (2015). As this is a preliminary study, only GPS data for stations in Onsala, Sweden (ONSA) and Wettzell, Germany (WTZR) were used.

3 Comparison of ZWD

The ZWD time series of VLBI and GPS data for Wettzell can be seen in Fig. 1, although more details become visible when calculating the difference w.r.t. the GPS data (Fig. 1, lower plot, and Fig. 2). The differences between data sets are computed by linearly interpolating all data sets to 5 min intervals. Corresponding plots for Onsala are included in Figs. 3-4.

Statistics about the differences can be found in Table 1. The RMS is calculated without removing the bias, while the standard deviation (STD) has the bias removed. The biases w.r.t. GPS reach 1.6 mm, and vary among the VLBI solutions by 0.2 mm. For Wettzell, the biases are slightly smaller for the LSM solution. While the average ZWD from LSM is closest to the 5 min GPS solution for Onsala, the station-based Kalman filter solution agrees better with the 1 h GPS solution. Overall, the biases among the VLBI solutions are much smaller than among the GPS solutions, which can reach up to 2 mm. The reason is most likely that the GPS solutions are based on different software packages, while both VLBI solutions are computed with VieVS@GFZ, just applying different estimation algorithms.

In the case of RMS and STD, the results are more decisive. In all cases, the station-based Kalman filter solution performs best, followed by the standard Kalman filter solution. Averaged over both stations and both GPS solutions, the improvement gained by using station-based noise modeling instead of a constant noise in the Kalman filter amounts to 7.3 % in terms of STD. An impact of this magnitude is not surprising as the noise level in the station-based solution for the two stations (Wettzell: $9.3 \text{ cm}^2/\text{day}$, Onsala: $6.0 \text{ cm}^2/\text{day}$) is 2-3 times smaller than in the standard solution ($19 \text{ cm}^2/\text{day}$). When comparing the STD for the standard Kalman filter and LSM solutions, the improvement is 5.5 % in favor of the Kalman filter. Possible explanations are that the stochastic state-based approach in Kalman filtering is closer to reality than deterministic modeling as used

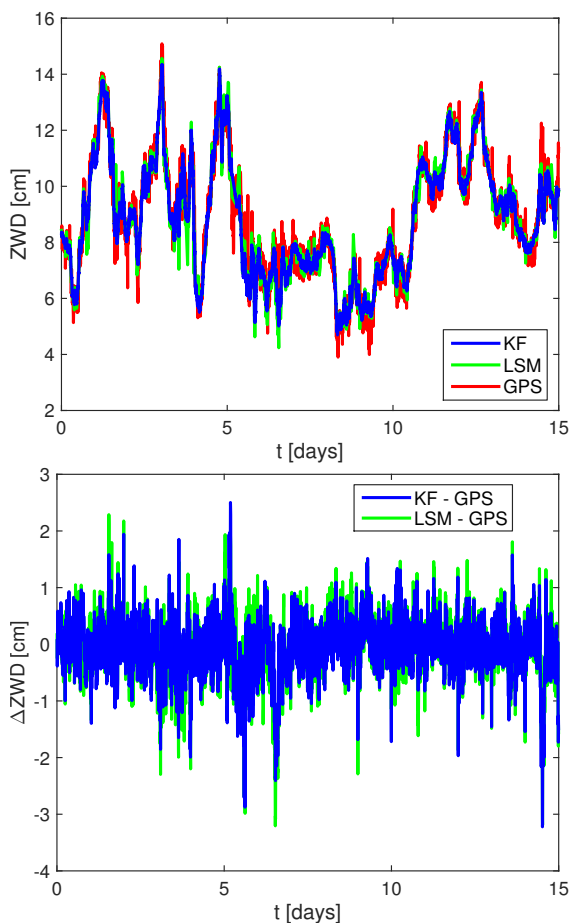


Fig. 1 ZWD and their differences are shown for Wettzell during CONT14. The GPS data in both plots have a temporal resolution of 5 min.

Table 1 Statistics about the ZWD differences during CONT14 are shown. All values are given in units of mm.

Solution	Bias RMS STD			Bias RMS STD		
	Wettzell			Onsala		
GPS 5 min						
LSM	-0.77	5.42	5.36	-1.06	4.97	4.86
KF _{standard}	-0.82	5.10	5.03	-1.11	4.64	4.51
KF _{stat.bsd.}	-0.91	4.97	4.88	-1.15	4.41	4.26
GPS 1 h						
LSM	-1.43	5.29	5.10	1.27	5.36	5.21
KF _{standard}	-1.47	4.98	4.77	1.23	4.98	4.83
KF _{stat.bsd.}	-1.58	4.78	4.51	1.17	4.66	4.51

in least-squares adjustments or that the standard parametrization and soft constraints applied in VIE.LSM are not flexible enough and could be optimized.

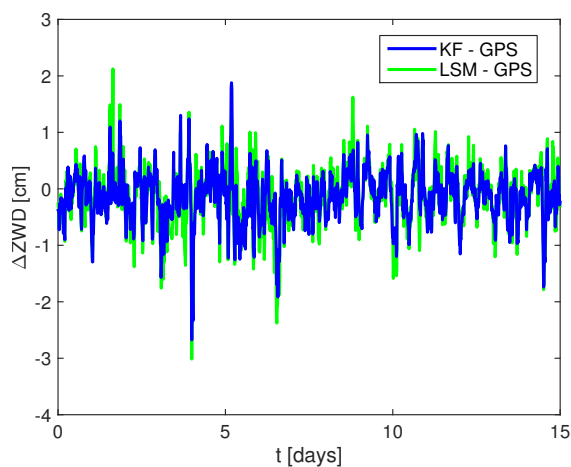


Fig. 2 ZWD differences for Wetzell during CONT14 are shown, with GPS data given at 1 h intervals.

4 GPS data in the VLBI analysis

In the Kalman filter implementation in VieVS@GFZ, it is possible to include external data in the estimation process. We computed a solution, for which we fixed the ZWD of stations Wetzell and Onsala to the values from the 5 min GPS ZWD time series. For this task it was necessary to interpolate the GPS time series to the VLBI observation epochs. For simplicity, no ZWD bias between GPS and VLBI, except for correcting for the height difference, was applied or estimated, but this decision should be investigated in future studies. Besides the inclusion of GPS data, the parametrization is identical to the standard Kalman filter solution described above.

To investigate the effect on station coordinates, we calculated station coordinate repeatabilities (WRMS) for all participating stations. Figures 5 and 6 show the results for Wetzell and Onsala, respectively. As an example of a station that was not calibrated by GPS data, Fig. 7 depicts the repeatabilities for Ny-Ålesund. The numerical values for these stations, as well as average values for all stations participating in CONT14, can be found in Table 2.

For both Wetzell and Onsala, the 3D WRMS is reduced when using GPS data in the Kalman filter. Onsala shows improvements in WRMS for all three coordinates, while for Wetzell, only the north component is positively affected. Here, the WRMS is smaller by more than a factor of two, what compensates the worse performance in radial and east components. This finding is interesting because one could expect that the vertical component would be affected most by introducing external ZWD data. Stations, for which ZWD were estimated as usual, show smaller differences in WRMS, and some, e.g. Ny-Ålesund, have better repeatabilities when no GPS data is used at all. On average, however, the 3D WRMS for the Kalman filter solution utilizing GPS data is smaller by 3 % compared to the standard solution. Hence, it seems that additional systematic errors introduced by the GPS

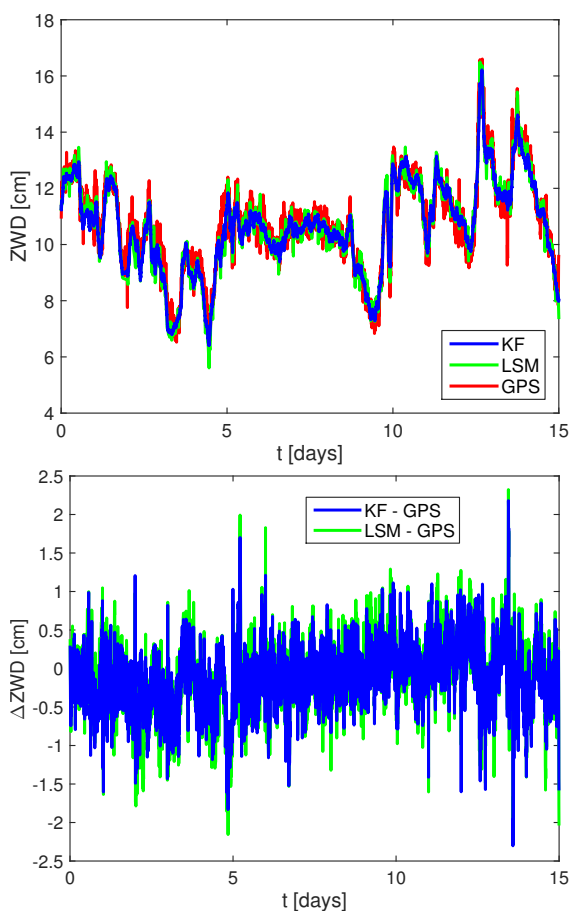


Fig. 3 ZWD and their differences are shown for Onsala during CONT14. The GPS data in both plots have a temporal resolution of 5 min.

data are of less significance compared to the stabilizing nature of external calibration.

For reference, also the repeatabilities for the LSM solution are shown in Figs. 5-7 and Table 2. Kalman filtering performs slightly better in terms of WRMS for all components, on average by about 2 %.

5 Conclusions

Comparisons to GPS solutions with different temporal resolution show that ZWD from Kalman filtered VLBI data are more accurate than those from a consistent least-squares adjustment. The average standard deviation is improved by more than 5 %. Furthermore, station-based noise modeling for the tropospheric parameters improves the differences w.r.t. GPS by another 7% on average. While the Kalman filter solution also performs better than LSM in terms of station coordinate repeatabilities, an

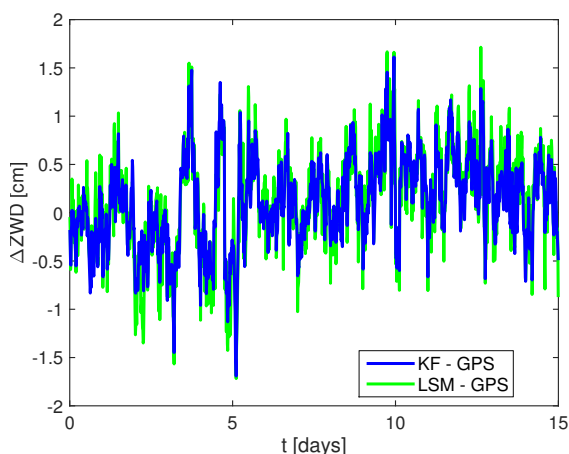


Fig. 4 ZWD differences for Onsala during CONT14 are shown, with GPS data given at 1 h intervals.

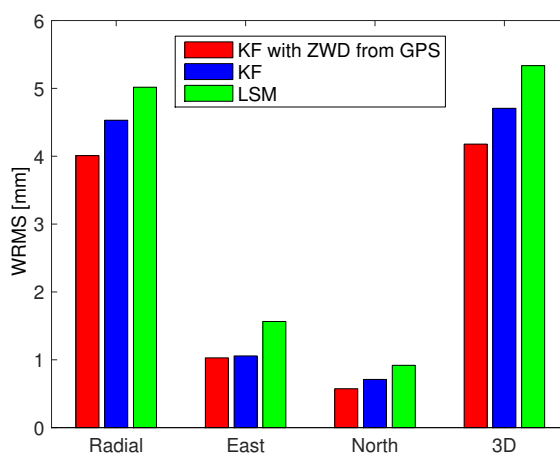


Fig. 6 CONT14 station coordinate repeatabilities for Onsala

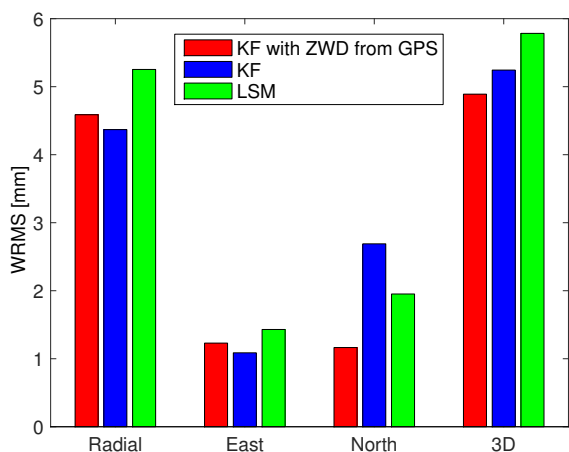


Fig. 5 CONT14 station coordinate repeatabilities for Wettzell

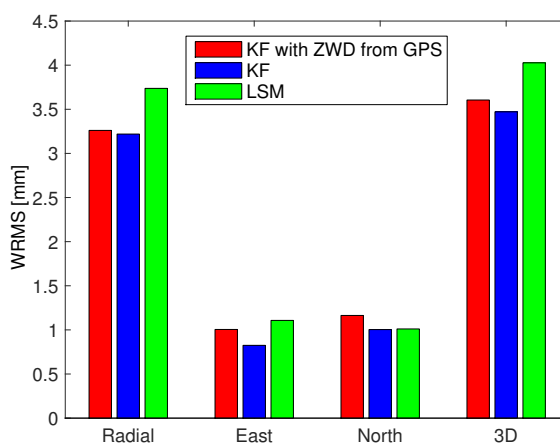


Fig. 7 CONT14 station coordinate repeatabilities for Ny-Ålesund

incorporation of ZWD from GPS in the VLBI analysis brings further improvement not only to directly calibrated stations, but also on average.

Future plans include extending the GNSS data in use, not only in terms of more stations, but also by investigating the impact of different satellite systems, i.e. GLONASS, Beidou, and Galileo, and combinations thereof. The investigations regarding inclusion of external data in the Kalman filter can also be extended, for instance by estimating biases and by weighting the different data sets.

Table 2 CONT14 station coordinate repeatabilities are given in units of mm. "Average" refers to the average value determined from all CONT14 stations.

Station/Solution	Radial	East	North	3D
Wettzell				
LSM	5.25	1.43	1.95	5.78
KF _{standard}	4.37	1.09	2.69	5.24
KF _{ZWD from GPS}	4.59	1.23	1.16	4.89
Onsala				
LSM	5.01	1.56	0.92	5.34
KF _{standard}	4.53	1.06	0.71	4.71
KF _{ZWD from GPS}	4.01	4.01	0.57	4.18
Ny-Ålesund				
LSM	3.74	1.11	1.01	4.03
KF _{standard}	3.22	0.82	1.00	3.47
KF _{ZWD from GPS}	3.26	1.00	1.16	3.61
Average				
LSM	7.50	2.26	3.31	8.62
KF _{standard}	7.31	2.35	3.18	8.44
KF _{ZWD from GPS}	7.14	2.55	2.78	8.19

References

- Böhm J, Werl B, Schuh H (2006) Troposphere mapping functions for GPS and very long baseline interferometry from European Centre for Medium-Range Weather Forecasts operational analysis data. *J Geophys Res*, 111(B02406), DOI 10.1029/2005JB003,629.
- Gendt G, Dick G, Reigber C, Tomassini M, Liu Y, Ramatschi M (2004) Near Real Time GPS Water Vapor Monitoring for Numerical Weather Prediction in Germany. *J Meteorol Soc Jpn*, 82(1B):361–370.
- Heinkelmann R, Soja B, Nilsson T, Dick G, Zus F, Willis P, Wickert J, Schuh H (submitted 2015) Comparison of atmospheric gradients from space geodetic techniques, numerical weather models, and water vapor radiometer during CONT14. submitted to *J Geod*.
- Herring TA, Davis JL, Shapiro II (1990) Geodesy by radio interferometry: The application of Kalman Filtering to the analysis of very long baseline interferometry data. *J Geophys Res: Solid Earth*, 95(B8):12,561–12,581, DOI 10.1029/JB095iB08p12561, URL <http://dx.doi.org/10.1029/JB095iB08p12561>
- Karbon M, Soja B, Nilsson T, Heinkelmann R, Liu L, Lu C, Mora-Diaz J, Raposo-Pulido V, Xu M, Schuh H (2014) ERP estimation using a Kalman Filter in VLBI. In: D. Behrend, K. Bayer, K. Armstrong (eds.) *Proc. Eighth IVS General Meeting*, 298–301.
- Li X, Ge M, Zhang H, Wickert J (2013) A method for improving uncalibrated phase delay estimation and ambiguity-fixing in real-time precise point positioning. *J Geod*, 87(5):405–416, DOI 10.1007/s00190-013-0611-x, URL <http://dx.doi.org/10.1007/s00190-013-0611-x>.
- Lu C, Li X, Ge M, Heinkelmann R, Nilsson T, Soja B, Dick G, Schuh H (2015) Estimation and evaluation of real-time precipitable water vapor from GLONASS and GPS. *GPS Sol*, 1–11, DOI 10.1007/s10291-015-0479-8, URL <http://dx.doi.org/10.1007/s10291-015-0479-8>
- Nilsson T, Soja B, Karbon M, Heinkelmann R, Schuh H (2015) Application of Kalman filtering in VLBI data analysis. *Earth Planets Space*, 67(1):136, DOI 10.1186/s40623-015-0307-y, URL <http://www.earth-planets-space.com/content/67/1/136>.
- Soja B, Nilsson T, Karbon M, Zus F, Dick G, Deng Z, Wickert J, Heinkelmann R, Schuh H (2015) Tropospheric delay determination by Kalman filtering VLBI data. *Earth Planets Space*, 67(1):144, DOI 10.1186/s40623-015-0293-0, URL <http://www.earth-planets-space.com/content/67/1/144>

Combining VLBI and GPS for inter-continental frequency transfer

T. Hobiger, C. Rieck, R. Haas, Y. Koyama

Abstract For decades the Global Positioning System (GPS) has been the only space geodetic technique routinely used for inter-continental frequency transfer applications. In the past VLBI has also been considered for this purpose and the method's capabilities were studied several times. However, compared to GPS current VLBI technology only provides few observations per hour, thus limiting its potential to improve frequency comparisons. We therefore investigate the effect of combining VLBI and GPSI on the observation level in order to draw the maximum benefit from the strength of each individual technique. As a test-bed for our study we use the CONT11 campaign observed in 2011. We perform a combined analysis of VLBI and GPS data on the observation level and demonstrate that our combination approach leads to small but consistent improvements for frequency transfer of up to 10%, in particular for averaging periods longer than 3000 s w.r.t. the GPS single technique solution. We discuss the implications of these findings and present our ideas about how VLBI can contribute to international frequency transfer tasks.

Keywords VLBI, GPS, frequency transfer, CONT11

1 Introduction

Given the fact that VLBI stations are equipped with highly precise and short-term stable frequency standards, usually hydrogen masers, comparing these atomic clocks appears to be straightforward. Since the early days of VLBI, several studies have dealt with the topic of applying this technology for time and frequency

Thomas Hobiger, Rüdiger Haas

Chalmers University of Technology, Department of Earth and Space Sciences, Onsala Space Observatory, Onsala SE-439 92, Sweden

Carsten Rieck

SP Technical Research Institute of Sweden, Box 857, Borås SE-501 15, Sweden

Yasuhiro Koyama

National Institute of Information and Communications Technology, 4-2-1 Nukui-Kitamachi, Koganei, 184-8795 Tokyo, Japan

transfer (e.g., Clark (1972)). Also in Koyama (2012) the use of VLBI for time and frequency metrology is discussed and the potential of this technique is pointed out. However, it has been stated that VLBI systems have several drawbacks that compromise the application of VLBI for such purposes on a routine basis. First, current VLBI systems are not operating continuously. Observation sessions are usually scheduled to last for only 24 hours, which prevents frequency comparisons on time scales longer than one day. Second, as most of the cable and electrical path lengths in the VLBI system are not calibrated in an absolute sense and are designed to be variable, this technology cannot directly be utilized for time comparisons. Frequency transfer is still possible on time scales shorter than the variation, estimated to result in a few ns variation over several days.

Thus, VLBI is in principle able to directly determine the differences between clocks at two sites, if the Earth's orientation, the station positions, as well as ionospheric and tropospheric delays are known or simultaneously fitted.

1.1 Clock differences as a by-product of geodetic VLBI analysis

No technique is capable of providing absolute clock parameters at each site. Therefore it is necessary that one clock at one selected station in a network is kept fixed and all other clocks of the other stations in the network will be related to this reference clock. By doing so, clock differences can be obtained from geodetic post-processing, i.e. the adjustment of the unknown parameters. Since the clock difference parameters need to be estimated together with the other unknowns, one needs to pay attention that neither unmodeled effects bias the clock estimates, nor correlations among the unknowns absorb clock variations in other parameters. Moreover, the parametrization of the clock unknowns has to reflect the physical behaviour of the clock, i.e. providing a temporal sampling which can follow a random walk (in phase) noise process.

1.2 Space geodetic data analysis with c5++

The software package "c5++" has been developed with the purpose of supporting the combination of space geodetic data from VLBI, GPS and SLR on the observation level, and also to allow processing of single-technique solutions. Since c5++ uses consistent geodetic/geophysical models for all space geodetic techniques and all analysis steps, it is guaranteed that differences of the estimated parameters that are derived from e.g. VLBI and GPS do not originate from different models or inconsistent corrections, but are directly related to the performance of each technique. Moreover, the possibility to combine data on the observation level allows to study the impact of combining techniques, with the purpose to improve the target parameters. The concept of combination on the observation level has been successfully demonstrated in Hobiger and Otsubo (2014) and will be applied here.

2 Frequency transfer during CONT11

In total 14 VLBI stations participated in the CONT11 campaign, but only 11 of the network stations shared a common frequency standard with a co-located GPS receiver (Rieck et al., 2012). Furthermore, unfortunately some of the stations were excluded because they experienced technical or observational problems. For example, the stations Badary and Zelenchukskaya experienced strong radio frequency interference (RFI) disturbances in several of the observed frequency bands. The station Tigo Concepción performed rather poorly, mainly due to its small antenna size, and several other sites had clock jumps of the VLBI equipment or missing GPS data. Although small antennas, like Tigo, are very attractive as they can be easily deployed at arbitrary sites, technology which was available during CONT11 causes a significant performance degradation that comes with shrinking the antenna diameter w.r.t. the average size of the other VLBI dishes in the network. This drawback is currently being worked on and thought to be overcome by switching to broad-band receiving systems (cf. Sec. 3). Thus, the further analysis concentrates in the following mainly on a sub-set of 6 of the CONT11 stations. As study from Rieck et al. (2012) compare the potential of frequency transfer of each technique, showing that VLBI and GPS perform similarly with best case one day instabilities on the order of 10^{-15} . Fig. 1 depicts the clock estimates from two single-technique solutions on a particular baseline.

2.1 VLBI and GPS analysis with c5++

In order to assess both short- and long-term frequency stabilities, the data were processed with c5++ in non-overlapping batch solutions with three consecutive days, i.e. covering a period of 72 hours each. Thus, the whole CONT11 campaign could be anal-

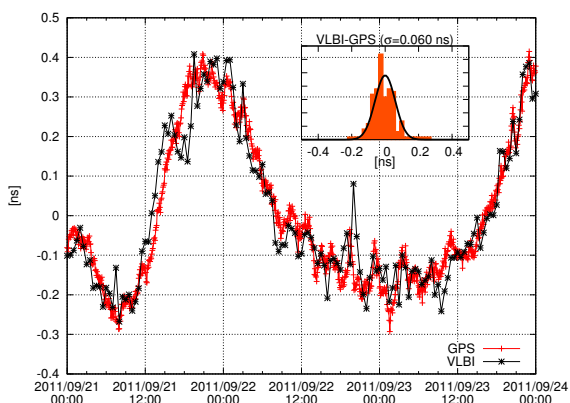


Fig. 1 Clock differences (after reducing a quadratic trend) as obtained from a 3-day batch solution for VLBI-only (red) and GPS-only (black) on the Wettzell-Westford baseline.

ysed in five 72 hour batches. This was possible since the whole campaign had been re-correlated with a consistent delay model that prevents discontinuities at the day boundaries. As mentioned before, VLBI analysis requires that one station clock in the network is fixed to an arbitrary constant value, which is chosen normally to be zero. Doing so, all estimated clocks in the network represent the clock difference between that station's clock and the clock of the reference site. The clock reference should be assigned to a station which is known to show no clock break during an entire session. The clock at Wettzell (Germany) was selected as reference. Another characteristic of VLBI analysis relating to clock estimates is the irregular temporal spacing of the original observational data. Depending on antenna and receiver characteristics and the flux density of the observed radio sources, optimized observation schedules require different scan-length and varying idle/slewing times. Moreover, hardware problems or operational problems can lead to larger temporal gaps during which a single station is not observing together with the other network sites. Therefore, constraints on the clock rate were chosen to reflect the physical variation of the atomic clock at the VLBI site. In addition, zenith wet delays (ZWDs), troposphere gradients and station coordinates need to be estimated in order to obtain clock estimates that are not degraded by the correlations among these parameters. The c5++ software allows to process un-differenced GPS observations with the precise-point positioning (PPP) approach, using the same geophysical models as used for VLBI analysis. PPP does not require GPS satellites in common-view, and becomes independent of the length of the baselines that are defined by the VLBI network geometry. Thus, even inter-continental frequency links can be established by this analysis method. However, satellite orbits and clocks need to be fixed to IGS final products since such parameters can not be estimated for this study, due to the small number of GPS receivers within the CONT11 network.

Since GPS observations are available with a regular and high sampling rate, clock parameters can be estimated without constraints. Moreover, PPP allows to directly access the behaviour of the station clock, and frequency transfer between two stations

can be performed by differencing the PPP clock solutions of the two sites. Other parameters like zenith troposphere delays or station coordinates have to be estimated together with the clock model, subject to the same correlations as VLBI.

2.2 Combining VLBI and GPS data on the observation level

Combination on the observation level reflects the concept of using all available geodetic data at a site in order to overcome potential deficits of a single technique. Since co-located instruments often share the same infrastructure (e.g. frequency standards) and are expected to experience the same environmental conditions, in particular the atmospheric conditions, one can estimate parameters related to these influences in a common model which only considers biases between the different techniques. It was demonstrated in Hobiger and Otsubo (2014) that the combination of GPS and VLBI on the observation level leads to a small but significant improvement of the geodetic target parameters and in particular improves the stability of the site coordinate time series. Since troposphere and clock parameters were estimated in Hobiger and Otsubo (2014) by a station-wise model it was obvious to investigate how the combination of these two techniques on the observation level can be utilized for the benefit of frequency transfer. As described in Hobiger and Otsubo (2014), troposphere parameters can be estimated with a common model that considers an offset between GPS and VLBI, caused by the height difference between the VLBI and GPS reference points, resulting in a hydrostatic delay difference which remains very stable over time.

On the other hand, a common clock model can be estimated by combining VLBI and GPS only if one considers that instrumental delays are not stable over time but are influenced by temperature-induced changes in reflections (cable multipath) and electrical lengths; for VLBI these can also depend upon the orientation of the antenna. It was suggested in Hobiger and Otsubo (2014) to estimate these inter-technique delay changes by a PLO model with a temporal resolution that is sufficient for representing at least a diurnal signal. A low temporal resolution, i.e. with a PLO step-width of more than 12 hours, bears the risk of not modelling all inter-technique delay changes properly. However, a high temporal resolution reduces the benefit of combining GPS and VLBI since a large fraction of the information provided by the second technique gets absorbed into this parameter. Therefore, the proper choice of the temporal resolution for this crucial parameter is explored in Sec. 2.4.

Another issue that arises from the combination of different observation types is related to the question on how to weight the data of each technique. In order to handle this problem with a proper stochastic model one needs to select an estimation strategy as described in the following.

2.3 Results from combined analysis with c5++

Combining VLBI and GPS on the observation level is the most natural way to estimate common parameters at geodetic co-location sites. With this approach, biases and technique-specific considerations can be taken into account before the observations are combined directly within the adjustment process. Two of such inter-technique biases are those related to troposphere and clock variability. The former one being mainly caused by different heights of the reference points of co-located instruments, which translate into a hydrostatic delay that can be either modeled or, as done in the present study, estimated as a constant offset during each 72 hours batch analysis. The latter offset, hereafter denoted as $\Delta_{clk}(t)$, is expected to be caused by temperature-induced cable delay variations and can either be estimated as a constant offset or parametrized by a PLO model with sufficient temporal resolution to follow cable delay changes. It is obvious that the choice of this inter-technique delay potentially absorbs any benefit that could result from the estimation of a common clock between the two techniques. A too-short temporal resolution of $\Delta_{clk}(t)$ bears the risk that a large fraction of valuable information from the second technique is not being reflected in the estimated clock. On the other hand, an insufficient model representation of the mostly diurnal cable length changes potentially degrades the combined solution and the obtained clock parameters. Therefore, different choices for the temporal resolution of the inter-technique cable delay model $\Delta_{clk}(t)$ have been used and their impact on the frequency transfer stability has been evaluated.

2.4 The impact of the choice for the temporal resolution of the inter-technique cable delay model

In order to evaluate whether the combination of VLBI and GPS leads to an improvement of the frequency transfer stability w.r.t. the GPS-only solution, the ratio

$$\kappa(\tau) = \frac{\frac{1}{N} \sum_N \text{MDEV}_{GPS}(\tau)}{\frac{1}{N} \sum_N \text{MDEV}_{GPS+VLBI}(\tau)} \quad (1)$$

is defined, where N is the number of baselines that are averaged. The ratio $\kappa(\tau)$ describes the average improvement/degradation when combining VLBI with GPS on the observation level for frequency transfer, compared to a GPS-only solution. Since the intervals for the PLO clock model were set to 5 minutes in both solutions one can compute $\kappa(\tau)$ in a straightforward way. Improvements in the overall frequency transfer performance will then be reflected as $\kappa(\tau) > 1$, whereas degradations can be recognized when $\kappa(\tau) < 1$. Figure 2 depicts $\kappa(\tau)$ for solutions with different choices for the temporal resolution of the inter-technique

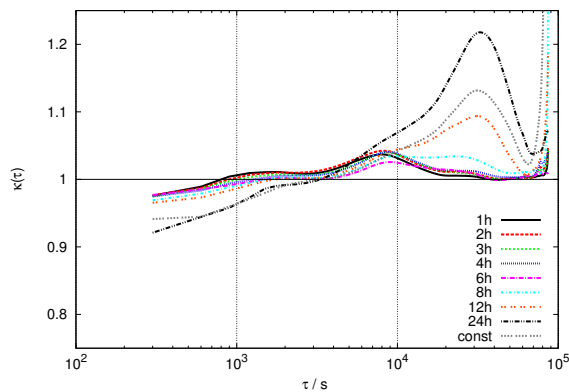


Fig. 2 Average improvement/degradation of the frequency transfer stability, measured as ratio $\kappa(\tau)$, when comparing the combined GPS-VLBI solutions against the GPS-only solution. Results are shown for different temporal resolutions (1 h, 2 h, 3 h, 4 h, 6 h, 8 h, 12 h and 24 h) of the inter-technique delay model as well as for the parametrization with a constant cable delay between the two techniques. Values of $\kappa(\tau) > 1$ indicate improvement

cable delay model $\Delta_{clk}(t)$. Overall, it can be seen that the combination of VLBI with GPS tends to improve the average frequency transfer stability w.r.t. the GPS-only solution. However, as anticipated in the previous section, the choice of the temporal resolution of $\Delta_{clk}(t)$ is crucial. The use of an interval length of 1 hour for the PLO of $\Delta_{clk}(t)$ absorbs almost all benefit gained from adding VLBI. On the other hand, it is clearly visible that daily estimates or parametrization as a constant lead to a degradation of the short term stability while improving the long-term stability more than any of the other choices for the temporal resolution of $\Delta_{clk}(t)$. In general, one can see that VLBI improves the frequency transfer stability for averaging periods between 3,000 and 20,000 seconds as well as for periods close to one day. The latter improvement can be explained by the fact that VLBI helps to smooth the jumps introduced by day boundary discontinuities of the used IGS orbit and clock products. However, one needs to consider also the lower significance (higher uncertainty) of the MDEV at the far end of the long averaging period domain. The improvement between 3,000 and 30,000 seconds is thought to have its origin in the parametrization of tropospheric estimates, which become more robust against data artifacts, when combining VLBI and GPS. In addition, a temporal resolution of 12 hours or longer for $\Delta_{clk}(t)$ leads to an improvement for averaging periods of 12 hours, which might relate to the orbital period of GPS satellites.

3 Discussion and outlook

On average the combination approach performs consistently better than the GPS-only solution, revealing an improvement of the frequency transfer stability of up to 10 %. This leads to

the question how VLBI can efficiently contribute to efforts of precise inter-continental frequency transfer.

It is very unlikely that time and frequency laboratories will deploy expensive and difficult to maintain radio telescopes which are necessary for VLBI operations. However, one could imagine a mutual benefit if a VLBI site is located in the vicinity of a timing laboratory and frequency is provided from this time lab over fiber to that VLBI site. This would imply that frequency standards at the VLBI sites can be omitted and the remotely provided frequency signals from the timing lab could be used for VLBI operations. One could then use global VLBI experiments to support inter-continental frequency transfer by a combination of GPS and VLBI on the observation level, as described in this study. However, the cable delay changes of the VLBI hardware and other time-dependent delays have to be monitored in order to gain benefit from adding VLBI. Estimation of such biases and delays, as performed in this study, helps to a certain extent, but monitoring and calibration of these inter-technique delays is crucial for the estimation of a common clock model among different space geodetic techniques. This requires efforts to study all back-end components and their delay characteristics, a task which is expected to be more straightforward when phasing out analog systems and replacing them with digital equipment. In addition, one needs also to raise the awareness of such a demand in the geodetic VLBI user community in order to develop and deploy such delay calibration and monitoring systems.

Note: This paper summarizes the main findings of a study which has been published as Hobiger et al. (2015).

References

- Clark T (1972) Precision Timing and Very Long Baseline Interferometry, *Proc. 4th PTTI*, 74–89.
- Hobiger T, Otsubo T (2014) Combination of GPS and VLBI on the observation level during CONT11 - common parameters, ties and inter-technique biases, *J Geod*, 88(11), 1017–1028.
- Hobiger T, Rieck C, Haas R, Koyama Y (2015) Combining GPS and VLBI for inter-continental frequency transfer, *Metrologia*, 52(2), 251–261.
- Koyama Y (2012) The Use of Very Long Baseline Interferometry for Time and Frequency Metrology, *MAPAN*, 27(1), 23–30.
- Rieck C, Haas R, Jarlemark P, Jaldehag K (2012) VLBI frequency transfer using CONT11, *Proc. European Frequency and Time Forum (EFTF)*, 163–165, doi: 10.1109/EFTF.2012.6502358.

Baseline dependent weights in VieVS

M. Uunila, H. Krásná, J. Gipson

Abstract It is well known that in processing VLBI data χ^2 is usually larger than 1, typically in the range of 4-8. This results from either too small measurement errors or mismodeling the data. By reweighting the data, that is, by increasing the errors of the observation, we can make $\chi^2 \sim 1$ (Gipson et al., 2008). In Solve's (Ma et al., 1990) operational solutions baseline dependent weights are always applied. Vienna VLBI Software (VieVS, Böhm et al. (2009)) uses global weighting, i.e., a constant weight is added to each observation. Adding baseline dependent weights in VieVS is a two step process. Firstly, we calculate the reweights for each baseline in an observation, secondly, we run the least squares adjustment a second time. Our study shows that baseline dependent weighting improves baseline length repeatability significantly. The Weighted Root Mean Square (WRMS) values of 71% of the baselines participating in CONT08 improved. UT1 adjustment scatter, and discrepancy between VieVS and Solve are also reduced.

Keywords Reweighting, UT1, VieVS, Solve, IVS

1 Introduction

There are many other error sources besides measurement noise which can affect the χ^2 (Gipson et al., 2008):

1. phase cal errors;
2. RFI in the signals;
3. other correlator related errors;

Minttu Uunila

Aalto University Metsähovi Radio Observatory, Metsähovintie 114, FI-02540 Kylmälä, Finland

Hana Krásná

Technische Universität Wien, Department of Geodesy and Geoinformation, Gusshausstrasse 27-29, 1040 Vienna, Austria

John Gipson

NVI Inc., NASA Goddard Space Flight Center, 7257D Hanover Parkway, Greenbelt, Maryland 20770, USA

4. source structure;
5. source position errors;
6. errors in geophysical models;
7. mis-modeling clocks and/or atmospheres;
8. underparametrizing the time variation of clocks and/or atmospheres;
9. etc.

All of the listed errors increase the noise of individual observations, which leads to χ^2 of being too large, e.g., in the range of 4-8. The data needs to be reweighted to bring $\chi^2 \sim 1$. In other words an additional noise term needs to be added to the observations.

In our study we will use two data sets; CONT08, and one year of International VLBI Service for Geodesy and Astrometry (IVS, Schuh and Behrend (2012)) Intensive series data. We will evaluate the effect caused by reweighting the data by analyzing baseline length repeatability, calculating VieVS minus Solve UT1 adjustment values, and calculating Weighted Root Mean Square (WRMS) differences between VieVS and Solve results.

2 Adding noise

There are three common ways to add noise to VLBI measurements (Gipson et al., 2008):

1. Global reweights, e.g., 33 ps for all observations, which is the VieVS default;
2. Station reweights, which depend only on the stations in an observation;
3. Baseline reweights, which only depend on the baselines in an observation.

Weight is added to the observations as follows.

$$\sigma_{t,ij,obs}^2 = \sigma_{t,ij,meas}^2 + \epsilon_{t,ij}^2 \quad (1)$$

where $\sigma_{t,ij,meas}$ is the actual measured value, and $\epsilon_{t,ij}$ is the re-weight constant.



Fig. 1 The 11 stations participating in CONT08 (Schuh and Behrend, 2012).

All three ways can be chosen in Solve. In operational solutions baseline dependent weighting is always used. VieVS deploys global reweights by default, but one can choose to use baseline dependent weighting in the latest version of VieVS, 2.2.

In VieVS we used the baseline dependent weights calculated as follows:

$$\epsilon_{ij}^2 = \frac{1}{n_{ij}} \sum v_{ij}^2 \quad (2)$$

Where the sum is over all observations involving baseline ij , n_{ij} are the number of observations involving this baseline, and v_{ij} are the residuals in pico-seconds.

3 Data sets

We use two different data sets; one to study baseline length repeatability, and another to calculate WRMS differences between VieVS and Solve solutions. The data sets are described in the following subsections.

3.1 Baseline length repeatability

We chose CONT08 as the data set for investigating the baseline length repeatability. CONT08 was a two-week campaign of continuous VLBI sessions, scheduled for observing during the second half of August 2008. The 11 stations that participated in CONT08 are displayed in Fig. 1 (Schuh and Behrend, 2012). The CONT08 campaign continued the series of the very successful continuous VLBI campaigns that were observed at irregular intervals: CONT94 (January 1994), CONT95 (August 1995), CONT96 (fall 1996), CONT02 (October 2002), and CONT05 (September 2005). After CONT08 two CONT series have been measured, CONT11 (September 2011) and CONT14 (May 2014).

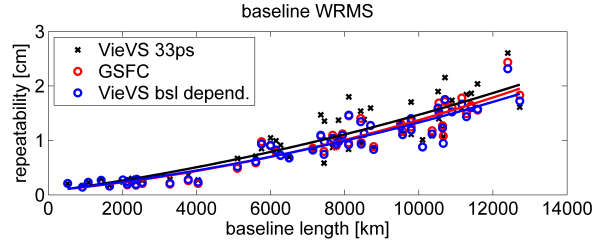


Fig. 2 WRMS of baseline length repeatability. Baseline length repeatability using global weights in VieVS is marked with black x's, VieVS using baseline weight files from Solve are marked with red circles, and from implementing a function to calculate baseline dependent weighting in VieVS are marked with blue circles, respectively.

3.2 VieVS minus Solve UT1 adjustments

For the VieVS minus Solve data set, we chose all Intensives from 2012 that had 12 or more observations. Weighted Root Mean Square (WRMS) values were calculated as follows.

$$WRMS = \sqrt{\frac{\sum_{i=1}^N \frac{(UT1_{VieVS,i} - UT1_{Solve,i} - WM)^2}{\sigma_{VieVS,i}^2 + \sigma_{Solve,i}^2}}{\sum_{i=1}^N \frac{1}{\sigma_{VieVS,i}^2 + \sigma_{Solve,i}^2}}} \quad (3)$$

Here, $UT1_{VieVS,i}$, and $UT1_{Solve,i}$ denote the estimates of the UT1 from VieVS and Solve analysis, respectively, and $\sigma_{VieVS,i}$ and $\sigma_{Solve,i}$ denote their respective formal uncertainties.

4 Results

We used VieVS version 2.2 and Solve release 2014.02.21 in our analysis. We calculated baseline length repeatability from VieVS solutions using CONT08 data with three different weighting schemes:

1. VieVS using global weights, e.g. a constant of 33 ps is added to each observation (VieVS 33 ps);
2. VieVS using external baseline dependent weight files calculated with Solve (GSFC);
3. VieVS deploying baseline dependent weights using a dedicated function (VieVS bsl depend.).

The WRMS improved in 64 % of the baselines when external weight files created by Solve were used, and in 71 % of the baselines when VieVS used baseline dependent weights (Fig. 2). The effect is larger with longer baselines.

We calculated baseline length repeatability differences with the respect to VieVS using global weights in two cases: 1) VieVS using Solve's baseline weight files, and 2) VieVS using a function to calculate baseline dependent weights. Baseline length repeatability differences are shown in Fig. 3.

Additionally, one year (2012) of data from IVS intensive sessions was analyzed with VieVS and Solve in order to see the effect on baseline weighting in UT1 results. VieVS minus

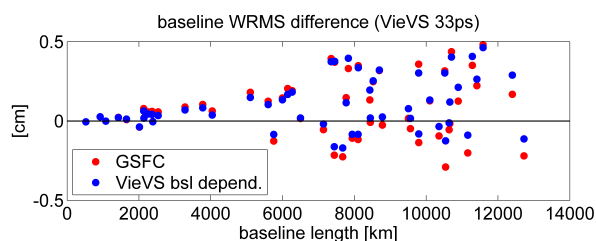


Fig. 3 Baseline length repeatability difference with respect to VieVS using global weights. Results using baseline weight files from Solve are marked with red dots, and from implementing a function to calculate baseline dependent weighting in VieVS are marked with blue dots, respectively. Baselines where the baseline weight solution are improved are above the horizontal axis.

Table 1 Weighted Root Mean Square (WRMS) differences in microseconds between VieVS and Solve.

setup	WRMS: All INTs	WRMS: INT01s
default	8.84	7.38
baseline weights	7.14	5.18

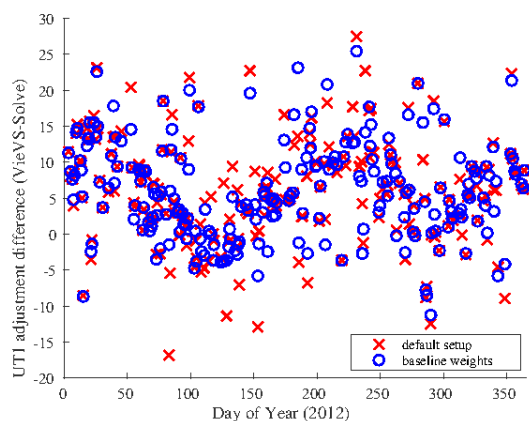


Fig. 4 VieVS minus Solve UT1 adjustments in microseconds. VieVS minus Solve UT1 adjustment values using the default setup of VieVS are shown with red x's, and VieVS minus Solve values with using baseline dependent weighting in VieVS are marked with blue circles.

Solve UT1 adjustment values using the default setup of VieVS are shown with red x's, and VieVS minus Solve values with using baseline dependent weighting in VieVS are marked with blue circles, Fig. 4. Most data points from deploying baseline dependent weights also in VieVS show noticeable improvement in comparison to VieVS using a constant weight of 33 ps in each observation.

The use of baseline weighting reduces the discrepancy between VieVS and Solve's estimates of UT1 adjustments in the IVS Intensive session solutions as shown in Table 1 and Fig. 4. WRMS differences reduced from 8.84 to 7.14 microseconds in the case of Intensives solutions, and from 7.38 to 5.18 microseconds in the case of INT01 solutions (Kokee–Wetzell baseline).

5 Conclusions

The WRMS improved in 64 % of the baselines of the CONT08, when we used weight files created with Solve. When we used baseline dependent weighting in VieVS, the WRMS reduced even more as 71 % of the baselines showed improvement. Fig. 2 shows significant improvement in the baselines length repeatability after implementing baseline dependent weights in VieVS.

UT1 WRMS difference between the two software packages reduced 19 % for all Intensive sessions and 30 % for INT01 sessions when baseline dependent weighting was used also in VieVS, when we analyzed one year of IVS Intensive sessions data.

In the future it would be worthwhile to add more iterations to the weighting process when necessary. We could also test using partial redundancy of baselines instead of Eq. 2, and see if it affects on the results. To derive baseline-dependent variance components using partial redundancy, the squared sum of the residuals is calculated for each baseline and scaled by the partial redundancy of this particular baseline (Artz et al., 2012).

Acknowledgements

The authors wish to express their gratitude to Karen Bayer at NVI Inc. NASA Goddard Space Flight Center for providing the Solve solutions used in the analysis to calculate the VieVS minus Solve Weighted RMS differences.

References

- Artz T, Leek J, Nothnagel A, Schumacher M (2012) VLBI Intensive Sessions Revisited. *IVS 2012 General Meeting Proc.*, NASA/CP-2012-217504, <http://ivsc.gsfc.nasa.gov/publications/gm2012/artz.pdf>
- Böhm J, Böhm S, Nilsson T, Pany A, Plank L, Spicakova H, Teke K, Schuh H (2009) The new Vienna VLBI Software VieVS. In: S. Kenyon, M. C. Pacino, U. Marti (eds.), *Proc. IAG Scientific Assembly 2009*, IAG Symposia Series 136, 1007–1011, doi: 10.1007/9783642203381_126
- Gipson J, MacMillan D, Petrov L (2008) Improved Estimation in VLBI through Better Modeling and Analysis. In: A. Finkelstein, D. Behrend (eds.), *IVS 2008 General Meeting Proc.*, 157–162.
- Ma C, Sauber J, Clark T, Gordon D, Himwich W E, Ryan J W (1990) Measurement of horizontal motions in Alaska using very long baseline interferometry. *J Geophys Res*, 95, B13, 21991–22011
- Schuh H, Behrend D (2012) VLBI: A fascinating technique for geodesy and astrometry. *J Geodyn*, 61, 68–80, doi: 10.1016/j.jog.2012.07.007.

Combination of common parameters for co-located VLBI antennas

T. Nilsson, R. Heinkelmann, S. Glaser, B. Soja, M. Karbon, H. Schuh

Abstract In this work we investigate the possibility to combine clock parameters and tropospheric parameters of co-located VLBI telescopes in the VLBI data analysis. This is done by simulation of a future VGOS network as well as analysis of real data from the CONT14 campaign. It is found that the combination of tropospheric parameters improve the station position repeatabilities of the co-located telescopes by about 15%. Similar improvements can be obtained when combining clock parameters, however only if the clocks can be completely combined and no offset between them needs to be estimated.

Keywords VLBI, troposphere, clocks, twin telescopes, CONT14

1 Introduction

In the global geodetic VLBI network there are several stations equipped with two (or more) VLBI radio telescopes. In the data analysis of VLBI sessions where co-located stations are participating with both telescopes, it is possible to combine common parameters for these telescopes. For example, if the distance between the telescopes is short, it can be assumed that the tropospheric parameters are equal. If the telescopes are also connected to the same frequency standard, it is possible to estimate a common clock function. Furthermore, if the local tie vector between the telescopes are precisely known, the vector between the telescopes can be fixed to this value in the analysis, thus just one station position offset valid for both stations will be estimated. VLBI sessions with co-located antennas will be very common in the future, since the VGOS (VLBI Geodetic Observing System,

Tobias Nilsson, Robert Heinkelmann, Benedikt Soja, Maria Karbon, Harald Schuh

GFZ German Research Centre for Geosciences, Telegrafenberg A17, D-14473 Potsdam, Germany

Susanne Glaser, Harald Schuh
Institut für Geodäsie und Geoinformationstechnik, Technische Universität Berlin, Straße des 17. Juni 135, D-10623 Berlin, Germany

Petrachenko et al. 2009) network will contain several so-called twin telescopes.

Recently, Nilsson et al. (2015a) investigated how much the combination of tropospheric parameters improve the station position estimates. This was done by analyzing simulated observations for a potential VGOS network containing one twin telescope in Wettzell. An improvement of 15% in the station position repeatability of the twin telescope was found, as long as the telescope distance was less than 1 km. The main improvement was in the repeatability of baseline vector between the two Wettzell telescopes, which was more than 50%. These results were validated by analyzing the CONT14 campaign, where two telescopes in Hobart, Australia (HOBART12 and HOBART26) participated. Furthermore, the improvements when combining the station positions and/or clock parameters were briefly investigated. It was found that the combination of one of these parameters gave about the same improvement in the station position repeatability as combination of tropospheric parameters. However, no further improvement could be achieved when more than one parameter group was combined.

In this work we extend the Nilsson et al. (2015a) study by taking a closer look at the effects of combining the clock parameters. This is done both through simulations (Section 3) and analysis of real observations from the CONT14 campaign (Section 4).

2 Data analysis

For the data analysis we used the GFZ version of the Vienna VLBI Software (Böhm et al., 2012), VieVS@GFZ (Nilsson et al., 2015b). In the data analysis, we have the possibility to set common parameters for co-located telescopes equal. The following possibilities were implemented:

None: No common parameters were combined

Clk 0: The clock parameters of the co-located telescopes were set to be equal.

Clk 1: As *Clk 0*, but a constant clock offset between the co-located telescopes was also estimated for each session.

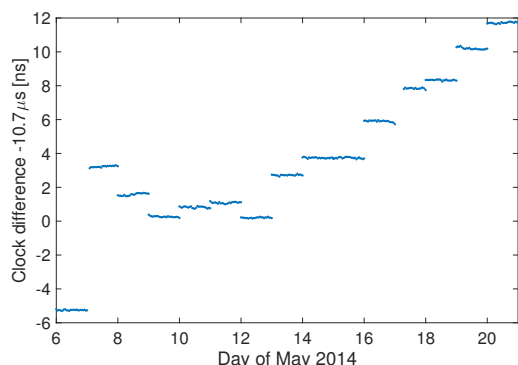


Fig. 1 Differences between the estimated clock functions of the HOBART12 and HOBART26 telescopes during CONT14.

Clk 2: The clock differences between the two telescopes was modeled as a piece-wise linear function, with 1 h intervals and relative constraints of 0.8 ns/h.

Trop: The zenith wet delays (ZWD) and gradients of the co-located telescopes were set equal. The tropospheric tie due to the height difference between the telescopes was applied a priori (Teke et al., 2013)

The estimation of a constant offset or a polynomial, as done in the *Clk 1* and *Clk 2* options, should theoretically not be needed when both telescopes are connected to the same clock. However, in reality the estimated clock error of a VLBI telescope does not only contain the true errors of the station clock, but also other clock-like contributions to the observed delay. This could for example be uncalibrated delays in cables and the receiving equipment. Thus it is likely that we need to take into account an unknown offset between the clocks (as done by *Clk 1*), and it is also possible that this offset have noticeable variation in time due to, e.g, thermal variations (*Clk 2*). This is demonstrated in Fig. 1 where the difference between the estimated clock errors of the co-located HOBART12 and HOBART26 telescopes during the CONT14 campaign is plotted. As we can see there is a huge offset (10.7 μ s), probably due to cable delays (none of the telescopes uses a cable calibration system). Furthermore, this offset is slightly different for each 1-day session; this is likely caused by the fact that each session is correlated individually, but further investigations are needed to find the exact reason. If we look carefully it is also possible to notice small variations over one session. Thus it is clear that we at least need to estimate an offset between the clocks for each session, and perhaps also some variations.

3 Simulations of a VGOS network

We made simulations for a potential future VGOS network consisting of 23 globally distributed stations; 22 single-telescope sites and one twin telescope in Wettzell. All telescopes were assumed to be very fast VGOS antennas with slew speed of

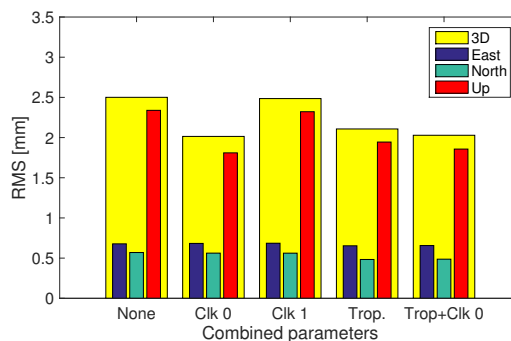


Fig. 2 Station position repeatabilities of the Wettzell twin telescope obtained from analysis of the simulated data. The x-axis give the analysis option applied (see Section 2).

12°/s in azimuth and 6°/s in elevation. For more details on the network, see Nilsson et al. (2015a). Observing schedules were generated using the scheduling tools in VieVS@GFZ, VIE_SIM (Sun et al., 2014), applying the source-based scheduling strategy with 4 sources schedule simultaneously and the multi-directional approach for the twin telescope (see Sun et al. (2014) and Nilsson et al. (2015a) for details). Simulated observations were generated using the simulation tools in VieVS@GFZ, VIM_SIM, applying the algorithms described in Pany et al. (2011) and Nilsson et al. (2015a). The same noise parameters as in Nilsson et al. (2015a) were used. These observations were then analyzed with VieVS@GFZ. In total we made 100 independent simulations, which should be enough to get good statistics.

Figure 2 shows the station position repeatability for the Wettzell twin telescope obtained from the simulations, and applying the different estimation options given in Section 2. We can see that in particular the repeatability of the height component improves by about 15% when the *Clk 0* or *Trop* option is applied. However, the *Clk 1* and *Clk 2* (not shown) options do not result in any noticeable improvement. This shows that the combination of the clock parameters can improve the solution, however, only if the mean offsets between the clocks can be fixed. This was possible for the simulations, where no clock difference between the station was simulated. Furthermore, we do not get any significant further improvement when combining both the clock and the tropospheric parameters (*Trop+Clk 0*), what confirms the results from Nilsson et al. (2015a).

In Fig. 3 the repeatabilities of the baseline length and height difference between the two Wettzell telescopes are shown. We can see here that the *Clk 0* and *Trop* options give significant improvements. For the baseline length the *Trop* option gives the largest improvement, while the *Clk 0* is better for the height difference. Also here there is no improvement when applying the *Clk 1* or *Clk 2* options. However, we can note that the best results are clearly obtained when applying both the *Clk 0* and *Trop* options.

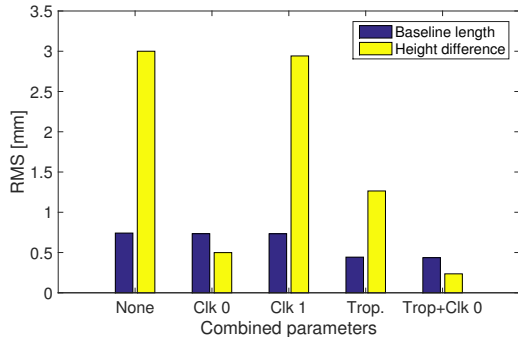


Fig. 3 Repeatabilities of the baseline length and height difference between the two Wettzell telescopes, obtained from analysis of the simulated data. The x-axis give the analysis option applied (see Section 2).

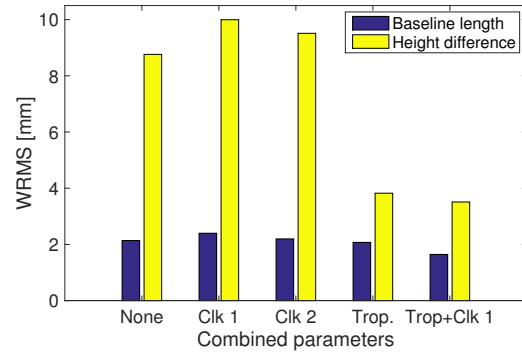


Fig. 5 Repeatabilities of the baseline length and height difference between the HOBART12 and the HOBART26 telescopes, obtained from analysis of the CONT14 data. The x-axis give the analysis option applied (see Section 2).

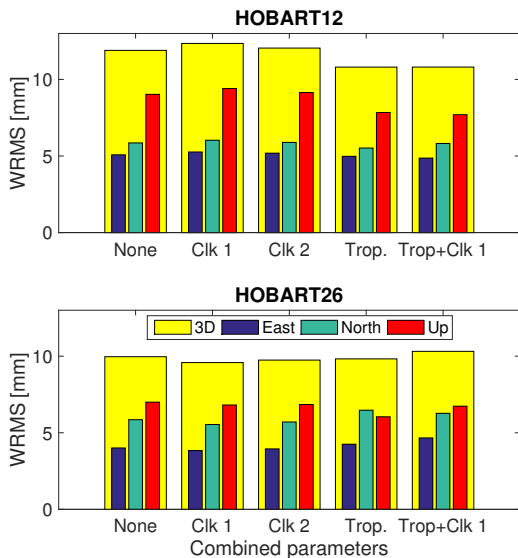


Fig. 4 Station position repeatabilities of the of the HOBART12 (top) and the HOBART26 (bottom) telescopes, obtained from analysis of the CONT14 data. The x-axis give the analysis option applied (see Section 2).

4 The Hobart telescopes in CONT14

We also tested the different analysis options on real data from the CONT14 campaign (6–20 May, 2014) (Behrend et al., 2014). In this campaign, both telescopes at the Hobart station, HOBART12 and HOBART26, participated, and both were connected to the same hydrogen maser. Figure 4 shows the station position repeatabilities of the Hobart telescopes when applying the different options. The results when applying option *Clk 0* are not shown since there is a big ($10.7 \mu\text{s}$) clock offsets between the two telescopes (see Fig. 1); thus it is clear that this option is not appli-

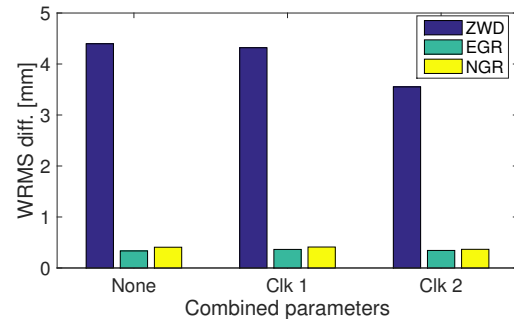


Fig. 6 WRMS difference between the ZWD and Gradient (EGR and NGR) estimates of the HOBART12 and HOBART26 telescopes, obtained from analysis of the CONT14 data. The x-axis give the analysis option applied (see Section 2).

cable. We can see that the *Clk 1* and *Clk 2* options make the repeatabilities slightly worse for HOBART12, but improve them slightly for HOBART26. Thus no obvious improvement is found when applying any of them, confirming the results of the simulations. Applying the *Trop* option improves the repeatabilities, especially for HOBART12.

We also investigated the repeatability of the baseline between the two Hobart telescopes. In Fig. 5 the repeatabilities of the baseline and height difference are shown. As already shown in Nilsson et al. (2015a), the *Trop* option improved the repeatability of the height difference significantly. However, the results gets slightly worse when the *Clk 1* and *Clk 2* options are applied. This could indicate that the clocks are effectively not exactly the same for the two telescopes, even though they are connected to the same hydrogen maser. On the other hand, the best results are obtained when applying both the *Trop* and *Clk 1* options, although this is only marginally better than applying only *Trop*.

Another way to assess the performance of the options for combining the clock parameters is to look at the estimated tropospheric parameters. Since the distance between the two co-

located telescopes is short (295 m for the Hobart telescopes), the estimated tropospheric parameters should be more or less equal (after applying tropospheric tie corrections, Teke et al. (2013)). Thus, by studying the difference between the two telescopes of the estimated tropospheric parameters, we get an indication of the quality of the solution. Fig. 6 shows the WRMS differences of the ZWD and gradients estimates of the HOBART12 and HOBART26 telescopes when applying the *None*, *Clk 1*, and *Clk 2* options. We can see that there is no effect on the WRMS differences when applying *Clk 1*, while when applying *Clk 2* the WRMS difference for the ZWD decreases. This indicates that the combination of clocks can improve the estimation of tropospheric parameters. However, the differences between the clocks is not exactly constant in time, thus *Clk 1* does not result in any improvement. The variations in the clock difference are better captured in the *Clk 2* solution, thus an improvement can be seen for the ZWD difference.

5 Conclusions

The results of this study show that the combination of clock parameters for co-located antennas connected to the same frequency standard can improve the station position repeatabilities and other parameters. For the station coordinates, however, there is only an improvement if no clock offset between the two telescopes needs to be estimated, while there are no significant improvements from just setting the variations over a session equal. This is probably because the station coordinates are estimated per session, hence the mean clock offsets over the session is mostly important. If the station coordinates would be estimated with higher resolution, options *Clk 1* and *Clk 2* might improve the results. As seen in Section 4, combining the clock variations can improve the estimation of time varying parameters like the ZWD.

References

- Behrend D, Thomas C, Himwich E, MacMillan D (2014) CONT14: Preparation and prospects. In: D. Behrend, K. D. Baver, K. Armstrong (eds.), *IVS 2014 General Meeting Proc.*, Science Press (Beijing), 196–200, URL ftp://ivscc.gsfc.nasa.gov/pub/general-meeting/2014/pdf/042_Behrend_etal.pdf.
- Böhm J, Böhm S, Nilsson T, Pany A, Plank L, Spicakova H, Teke K, Schuh H (2012) The new Vienna VLBI software. In: S. Kenyon, M. C. Pacino, U. Marti (eds.), *Proc. IAG Scientific Assembly 2009*, IAG Symposia Series 136, 1007–1011, doi: 10.1007/978-3-642-20338-1_126.
- Nilsson T, Karbon M, Soja B, Heinkelmann R, Lu C, Schuh H (2015) Atmospheric modeling for co-located VLBI antennas and twin telescopes. *J Geod.*, 89:655–665, doi: 10.1007/s00190-015-0804-6.
- Nilsson T, Soja B, Karbon M, Heinkelmann R, Schuh H (2015) Application of Kalman filtering in VLBI data analysis. *Earth Planets Space*, 67(136), 1–9, doi: 10.1186/s40623-015-0307-y.
- Pany A, Böhm J, MacMillan D, Schuh H, Nilsson T, Wresnik J (2011) Monte Carlo simulations of the impact of troposphere, clock and measurement errors on the repeatability of VLBI positions. *J Geod.*, 85, 39–50, doi: 10.1007/s00190-010-0415-1.
- Petrachenko B, Niell A, Behrend D, Corey B, Böhm J, Charlot P, Collioud A, Gipson J, Haas R, Hobiger T, Koyama Y, MacMillan D, Malkin Z, Nilsson T, Pany A, Tuccari G, Whitney A, Wresnik J (2009) Design aspects of the VLBI2010 system. In: D. Behrend, K. Baver (eds.), *IVS 2008 Annual Report*, NASA/TP-2009-214183, xx-yy.
- Sun J, Böhm J, Nilsson T, Krásná H, Böhm S, Schuh H (2014) New VLBI2010 scheduling strategies and implications on the terrestrial reference frames. *J Geod.*, 88(5):449–461, doi: 10.1007/s00190-014-0697-9.
- Teke K, Nilsson T, Böhm J, Hobiger T, Steigenberger P, Garcia-Espada S, Haas R, Willis P (2013) Troposphere delays from space geodetic techniques, water vapor radiometers, and numerical weather models over a series of continuous VLBI campaigns. *J Geod.*, 87(10-12), 981–1001, doi: 10.1007/s00190-013-0662-z.

VLBI Analysis at BKG

V. Thorandt, G. Engelhardt, D. Ullrich

Abstract The VLBI group of the Federal Agency for Cartography and Geodesy (BKG) in Leipzig is part of the jointly operated IVS Analysis Center of BKG and the Institute for Geodesy and Geoinformation of the University of Bonn (IGGB). BKG is responsible for regular submissions of time series of Earth Orientation Parameters (EOP) and tropospheric parameters, the generation of daily SINEX (Solution INdependent EXchange format) files for 24-hours sessions and Intensive VLBI sessions, quarterly updated solutions to produce terrestrial and celestial reference frame realizations (TRF, CRF), and generating Intensive schedules (mainly Tsukuba-Wetzell). Additionally, the BKG Analysis Center has generated input in the form of daily SINEX files for the ITRF2014 VLBI combination solution. The data processing steps are explained and also some activities in the technologies of data analysis are pointed out.

Keywords Data Analysis, Time Series, SINEX Files

1 General Information on Data Analysis

At BKG, the Mark 5 VLBI data analysis software system Calc/Solve, release 2014.02.21 (GSFC, 2014), has been used for VLBI data processing. It is running on a Linux operating system.

Calc/Solve allows to generate so-called TRP files derived from the Vienna Mapping Function (VMF1) data. They contain external information about the troposphere on a scan-by-scan basis, specifically the a priori delay, dry and wet mapping functions, and gradient mapping functions. The BKG VLBI group uses TRP files to input data related to VMF1. The VMF1 data were downloaded daily from the server of the Vienna University of Technology.

Additionally, the technological software environment for Calc/Solve has been refined to link the Data Center management with the pre- and post-interactive parts of the EOP series pro-

Volkmar Thorandt, Gerald Engelhardt and Dieter Ullrich
Bundesamt für Kartographie und Geodäsie (BKG), Karl-Rothe-
Str. 10-14, D-04105 Leipzig, Germany

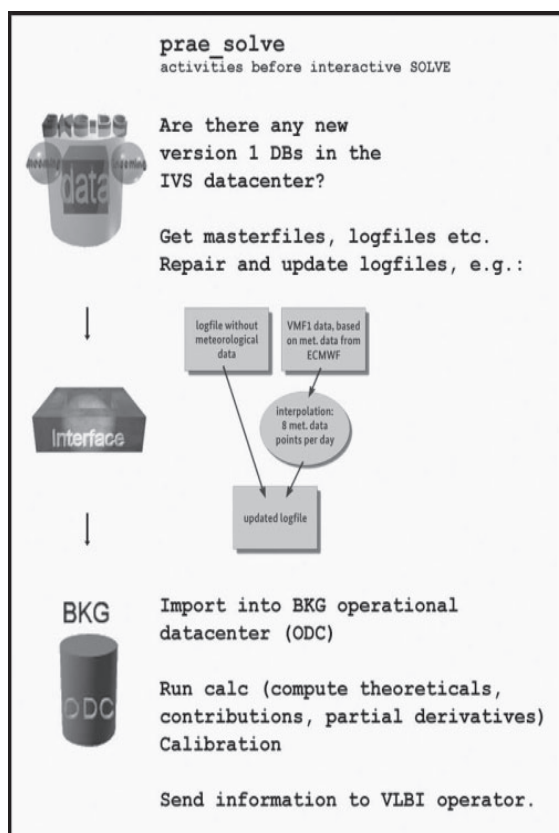


Fig. 1 Activities before interactive SOLVE, prae_solve

duction and to monitor all Analysis and Data Center activities (s. Fig. 1 and Fig. 2).

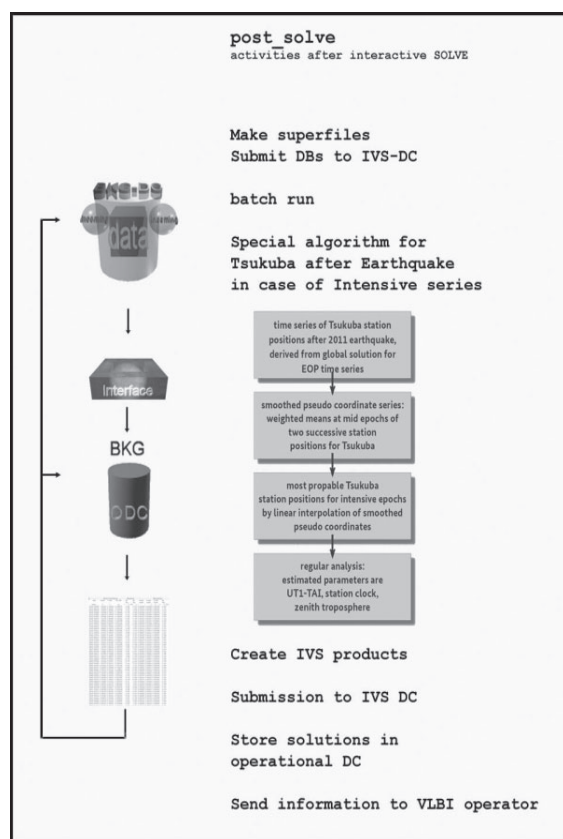


Fig. 2 Activities after interactive SOLVE, post_solve

2 Processing of Correlator Output

One important task in data analysis at BKG is the generation of calibrated databases for the sessions correlated at the MPIFR/BKG Astro/Geo Correlator at Bonn (e.g. EURO, OHIG, T2) and submitted them to the IVS Data Centers.

3 Scheduling

BKG is responsible for scheduling the INT2 Intensive sessions, which are observed on the TSUKUBA-WETTZELL baseline by using the program system SKED developed by John Gipson (NVI, Inc/NASA Goddard Spaceflight Center). Due to maintenance of the TSUKUBA antenna in 2014, two schedule files for baseline KASHIM34-WETTZELL were also made available.

4 IVS EOP Time Series bkg00014

The BKG EOP time series bkg00013 was replaced by the new one bkg00014. One main difference to the former solution was the use of the IERS2010 conventions. The solution for generating the EOP series based on a global solution mode with common estimation of all parameter types. The EOP are one part of the arc-parameters, i.e. estimations for each experiment session. The global parameter adjustments refer to the entire data set, e.g. station positions and velocities or source positions.

Each new VLBI session issued from correlator as database version 1 is processed and after that a new global solution with 24-hours sessions since 1984 is computed. Then the EOP time series bkg00014 is extracted.

Some topics of solution bkg00014 are:

- number of sessions more than 4800,
- datum definition is realized by applying no-net-rotation and no-net-translation conditions for 25 selected station positions and velocities with respect to VTRF2008a and no-net-rotation condition for 295 defining sources with respect to ICRF2,
- global parameter types are station coordinates and velocities, radio source positions
- local parameter types in each session, e.g. EOP, tropospheric parameters (zenith wet delays at 1 hour intervals), coordinates of some unstable or infrequently observed sources, local station coordinates for AIRA (Japan), CHICHI10 (Japan), CTVASTJ (Canada), DSS13 (USA), HART15M (South Africa), ISHIOKA (Japan), KASHIM11 (Japan), KASHIM34 (Japan), KOGANEI (Japan), KUNMING (China), PT.REYES (USA), RAEGYEB (Spain), SEJONG (Korea), SEST (Chile), SINTOTU3 (Japan), TIANMA65 (China), TIGOCONC (Chile), TSUKUB32 (Japan), UCHINOUR (Japan), VERAISGK (Japan), VERAMZSW (Japan), WIDE85_3 (USA), and YEBES40M (Spain).

Furthermore the fact of unavailable meteorological data in station logfiles could be compensated by using of meteorological data from European Centre for Medium-Range Weather Forecasts (ECMWF) contained in VMF1 data files. This procedure was integrated in the technological process of the EOP series generation.

5 IVS UT1 Time Series bkgint14

The UT1-UTC time series bkgint09 was replaced by bkgint14 in consideration of the IERS2010 conventions. The series bkgint14 based on independent session solutions with fixed TRF (VTRF2008a) and fixed ICRF2. The a priori EOP are taken from final USNO series (USNO, 2014). The estimated parameter types are only UT1-TAI, station clock, and zenith troposphere. The algorithms of the semi-automatic process for handling the Intensive sessions Int2/3 with station TSUKUBA after the Japan earthquake (Engelhardt et al., 2013) have been further used, i.e.

before the regular analysis can be started most probable station positions of TSUKUBA for the epochs of Int2/3 sessions have to be estimated.

6 Quarterly Updated TRF and CRF Solutions for Submission to IVS

Every year quarterly updated solutions for the IVS products TRF and CRF are computed. There are no differences in the solution strategy compared to the continuously computed EOP time series bkg00014. The results of the radio source positions are submitted to IVS in IERS format. The TRF solution is available in SINEX format, version 2.1 and includes station coordinates, velocities, and radio source coordinates together with the covariance matrix, information about constraints, and the decomposed normal matrix and vector.

7 Tropospheric Parameters

The VLBI group of BKG continues regular submissions of long time series of tropospheric parameters to the IVS (wet and total zenith delays, horizontal gradients) for all available VLBI sessions since 1984. The tropospheric parameters are extracted from the standard global solution for the EOP time series bkg00014 and transformed into SINEX format.

8 Daily SINEX Files

In addition to the global solutions, daily SINEX files for all available 24-hours sessions as base solutions for the IVS time series of baseline lengths and for combination techniques are submitted. Independent session solutions (bkg2014a) are computed for the parameter types station coordinates, radio source coordinates except for 295 defining sources of ICRF2, and EOP including the X,Y-nutation parameters. The a priori datum for TRF is defined by the VTRF2008a, and ICRF2 is used for the a priori CRF information.

9 SINEX Files for Intensive Sessions

IVS SINEX files for Intensive sessions (bkg2014a) are created and submitted to IVS. The parameter types are station coordinates, pole coordinates and their rates, and UT1-TAI with rate. Only the normal equations stored in the SINEX files are important for further intratechnique combination or combination with other space geodetic techniques.

10 Conclusions and Outlook

The main task of BKG VLBI Analysis Center is the generation of all IVS products. This also requires the further development of the semi-automatic software environment for Calc/Solve. Besides the usage of VLBI data analysis software system Calc/Solve the new developed software ν Solve for interactive processing of a single geodetic VLBI session will also be used in the future. It is a part of Calc/Solve release (Calc/Solve, 2008). Additionally tests with the new vgosDB format (IVS-WG4, 2013) are planned.

References

- Engelhardt G, Thorandt V, Ullrich D (2013) Rapid UT1 Estimation Derived from Tsukuba VLBI Measurements after 2011 Earthquake. In: N. Zubko, M. Poutanen (eds.) *Proc. 21st EVGA Working Meeting*, 85–87.
- GSFC, NASA (2014) Release of Mark 5 VLBI Analysis Software Calc/Solve from February 21, 2014. <http://gemini.gsfc.nasa.gov/solve>.
- IVS-WG4, John Gipson et al. (2013) Final Report of IVS Working Group 4 (WG4) on Data Structures. <ftp://ivscc.gsfc.nasa.gov/pub/annual-report/2013/pdf/spc1-wg4.pdf>.
- USNO (2014) Earth orientation parameters series from finals USNO series 2014. http://gemini.gsfc.nasa.gov/500/oper/solve/_apriori_files/usno_finals_erp.

Combination products and the IVS contribution to ITRF2014

L. Messerschmitt, S. Bachmann, D. Thaller

Abstract The IVS is responsible for providing the VLBI contribution to the new International Terrestrial Reference Frame, i.e., the ITRF2014. Nine IVS Analysis Centers provided session-wise, datum-free normal equations in SINEX files to the IVS Combination Center, which then generated the combined IVS contribution to ITRF2014. The sessions analyzed for ITRF2014 cover a time span from 1979 until the end of 2014, and the quality of the derived station coordinates is at the level of a few millimeters. This paper summarizes the combination process, and characterizes the resulting VLBI contribution to ITRF2014.

Keywords International Terrestrial Reference Frame 2014, IVS combination, VLBI, Earth Orientation Parameter

1 Introduction

The International Terrestrial Reference Frame (ITRF) is the accurate realization of the International Terrestrial Reference System (ITRS), and was adopted by the XXIst General Assembly of the International Astronomical Union (IAU) in Buenos Aires, Argentina, in 1991.¹ The ITRF has more than four hundred globally distributed 3-dimensional cartesian reference points. Very Long Baseline Interferometry (VLBI), together with Satellite Laser Ranging (SLR), are essential for the determination of the scale, because they are the only techniques with undisturbed access to this parameter. With the transformation to 12h UT, which is used by every space geodetic technique, it is possible to use these techniques in complement to each other, so that the weaknesses of one technique can be cancelled out by the strengths of another technique, for example such as the poor occurrence of VLBI Stations in the southern hemisphere.

The results were generated in cooperation of geodetic institutes and with use of four space geodetic techniques.

Linda Messerschmitt, Sabine Bachmann and Daniela Thaller
Bundesamt für Kartographie und Geodäsie, BKG, Richard-Strauss-Allee 11, D-60598 Frankfurt am Main, Germany

¹ <http://www.iers.org/IERS/EN/Science/Recommendations/resolutionCTRS.html?nn=12932>

- Global Navigation Satellite System (GNSS)
- Satellite Laser Ranging (SLR)
- Very Long Baseline Interferometry (VLBI)
- Doppler Orbitography and Radiopositioning Integrated by Satellite (DORIS)

Every space geodetic technique independently implements their own international measuring campaigns and the observations of all techniques are summarized at regular time intervals in an ITRF. The annually renewed campaign schedule for the VLBI is led by the International VLBI Service for Geodesy and Astrometry (IVS), and can be found at the following link (<http://lupus.gsfc.nasa.gov/sess/>).

In February 2013, the ITRS Data Center of the International Earth Rotation and Reference Systems Service (IERS) decided to process a new ITRF2014, supported by the individual contributions of the IAG space geodetic technique services. The IERS Convention Center, an collaborative effort of the Bureau International des Poids et Mesure (France) and the U.S. Naval Observatory (USA), regularly publishes the IERS Conventions.

For example, the current IERS Conventions (2010) (Petit and Luzum, 2010(@)) comprise astronomical constants (IAU2009), the definition of the ICRS and International Celestial Reference Frame (ICRF), as well as the realization of the ITRF. The data collection, analysis procedure, and the combination must comply with these formalities.

Every interested scientific institute can participate in the IVS contribution to the ITRF2014 under the conditions of both the IERS conventions and the IVS internal guidelines set by the IVS Analysis Coordinator.²

2 Input for IVS Combination

Eleven Analysis Centers submitted their contributions to the ITRF2014 as 24h sessions in the form of datum-free normal equations in SINEX files. These files contain coordinates of the involved VLBI stations as well as Earth Orientation Parameters (EOP), taken from sessions covering the time span of 1979 until

² http://lupus.gsfc.nasa.gov/files_IVS-AC/ITRF2013_checklist_v2014Feb07.pdf

Table 1 IVS Analysis Centers, their software package and contribution to operational IVS products and to the ITRF2014.

AC	Name	Software	Operational	ITRF2014	
				AC	submitted included
AUS	Geoscience Australia, Australia	OCCAM	no	yes	no
BKG	Federal Agency for Cartography and Geodesy, Germany	Calc/Solve	yes	yes	yes
CGS	Centro di Geodesia Spaziale, Italy	Calc/Solve	under review	yes	yes
DGFI	German Geodetic Research Institution	OCCAM	yes	no	no
GFZ	German Research Center for Geosciences	VieVS	under review	yes	yes
GSFC	Goddard Space Flight Center, USA	Calc/Solve	yes	yes	yes
IAA	Institute of Applied Astrometry, Russia	Quasar	yes	yes	yes
NMA	Norwegian Mapping Authority, Norway	GEOSAT	no	yes	no
OPAR	Observatory of Paris, France	Calc/Solve	yes	yes	yes
SHAO	Shanghai Observatory, China	Calc/Solve	no	yes	yes
USNO	US Naval Observatory, USA	Calc/Solve	yes	yes	yes
VIE	Vienna University of Technology, Austria	VieVS	no	yes	yes

the end of 2014. The IVS Combination Center (CCIVS) combined the AC contributions into a unified solution due to different software, analysis procedures, and strategies among the Analysis Centers. Table 2 depicts the determining parameters of each space geodetic technique used in the analysis. All combined SINEX files include the EOPs and station coordinates. There were two noted abnormalities regarding the combination of contributions of the ACs to ITRF2014: firstly, the Norwegian Mapping Authority detected a bug in their software, GEOSAT, and secondly, the Australian data had a possible degrading influence on the station weighted root mean square (WRMS) of the combination. Because of this, these two AC contributions were excluded from the IVS ITRF2014 combined contribution, which reduced the number of participating ACs to nine. In the time span of 1979 to the end of 2014, 5796 VLBI sessions were processed and submitted to the IERS ITRS Center. Table 1 summarizes all VLBI Analysis Centers with their contribution and their respective software packages.

Eight Analysis Center contribute regularly to the rapid combination. The German Geodetic Research Institute/Technical University of Munich (DGFI-TUM) is diligently involved in the rapid combination, but did not submit data for the ITRF2014. The Analysis Centers of Norway, Vienna, Shanghai, and Australia have not yet taken part in the rapid combination. Additionally, the Centro di Geodesia Spaziale (CGS) in Italy and the German Research Center for Geosciences (GFZ) are still under review for the rapid process, but it is anticipated that they will be fully integrated into the combination soon.

3 Analysis Strategy

The standards for compiling all AC contributions are defined by the IVS Analysis Coordinator.

The contributions, in the form of datum-free normal equations, are provided in SINEX and contain station coordinates as well as EOPs. Figure~1 depicts the strategy for the intra-technique combination, consisting of seven steps. The technical

Table 2 Parameters by the space geodetic techniques.

	Parameter type	VLBI	GNSS	SLR	LLR	DORIS
CRF	Quasar positions	X				
	Orbits (satel., moon)	X	X	X	X	X
EOP	Nutation	X			X	
	Nutation rates	X	X	X	X	X
	UT1-UTC	X				
	LOD	X	X	X	X	X
TRF	Polar motion	X	X	X	X	X
	Station positions	X	X	X	X	X
	Gravity field Geocenter		X	X		X
	Low-degree		X	X	X	X
Atmosphere	Troposphere	X	X			X
	Ionosphere	X	X			X

realization of the combination process was done by Böckmann et al. (2010), whose described procedure was used to compute the contribution to ITRF2008. In the meantime, the combination process has been refined, especially the outlier test. More details can be found in Bachmann et al. (2015).

The combination is implemented using the following steps:

1. The session-wise datum-free normal equation systems are transformed to 12h UT
2. Transformation of equal a priori station coordinates, i.e., VTRF2008
3. Robust outlier testing for station coordinates and for earth orientation parameters, using
 - a. detection by Least Median of Square (LMS) method with identical epochs and a priori values
4. Variance component estimation (VCE) for determining the weighting factor for each AC, using
 - a. the Operator-Software-Impact (OSI) method
5. Accumulating the weighted individual normal equations of all ACs in the IVS combined session

6. Determining the datum defects of the normal equations by using the datum NNR and NNT
7. Inverting the normal equations to get the combined solution for each VLBI session

When generating long-term series, systematic behavior may also be discovered. The combination process is based on the orbit and geodetic parameter estimation software (DOGS-CS) of the German Geodetic Research Institute/Technical University of Munich (DGFI-TUM). The differences between the standards used for the IVS contribution to ITRF2014 and ITRF2008 are mainly the use of IERS Conventions 2010 instead of 2003. The Nutation model changed from IAU2000A to the newer model IAU2006A. The site eccentricities have been taken into account with a new linear model developed specially for the ITRF2014 processing. No correction of the permanent tide has been applied. The combined SINEX files can be found in the IVS database.³

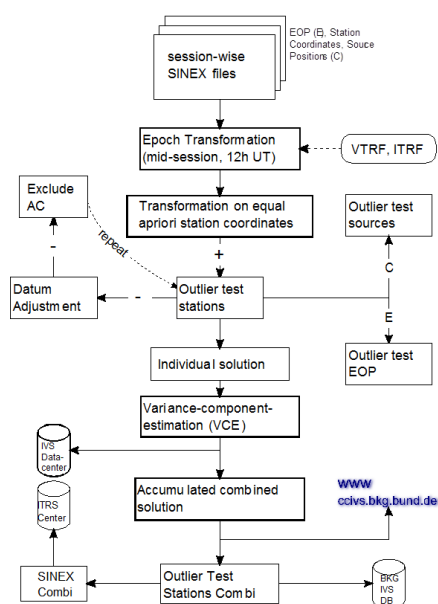


Fig. 1 Overview of VLBI combination process

4 Results of IVS Contribution to ITRF2014

In this section, results of station coordinates, EOPs and the VTRF will be shown.

³ ftp://ivs.bkg.bund.de/pub/vlbi/ITRF2013/daily_sinex/ivs2014a/

4.1 Station Coordinates

The first quality check for the estimated station coordinates is done by comparing the coordinates derived from each individual AC solution with the IVS combined solution for the respective session. Figure 2 shows this comparison for the observatory Wettzell (Germany) as one example. In the early years, the differences were up to 15mm, due to smaller networks with worse global distribution. However, starting with the 1990s, the quality of the station coordinates greatly improved with differences of only a few millimeters. In order to evaluate station accuracy and repeatability, a WRMS of the session-wise coordinate residuals has been computed for each station. The WRMS of the combined solution amounts to 3-4mm in horizontal and 7mm in vertical direction. The individual AC solutions are at the same level of quality.

4.2 Earth Orientation Parameters

VLBI is the only method that provides a complete set of EOP. Table 2 shows that VLBI determines UT1-UTC (dUT) as well as the nutation in contrast to all other space geodetic techniques. This reinforces the importance of VLBI to successful determination of the ITRF. Parameters like coordinates of the x-pole and y-pole and the length of day (LOD) can also be estimated by VLBI.

In order to evaluate the quality of the VLBI-derived EOPs, the time series of the individual AC solutions are compared to the IVS combination. Figure 3 shows the WRMS of these differences for dUT and the pole coordinates. The WRMS of the x- and y-pole amount to 0.05-0.10 mas, and the WRMS of the dUT differences amount to 0.04-0.15 ms.

4.3 VTRF

The VTRF is a geocentric reference frame which co-rotates with the earth. Its origin is located close to the center of mass, the Z axis is the direction of the pole along the earth rotation axis, and the orientation of the X axis is directed to the Greenwich meridian. The Y axis is orthogonal to the Z and X axis. The VTRF contains piece-wise linear station coordinates and velocities of station positions. Using VTRF, we can notice a drift of 1.5 cm per year for the Wettzell station in Germany and a higher drift in the Australian area of 5 cm per year for the Yarragadee station.

Table 3 lists the transformation parameters between VTRF2014 and ITRF2008 (Altamimi et al., 2011). VLBI is not sensitive to origin and rotation, thus, the translation and rotation parameters only show the quality of the datum realization. The scale difference with respect to the second ITRS combination center, i.e., the DTRF2008 solution is smaller: only 0.11 ppb with a linear drift of 0.02 ppb/y.

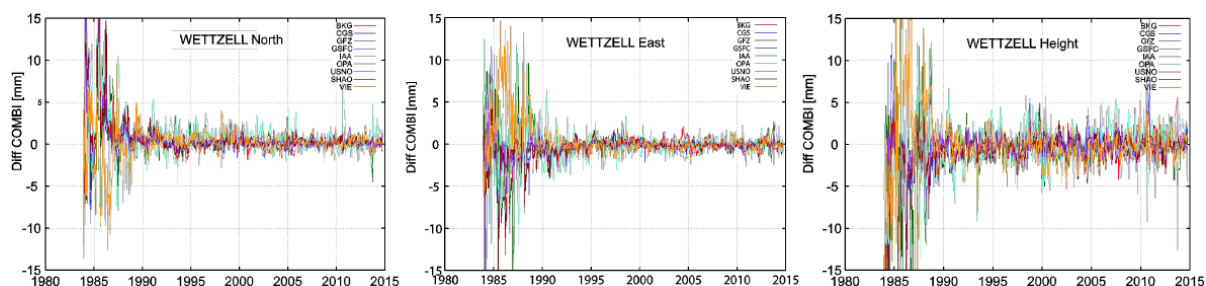


Fig. 2 VLBI Station coordinates timeseries of Wetzell, Germany

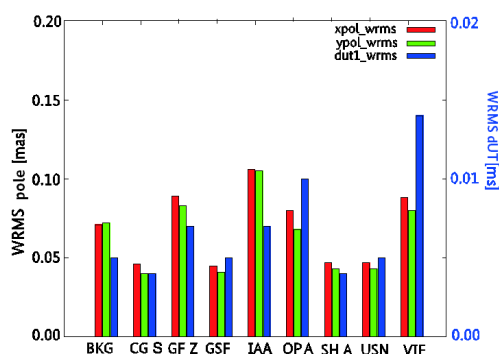


Fig. 3 WRMS of the differences between the individual AC and the combined EOP solutions

Table 3 Transformation parameters between VTRF2014 and ITRF2008.

Parameter	Position	Velocities (per year)
Tx[mm]	-0.4 (± 0.6)	-0.4 (± 0.6)
Ty[mm]	0.6 (± 0.6)	-0.4 (± 0.6)
Tz[mm]	-1.3 (± 0.5)	-0.1 (± 0.5)
Rx[mas]	-0.003 (± 0.002)	-0.0008 (± 0.002)
Ry[mas]	0.001 (± 0.002)	0.0003 (± 0.002)
Rz[mas]	0.0002 (± 0.002)	0.0008 (± 0.002)
Scale[ppb]	0.44 (± 0.09)	-0.02 (± 0.09)

5 Conclusions and Outlook

Interest in contributing to the International Terrestrial Reference Frame from scientific institutes has increased in recent years. A total of 5796 sessions from nine Analysis Centers spanning from 1979 to late 2014 and using three different software packages, were successfully transmitted to the IERS Data Center. In comparison to the ITRF2008 contribution a significant increase of 20 percent was noticed regarding the number of sessions and the participating Analysis Centers. The new generation of smaller VLBI telescopes, such as 12 or 13 meter dishes, will increase the number of stations in the future, due to lower costs. Because of this, it can be expected that the network infrastructure will be

densified in the southern hemisphere, thereby greatly improving network stability. More details and results of the IVS contribution to ITRF2014 are summarized in Bachmann et al. (2015).

References

- Altamimi Z, Collilieux X, Metivier L (2011) ITRF2008: an improved solution of the international terrestrial reference frame. *J Geod*, 85, 457–473, doi: 40410.1007/s00190-011-0444-4.
- Bachmann et al. (2015) submitted to *J Geod*
- Böckmann S, Artz T, Nothnagel A (2010) VLBI terrestrial reference frame contributions to ITRF2008. *J Geod*, 84, 201–219, doi: 10.1007/s00190-009-0357-7.
- Petit G, Luzum B (eds.) (2010) IERS Conventions 2010. *IERS Technical Note*, 36, International Earth Rotation and Reference Systems Service (IERS), http://www.iers.org/IERS/EN/DataProducts/Conventions/conventions_cont.html

Analysis of GPS, VLBI and DORIS input time series for ITRF2014

V. Tornatore, E. Tanır Kayıkçı, M. Roggero

Abstract In this work we have compared the Up component time series reprocessed in view of the new ITRF2014. The solutions that we have considered are the combinations of individual submissions of the Operational Analysis Centers (ACs) as official IVS, IGS and IDS products. We have modelled time series as discrete-time Markov processes, we have detected and removed discontinuities from data time series and estimated trends (long term signals). A frequency analysis making research of residual periodic signals and identification of the common ones to all the three space geodetic techniques has been performed. Preliminary results on co-located sites are shown.

Keywords VLBI, GPS, DORIS, time series, harmonic analysis, ITRF2014

1 Introduction

A new determination of ITRF (called ITRF2014) is underway, at this aim several Analysis Centers of IVS, ILRS, IGS, IDS reprocessed all data available till the end of 2014. Reprocessing efforts continued with the approach, started with ITRF2005 and continued with ITRF2008, of using time series of station positions and Earth Orientation Parameters (EOPs) to take into account for realization of ITRF both for station non-linear motions and discontinuities (Altamimi et al., 2007), and also to evaluate the stability over time of frame parameters (origin and the scale) important for studies of Earth sciences. All the space geodetic techniques contributing to ITRF2014 used recommendation indicated in the call for participation (see http://itrf.ensg.ign.fr/ITRF_solutions/2013/CFP-ITRF2013-27-03-2013.pdf).

Vincenza Tornatore Politecnico di Milano, Dipartimento di Ingegneria Civile e Ambientale (DICA), Piazza Leonardo da Vinci 32, I-20133 Milano, Italy

Emine Tanır Kayıkçı Karadeniz Technical University, Department of Geomatics Engineering, T-61080 Trabzon, Turkey
Marco Roggero Politecnico di Torino, Dipartimento di Architettura e Design (DAD), Castello del Valentino, Viale Mattioli 39, I-10125 Torino, Italy

The solutions were calculated using IERS Conventions IERS (2010), including updates at <http://tai.bipm.org/iers/convupdt/convupdt.html>. It was not required to apply any geophysical fluid loading effect correction, except tidal load and other displacements for which the models are given in IERS Conventions 2010. However, it is envisaged that the individual Analysis Center solution will be corrected for non-tidal atmospheric loading during the ITRF generation, using a unique loading model provided by the IERS Global Geophysical Fluid Center (GGFC).

In this study we have analysed intra-technique combined solutions of the Up component time series for all the stations, whose coordinates have been estimated in the ITRF2014 solutions, belonging to the international space geodetic technique Services: IVS, IDS, IGS. The SLR time series are not included because at the time of this study the official solution for coordinate time series was not yet ready, it is planned to carry out a study also on SLR solutions once they will be officially available.

VLBI, GPS and SLR stations co-located with DORIS sites are shown in Fig. 1. For each technique Up component time series are modeled as discrete-time Markov processes, see Sec. 2.

The method we have used for the time series analysis and the detection of periodic signals is that described in Roggero (2015). Some examples will be given for the Ponta Delgada site where GPS/GLONASS and DORIS stations are co-located since several years. The presence of anomalous behaviours common to the three techniques is investigated for the Up component time series by analysing in frequency and amplitude the signals of the permanent stations. The harmonic analysis has been carried out globally for stations (belonging to each VLBI, GPS and DORIS network), having with a long time history and good sampling. Comparisons among obtained results for each of the three techniques have been made in Sec. 3

2 Time series analysis

To obtain high accuracy multi-year solutions one key task is to assess the quality of the underlying coordinate time series. The new calculation of ITRF2014 represents a good opportunity for



Fig. 2 GPS/GLONASS station at Ponta Delgada, Sao Miguel, Azores



Fig. 3 DORIS station at Ponta Delgada, Sao Miguel, Azores

known discontinuity: antenna and receiver change. A mean velocity of -1.79 mm/yr has been estimated for the GPS station.

Concerning the DORIS site (see picture shown in Fig. 3) it is also installed on concrete beam on the roof of a 3 storied building. The first station called PDLB was installed on the 02/11/1998 and removed 21/08/2001, then the present PDMD station was installed on the 22/08/2001.

A co-location between the two stations PDLB and PDMD was measured giving a negligible distance in X,Y,Z of a few millimeter each (precision 1 mm) reported in the logfile of the station. A little jump of 4.3 mm has been estimated in the Up component at the epoch when the station was changed, see the two time series of PDLB and PDMD stations displayed together in Fig. 5. In the DORIS time series clearly appear also gaps in data acquisition that according to logfile are generically due to corrupted data and failures.

The values of the estimated velocity is -2.16 mm/yr for the present PDMD station, this value is not very different from that found for GPS antenna (-1.79 mm/yr) PDEL, showing a good agreement on estimated velocities by the co-located GPS and DORIS techniques. However the PDMD value is very different from that of the previous DORIS station PDLB that is equal to -

8.57 mm/yr. It has to be noticed that data of PDLB are more scattered than those of PDMD and the covered time interval is very short. This confirms how estimated velocity values can change according to time interval considered, especially when it is very short and data are very noisy the values of the estimated velocities can not be very reliable. At the site of Ponta Delgada also meteorological instrumentations are present like humidity, pressure and temperature sensors. The co-location measurement carried out at the site are:

1. Tide Gauge co-location with DORIS station (measured 10/1998 and 08/2001)
2. GNSS and current DORIS PDMD distance in X,Y,Z a few meters, accuracy 10 mm, tie measured on 01/08/2001
3. VLBI-GNSS (VLBI portable observation at the level of 10 mm accuracy)

More details on values of these past co-locations can be found on the logfile of the stations both for PDEL and PDMD. Anyway all the local tie campaigns are quite dated, it would be useful to repeat co-location campaigns also in view of the new VLBI Global Observing System (VGOS) antenna recently installed at Santa Maria island.

3 Harmonic Analysis

The procedure applied for the analysis of all time series (Up component) estimated in view of ITRF2014 for the sites belonging to networks of IVS, IGS and IDS, had the aim to remove discontinuities, estimate velocities, remove non linear long term trends and residual calculation.

This was done to obtain residuals having statistical properties that vary cyclically with time so that harmonic analysis could be applied. However obtained residuals still present some limitations to apply harmonic analysis, since they do not fulfill completely all the requirements of a standard harmonic analysis, like long time series, constant sampling rate, equally weighted data values, no presence of gaps.

For all of these reasons we carried out residual harmonic analysis using the non linear least square algorithm implemented in the software called FAMOUS (?). The signals estimated by FAMOUS were studied in frequency and amplitude stacking the power spectra in order to detect the most significant effects. Then a global analysis of detected signals over the total number of stations was performed, excluding only those sites having time history shorter than 10 years.

The results of our harmonic analysis presented three classes of signals, related to seasonal, orbital (GPS draconitic) and tidal effects. The minimum sampling frequency (Nyquist frequency) for weekly time series is 14 days, around this value a strong signal has been also detected and can also be attributed to tidal model errors. Values for the detected signals, period and amplitude, for GPS, VLBI and DORIS sites (only signals that passed FAMOUS significance tests are reported) can be found in Tab. 1 and in Tab.2. The values inside square brackets in Tab.1 are the percentages of incidence, that is the number of stations in which the signal has been detected over the total number of stations. All

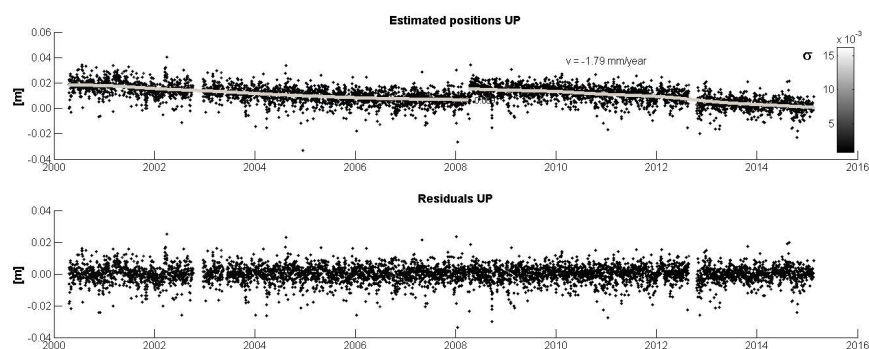


Fig. 4 Up component time series plus estimated long term signal (top), and residuals almost cyclostationary (bottom) for Ponta Delgada GPS station (PDEL). The grayscale color bar represents the σ of the Up component

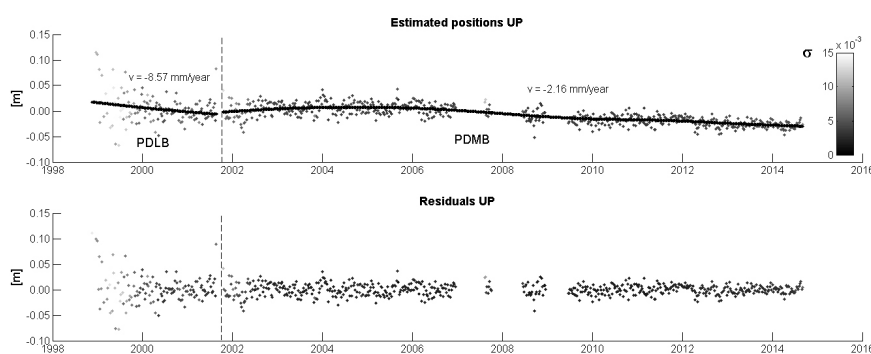


Fig. 5 Up component time series plus estimated long term signal (top), and residuals almost cyclostationary (bottom) for Ponta Delgada DORIS stations (PDLB and PDMD). The grayscale color bar represents the σ of the Up component, that is higher during the first years of PDLB observations

expected and detected draconitic, solar and tidal harmonic have comparable periods for the GPS technique. Among all the detected annual signals two of them with 14 days and 1 year (solar) period are common to all the 3 techniques.

4 Conclusions

In view of the calculation of ITRF2014, input time series from the four space geodetic techniques have been reprocessed till the end of the 2014 according to same recommendation. Therefore combined intra-technique time series solutions constitute a huge homogeneous data set. In this work we have applied the same method for time series analysis in particular of the Up component of GPS, DORIS and VLBI sites estimated during reprocessing procedure. Once we have detected and removed time series discontinuities, we have estimated trends and removed them obtaining almost cyclostationary stochastic process, whose statistical properties vary periodical.

The adopted algorithms, in this work, have made harmonic analysis possible and reliable almost on all our set of data even when we do not have constant sampling rate, and short gaps are still present in the time series. Among the detected annual signals two of them with 14 days and 1 year (solar) periods are common to all the 3 techniques, detailed investigation on the geophysical origin of these signals nature are necessary to make a correct interpretation.

An extended version of this work is going to be published on the Journal Advances in Space Research (ISSN: 0273-1177), Special Issue: Applications of DORIS data.

Table 1 Signal mean amplitudes estimated for GPS, DORIS and VLBI sites (only signals that passed FAMOUS significance tests are reported).

cpy	mean amplitude [mm]						
	GPS			DORIS		VLBI	
	draconitic	solar	tidal	solar	tidal	solar	tidal
1	3.5 [1.7%]	4.4 [50.2%]	1.3 [3.1%]	10.3 [15.0%]		2.5 [5.5%]	
2	1.7 [37.5%]	1.9 [15.1%]	2.9 [4.0%]	8.8 [3.9%]			
3	1.5 [20.2%]	1.6 [7.5%]		7.5 [9.2%]			
4	1.6 [27.7%]	1.2 [1.9%]	1.2 [1.9%]				
5	4.1 [4.0%]						
6	1.0 [7.1%]						
7	1.4 [2.2%]						
12			7.3 [6.5%]		6.1 [18.3%]		4.7 [8.2%]

Table 2 Expected and estimated signal periods at GPS, DORIS and VLBI sites (only signals that passed FAMOUS significance tests are reported).

cpy	Period [days]									
	Expected			GPS			DORIS		VLBI	
	draconitic	solar	tidal	draconitic	solar	tidal	solar	tidal	solar	tidal
1	351.2	365.3	164.0	350 ±1	365±5	163±2	363±10		365±2	
2	175.6	182.6	82.0	176±3	182±2	82±1	183±3			
3	117.1	121.8		117±1	122±1		118±3			
4	87.8	91.3	41.0	88±1	91±1	41±1				
5	70.2			70±1						
6	58.5			59±1						
7	50.2			50±1						
12			13.7			14±1		15±1		13±2

5 Acknowledgments

The authors wish to thank Guilhem Moreaux (CLS, Collecte, Localisation, Satellites, France) Sabine Bachman and Linda Messerschmitt (BKG, Bundesamt für Kartographie und Geodäsie Germany), Paul Rebischung (IGN, Institut National de l'information géographique et forestière, France), for having provided time series coordinate, from intra-technique combined solutions calculated for ITRF14, respectively for DORIS, VLBI, and GPS sites. We thank also for very useful information and discussions on how the solutions have been calculated.

References

- Albertella A, Betti B, Sansó F, Tornatore V (2005) Real Time and Batch Navigation solutions: alternative approaches. *Bollettino SIFET N. 4/2005*, Cagliari, ISSN 1721-971X, 85–102.
- Altamimi Z, Collilieux X, Legrand J, Garayt B, Boucher C (2007) ITRF2005: a new release of the international terrestrial reference frame based on time series of station positions and earth orientation parameters. *J Geophys Res*, 112 (B09401).
- Mignard F (2003) FAMOUS, Frequency Analysis Mapping On Unusual Sampling, (OCA Cassiopee), Software.
- Petit G, Luzum B (eds.) (2010) *IERS Conventions 2010, IERS Technical Note 36*. Frankfurt am Main: Verlag des Bundesamts für Kartographie und Geodäsie, 2010.
- Roggero M (2012) Discontinuity detection and removal from data time series. *VII Hotine Marussi Symposium on Theoretical and Computational Geodesy*, Springer-Verlag Berlin and Heidelberg GmbH & Co. K (DEU), ISBN: 9783642220777
- Roggero M (2015) Extensive analysis of IGS REPRO1 coordinate time series. *VII Hotine-Marussi Symposium on Mathematical Geodesy* 06/2015; 142.
- Teunissen P (1998) Quality control and GPS. *GPS for Geodesy*, P. J. G. Teunissen, A. Kleusberg (eds.), Springer-Verlag, Berlin, Heidelberg, New York, ISBN 3-540-63661-7.
- Tornatore V, Cazzaniga N (2009) GPS-aided inertial navigation algorithms: new approaches. *Int J Pure Appl Math*, ISSN 1311-8080, 51(2), 171-179.

VLBI Phase-referencing Experiments for Deep Space Probes

W. Zheng, F. Tong, J. Zhang, F. Shu, L. Liu

Abstract Chinese VLBI Network (CVN) carried out several phase-referencing experiments to validate its ability of accurate deep space probe positioning. At ChangE-3 lunar surface working stage, under the special same-beam observation condition, the phase-referencing imaging results were performed. From visibility data outputted by CVN software correlator, the angle positions can be got by Difmap, and then the relative positions between Rover and Lander were got. The accuracy of relative position is confirmed to be at the level of 0.5 mas. The phase-reference positioning experiments of Mars Express (MEX) and Chang'E-5T1 probes (CE-5T1) were also performed successfully. The positioning accuracy of CE-5T1 is within the orbit accuracy, but the accuracy of MEX is about 40 mas. Compared with the accurate MEX orbit provided by European Space Agency (ESA), a systematic angle position error of MEX was found, which was caused by the near-field target delay prediction error.

Keywords VLBI phase-referencing positioning, near-field delay model, lunar probe, MEX, CVN

1 Introduction

Chinese VLBI network (CVN) has played important roles in the Chinese Lunar exploration projects (Zheng et al., 2014; Huang et al., 2014). It has 4 VLBI antennas which located in Shanghai, Beijing, Kunming, Urumqi, and one VLBI data processing center (VLBI center) owned by Shanghai Astronomy Observatory, Chinese Academy of Sciences. In VLBI center, there are two sets of data processing and orbit determination pipelines including

Weimin Zheng, Fengxian Tong, Juan Zhang,
Fengchun Shu, Lei Liu;
Shanghai Astronomical Observatory,
Chinese Academy of Sciences;
Key Laboratory of Radio Astronomy,
Chinese Academy of Sciences;
University of Chinese Academy of Sciences;
E-mail: zhwm@shao.ac.cn

configuration items like, schedule, software/hardware correlator, media correction, post-processing, and orbit/position determination. In Chang'E-3 (CE-3) critical mission, the real-time VLBI group delay and the ranging data were used for orbit/position determination. After CE-3 Lander soft-land on the Moon, we performed an in-beam VLBI phase-referencing experiment and got the Rover relative positions with the accuracy of about 1 m (Tong et al., 2014). This result indicates that VLBI phase-referencing method has a great potential of accurate deep spacecraft navigation, so more experiments are carried out.

Four CVN antennas joined the CE-5T1 phase-referencing experiment in 2014 and another Russian VLBI antenna – Badary (BD) joined the MEX observation in 2015. The nearby extragalactic radio sources were selected as the calibrators with the separation angle of ~ 2.5 degree for MEX, and ~ 1.2 degree for CE-5T1, respectively. After correlation, the visibility data was converted to FITS-IDI format for data calibration and imaging.

This paper shows the results of phase-referencing experiments of CE-3, MEX, and CE-5T1. MEX experiments also indicate that for accurate phase-referencing positioning, the predicted delay should be as accurate as possible both for quasar and the near-field target.

According to the VLBI imaging theory, the brightness distribution of target can be got by performing the Fourier transform of visibility data (Thompson et al., 2001):

$$A(l, m) \cdot I(l, m) = \iint V(u, v) e^{j2\pi(ul+vm)} du dv \quad (1)$$

However, the actual visibility data are discrete in the UV plane. After Fourier transform, the dirty image of a target is produced. From the dirty image, the target angle offset from the priori phase center will be determined.

AIPS and Difmap were used to do visibility calibration and imaging. The visibility data were loaded into AIPS for calibration, and then Difmap was used for probe imaging.

2 CE-3 Relative positioning of Rover

After CE-3 probe soft-land on the east of Sinus Iridum area on Dec. 14, 2013, Lander and Rover signals were covered by all

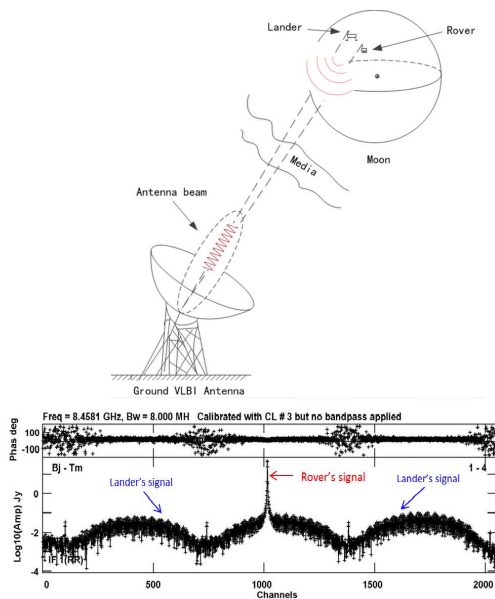


Fig. 1 In the same beam mode, CE-3 Lander and Rover signals were observed within the same IF.

CVN antennas beam. In such same beam condition, both signals were even in the same IF (Fig. 1). After Dec. 14, Lander released Rover. And then Rover moved around Lander for photograph one another at site A, B, C, D, E in a distance about 10 m through Dec. 15 to 21.

Raw data were sent to VLBI center through Internet. The software correlator and delay prediction software were used for correlation, and the visibility data were stored in FITS-IDI format. The phase-reference imaging method was used that choose Lander as calibrator and Rover as target to get the relative positions of Rover at site A, B, C, D, E (Tong et al., 2014).

3 MEX and CE-5T1 Observation

In 2010, EVN arranged a phase-referencing observation of MEX, and the got position accuracy better than 1 mas (Duev et al., 2012; Molera et al., 2010). In order to test CVN phase-referencing positioning ability, we arranged a ~ 8 h CVN phase-referencing experiment of CE-5T1 on December 23, 2014 and another ~ 1.5 h phase-referencing experiment of MEX using CVN and BD station, on January 5, 2015.

The nearby extragalactic radio sources, '2155-152' and '1920-211', were selected as the calibrator for MEX and CE-5T1 respectively, with about 0.8 Jy flux at X band, and 0.1 mas angle position error. MEX and CE-5T1 emit signals at the frequency of ~ 8.4 GHz (Fig. 2), and the signals were observed by two Digital Base Band Converter (DBBC) IFs with 4 MHz bandwidth. In this experiment, the distance from Earth to MEX and CE-5T1 was about 1.9895 AU and 400,000 km respectively.

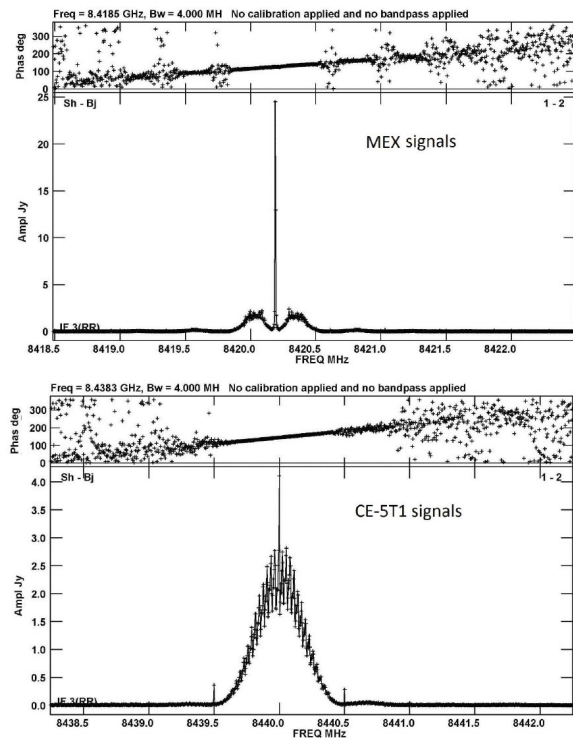


Fig. 2 Telemetry signal of MEX and digital signal of CE-5T1

The mean angle position of MEX and CE5-T1 was about 21h58m06s at right ascension and $-15d01m09s$ at declination, and about 19h28m18s at right ascension and $-21h00m03s$ at declination, respectively. The fast-switch observation mode was adopted for the phase-referencing experiment with the switching cycle time 170 s for MEX, and 138 s for CE-5T1.

4 Results and Analysis

Figure 3 and Tab. 1 showed the cleaned image of CE-3 Lander and Rover phase-referencing results. The relative position accuracy between Lander and Rover is about 0.5 mas. This accuracy keep consistent with the visual results obtained by the stereo camera installed on lander and Rover, and the visual results accuracy is about 4 % distance of Rover's each movement which is less than 10 m.

Figure 4 shows the dirty image of MEX and CE-5T1. The MEX angle offset is about 40 mas. MEX accurate orbit provided by ESA with accuracy better than 100 m. Considering the 1.9895 AU distance from Earth to MEX, the corresponding angle offset should be at a level of 0.07 mas. So, the 40 mas angle offset is much bigger than the real angle offset (0.07 mas) is. Compared with CE-5T1 orbit accuracy which was about tens of mas, the CE-5T1 angle offset was within the orbit accuracy.

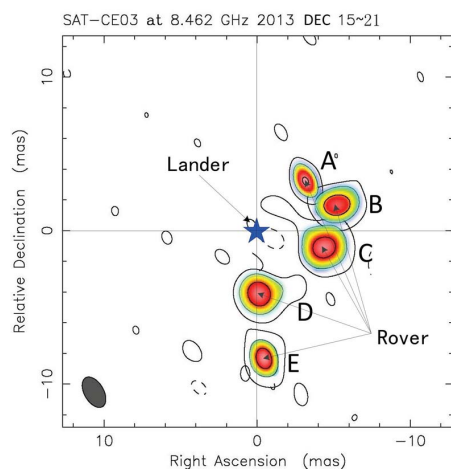


Fig. 3 Phase-referencing results of CE-3's Lander and Rover.

Table 1 In-beam phase-referencing position results vs. visual results, unit: meter.

Site	Visual results	Imaging results	Differences	
A	North	9.030	9.194	-0.164
	East	1.550	1.341	0.209
B	North	5.000	5.252	-0.252
	East	8.900	9.207	-0.307
C	North	-5.650	-5.245	-0.405
	East	8.360	8.812	-0.452
D	North	-9.750	-9.728	-0.022
	East	0.270	0.599	-0.329
E	North	-19.770	-19.533	-0.237
	East	-0.200	-0.159	-0.041

According to the relationship between angle error and time delay (Pradel et al., 2006), 40 mas angle error equals to about 1.9 ns at baseline length 3000 km. The comparison between CVN software correlator far-field target delay with that of Vienna VLBI Software (VieVS) indicates that the difference is at a level of a few picoseconds. However, the CVN software correlator near-field target delay calculation precision is known at a level of nanoseconds. It should be the accuracy of near-field delay prediction error caused the MEX obvious angle deviation. To improve MEX positioning accuracy, the more accurate near-filed delay prediction model is necessary.

5 Conclusions

We have performed several phase-referencing experiments of CE-3, MEX, and CE-5T1. The in-beam phase-referencing conditions have removed almost all common errors, so the relative position of CE-3 Rover is achieved with an accuracy of 0.5 mas. However, due to the accuracy limitation of the existing near-

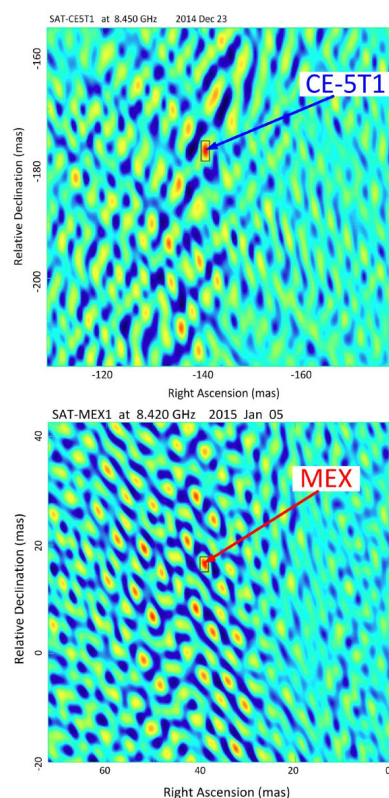


Fig. 4 Dirty image of CE-5T1 and MEX.

field target delay prediction software, the non-in-beam phase-referencing results (MEX, CE-5T1) have systematic deviations even up to tens of mas. The work to improve the accuracy of near-field delay software is in progress. The experiments also show that the accuracy of delay prediction is very important for phase-referencing positioning. The higher accuracy delay is, the higher position accuracy is.

Acknowledgements

We would like to express our sincere gratitude to Dr. Sergei Pogrebenko of Joint Institute for VLBI in Europe (JIVE) for MEX observation coordination and position result comparison.

References

- Duev D A, Molera Calvés G M, Pogrebenko S V, Gurvits L I, Cimo G, Bocanegra Bahamon T (2012) Spacecraft VLBI and Doppler tracking: Algorithms and implementation. *Astron Astrophys*, 541, 849–858.

- Huang Y, Chang S Q, Li P J, Hu X, Wang G, Liu Q, Zheng W, Fan M (2014) Orbit determination of Chang'E-3 and positioning of the lander and the rover. *Chinese Sci Bull*, 59, 3858–3867.
- Molera Calvés G, Pogrebenko S V, Wagner J, Cimo G, Gurvits L I, Duev D (2010) Tracking of Venus Express and Mars Express spacecraft with VLBI radio telescopes. *AGU Fall Meeting 2010*, abstract #P51D-1479.
- Pradel N, Charlot P, Lestrade J F (2006) Astrometric accuracy of phase-referenced observations with the VLBA and EVN. *Astron Astrophys*, 452, 1099–1106.
- Thompson A R, Moran J M, Swenson J W (2001) *Interferometry and Synthesis in Radio Astronomy*. Wiley-Interscience
- Tong F X, Zheng W M, Shu F C (2014) Accurate relative positioning of Yutu lunar rover using VLBI phase-referencing mapping technology (in Chinese). *Chinese Sci Bull* (Chinese Version), 59, 3362–3369.
- Zheng W M, Zhang J, Yu Y, Wang W, Li T (2014) Software correlator in the Chang'E-3 mission. In: D. Behrend, K. D. Baver, K. L. Armstrong (eds.), *IVS 2014 General Meeting Proc.*, Science Press (Beijing), 188–190.
- Zheng W M, Huang Y, Chen Z, Wang G L, Liu Q, Tong F, Li P, Tong L, Shu F (2014) Real-time and high accuracy VLBI in CE-3 mission. In: D. Behrend, K. D. Baver, K. L. Armstrong (eds.), *IVS 2014 General Meeting Proc.*, Science Press (Beijing), 466–472.

A Celestial Reference Frame at 22 GHz (K-band)

A. de Witt, A. Bertarini, C. S. Jacobs, J. Quick, S. Horiuchi, J. E. J. Lovell, J. M. McCallum, T. Jung, G. Bourda, P. Charlot

Abstract Relative to observations at the standard S/X (2.3/8.4 GHz) observing bands, at higher radio frequencies, sources that make up the International Celestial Reference Frame (ICRF) are expected to exhibit more compact source morphology and the effect of core-shift is expected to be smaller. This reduction in astrophysical systematics should allow for a more well-defined and stable reference frame at higher frequencies, and also be advantageous in tying the VLBI reference frame to future optical reference frames such as Gaia. The current K-band reference frame consists of only 279 sources with weak coverage in the Southern Hemisphere and several localised regions with no sources, especially near the ecliptic and galactic planes. We present an overview of our plans to improve the accuracy and coverage of the K-band celestial reference frame and present ongoing results from our observational efforts. Specifically, dedicated high-resolution imaging and astrometric observations are currently underway to complete sky coverage in the south using South Africa to Australia baselines and to improve the K-band celestial reference frame in the North using the VLBA to densify the

spatial coverage of sources. Our goal is to achieve a frame of at least 500 sources.

Keywords Celestial Reference Frame, VLBI, astrometry, K-band

1 Introduction

High precision Very Long Baseline Interferometric (VLBI) measurements of positions of extragalactic radio sources define and maintain the current International Celestial Reference Frame (ICRF-2, Ma et al., 2009), which forms the underlying basis for positional astronomy. The ICRF-2 is based on dual frequency S-band (2.3 GHz) and X-band (8.4 GHz) VLBI observations of 3414 extragalactic radio reference sources. Catalogs of positions of extragalactic radio reference sources with the highest precision, such as the ICRF, are needed for many applications. Among these are imaging of faint radio sources in phase-referencing mode, accurate differential astrometry, spacecraft tracking, space navigation and space geodesy. Extragalactic radio sources that are relatively bright at the frequency of observation, compact or core-dominated on VLBI scales, with no or little detectable motion and which have accurately known positions, stable at the sub-milliarsecond level, are well suited for high-accuracy reference frame work. Quasars being at great distances do not exhibit any measurable proper motion or parallax, making them ideal reference sources.

Unfortunately, at the standard S/X frequencies, many ICRF sources exhibit spatially extended intrinsic structures that may vary with time, frequency and baseline projection. Such structure can introduce significant errors in the VLBI measurements thereby degrading the accuracy of the estimated source positions (Charlot, 1990). Extended source structures, if not corrected for, will limit the ability to further improve the accuracy of individual VLBI source positions and thus the improved stability of future celestial reference frames. However, mapping the structures on a regular (approximately monthly) basis for 100s of sources has proven to be too resource intensive to be a sustained solution.

Aletha de Witt, Jonathan Quick
Hartebeesthoek Radio Astronomy Observatory, PO Box 443
Krugersdorp, 1740, South Africa
Alessandra Bertarini
Max-Planck-Institut für Radioastronomie, Auf dem Hugel 69,
Bonn, Germany
Christopher Jacobs
Jet Propulsion Laboratory, California Institute of Technol-
ogy/NASA, Pasadena, CA, U.S.A.
Shinji Horiuchi
C.S.I.R.O./Canberra Deep Space Communications Complex,
Australia
Jim Lovell, Jamie McCallum
University of Tasmania, Sandy Bay Campus, Maths-Physics
Building, Private Bag 86, HOBART TAS 7001, Tasmania
Taehyun Jung
Korea Astronomy and Space Science Institute, Daejeon, Repub-
lic of Korea
Geraldine Bourda, Patrick Charlot
University of Bordeaux, LAB, UMR 5804, F-33270, Floirac,
France

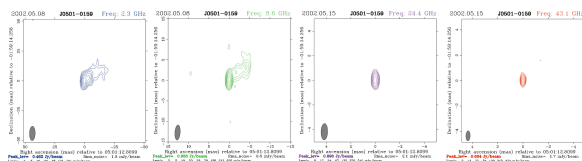


Fig. 1 Source structure versus frequency. VLBI images of the source J0501-0159 at S-band (2.3 GHz), X-band (8.4 GHz), K-band (24.4 GHz) and Q-band (43.2 GHz). The structure of quasars can vary dramatically with frequency, with sources generally appearing more compact at higher radio frequencies on VLBI scales. Image credit: Alexandr Pushkarev, Charlot et al. (2010).

It may, however, be possible to reduce source structure effects by transitioning to higher frequency VLBI observations of the radio celestial reference frames. On VLBI scales sources generally appear more compact at higher radio frequencies (e.g., Bietenholz, Bartel and Rupen, 2004; Charlot et al., 2010, see Fig. 1). Very long baseline observations of extragalactic radio sources have also shown that the location of the peak brightness point often varies with observing frequency due to opacity effects, a phenomenon sometimes called “core-shift”. In particular, VLBI images of Active Galactic Nuclei (AGN) show that the observed position of the peak brightness point moves closer to the central black hole as the frequency increases (e.g., Sokolovsky et al., 2011). The topic of core shifts in AGN is of growing interest and more accurate models of the shift of the peak brightness point with observing frequency will be very useful to match the radio positions of reference sources, that currently define the ICRF, to future optical catalogues such as Gaia (Kovalev et al., 2008).

In 2012, the need for the ICRF-2 to have a more uniform spatial coverage of sources and uniform accuracy in source coordinates led to the formation of an International Astronomical Union (IAU) working group, with the goal of the realisation of the next generation celestial reference frame (ICRF-3). A review of the needs for a next generation celestial reference frame motivated for the creation of celestial reference frames at higher radio frequencies such as K-band (22-24 GHz) and Ka-band (32 GHz), where sources tend to become more core dominated and the effects of core-shift is reduced. The goals of the ICRF-3 working group is to improve the precision as well as the spatial and frequency coverages relative to the ICRF-2 by 2018, in time for comparisons and alignment with the Gaia optical frame (Jacobs et al., 2014a).

In this paper, we present an overview of our plans to improve the accuracy and coverage of the K-band celestial reference frame and present ongoing results from our observational efforts.

2 Celestial Reference Frames at High Radio Frequencies

At present there are far fewer observations of reference sources at high radio frequencies compared to the standard S/X observing bands. One of the major challenges of observing at higher radio frequencies is the decrease in system sensitivity. At higher radio frequencies the sources themselves are in general weaker and many sources are resolved, antenna performance (e.g. antenna pointing) become degraded, system temperatures are higher and more susceptible to degradation from bad weather, and coherence times are shorter. Fortunately the rapidly decreasing costs of recording higher data rates allows us to compensate for sensitivity issues that result from observing at higher radio frequencies. In the last few years considerable work has been done and significant progress made on defining reference frames at higher radio frequencies.

Astrometric VLBI observations at Ka-band, a combined project of NASA’s Deep Space Network and ESA, have already developed a catalogue of ~631 observable sources (134 south of -45° declination) with highly accurate positions for improved deep-space navigation (Jacobs et al., 2014b), showing that there are sufficient strong sources suitable for astrometric use at higher frequencies. However, all the data from the Ka-band effort is from single baseline passes only and thus no source images could be made.

Ka-band receivers are typically only available at tracking stations which are very few in number. The advantage of observing at K-band is that many radio observatories typically have K-band receivers, allowing for simultaneous astrometric and imaging observations. For VLBI observations at K-band, calibrator sources are also needed in particular for trigonometric parallaxes and proper motions of H_2O (22 GHz) masers (e.g., Reid et al., 2014), as well as phase-referenced observations to image and study the sub-milliarcsecond structure of the most compact regions of emission in AGN. There is also a growing interest in studying AGN across a wide range of frequency, for example studies to measure the core shift of AGN as a function of frequency, as mentioned previously, and to study correlations of K-band light curves with FERMI gamma-ray light curves in order to shed light on the origin of high energy emissions in AGN.

Astrometric and imaging observations by Lanyi et al. (2010) and Charlot et al. (2010) provided a foundation for the development of a reference frame at K-band. However, the current catalogue consists of only 279 sources with weak coverage in the Southern Hemisphere, several localised regions with no sources, especially near the ecliptic and galactic plane and uncertainties in source positions at the ~ 100 micro-arcsecond level (see Fig. 2). Additional observations to improve the precision and spatial coverage of the K-band celestial reference frame is thus needed. Dedicated astrometric and imaging observations to improve the K-band celestial reference frame are currently underway (e.g. de Witt et al., 2014a,b) and recent results are discussed in § 3 and 4.

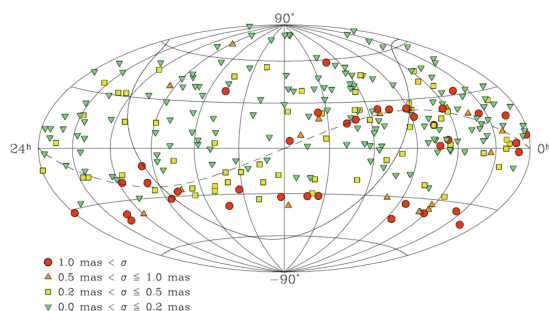


Fig. 2 The distribution of CRF sources at 24 GHz from ten, 24 observing sessions with the VLBA (Lanyi et al., 2010). The catalogue consists of 274 sources. The measured median formal uncertainties of right ascension (α) and declination (δ) are 0.08 and 0.15 milliarcseconds, respectively. The uncertainties of $\alpha \cos \delta$ are about a factor of 2 smaller than that in δ .

3 Towards a Full Sky Celestial Reference Frame at K-band

We have formed a collaboration with the goal of completing sky coverage of the K-band celestial reference frame in the south and to improve the precision and spatial coverage of the K-band celestial reference frame in the north. Dedicated observations to image the structure of potential reference source at K-band and astrometric observations to improve the precision of the K-band celestial reference frame are currently underway. Below is a summary of our K-band observations that have been completed or approved to date;

1. **Astrometric Test Observations in the South:** Our first astrometric test observations ran for four hours on 23 August 2013, using the HartRAO 26m, Hobart 26m and the Tamna 21m antennas. We observed 20 source south of -20° declination and we found fringes to all stations. The flux cut-off was set to be 500 mJy. For more details see de Witt et al. (2014a).
2. **Astrometric Trial Observations in the South:** Given our successful test observations we proceeded with a similar 24-hour experiment that started on 21 December 2013, in which we observed 106 sources south of -20° declination. These observations also included the Tidbinbilla 70m antenna. We demonstrated that data taken with the the Tamna digital backend and the Tidbinbilla Deep Space Station VLBI Processor (DVP) backend system can be successfully correlated with DiFX (Deller et al., 2007). For more details see de Witt et al. (2014b). We observed the same 106 sources during another similar 24-hour experiment, that started on 04 May 2014, in which we successfully tested the newly installed cryogenically cooled K-band receiver on the HartRAO 26m antenna, that replaced the experimental ambient receiver. The astrometric data analysis is in progress. Further Improvements in instrumental calibration on the HartRAO 26m antenna also provides hope that significant progress in the Southern Hemisphere is achievable in the next one or two years.

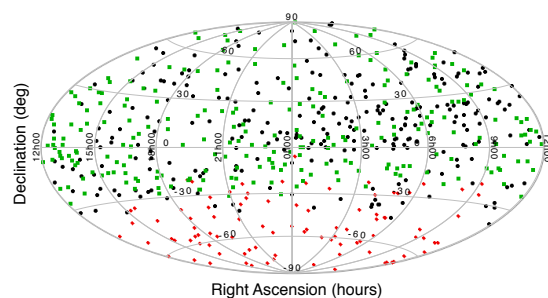


Fig. 3 The 279 sources from Lanyi et al. (2010) and Charlot et al. (2010) are shown in black. The 106 sources from the southern astrometric observations are shown in red. The 246 sources to be observed using the VLBA are shown in green.

3. **Imaging Observations in the South:** A proposal to image the source structure of potential southern K-band reference sources using the Long Baseline Array (LBA) was approved (proposal code v521a). Observations ran for 21 hours on 22 September 2014. The details of the observations and data reduction are discussed in § 4 and preliminary imaging results are shown. A proposal for additional imaging observations was submitted (proposal code v521b), and 12 hours on the LBA have been approved. These observations are scheduled for 25 September 2015.
4. **Astrometric and Imaging Observations in the North:** The Very Long Baseline Array (VLBA) approved four, twenty-four hour session for astrometric and imaging observations to improve the K-band celestial reference frame in the north (proposal code VLBA/15A-187). We will observe 246 sources north of about -30° declination. The source list is based on the X/Ka catalogue and the flux cut-off is set to be 100 mJy.

In Fig. 3 we show the sky distribution of the 106 sources from our astrometric observations in the south as well as the 246 sources that we will observe in the 4 astrometric and imaging sessions using the VLBA in the north. We also show the sky distribution of the 279 sources from the original Lanyi et al. (2010) and Charlot et al. (2010), K-band catalogue.

4 K-band Imaging Observations in the South: Data Reduction and Preliminary Results

We observed 32 potential K-band reference sources on 22 September 2014, using six of the LBA antennas; ATCA, Mopra, Parkes, Hobart, Ceduna and HartRAO. We observed at a frequency of 22.3 GHz with a total bandwidth of 32 MHz per polarization in two intermediate frequencies. The data were recorded in both senses of circular polarization (RCP and LCP). The 32 target sources were observed in 5 minute scans, and we obtained between 3 and 6 scans per source. The correlator

integration time was 2 seconds and the data was correlated at the Curtin University of Technology using the DiFX software correlator.

The data reduction was carried out with the NRAOs Astronomical Image Processing System (AIPS) software suite of programs. The amplitude gains were calculated from the system temperature and gain curve information contained in the tables generated during observations. Data inspection, editing and fringe fitting were done in the standard manner. The visibility data for each source were Fourier inverted and deconvolved

using the CLEAN algorithm, and amplitude gains were further refined by self-calibration using CLEAN models. For the final CLEAN images we used a weighting function of the visibilities in between uniform and natural weighting and using the square root of the statistical visibility weights. In Fig. 4 we show preliminary imaging results for the sources J1427-4206 and J1829-5813.

5 Summary and Goals

Extragalactic radio sources generally exhibit more compact source morphology and reduced core-shift at higher radio frequencies. Therefore, astrometric VLBI observations at K-band will allow for a more accurate and stable reference frame to be constructed. For this reason, we initiated an observational program to densify the K-band celestial reference frame at K-band.

Our goal is the realisation of a full-sky, K-band celestial reference frame by 2018, in time for the Gaia optical reference frame. In order to achieve this goal we need to obtain comparable density and accuracy in the south to that obtained from the astrometry that was done with the VLBA in the north. In addition we need to improve the accuracy and coverage of the K-band celestial reference frame in the north using the VLBA. Our ultimate goal is to achieve a frame of at least 500 sources and to reach accuracies better than $70 \mu\text{as}$ to match the Gaia predicted accuracy for $V=18$ visual magnitude quasars.

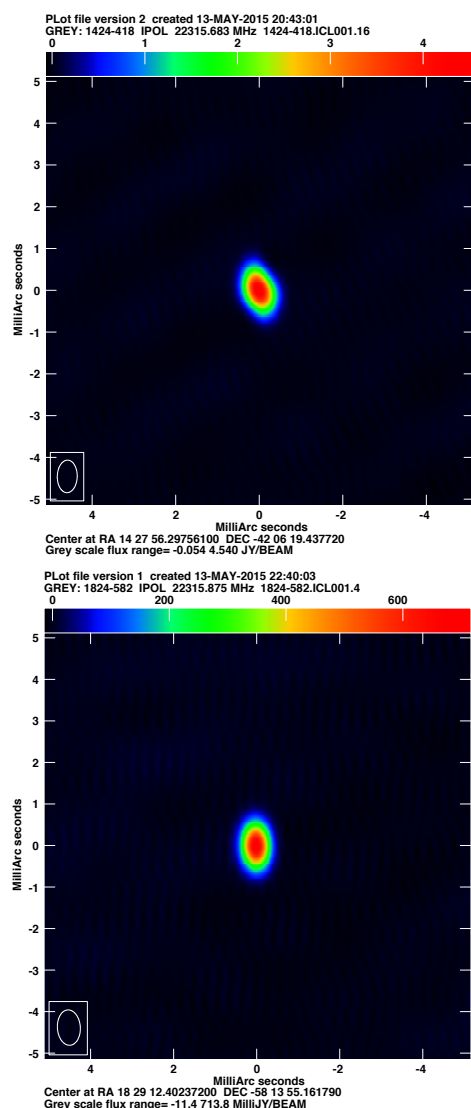


Fig. 4 Top: A map of the source J1427-4206. The peak flux density is 5.59 Jy and the rms noise is 17.8 mJy/beam. Bottom: A map of the source J1829-5813. The peak flux density is 0.69 Jy and the rms noise is 3.08 mJy/beam. North is up and East is to the left.

References

- Bietenholz M F, Bartel N, Rupen M P (2004) The location of the core in M81. *Astrophys J*, 615, 173.
- Charlot P (1990) Radio-source structure in astrometric and geodetic very long baseline interferometry. *Astron J*, 99, 1309.
- Charlot P, Boboltz D A, Fey A L, Fomalont E B, Geldzahler B J, Gordon D, Jacobs C S, Lanyi G E, Ma C, Naudet C J, Romney J D, Sovers O J, Zhang L D (2010) The celestial reference frame at 24 and 43 GHz. II. Imaging. *Astron J*, 139, 1713.
- Deller A T, Tingay S J, Bailes M, West C (2007) DiFX: A Software Correlator for Very Long Baseline Interferometry Using Multiprocessor Computing Environments. *Publ Astron Soc Pac*, 119, 318.
- de Witt A, Bertarini A, Horiuchi S, Jacobs C, Jung T, Lovell J, McCallum J, Quick J, Sohn B W, Ojha R (2014a) Extending the K-band celestial frame emphasizing Southern hemisphere, In: N. Capitaine (ed.) *Proc. Journées 2013, Systèmes de référence spatio-temporels*, 61–64, www.syrte.obspm.fr/journées2013/pdf/deWitt.pdf.
- de Witt A, Bertarini A, Horiuchi S, Jacobs C, Jung T, Lovell J, McCallum J, Quick J, Sohn B W, Phillips C, Ojha R (2014b) Completing the K-band Celestial Reference Frame

- in the Southern Hemisphere. In: D. Behrend, K. D. Baver, K. L. Armstrong (eds.), *IVS 2014 General Meeting Proc.*, Science Press (Beijing), 433–437, <http://ivs.nict.go.jp/mirror/publications/gm2014/>.
- Jacobs C S, Arias F, Boboltz D, Böhm J, Bolotin S, Bourda G, Charlot P, de Witt A, Fey A, Gaume R, Gordon D, Heinkelmann R, Lambert S, Ma C, Malkin Z, Nothnagel A, Seitz M, Skurikhina E, Souchay J, Titov O (2014a) ICRF-3: Roadmap to the next generation ICRF. In: N. Capitaine (ed.) *Proc. Journées 2013, Systèmes de référence spatio-temporels*, 51–56, www.syrte.obspm.fr/journees2013/pdf/Jacobs.pdf.
- Jacobs C S, Clark J E, Garcí-Miró C, Goodhart C E, Horiuchi S, Madde R, Mercolino M, Naudet C J, Snedeker L G, Sotuela I, White L A (2014b) The X/Ka Celestial Reference Frame: Results from combined NASA-ESA baselines including Malargüe, Argentina. Abstract submitted to: *8th IVS General Meeting*, www.adsabs.harvard.edu/abs/2014ivs.confE...2J.
- Kovalev Y Y, Lobanov A P, Pushkarev A B, Zensus J A (2008) Opacity in compact extragalactic radio sources and its effect on astrophysical and astrometric studies. *Astron Astrophys*, 483, 759.
- Lanyi G E, Boboltz D A, Charlot P, Fey A L, Fomalont E B, Geldzahler B J, Gordon D, Jacobs C S, Ma C, Naudet C J (2010) The celestial reference frame at 24 and 43 GHz. I. Astrometry. *Astron J*, 139, 1695.
- Ma C, Arias E, Bianco G, Boboltz D, Bolotin S, Charlot P, Fey A, Gaume R, Gontier A, Heinkelmann R, Jacobs C, Kurdubov S, Lambert S, Malkin Z, Nothnagel A, Petrov L, Skurikhina E, Sokolova J, Souchay J, Titov O, Zharov V (2009) The Second Realization of the International Celestial Reference Frame by Very Long Baseline Interferometry. In: A. Fey, D. Gordon, C. S. Jacobs (eds.), *IERS Technical Note, No. 35*, IERS, BKG, Frankfurt am Main, Germany, www.iers.org/documents/publications/tn/tn35/tn35.pdf.
- Reid M J, Menten K M, Brunthaler A, Zheng X W, Dame T M, Xu Y, Wu Y, Zhang B, Sanna A, Sato M, Hachisuka K, Choi Y K, Immer K, Moscadelli L, Rygl K L J, Bartkiewicz A (2014) Trigonometric Parallaxes of High Mass Star Forming Regions: The Structure and Kinematics of the Milky Way. *Astron Astrophys*, 783, 130.
- Sokolovsky K V, Kovalev Y Y, Pushkarev A B, Lobanov A P (2011) A VLBA survey of the core shift effect in AGN jets. I. Evidence of dominating synchrotron opacity. *Astron Astrophys*, 532, A38.

Observing Gaia transfer sources in R&D and RDV sessions

K. Le Bail, D. Gordon, J. M. Gipson, D. S. MacMillan

Abstract The ESA mission Gaia was successfully launched on December 19, 2013. Over its five year mission, it is expected to observe and map billion of objects, including 500 000 quasars. The Laboratory of Astrophysics of Bordeaux (LAB) identified 195 sources to link the Gaia-optical frame and the VLBI radio frame. They submitted a proposal that was approved in 2012 to include these sources in the IVS monitoring program and observe them regularly. Of the 195 sources, sixty-six were not sufficiently observed and forty were not part of the IVS monitoring program. We included the sources in the IVS monitoring program in two steps. First, we modified the observation target of all the sources to twelve successful sessions per year. Second, as the forty sources not initially in the IVS monitoring program were mostly weak, we specifically scheduled them in R&D and RDV sessions. We are now able to see significant improvements in position uncertainties from the beginning of this effort in 2013 and we have better flux values of the 195 transfer sources. We were also able to identify a set of sources too weak to be observed in regular IVS sessions. This paper explains the observing strategy developed, shows the significant improvements resulting from our observing, and discusses the next steps, taking into account the updates of the Gaia mission.

Keywords ICRF2 Gaia transfer sources

1 The set of 195 potential Gaia transfer sources identified by the Laboratory of Astrophysics of Bordeaux

In 2012, the Laboratory of Astrophysics of Bordeaux (LAB) submitted a proposal to the IVS to observe 195 ICRF2 transfer sources in the context of the Gaia mission. These 195 sources were selected within the ICRF2 catalog for their optical magnitude and astrometric suitability (Bourda et al., 2008; Charlot

Karine Le Bail, David Gordon, John M. Gipson and Daniel S. MacMillan
NVI, Inc., Greenbelt, MD 20771, United States of America

et al., 2013). Based on the GSFC catalog 2012a and the list of sources of the IVS monitoring program provided at the time of the proposal, these 195 sources were divided into four different categories:

- Category 1 (89 sources): sources in the IVS monitoring program and sufficiently observed.
- Category 2 (66 sources): sources in the IVS monitoring program but not sufficiently observed.
- Category 3 (16 sources): sources not in the IVS monitoring program and with good position accuracy (< 200 microarcseconds).
- Category 4 (24 sources): sources not in the IVS monitoring program and with poor position accuracy.

The initial request of the LAB was to observe the Gaia transfer sources at least once a month to obtain an observation frequency comparable to the Gaia catalog. We set the target for all 195 sources to twelve successful sessions per year.

The 24 category 4 sources have been observed in dedicated R&D and RDV sessions to improve their position accuracy. The RDVs use the VLBA combined with non-VLBA geodetic stations. In August 2014, the set of Gaia transfer sources scheduled specifically in R&D and RDV sessions was increased to 33. 1) One source in category 1 and four sources in category 2 had not been observed in the preceding twelve months. They were included in the list to determine if they could be detected in the usual R&D and RDV station network so that their fluxes and positions could be updated. 2) Four sources in category 3 had large position uncertainties. They were included in the set to improve their uncertainties.

2 Scheduling in R&D and RDV sessions

The observing schedules were made using the software *sked*.

For the R&D sessions, the recording mode is 512 Mbps except for RD1307 and RD1308 which used a 256 Mbps recording mode. The source flux values are either from 1) the current *sked* flux catalog, 2) the BVID catalog, or 3) a composite catalog taking into account the two catalogs in 1) and 2) and the detection rate of the sources in previous R&D sessions.

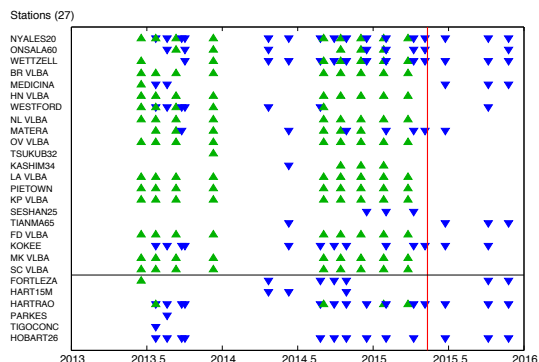


Fig. 1 R&D sessions dedicated to the observation of 33 specific Gaia transfer sources (blue triangles) and RDV sessions including the observation of these 33 sources (green triangles). The red line indicates the sessions planned from now until the end of 2015.

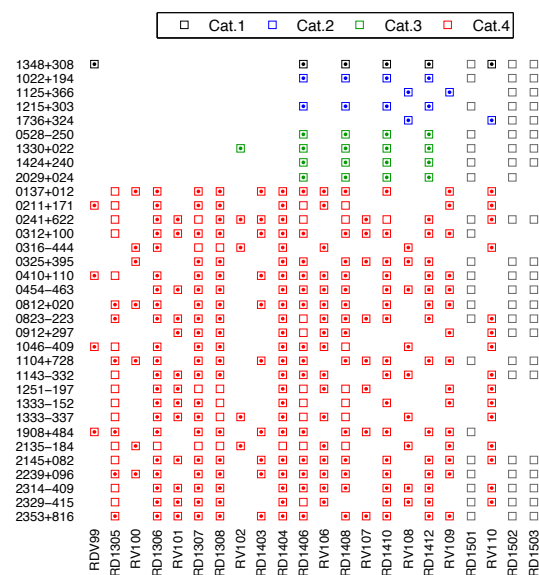


Fig. 2 The 33 Gaia transfer sources specifically scheduled in some R&D and RDV sessions. The squares mean that the source was scheduled and the dotted squares mean that the source observations were good enough to be used in a VLBI data solution.

The RDV sessions were recorded at 256 Mbps. Scheduling was done using a combination of auto-scheduling for most sources and manual scheduling for the Gaia transfer sources.

Figure 1 shows that most of the stations are in the Northern hemisphere. The antenna diameters are on average 25 meters, except for two stations: Parkes (64 meters) and Tianma65 (65 meters) that were each used only once (in RD1306 and RD1404). In Figure 2, we can see that these two sessions were the most successful: 21 out of 22 sources were successfully observed in RD1306 and 23 out of 24 sources in RD1404.

3 Source observation frequency and position accuracy

Figure 3 illustrates the number of successful sessions over the past year for each of the 195 Gaia transfer sources from January 1st, 2011 to May 1st, 2015. For example, when looking at category 4 sources, we can see in October 2013 that thirteen sources were observed in four to six sessions in the previous year (October 2012 to October 2013), and eleven sources were observed in one to three sessions in the previous year.

These plots show the improvement in the number of successful sessions in which the Gaia transfer sources were observed since 2011. Since October 2013, the number of successful sessions have increased, especially for categories 2, 3 and 4. The target of 12 successful sessions per year is reached for a third of the category 2 sources and a quarter for the category 3 sources. The category 4 sources are now observed in an average of seven successful sessions per year.

All sources in categories 1, 2 and 3 have position uncertainties less than 100 microarcseconds, except 0454+844 (cat. 1), 2353-686 and 0522-611 (cat.2). (See Figure 4.) These three sources are either far North or far South. They are not weak sources but they have not been observed much in the past year. They will be added to the list of sources to be observed in the next R&D and RDV sessions. For the sources in category 4, 9 sources (out of 24) have position uncertainties smaller than 100 microarcseconds, 11 sources between 100 and 200 microarcseconds, 2 sources between 200 and 300 microarcseconds, and two sources (0316-444 and 2135-184) still have poor position accuracy, greater than 300 microarcseconds.

4 Discussion: the importance of having more stations with large dishes

In Figure 2, we showed that RD1404 is one of the most successful R&D sessions dedicated to the observation of 33 of the Gaia transfer sources. RD1404 network contains Tianma65 (T6). A solution was made with and without the Tianma65 baselines in the solution. Table 1 is an accounting of the differences in the number of observations of each of the category 4 sources. Flux values from the *sked* catalog are indicated in the fourth and fifth columns. These sources are mostly weak sources with flux lower than 0.10 Jy. Most of these sources got significantly more observations using Tianma65, and quite a few would not have enough observations to be useful without Tianma65.

Figure 5 illustrates which sources can be detected depending on the baseline observing them. In our case, with the mode we use in *sked* for the R&D sessions (SNR of 20 in X-band, 15 in S-band), the baseline T6-Ny can observe sources with a flux of 0.05 Jy, while the baseline On-Ny can only observe sources with flux values larger than 0.10, and the baseline Ft-Ny can only observe sources with flux values larger than 0.30. The three baselines T6-Ny, On-Ny and Ft-Ny were chosen to illustrate the best

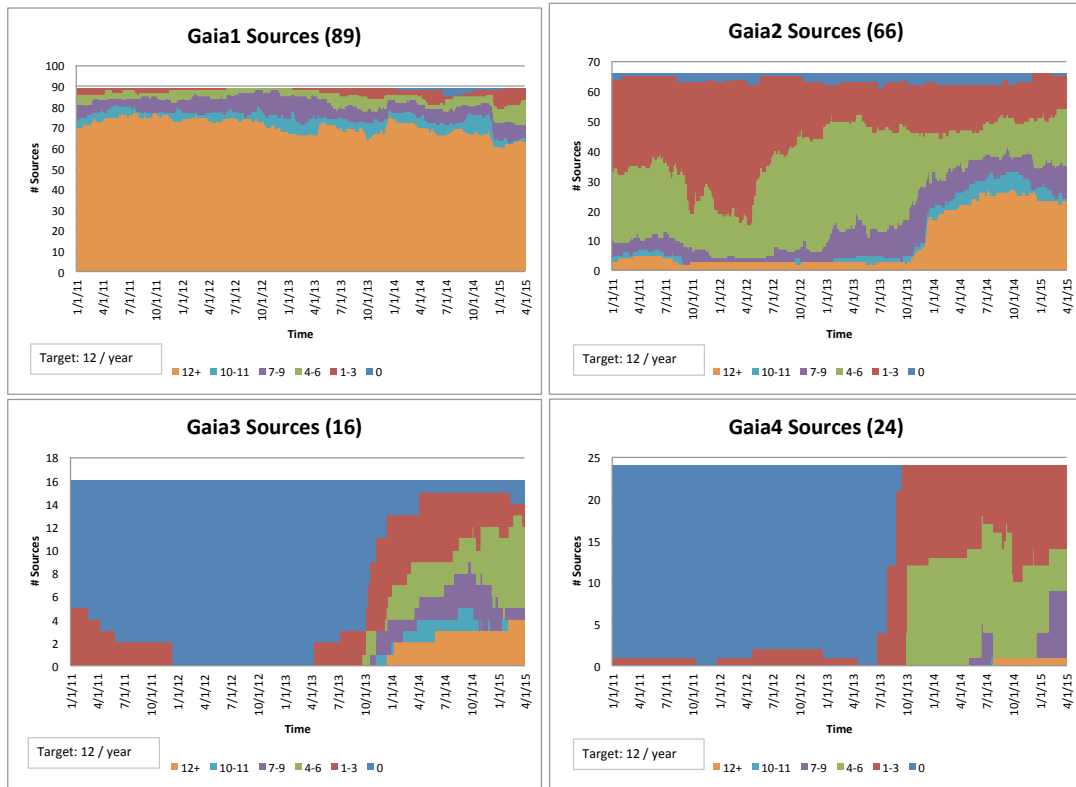


Fig. 3 Number of successful sessions in the past year for each of the 195 Gaia link sources in each category.

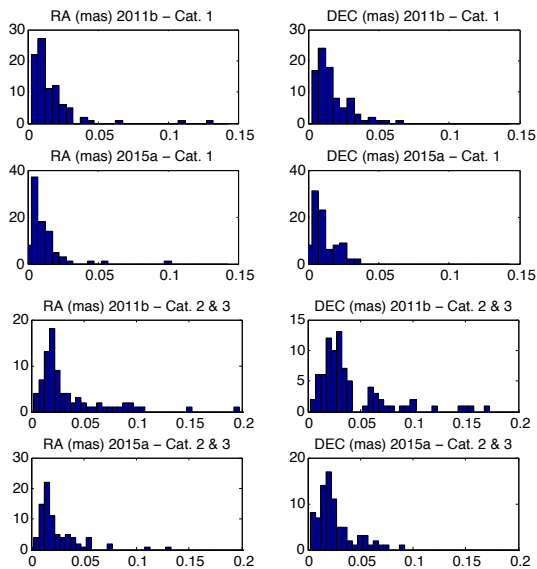


Fig. 4 Position accuracy comparison between GSFC solutions 2011b and 2015a for Gaia transfer sources in categories 1, 2 and 3.

case (using the large dish T6), the average case (On-Ny) and a baseline with less sensitivity (Ft-Ny).

Since 2013, the observation of the 195 Gaia transfer sources has improved significantly: more observations, better position uncertainties and a better knowledge of the flux of the sources. However, to be able to observe all of the 195 Gaia transfer sources at the same level, we need more stations with better SEFDs (larger dish and higher sensitivity), and we need more stations in the South.

Table 1 Number of successful observations of the 24 Gaia transfer sources in category 4 when using Tianma65 (T6) in the network or not. Flux values are indicated for reference.

Sources	Number of obs		Flux (Jy)	
	w/ T6	w/o T6	S-band	X-band
2135-184	0	0	0.03	0.10
0316-444	4	0	0.05	0.05
0211+171	10	3	0.06	0.06
1251-197	22	7	0.07	0.07
1333-152	28	9	0.07	0.10
0325+395	9	0	0.07	0.33
0912+297	43	22	0.08	0.07
0137+012	57	34	0.08	0.17
0312+100	74	57	0.09	0.10
1046-409	7	2	0.09	0.12
1333-337	20	6	0.09	0.17
1908+484	69	39	0.10	0.06
1143-332	15	5	0.13	0.16
2329-415	7	2	0.14	0.13
1104+728	84	56	0.16	0.12
0410+110	102	76	0.16	0.15
0812+020	99	68	0.20	0.13
2145+082	23	10	0.22	0.09
0241+622	20	18	0.24	0.52
2314-409	10	1	0.30	0.15
2239+096	59	45	0.33	0.23
0823-223	20	11	0.40	0.76
2353+816	106	89	0.49	0.36
0454-463	3	0	0.74	0.50
Average	37	23		

Charlot P, Bellanger A, Bouffet R, Bourda G, Collioud A, Baudry A (2014) Report for 2013 from the Bordeaux IVS Analysis Center. In: K. D. Baver, D. Behrend, K. L. Armstrong (eds.), *IVS 2013 Annual Report*, 253–256.

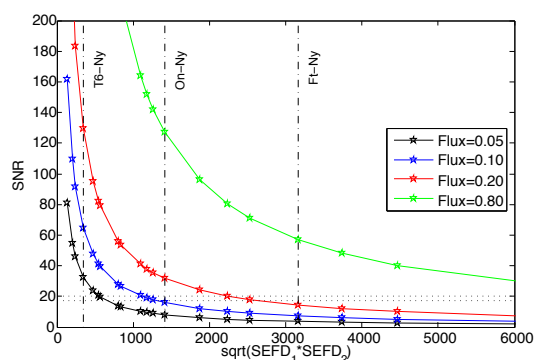


Fig. 5 SEFD vs. SNR. Four different cases are illustrated for sources with flux values of 0.05, 0.10, 0.20 and 0.80 Jy. Baselines T6-Ny, On-Ny and Ft-Ny are indicated as a reference.

References

Bourda G, Charlot P, Le Campion J F (2008) Astrometric suitability of optically-bright ICRF sources for the alignment with the future Gaia celestial reference frame. *Astron Astrophys*, 490, 403–408.

EVGA 2015 scientific programme

18 May 2015

09:00-09:15	Welcome	B. Pacheco and V. Fraga
Session-T1	Chair: Alessandra Bertarini	
09:15-09:30	VGOS Operational Readiness	B. Petrachenko
09:30-09:45	Broadband VLBI at 6 GHz to 14 GHz frequency between Kashima 34 m and Ishioka 13 m	K. Takefuji
09:45-10:00	Technological Developments for VGOS from IGN & Yebes Observatory	J. A. López Fernández
10:00-10:15	Results from the TWIN Commissioning Phase	T. Schüler
10:15-10:30	Toward VGOS with the AuScope array	J. McCallum
10:30-11:00	Coffee break	
Session-T2	Chair: José Antonio López Fernández	
11:00-11:15	The 13 m Yebes antenna. Telescope control, commissioning and tests	P. de Vicente
11:15-11:30	DBBC3L - A full compliant VGOS backend	G. Tuccari
11:30-11:45	Development of Multipurpose Digital Backend for "Quasar" network radio telescopes	E. Nosov
11:45-12:00	Results from the test realization of a system monitoring for seamless auxiliary data	A. Neidhardt
12:00-12:15	Expanding the Bonn Correlator for VGOS and summary of recent activities	W. Alef
12:15-12:30	IAA VGOS GPU-based software correlator: current status and broadband processing	V. Ken
12:30-14:00	Extended lunch and poster viewing	
Session-O1	Chair: Hayo Hase	
14:00-14:15	Status of the Spanish/Portuguese RAEGE project	F. Colomer
14:15-14:30	The southern hemisphere AUSTRAL program: A pathway to VGOS	J. Lovell
14:30-14:45	GSI's regional stations and AOV activities	R. Kawabata
14:45-15:00	First geodetic result of Ishioka VGOS Station in Japan	Y. Fukuzaki
15:00-15:15	On the role of Tianma radio telescope for improving celestial reference frames	F. Shu
15:15-15:45	Coffee break	
Session-O2	Chair: Rüdiger Haas	
15:45-16:00	Russian radio interferometer of new generation	Y. Bondarenko
16:00-16:15	Status report on observations with the GGAO-Westford VGOS systems	A. Niell

16:15-16:30	Contributions of HartRAO to Space Geodesy, Astrometry and related disciplines	L. Combrinck
16:30-16:45	Geodetic Italian VLBI: first tests	M. Stagni
16:45-17:00	An Observation and Analysis Scenario for VGOS in 2020	H. Hase
17:00-17:30	”Stretch your legs” break	
Session-O3	Chair: Yuri S. Bondarenko	
17:30-17:45	Practical Uses of VGOSDB format	J. Gipson
17:45-18:00	Scheduling VLBI observations to satellites with the Vienna VLBI Software (VieVS)	A. Hellerschmied
18:00-18:15	GLONASS-VLBI: Onsala-Wettzell test observations	R. Haas
18:15-18:30	Software Development for D-VLBI Scheduling and Analysis of Spacecraft Observations	J. M. Anderson

19 May 2015

08:45-09:30	Inauguration of the geodetic VLBI station in Zelenchukskaya (Russia)	
Session-A1	Chair: Thomas Hobiger	
09:30-09:45	GNSS zenith delays and gradients in the analysis of VLBI Intensive sessions	K. Teke
09:45-10:00	Observing GNSS L-band signals: ionospheric corrections by co-located GNSS measurements	B. Männel
10:00-10:15	VLBI-like GNSS delays in the analysis of CONT11	Y. Kwak
10:15-10:30	Influence of the horizontal resolution of numerical weather models on ray-traced delays for VLBI analysis	A. Hofmeister
10:30-10:45	Augmenting the stochastic model in VLBI data analysis by correlations from atmospheric turbulence models	S. Halsig
10:45-11:15	Coffee break	
Session-A2	Chair: Johannes Böhm	
11:15-11:30	Atmospheric refractivity gradients from VLBI compared to those from GNSS, DORIS, WVR, and NWM	R. Heinkelmann
11:30-11:45	Subdaily station motions from Kalman filtering VLBI data	B. Soja
11:45-12:00	Antenna axis offsets estimated in VLBI data analysis	T. Nilsson
12:00-12:15	Numerical issues of VLBI data analysis	T. Artz
12:15-12:30	Sophistication in UT1-Intensive Scheduling by Using Impact Factors - First Results of Field Tests	A. Nothnagel
12:30-12:45	The CONT campaigns as a precursor to VGOS observing	D. MacMillan
12:45-13:00	CONT14 as a testbed for the combination of VLBI and GPS data on the observation level	T. Hobiger

13:00-14:15	Extended lunch and poster viewing	
Session-A3	Chair: Géraldine Bourda	
14:15-14:30	Earth Orientation Parameters for VLBA Calibrator Survey Sessions	D. Mayer
14:30-14:45	Revisiting the VLBA Calibrator Surveys, VCS-II	D. Gordon
14:45-15:00	ICRF-3: Status, Plans, and Multi-wavelength Progress towards the next generation ICRF	C. Jacobs
15:00-15:15	Assessment of CRF Solutions from Session-wise Normal Equation Systems	A. Iddink
15:15-15:45	Coffee break	
Session-A4	Chair: Bill Petrachenko	
15:45-16:00	Studying impacts of strategy choices concerning the Celestial Reference Frame on the estimates of nutation time series during geodesic VLBI Analysis	C. Gattano
16:00-16:15	Reducing the impact of source structure on the celestial frame: modeling or mitigation strategies?	P. Charlot
16:15-16:30	On the estimation of a celestial reference frame in the presence of source structure	L. Plank
16:30-16:45	Imaging the IYA09 VLBI super-session	A. Collioud
16:45-17:15	"Stretch your legs" break	
Session-A5	Chair: P. Charlot	
17:15-17:30	Aligning VLBI and Gaia Extragalactic Celestial Reference Frames	G. Bourda
17:30-17:45	Estimating the velocity of the Solar barycenter from VLBI observations	M. Xu
17:45-18:00	The CVN Geodetic Observation and its Result	G. Wang
18:00-18:15	Preliminary results of pulsar astrometry with CVN	P. Jiang
18:15-18:30	Closing session	F. Abreu, R. Haas

EVGA 2015 poster contributions

Technology

P1-01	QRFH Wideband Cryogenic Receivers	R. Rayet
P1-02	Ultra Wide-Band HTS filter for new geodetic VLBI front-ends	A. Caddemi
P1-03	The new release of e-RemoteCtrl	A. Neidhardt
P1-04	The German Antarctic Receiving Station O'Higgins - upgrades of the VLBI-capabilities for future challenges	C. Plötz

Observations

P2-01	Hb-Ho: observations with the sibling telescopes in Hobart	L. Plank
P2-02	The Asia-Oceania VLBI Group for Geodesy and Astrometry	J. Lovell
P2-03	An experimental scanning of the Metsähovi radio telescope dish	U. Kallio
P2-04	The contribution of the Twin Telescopes at Onsala and Wettzell to the VGOS System	C. Schönberger
P2-05	Contributions of the Onsala Space Observatory to the GGOS	R. Haas
P2-06	Spacecraft VLBI Phase Referencing Tracking with the Chinese VLBI Network and Deep Space Network	H. Zhou
P2-07	Local Tie works in Yebes Observatory	B. Córdoba
P2-08	Coordinate Based Bundle Adjustment - Advanced Network Adjustment Model for Polar Measurement Systems	M. Lösler
P2-09	A GPS-based local-tie vector at the Onsala Space Observatory	T. Ning
P2-10	Determining HartRAO antenna reference point and axis offset parameters using VieVS	M. Nickola
P2-11	Continuous VLBI Scheduling: The CONT14 Example	D. Behrend
P2-12	Implementation of VGOSDB format	S. Bolotin
P2-13	Current status and future plans for the Vienna VLBI Software (VieVS)	A. Hellerschmied

Analysis

P3-01	Minimization of the UT1 Formal Error through Minimization Algorithms	J. Gipson
P3-02	Automated analysis of Kokee-Wettzell intensive sessions	N. Kareinen
P3-03	Applying Kalman filtering to investigate tropospheric effects in VLBI analysis	B. Soja
P3-04	Combining VLBI and GPS for inter-continental frequency transfer	T. Hobiger
P3-05	Atmospheric tidal effects in Earth rotation observed by VLBI	A. Girdiuk
P3-06	Baseline dependent weights in VieVS	M. Uunila
P3-07	Combination of common parameters for co-located VLBI antennas	T. Nilsson
P3-08	VLBI Analysis at BKG	V. Thorandt
P3-09	IVS Combination Center at BKG: Combination products and the IVS contribution to ITRF2014	L. Messerschmitt
P3-10	CONT14 analyzed by a Kalman filter: a test case	M. Karbon
P3-11	Comparison of VLBI and DORIS solutions in view of ITRF2014	V. Tornatore
P3-12	Status Report of VLBI Measuring System based on China Deep Space Network	K. Xu
P3-13	First determination of the locations of the Chinese Deep Space Stations – JIAMUS66 and KASHI35 using Geodetic VLBI	D. Xu
P3-14	dDOR Data Processing and Analysis in CE-3 Mission	D. Zhang
P3-15	A Celestial Reference Frame at 22 GHz (K-band)	A. de Witt

P3-16	CVN High Accuracy VLBI Phase-referencing Positioning experiment for Deep Space Probe	W. Zheng
P3-17	The X/Ka-band (8.4/32 GHz) Celestial Frame: Can it be more accurate than the ICRF2?	C. Jacobs
P3-18	Source structure influence on GeoVLBI observations	N. Zubko
P3-19	Observing Gaia transfer sources in R&D and RDV sessions	K. Le Bail

This page is intentionally left blank.

EVGA 2015 list of participants

Name	Affiliation and Email address
Alef, Walter	Max Planck Institute for Radio Astronomy, Germany walef@mpifr-bonn.mpg.de
Anderson, James M	Deutsches GeoForschungsZentrum GFZ, Germany anderson@gfz-potsdam.de
Antunes, Marlene	Direção Regional das Obras Públicas e Comunicações, Portugal, marlene.cs.antunes@azores.gov.pt
Artz, Thomas	University of Bonn, Germany artz@igg.uni-bonn.de
Behrend, Dirk	NVI, Inc./NASA GSFC U.S.A. dirk.behrend@nasa.gov
Bertarini, Alessandra	University of Bonn, Germany abertari@mpifr-bonn.mpg.de
Böhm, Johannes	Technische Universität Wien, Austria johannes.boehm@tuwien.ac.at
Bolaño Gonzalez, Ruben	Instituto Geografico Nacional / RAEGE Santa Maria, Portugal, ruben.b.gonzalez@azores.gov.pt
Bondarenko, Yuri	Institute of Applied Astronomy, Russia bondarenko@ipa.nw.ru
Bourda, Geraldine	Laboratoire d'Astrophysique de Bordeaux, France bourda@obs.u-bordeaux1.fr
Casotto, Stefano	University of Padua, Italy stefano.casotto@unipd.it
Charlot, Patrick	Laboratoire d'Astrophysique de Bordeaux, France charlot@obs.u-bordeaux1.fr
Cho, Jung-ho	Korea Astronomy & Space Science Institute, South Korea, jojh@kasi.re.kr
Collioud, Arnaud	Laboratoire d'Astrophysique de Bordeaux, France collioud@obs.u-bordeaux1.fr
Colomer, Francisco	Instituto Geografico Nacional, Spain f.colomer@oan.es
Combrinck, Ludwig	Hartebeesthoek Radio Astronomy Observatory, South Africa, ludwig@hartrao.ac.za
de Vicente, Pablo	Instituto Geográfico Nacional - Yebes, Spain p.devicente@oan.es
de Witt, Aletha	Hartebeesthoek Radio Astronomy Observatory, South Africa, alet@hartrao.ac.za
Engelhardt, Gerald	Federal Agency for Cartography and Geodesy, Germany, gerald.engelhardt@bkg.bund.de
Eschelbach, Cornelia	Frankfurt University of Applied Sciences, Germany cornelia.eschelbach@fb1.fra-uas.de
Fukuzaki, Yoshihiro	Geospatial Information Authority of Japan, Japan fukuzaki-y96pe@mlit.go.jp
García-Espada, Susana	Instituto Geografico Nacional / RAEGE Santa Maria, Portugal, susana.g.espada@azores.gov.pt
Gattano, César	Observatoire de Paris, SYRTE, France cesar.gattano@obspm.fr

Gaume, Ralph	U.S. National Science Foundation, U.S.A. rgaume@nsf.gov
Gipson, John	NASA GSFC/NVI, Inc, U.S.A. John.M.Gipson@nasa.gov
Gomez-Gonzalez, Jesus	Instituto Geografico Nacional, Spain jggonzalez@fomento.es
Gordon, David	NVI Inc./NASA GSFC, U.S.A. David.Gordon-1@nasa.gov
Haas, Rüdiger	Chalmers University of Technology, Sweden rudiger.haas@chalmers.se
Halsig, Sebastian	University of Bonn, Germany halsig@igg.uni-bonn.de
Hase, Hayo	Bundesamt für Kartographie und Geodäsie, Germany, hayo.hase@bkg.bund.de
Heinkelmann, Robert	GFZ Potsdam, Germany heinkelmann@gfz-potsdam.de
Hellerschmied, Andreas	Vienna University of Technology, Austria andreas.hellerschmied@geo.tuwien.ac.at
Hobiger, Thomas	Chalmers University of Technology, Sweden thomas.hobiger@chalmers.se
Hofmeister, Armin	Technische Universität Wien, Austria armin.hofmeister@tuwien.ac.at
Iddink, Andreas	University of Bonn, Germany aiddink@uni-bonn.de
Jacobs, Christopher	JPL, U.S.A. Christopher.S.Jacobs@jpl.nasa.gov
Kawabata, Ryoji	Geospatial Information Authority of Japan, Japan kawabata-r96aq@milit.go.jp
Ken, Voytsekh	IAA RAS Russia voitsekh@gmail.com
Kwak, Younghee	Vienna University of Technology, Austria younghee.kwak@tuwien.ac.at
Lanotte, Roberto	E-GEOS Centro di Geodesia Spaziale CGS/ASI Matera, Italy, roberto.lanotte@e-geos.it
Lopez Fernandez, José Antonio	Instituto Geográfico Nacional - Yebes, Spain jalfernandez@fomento.es
Lösler, Michael	Frankfurt University of Applied Sciences, Germany michael.loesler@fb1.fra-uas.de
Lovell, Jim	University of Tasmania, Australia Jim.Lovell@utas.edu.au
Ma, Chopo	NASA Goddard Space Flight Center, U.S.A. chopo.ma@nasa.gov
MacMillan, Daniel	NVI, Inc., U.S.A. daniel.s.macmillan@nasa.gov
Männel, Benjamin	ETH Zürich, Switzerland maennelb@ethz.ch
Mayer, David	Technische Universität Wien, Austria david.mayer@tuwien.ac.at
McCallum, Jamie	University of Tasmania, Australia jamie.mccallum@utas.edu.au

Messerschmitt, Linda	Federal Agency for Cartography and Geodesy, Germany, linda.messerschmitt@bkg.bund.de
Mestre, Rita	Volcanology and Geological Risk Assessment, Portugal, titamendo@gmail.com
Mey, Philip	Hartebeesthoek Radio Astronomy Observatory, South Africa, philip@hartrao.ac.za
Müskens, Arno	University of Bonn, Germany mueskens@mpifr.de
Neidhardt, Alexander	FESG, TU Muenchen, Germany neidhardt@fs.wettzell.de
Nickola, Marisa	Hartebeesthoek Radio Astronomy Observatory, South Africa, marisa@hartrao.ac.za
Niell, Arthur	MIT Haystack Observatory, U.S.A. aniell@haystack.mit.edu
Nilsson, Tobias	GFZ German Research Centre for Geosciences, Germany, nilsson@gfz-potsdam.de
Nosov, Evgeny	Institute of Applied Astronomy, Russia e84@mail.ru
Nothnagel, Axel	University of Bonn, Germany nothnagel@uni-bonn.de
Petrachenko, Bill	Natural Resources Canada, Canada Bill.Petrachenko@nrc.gc.ca
Plank, Lucia	University of Tasmania, Australia Lucia.Plank@utas.edu.au
Porcas, Richard	Max-Planck-Institut für Radioastronomie, Germany, porcas@mpifr-bonn.mpg.de
Rayet, Rémi	CALLISTO, France remi.rayet@callisto-space.com
Sa, Nuno	Universidade dos Acores, Portugal nunosa@uac.pt
Santos, Luis R.	Direção Regional das Obras Públicas e Comunicações, Portugal, luis.r.santos@azores.gov.pt
Schuh, Harald	GFZ German Research Centre for Geosciences, Germany schuh@gfz-potsdam.de
Schüler, Torben	Geodetic Observatory Wettzell, Federal Agency for Cartography and Geodesy, Germany, schueler@fs.wettzell.de
Shu, Fengchun	Shanghai Astronomical Observatory,, China sfc@shao.ac.cn
Soja, Benedikt	GFZ German Research Centre for Geosciences, Germany bsoja@gfz-potsdam.de
Stagni, Matteo	IRA - INAF, Italy mstagni@ira.inaf.it
Takefuji, Kazuhiro	National Institute of Information and Communications Technology, Japan, takefuji@nict.go.jp
Teke, Kamil	Hacettepe University, Turkey kteke@hacettepe.edu.tr
Thorandt, Volkmar	Federal Agency for Cartography an Geodesy, Germany volkmar.thorandt@bkg.bund.de
Tornatore, Vincenza	Politecnico di Milano, Italy vincenza.tornatore@polimi.it

Tuccari, Gino	INAF-Istituto di Radioastronomia, Italy, and Max Planck Institut für Radioastronomie, Germany, g.tuccari@ira.inaf.it
Uunila, Minttu	Aalto University, Finland minttu.uunila@aalto.fi
Wang, Guangli	Shanghai Astronomical Observatory , China wgl@shao.ac.cn
Wu, Jiang	Shanghai Astronomical Observatory, China jiangwu@shao.ac.cn
Xu, Ke	China State Key Laboratory of Astronautic Dynamics, China, xk361@163.com
Xu, Minghui	Shanghai Astronomical Observatory, China mhxu@shao.ac.cn
Zhang, Dong	China State Key Laboratory of Astronautic Dynamics, China, sandmanzd@163.com
Zheng, Weimin	Shanghai Astronomical Observatory , China zhwm@shao.ac.cn
Zubko, Nataliya	Finnish Geospatial Research Institute, Finland nataliya.zubko@nls.fi

EVGA 2015 organization



Governo dos Açores



EVGA 2015 sponsors



Autoridade Nacional de Comunicações (ANACOM) is responsible for the regulation of the communications sector, including electronic and postal communications, along with assisting the Government in these areas. In its operations, it is guided by values such as quality, competence, efficiency, transparency, proximity and responsibility.



SATA is an air travel group composed by five companies: two airlines (Azores Airlines and SATA Air Aores); two tour operators, one in Canada (Azores Airlines Canada) and another in the United States (Azores Airlines America); and an entity in charge of managing various airport infra-structures in the Azores archipelago (SATA Gesto de Aerodromos). Connecting the Azores to the world for over sixty-five years, SATA focuses on its clients and on guaranteeing a service of excellence based on its corporate values of Friendliness, Reliability and Innovation, highly committed to the safety and comfort of its passengers. In 2013, SATA provided the biggest connectivity ever between the Azores and the rest of the world opening new routes, reinforcing frequencies, creating commercial representations in new markets and establishing new partnerships with airlines of reference, carrying more than one million passengers in a year to dozens of destinations in Europe, Canada and the United States.



GlobalEDA is a technology-based company acting in the telecommunications and information systems areas, involving worldwide well known partners and developing an attested sustained knowledge on the trading aspects, design, supply, installation, operation and maintenance. It has a close relationship with scientific and technological entities, and promotes initiatives such as EVGA, where it shares experiences, expertise and information, with the worlds top companies in Information and Communication Technologies (ICT).



PT Portugals operations cover all segments of the telecoms sector: fixed, mobile, multimedia, data, data center and cloud, as well as enterprise solutions, having a diversified business portfolio in which quality, innovation and service excellence are key factors. It is a client oriented company, focused on innovation and execution that meet the needs of the digital consumer, and it is organized by customer segments promoting collaboration between functions and platforms to ensure a convergent experience with high quality levels. Next generation access networks and data centers have long been an area of expertise of PT Portugal, effectively establishing the company as a provider of value-added services at a global scale and the country as a test bed for leading-edge solutions.



NOS is a communications company that was born from the fusion of ZON and Optimus, the two biggest enterprises of communications in Portugal. Because of that, NOS is a strong and responsible company, focused in the future and clearly committed to the excellency of its services, as well as to the customers satisfaction. In order to provide a faster, safest and innovative service, NOS has joined, into one strong and integrated structure, all fixed and mobile communications, using the smartest and most advanced networks of our country.



EDA is a company operating in production, distribution and trading of electricity. Recognized by their customers for the efficiency and quality of the services provided, EDA plays a key role in the Azores development process, safeguarding the environmental and cultural heritage and electing as its strategic areas, telecommunications, information systems and electrical and mechanical maintenance. On what concerns to the electrical sectors, EDAs growing commitment is to renewable energies.



The main mission of Teatro Micaelense is to assure the providing of a public service within the field of cultural promotion, through the presentation, production and co-production of activities from the most diverse artistic strains. In parallel, Teatro Micaelense takes on its place as a privileged instrument for the development of the Meetings and Incentives sector in the Azores, allowing for the holding of conferences, business meetings and other social events.



The Technical Engineers Order OET - is the representative association for the Technical Engineers, which are skilled professionals with a 1st cycle degree of an Engineering graduation or equivalent training. These professionals practice in the engineering area and have skills, technical and scientific knowledge and a high practical sense that enable them to perform on their expertise areas.

ISBN 978-989-20-6191-7



9 789892 061917